Using Zebrafish to Assess the Role of Inflammation-Linked Parkinson's Disease Risk Genes in Neurodegeneration

The University of Sheffield

Faculty of Medicine, Dentistry and Health
Department of Neuroscience

Emma May Fargher

A thesis submitted in fulfilment of the requirements for the degree of Doctor of Philosophy

Submission Date: February 2022

Primary Supervisor: Professor Oliver Bandmann
Secondary Supervisors: Dr Fredericus van Eeden and Dr Ryan MacDonald

Acknowledgments

I would like to thank NZP for providing the funding for this project which has allowed me to develop practical skills, knowledge and resilience beyond what I ever expected.

It would not have been possible to complete this doctorate without the support of those around me. My utmost gratitude goes to my supervisor, Professor Oliver Bandmann, for his support, encouragement, guidance and patience, particularly during the coronavirus pandemic. I would also like to thank my second supervisor, Dr Freek van Eeden, who has been exceptionally helpful with his vast knowledge of zebrafish.

My thanks must also go to Dr Ryan MacDonald and Dr Aaron Savage who welcomed me into their group despite my complete lack of experience and taught me the lab skills I needed to complete my PhD. This also extends to all members of the Bandmann group and C10 who have always been around for lab support and stimulating academic discussion.

To all my friends at the Bateson centre, particularly to Dhee, without your encouragement of coffee breaks or after work drinks my experience as a postgrad would not have been the same. This also applies to my friends outside of work, past and present, who have always been there for emotional support and a reminder to relax and have fun. Jess, your friendship during this write up period has been amazing. I cannot thank you enough. This list would not be complete without a special mention to Dom and Charlotte who were the best housemates throughout lockdown, providing a perfect balance between a quiet work environment and 12-hour bottomless brunches!

Of course none of this would have been possible without the love and support of my parents who enabled me to pursue this academic route or my college lecturers who helped me to recognise my potential. I also must thank my brother, Tom, from the bottom of my heart. Not only has he provided financial, emotional and career support over the years, but he has also set an almost unachievably high bar of success which has always driven me to work hard and be the best that I can!

And finally, my thanks must go to my husband, Sam, who has put up with my changing work patterns, late nights, 4am starts and a number of stressful weeks without complaint. Your understanding, grounding and distraction has been invaluable.

Abstract

Parkinson's disease (PD), a neurodegenerative movement disorder characterised by the loss of dopaminergic neurons in the substantia nigra, has been unequivocally linked to neuroinflammation. Polymorphisms in or near over 90 PD risk genes have been linked with altering the likelihood of developing PD and a number of these genes can also be linked to inflammation. This thesis primarily explores the role of two inflammation-linked risk genes (*leucine-rich repeat kinase 2* (*LRRK2*) and *α-amino-β-carboxymuconate-ε-semialdehyde decarboxylase* (*ACMSD*)) using the zebrafish as a model system. *acmsd* and *lrrk2* were shown to be expressed in larval and adult zebrafish, and zebrafish carrying loss-of-function mutations in both genes were generated using CRISPR-Cas9 technology. Homozygous mutants were viable, fertile and exhibited no abnormalities in movement, dopaminergic neurons or microglia. They also demonstrated no change in susceptibility to hepatotoxic, neurotoxic or pro-inflammatory compounds. Metabolomics analysis identified an increase in kynurenine aminotransferase activity in *acmsd* mutant zebrafish, offering an attractive hypothesis to explain the lack of phenotype in this line; kynurenic acid, the product of kynurenine aminotransferase, can antagonise quinolinic acid, which may reduce the toxic effects of the increase in quinolinic acid detected in both larval and adult *acmsd* mutants. Additionally, several new *lrrk2*-mutant zebrafish lines were successfully created using a novel genetic editing technique. This site-directed mutagenesis enabled the induction of specific amino acid changes that recapitulate pathogenic mutations of *LRRK2* in PD. This methodology could also now be applied to other genes and research areas, increasing the relevance of zebrafish as a model for human disease. To conclude, whilst both *lrrk2* and *acmsd* are expressed throughout life in zebrafish, a loss of their expression did not result in a PD-like phenotype. A possible explanation for this was identified for *acmsd* and new stable mutants carrying distinct point mutations were generated for *lrrk2*.

Table of Contents

1 Table of Abbreviations

Abbreviation	Full name	Abbreviation	Full name
6-OHDA	6-hydroxydopamine	KAT-1	Kynurenine aminotransferase 1
aa	Amino acid	LPS	Lipopolysaccharide
ACMS	α-amino-β-carboxymuconate-ε-semialdehyde	LRR	Leucine-rich repeat
ACMSD	α-Amino-β-Carboxymuconate-ε-Semialdehyde Decarboxylase	LRRK1	Leucine-rich repeat kinase 1
AMS	α-aminomuconate semialdehyde	MAPKKK	Mitogen-activated protein kinase kinase kinase
ANOVA	Analysis of variance	MCP1	Monocyte chemoattractant protein 1
BBB	Blood-brain barrier	Mmp9	Matrix metallopeptidase 9
BH4	Tetrahydrobiopterin	MPP+	1-methyl-4-phenylpyridinium
BLAST	Basic Local Alignment Search Tool	MPTP	1-methyl-4-phenyl-1,2,3,6-tetrahydropyridine
BLASTN	Nucleotide Basic Local Alignment Search Tool	mRNA	Messenger RNA
BLASTP	Protein Basic Local Alignment Search Tool	NAD+	Nicotinamide adenine dinucleotide
bp	Basepairs	NADH	Reduced nicotinamide adenine dinucleotide
BSA	Bovine Serum Albumin	NaOH	Sodium Hydroxide
cAMP	Cyclic adenosine monophosphate	NFκB	Nuclear factor kappa B
Cas9	CRISPR-associated protein 9	NHEJ	Non-homologous end joining
cDNA	Complementary DNA	NMDA	N-Methyl-D-aspartic acid or N-Methyl-D-aspartate
CNS	Central nervous system	NO	Nitric Oxide
CRISPR	Clustered, Regularly-Interspaced, Short, Palindromic Repeats	NOS	Nitric Oxide Synthase
crRNA	CRISPR RNA	NSAIDs	Non-steroidal anti-inflammatory drugs
CSF	Cerebral Spinal Fluid	O_2^-	Superoxide
CXCL8	C-X-C Motif Chemokine Ligand 8	PAM	Protospacer Adjacent Motif
DAPI	4’,6-diamidino-2-phenylindole	PBS	Phosphate buffered saline
DEPC	Diethyl Pyrocarbonate	PBStw	Phosphate buffered saline with 0.01% tween
DMSO	Dimethyl sulfoxide	PCR	Polymerase chain reaction
DNA	Deoxyribonucleic acid	PD	Parkinson’s disease
Dpf	Days post fertilisation	PET	Positron emission tomography
DTT	Dithiothreitol	PIC	Picolinic acid
FABP	Fatty acid binding protein	PXR	Pregnane X receptor
FXR	Farnesoid X receptor	qPCR	Quantitative polymerase chain reaction
GAK	Cyclin G Associated Kinase	QUIN	Quinolinic Acid
GCH1	GTP Cyclohydrolase 1	RBC	Red blood cell
gDNA	Genomic DNA	RBI	Rostral blood island
GDP	Guanosine diphosphate	RFLP	Restriction fragment length polymorphism
GI	Gastrointestinal	RNA	Ribonucleic acid
gRNA	Guide RNA	Roc	Ras of complex protein
GTP	Guanosine triphosphate	ROS	Reactive Nitrogen Species
GUDCA	Glycoursodeoxycholic Acid	RT	Room temperature
GWAS	Genome-wide association studies	SEM	Standard error of the mean
HAG	Highly active guide	SNpc	Substantia nigra pars compacta
HCl	Hydrochloric acid	SNPs	Single nucleotide polymorphisms
HDR	Homology directed repair	SSC	Saline sodium citrate
HLA-DR	Human Leukocyte Antigen – DR isotype	ssODN	Single-stranded donor oligonucleotide
IBD	Inflammatory Bowel Disease	TALEN	Transcription activator-like effector nucleases
ICSBP	Interferon consensus sequence binding protein	TGF-α	Transforming growth factor alpha

IDT	Integrated DNA technologies
IFN-γ	Interferon gamma
IHC	Immunohistochemistry
IL-10	Interleukin-10
IL-12	Interleukin-12
IL-1α	Interleukin-1 alpha
IL-1β	Interleukin-1β
IL-6	Interleukin-6
IL-8	Interleukin-8
Irf8	Interferon regulatory factor 8
TGF-β	Transforming growth factor beta
TH1	Tyrosine Hydroxylase 1
TNBS	2,4,6-Trinitrobenzenesulfonic acid
TNF-α	Tumour Necrosis Factor - alpha
TUDCA	Tauroursodeoxycholic acid
UDCA	Ursodeoxycholic acid
VDA	Ventral wall of dorsal aorta
WISH	Wholemount in situ hybridisation
WT	Wildtype

2 Introduction

Parkinson's disease (PD) is a progressive neurodegenerative disorder. It is characterised by the degeneration and death of dopaminergic neurons in the substantia nigra pars compacta (SNpc) and the deposition of misfolded protein aggregates, named Lewy Bodies (Braak et al., 2004). These cellular changes lead to a progressive loss of nervous system function, resulting primarily in bradykinesia, rigidity and tremor, although PD is also associated with non-motor symptoms including insomnia, depression, loss of smell and constipation (Postuma et al., 2015).

At present, PD is the most prevalent neurodegenerative movement disorder, effecting 0.1% of the global population, with predictions of worldwide incidence reaching 9.3 million by 2030 (Dorsey et al., 2007). The most important risk factor for PD is age, where the likelihood of developing the disease increases over time (Hirsch et al., 2016), although environmental and genetic risk factors, discussed below, have also been recognised to play considerable roles.

Despite the vast amount of research attention and funding that PD has received, there is still no cure available to prevent or reverse dopaminergic neuron degeneration. Currently available treatments focus purely on symptom reduction whilst carrying a high risk of serious side effects, such as dyskinesia (Thanvi et al., 2007). Supplementation with the dopamine precursor L-DOPA is the primary treatment option for people with PD and whilst successful in symptomatic treatment during early stages of disease, its efficacy diminishes over time and patients continue to decline (Parkinson Study Group, 2000; Rajput et al., 2002). Whilst PD is not recognised as a disease of mortality, it is progressive. Patients experience continued reductions in their quality of life with little treatment options available to them. The risk of physical injury or aspiration increases over time due to reductions in motor control, swallowing and coordination, possibly resulting in premature death (Matsumoto et al., 2014).

Given the severity and prevalence of this devastating disease, the need to continue research into PD is clear. It is likely that at the time of clinically manifest symptoms extensive dopamine has already been depleted, since 50% of dopaminergic neurons are lost by 12-months post diagnosis (Kordower et al., 2013). Focussing on a means to target disease processes early, perhaps even prior to clinical diagnosis, could enable those with PD to never develop the life changing symptoms associated with advanced stage disease.

2.1 Neuroinflammation in Parkinson's Disease

The central nervous system (CNS) is built up of multiple, interconnected cells; within this organised network lies another central bodily system, the immune system (Kipnis & Filiano,

2018). The immune system plays a vital role in protecting the body from invading pathogens and foreign material. Within the brain, specialised immune cells reside, protecting the CNS in the same way that other members of the immune system protect the rest of the body, creating a new field of research known as neuroimmunology. Under certain conditions, peripherally located immune cells can cross the blood brain barrier (BBB), contributing to the immune response of the brain to infections, damage and toxins (Larochelle et al., 2011).

The CNS demonstrates an inflammatory response in a similar way to the rest of the body, a process referred to as neuroinflammation. Over the last two decades accumulating evidence has emerged that suggests a contribution of neuroinflammation to the development of PD. Animal research and epidemiological data (discussed below) strongly suggest that inflammation occurs as an early indication of the disease, possibly before overt Parkinsonian symptoms appear. However, it is still not fully understood whether inflammation represents a cause or consequence of PD.

Microglia are the principle, brain resident, innate immune cells in charge of maintaining homeostasis in the CNS. Identified by Achucarro and del Rio-Hortega in the early 20th century (Tremblay et al., 2015), microglia act as a first line of defence against invading pathogens. Microglial activation occurs following injuries or immune insults, resulting in increased numbers

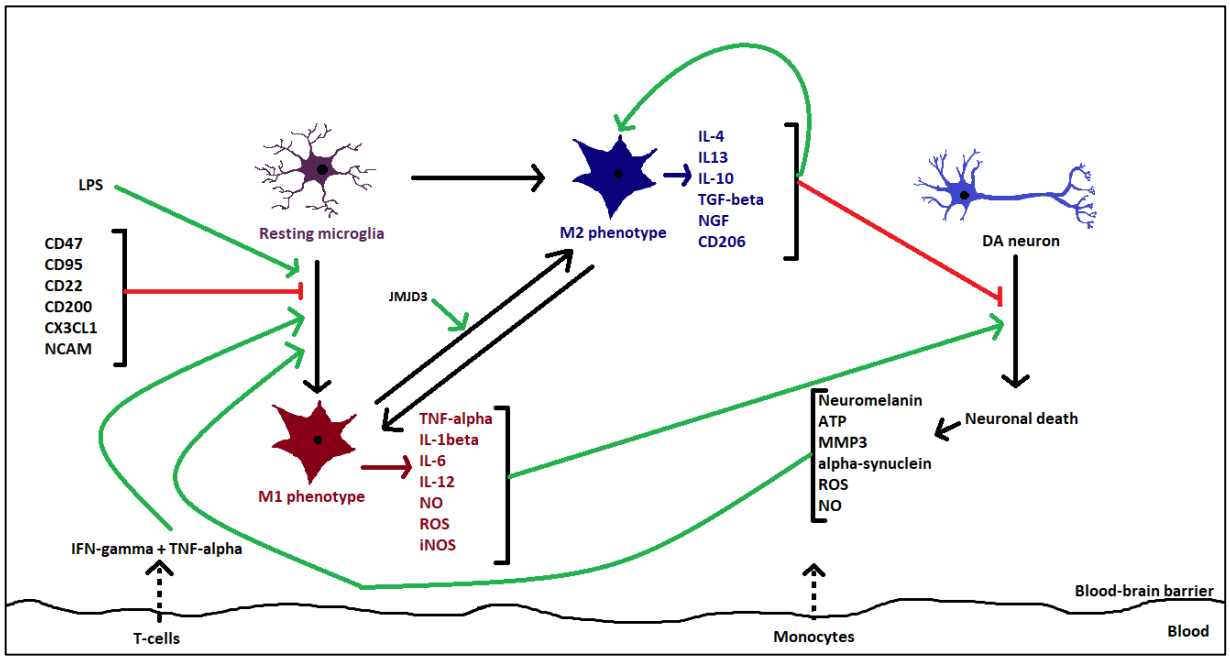

Figure 1. The Role of Microglial Cytokines in Dopaminergic Neuronal Death. *Microglia adopt two distinct phenotypes, associated with two opposing roles in the central nervous system. The M1 phenotype enables the production of proinflammatory cytokines which contribute to the death of dopaminergic neurons, whilst the M2 phenotype has an opposing role. Dying neurons produce factors which further push microglia towards a proinflammatory phenotype, resulting in a positive feedback loop. Other factors, such as Jumonji domain containing 3 (Jmjd3) (Tang et al., 2014) and peripheral immune cells (Wong et al., 1999), are also able to alter microglial polarisation via cytokine-independent mechanisms Original image. For additional references, see text.*

of macrophage-like cells with phagocytic ability (Stence et al., 2001). Activated microglia are usually associated with a negative role in the brain due to the production of reactive oxygen species (ROS), reactive nitrogen species and proinflammatory cytokines, including interleukin-1β (IL-1β), interleukin-6 (IL-6) and tumour necrosis factor-alpha (TNF-α) (Li et al., 2004). However, evidence also suggests that microglia demonstrate a protective role in the CNS via the production of neurotrophic factors (Elkabes et al., 1996) and anti-inflammatory cytokines, such as interleukin-10 (IL-10) and transforming growth factor beta (TGF-β) (da Cunha et al., 1993; Seo et al., 2004), which act as neuronal survival signals (Martinou et al., 1990). To complement these apparently conflicting roles, microglia have been shown to possess two distinct activated phenotypes. The M1, or macrophagic, phenotype is said to be proinflammatory, whilst the M2, or antigen presenting, phenotype is thought to be anti-inflammatory (**figure 1**). This basic view of two distinct microglial phenotypes may be outdated. It is now more commonly recognised that there are multiple phenotypic stages during microglial activation and that amoeboid cells lacking processes can be considered active (A. Karperien et al., 2013).

There are many ways in which neuroinflammation can result in the death of dopaminergic neurons, including cytokine-dependent toxicity and inflammation-derived oxidative stress. During neuronal death nearby microglia proliferate and become highly phagocytic accompanied by an acute transcriptional response, identified by RNA sequencing (Oosterhof et al., 2017). To perpetuate matters, dying neurons release inflammation-inducing factors, such as matrix metalloproteinase-3, α-synuclein and neuromelanin, which further activate microglia, leading to a snowball effect that creates a chronic inflammatory state in the CNS (Zecca et al., 2003; Zhang et al., 2013). It is this out-of-control neuroinflammatory feedback loop that has recently been suggested to contribute to the relentless progression of PD.

Inflammation may also worsen some of the symptoms of PD associated with significant reductions in quality of life, such as fatigue (Herlofson et al., 2018). By targeting neuroinflammation, it may be possible to not only alter the degenerative process but also relieve some of the pre-existing symptoms experienced by patients. The role of neuroinflammation in PD is supported in both human patient research and animal models of the disease:

2.1.1 Evidence from Research in Patients

There is clear evidence for inflammatory processes being upregulated in people with PD, including increased plasma levels of proinflammatory cytokines like IL-6 and TNF-α (Brodacki et al., 2008). This can be extended to demonstrate inflammation specifically within the CNS, where

proinflammatory cytokines have been shown to be increased in the ventricular cerebral spinal fluid (CSF) (Mogi et al., 1995; Mogi et al., 1996; Mogi, Harada, Riederer, et al., 1994). Similar cytokines, namely TGF-β1, TNF-α, IL-1β, IL-6 and TGF-α, were also exclusively increased in striatal areas of the PD brain, including the caudate nucleus and putamen, remaining at normal levels in the cerebral cortex (Mogi et al., 1995; Mogi, Harada, Kondo, et al., 1994). The upregulation of such cytokines strongly suggests that neuroinflammation is a pathological feature of PD and the upregulation specifically in areas targeted by the disease suggests that this is not an unrelated phenomenon.

Microglial activation has been identified in many neurodegenerative diseases including PD, Alzheimer's disease and multiple sclerosis (Airas et al., 2018; McGeer et al., 1988; Ouchi et al., 2005). Post mortem studies were the first to indicate the involvement of microglia in PD, discovering Human Leukocyte Antigen DR isotype (HLA-DR)-positive microglia in the SNpc of patients (McGeer et al., 1988). Later studies corroborated these data, demonstrating that activated microglia are more numerous in PD patient brains when compared to healthy controls, particularly in the substantia nigra and putamen (Imamura et al., 2003). Positron emission tomography (PET), enabling the study of living patients, also showed that activated microglia are present in the brains of PD patients, irrespective of the number of years since diagnosis (Gerhard et al., 2006). Positive correlations exist between the number of active microglia and the extent of neurodegeneration (Imamura et al., 2003), as well as the severity of motor symptoms (Ouchi et al., 2005), hinting that microglia are, at least in part, responsible for Parkinsonian symptoms. However, these correlations are not supported in all studies assessing disease severity (Gerhard et al., 2006), implying that mechanisms besides microglial activation are also involved in PD neurodegeneration.

Additional links between inflammation and PD can be made from genome wide association studies (GWAS), as single nucleotide polymorphisms (SNPs) resulting in an increased risk of PD or various inflammatory diseases have been identified in the same genes. Seventeen overlapping loci have been identified between PD and inflammatory diseases including type 1 diabetes, Crohn’s disease, ulcerative colitis and rheumatoid arthritis (Witoelar et al., 2017). Such data implicates common genes in the processes which lead to neurodegeneration as well as inflammation, reinforcing the idea that these two areas are fundamentally linked.

To further support a role for inflammation in the development of PD, hypersensitivity diseases, such as allergic rhinitis and hay fever, may be more common in people with PD versus healthy controls (Bower et al., 2006). It is interesting to note, however, that many other diseases involving the immune system, including systemic lupus erythematosus and rheumatoid arthritis, have not been linked to PD (Bower et al., 2006). It could be hypothesised that patients with hypersensitivity diseases that cause activation of the systemic immune system are predisposed to overreact to antigens, which may lead to an exaggerated immune response resulting in dopaminergic neuron loss in the CNS. This theory is supported by other studies that have identified severe influenza as a risk factor for PD, carrying an odds ratio of 2.01 (Harris et al., 2012). The acute immune response to influenza may well prime the immune system for over-reactivity to future infections. Although interesting, the data reported by Harris et al (2012) must be carefully interpreted. This study was not controlled and relied on self-reporting which introduces considerable bias. In particular, problems may arise with patients differentiating between influenza and the common cold, for which this study found a negative correlation with PD. Furthermore, many other immune diseases included in this report were not associated with PD, or even inversely associated.

The hypothesis of increased sensitivity to immune insults is supported by human cell-based models. Monocytes from PD patients have been identified as hyperactive to certain triggers, including lipopolysaccharide (LPS) (Grozdanov et al., 2014). The application of LPS to monocytes to initiate their activation saw those monocytes from PD patients respond excessively compared to those from healthy controls, producing increased levels of proinflammatory cytokines. Grozdanov et al. (2014) used this information to develop the idea that a “second hit” is needed on top of a predisposition that created primed monocytes, a similar scenario to that which is thought to increase the risk of PD in those with hypersensitivity disorders.

2.1.1.1 The Gut-Brain Axis

A more recent area in the study of inflammation in PD focusses on a putative link between the inflammatory state of the gastrointestinal (GI) system and the function of the brain. An obvious relationship between GI functioning and PD exists, since GI symptoms are a common complaint in PD, with up to 50% of patients experiencing constipation (Chen et al., 2015). Additionally, constipation may also act as a predictor of PD, with a large-scale study indicating that those with constipation are twice as likely to develop PD later in life (Adams-Carr et al., 2016).

These data have been expanded to describe the possible connection between enteric inflammation and CNS function, whereby immune responses in the intestine may lead to the development of neuroinflammation and neurodegenerative disease. Over a decade ago, Braak's hypothesis proposed that the α-synuclein pathology associated with PD was initiated in the submucosal plexus of the enteric nervous system, which then translates to the brain via the vagus nerve (Braak et al., 2006). This hypothesis has been supported in more recent research by the identification that α-synuclein is, in fact, able to be retrogradely transported along the vagus nerve *in vivo* (Holmqvist et al., 2014). Additionally, truncal vagotomy, although not selective vagotomy, is negatively associated with PD risk (Liu et al., 2017), further suggestive of an important role for the GI system and vagus nerve in early PD pathology.

Further investigations into GI inflammation followed, identifying increases in calprotectin, a marker for GI inflammation, in the intestine (Schwiertz et al., 2018) as well as proinflammatory cytokines, namely IL-1α, and interleukin-8 (IL-8), in PD patient stool (Houser et al., 2018). Colonic biopsies from PD patients also support the theory of GI inflammatory involvement in the disease, with increased expression of proinflammatory cytokines and glial markers, which appeared independent of clinical severity (Devos et al., 2013). The microbiota found in the GI tract of PD patients has also been identified as abnormal, with decreases in anti-inflammatory associated microbes and increases in inflammation-inducing bacteria (Keshavarzian et al., 2015). The overgrowth of bacteria in the small intestine has been associated with worse motor function in PD patients (Scheperjans et al., 2015; Tan et al., 2014), suggesting that the altered microbiome is somehow related to the motor phenotype and disease severity. The prevailing theory for which GI inflammation may increase the risk of PD, besides the involvement of α-synuclein (Braak's hypothesis), is that inflammation in the GI system is able to penetrate the brain due to the leaky BBB observed in PD patients (Gray & Woulfe, 2015). A model for this was developed by Houser and Tansey (2017).

Another interesting finding is that inflammatory bowel disease (IBD) has been recognised as a comorbidity of PD, with SNPs identified by GWAS as being common to PD and both Crohn's disease and ulcerative colitis (Witoelar et al., 2017), although these are not evident in all populations (Camacho-Soto et al., 2018; Fujioka et al., 2017). A possible reason for this discrepancy may be due to the anti-inflammatory treatment received by Crohn's disease patients, particularly since TNF-α blockers taken by patients with Crohn's disease are associated with a reduced PD risk (Peter et al., 2018). More controlled studies, taking into account the

medication of the participants, will reveal whether this genetic association between IBD and PD indeed exists.

Despite the above data suggesting a correlation between GI inflammation and PD, cause and effect cannot be established. It is possible that gut inflammation may be an epiphenomenon or an effect of PD treatments rather than a causal factor in PD pathology. However, much research has identified GI inflammation in very early cases of PD (Tan et al., 2014), indicating that it occurs concomitantly, or perhaps even prior, to PD diagnosis. This substantiates the theory that GI inflammation may be a cause, or at least contributing factor, as opposed to a consequence, of PD.

2.1.2 Animal Models and The Role of Peripheral Inflammation

Various toxin-induced animal models of PD, including 1-methyl-4-phenyl-1,2,3,6 tetrahydropyridine (MPTP), 6-hydroxydopamine (6-OHDA), LPS, paraquat and rotenone, have been useful in establishing a possible mechanism by which neuroinflammation may be linked to the disease (**figure 2**) (Castaño et al., 1998; Cicchetti et al., 2002; Emmrich et al., 2013; Kalkonde et al., 2007; Liberatore et al., 1999; Mangano et al., 2012).

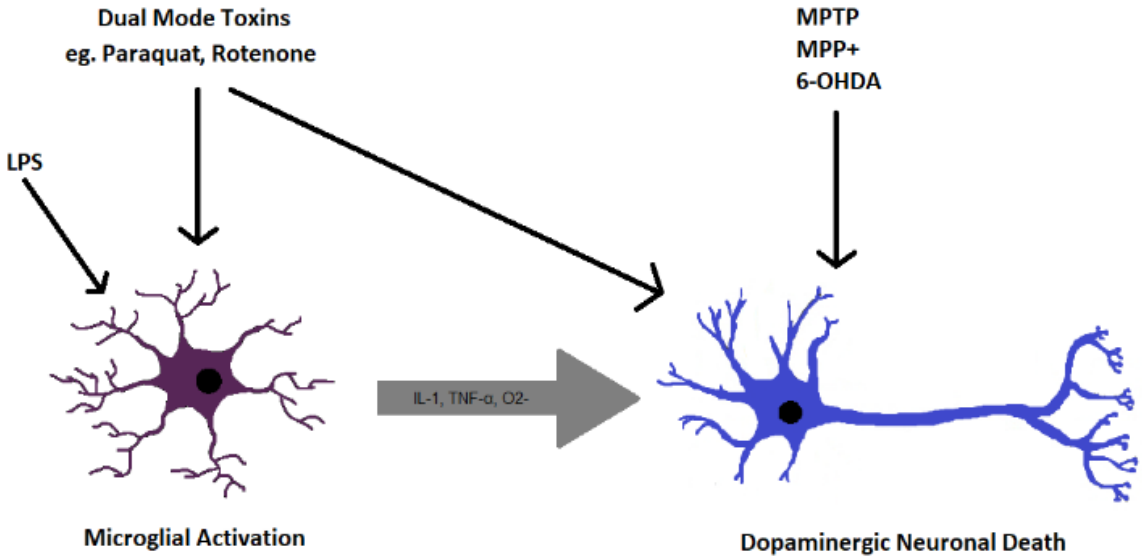

Figure 2. The Mechanism of Action of Neurotoxin Models of Parkinson's Disease. *Toxins can lead to the death of dopaminergic neurons, resulting in Parkinson's disease-like pathology in animal models. Dual mode toxins can cause dopaminergic toxicity directly as well as via microglial activation, leading to the release of proinflammatory factors including interleukin 1 (IL-1), tumour necrosis factor alpha (TNF-α) and superoxide (O_2^-). Original image, adapted from Block and Hong (2005). MPTP, 1-methyl-4-phenyl-1,2,3,6 tetrahydropyridine; 6-OHDA, 6-hydroxydopamine; LPS, lipopolysaccharide; MPP+, 1-methy-4-phenylpyridinium.*

One important finding from these models was the identification that neither MPTP nor its active metabolite, 1-methy-4-phenylpyridinium (MPP+), could directly activate microglia, yet both are able to induce significant neurodegeneration (Gao et al., 2003). This enabled the establishment of the paradigm that neuronal damage leads to the activation of microglia and that inflammation may be a result of neuronal cell death rather than a cause.

Due to its well-known ability to induce peripheral inflammation, LPS, a bacterial endotoxin, has proven critical to enhancing the understanding of this emerging research area. When administered systemically, LPS has the ability to cause nigral neurodegeneration, resulting in Parkinsonian symptoms in animal models. The capability of a peripheral inflammatory cue to result in CNS inflammation has been suggested to be a result of susceptible microglia undergoing phenotype switching to produce proinflammatory cytokines (Cunningham et al., 2009). Despite focussing on dementia, this study demonstrates how systemic inflammation can prime the CNS to cultivate a proinflammatory state and how this can lead to both biochemical and symptomatic worsening of neurodegeneration. Furthermore, LPS has been found to compromise the BBB (Cardoso et al., 2012; Erickson et al., 2012), enhancing the ability of activated immune cells from the periphery to enter the CNS and cause neuroinflammation.

More recent research has also taken advantage of animal models to demonstrate further the risk of peripheral inflammatory processes to developing PD. Inhibiting peripheral inflammation in the liver of an MPTP model reduced the amount of dopaminergic neuronal degeneration in the midbrain (Qiao et al., 2018), clearly linking the presence of inflammation outside of the CNS to effects within it. Combining an MPTP model of PD with LPS, García-Domínguez et al. (2018) have been able to collate earlier research findings, creating a mechanism by which peripheral inflammation may lead to the development of PD. In their model, MPTP created a basal neuroinflammatory state which primed microglia to respond to proinflammatory cues. Systemic inflammation by LPS broke down the BBB, enabling peripheral immune cells and cytokines to pass into the CNS and activate these primed microglial cells. An up-regulation of proinflammatory cytokines was evident in the brain alongside activated microglia and astrocytes, eventually leading to the loss of dopaminergic neurons in the substantia nigra.

The exploitation of genetic techniques to inhibit microglial activation in animal models, for example by knocking out class II transactivator, supports human data for microglia being the driving force of neuroinflammation in PD (Williams et al., 2018). The reduction in

neurodegeneration in these murine models powerfully demonstrates that neuroinflammation, namely microglial activation, can indeed result in neurodegeneration.

2.1.3 Dopaminergic Predisposition to Inflammation

Dopaminergic neurons may be predisposed to death by inflammation, which may be acutely linked to microglial activity. Microglia are present at different concentrations in different areas of the brain, with the highest concentration in the mesencephalon (Kim et al., 2000). When comparing the effects of LPS injected into different areas of rat brains, or directly to neuron-glia cultures isolated from these areas, it has been found that neuronal death is differentially responsive to LPS depending on region (Kim et al., 2000). For example, mesencephalic neurons are more likely to die in response to LPS than in other areas of the brain, suggesting that these neurons are more susceptible to inflammation-induced neurodegeneration. Additionally, it was noted that a dose-dependent increase in cytokine production, namely NO and TNF-α, occurred in mesencephalic cultures more so than in cortical or hippocampal neurons, suggesting that this cytokine production may be responsible for the observed neuron death. Adding additional microglia to cultures of cortical or hippocampal neurons increased the neurotoxic effects of LPS (Kim et al., 2000), demonstrating that differences in LPS toxicity are due to the microglia present in different brain regions and not differences in the neurons per se.

2.1.4 Monogenetic Parkinson's Disease Genes and Inflammation

PD can be separated into two core subtypes; familial, where the disease results from inherited genetic mutations, or idiopathic, where there is no evidence of family history of disease. Several genes that are responsible for monogenetic forms of PD have now been identified (see **table 1**). These Mendelian subtypes are relatively rare, responsible for only 5-10% of all PD cases (Thomas & Beal, 2007), although their possible relationships to neuroinflammation is interesting in this context.

The first mutation to be confirmed as a cause of monogenic PD was a G209A substitution in *SNCA*, the gene encoding α-synuclein, which results in autosomal dominant PD (Polymeropoulos et al., 1997). Part of the pathological response to this mutation may be the induction of neuroinflammation. A key feature of PD is the presence of Lewy Bodies, made up of filamentous α-synuclein (Spillantini et al., 1998). Whilst these Lewy Bodies can be directly responsible for neuronal death, the aggregated α-synuclein also plays a role in activating proinflammatory responses in the CNS, which further instigates this death (W. Zhang et al., 2005). A correlation between α-synuclein levels and microglial activation, as measured by MHC-II staining, has been

identified in human brains (Croisier et al., 2005). Although distinguishing cause and consequence is not possible from such data, mice overexpressing α-synuclein demonstrate an activation of microglia (Su et al., 2008), suggesting that α-synuclein does indeed induce this activation. Further studies have suggested a mechanism of action for this (**figure 3**), highlighting a central role for neuroinflammation in this Mendelian case of PD.

Additionally, other genes implicated in familial PD, such as *Parkin* (Lücking et al., 2000), can be linked to neuroinflammation by analysing their expression in immune cells. Parkin has been detected in microglia and peripheral macrophages (Tran et al., 2011), where it has been suggested to act as a suppressor of inflammation (Dionísio et al., 2019; Singh et al., 2018; Tran et al., 2011). Parkin may prevent the persistence of activated microglial cells by inducing their necroptosis (Dionísio et al., 2019), reducing the number of cells available to release cytokines into the CNS, thereby lessening further inflammation. There is controversy over whether Parkin has a proinflammatory (de Leseleuc et al., 2013; Letsiou et al., 2017) or anti-inflammatory role in the CNS, but it is clear that Parkin is implicated in some way in neuroinflammation as well as in PD.

Links between other monogenetic PD genes and neuroinflammation have been identified; those available as stable zebrafish lines in the Bandmann Laboratory are outlined briefly in **table 1**.

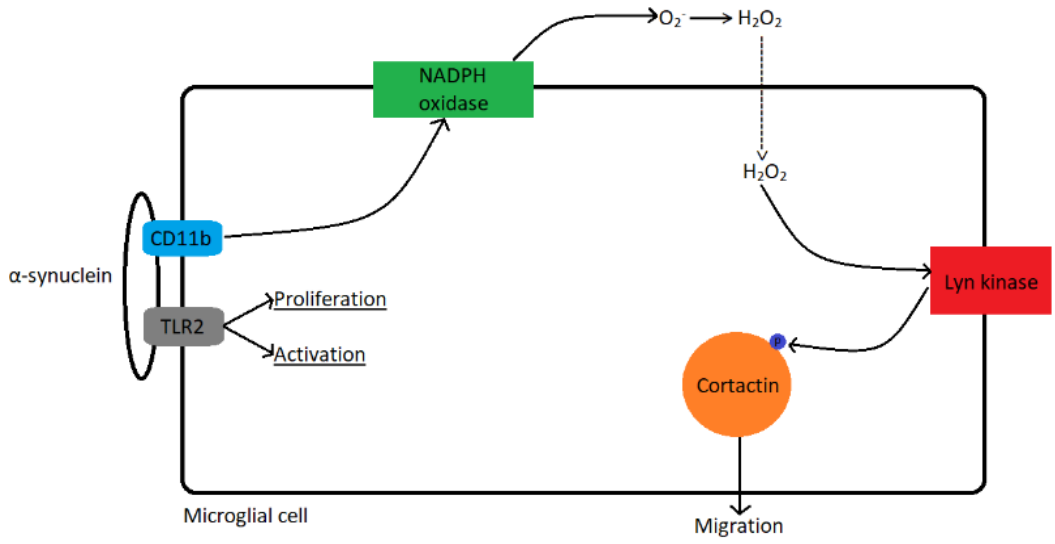

Figure 3. Schematic Representation of the Mechanism of Action by Which α-Synuclein Enables the Activation and Migration of Microglia. *α-synuclein binds directly to CD11b on the surface of microglia, activating NADPH oxidase, with the downstream consequence of producing O_2^-. This is converted to hydrogen peroxide (H_2O_2) which is membrane permeable, creating a concentration gradient from outside to inside the cell, leading to microglial migration. Cortactin phosphorylation by Lyn kinase, induced by the H_2O_2 released, causes the actin cytoskeleton to rearrange which determines the direction of microglial migration. Additionally, the binding of α-synuclein to toll-like receptor 2 (TLR2) causes increased proliferation and cytokine production. Original image, data taken from Wang et al. (2015), Kim et al. (2014) and W. Zhang et al. (2005).*

Table 1. Some of the Genes Thought to be Causative of Inherited Forms of Parkinson's Disease and Their Possible Role in Neuroinflammation.

Gene	Protein	Inheritance and disease onset	Link to neuroinflammation?
SNCA	Encodes for α-synuclein, a pre-synaptic neuronal protein involved in synaptic vesicle clustering to aid neurotransmitter release (Diao et al., 2013).	AD early and late-onset PD (Polymeropoulos et al., 1997)	α-synuclein activates microglia (W. Zhang et al., 2005), leading to the production of proinflammatory mediators (Su et al., 2008), as well as potentiating the CNS response to systemic inflammation (Gao et al., 2011).
LRRK2	Encodes for leucine-rich repeat kinase 2, a kinase, GTPase and a scaffolding protein important in regulation of the cytoskeleton, among other things (Li et al., 2014).	AD late-onset PD (Zimprich et al., 2004)	Discussed in chapter 5.
PARKIN	Encodes for parkin, an E3 ubiquitin ligase, responsible for targeting proteins for degradation via the ubiquitin-proteasome pathway (Shimura et al., 2000).	AR early-onset PD (Lücking et al., 2000) and AR juvenile Parkinsonism (Kitada et al., 1998)	Parkin is expressed in microglia and macrophages, at levels that vary depending on the inflammatory state of the surrounding area (Tran et al., 2011). Controversy exists over whether Parkin plays a proinflammatory (de Leseleuc et al., 2013; Letsiou et al., 2017) or anti-inflammatory (Dionísio et al., 2019; Tran et al., 2011) role in the CNS. Most studies suggest that Parkin prevents cytokine release from astrocytes and microglia and induces their necroptosis (Dionísio et al., 2019; Singh et al., 2018).
PINK1	Encodes for phosphatase and tensin homolog-induced putative kinase 1, a mitochondrial serine/threonine kinase (Valente et al., 2004).	AR early-onset PD (Valente et al., 2004)	The role of PINK1 in neuroinflammation is unclear. It may be proinflammatory, stimulating NFκB signalling and increasing the production of cytokines (Lee & Chung, 2012) and reactive oxygen species (Heeman et al., 2011). However, PINK1 deficiency is also thought to lead to neuroinflammation as a consequence of cytokine alterations (Akundi et al., 2011; Sliter et al., 2018), T cell number and function (Ellis et al., 2013; Saunders et al., 2012) and the aggregation of α-synuclein (Liu et al., 2009).
DJ-1	Encodes for protein deglycase DJ-1, a multifunctional protein involved in a varied range of processes (Bonifati et al., 2004).	AR early-onset PD (Bonifati et al., 2003)	DJ-1 appears to be involved in the production of cytokines in astrocytes (Ashley et al., 2016), which may contribute to gliosis and inflammation in the CNS.
ATP13A2	Encodes for ATPase cation transporting 13A2, a neuronal P-type ATPase involved in cation homeostasis and maintaining neuronal integrity (Ramonet et al., 2011).	AR early-onset PD and Kufor-Rakeb syndrome (Ramirez et al., 2006)	Little research has explored ATP13A2 in neuroinflammation. ATP13A2 may inhibit astrocyte production of proinflammatory cytokines, whilst inducing production of anti-inflammatory cytokines, by preventing the activation of the NLRP3 inflammasome (Qiao et al., 2016).
VPS13C	Encodes for vacuolar protein sorting 13 homolog C. This is a lipid transport protein bound to the endoplasmic reticulum (Kumar et al., 2018)	AR PD (Schormair et al., 2018)	Unknown / not reported.

Table outlining some common monogenic causes of Parkinson's disease, with reference to their protein function and implications in neuroinflammation. AD, autosomal dominant; AR, autosomal recessive; CNS, central nervous system; PD, Parkinson's disease.

2.1.5 Parkinson's Disease Risk Genes and Neuroinflammation

Most cases of PD are classed as sporadic (Thomas & Beal, 2007), where there is no evidence of family history of disease. GWAS have been critical to unearthing possible genetic risk factors associated with sporadic PD. This relatively recent study design identifies SNPs, variations in just one nucleotide, that are more common in those with a disease than in those without. In 2014, a meta-analysis of GWAS identified 24 loci implicated in sporadic PD, with a total of 28 risk variants (Nalls et al., 2014). This was further increased to 35 loci in a similar meta-analysis (Chang et al., 2017) and even more recently to a total of 90 (Nalls et al., 2019). This most recent meta-analysis identified 7.8 million SNPs from 17 previous studies, totalling nearly 1.5 million individuals. It is possible that even more variants will be identified as research develops further and more genomes are fully sequenced.

Table 2 summarises risk genes that are available as stable zebrafish knockout lines in the Bandmann Laboratory; those used in this project are discussed in more detail within their relevant chapters. Although it is probable that SNPs confer an additive risk to disease development, developing a loss-of-function system for each gene independently enables a better understanding of how this might be the case. Many PD risk genes are expressed in immune cells of the CNS and the ability to link these SNPs to inflammation further supports the paradigm that neuroinflammation plays a central role in PD pathogenesis.

Table 2. Some of the Parkinson's Disease Risk Genes Identified by Genome Wide Association Studies and Their Possible Role in Neuroinflammation.

Gene	Normal function	Reference that shows risk of SNPs	Link to neuroinflammation?
ACMSD	Encodes for α-amino-β-carboxymuconate-ε-semialdehyde decarboxylase, an enzyme involved in tryptophan degradation (Pucci et al., 2007).	(Nalls et al., 2014)	Discussed in chapter 4.
FYN	Encodes for a kinase involved in T-cell signalling (Palacios & Weiss, 2004).	(Nalls et al., 2019)	Required for microglial activation in response to LPS and the subsequent release of cytokines (Panicker et al., 2015).
GAK	Encodes for cyclin G associated kinase, a serine/threonine kinase that plays a vital role in clathrin-mediated intracellular transport (C. X. Zhang et al., 2005).	(Nalls et al., 2019; Nalls et al., 2014)	Discussed in chapter 6.
GBA	Encodes for glucocerebrosidase, a lysosomal enzyme that hydrolyses the glycolipid glucocerebroside to ceramide and glucose (Vielhaber et al., 2001).	(Chang et al., 2017; Nalls et al., 2019; Nalls et al., 2014)	Prevents microglial activation and expression of proinflammatory cytokines (Farfel-Becker et al., 2011; Vitner et al., 2014) whilst also inhibiting the accumulation of α-synuclein (Du et al., 2015; Yun et al., 2018).
GCH1	Encodes for GTP cyclohydrolase 1, the rate-limiting enzyme in	(Chang et al., 2017; Nalls et al.,	Discussed in chapter 6.

	tetrahydrobiopterin synthesis. Tetrahydrobiopterin is required for dopamine synthesis (Werner et al., 2011).	2019; Nalls et al., 2014)	
INPP5F	Encodes for inositol polyphosphate-5-phosphatase F, an enzyme found in the endosome (Nakatsu et al., 2015).	(Nalls et al., 2019; Nalls et al., 2014)	Unknown / not reported
LRRK2	Encodes for leucine-rich repeat Kinase 2, a kinase, GTPase and scaffolding protein important in regulation of the cytoskeleton, among other things (Li et al., 2014).	(Chang et al., 2017; Nalls et al., 2019; Nalls et al., 2014)	Discussed in chapter 5.
MCCC1	Encodes for methylcrotonoyl-CoA carboxylase 1, an enzyme found in the mitochondria that is required for the catabolism of leucine and isovalerate (Obata et al., 2001).	(Chang et al., 2017; Nalls et al., 2019; Nalls et al., 2014)	MCCC1 is expressed in peripheral immune cells as well as glial cells in the CNS (Murín et al., 2006; Obata et al., 2001). A role for MCCC1 has been identified in innate immunity, whereby it possesses an antiviral role (Cao et al., 2016), although a direct link to neuroinflammation has not been reported.
SIPA1L2	Encodes for signal induced proliferation associated 1 Like 2, a GTPase-activating protein involved in the functioning of the synapse (Spilker & Kreutz, 2010).	(Chang et al., 2017; Nalls et al., 2019; Nalls et al., 2014)	Unknown/not reported
SNCA	Encodes for α-synuclein, a pre-synaptic neuronal protein involved in synaptic vesicle clustering to aid neurotransmitter release (Diao et al., 2013).	(Chang et al., 2017; Nalls et al., 2019; Nalls et al., 2014)	See table 1
STX1B	Encodes for syntaxin-1 which controls synaptic vesicle fusion at neuronal synapses, assisting in the release of neurotransmitters (Gerber et al., 2008).	(Nalls et al., 2014)	A loss of STX1B may lead to glial dysfunction, including disrupted release of neurotrophic factors (Kofuji et al., 2014). However, later studies suggest STX1B deficiency leads to neuron death via non-glia mechanisms (Vardar et al., 2016). Further work is needed to clarify this mechanism of action and establish a clearer link to neuroinflammation.
TMEM175	Encodes for transmembrane protein 175, a potassium channel found on the lysosome (Cang et al., 2015).	(Chang et al., 2017; Nalls et al., 2019; Nalls et al., 2014)	Deficiency can lead to the aggregation of α-synuclein (Jinn et al., 2017), which may be responsible for inducing neuroinflammation.
VPS13C	Encodes for vacuolar protein sorting 13 homolog C. This is a lipid transport protein bound to the endoplasmic reticulum (Kumar et al., 2018).	(Chang et al., 2017; Nalls et al., 2019; Nalls et al., 2014)	See table 1

Table showing some of the risk genes identified for Parkinson's disease, their normal function and their possible links to neuroinflammation.

2.2 Zebrafish as an Animal Model for Parkinson's Disease

Model organisms are used to study human disease *in vivo*. Animal models have benefits over *in vitro* models in that they take into account the complex interplay between bodily systems, a more valid representation of the human condition. However, they are often more difficult to manipulate and isolating single biological processes is challenging due to compensatory and protective mechanisms often present in living organisms. Simple invertebrate models, such as *C.elegans* and Drosophila, are well characterised, easy to genetically manipulate and are not under regulatory control. However, due to the substantial differences to humans, such simple animal models may not accurately recapitulate human disease. Complex mammalian systems, which are biologically the most similar to humans, are under tighter regulatory control and are often more difficult to work with, both experimentally as well as practically in terms of the level of care needed, cost to keep, space required and ethical considerations.

Zebrafish (*Danio rerio*), as a non-mammalian vertebrate, represent a compromise between these simple and more complex models, with intermediate levels of regulatory control and ease of working but at the cost of increased dissimilarities to humans compared to mammalian models. They are, however, genetically very similar to humans. The zebrafish genome is comparable to that of humans in terms of its chromosome number and organisation (Ehrlich et al., 1997; Postlethwait et al., 2000). This conservation extends to pathological conditions, with 82% of human disease causing genes having a zebrafish orthologue (Howe et al., 2013). One phenomenon to bear in mind when working with zebrafish is the concept of whole genome duplication. Around 20% of zebrafish genes exist in duplicate (Postlethwait et al., 2000), which makes studying these specific genes more difficult due to possible compensation from corresponding paralogs.

Benefits of zebrafish as a research model of human disease are their short generation time and production of large batches of transparent embryos that develop externally, enabling easy observation and manipulation. Furthermore, embryonic development is complete by 72 hours post fertilisation (hpf) (Kimmel et al., 1995), enabling a relatively high-throughput approach for *in vivo* experiments. Multiple experimental techniques can be employed in zebrafish for the study of disease processes, including the use of fluorescent dyes, transgenic animals, in situ hybridisation, immunohistochemistry and various imaging techniques. These allow for the study of biological events in both tissue as well as in living embryos, enabling observation of disease processes in real-time.

Zebrafish represent an excellent organism for studying neurodegenerative diseases. Not only are their embryos easy to manipulate and study, the zebrafish nervous system is highly comparable to the nervous system of humans. For the study of PD, it is relevant that the zebrafish dopaminergic system is well characterised, making deviations from the norm relatively easy to recognise. Dopaminergic neurons first appear in the zebrafish embryo around 18hpf in the ventral diencephalon (Holzschuh et al., 2001), allowing research into dopaminergic neurodegeneration to begin just 1 day after collecting embryos. These neurons also undergo rapid development, with axonal projections being formed by 3-days post fertilisation (dpf) (Du et al., 2016).

The dopaminergic system of zebrafish shares similarity to that of humans. Approximately 25 neurons have been identified in the posterior tuberculum that project to the subpallium; this population (named the diencephalic (DC) group) is thought to be analogous to the human SNPc and can be easily distinguished and counted following in situ hybridisation (Du et al., 2016; Jay et al., 2015; Rink & Wullimann, 2001, 2002; Tay et al., 2011). In mammals, the *ORTHOPEDIA* homeobox gene-expressing A11 dopaminergic neuronal group is thought to be responsible for movement and sensory inputs (Koblinger et al., 2018). In zebrafish, DC2/4/5 neurons have also been found to express *orthopedia* and demonstrate conserved location, morphology and projection patterns to the A11 mammalian group (Ilin et al., 2021; Ryu et al., 2007; Tay et al., 2011). By axonal tracing, electrophysiology and laser ablation of DC2/4/5 in zebrafish larvae, it has been found that these groups also innervate the spinal cord and sensory structures, with a decrease in movement seen in their absence (Jay et al., 2015). Studying this population in zebrafish is, therefore, both simple and relevant.

Additionally, the assessment of microglial morphology and number can be utilised as a readout for neuroinflammation in zebrafish. Activated microglia retract their branches and become amoeboid (Audrey Karperien et al., 2013) which can be observed via wholemount immunohistochemistry due to the transparency of zebrafish larvae. This is an obvious advantage to other models, where glia are often only able to be observed in sections.

However, it is important to take into consideration the lack of α-synuclein in zebrafish when studying neurodegenerative diseases, in particular PD, where α-synuclein-containing Lewy Bodies are central to pathology. Zebrafish may not fully represent PD pathological processes due to the lack of this important protein, possibly generating data that is invalid when applied to the human condition. However, this lack of α-synuclein can also be viewed as advantageous as it

enables the study of disease processes that may be masked by this dominant pathological phenomenon, aiding the understanding of mutated proteins that cannot be studied in other animal models.

2.2.1 CRISPR-Cas9 Genome Editing

CRISPR (clustered, regularly-interspaced, short, palindromic repeats) was first identified as a defence mechanism of bacteria and archaea to phages (bacterial viruses) and has recently been exploited as a mutagenic technique in a number of animal models. CRISPR-Cas9 mutagenesis results from double-stranded DNA breaks by CRISPR associated protein 9 (Cas9) nuclease, in gene regions specifically targeted by a guide RNA (gRNA, **figure 4**). Cas9 is a protein that recognises a protospacer-adjacent motif (PAM), in this case NGG, to initiate double-stranded breaks in DNA which occur at its two sites of nuclease activity (Gasiunas et al., 2012; Jinek et al., 2012). Once Cas9 binds to the PAM, CRISPR-RNA (crRNA) binds to the adjacent sequence which causes the DNA to unwind, a process that can only occur in the presence of trans-activating crRNA (tracrRNA) (Jinek et al., 2012). Cas9 cleaves 3bps upstream of the PAM site on the complementary strand or 3-8bps upstream on the non-complementary strand (Jinek et al., 2012). Attempts by normal, error-prone DNA repair pathways, such as non-homologous end joining (NHEJ), to fix this double-stranded break results in the creation of indel mutations in the gene of interest. CRISPR-Cas9 mutagenesis is well established in zebrafish, with high efficiency (up to 99%) and mutations resulting in germline transmission (Jao et al., 2013). This enables zebrafish harnessing disease-relevant mutations to be created with relative ease.

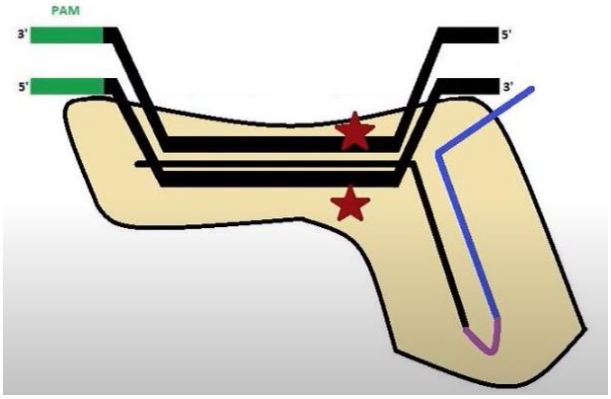

Figure 4. Schematic Representation of CRISPR-Cas9 Mediated Genetic Mutagenesis. *Diagram showing the process of double-stranded DNA (thick black lines) breakage at two sites of nuclease activity (stars) in the Cas9 protein (yellow). Cas9 binds to DNA at the protospacer-adjacent motif (PAM) site (green) and CRISPR-RNA (crRNA, thin black line) binds to the subsequent DNA sequence to unwind it. This crRNA is held in place by trans-activating crRNA (tracr-RNA, thin blue lines). The combination of crRNA and tracr-RNA is known as guide RNA (gRNA), and has been artificially joined for ease of production. Cas9 cuts DNA 3 basepairs upstream of the PAM site. Original Image.*

CRISPants, a form of creating genetic mutations in the F0 generation, are also useful in zebrafish research. Injecting gRNA targeting genes of interest into single-cell zebrafish embryos results in the creation of a mosaic animal, whereby some cells will carry mutations in the gene of interest and others may not. By using highly-active guides (HAGs), mosaic animals can be created that harbour mutations in the majority of their cells, essentially creating a mutant zebrafish (Wu et

al., 2018). By injecting multiple guides directly into the yolk of a recently fertilised zebrafish embryo, effective biallelic gene disruption within hours of injection has been achieved that can sometimes even be carried into adulthood (Wu et al., 2018). This method has been demonstrated to reproduce mutant phenotypes resulting from standard mutation methods. As these mutations remain in the fish longer than the oligomers used for morpholino studies, which often do not persist past 3dpf (Wu et al., 2018), CRISPants are useful in assessing the relevance of potential loss-of-function stable mutants in a time and cost – saving way. It also allows for the quick analysis of gene-gene interaction models where one stable mutant already exists. CRISPant guides can be injected into mutant embryos to assess additive or rescue effects of combinations of genetic mutations. However, it is generally expected that phenotypes discovered in this way are confirmed by stable mutants, to account for any possible off-target effects resulting from the injection of CRISPant mixes.

2.3 Hypotheses

Neuroinflammation may be the shared variable linking monogenic, environmental and risk gene-linked cases of PD. Many genes associated with PD, particularly those that fall under the 'risk gene' category, have not yet been studied with regards to inflammation and there are currently no drugs available to patients that target this directly. The more evidence that emerges to suggest an involvement of neuroinflammation in PD, the closer science can move towards identifying disease-modifying treatments, ultimately giving patients a better quality of life.

The aim of this thesis is to test the following hypotheses;

1. Zebrafish carrying functionally inactivating mutations in PD risk genes that can also be linked to inflammation will display a PD-relevant phenotype.

2. Zebrafish carrying functionally inactivating mutations in PD risk genes that can also be linked to inflammation will display an inflammatory phenotype.

3. Zebrafish carrying functionally inactivating mutations in PD risk genes will be more susceptible to additional, external triggers.

4. Inhibiting neuroinflammation, either pharmacologically or otherwise, will be able to, at least partially, rescue the phenotype of PD mutant zebrafish.

We know already that inflammation is involved in human PD and this has also now been demonstrated in PD mutant zebrafish lines (Keatinge et al., 2015; Larbalestier et al., 2021).

ACMSD acts to reduce neuroinflammation under normal conditions, and therefore it was hypothesised that *acmsd*$^{-/-}$ zebrafish would demonstrate an increased inflammatory phenotype. Conversely, since the most common *LRRK2* mutation identified in human PD patients results in a gain of LRRK2 function, it was hypothesised that *lrrk2*$^{-/-}$ zebrafish would show a reduced susceptibility to inflammation. If inflammation truly is one of the driving forces behind PD and the phenotypes seen in PD-relevant knockout zebrafish, then preventing its development should lead to a partial rescue of these abnormalities.

2.4 Objectives

To address these hypotheses, there were four main objectives of this project, outlined below.

Objective 1: To characterise novel zebrafish models of PD. The primary aim of this project was to characterise two zebrafish lines that carry knockout mutations of PD relevant genes*; leucine-rich repeat kinase 2* (*lrrk2*$^{-/-}$) and *α-amino-β-carboxymuconate-ε-semialdehyde decarboxylase* (*acmsd*$^{-/-}$).

Objective 2: To determine whether inflammation, particularly that mediated by microglia, drives the phenotype of these models. A further aim of this project was to assess the role of microglia and inflammation in contributing to the phenotype of PD mutant zebrafish. Various measures of inflammation, including the susceptibility to external inducers of inflammation, would assist in answering this question and by preventing the development of microglia, their role in this process could be better understood.

Objective 3: To target inflammation pharmacologically using known anti-inflammatory drugs, bile acids and novel compounds. Bile acids are known to have anti-inflammatory effects in humans and be useful in the treatment of PD. This project aimed to identify whether these compounds could reduce inflammation in zebrafish and if this could subsequently rescue the phenotype of PD mutant lines. The overall wider aim was to help establish whether inhibiting neuroinflammation can have a disease-modifying impact in PD.

Objective 4: Develop new, more relevant PD zebrafish lines. The final aim of this project was to establish a number of new *lrrk2* zebrafish lines that harbour mutations in the *lrrk2* gene that recapitulate pathogenic mutations identified in human PD. These lines could be more relevant to study PD than complete loss-of-function models.

3 Materials and Methods

3.1 Zebrafish Husbandry

3.1.1 Adult Zebrafish Husbandry

Adult zebrafish were maintained at 28°C in the Bateson Centre at the University of Sheffield. Fish were fed a diet of Zebrafeed [SPAROS] and live Rotifers and subjected to a light-dark cycle of 14 and 10 hours, respectively. Regulated procedures followed the UK Home Office Animals (Scientific Procedures) Act 1986 under project licence PP6422743 (Professor Oliver Bandmann) and Personal Licence IE398CC2C (Emma Fargher).

3.1.2 Zebrafish Lines

Wildtype (WT) zebrafish used in this project were strain AB, unless otherwise stated. Loss-of-function PD mutant lines were created in house by Dr Marcus Keatinge using the CRISPR-Cas9 system and maintained as heterozygous colonies in the AB background (see **table 3**).

Table 3. The Parkinson's Disease Mutant Zebrafish Lines Used for This Project

Zebrafish Line	Mutation induced / reference	Allele Code	Filial numbers used
Loss-of-function of GTP cyclohydrolase 1 *(gch1$^{-/-}$)*	94bp deletion in exon 1 resulting in nonsense-mediated decay of mRNA and a truncated protein (Larbalestier et al., 2021).	sh460	f6, f7 and f8
Loss-of-function of cyclin g associated kinase *(gak$^{-/-}$)*	50bp deletion, 4bp insertion in exon 11 resulting in nonsense-mediated decay of mRNA and a truncated protein (unpublished data, Bandmann laboratory).	sh615	f3 and f4
Loss-of-function of α-amino-β-carboxymuconate-ε-semialdehyde decarboxylase *(acmsd$^{-/-}$)*	See chapter 4	sh619	f3, f4 and f5
Loss-of-function of *leucine-rich repeat kinase 2 (lrrk2$^{-/-}$)*	See chapter 5	sh609	f4, f5 and f6
lrrk2 R1441C knock-in	See chapter 5	sh669	
lrrk2 R1441G knock-in	See chapter 5	sh670	
lrrk2 I2020T knock-in	See chapter 5	sh668	
lrrk2 G2019S knock-in	See chapter 5	sh671	
tgBAC(*tnfa*:GFP)	(Marjoram et al., 2015)	pd1028tg	
tg(*mpx*:GFP)	(Renshaw et al., 2006)	i114	
ETvmat2:GFP	(Wen et al., 2008)	pku2Et	

Mutations listed were introduced into AB strain zebrafish using CRISPR-Cas9 technology. Filial generations of heterozygous colonies were created by outcrossing previous generations to AB wildtype zebrafish.

3.1.3 Embryonic Zebrafish Husbandry

Zebrafish embryos were obtained by pair mating or marbling adult fish and collecting offspring around noon the following day. Larvae up to 10 days-post fertilisation (dpf) were maintained at 28°C in 10cm petri dishes with ~40mL E3 media (water with 500µM NaCl, 17µM KCl, 33µM CaCl and 33µM $MgSO_4$). For fish not undergoing drug treatments, methylene blue was added as an antifungal agent to a final concentration of 20µL per litre of E3. Unfertilised and dead embryos were identified and removed at 1dpf. Zebrafish between 5-10dpf were subject to light/dark cycles, underwent daily media changes and were fed Zebrafeed [SPAROS] every 24 hours.

3.1.4 Depigmentation of Larvae

For use in in situ hybridisation (ISH) or whole mount immunohistochemistry (IHC) experiments, larvae pigmentation was prevented by the addition of 0.003% phenylthiourea [fluorochem] from approximately 12hpf. Phenylthiourea was initially dissolved in DMSO to a stock concentration of 75mg/mL and stored at 4°C. 12µL of this was added to each plate of embryos to prevent pigmentation.

3.1.5 Anaesthesia and Culling

Anaesthesia of zebrafish was obtained by immersing fish in 4.2% tricaine (MS222) dissolved in E3. To cull unneeded zebrafish under 5.2dpf, anaesthetised larvae were disposed of in bleach; those over 5.2dpf were culled using approved schedule 1 methods, usually an overdose of anaesthesia (30mL tricaine per 100mL E3) followed by confirmation of cessation of circulation. Immersion fixation (see below) was used to cull fish when tissue integrity was to be maintained.

3.1.6 Fixation of Larvae

Following anaesthesia, larvae were fixed by submersion in 4% paraformaldehyde in phosphate buffered saline (PBS) at 4°C overnight. For sectioning, larvae were washed three times in PBS before cryoprotecting in 30% sucrose in PBS at 4°C for at least 24 hours. For in situ hybridisation, paraformaldehyde-fixed embryos were transferred into methanol by serial dilution (30%; 50%; 70%; 100% methanol in PBSTw (phosphate buffered saline, 0.1% Tween-20)) and stored at -20°C for at least 12 hours.

3.2 Genotyping

3.2.1 Finclipping Technique

To genotype live zebrafish larvae, finclips were taken at 3dpf from anaesthetised fish. The tip of the caudal fin (**figure 5**) was cut using a scalpel under a stereo microscope [Leica] and placed in a 96-well polymerase chain reaction (PCR) plate with 20µL sodium hydroxide (NaOH). Larvae were placed in corresponding wells of an E3 filled 96-well plate whilst genotyping was conducted.

Clipping below the area of blood flow ensures limited damage to the fish and allows the clipped area to regenerate.

Finclipping was also used to genotype fixed embryos where heads and/or bodies were needed for further experiments. For this, less accurate clips were taken using the same methodology. If embryos were not needed, this step was skipped and whole fish were used for genotyping.

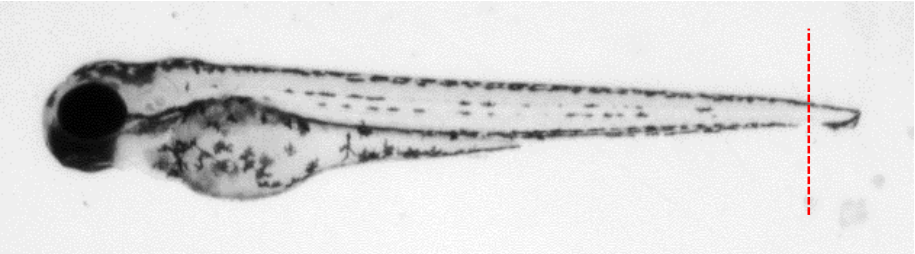

Figure 5. Finclipping Protocol for the Genotyping of Larval Zebrafish*. Brightfield image of a 3dpf zebrafish with the red dashed line representing where the caudal fin is cut during the finclipping procedure used for genotyping. This finclip is used to extract DNA for amplification using polymerase chain reaction whilst the fish is placed in the corresponding well of a 96-well plate to recover.*

3.2.2 DNA Extraction

To extract genomic DNA (gDNA), finclips were boiled in 20µL 50mM NaOH for 10 minutes at 95°C. If whole embryos were used, NaOH was increased to 50µL to avoid over-concentrated DNA samples. PCR plates were then vortexed and the solution neutralised by the addition of 1/10th the volume of 1M Tris-HCl (pH8).

3.2.3 Polymerase Chain Reaction (PCR)

Amplification of gDNA was obtained by standard PCR. 1µL gDNA sample was added to 1µL 10µM forward primer, 1µL 10µM reverse primer, 2µL MilliQ and 5µL BioMix Red [Bioline] in one well of a PCR plate. Genotyping primers, outlined in **table 4**, were obtained from Integrated DNA Technologies.

Table 4. Primers Used for Genotyping Mutant Zebrafish.

Genotype	Forward Primer	Reverse Primer
gch1$^{-/-}$	AAACTGACGGAGCGATCAAC	TCTCCTGGTATCCCTTGGTG
gak$^{-/-}$	GTATGACACAGACCCGACCA	AACCAAGGCAAGCTGAAACG
acmsd$^{-/-}$	CCCCAGAGCTGTTTCCTGTC	CCGTGAGCAAAGCAGACCTT
lrrk2$^{-/-}$	CTTCAGGCGTTCATGAGCAGC	GAGGCCTTCATGTGTCCGAT

Primer sequences used for polymerase chain reaction amplification of genomic DNA for use in the genotyping of zebrafish. Primers were obtained from Integrated DNA Technologies and diluted 1:10 into MilliQ to create working solutions. 100µM stock solutions were stored at -20°C and 10µM working solutions at room temperature. All primer sequences are written 5'-3'.

PCR plates were placed in a MultiGene Optimax Thermal Cycler [LabNet International] - the temperature cycle is outlined in **table 5**, where stages 2-5 were repeated 30 times. Following PCR, 3µL of each sample was placed in a well of a 2% agarose gel containing 1µL/50mL ethidium bromide [Alfa Aesar] and run by gel electrophoresis for 40 minutes at 120 volts. Gels were visualised using a Benchtop UV Transilluminator [UVP]. For genotyping *lrrk2*$^{-/-}$, an additional digest step was performed. 1µL of a 1:3 (enzyme:MilliQ) dilution of Bsl1 [NEB] was added to 3µL of PCR product and digested for 3 hours at 37°C. This reaction mix was then visualised by gel electrophoresis, as above.

Table 5. The Temperature Cycle Used in Polymerase Chain Reaction.

Stage	**Temperature (°C)**	**Length of time**
1	93	3 minutes
2 Denaturing	95	30 seconds
3 Annealing	60 (65 for *acmsd*$^{-/-}$)	30 seconds
4 Extension	72	30 seconds
5 Incubation	72	5 minutes

The temperature cycle used during polymerase chain reaction in this project to amplify DNA for genotyping. Stages 2-4 were repeated 30 times before moving to stage 5. Samples were held at 10°C at the end of this process until run by gel electrophoresis.

3.3 Sequencing of DNA

To sequence DNA, PCR-amplified products were cleaned up using the QIAquick PCR Purification Kit [QIAGEN]. Here, a high-salt binding buffer is added to the PCR mixture at a 5:1 ratio and applied to the QIAquick spin column containing a silica membrane. Columns are spun for 1 minute to pass the liquid through the membrane to which nucleic acids adsorb. Following wash steps using the wash buffer, pure DNA is eluted by the application of 30µL of elution buffer and collected into a 1.5mL Eppendorf tube. For cDNA sequencing, samples were gel extracted to exclude gDNA contamination. This was done using the QIAquick Gel Extraction Kit [QIAGEN]. Briefly, samples were cut out of a gel using a scalpel blade, dissolved in buffer and processed through a silica-based column. The purity and concentration of DNA was determined by NanoDrop 1000 Spectrophotometer [Thermo Scientific] and samples were sequenced using Sanger sequencing by Genewiz/Azenta.

3.4 Adult Zebrafish Organ Dissection

Anaesthetised adult zebrafish were first decapitated in line with 'Regulated Killing' procedures. Dissection was carried out on a polystyrene board using dissection scissors, needles and forceps, and viewed using a stereomicroscope [Leica]. All organs (**figure 6**) were flash frozen on dry ice immediately following dissection and stored at -80°C.

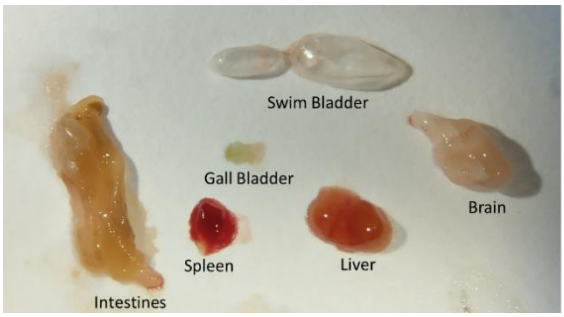

Figure 6. Dissected Zebrafish Organs. *Photograph of adult zebrafish organs dissected during this project. Own image.*

The heart was removed first as it was usually exposed following decapitation. It was placed in a dish of PBS to separate it from the surrounding vasculature and other tissue. Next, an incision was made from the decapitation site to the anus using dissection scissors. Skin and muscle were then pinned to the dissection board, exposing the organs from the ventral side. In females, the cavity was first cleared of oocytes, which prevent visualisation of other organs, by removing the ovaries and oocytes using forceps. In males, the testes were removed first and placed in PBS to enable the removal of fat cells from the testis tissue. Next, the gastrointestinal system was removed whole and placed on the dissection board. The liver, spleen, gall bladder and intestines were separated. The swim bladder was then removed from the body, revealing the kidney. A sample of kidney was removed by scraping forceps along the dorsal wall of the body cavity. Brains were then extracted from severed heads by breaking and removing the skull to expose the entire brain and gently scooping using forceps.

3.5 Quantitative Polymerase Chain Reaction (qPCR)

3.5.1 RNA Extraction

RNA was extracted from whole larvae or adult tissue using TRIzol Reagent [Sigma]. 15 larvae of the same genotype, usually determined via the tailfin clip method at 3dpf, were used per reaction. Larvae were homogenised in 250µL TRIzol Reagent using a 25-gauge needle and syringe and left at room temperature (RT) for 3 minutes. 50µL of chloroform [Sigma] was added to the Eppendorf, the tube inverted and incubated for 3 minutes at RT. Following 4°C 15-minute centrifugation at 13000rpm, the top aqueous phase was placed into a new tube with the addition of the same volume of isopropanol. Samples were then incubated at RT for 10 minutes. To collect the pellet, 15-minute centrifugation at 4°C was used and the supernatant removed. Pellets were washed using 150µL 70% ethanol and centrifuged for 5 minutes at 4°C. After air-drying, RNA

pellets were resuspended in 15µL DEPC-treated water [Invitrogen]. RNA concentrations were determined by spectrophotometry using a NanoDrop 1000 Spectrophotometer [Thermo Scientific]. RNA was stored at -80°C.

3.5.2 Complementary DNA (cDNA) Synthesis

cDNA was created using the Verso cDNA Synthesis Kit [Thermo Scientific] as per manufacturer's instructions. Briefly, 1µg RNA was added to 4µL 5X reaction buffer, 2µL dNTPs, 1µL RT enhancer, 1µL Verso enzyme and 1µL Oligo dT primer to a total volume of 20µL (DEPC-treated water [Invitrogen] was used if volumes were less than this). Samples were heated to 42°C for 30 minutes to synthesise the cDNA and then held at 95°C for 2 minutes to deactivate the enzyme. cDNA was stored at -20°C.

3.5.3 qPCR

mRNA transcript levels were quantified by qPCR using a CFX96 Touch Real-Time PCR Detection System [BioRad] and Brilliant III Ultra-Fast SYBR Green qPCR Master Mix [Agilent Technologies]. *rps29* served as a reference gene to which expression data was normalised. *ef1α* was used as a reference gene by previous laboratory members, for which some data is included in this thesis; this is clearly specified when used in results sections. Primers (**table 6**) were designed using Primer3 software (http://primer3.ut.ee/) and checked using Primer BLAST (NCBI). *il-1β*, *cxcl8* and *mmp9* sequences were taken from López Nadal et al. (2018) but re-optimised for use in the current project. All primers were first tested by gradient PCR using wildtype cDNA to ensure primer specificity and to select the most appropriate temperature for qPCR reactions. Specificity was again checked by the presence of a single peak on the melt curve after each reaction. Primers were optimised by varying primer and DNA concentration to create a standard curve. The lowest concertation of primer that achieves efficiency near 100% was used for subsequent reactions. 19µL of qPCR reaction mix (50% SYBR green, 5% DMSO, primers at desired concentration and made up to 19µl with nuclease-free water) was added to each well of a 96-well plate [Appleton Woods] with 1µL cDNA. Plates were sealed with strip caps [Sarstedt] and centrifuged to ensure solution mixing and reduce bubbles. Plates were loaded into the qPCR machine and cycled as outlined in **table 7**. Three technical replicates per data point were run and the average Ct used for analysis.

Table 6. Primer Sequences used for Quantitative Polymerase Chain Reaction

Gene	Forward Primer	Reverse Primer	Product Size
acmsd pair 1	ATCCAAGAGAACTGCTGGGATC	TAACCCAACGAAGCGCTTTG	198 bp
acmsd pair 2	ACATTCACAACAGCGCAAGG	ATCCCAGCAGTTCTCTTGGATC	242 bp
lrrk2	CCACAGGAGCGCGATATTCA	TTTGTGTTTCCGCACAGAGC	129 bp
lrrk1 pair 1	AGTCCTGGCTGCTCAACATC	TCCAGGTGATGTCCGGGTAT	186 bp
lrrk1 pair 2	TGCGAAAATAGCGGTGGAGT	GCTCTCTGACCACCGTTTGA	186 bp
il-1β	TGCGGGCAATATGAAGTCA	TTCGCCATGAGCATGTCC	272 bp
mmp9	ACGGCATTGCTGACAT	TAGCGGGTTTGAATGG	184 bp
cxcl-8a	TGTTTTCCTGGCATTTCTGACC	TTTACAGTGTGGGCTTGGAGGG	151 bp
rps29	TTTGCTCAAACCGTCACGGA	ACTCGTTTAATCCAGCTTGACG	110 bp
ef1α	TGGTACTTCTCAGGCTGACT	TGACTCCAACGATCAGCTGT	146 bp

Primers were obtained from Integrated DNA Technologies and diluted 1:20 into DEPC-treated water to create working solutions. Stock solutions were stored at -20°C and working solutions at room temperature. All primer sequences are written 5'-3'. bp, base pairs.

Table 7. The Temperature Cycle Used in Quantitative Polymerase Chain Reaction.

Stage	Temperature (°C)	Length of time
1 Initial Denaturation	95	3 minutes
2 Denaturing	95	10 seconds
3 Annealing	55-65	30 seconds
4 Plate read		
5	95	1 minute
6	55	30 seconds
7 Melt Curve	55-95 (increments of 0.5)	

The temperature cycle used during quantitative polymerase chain reaction in this project to measure gene expression via the detection of RNA levels. Stages 2-4 were repeated 39 times before moving to stage 5. A melt curve analysis was then performed on the samples following final cycle.

Data were analysed using the delta-delta Ct method:

1. delta Ct (dCt) = Average GOI Ct – average reference gene Ct
2. delta-delta Ct (ddCt) = dCt – the average of control group dCt
3. Fold change = 2^(-ddCt)
4. Normalised fold change = Fold change / average fold change of control groups

3.6 Reverse Transcription Polymerase Chain Reaction (RT-PCR)

cDNA from 1-5dpf wildtype embryos was obtained as described above. Standard PCR (**section 3.2.3**) using qPCR primers (**table 6**) was used to amplify cDNA, which was visualised using a Benchtop UV Transilluminator [UVP] following agarose gel electrophoresis. *rps29* was used as a reference gene. *ef1α* was used as a reference gene by previous laboratory members, for which some data is included in this thesis; this is clearly specified when used in results section.

3.7 Movement Analysis

3.7.1 Larval Movement Analysis

Mixed genotype embryos were obtained by incrossing heterozygous parents. At 5dpf, larvae were transferred to a 48-well plate in 500µL E3 without methylene blue. Movement was analysed using the ZebraBox [Viewpoint Life Sciences] following a 30-minute habituation period. Movement was recorded over 60 minutes; 30 minutes in light conditions followed by 30 minutes of alternating 5-minute dark-light cycles. Siblings were then genotyped using sacrificed whole larvae, as described in **section 3.2**.

3.7.2 Adult Movement Analysis

Adult zebrafish of known sex and genotype were placed in single tanks with aquarium water. Movement was recorded continuously for 7 hours using a camera and tracked by the ViewPoint software. For analysis, the first hour of the recording was omitted as fish were habituating to the environment.

3.8 Whole-Mount In Situ Hybridisation (WISH)

3.8.1 WISH Probe Design

WISH probes were designed from the cDNA sequence, obtained from Ensembl, of genes of interest. Primers, outlined in **table 8**, were generated using Primer3 software (http://primer3.ut.ee/). The only exceptions are *lrrk2* probe 1 primers, which were taken from Sheng et al. (2010) and *fabp10a* primers, which were designed by Dr Emily Reed. All primers were obtained from Integrated DNA Technologies (IDT). To transcribe sense probes from cDNA (see **section 3.8.2**), reverse primers were tagged with the T7 sequence (taatacgactcactataggg) and to transcribe antisense probes, forward primers were tagged with T7.

Table 8. Primers Used for Whole Mount In Situ Hybridisation Probe Synthesis

Target	Forward Primer	Reverse Primer	Length of Riboprobe
th1	AGTGCACCTGTCGGATGTTA	GCGTCCACAAAGCTTTCTGA	915 bases
lrrk2 (probe 1)	TGCAAACGGAGGTAAAAACC	AGATGATCCTGGTCCCACAG	506 bases
lrrk2 (probe 2)	TTCTGGATGAGGAGGAATGG	AGCAGCTTGGAAAACCTTCA	824 bases
acmsd (probe 1)	AGGCGGTGCTTTTCCATACA	GCAAGAAGGTCGCTGTTTCG	723 bases
acmsd (probe 2)	TCAATGCCCCAGAGCTGTTT	TGGCTTTGCATGTGTTCGTG	905 bases
acmsd (probe 3)	CCAAGGGAATGGCCAGACTT	AGCACAAAGATCAGGTCGCA	714 bases
acmsd (probe 4)	GATCCAGAGGCTCGGATTCG	CCAGAGCATTTCCAGCAAGC	814 bases
fabp10a	AGCTTCTCCAGAAAGCATGG	TCCTGATCATGGTGGTTCCT	376 bases

The primer sequences generated from Primer3 software for use in the generation of whole mount in situ hybridisation probes. Lrrk2 probe 1 primer sequences were taken from (Sheng et al., 2010). All primer sequences are written 5'-3'.

3.8.2 Making WISH Probes from cDNA

Digoxigenin (DIG)-labelled riboprobes were generated using wildtype zebrafish cDNA as a template. A gradient PCR was initially used to identify optimum annealing temperatures for each primer pair (primers without T7 tags were used for this). Standard PCR (see **section 3.2.3**) at this temperature was then used to amplify cDNA and the presence of the correct product was confirmed by gel electrophoresis. PCR products were cleaned up using the QIAquick PCR Purification Kit [QIAGEN], described in **section 3.3**. Some probes required gel extraction and the design of nested primers, discussed in results sections. The purity and concentration of DNA was estimated by gel electrophoresis and spectrophotometry using the NanoDrop 1000 Spectrophotometer [Thermo Scientific].

3.8.2.1 WISH Probe Transcription and Purification

RNA transcription of WISH probes was achieved by the addition of 1µg of PCR-amplified DNA to 2µL DIG-labelled NTPs, 2µL dithiothreitol (DTT), 4µL 5X transcription buffer, 1µL RiobLock RNAse inhibitor [Thermo Scientific], 2µL of T7 polymerase and made up to 20µL with DEPC-treated water [Invitrogen]. After incubating at 37°C overnight, 2µL of DNase I [NEB] was added and samples incubated for a further 30 minutes. RNA was precipitated at -20°C for 30 minutes in an equal volume of isopropanol and 1/10th volume of 7.5M ammonium acetate. Pellets were generated by centrifuging at 4°C for 30 minutes and removing the supernatant. Washes using 500µL of 75% ice-cold ethanol were performed by centrifuging for 10 minutes at 4°C. After air drying, pellets were resuspended in 20µL DEPC-treated water [Invitrogen]. RNA concentration was estimated by NanoDrop 1000 Spectrophotometer [Thermo Scientific] measurements. Probes were diluted in hybridisation buffer A (Hyb-A; 50% deionised formamide [Invitrogen, Fisher Scientific UK Ltd], 50µg/mL heparin [Sigma], 5X Saline Sodium Citrate (SSC) [Sigma], 0.1% Tween-20, 500µg/mL yeast tRNA [Sigma], using citric acid to correct pH to pH6) to a final concentration of 1ng/µL. These were stored at -20°C.

3.8.3 WISH Protocol

The WISH protocol was adapted from Thisse and Thisse (2008). Paraformaldehyde-fixed embryos were successively rehydrated by 5-minute washes in methanol:PBSTw at ratios of 70:30, 50:50 and 30:70, followed by four 5-minute PBSTw washes. Embryos were then digested with 10µg/mL proteinase K [Invitrogen] for the time specified in **table 9**.

Digested embryos were re-fixed at RT in 4% paraformaldehyde for 20 minutes on the rocker, followed by five 5-minute washes in PBSTw. Fish were left to prehybridise in 70°C Hyb-A for at

Table 9. Proteinase K Timings Used During In Situ Hybridisation Experiments.

Days post fertilisation	Time digested in Proteinase K
1	5-10 minutes
2	15 minutes
3	30 minutes
4	40 minutes
5	1 hour

Length of time embryos were digested in proteinase K during in situ hybridisation. The length of time of proteinase K was altered depending on the age of the embryo.

least 2 hours before applying the probe at 70°C overnight. Embryos were then washed in Hyb-B (Hyb-A without heparin or yeast tRNA) followed by 15-minute successive 70°C washes into 2X SSC at ratios of 75:25, 50:50, 25:75 (Hyb-B:SSC), followed by two 30-minute washes in 0.2X SSC. Samples were then moved to RT to wash into PBSTw by 10-minute washes in 0.2X SSC:PBSTw at ratios of 75:25, 50:50, 25:75 and 0:100. Embryos were then blocked in blocking buffer (PBSTw with 2% sheep serum and 2mg/mL BSA) for at least 2 hours before incubating overnight with Anti-Digoxigenin-AP, Fab fragments [Roche] diluted 1:5000 into blocking buffer. Embryos were washed for 15 minutes in PBSTw eight times prior to incubating in NTMT staining buffer (0.1M Tris-HCl pH9.5, 50mM $MgCl_2$, 0.1M NaCl, 0.1% Tween-20) by three 5-minute washes. During the final wash, embryos were transferred to an opaque 12-well plate. Staining solution was made by diluting 3.5µL Nitro Blue Tetrazolium (NBT) [Roche] and 4.5µL 5-Bromo-4-chloro-3-indolyl phosphate (BCIP) [Roche] per 1mL NTMT; 1mL was applied to each well and the plate kept in the dark at RT on the rocker. Staining was checked regularly and stopped by washing in PBSTw three times for 5-minutes each. Embryos were then fixed in 4% paraformaldehyde for 20 minutes and successively washed into 75% glycerol at RT for imaging. A Nikon SMZ1500 stereomicroscope was used to image fish in 100% glycerol. *Th1* stained fish were imaged as described below.

3.9 Methyl-4-phenylpyridinium (MPP+) Toxin Exposure

1dpf embryos, obtained from a single heterozygous incross, were dechorionated and placed in 3cm petri dishes containing 2.7mL E3 without methylene blue. Zebrafish were treated with 3mM MPP+ [Sigma] from 1-3dpf by constant immersion. This was achieved by the addition of 300µL 30mM MPP+ (100mg MPP+ powder dissolved in 11.2mL MilliQ), to a total volume of 3mL per dish. The media and MPP+ were replenished daily and 0.003% phenylthiourea [Sigma-Aldrich] was used to prevent pigmentation. Control embryos were treated with an equal volume of MilliQ water. Plates were wrapped in foil due to the light sensitive nature of MPP+ and kept at 28°C. At 3dpf, larvae were washed out of MPP+ and fixed by immersion fixation in paraformaldehyde before being transferred to methanol and stored at -20°C. Larvae were used for *th1* WISH and dopaminergic neuron counting (described below).

3.10 Dopaminergic Neuron Counting

Following WISH for *th1*, decapitated zebrafish heads were mounted on slides in 100% glycerol and visualised on an AxioPlan Microscope with a Plan-NEOFLUAR 20x Ph2 objective [Zeiss]. Larval tails were retained for genotyping. *th1*+ neurons from DC2 and DC4/5 populations, as described by Rink and Wullimann (2002), were counted. To remove bias, this was done blinded to genotype and treatment group (if counting post-MPP+ exposure) until the data analysis stage. To obtain representative images, slides were imaged using an Epifluorescence Microscope [Olympus].

In 5dpf zebrafish, the transgenic reporter line *ETvmat2:GFP* was used to visualise the DC groups of neurons. This line labels the vesicular monoamine transporter 2 (Vmat2), and therefore enables visualisation of monoaminergic neurons, including the DC populations (Jay et al., 2015). *acmsd*$^{+/-}$*;ETvmat2:GFP* zebrafish were crossed with either *acmsd*$^{+/+}$ or *acmsd*$^{-/-}$ zebrafish. Larvae were selected for fluorescence at 24hpf and finclipped for genotyping at 3dpf. Larvae were imaged using an AiryScan confocal microscope [Zeiss] with a 10X objective lens. As before, cell counts were conducted blinded to genotype to avoid bias.

3.11 Sectional Immunohistochemistry

14µm cryosections were obtained using a Leica cryostat from zebrafish mounted in frozen Cryomatirx OCT [CellPath]. Once air-dried, slides were stored at -20°C. Frozen slides were rehydrated in PBS-filled coplin jars for 5 minutes at RT. Slides were then immediately blocked (untreated condition) or treated with Tris-HCl (pH9) or sodium citrate (pH6) for antigen retrieval. This was achieved by placing slides in Tris-HCl or sodium citrate filled coplin jars and heating in a rice cooker for 20 minutes. Treated slides were then washed in PBS for 5 minutes. All conditions were blocked using 150µL IHC blocking solution (10% sheep serum, 1% BSA, 0.3% Triton-X, 0.5% Tween-20) applied directly to the slide and covered with parafilm for 1 hour. Immunostaining was achieved using 150µL of the following primary antibodies diluted in blocking solution overnight at 4°C: rabbit polyclonal anti-L-Plastin (LCP1; 1 in 200; GTX124420; GeneTex) or mouse anti-4c4 (a gift from Alexander McGown, The University of Sheffield).

Slides were then washed three times in PBS for 20 minutes. Alexa Fluor–conjugated secondary antibodies [Invitrogen] were diluted 1:500 into IHC block and 150µL applied to slides for 2.5 hours. Slides were washed three times for 20 minutes, ensuring slides were protected from light. 10µL 5mg/mL 4’,6-diamidino-2-phenylindole (DAPI) [Roche] was added to the final PBS wash step for nuclear staining. Samples were then mounted under a glass coverslip by the addition of three

drops of FluorSave reagent [Calbiochem]. Slides were dried at RT overnight and imaged the following day using a Leica SP5 confocal microscope with a 40X oil immersion lens.

3.12 Microglial Analysis

3.12.1 Whole Mount Immunohistochemistry

Immunohistochemistry against 4c4 (microglial marker; antibody gifted from Dr Alexander McGown, The University of Sheffield) was conducted as previously described (Inoue & Wittbrodt, 2011). Paraformaldehyde-fixed embryos were serially rehydrated by 5-minute washes in methanol:PBSTw at ratios of 70:30, 50:50 and 30:70, followed by four 5-minute PBSTw washes. Antigen retrieval was achieved by placing ~20 embryos in 1.5mL Eppendorfs with 500µL 150mM Tris-HCL (pH9). Embryos were heated to 70°C for 15 minutes and then washed twice in PBSTw followed by two 5-minute washes in MilliQ. Embryos were then acetone cracked at -20°C for 20 minutes and re-washed at RT by two 5-minute washes in MilliQ and three 5-minute washes in PBSTw. Blocking solution was made up in PBSTw (10% sheep serum, 0.8% Triton X-100, 1% BSA) and 500µL applied to larvae overnight at 4°C on the rocker. Blocking solution was removed and larvae incubated in 500µL mouse anti-4c4 mix (1:50 dilution of 4c4 in a modified block solution: 1% sheep serum, 0.8% Triton X-100, 1% BSA made up in PBSTw) at 4°C on the rocker for 3-4 days. Unbound primary antibody was washed off by three 1-hour washes in PBS containing 10% sheep serum and 0.1% Triton X-100 at RT on the rocker. Following two 10-minute washes in PBS-Triton (0.1% Triton X-100 in PBS), 500µL anti-mouse AlexaFluor 488 secondary antibody [Invitrogen] (1:200; antibody:PBSTw) was applied to larvae for 3 days at 4°C on the rocker. If nuclear staining was required 5mg/mL DAPI [Roche] at a dilution of 1:100 was also added alongside the secondary antibody. Unbound secondary antibody was washed off by three 1-hour washes in PBSTw and embryos imaged immediately.

3.12.2 Imaging

Following immunostaining, decapitated larval heads were mounted in 2% low melting point agarose in a clear bottomed 96-well plate [Greiner], placing the dorsal head flush against the bottom of each well. The body was retained for genotyping. Imaging was conducted using the Opera Phenix High Content Screening System [Perkin-Elmer] using a 20x objective and an 80 image z-stack.

3.12.3 Image Analysis

Images were analysed blinded to genotype using ImageJ software. Cells were manually counted by scrolling through z-stacks to prevent issues of overlapping cells being missed in z-stack projections. 4c4+ cells were counted in the midbrain and forebrain. Microglial activation was

assessed using 4c4+ cell morphology (**figure 7**) and calculated as the number of activated cells (cells with an amoeboid morphology) divided by the total number of 4c4+ cells.

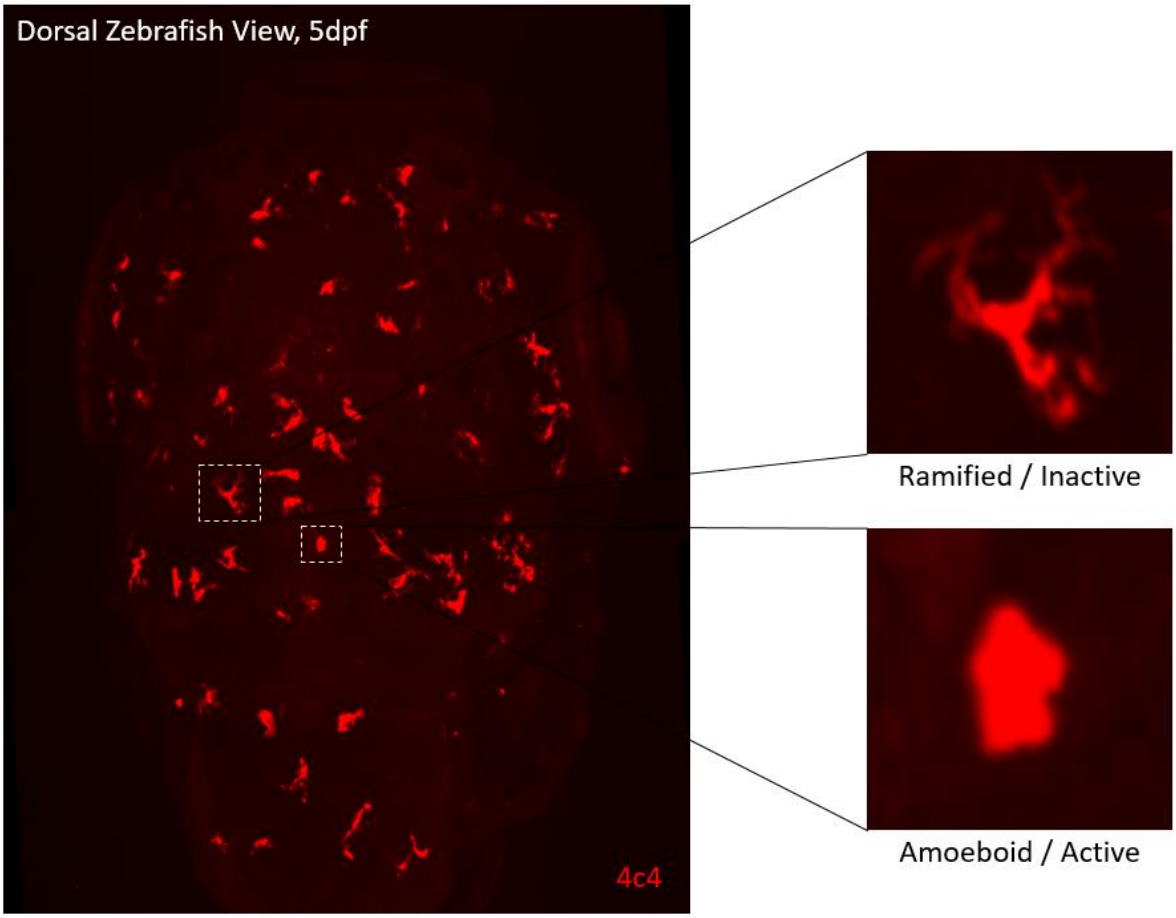

Figure 7. Cell Morphology Used to Determine Activation State of Microglia in Zebrafish Brain. *Microglia were labelled using immunohistochemistry against 4c4 in wholemount zebrafish larvae. Each cell was classified into one of two activation states; inactive (ramified cell shape, top panel) or active (amoeboid cell shape, bottom panel).*

3.13 CRISPR

3.13.1 Designing Guide RNA for Knockouts

For targeting of *irf8*, guide RNAs (gRNAs) of 20bps were designed using ChopChop (Montague et al., 2014) and obtained from Sigma-Aldrich. gRNAs were diluted in DEPC-treated water [Invitrogen] to concentrations of 100µM and stored at -20°C. To create the CRISPR injection mixture, an equal molarity of gRNA and trans-activating crRNA (tracrRNA) (1µL of each) were added to 0.5µL Cas9, creating a final concentration of gRNA of ~50µM. For triple targeting gRNAs, 0.5µL of each guide was added to 1.5µL of tracrRNA. The i*rf8* sequences used for CRISPR in this project are shown in **table 10**. i*rf8* guide 1 sequence was kindly provided by Dr Daniel Lysko.

For the creation of *lrrk1* and *lrrk2* CRISPants, guides were manually designed. This was achieved by the identification of Cas9 PAM sites (NGG, CCN) within the gene of interest, starting in exon 1. Guides were designed such that successful Cas9 cleavage would result in the loss of a

restriction enzyme site, assessed by the use of primers targeting either side of the cut site (see below). As there are two *lrrk1* transcripts produced from a single *lrrk1* gene, guides were designed using the shorter transcript to ensure that both were affected following mutation. Stock gRNA was diluted in DEPC-treated water [Invitrogen] to a final concentration of 20µM and stored at -20°C. tracrRNA for use here was stored as a 20µM concentration at -20°C. Injection mixtures consisted of 1µL of each gRNA, 1µL tracrRNA, 1µL Cas9 and 1µL of DEPC-treated water [Invitrogen].

3.13.2 Microinjection

Microinjection needles made from borosilicate glass capillaries (Kwik-Fil, World Precision Instruments, Inc., Hertfordshire, UK) were pulled using a micropipette puller (Model P-97, Sutter Instrument Co., USA). Needles were loaded with the injection mixtures described above and broken using forceps to a size appropriate to produce drop of 0.5nL from an injector pump (Pv 820 Pneumatic pico-pump, WPI), measured using an oil-filled graticule. Injection mixtures were injected into the yolk of one-cell stage zebrafish embryos which were then collected and kept in E3 media.

3.13.3 Guide Efficiency Testing

gRNA was designed so that the Cas9 cut site would disrupt a restriction enzyme site so that efficiency could be determined via restriction fragment length polymorphism (RFLP). DNA was obtained from 1dpf embryos and amplified by standard PCR. PCR products were then digested with appropriate restriction enzymes (**table 11**) for 3 hours. Products were visualised via gel electrophoresis. For *irf8*, efficiency was determined by the loss of microglia as determined by neutral red staining or 4c4 wholemount immunohistochemistry.

Table 10. Guide RNA Sequences Used for CRISPR-Cas9

Guide	Target	Sequence	Forward	Reverse	Restriction Enzyme
irf8 guide 1	Exon 1	GCGGTCGCAGACTGAAACAG(TGG)	N/A	N/A	N/A
irf8 guide 2	Exon 1	GTCTACAAGATGAACTCGGG(CGG)	N/A	N/A	N/A
irf8 guide 3	Exon 1	GCACTATGTTTCGAATCCCC(TGG)	N/A	N/A	N/A
lrrk1 guide 1	Exon 1	ATACGGATGGCGAGGACCAG(AGG)	TGCTCCTGCTCCTCCAGTAT	ACCGCTATTTTCGCAGGACA	AvaII
lrrk1 guide 2	Exon 2	(CCA)GCCGTTCTAGCAGCACATCA	TCGACTCCGTTCGGTTTCTG	GTGACTATTGTGGGTGCACC	MwoI
lrrk1 guide 3	Exon 3	TTTAGACGTGGTGAAGCTCC(TGG)	CCCGCCCCTTTTTGATGTCT	GAATGAACAGCACAGCCGTC	AluI
lrrk1 guide 4	Exon 4	(CCT)CGTACACACTGATGGATCAC	AGGAGATTGCGTGTTTTCTGC	GGGGCCTAACAGGTCACATT	RsaI
lrrk1 guide 4 (new)	Exon 4	TTTCTCCTCGTACACACTGA(TGG)	AGGAGATTGCGTGTTTTCTGC	GGGGCCTAACAGGTCACATT	MslI
lrrk1 guide 5	Exon 2	(CCT)GTGTTTGGCAGCTCAGAATG	TTTTGGCACTGTGGGCTTCA	GCTCTCTGACCACCGTTTGA	BslI
lrrk1 guide 6	Exon 3	GTTGGCTACGGCGTCTCAGC(AGG)	TGAGTTCTTCTTGTGCTGCG	CGCAGCATACAGAGGCAAAC	DdeI
lrrk1 guide 7	Exon 5	CTGCCGTCTGTGGTGCCGTG(GGG)	GCTGTGCATGTTGACTGGTC	ATGATCTGCTGTGAGGACGC	BtgI
lrrk1 guide 8	Exon 7	TCTGCGCAAACTGCAGGGTC(TGG)	CTGCCTGGAGTCACGTCATA	TCAGGAAAGCGGCTCAGTTT	AlwNI
lrrk2 guide 1	Exon 1	GACTGAAGAAGCTACTGGTG(AGG)	TGTGAAATCTGCGGGGATGTTA	TATGATCTGCACCATTGTCCCC	BsrI
lrrk2 guide 2	Exon 6	CGAGAAGAAGGACCATGAGG(TGG)	GTGTCAGTTCTGCCCATTTGAC	GTGGTATGAGGACCTTCAGAGC	BslI
lrrk2 guide 3	Exon 5	TGAGATCAAGATGCAGGTTC(TGG)	AAGACGCCAAGATGATGATGGT	GTCTGCAGCAGTGGTTGTAAAG	AlwNI
lrrk2 guide 4	Exon 9	GGTAAAGAAAGAAGCCGCTC(AGG)	CCTACTTGTCTTTCGAAGGCCT	ACTTTGACGTCTTCAGCATGTC	MwoI

CRISPR guide RNA sequences for irf8 were obtained using the Chop-Chop software, others were designed by hand in Snapgene. PAM sequences are provided in brackets. All sequences are given 5'-3'. If PAM is CCN, the sequences were reverse complemented prior to ordering.

Table 11. Guide RNA Sequences Used for CRISPR-Cas9 Induction of Single Amino Acid Substitutions

Guide	Sequence	Forward	Reverse	Restriction Enzyme
G2019S and I2020T	GTCGCTAAAATCACAGACTA	TGATCATCTACCGAGACCTGAA	TATGGGTAAATGAGCGAGACCT	N/A
R1441C/G/H	TGTGTTTCTCCAGGCTGTAG	TCACCACATGCTTTGATCCA	GTAGGTGGCGCTCTTCACAC	sfcI
Y1699C	TGAGATGCCATATTTTCCGA	GACCACAGGCCAGTGATTGA	TGCCATAGAGCAGGAATGCA	Hpy188I
N1437H	ACCCTGGCTCTTTAACATTA	AGGTGGTGAAGAGTGCAGTG	AGAAAGTCTGGTTTTATTTCGGCT	mslI

Guides were stored as 100μM stock solutions and diluted with an equal molarity of tracrRNA and 0.5μL Cas9 to create an injection mixture. PAM sequences are provided in brackets. All sequences are given 5'-3'. If PAM is CCN, the sequences were reverse complemented prior to use.

3.13.4 Generation of Single Amino Acid Change Mutants

CRISPR-Cas9 was also used to create single amino acid changes in zebrafish that recapitulate mutations seen in PD. Following protein-protein alignments in SnapGene to identify equivalent amino acids in zebrafish, *in silico* transcription of the DNA sequence was carried out to find the corresponding codon using known flanking amino acids. Possible guides were identified by the presence of NGG or CCN, whereby the Cas9 cut site was within 10 bases of the codon of interest. Guide efficiency was checked either by restriction digest (as described above) or by evidence of smearing on a high percentage gel following injection into wildtype embryos.

If a successful guide was identified, 127bp single-stranded donor oligonucleotides (ssODNs) were designed around the PAM site (85 bases 3' and 42 bases 5' of PAM) to act as a template for homology-directed repair (HDR). These oligonucleotides contained the mutation of interest as well as mutations in the PAM site (to prevent Cas9 cleavage of successfully mutated DNA), the induction of a restriction site (for later identification of mutants) and alterations of wobble bases to enable the design of primers that will only amplify DNA after successful HDR and insertion of the new DNA sequence.

Due to codon redundancy, multiple new codons could be introduced that result in the correct amino acid change. A codon preference table (https://www.kazusa.or.jp/codon/cgi-bin/showcodon.cgi?species=7955) was used to assist in choosing which codon to include; rare codons were avoided. Oligonucleotides satisfying all of the above requirements were reverse complemented and ordered from IDT. They were phosphorothioated on the first and last two bases to enhance stability and prevent nuclease breakdown once injected. Corresponding primers were checked using Primer-BLAST and tested on wildtype zebrafish DNA upon arrival to ensure they had no ectopic binding sites and no products are generated in non-mutated DNA.

Finally, co-injections of active guides and ssODNs were performed and DNA assessed at 1dpf using the novel primers designed and/or induced restriction sites. If HDR was successful in injected embryos, large numbers were raised to identify founders that demonstrate germline transmission of the mutation. This was achieved by outcrossing G0 zebrafish with wildtype zebrafish and assessing the offspring using the novel primers and induced restriction sites. Successfully transmitting fish were outcrossed and offspring raised to generate a stable mutant line.

3.14 Neutral Red Staining

Neutral red staining was conducted as described by Herbomel et al. (2001), but without the addition of phenylthiourea. Briefly, 3dpf or 4dpf larvae were submersed in neutral red [Sigma Aldrich] at a final concentration of 2.5µg/mL of E3 for 6 hours at 28°C. Larvae were washed by refreshing the media twice and fish imaged immediately using a Nikon SMZ1500 stereomicroscope after mounting in 1% low melting point agarose. Quantification of microglial number was achieved by subjectively counting the number of distinct red dots from brightfield images using ImageJ software.

3.15 Toxicity Trials and Drug Treatments

3.15.1 Anti-inflammatory Compounds

A number of compounds were used for their anti-inflammatory properties (**table 12**). These compounds were added to E3 media for treatment of zebrafish larvae from 1-12dpf. Toxicity trials on wildtype zebrafish were always conducted prior to the treatment of any mutant zebrafish to establish maximum tolerated doses (see below).

Table 12. Anti-inflammatory Compounds Used in This Thesis

Drug Name	Source	Tested	Used in experiments
UDCA	Sigma-Aldrich	Yes	No
TUDCA	Sigma-Aldrich	Yes	Yes
GUDCA	Gift from Dr Heather Mortiboys laboratory	Yes	No
Jed135	Dextra/NZP synthesised compound	Yes	No
Jed666	Dextra/NZP synthesised compound	Yes	Yes
Dexamethasone	Sigma-Aldrich	Yes	Yes
Quinacrine Dihydrochloride	Sigma-Aldrich	Yes	No

Table outlining the compounds used in this thesis to treat zebrafish due to their predicted anti-inflammatory effects.

3.15.1.1 Assessing Solubility

To assess the ability of drugs to dissolve into E3 media, various concentrations were added to 3mL E3 containing either 1% or 0.5% DMSO and left at 28°C overnight. The following day, crystal formation was analysed under a stereomicroscope [Leica].

3.15.1.2 Toxicity Trials

Drugs were dissolved in DMSO and administered to groups of 20 dechorionated zebrafish larvae via constant immersion by applying directly to the E3 media (final DMSO concentration of 1%). Media and drug were refreshed daily and fish over 5dpf fed with Zebrafeed [Sparos]. The pH of the media was checked once drugs applied. Survival in toxicity trials of 1-5dpf zebrafish was measured by the presence of a heartbeat. In 1-10dpf or 5-10dpf trials, fish were culled (classed as death) if they no longer responded to touch. This is due to home office regulations meaning

that death cannot be an endpoint of experiments over 5dpf. Husbandry (untreated wildtype) and DMSO controls were included in all trials. Fish were kept at 28°C throughout.

3.15.1.3 Drug Treatment Experiments

The treatment of mutant zebrafish was conducted as above, whilst blinded to both genotype and condition (treatment vs control). Fish were genotyped at the end of the experiment to prevent experimenter bias.

3.15.2 Hepatotoxicity Experiments

Paracetamol (acetaminophen) [Sigma] was used to induce liver damage in zebrafish larvae. Initially, toxicity trials were conducted using previously published data as a guide. Liver damage was assessed by two means; firstly, livers were examined under brightfield microscopy to look at changes in liver colour. Secondly, fish were fixed following treatment and assessed using in situ hybridisation against *fabp10a* (see **section 3.8.3**). Images were obtained and liver area was measured in ImageJ by setting a colour threshold and creating a region of interest.

3.15.3 Induction of Inflammation

Pharmacological induction of inflammation was achieved in zebrafish embryos by exposure to a number of compounds. Methodologies for treatment were developed by combining published protocols with advice from Dr Sylvia Brugman. For all toxicity trials, 20 dechorionated larvae were exposed to compounds from 2 or 3dpf in 3mL E3 without methylene blue. Media, including compounds, was refreshed daily. Fish were kept at 28°C and monitored for survival.

3.15.3.1 The Dextran Sodium Sulfate Model

Dextran Sodium Sulfate (DSS, MW ~40, 000) [Sigma-Aldrich] was dissolved into E3 media to create a 10mg/mL stock solution which was then directly added to E3 at required concentrations. Protocols were adapted from Oehlers et al. (2013) but with markedly reduced concentrations as suggested by Dr Brugman. Larvae were exposed to DSS from 3-5dpf by constant immersion in 3mL E3, refreshed daily. RNA was extracted from 5dpf larvae following exposure.

3.15.3.2 The Trinitrobenzene Sulfonic Acid Model

Trinitrobenzene Sulfonic Acid (TNBS) [Sigma-Aldrich] was purchased as a 1M stock solution and added directly to E3 media to desired concentrations. Protocols were adapted from Oehlers et al. (2013). Larvae were exposed to TNBS from 3-5dpf by constant immersion in 3mL E3, refreshed daily. RNA was extracted from 5dpf larvae following exposure.

3.15.3.3 The Saponin Model

Extra pure saponin [Thermo Fisher Scientific] was dissolved into E3 to create a stock solution which was added directly to E3 media containing zebrafish larvae at desired concentrations. Protocols were adapted from López Nadal et al. (2018). Larvae were exposed to saponin from 3-5dpf by constant immersion in 3mL E3. Drug and media were refreshed daily. RNA was extracted from 5dpf larvae following exposure.

3.16 NAD/NADH Assay

NAD/NADH assays, including data analysis, were conducted on adult zebrafish by Mr Oluwaseyi Pearce. Brains were extracted as described previously, weighed and used fresh. Levels of NAD+ and NADH were measured using a colourimetric NAD/NADH Assay Kit (ab6534) [abcam]. The assay was performed as per manufacturer's instructions, with minor alterations following optimisation for zebrafish tissue. Briefly, brains were washed using 400µL PBS and homogenised in 400µL NADH/NAD extraction buffer using a Dounce homogeniser. Following centrifugation at 4°C for 5 minutes, the supernatant was collected into a clean tube. Samples were centrifuged in 10kD spin columns (ab93349) at 4°C for approximately 1.5 hours. Filtrate volume was measured and split (half for NADH measurement and half for total NAD measurement). Samples for NADH measurement were incubated at 60°C for 30 minutes to decompose NAD+ prior to plate reads. Samples or standards were added into wells of a clear bottomed 96-well plate [Greiner] with 100µL reaction mix (98µL NAD cycling buffer and 2µL NAD cycling enzyme mix). Some wells were used to measure background activity; to these wells only NAD cycling buffer was added (100µL). Plates were incubated for 5 minutes at RT to convert NAD+ to NADH. 10µL NADH developer was added to each well and the plate shaken for 5 minutes. Plates were read using a plate reader [Pherastar] with OD450nm readings made every 15 minutes for a total of 210 minutes. Protein concentration within samples was determined via a Bradford assay on the initial supernatant. Here, 5µL BSA standards or samples were added to each well of a 96-well plate with 195µL Bradford reagent. Plates were shaken in the dark for 3 minutes and absorbance measured at OD595nm. Data were analysed as described in manufacturer's instructions, using a paired t test between biological replicates assayed on the same day.

3.17 Metabolomics Assay

Kynurenine pathway metabolite analysis was carried out by Charles River Laboratories in the Netherlands using mass spectrometry. For larval analysis, five 5dpf larvae of known genotype were combined in an Eppendorf and flash frozen. For adult analysis, brains and liver were extracted from adult zebrafish of known genotype, weighed and flash frozen. Five biological

replicates were conducted for each experiment. Samples were shipped on dry ice. Additional wildtype samples were sent to optimise assays for use in zebrafish. Larval extract was obtained by homogenising larvae in 100µL extraction solvent using sonication. Homogenates were centrifuged and the supernatants stored as larval extract. Metabolites are reported as the concentration in this extract, which could be converted to concentration per larva. For adult tissue, 5µL extraction solvent was added to each mg of tissue and the sample homogenised using a Precellys homogeniser. Homogenates were centrifuged and the supernatants stored as extracts. Since these samples were weighed, metabolites are reported as tissue content (ng/g tissue).

3.18 In Silico Research

Initial *in silico* research of human and zebrafish genes was conducted using Ensembl software. Basic Local Alignment Search Tool (BLAST) programs were utilised to find orthologous genes by aligning protein sequences against the proteome of the opposite species. Nucleotide BLAST (BLASTN) was used to compare nucleic acid sequences between orthologous genes. Protein BLAST (BLASTP) was used to compare amino acid sequences, as well as specific protein domains using the "subrange" setting. The Needleman–Wunsch algorithm in SnapGene was also used to compare protein sequences and generate images used in this thesis. InterPro software (Mitchell et al., 2019), which combines information from multiple databases, was used to identify specific protein domains within amino acid sequences. EMBOSS Transeq (Madeira et al., 2019) was used to translate mutated nucleic acid sequences to their peptide sequences for comparison to wildtype proteins. An online exon-intron graph tool was used to create genomic figures, whilst protein schematics were created by hand in Adobe Illustrator, using pixel size for correct scaling. Synteny was assessed by "region comparison" on Ensembl, covering 1Mb of DNA surrounding the gene of interest.

3.19 Statistics

Where possible, experiments were completed in at least triplicate. Biological replicate refers to the use of embryos from separate parental batches. Graphs and statistical analyses were conducted in GraphPad Prism 7. Graphs other than survival curves are shown as means ± standard error of the mean (SEM). Statistical tests used are described per graph. Where relevant, normality was assessed using a Shapiro-Wilk test. Statistical significance was determined as $P<0.05$.

4 α-Amino-β-Carboxymuconate-ε-Semialdehyde Decarboxylase and Parkinson's Disease

4.1 Introduction

α-Amino-β-carboxymuconate-ε-semialdehyde decarboxylase (ACMSD) lies under a GWAS peak on chromosome 2 (Nalls et al., 2014), suggesting that SNPs in this gene may alter the risk of developing PD. This meta-analysis of GWAS reported this locus as "*ACMSD/TMEM163"*, although an updated meta-analysis (Nalls et al., 2019) dropped *ACMSD*, reporting this locus solely as *TMEM163*; the significant SNPs also differed from the original report. However, multiple SNPs have been discovered that lie closer to *ACMSD* than *TMEM163* and the association of these SNPs with PD appears to vary by population (**table 13**). This heterogeneity across populations has been suggested as the reason that some studies do not report *ACMSD* as a significant risk locus, despite its likely role in altering susceptibility to PD (Lill et al., 2012; Nalls et al., 2011).

To further support the proposal that *ACMSD* is indeed the gene responsible for altering PD risk at this locus, additional links between *ACMSD* and PD can be made, which is not the case for *TMEM163* (a PubMed search of "TMEM163 and Parkinson's" produced no results outside of GWAS). A pathogenic mutation in *ACMSD* (E298K) has been reported in a patient with late onset sporadic PD (Vilas et al., 2017), suggesting that other variations in *ACMSD* may also have effects relevant to the disease. Exploring Parkinsonian-like disorders also reinforce suggestions that *ACMSD* may play a role in PD. The screening of a three generation pedigree of a family with cortical myoclonic tremor, epilepsy and Parkinsonism identified that a W26*(Stop) mutation in *ACMSD* was likely responsible (Martí-Massó et al., 2013). Additionally, metabolites of the kyurenine pathway have been identified as dysregulated in PD patients (discussed in detail below), further suggesting that *ACMSD* is indeed the gene of interest at this locus.

Table 13. The Significance of Single Nucleotide Polymorphisms in α-Amino-β-Carboxymuconate-ε-Semialdehyde Decarboxylase in Various Studies

Study	Population	SNP	Odds Ratio	Significant?
(Nalls et al., 2014)	Multiple	rs6430538	<1	Yes
(Wang et al., 2019)	Chinese	rs6430538	>1	No
(Chang et al., 2019)	Taiwanese	rs6430538	<1	No
(Lill et al., 2012)	Multiple	rs6723108	<1	Yes (not conclusive)
(Bandrés-Ciga et al., 2016)	Spanish	rs6430538	>1	Yes
(Tejera-Parrado et al., 2019)	Spanish	rs6430538	>1	Yes
(Nalls et al., 2011)	Caucasian	Rs6710823	>1	Yes
(Pihlstrøm et al., 2013)	Scandinavian	rs10928513	<1	Yes

Published data on single nucleotide polymorphisms (SNPs) identified at either the ACMSD/TMEM163 or ACMSD alone loci. Significance was assumed at P<0.05.

ACMSD is an enzyme expressed in the kidneys, liver, and brain (Fukuoka et al., 2002) acting at a critical branching point in the catabolism of tryptophan via the kynurenine pathway. ACMSD is described as a homodimeric enzyme, with dimerisation being a requirement for decarboxylase function (Huo et al., 2013). The enzymatic activity of ACMSD is further increased by the formation of a dimer-dimer tetramer, responsible for stabilising an additional active site in each monomer, establishing eight active sites per tetramer (Yang et al., 2019).

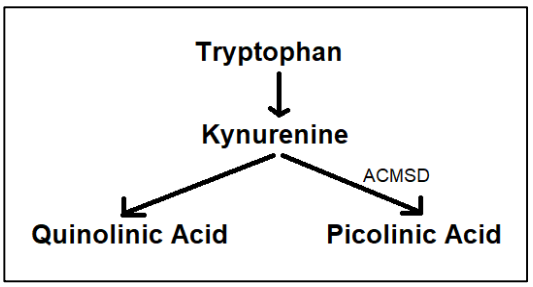

Figure 8. The Role of α-Amino-β-Carboxymuconate-ε-Semialdehyde Decarboxylase in the Degradation of Tryptophan.
α-amino-β-carboxymuconate-ε-semialdehyde decarboxylase (ACMSD) is required at a critical branching point in the kynurenine pathway where it acts to convert kynurenine to picolinic acid. In the absence of ACMSD, kynurenine is non-enzymatically degraded to quinolinic acid. Some pathway steps are not shown.

ACMSD acts in the kynurenine pathway to determine which of two key metabolites result from the degradation of tryptophan, picolinic acid (PIC) or quinolinic acid (QUIN) (**figure 8**). More specifically, ACMSD acts to convert α-amino-β-carboxymuconate-ε-semialdehyde (ACMS) to α-aminomuconate semialdehyde (AMS), which results in the final pathway product of PIC, a stable, non-metabolised metal chelator. For further pathway details, see **figure 9**.

Importantly, ACMS is an unstable molecule that will dehydrate to form QUIN in the absence of ACMSD. QUIN is a precursor for nicotinamide adenine dinucleotide (NAD+) synthesis but also acts as a potent neurotoxin. Due to its importance in cell survival, via NAD+ production, but also its neurotoxic nature, the production of QUIN must be tightly controlled; this regulation can be achieved at the level of ACMSD by modulating both the expression and activity of this enzyme. ACMSD monomers are held together by hydrogen bonds and salt bridge formation between key arginine residues that form the active site of the dimer and higher order structures (Huo et al., 2013). This quaternary structure is partially dependent on the pH and ionic strength of the surrounding solution (Yang et al., 2019). Aside from expression levels, this offers a further level of control over the activity of ACMSD and, therefore, the levels of QUIN produced.

NAD+ is a co-enzyme present in all species that is primarily involved in energy metabolism but is also recognised as an important molecule in DNA repair and epigenetics, where it acts as a co-enzyme for histone deacetylases. During redox reactions, critical for energy generation, NAD+ cycles between its oxidised and reduced states. However, in other reactions NAD+ is irreversibly cleaved, requiring the generation of new molecules to maintain adequate NAD+ levels. This occurs via three pathways: The Preiss-Handler pathway, the Salvage Pathway and the Kynurenine

Pathway, which is also known as the *de novo* Pathway here. The kynurenine pathway leads to the production of NAD+ from QUIN via quinolinate phosphoribosyl transferase and nicotinamide mononucleotide adenylyl transferase and this process can be directly linked to ACMSD activity – the greater the activity of ACMSD, the less NAD+ produced. This has been demonstrated in human and mouse cell-based models as well as *in vivo* in *C.elegans* and mice (Katsyuba et al., 2018). Using RNAi to reduce the expression of *acmd-1* (the orthologue of *ACMSD*) in *C.elegans*, resulted in 1.2x higher levels of NAD+ expression (Katsyuba et al., 2018). Furthermore, this increase in NAD+ was responsible for an increased lifespan that was dependent on Silent Information Regulator 2.1 (SIR2.1) and activation of the mitochondrial stress defence response via DAF-16, the sole orthologue of FOXO (Forkhead Box Protein O) family of transcription factors in *C.elegans*. This same effect was demonstrated by increasing dietary tryptophan, which would also result in increased levels of NAD+, although interestingly combining *acmd-1* knockdown and increased tryptophan did not appear to have additive effects. These data were supported in cell-based assays using both human and mouse cells, where a 98% reduction of ACMSD activity resulted in a 1.4x increase in NAD+ levels (Katsyuba et al., 2018). This appeared to be important for mitochondrial function, protection against steatosis and fatty-acid induced apoptosis as well as resulting in reduced levels of ROS. As with *C.elegans*, nearly all of the observed effects were sirtuin 1 (human orthologue of SIR2.1) dependent. However, in mammalian *in vivo* experiments the effects of inhibiting ACMSD appeared to vary by organ. As expected, increases in NAD+ were only present in areas where ACMSD is expressed (brain, liver, kidney), but the effects on QUIN, which was increased to below toxic levels, was only seen in the brain and mitochondrial effects only occurred in the liver.

Despite the important relationship between QUIN and NAD+ production, it is well recognised that QUIN is a neurotoxic molecule and so its levels must be controlled, even at the detriment of energy generation. Humans therefore rely on dietary niacin, creating NAD+ via the salvage pathway, rather than the kynurenine pathway, so that levels of QUIN can be kept to a minimum. In other animals, including mice, the kynurenine pathway alone is enough to produce sufficient NAD+ for cellular processes, but this comes at the cost of increased levels of QUIN. This represents a source of species variation, an important factor to bear in mind when choosing model organisms to study this pathway. This difference can be seen experimentally; mice that overexpress human ACMSD develop dependency on dietary niacin for NAD+ synthesis, becoming NAD+ deficient on niacin-free diets (Palzer et al., 2018). In this model, NAD+ deficiency also

depended on the tryptophan content of the diet, suggesting that some NAD+ is still synthesised via the kynurenine pathway despite high levels of ACMSD driving ACMS towards PIC production.

The neurotoxic effect of QUIN is conferred via a number of mechanisms, but is primarily thought to act via the direct activation of NMDA receptors. Whilst less potent than NMDA and glutamate, QUIN may be less quickly degraded, remaining available to activate receptors for extended periods of time (de Carvalho et al., 1996; Stone & Perkins, 1981). QUIN is widely accepted to result in differing neurotoxicity depending on brain region. This is commonly thought to be NMDA receptor subtype-specific, with only those containing NR2A or NR2B subunits susceptible to QUIN-induced toxicity (de Carvalho et al., 1996). This concept is particularly interesting since NR2B subunits are found on dopaminergic neurons (Jones & Gibb, 2005), suggesting they are at particular risk of excitotoxic NMDA receptor activation. However, ex vivo, QUIN can induce neurotransmitter release from noradrenergic but not dopaminergic neurons (Pittaluga et al., 2001). Aside from suggesting that direct excitotoxicity may not explain QUIN-induced dopaminergic neurodegeneration, the specificity of QUIN for NMDA receptor subtypes is also questioned by these data. NMDA receptors in both neuronal populations contain NR2B subunits and yet are differentially susceptible to QUIN. Pittaluga et al. (2001) suggest that splice variants of the NR1 subunit may actually be responsible for determining QUIN sensitivity. It is also possible that specific combinations of subunits are required for QUIN-induced NMDA receptor activation.

QUIN also induces excitotoxicity by increasing the release, and inhibiting the reuptake and degradation, of glutamate in synaptic regions (Tavares et al., 2005; Tavares et al., 2002; Tavares et al., 2000; Ting et al., 2009). Increased local glutamate concentrations result in the activation of glutamate receptors irrespective of subtype composition. Both the direct activation of NMDA receptors by QUIN and the enhanced availability of glutamate results in an increased calcium flux into neurons and glia, ultimately leading to the dysregulation of mitochondria and cell death (Duchen, 2012; Lee et al., 2010; S. Vandresen-Filho et al., 2015). Mitochondrial dysfunction, namely a reduction in complex 1 activity, is evident in the brain of live rats injected with QUIN (Hosoi et al., 2021), which may be a result of increased cytosolic calcium levels.

Whilst microglia and macrophages are the primary source of QUIN, they also directly respond to pathological levels. Exposure to exogenous QUIN results in the activation of microglia in the surrounding area (Hosoi et al., 2021; Minghetti et al., 2007; Moresco et al., 2008). Whilst this may be a secondary effect of degenerating neurons, the identification of microglial activation in response to QUIN in primary microglial cultures suggests that this is likely a direct effect on

microglia themselves (Feng et al., 2017). Although not fully understood, QUIN-induced microglial activation may be the result of NFκB translocation to the nucleus, causing the increased expression of proinflammatory mediators, including IL-1β and TNF-α (Feng et al., 2017). Pharmacological inhibition of the NMDA receptor is unable to prevent this activation, suggesting that it occurs via an NMDA receptor-independent mechanism (Pierozan et al., 2018). Interestingly, conditioned media from QUIN-activated microglia is able to induce neuronal death and the inhibition of microglial activation reduces QUIN-induced neuronal toxicity (Feng et al., 2017). These data suggest that the inflammatory effect of QUIN may play a larger role in QUIN-induced neurotoxicity than direct NMDA receptor activation.

QUIN can also enhance neuroinflammation by inducing the production of monocyte chemoattractant protein 1 (MCP1), IL-8 and TNF-α from astrocytes (Guillemin et al., 2003; Pierozan et al., 2018). Generally, astrocytes are considered neuroprotective in the kynurenine pathway due to their production of anti-inflammatory kynurenic acid and PIC, which can minimise QUIN production and act as an NMDA receptor antagonist (Guillemin et al., 2001). However, microglia can acquire the kynurenine generated in astrocytes and drive it down the neurotoxic, proinflammatory pathway, terminating with the production of QUIN (**figure 9**). QUIN can then act on the astrocytes, increasing their production of proinflammatory mediators.

Oxidative stress is another key mechanism involved in QUIN-induced toxicity. QUIN has been widely demonstrated to increase ROS and reactive nitrogen species (RNS) in astrocytes, microglia and neurons (Braidy et al., 2009; Hosoi et al., 2021; Ryu et al., 2004; Samuel Vandresen-Filho et al., 2015). Enhanced production of RNS can be attributed to the increased expression of iNOS and nNOS following exposure (Braidy et al., 2009; Ryu et al., 2004). Increased ROS may result from the transfer of electrons from QUIN-iron complexes to oxygen (Pláteník et al., 2001). Oxidative stress induced following QUIN exposure also differs by brain region, although, relevant to PD, increased ROS has been identified in the striatum (Samuel Vandresen-Filho et al., 2015). This varying sensitivity of different brain regions has been suggested to result from differing antioxidant capacities (Samuel Vandresen-Filho et al., 2015).

QUIN can also cause cytoskeletal disruptions in neurons and astrocytes, resulting in a disrupted morphology and loss of cell-cell interactions (Pierozan et al., 2012). Blocking NMDA receptors has no effect in preventing QUIN-induced changes to neuronal morphology (Pierozan et al., 2018), suggesting this aspect of toxicity also occurs independently of NMDA receptors. Finally, QUIN may also result in disruption of the BBB (Reynolds & Morton, 1998; St'astný et al., 2000), enabling

the infiltration of potentially damaging compounds into the CNS which may contribute to neurodegeneration.

ACMSD appears to have conflicting roles in the CNS. On one hand, ACMSD can be thought of as an anti-inflammatory molecule. During an immune insult, increased ACMSD acts to limit the production of QUIN and, therefore, the neuronal damage caused by the resulting neurotoxicity and inflammation (Thirtamara-Rajamani et al., 2017). On the other hand, excessive ACMSD activity can result in NAD+ deficiency. It is clear that ACMSD activity needs to be carefully balanced. Humans have developed a dependency on dietary niacin for NAD+ production to overcome this issue, allowing for increased ACMSD activity to prevent QUIN build up, whilst generating enough NAD+ for survival. However, this reliance on niacin results in an increased risk of Pellagra, which in itself is linked to neurodegeneration, particularly in the form of dementia (Morris et al., 2004).

It is possible that both increases and decreases in ACMSD may alter the risk of developing PD, either by reducing the production of NAD+ or increasing the vulnerability of the CNS to inflammation in response to an initial immune insult, such as exposure to toxins or infections. This theory is also supported by the study of other members of the kynurenine pathway, some of which have been identified as dysregulated in PD. In MPTP treated mice, decreased kynurenine aminotransferase 1 (KAT-1) has been found in the SNPc (Knyihár-Csillik et al., 2004), suggesting that levels of kynurenic acid and other downstream metabolites are also likely to be dysregulated. In human PD, tryptophan has been found to be decreased and 3-hydroxykynurenine increased in patient serum and CSF (Han et al., 2017; Klatt et al., 2021; Lewitt et al., 2013; Widner et al., 2002). Kynurenine also tends to be decreased in the blood of PD patients (Han et al., 2017; Klatt et al., 2021), but levels within the CSF have been shown to be increased (Iwaoka et al., 2020). Levels of kynurenic acid varies by publication, with reports of this being both increased and decreased in PD patients (Oxenkrug et al., 2017; Sorgdrager et al., 2019). Within the brain itself, a decrease of kynurenine and kynurenic acid and an increase of 3-hydroxykynurenine have been found specifically within the substantia nigra of those with PD (Ogawa et al., 1992). Furthermore, levels of KAT-II, responsible for 75% of kynurenic acid production, has been found to be increased in RBCs taken from symptomatic PD patients (Hartai et al., 2005). A summary of kynurenine pathway metabolites in PD is shown in **table 18**, **section 4.3**. The changes to kynurenine pathway metabolites in the blood, brain and CSF of patients

suggests that this pathway is dysregulated in the CNS as well as more widely in the body, although its direct link to ACMSD, or indeed cause and effect, cannot be shown.

4.1.1 The Zebrafish Liver

The liver is an organ with a primary role of detoxification and lipid processing. Since the highest expression of *ACMSD* in humans is reported in the liver, analysis of this organ in loss-of-function zebrafish mutants may provide further insight into the basic function of this protein.

As in humans, the zebrafish liver is also a metabolic and lipid storage organ. Liver budding begins at 24-28hpf in zebrafish larvae, and a functional liver containing all cell types is present by 4dpf (Field et al., 2003). Development recapitulates that of mammalian liver development and its final structure and function is mostly conserved. The primary difference is the seemingly random positioning of bile ducts, veins and arteries that are highly organised in the mammalian liver (Yao et al., 2012).

Fatty acid binding proteins (FABP), involved in the uptake, transport and intracellular targeting of fatty acids, represent a group of proteins with conserved structure but distinct expression patterns. Fabp10a was first identified in adult zebrafish as a 126aa protein specifically expressed in the liver (Denovan-Wright et al., 2000) although later research suggests that its expression pattern also includes the intestines and testis (Sharma et al., 2006). In zebrafish larvae, *fabp10a* is expressed exclusively in the liver, with signals detectable from 48hpf (Sharma et al., 2006; Venkatachalam et al., 2009). A duplicated gene, *fabp10b*, was discovered later (Venkatachalam et al., 2009) although its expression pattern differed significantly from *fabp10a*; *fabp10b* is expressed only in the olfactory vesicles of larvae and primarily in the muscle and heart of adult zebrafish (Venkatachalam et al., 2009). *fabp10a* expression can be used as a reliable readout of hepatotoxicity of some compounds in larval zebrafish (Mesens et al., 2015), making it a useful marker to use in this project.

Many compounds have been used to induce liver damage in zebrafish. The most commonly used is paracetamol (acetaminophen). Exposure of zebrafish larvae to toxic doses of paracetamol has been shown to result in decreased liver size (Cornet et al., 2017; He et al., 2013; M. Kim et al., 2018; Nguyen et al., 2017; Yamashita et al., 2019; Zhang et al., 2019) and yolk retention (He et al., 2013; M. Kim et al., 2018), a commonly used marker of liver damage or delayed liver development in zebrafish larvae. Paracetamol has also been reported to result in lipid accumulation in the yolk (Cornet et al., 2017), likely resulting from dysfunction of the liver, which usually acts to clear these lipids as it develops. At the cellular level, paracetamol results in the

appearance of vacuoles (M. Kim et al., 2018; Nguyen et al., 2017; Yamashita et al., 2019), swelling (M. Kim et al., 2018; Yamashita et al., 2019) and nuclear changes (M. Kim et al., 2018; Yamashita et al., 2019), ultimately leading to necrosis and a reduced number of hepatocytes (He et al., 2013; Yamashita et al., 2019). At the mRNA level, increased levels of *keap1/2* and *gstp1* are seen (Yamashita et al., 2019), suggesting oxidative stress plays a role in the hepatotoxicity. The toxicity of paracetamol in zebrafish larvae appears to be liver specific, with miR-122 (a microRNA known to be released from injured hepatocytes), increasing specifically in the liver and not in other organs (Nam et al., 2016). However, if the dose is further increased, cardiac effects become apparent (Zhang et al., 2014). By using a low concentration of paracetamol, hepatotoxicity can be induced in zebrafish larvae without effects on other organs (Mesens et al., 2015). Additionally, both immersion and injection into the yolk at 3dpf have been shown to be viable options to induce hepatotoxicity (Nguyen et al., 2017) and *fabp10a* can be used as readout (Mesens et al., 2015).

Zebrafish provide a great model system that can be used to explore the role of *ACMSD* as a putative PD risk gene owing to their genetic manipulability and relative ease of assessing PD-relevant readouts. The aims of this chapter are to describe the creation of a zebrafish line carrying a loss-of-function mutation in *acmsd* and the use of this model to investigate how Acmsd impacts normal zebrafish development and processes. In addition, the role of this enzyme in PD pathogenesis will be explored by assessing movement, dopaminergic neuron development and neuroinflammation as well as challenging this zebrafish line with additional stressors, including hepatotoxicity and environmental inflammation.

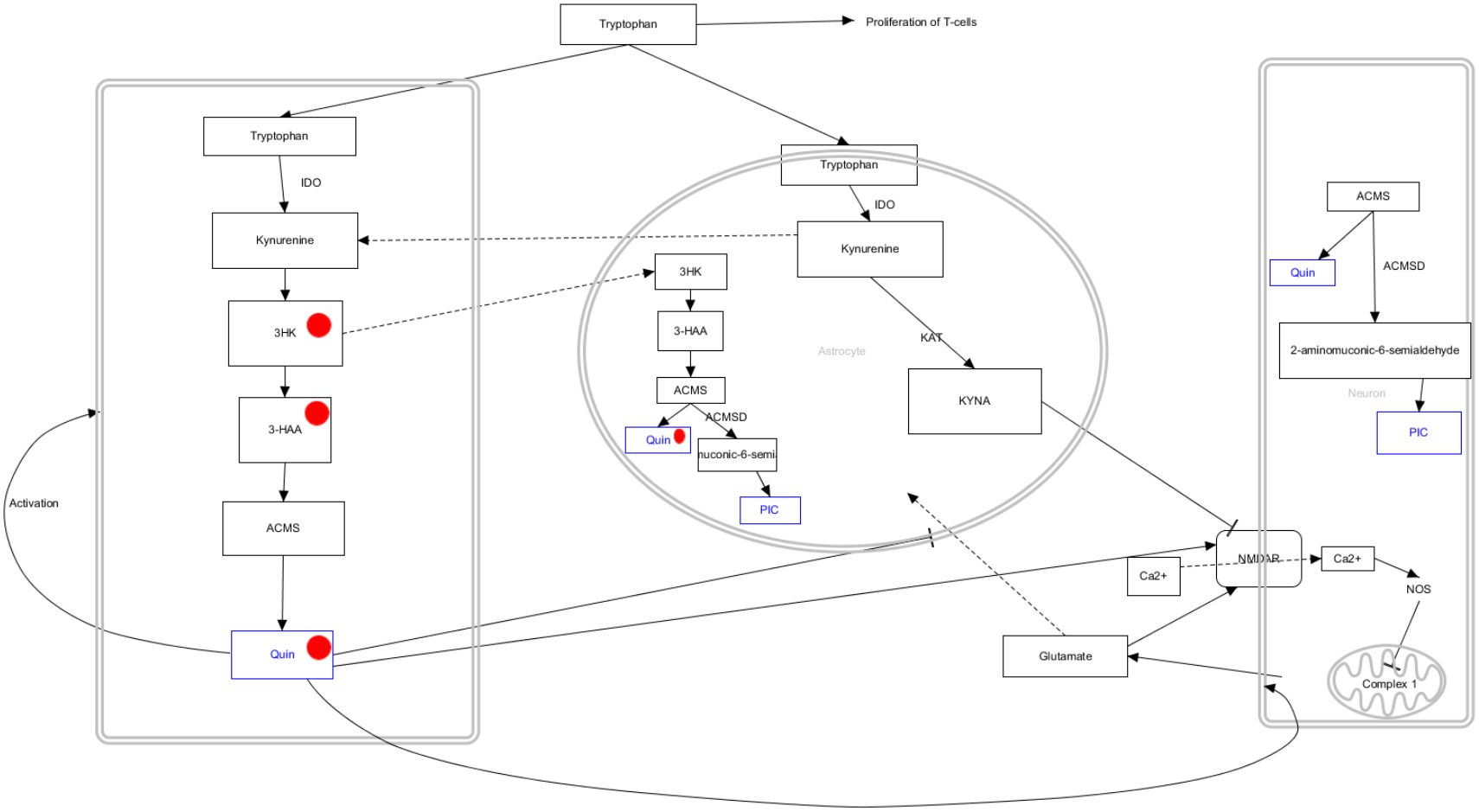

Figure 9. Schematic of the Kynurenine Pathway in the Central Nervous System. *The kynurenine pathway is responsible for the metabolism of tryptophan. This occurs in both the microglia (left) and astrocytes (central) although downstream metabolites vary depending on cell type. The presence of aminocarboxymuconate-semialdehyde decarboxylase (ACMSD) in neurons (right) and astrocytes leads to the production of picolinic acid (PIC), whilst its absence in microglia leads to the spontaneous production of quinolinic acid (QUIN). QUIN is proinflammatory and neurotoxic via a number of mechanisms including the activation of NMDA receptors, inhibition of glutamate re-uptake and increased glutamate release from neurons. Red dots represent neurotoxic metabolites. ACMSD, α-amino-β-carboxymuconate-ε-semialdehyde decarboxylase; IDO, indolamine 2,3-dioxygenase; 3HK, 3-hydroxykynurenine; 3-HAA, 3-hydroxyanthranilic acid; ACMS, alpha-amino-beta-carboxymuconate-epsilon-semialdehyde; Quin, Quinolinic* acid*; KAT, kynurenine aminotransferase; KYNA, kynurenic acid; PIC, picolinic acid; Ca2+, calcium; NMDAR, N-methyl-D-aspartate receptor; NOS, nitric oxide synthase. For references, see main text or review by Lugo-Huitrón et al., 2013*

4.2 Results

4.2.1 In Silico Research

The Ensembl database describes human *ACMSD* (ENSG00000153086) as a protein coding gene on chromosome 2 expressed as two splice variants; a 1307bp transcript, coding for a 278aa long protein, and a 1252bp transcript, coding for a 336aa protein (**figure 10**). Protein-Protein BLAST of these transcripts using BLASTP software identified a 100% conserved 252aa C-terminal between splice variants (**figure 10**). Needleman-Wunsch global alignment in SnapGene revealed a total protein identity of 77.1% when accounting for the differing N-terminal. InterPro software analysis of the full length ACMSD amino acid sequence predicted there were no conserved protein domains present, suggesting that ACMSD does not belong to a wider protein family.

To identify the zebrafish orthologue of ACMSD, the full length human ACMSD amino acid sequence was aligned to the zebrafish proteome using BLASTP software. The only result from this alignment was Acmsd, possessing 81.25% identity to the human protein (**figure 10**). The reverse analysis, aligning the zebrafish Acmsd protein sequence to the human proteome, also revealed ACMSD as a single result.

At the DNA level, Ensembl also identified *acmsd* (ENSDARG00000062549) on chromosome 9 as the single zebrafish orthologue to human *ACMSD* (**figure 10**). This highly conserved gene demonstrated 80.95% identity to *ACMSD* when compared using BLASTN. Zebrafish also express two splice variants of *acmsd*, a 1570bp and a 1568bp transcript, although both yield identical 336aa protein sequences. As with human ACMSD, InterPro analysis of conserved domains also failed to identify any specific protein domains within zebrafish Acmsd.

Genome synteny has been conserved between the human and zebrafish *ACMSD* loci, with a number of orthologous genes, including *CCNT2/ccnt2a* and *MAP3K19/map3k19,* present in a 1Mb region surrounding each gene (**figure 11**).

All of the above data suggest that zebrafish *acmsd* is the true orthologue of human *ACMSD*.

Table 14. Comparison of Human and Zebrafish α-Amino-β-Carboxymuconate-ε-Semialdehyde Decarboxylase.

	Human	**Zebrafish**
Transcript Base Pairs	1252	1570
Amino Acids	336	336
Exons	10	10
Protein Coding Splice Variants	2	2
Chromosome Number	2	9

A table outlining the basic features of the α-amino-β-carboxymuconate-ε-semialdehyde decarboxylase protein and gene and comparing these between human and zebrafish. The full length transcripts from both organisms were used for comparison.

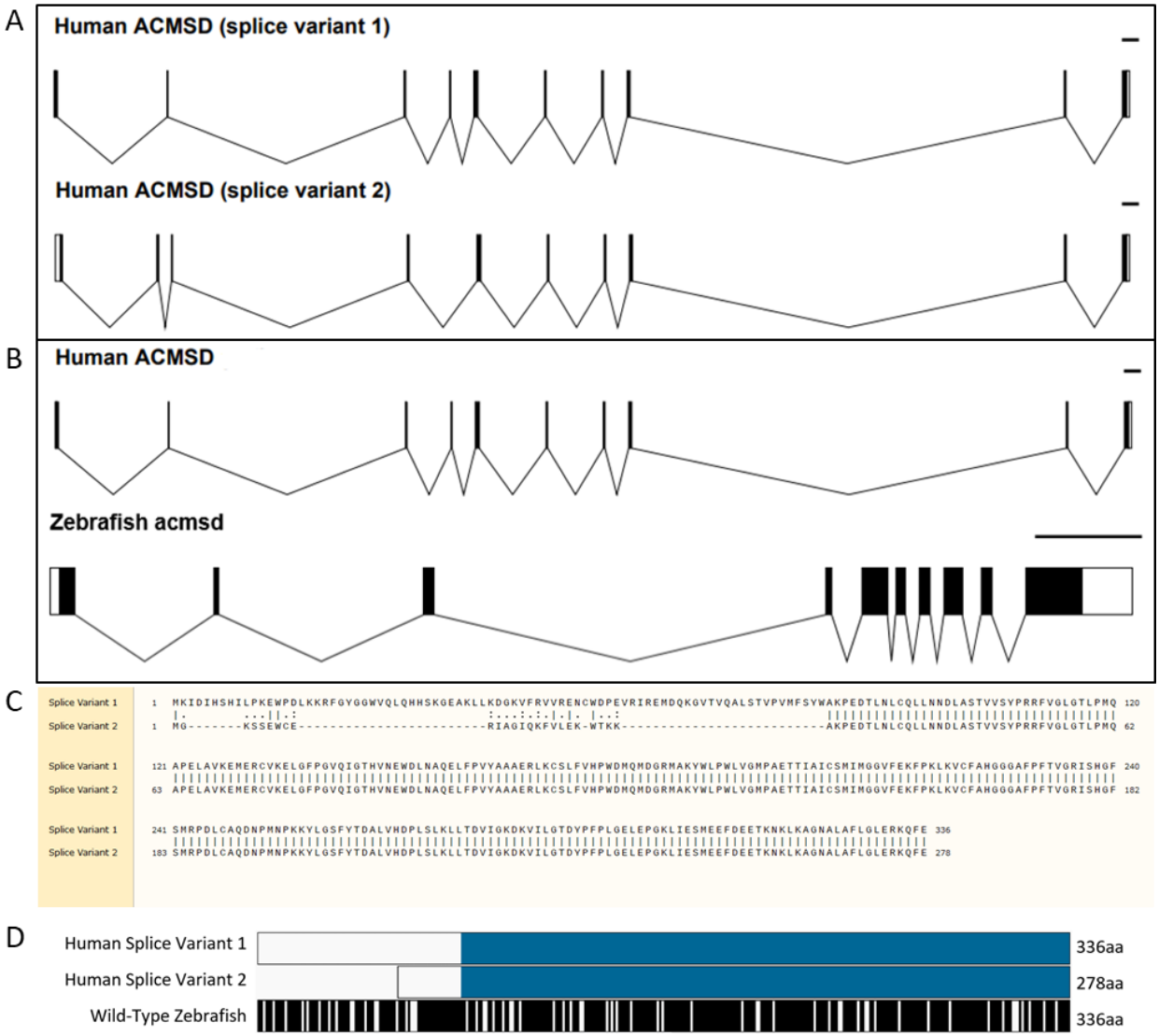

Figure 10. A Comparison of Human and Zebrafish α-Amino-β-Carboxymuconate-ε-Semialdehyde Decarboxylase Finds That Both Genes Share High Similarity. A*. Humans possess two splice variants of ACMSD which are schematised here at the DNA level. Both variants have 10 exons. White sections represent untranslated regions of sequence. Scale bar = 1Kb.* ***B.*** *Both organisms have a single gene encoding for ACMSD, comprised of 10 exons. The human orthologue has increased intron (thin lines) size, resulting in a DNA sequence length over 6-times that of zebrafish. Scale bar = 1Kb.* ***C.*** *The two splice variants found in humans result in proteins of either 336aa or 278aa in length. Screenshot from SnapGene shows conserved 253 amino acid C-terminal.* ***D.*** *Schematic comparison of human splice variants and zebrafish protein. Blue regions represent conserved amino acid sequences between human variants. The single zebrafish protein is 336aa long. Black regions of the zebrafish graphic symbolise conserved amino acids between the 336aa human splice variant and the zebrafish sequence, equating to 81.25% protein identity. Graphic is drawn to scale by equating 1 pixel to 1 amino acid. aa, amino acid; acmsd, α-amino-β-carboxymuconate-ε-semialdehyde decarboxylase.*

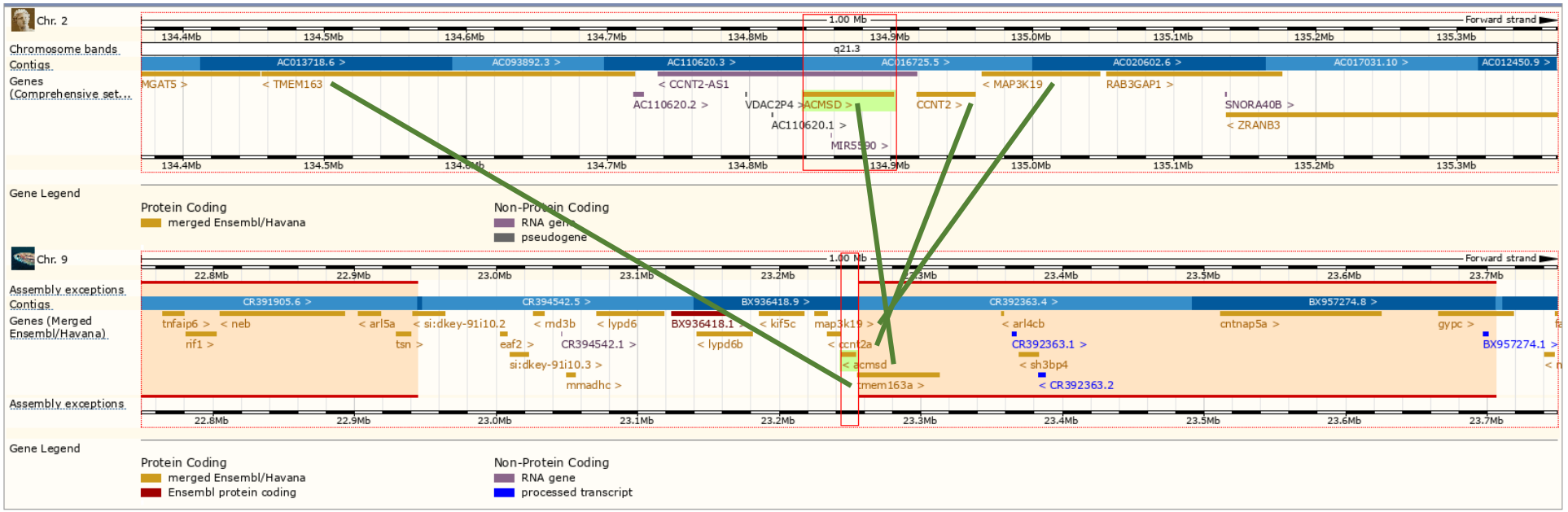

Figure 11. Synteny Around α-Amino-β-Carboxymuconate-ε-Semialdehyde Decarboxylase is Maintained Between Human and Zebrafish. *Screenshot of the results from the region comparison feature on Ensembl comparing 1Mb around the acmsd gene on human chromosome 2 and zebrafish chromosome 9. Genes labelled in red or yellow were used for synteny comparison. Green lines depict orthologous genes.*

4.2.2 Expression of *acmsd* in Wildtype Zebrafish

4.2.2.1 Reverse Transcriptase Polymerase Chain Reaction (RT-PCR)

To identify whether Acmsd may play a role in the early stages of zebrafish development, the expression of *acmsd* at this time was analysed. RT-PCR found that *acmsd* was expressed from 1-5dpf in wildtype zebrafish (**figure 12A**). The level of expression compared to the loading control (*rps29*) suggested that *acmsd* mRNA levels increase overtime. Expression was also assessed in adult zebrafish organs, finding highest expression in the liver and intestines of both sexes (**figure 12B).** *acmsd* also appeared to be expressed in the brain, kidney, gonads, gall bladder and possibly in the heart, although this band was faint in the female and not present in the male.

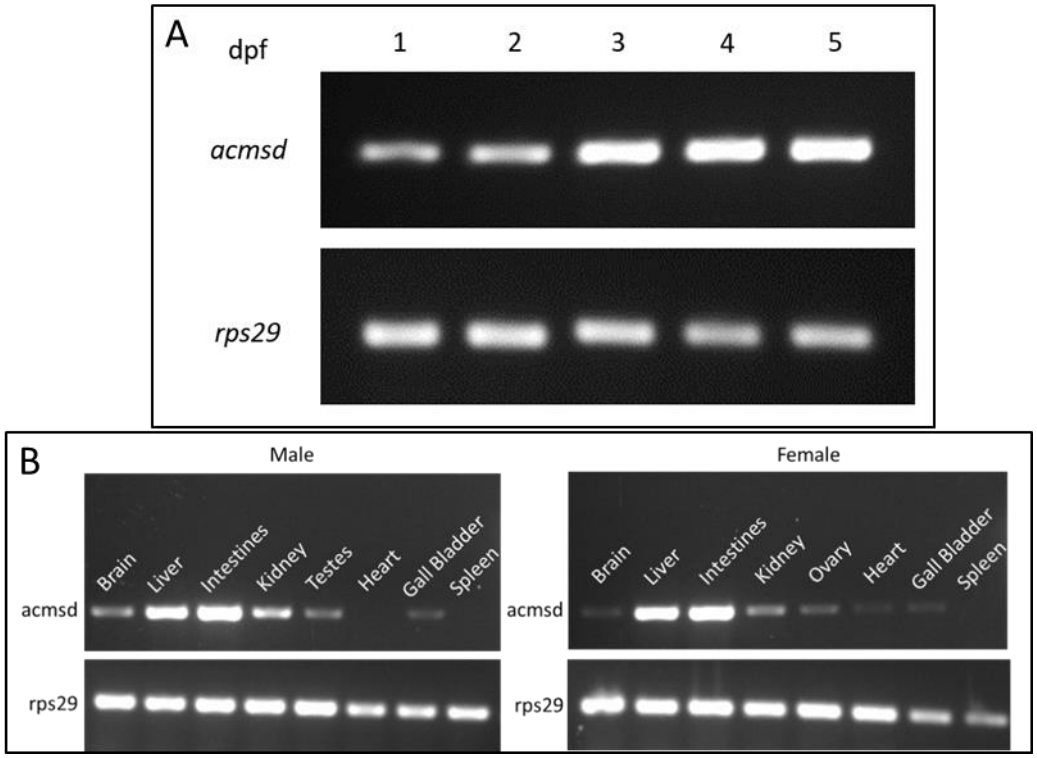

Figure 12. α-Amino-β-Carboxymuconate-ε-Semialdehyde Decarboxylase Expression in Wildtype Zebrafish. A. *RT-PCR shows that acmsd is expressed at an increasing concentration from 1-5dpf in wildtype zebrafish. 15 larvae were combined per age group for RNA extraction. rps29 was used as a loading control.* ***B.*** *RT-PCR of acmsd in adult zebrafish organs in a single male (left) and female (right) show similar patterns. acmsd appears to be expressed primarily in the liver and intestines. acmsd, α-amino-β-carboxymuconate-ε-semialdehyde decarboxylase; dpf, days post fertilisation; rps29, ribosomal protein S29.*

4.2.2.2 In Situ Hybridisation

In situ hybridisation primers were designed that did not cross the deletion site so that they could be used in later experiments to assess transcript levels in mutant larvae (**figure 13A**). Both sets of primers were tested using a gradient PCR, but even at higher temperatures were found to have non-specific amplification (**figure 13B,C**). Nested primers were therefore designed for each primer pair which enabled the amplification of only the product of interest following both PCRs. Probe 1 was used on wildtype samples to assess the expression of *acmsd* in zebrafish larvae at

3dpf. Staining was seen in the head region in both the sense and antisense probes, but staining within the liver was seen only with the antisense probe (**figure 13**).

Due to staining from the sense probe, new probes were designed to determine whether this staining pattern was real. Owing to the short length of *acmsd* cDNA, these probes had to cross the deletion site. These primers produced a single band when amplified by PCR, so nested primers were not necessary. Two new probes were tested in 3dpf wildtype zebrafish. Both demonstrated *acmsd* expression specifically in the liver, with some fish also showing staining in the gut (images from one probe shown in **figure 14**). No head staining was identified using these new probes.

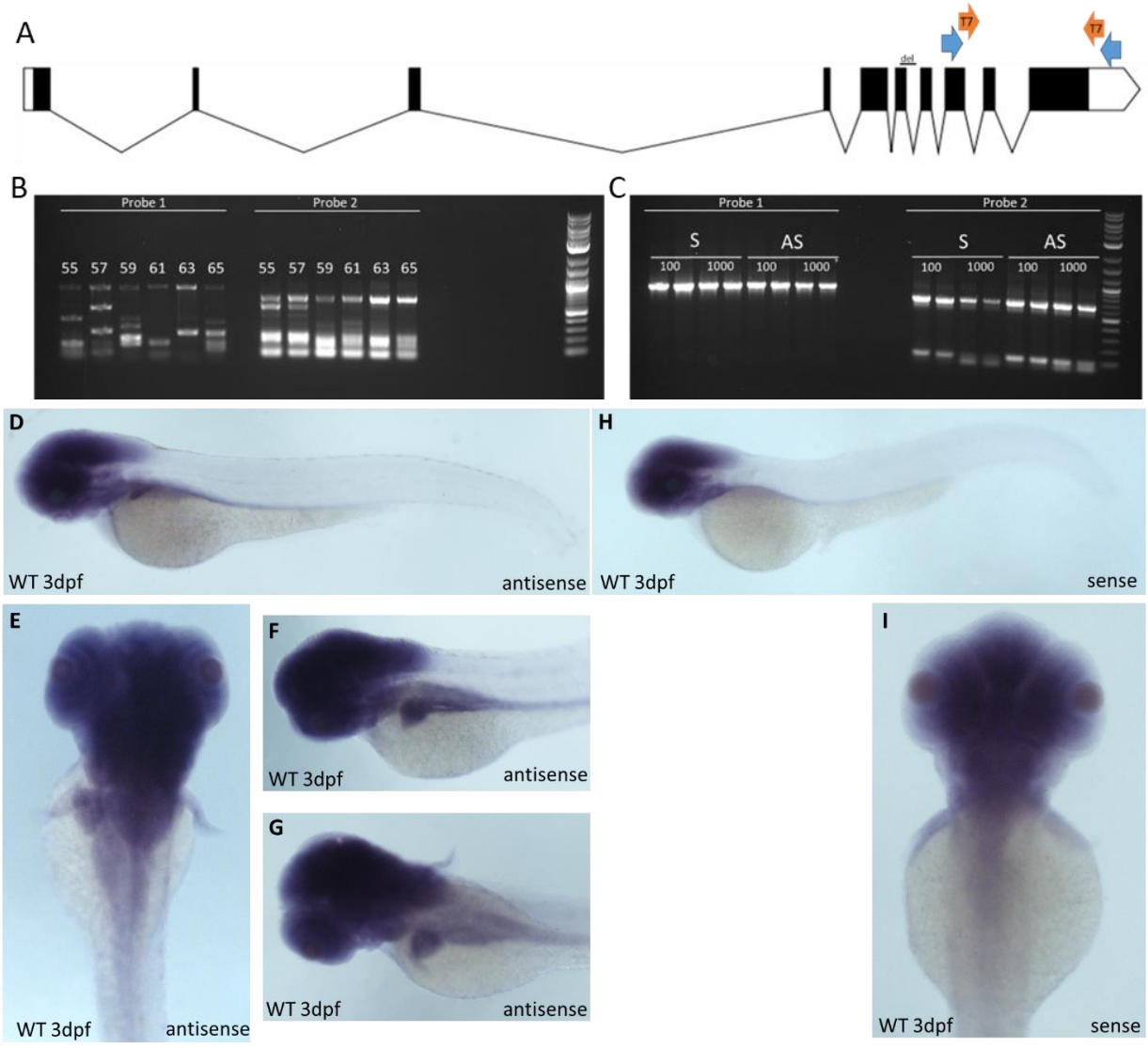

Figure 13. Designing In Situ Hybridisation Probes Against α-Amino-β-Carboxymuconate-ε-Semialdehyde Decarboxylase. A. *Target region of probes at the 3' end of the acmsd gene. Forward primers in exon 8 and reverse primers in the 3' UTR. Blue arrows depict the approximate region of initial primer pairs, orange shows approximate region of nested primers, tagged with T7 for transcription* ***B.*** *Gradient PCR using initial primer pairs on wildtype cDNA. 1kb plus ladder used.* ***C.*** *Electrophoresis gel showing specific product after using nested primers on initial PCR products. S, sense; AS, antisense; 100, used 100X dilution of initial PCR product; 1000, used 1000X dilution of initial PCR product. 1Kb plus ladder used* ***D.*** *In situ hybridisation in 3dpf wildtype larvae using both the antisense (**D-G**) and sense (**H-I**) probes from primer pair 1. dpf, days post fertilisation; WT, wildtype.*

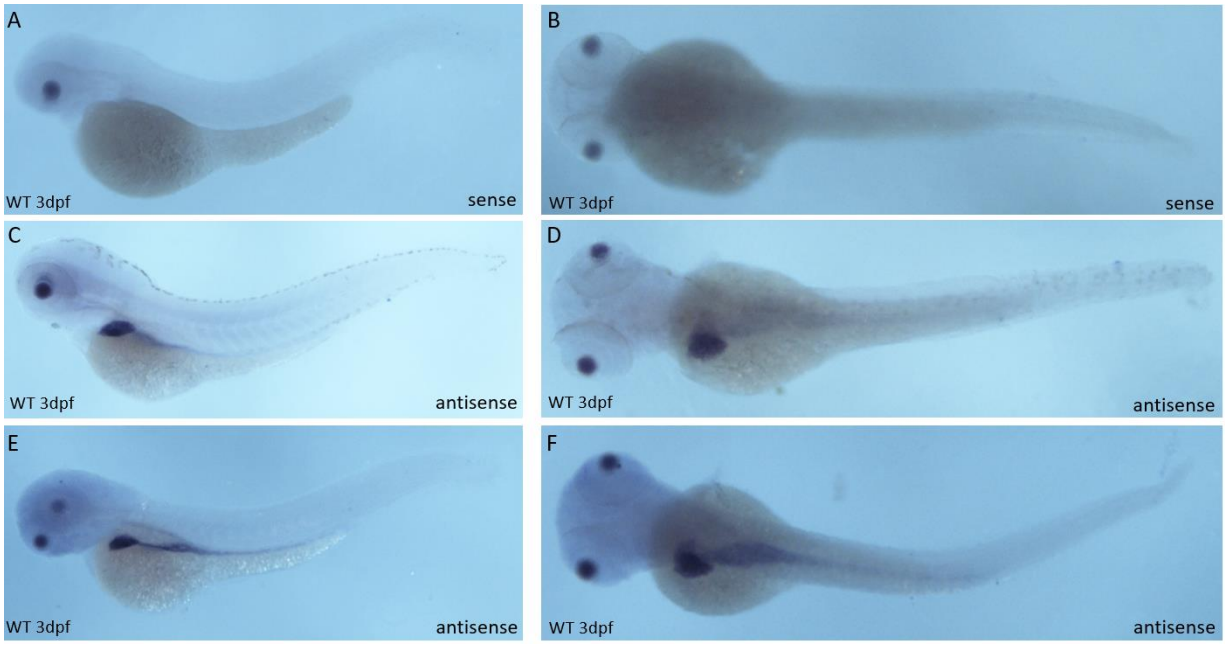

Figure 14. In Situ Hybridisation Demonstrates α-Amino-β-Carboxymuconate-ε-Semialdehyde Decarboxylase Expression Specifically in The Liver of 3-Days Post Fertilisation Wildtype Zebrafish. A-B. *Sense probe produced no staining as seen from lateral (**A**) and dorsal (**B**) view. **C-F.** Antisense probe staining from lateral (**C, E**) and dorsal (**D, F**) view. The liver can be seen stained as well as more faint staining in the gut. Some larvae had more obvious gut staining (**E, F**) dpf, days post fertilisation; WT, wildtype.*

4.2.1 α-Amino-β-Carboxymuconate-ε-Semialdehyde Decarboxylase Mutant Zebrafish

4.2.1.1 Generation of an acmsd$^{-/-}$ Mutant Zebrafish

The *acmsd*$^{-/-}$ mutant zebrafish line was created using CRISPR/Cas9 technology by Dr Marcus Keatinge prior to the commencement of this project. The resulting mutant had a 1bp insertion and 71bp deletion in exon 6 and into intron 6-7, resulting in the deletion of a 3' splice site (**figure 15**). The large 70bp reduction in gene length meant that this mutant was easily genotyped by standard PCR (**figure 15E**).

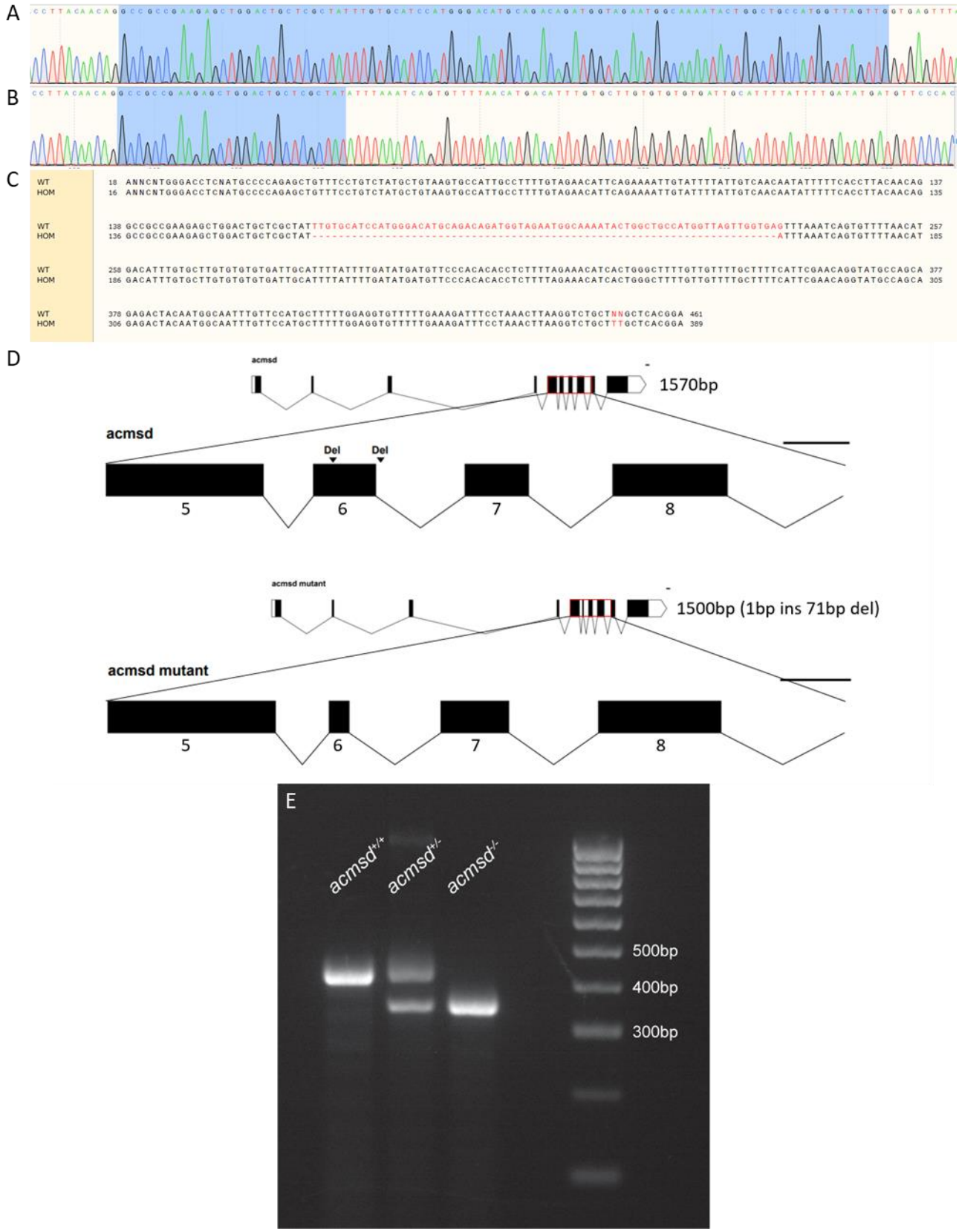

Figure 15. CRISPR-Generated Mutation in Exon 6 of α-Amino-β-Carboxymuconate-ε-Semialdehyde Decarboxylase in Zebrafish. ***A****. Chromatogram of sequenced wildtype DNA with exon 6 of acmsd highlighted in blue.* ***B.*** *Chromatogram of sequenced acmsd homozygous mutant DNA with exon 6 of acmsd highlighted in blue.* ***C.*** *Comparison of these sequences in SnapGene. Red bases represent those that differ between genotypes.* ***D.*** *Schematic representation of the mutation induced. 1bp was inserted at the 71bp deletion site ('del'), creating a DNA sequence 70bps shorter than wildtype acmsd and removing a 3' splice site. Scale bar = 100 bases.* ***E.*** *The resulting 70bp reduction in DNA length allows for genotyping via standard PCR. Wildtype zebrafish are identified by a single 425bp band (left), whist homozygous mutants are identified by a 355bp band (right). Heterozygous mutants appear as double bands (centre). acmsd, α-amino-β-carboxymuconate-ε-semialdehyde decarboxylase; bp, basepair; del, deletion; HOM, homozygous mutant; ins, insertion; WT, wildtype.*

4.2.1.2 Determining Mutation Effect

The mutation created includes the deletion of a 3' splice site as the 70bp deletion crosses an exon-intron boundary at the end of exon 6. The outcome of this splice site deletion could be that the exon is skipped, the 3' intron is inserted or there is activation of a cryptic splice site. To determine which occurs in this mutant, RT-PCR was conducted on homozygous mutant zebrafish cDNA using a primer pair that spanned from exon 5 to exon 7. The amplified cDNA was gel-extracted and sequenced in both directions. This revealed that exon 6 undergoes complete exon skipping without the retention of surrounding introns (**figure 16**). The flanking exon sequences were indistinguishable from wildtype. *In silico* transcription of *acmsd* cDNA sequences with and without exon 6 were conducted using SnapGene (**figure 16**). These suggest that the loss of exon 6 results in the production of a 227aa protein, with the 162aa N-terminal identical to wildtype. Importantly, this transcript induces a premature STOP codon into exon 8 which likely induces nonsense-mediated decay of the resulting mRNA. SnapGene also suggested that the loss of exon 6 induced an additional open reading frame, resulting in the production of a 156aa protein with the 142aa C-terminal identical to wildtype. However, this ATG was located towards the 3' end of the mRNA and creates a very small reading frame so is unlikely to be transcribed. Additionally, if the first open reading frame results in nonsense-mediated decay, there would only be very low levels of mRNA to transcribe this later variant from.

4.2.1.3 Confirmation of a Pathogenic Mutation

4.2.1.3.1 Using Quantitative PCR

4.2.1.3.1.1 Designing qPCR Primers

Two primer pairs for *acmsd* qPCR were designed using Primer3 and tested in a standard PCR reaction using wildtype cDNA as a template. Both pairs produced a single, clean band when run by gel electrophoresis (**figure 17A**), indicating primer specificity to *acmsd.* Therefore, optimisation steps were taken using both pairs.

Melt curves for both primer pairs produced single peaks above threshold level, confirming that only one target was amplified (**figure 17B,C**). Four concentrations of cDNA (5X dilutions) and three concentrations of primer (100nM, 250nM, 500nM) were used to create standard curves and identify the most appropriate primer concentration to use for experiments. Primer pair 1 at 500nM was chosen to take forward for qPCR as this had the highest efficiency and an r-squared value above 0.99; this was not the case for other combinations tested (**figure 17D-F**). Whilst *ef1α* was used during optimisation steps, *rps29* was chosen for use as a reference gene, at a previously tested concentration of 300nM, as others had reported issues with *ef1α.*

Figure 16. Effect of the CRISPR-Generated Mutation of α-Amino-β-Carboxymuconate-ε-Semialdehyde Decarboxylase at the Protein Level. A. *Chromatogram of wildtype acmsd cDNA. The end of exon 5 is highlighted in blue.* ***B.*** *Chromatogram of acmsd homozygous mutant cDNA. The end of exon 5 is highlighted in blue.* ***C.*** *5'-3' sequencing data of acmsd cDNA in 2 homozygous mutant (top) and 2 wildtype (bottom) zebrafish larvae. In acmsd mutants, the 3' end of exon 5 appears identical to wildtype, exon 6 is missing and the 5' end of exon 7 appears identical to wildtype. The sequencing data then becomes hard to interpret.* ***D.*** *3'-5' sequencing data of acmsd cDNA shows the same result, with exon 6 being completely lost.* ***E.*** *In silico transcription of wildtype acmsd shows that the codon for glycine (highlighted in blue) crosses the boundary between exons 6 and 7.* ***F.*** *Predicted protein sequences resulting from the loss of exon 6 from acmsd cDNA as determined via SnapGene, with a minimum open reading frame of 75 amino acids. Coloured amino acids represent identity to wildtype sequence.* ***G.*** *The likely protein created by this mutation is 227aa long, sharing complete identity to the 162aa N-terminal of wildtype Acmsd. The black fill in the wildtype protein represents conserved residues to human ACMSD. aa, amino acids; acmsd, α-amino-β-carboxymuconate-ε-semialdehyde decarboxylase; HOM, homozygous mutant; WT, wildtype.*

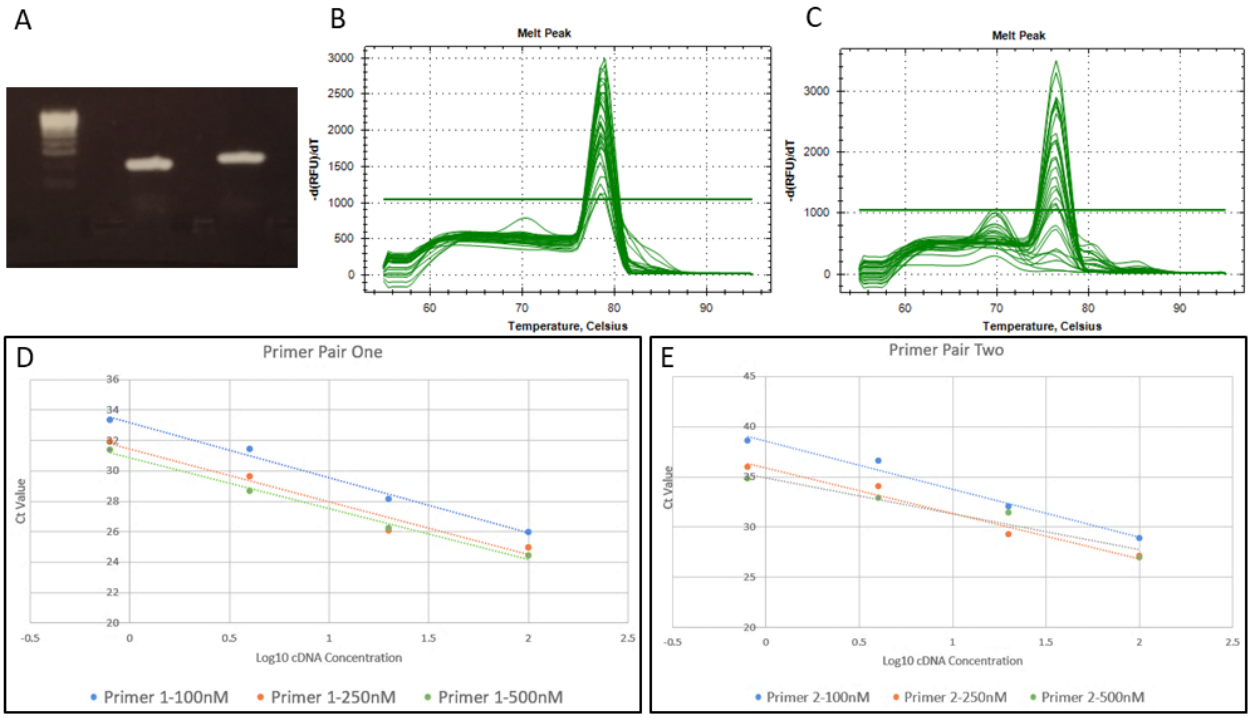

F	Primer 1 100nM	Primer 1 250nM	Primer 1 500nM	Primer 2 100nM	Primer 2 250nM	Primer 2 500nM	ef1α 100nM
R-squared	0.990	0.966	0.992	0.981	0.970	0.937	0.929
Slope	-3.617	-3.492	-3.348	-4.811	-4.484	-3.579	-2.833
Efficiency	89.0	93.4	98.9	61.4	67.1	90.3	125.4

Figure 17. A. *Electrophoresis gel of a PCR run using acmsd primer pair 1 (left) and acmsd primer pair 2 (right) using wildtype cDNA at 60°C.* ***B.*** *Melt curve obtained following qPCR using acmsd primer pair 1.* ***C*** *Melt curve obtained following qPCR using acmsd primer pair 2.* ***D.*** *Standard logarithmic curve created following efficiency testing using acmsd primer pair 1 at 3 concentrations; 100nM, 250nM and 500nM.* ***E.*** *Standard logarithmic curve created following efficiency testing using acmsd primer pair 2 at 3 concentrations; 100nM, 250nM and 500nM.* ***F.*** *Summary of values obtained from efficiency testing of both primer pairs. acmsd, α-amino-β-carboxymuconate-ε-semialdehyde decarboxylase; cDNA, complementary deoxyribose nucleic acid; nM, nanomolar; PCR, polymerase chain reaction.*

4.2.1.3.1.2 Quantitative Polymerase Chain Reaction (qPCR)

acmsd$^{-/-}$ mutant zebrafish have significantly reduced *acmsd* mRNA levels compared to their wildtype siblings, both in larvae, at 5dpf, and in adult brain tissue (**figure 18A**). In larvae, mRNA levels were 79.5% lower in *acmsd* homozygous mutants than in their wildtype siblings, suggesting that the CRISPR-Cas9 induced mutation triggers nonsense-mediated decay of the resulting transcript. In brain tissue taken from adult zebrafish, *acmsd* mRNA was expressed at 42.5% that of wildtype siblings, although a high variability in *acmsd* expression was found in wildtype brains (**figure 18B**).

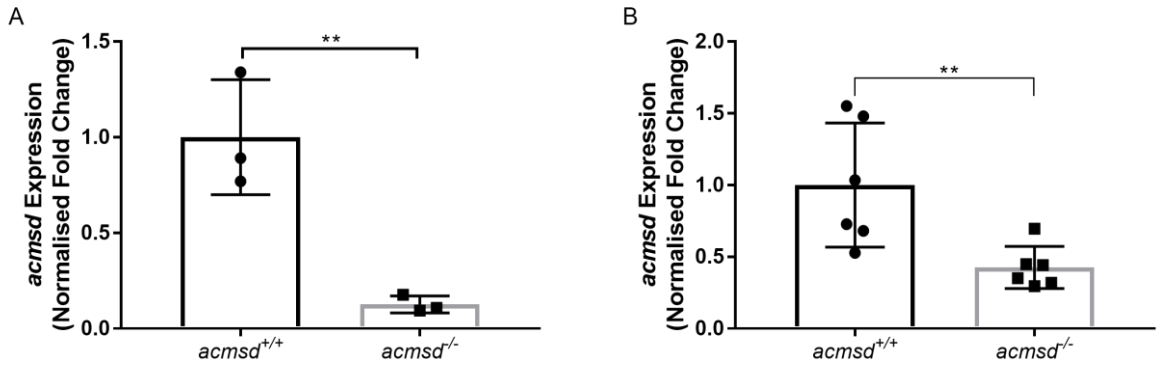

Figure 18. Quantitative Polymerase Chain Reaction of α-Amino-β-Carboxymuconate-ε-Semialdehyde Decarboxylase Transcript Levels Shows Nonsense-Mediated Decay of mRNA. A. *At 5dpf, acmsd$^{-/-}$ mutant zebrafish obtained from a heterozygous incross show significantly reduced expression of acmsd mRNA compared to their wildtype siblings (two-tailed t test using ddCt values, n=3 biological replicates (15 larvae per replicate), p=0.0012).* ***B.*** *Adult brain tissue obtained from* acmsd$^{-/-}$ *mutants shows significantly reduced mRNA expression compared to their wildtype siblings (two-tailed t test using ddCt values, n=6 biological replicates (1 brain per replicate), p=0.0040). rps29 was used as a reference gene in both datasets.* acmsd$^{-/-}$ *transcript levels are expressed as a percentage of averaged wildtype levels. All groups passed Shapiro-Wilk test for normality. acmsd, α-amino-β-carboxymuconate-ε-semialdehyde decarboxylase; dpf, days post fertilisation.*

4.2.1.3.2 In Situ Hybridisation

Both *acmsd* in situ hybridisation probes discussed in **section 4.2.2.2** were used to assess *acmsd* expression in 3dpf larvae obtained from an *acmsd* heterozygous incross. *acmsd* probe 1, although resulting in background staining, binds to *acmsd* outside of the predicted mutation site. This means that a reduction in staining using this probe would likely represent a reduction in RNA levels. a*cmsd* probe 2 binds across the predicted deletion site and therefore may not bind in mutants. A reduction in staining using this probe would likely represent an altered RNA sequence, but a reduction in total RNA levels could also be responsible.

A reduction in liver staining of *acmsd* homozygous mutants was seen using probe 1, although staining within the head remained the same across genotypes (**figure 19**). Liver staining also appeared reduced in heterozygous larve, although a complete absence in either genotype was difficult to conclude due to non-specifc staining in the surrounding areas. A complete loss of staining in *acmsd*$^{-/-}$ mutants was seen using probe 2 (**figure 20**). Heterozygous mutants displayed two phenotypes; most larvae appreared as wildtype, with obvious staining in the liver, but liver staining was absent in some larvae, making them indistinguishable from homozygous mutants (**figure 20**). This was never seen in wildtype larvae. Slight backgroud staining was apparent in some of the larvae during this experiment, unrelated to genotype. Methanol clearing was not attempted as this was unnoticed until imaging, at which point larvae were stored in glycerol.

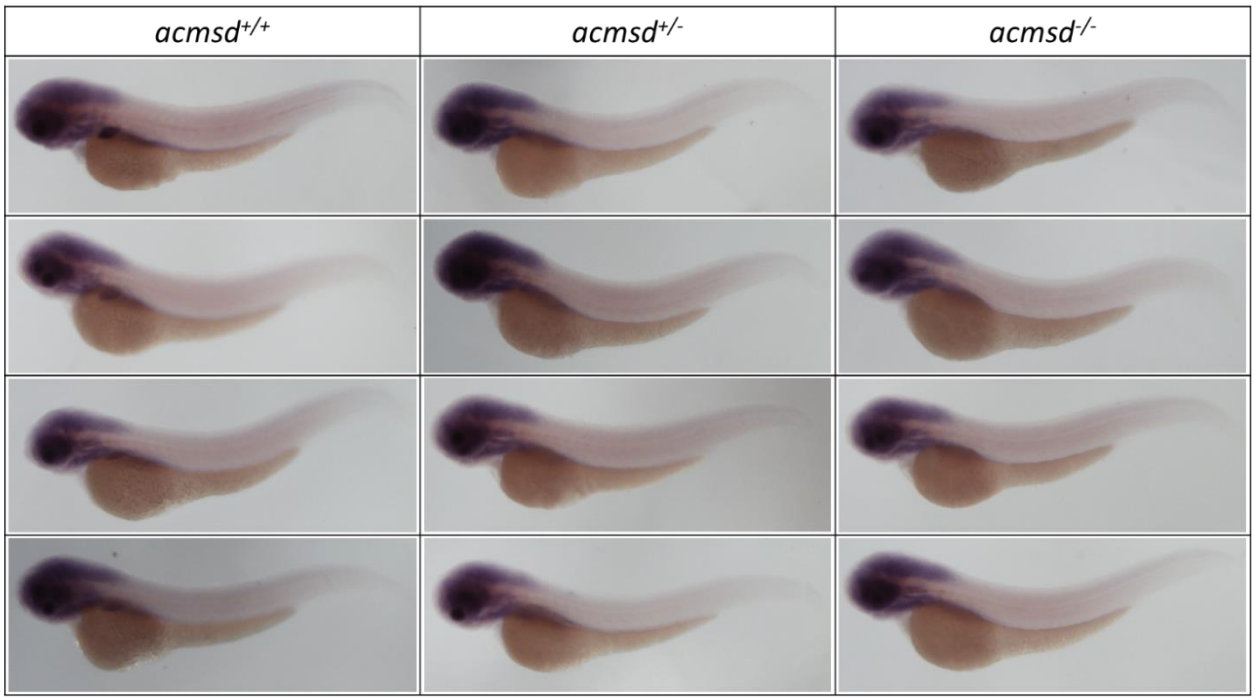

Figure 19. In Situ Hybridisation of α-Amino-β-Carboxymuconate-ε-Semialdehyde Decarboxylase Heterozygous Incross Larvae at 3-Days Post Fertilisation Using Probe 1 Demonstrates an Altered Staining Pattern Depending on Genotype. *Representative brightfield images of 3dpf larvae obtained from a single acmsd$^{+/-}$ incross following in situ hybridisation using acmsd probe 1. Staining is seen the head and liver of wildtype embryos (left) but liver staining is absent from acmsd heterozygous (middle) and homozygous (right) mutant larvae. Experiment carried out in a single Eppendorf tube, blinded to genotype. Larvae were genotyped following imaging. acmsd, α-amino-β-carboxymuconate-ε-semialdehyde decarboxylase; dpf, days post fertilisation.*

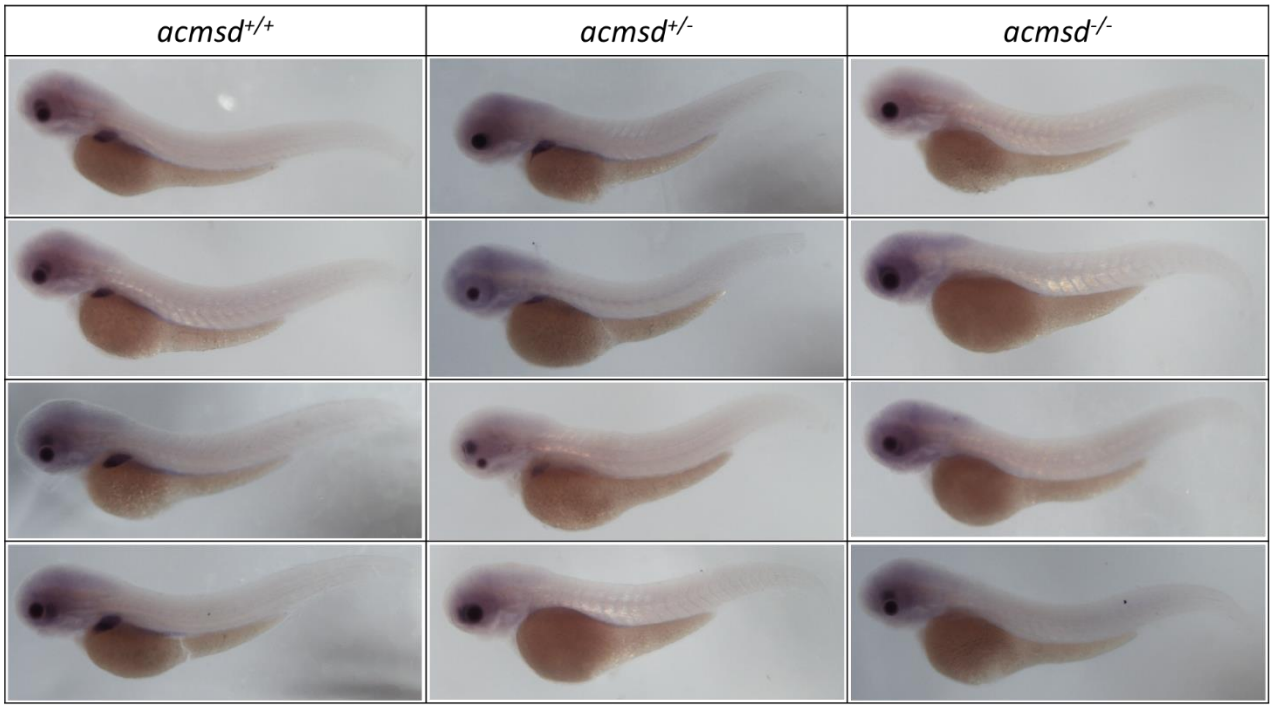

Figure 20. In Situ Hybridisation of α-Amino-β-Carboxymuconate-ε-Semialdehyde Decarboxylase Heterozygous Incross Larvae at 3-Days Post Fertilisation Using Probe 2 Demonstrates an Altered Staining Pattern Depending on Genotype. *Representative brightfield images of 3dpf larvae obtained from a single acmsd$^{+/-}$ incross following in situ hybridisation using acmsd probe 2. Staining is seen the liver of wildtype larvae (left) that is not seen in acmsd$^{-/-}$ larvae (right). acmsd$^{+/-}$ larvae show a mixed phenotype, with some fish showing liver staining (top middle) and some fish without liver staining (bottom middle). Experiment carried out in a single Eppendorf tube, blinded to genotype. Larvae were genotyped following imaging. acmsd, α-amino-β-carboxymuconate-ε-semialdehyde decarboxylase; dpf, days post fertilisation.*

4.2.2 Overall Morphological Phenotype

Despite *acmsd* being expressed throughout life in zebrafish and the successful generation of a loss-of-function mutation, adult homozygous *acmsd*$^{-/-}$ mutant zebrafish are viable and fertile. No obvious morphological differences in *acmsd*$^{-/-}$ zebrafish were identified at embryonic/larval stages (**figure 21**) or throughout adulthood.

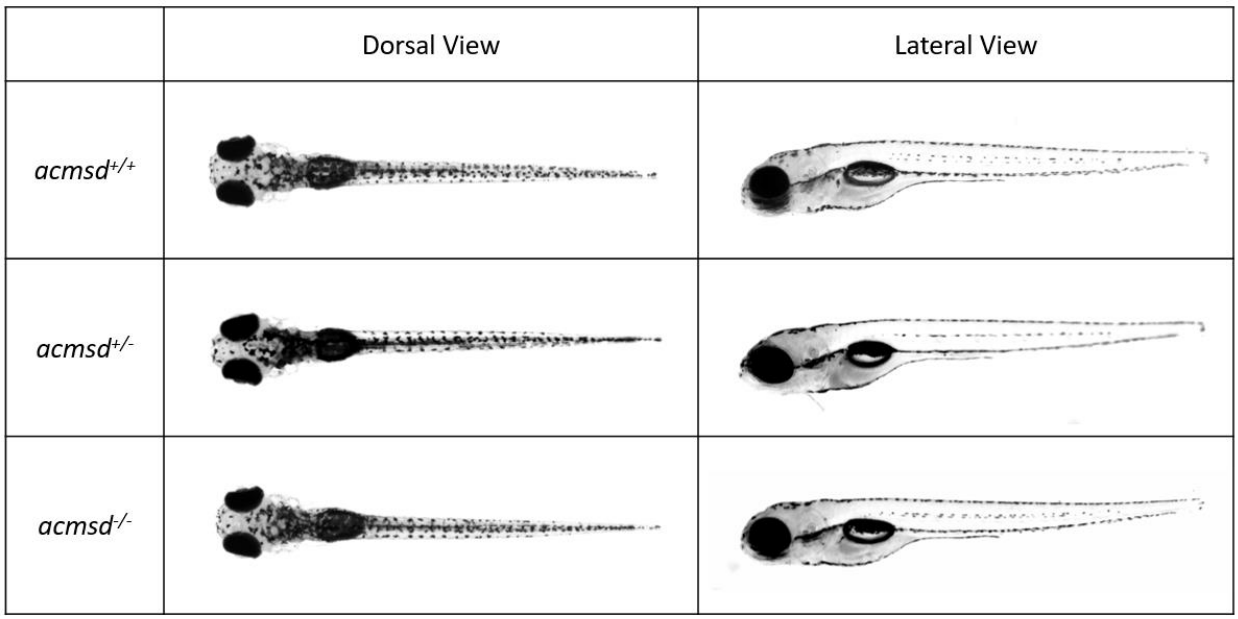

Figure 21. Comparing the Gross Morphology of α-Amino-β-Carboxymuconate-ε-Semialdehyde Decarboxylase Mutant Zebrafish Larvae. *Brightfield images of 5dpf zebrafish siblings showing normal gross morphology between genotypes. Larvae were anaesthetised using 4.2% tricaine for imaging and genotyped immediately after. acmsd, α-amino-β-carboxymuconate-ε-semialdehyde decarboxylase; dpf, days post fertilisation.*

4.2.3 Movement Analysis

4.2.3.1 Larval (5dpf) Movement Analysis

Movement analysis at 5dpf found no difference in swimming behaviour between *acmsd*$^{-/-}$ zebrafish and their heterozygous or wildtype siblings (**figure 22**). Movement was recorded over a 1-hour time period; following an unrecorded habituation period, larvae were maintained in light conditions for 30 minutes prior to alternating 5-minute dark-light cycles for 30 minutes. Analysis of distance travelled over time suggested there may be differences in the swimming behaviour of *acmsd*$^{-/-}$ homozygous mutants during the initial 30-minute light period as well as during dark phases (**figure 22A**). Therefore, the total distance travelled in each of these phases separately was quantified, finding no significant differences between genotypes during the initial 30-minute light period, the combined light phases, the combined dark phases or over the entire 1-hour recording period ($p>0.05$ for each phase, **figure 22B-E**).

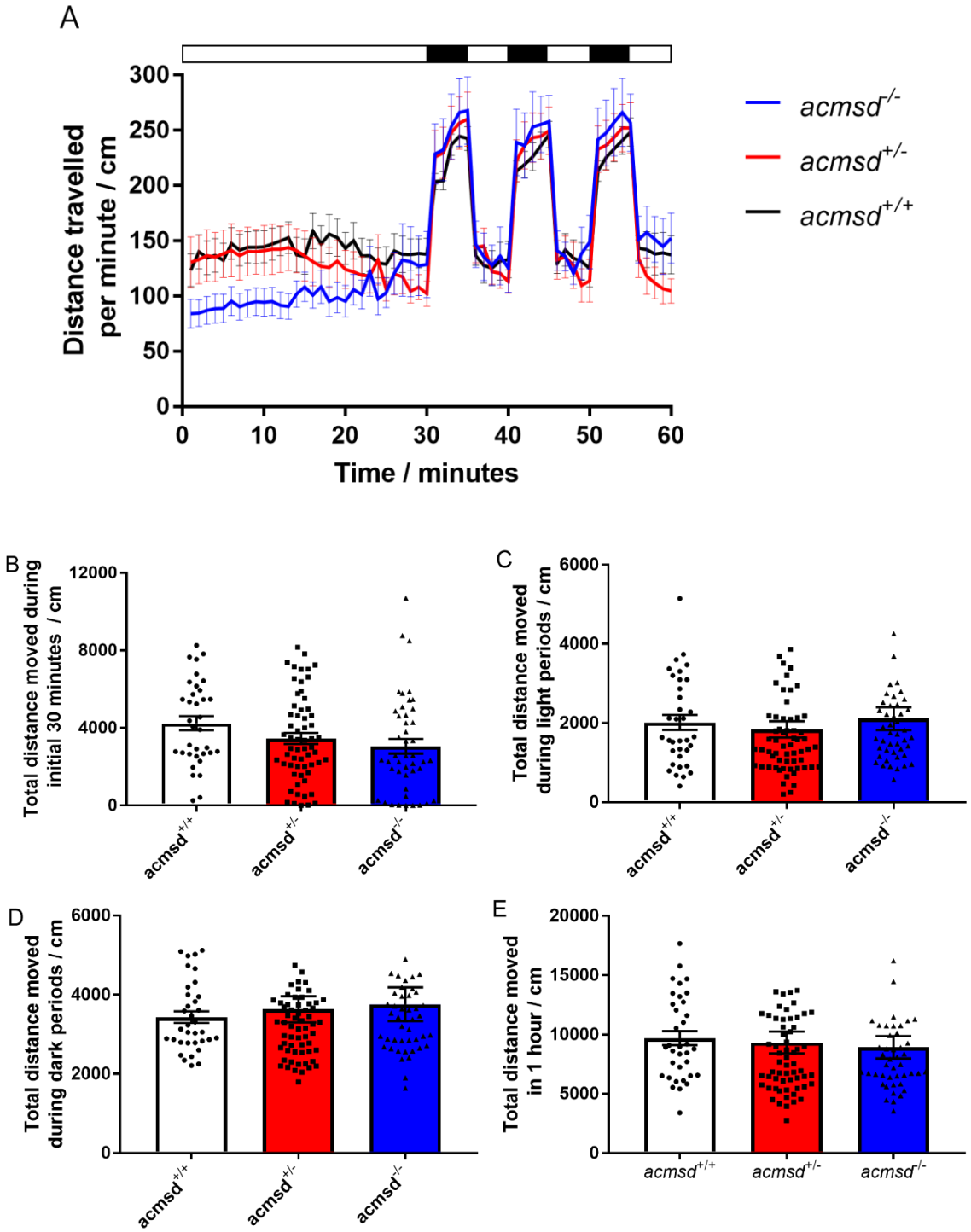

Figure 22. α-Amino-β-Carboxymuconate-ε-Semialdehyde Decarboxylase Mutant Zebrafish Demonstrate Normal Swimming Behaviour at 5-Days Post Fertilisation. *Larval zebrafish movement was recorded over a 1-hour time period at 5dpf. Following habituation, larvae were maintained in light conditions for 30 minutes prior to alternating 5-minute dark-light cycles for 30 minutes.* ***A.*** *Distance over time analysis between* acmsd$^{-/-}$, acmsd$^{+/-}$ *and their wildtype siblings. Horizontal white bar represents time zebrafish were in light conditions, black bar represents time in dark conditions.* ***B-E.*** *Comparing the distance travelled in each phase of the experiment found no differences between genotypes during (**B**) the initial 30-minute light period (one-way ANOVA, p=0.2160), (**C**) during the combined light phases (one-way ANOVA, p=0.6810), (**D**) during the combined dark phases (one-way ANOVA, p=0.0745) or (**E**) over the entire 1-hour recording period (one-way ANOVA, p=0.8594). Note different axis scales between graphs. n=45* acmsd$^{-/-}$*; 62* acmsd$^{+/-}$*; 35* acmsd$^{+/+}$ *from 3 biological replicates. acmsd, α-amino-β-carboxymuconate-ε-semialdehyde decarboxylase; cm, centimetre; dpf, days post fertilisation.*

4.2.3.2 Adult Movement Analysis

Movement was also assessed in adult (9mpf) zebrafish by recording the distance travelled by individually housed fish over 7 hours (**figure 23**). The first hour was used as a habituation period and therefore not used for further analysis. No significant difference was found in the distance travelled between *acmsd*$^{-/-}$ mutant zebrafish and their wildtype siblings over the 6-hour experimental time period (**figure 23**, p=0.1796).

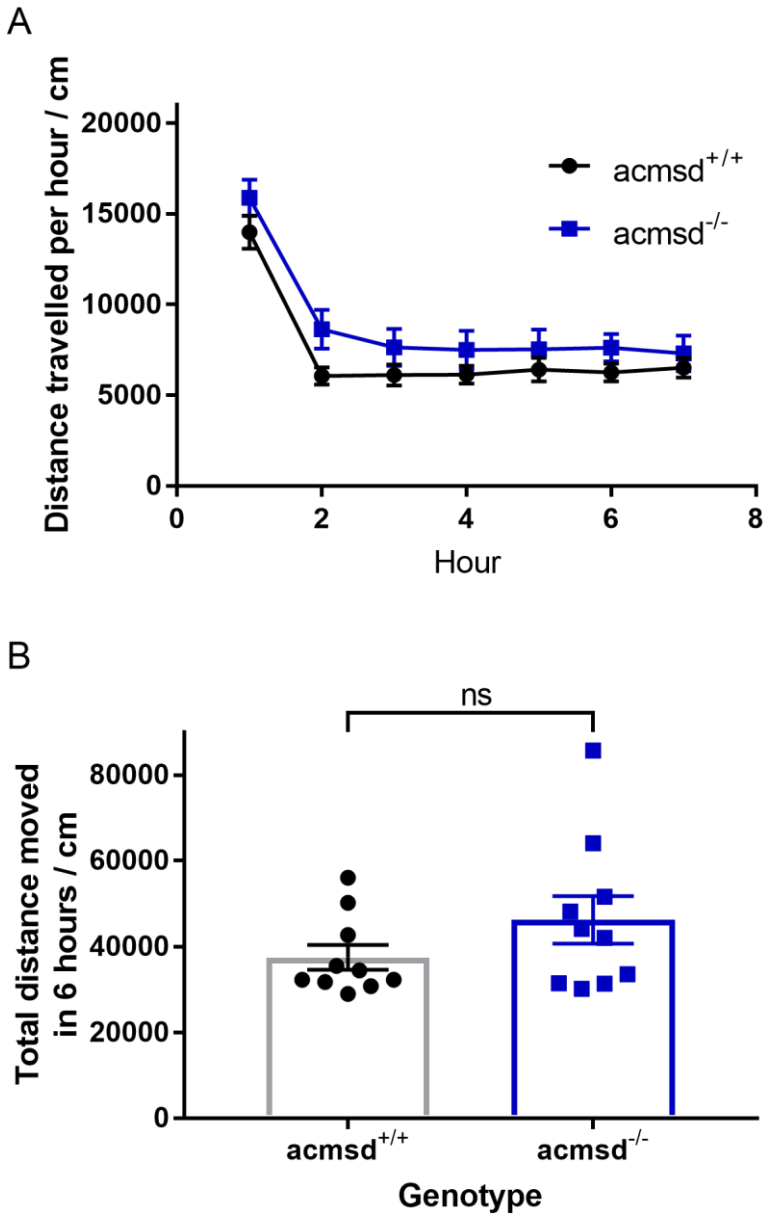

Figure 23. α-Amino-β-Carboxymuconate-ε-Semialdehyde Decarboxylase Mutant Zebrafish Demonstrate Normal Swimming Behaviour at 9-Months Post Fertilisation. *Adult zebrafish movement was recorded over a 7-hour time period at 9mpf. Zebrafish were maintained in light conditions for 7 hours, with the first hour counted as a habituation period.* ***A.*** *Distance travelled over time by* acmsd$^{-/-}$ *mutant zebrafish and their wildtype siblings. Data points represent mean±SEM values per genotype.* ***B.*** *Comparing the total distance travelled in hours 2-7 (removing the first hour for habituation) found no differences between genotypes (unpaired two-tailed t test, p=0.1796). Data points in this graph represent individual fish. n=10* acmsd$^{-/-}$*; 10* acmsd$^{+/+}$ *(equal male/female ratios between groups) taken at 2 different time points. acmsd, α-amino-β-carboxymuconate-ε-semialdehyde decarboxylase; cm, centimetre; mpf, months post fertilisation.*

4.2.1 Dopaminergic Neuron Quantification

4.2.1.1 th1+ Cell Counts

Tyrosine hydroxylase *(th1)* was used as a marker of dopaminergic neurons in 3dpf larval zebrafish. In situ hybridisation enabled the visualisation of *th1+* neurons in the ventral diencephalon (**figure 24**). Following in situ hybridisation against *th1*, decapitated heads from *acmsd*$^{+/-}$ incross larvae were mounted in glycerol and dopaminergic neuronal cell bodies were counted. The tails were used for genotyping. No significant difference in the number of *th1*+ cells in neuronal populations DC2 and DC4/5 was found between *acmsd*$^{-/-}$ mutant zebrafish and their wildtype siblings (p=0.9866, **figure 24**).

4.2.1.2 Methyl-4-phenylpyridinium (MPP+) Toxin Exposure

MPP+ produces a reduction in the number of *th1*+ cells in zebrafish and other animal models (Lam et al., 2005). Here, exposure to 3mM MPP+ from 1-3dpf resulted in significant reductions of *th1*+ cells in both wildtype (43.11% reduction) and *acmsd*$^{-/-}$ mutant zebrafish (43.43% reduction) (p<0.0001, **figure 24**). There was no significant difference between genotypes in the number of *th1*+ cells following exposure (p=0.9999, **figure 24**), suggesting that the effect of MPP+ on *th1+* cells was unaffected by genotype.

4.2.1.3 th1+ Cells in acmsd Homozygous Incross Larvae

The above experiment was repeated using three biological replicates of *acmsd*$^{-/-}$ mutant larvae obtained from *acmsd*$^{-/-}$ parents. For wildtype controls, larvae were obtained from wildtype siblings of the *acmsd*$^{-/-}$ parents, making experimental larvae cousins. The data remain the same as for heterozygous incross larvae (**figure 25**). No differences were seen the number of *th1+* cells between wildtype and *acmsd*$^{-/-}$ larvae (p=0.1638). Both genotypes were equally susceptible to the effects of MPP+, which significantly reduced the number of *th1+* cells by 38.28% in wildtype (p<0.0001) and 28.81% in *acmsd*$^{-/-}$ larvae (p<0.0001) following a 3-day exposure. No significant difference was identified in the number of *th1*+ cells following MPP+ exposure (p=0.2920).

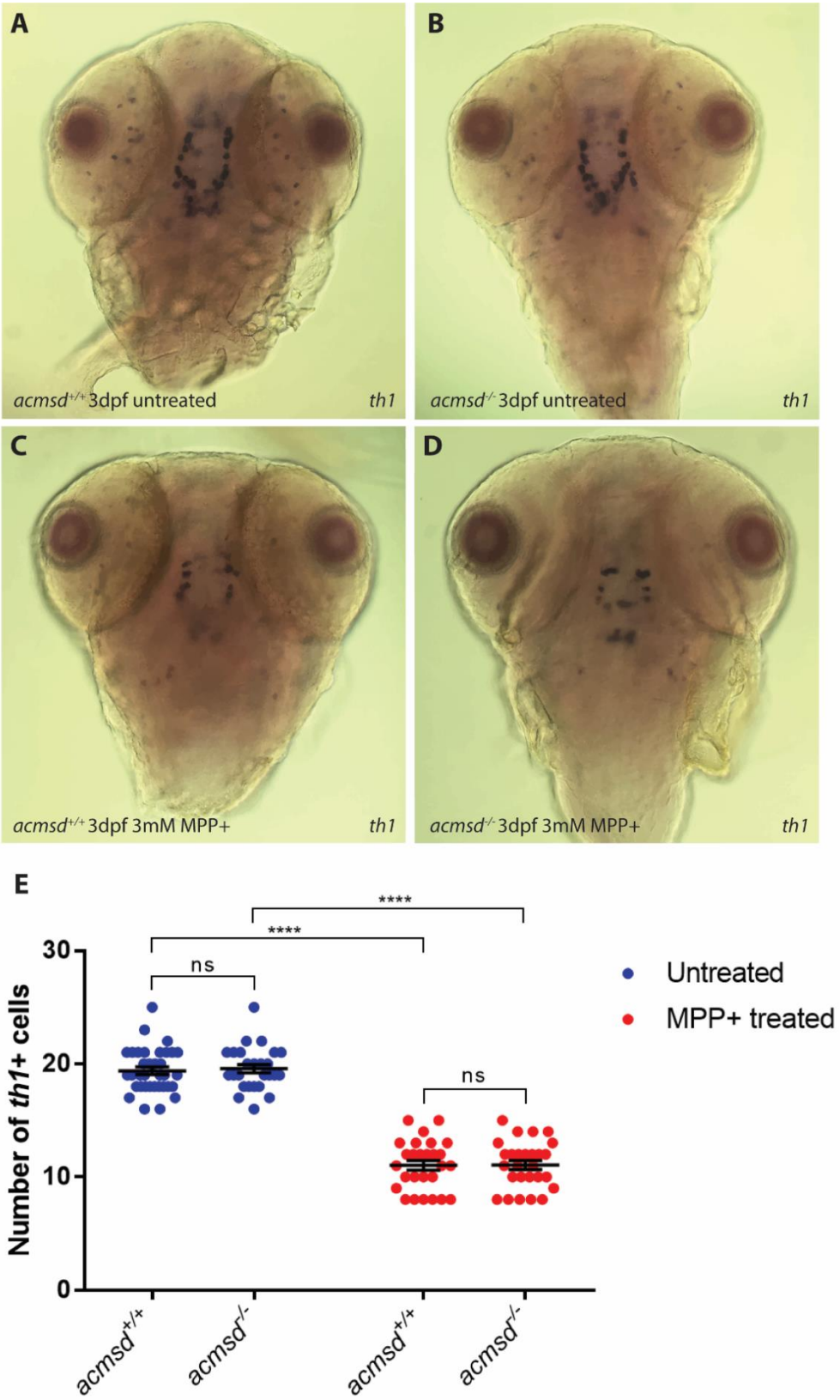

Figure 24. α-Amino-β-Carboxymuconate-ε-Semialdehyde Decarboxylase Mutant Zebrafish Retain Normal Dopaminergic Neuron Numbers and Susceptibility to MPP+. *In situ hybridisation against tyrosine hydroxylase (th1) shows no change in staining pattern between wildtype* ***(A)*** *and acmsd$^{-/-}$ mutant* ***(B)*** *zebrafish. MPP+ exposure resulted in clear reductions in th1+ cells in both wildtype* ***(C)*** *and acmsd$^{-/-}$ mutant* ***(D)*** *zebrafish* ***E.*** *th1+ neuron numbers in the ventral diencephalon show no difference between wildtype and* acmsd$^{-/-}$ *mutant zebrafish (p=0.9866). MPP+ exposure resulted in significant reductions in th1+ cells irrespective of genotype (43.11% in* acmsd$^{+/+}$*, p<0.0001; 43.43% in* acmsd$^{-/-}$*, p<0.0001). Total cell counts between groups following MPP+ exposure remained indistinguishable (p=0.9999). Data represented as mean±SEM. n=26-35 per group, from 3 biological replicates. Statistics from a two-way ANOVA with Tukey's multiple comparisons post-hoc test. All groups passed Shapiro-Wilk test for normality. acmsd, α-amino-β-carboxymuconate-ε-semialdehyde decarboxylase; dpf, days post fertilisation; mM, millimolar; MPP+, 1-methyl-4-phenylpyridinium; th1, tyrosine hydroxylase 1.*

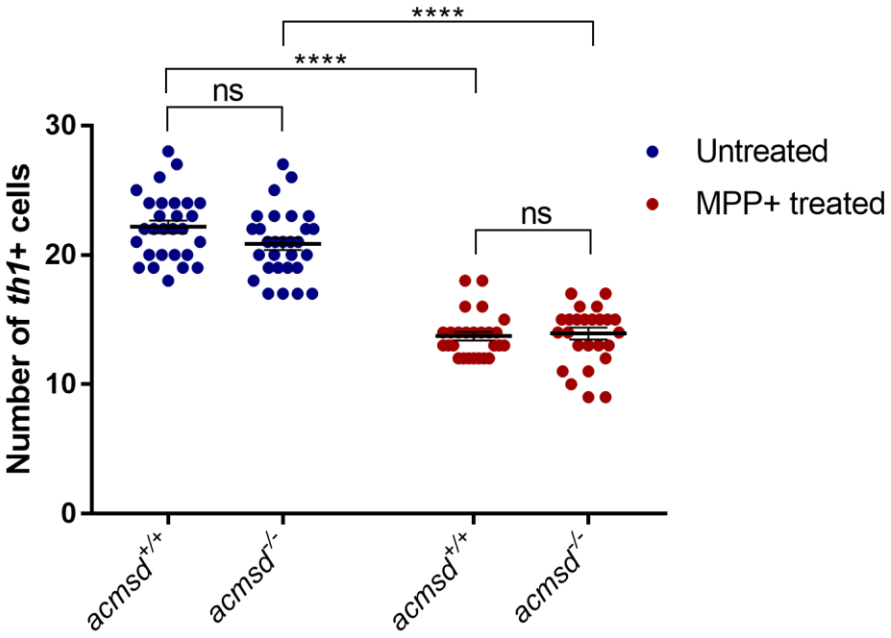

Figure 25. α-Amino-β-Carboxymuconate-ε-Semialdehyde Decarboxylase Mutant Larvae from Homozygous Parents Retain Normal Dopaminergic Neuron Numbers and Susceptibility to MPP+. *In situ hybridisation against tyrosine hydroxylase (th1) shows no change in staining pattern between wildtype and* acmsd$^{-/-}$ *mutant zebrafish. th1+ neuron numbers in the ventral diencephalon show no difference between wildtype and acmsd$^{-/-}$ mutant zebrafish (p=0.1638). MPP+ exposure resulted in significant reductions in th1+ cells irrespective of genotype (38.28% in* acmsd$^{+/+}$*, p<0.0001; 28.81% in* acmsd$^{-/-}$*, p<0.0001). Total cell counts between groups following MPP+ exposure remained indistinguishable (p=0.2920). Data represented as mean±SEM. n=26-29 per group, from 3 biological replicates. Statistics from a two-way ANOVA with Tukey's multiple comparisons post-hoc test. All groups passed Shapiro-Wilk test for normality. acmsd, α-amino-β-carboxymuconate-ε-semialdehyde decarboxylase; dpf, days post fertilisation; mM, millimolar; MPP+, 1-methyl-4-phenylpyridinium; th1, tyrosine hydroxylase 1.*

4.2.1.4 Using the ETvmat2:GFP Zebrafish Line

To assess dopaminergic neurons in 5dpf larvae, *acmsd*$^{-/-}$ mutant zebrafish were crossed with wildtype zebrafish carrying the *ETvmat2:GFP* transgene. This transgene results in the expression of green fluorescence wherever the vesicular monoamine transporter 2 (*vmat2*) gene is expressed, therefore enabling visualisation of monoaminergic neurons in the zebrafish brain. The resulting adults were heterozygous for the *acmsd* mutation and carried one copy of the *vmat2* transgene. An incross of these, whilst enabling the study of siblings, would result in larvae that carry one, two or no copies of the *vmat2* transgene; screening out those with no copy would be simple but distinguishing between one or two copies would be more difficult, adding a possible extraneous variable to this experiment. Therefore *acmsd*$^{+/-}$;*ETvmat2:GFP* adults were crossed to either *acmsd*$^{-/-}$ or *acmsd*$^{+/+}$ (siblings) adults. Larvae were selected for fluorescence at 24hpf and finclipped for genotyping at 3dpf. For imaging, larvae were anaesthetised in tricaine, mounted in imaging dishes with low melting point agarose and imaged using a 10X objective lens on the AiryScan confocal microscope [Zeiss]. This experiment was conducted on three biological replicates, with three fish per genotype per replicate.

No obvious difference in monoaminergic groups was seen in the brain of 5dpf *acmsd*$^{-/-}$ mutant larvae compared to that of wildtypes (**figure 26**). To view the DC groups, more ventral images were needed as these are located deeper than the nuclear groups visualised in the full brain. Using the caudal hypothalamus as a marker, zoomed in z-stacks ventral to the raphe nuclei were obtained. This enabled the visualisation of DC2 and DC4/5 (**figure 26**). Using z-stack images, neuronal cell bodies were counted, finding no difference in the number of dopaminergic neurons between wildtype and *acmsd*$^{-/-}$ mutant zebrafish at 5dpf (**figure 26E,** p=0.8126).

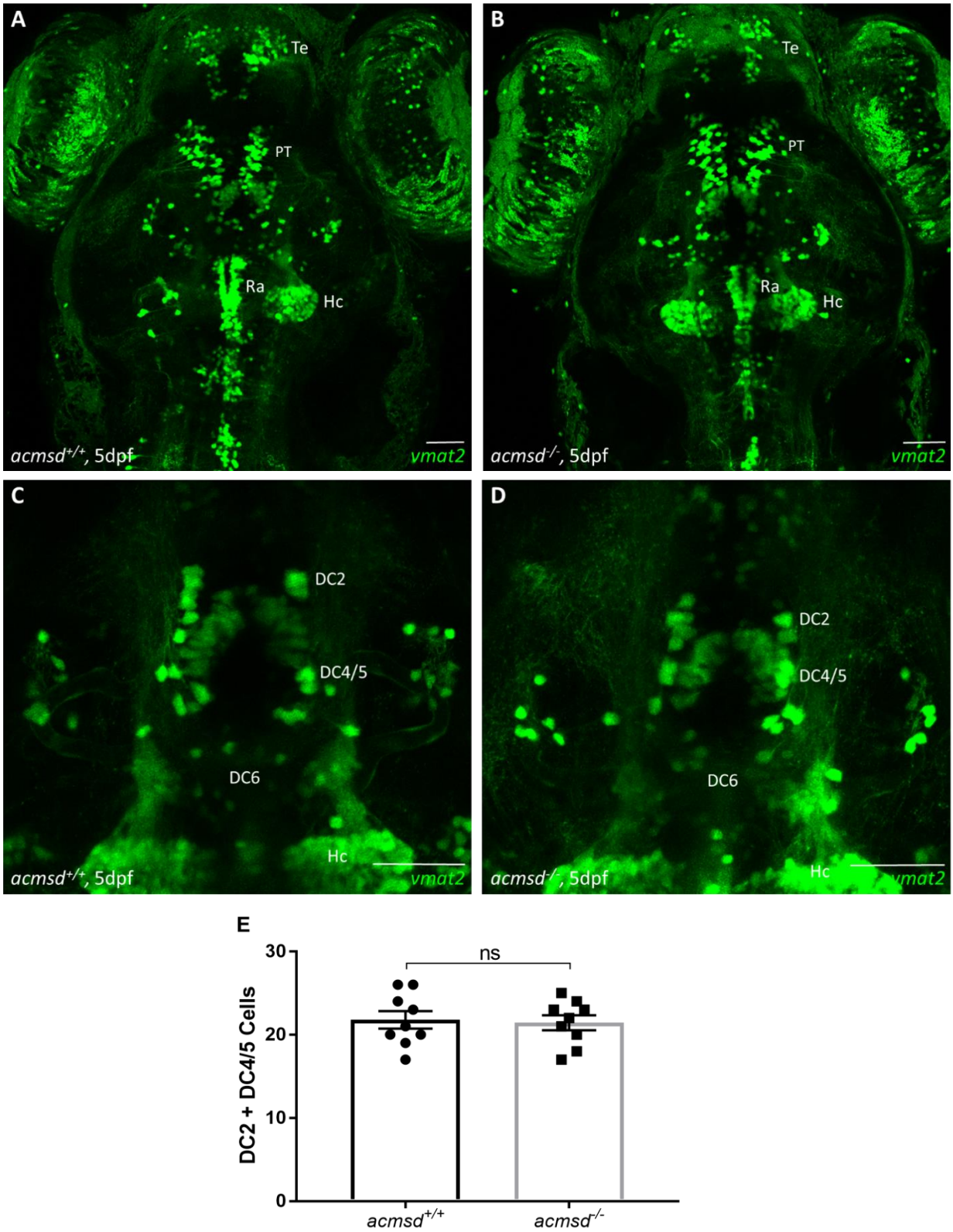

Figure 26. Monoaminergic Neurons in α-Amino-β-Carboxymuconate-ε-Semialdehyde Decarboxylase Mutant Larvae Visualised using the ETvmat2:GFP Transgenic Line. *Full dorsal head view of wildtype (**A**) and acmsd$^{-/-}$ mutant (**B**) zebrafish at 5dpf with labelled brain regions. Zoomed in images of DC neuronal groups in the ventral diencephalon of wildtype (**C**) and acmsd$^{-/-}$ mutant (**D**) zebrafish. All images were taken on anaesthetised larvae mounted in low melting point agarose using a 10X objective lens on the Zeiss AiryScan confocal microscope. Scale bar represents 50µm in all images. **D.** Neuronal cell bodies in DC2 and DC4/5 were counted from z-stack images. No difference in cell number was identified between wildtype and acmsd$^{-/-}$ mutant zebrafish (p=0.8126). Data represented as mean±SEM. n=9 larvae per group, from 3 biological replicates. Statistical analysis from an unpaired two-tailed t test following Shapiro-Wilk test for normality. acmsd, α-amino-β-carboxymuconate-ε-semialdehyde decarboxylase; DC, diencephalic neurons; dpf, days post fertilisation; Hc, caudal hypothalamus; PT, pretectal neural cluster; Ra, raphe nucleus; Te, telencephalic neurons; vmat2, vesicular monoamine transporter 2.*

4.2.2 Inflammation in acmsd$^{-/-}$ Mutant Zebrafish Larvae

4.2.2.1 Global Inflammation

Inflammation was assessed in whole zebrafish larvae to determine whether *acmsd*$^{-/-}$ mutant larvae possess increased inflammation under basal conditions. This was done using two methods; qPCR and fluorescent reporter lines.

4.2.2.1.1 Quantitative PCR

qPCR primers designed against three inflammatory markers were initially tested on wildtype cDNA using a gradient PCR to assess specificity. All annealing temperatures tested produced single bands following PCR (**figure 27A**). 60°C was selected for qPCR experiments. Primers were optimised as described for *acmsd* primers in **section 4.2.1.3.1.1** (data not shown), finding primer concentrations of 500nM optimal for all three primer pairs. qPCR was then conducted on three biological replicates of *acmsd*$^{+/-}$ incross larvae, finding no difference in the expression of *cxcl8* (p=0.9044), *il-1ϐ* (p=0.4583) or *mmp9* (p=0.3905) between *acmsd*$^{-/-}$ mutants and their wildtype siblings (**figure 27B-D**).

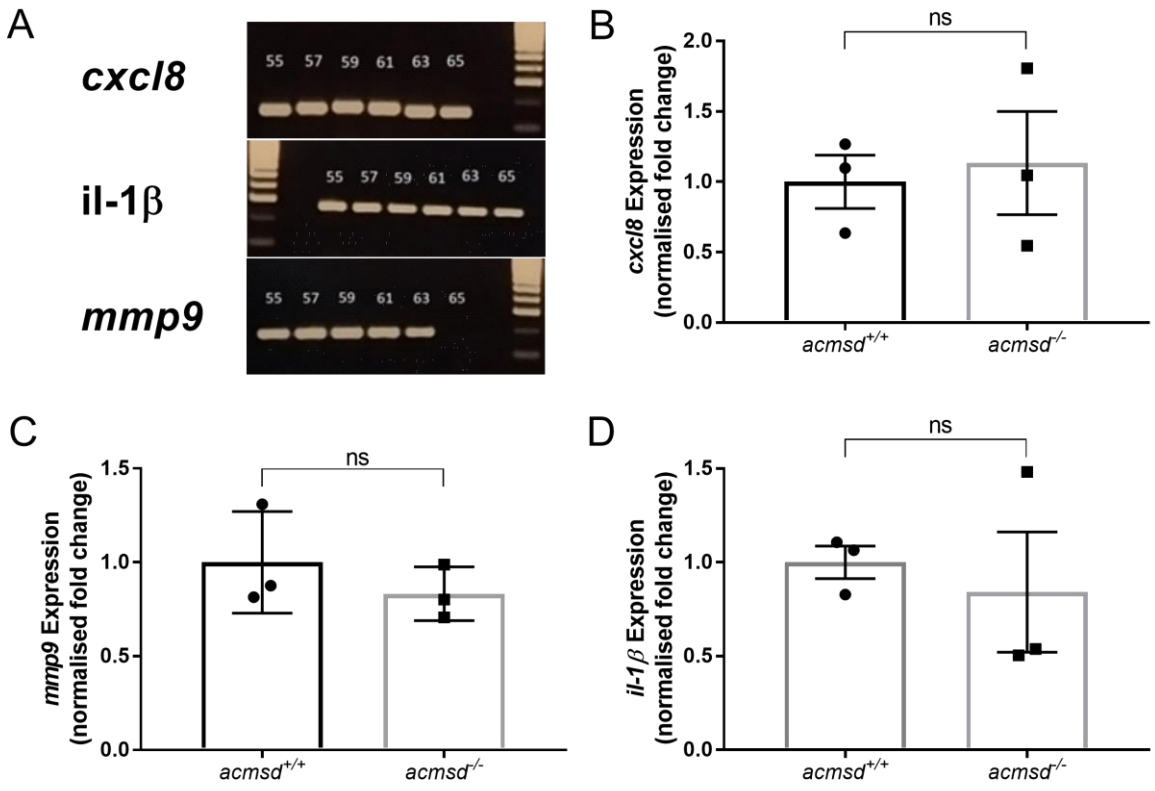

Figure 27. Quantitative Polymerase Chain Reaction for Markers of Inflammation Found No Evidence of an Altered Inflammatory State in α-Amino-ϐ-Carboxymuconate-ε-Semialdehyde Decarboxylase Mutant Larvae. A. *Gradient PCR test using wildtype cDNA as a template, showing single bands for all 3 genes. Numbers represent annealing temperatures used. 100bp ladder.* ***B-D.*** *No significant differences were identified between acmsd$^{-/-}$ homozygous mutant larvae and their wildtype siblings in the expression levels of cxcl8 (**B**, p=0.9044), mmp9 (**C**, p=0.3905) or il-1ϐ (**D**, p=0.4583) at 5dpf. n=3 biological replicates (15 larvae per replicate). Larvae were obtained from a heterozygous incross and genotyped by tailfin clip assay at 3dpf. ddCt values were used for statistical analysis using an unpaired t test but fold change values are shown on graphs. All groups passed Shapiro-Wilk test for normality. acmsd, α-amino-ϐ-carboxymuconate-ε-semialdehyde decarboxylase; cxcl8, c-x-c motif chemokine ligand 8; il-1ϐ, interleukin-1 beta; mmp9, matrix metalloproteinase 9.*

4.2.2.1.2 Fluorescently Labelled Reporter Lines

4.2.2.1.2.1 Visualising Neutrophils

acmsd$^{-/-}$ homozygous mutant adult zebrafish were crossed with the transgenic reported line, tg(*mpx*:GFP)i114, which enables the visualisation of neutrophils (Elks et al., 2011). Following selection and raising of offspring, acmsd$^{+/-}$;tg(*mpx*:GFP)i114 adults were incrossed and larvae imaged using a fluorescent microscope at 5dpf. Fish were genotyped following imaging. Although no quantification of these images was performed, there was no visually obvious difference in neutrophil number or location in *acmsd*$^{-/-}$ mutant zebrafish compared to their wildtype siblings (**figure 28**).

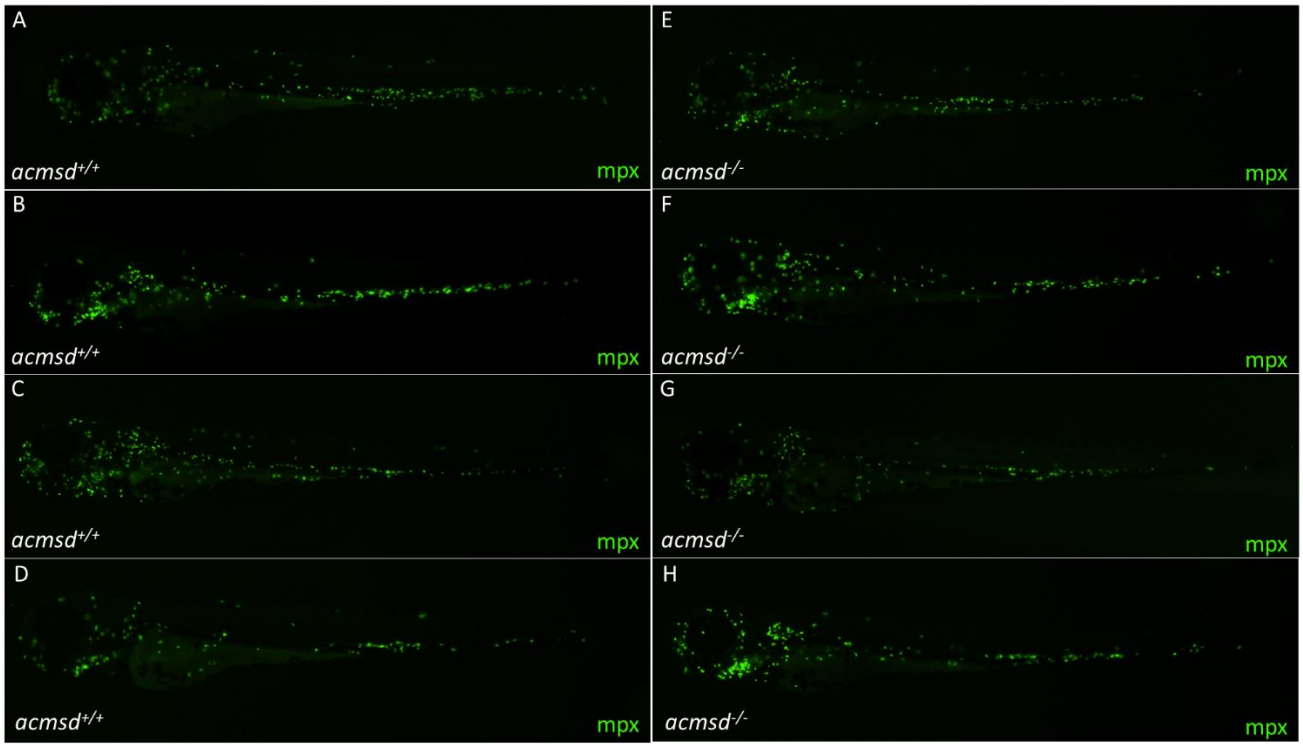

Figure 28. Neutrophil Number and Location Appear Grossly Normal in α-Amino-β-Carboxymuconate-ε-Semialdehyde Decarboxylase Mutant Larvae*. The transgenic line, tg(mpx:GFP)i114, was crossed into the acmsd background to enable visualisation of neutrophils within acmsd*$^{-/-}$ *mutant larvae (**E-H**) and their wildtype siblings (**A-D**) at 5dpf. acmsd, α-amino-β-carboxymuconate-ε-semialdehyde decarboxylase; dpf, days post fertilisation; mpx, myeloid-specific peroxidase.*

4.2.2.1.2.2 Tumour Necrosis Factor Alpha

acmsd$^{-/-}$ homozygous mutant adult zebrafish were crossed with the transgenic reported line, tgBAC(*tnfa*:GFP), a fluorescently labelled *tnf-α* line (Lewis & Elks, 2019). Following selection and raising, adult acmsd$^{+/-}$;tgBAC(*tnfa*:GFP) zebrafish were incrossed and larvae imaged using a fluorescent microscope. Fish were genotyped following imaging of the tailfin injury assay. *tnf-α* expression was seen in the yolk sac extension and hindbrain area, with no difference in expression pattern identified between *acmsd*$^{-/-}$ mutant larvae and their wildtype siblings (**figure 29**). 16 hours post tailfin injury, *tnf-α* expression was increased at the wound site (**figure 29**).

There was no obvious difference in expression following injury between *acmsd*$^{-/-}$ mutant larvae and their wildtype siblings, however this was not quantified due to low image quality.

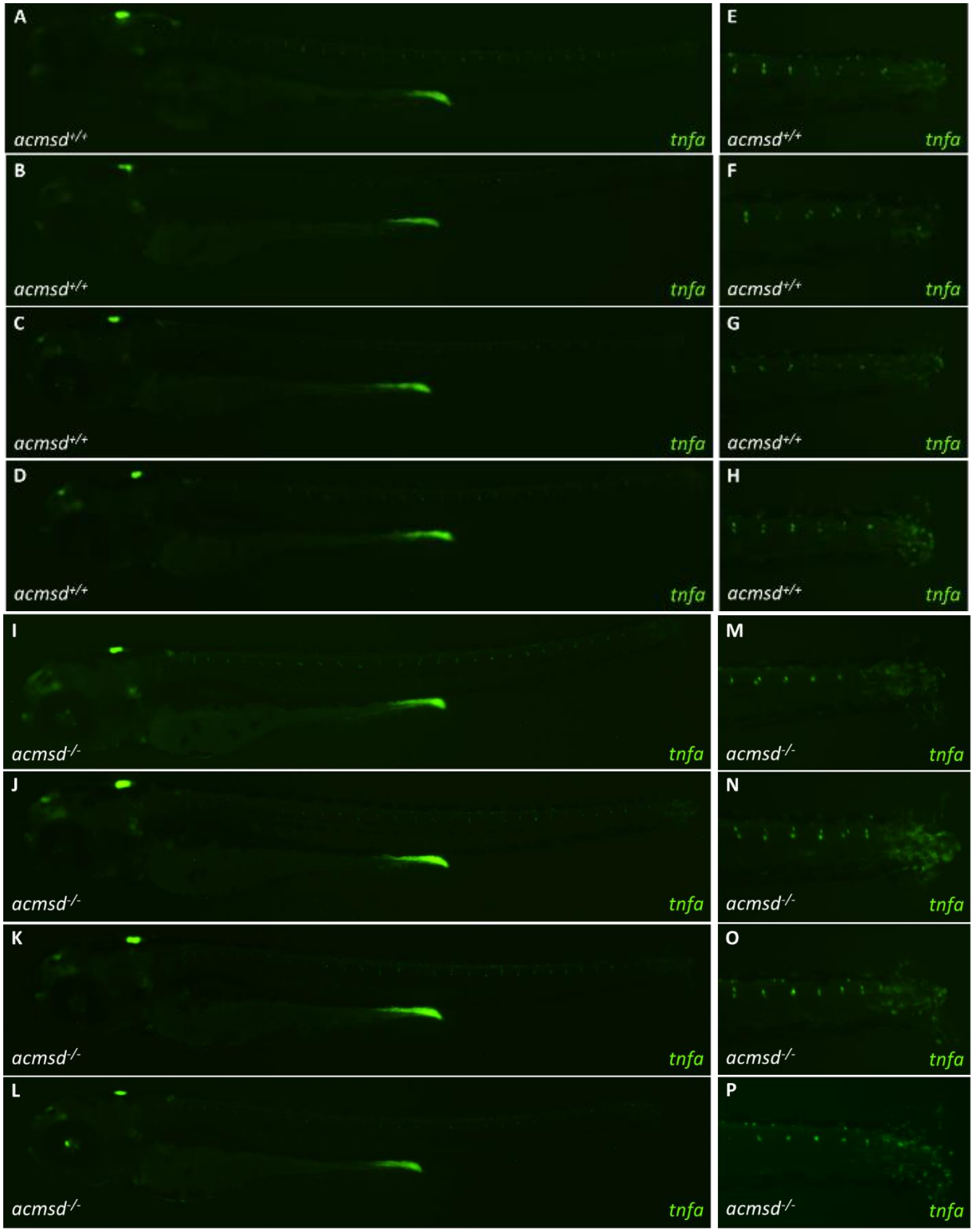

Figure 29. α-Amino-β-Carboxymuconate-ε-Semialdehyde Decarboxylase Mutant Larvae Demonstrate the Same Expression Pattern of Tumour Necrosis Factor Alpha as Their Wildtype Siblings. *The transgenic line, tgBAC(tnfa:GFP), was crossed into the acmsd background to enable visualisation of tnf-α within acmsd*$^{-/-}$ *mutant larvae (**I-P**) and their wildtype siblings (**A-H**). **A-D** and **I-L** shows fluorescence from whole larvae at 4dpf. **E-H** and **M-P** show expression in the tail 16-hours post tailfin injury. acmsd, α-amino-β-carboxymuconate-ε-semialdehyde decarboxylase; dpf, days post fertilisation; tnfa, tumour necrosis factor alpha.*

4.2.2.2 Microglial Analysis

To assess possible microglial changes in *acmsd*$^{-/-}$ mutant zebrafish, three approaches were used; L-plastin immunostaining on 5dpf midbrain sections, neutral red microglial stain on live 4dpf larvae and 4c4 wholemount immunohistochemistry on 5dpf fixed whole larvae.

4.2.2.2.1 L-plastin

Initially microglia were assessed using L-plastin immunostaining on 14µm sections of larval (5dpf) brain tissue. Staining patterns suggested a possible increase in the number of microglia in *acmsd*$^{-/-}$ zebrafish (**figure 30H,K**) compared to their wildtype siblings (**figure 30B,E**). Tyrosine hydroxylase was used as a positive control and to identify regions of the brain from sections. Quantification of staining was not carried out as sections were not from comparable brain regions and so further assessment would have been invalid.

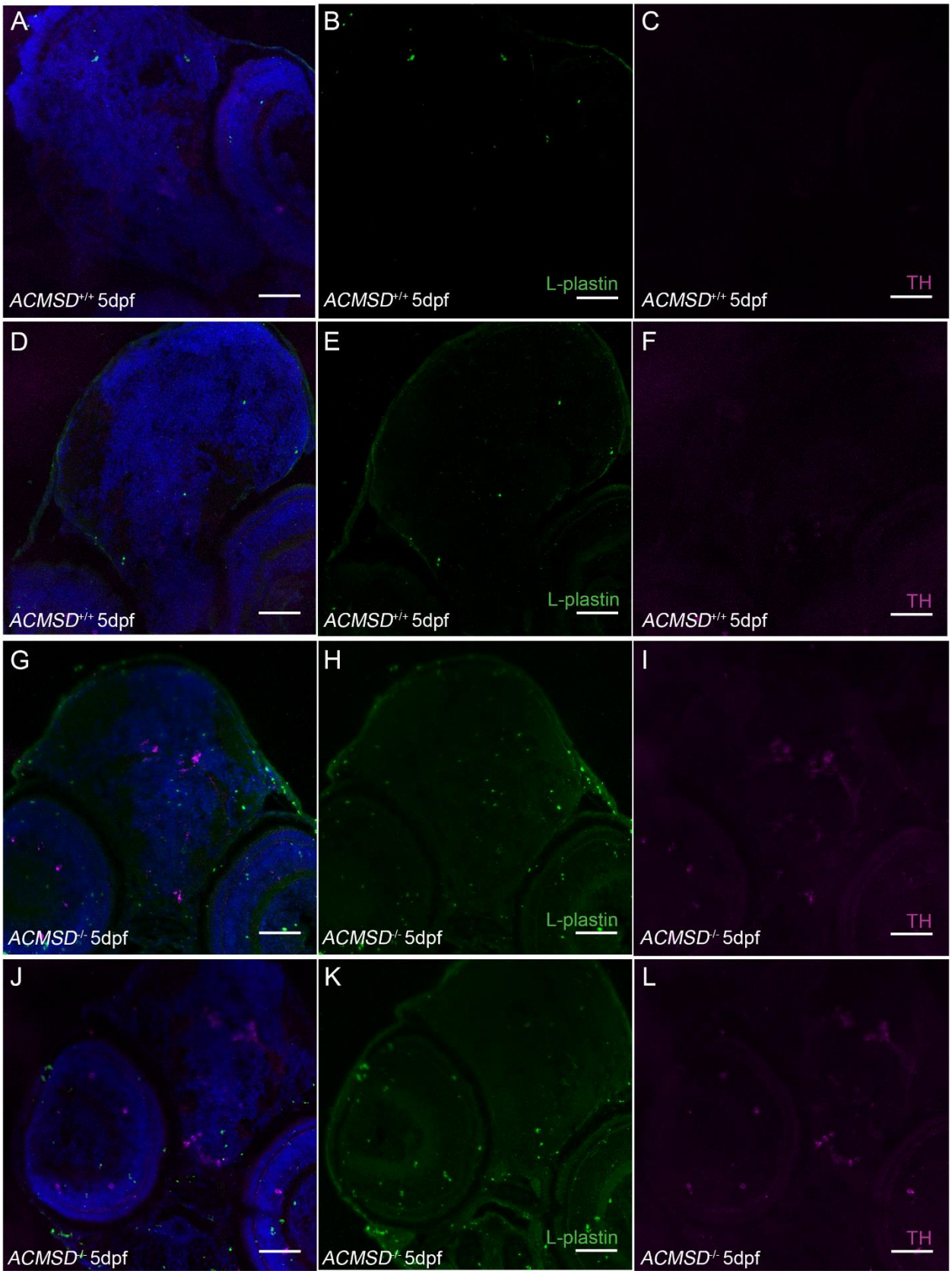

Figure 30. L-plastin Expression in 5-Days Post Fertilisation α-Amino-β-Carboxymuconate-ε-Semialdehyde Decarboxylase Homozygous Mutant Zebrafish and Their Wildtype Siblings. *Representative immunohistochemistry staining of L-plastin (green, **B,E,H,K**) in 14µm cryosections of 5dpf acmsd$^{-/-}$ homozygous mutant zebrafish brain (**G-L**) compared to their wildtype (acmsd$^{+/+}$) siblings (**A-F**). Co-stained with tyrosine hydroxylase (magenta, **C,F,I,L**) and DAPI (blue, **A,D,G,J**). Scale bar = 50µm. ACMSD, α-amino-β-carboxymuconate-ε-semialdehyde decarboxylase; DAPI, 4',6-diamidino-2-phenylindole; dpf, days post fertilisation; TH, tyrosine hydroxylase.*

4.2.2.2.2 Neutral Red Staining

To obtain a more valid representation of microglial number in *acmsd*$^{-/-}$ mutant zebrafish, neutral red staining was used to visualise microglia in the entire brain of living 4dpf larvae (**figure 31**). Following incubation in neutral red stain for 6 hours, larvae were anaesthetised using 4.2% tricaine and mounted in agarose for brightfield imaging. Larvae were genotyped after imaging. In contrast to single sections, imaging the entire brain allowed for quantification of microglial number by counting the neutral red stained dots directly from brightfield images using ImageJ software. The average number of microglia in homozygous *acmsd*$^{-/-}$ mutants was 40.2, an increase of 11.8 compared to their wildtype siblings (**figure 31G**). There also appeared to be a gene-dosage effect, with heterozygous *acmsd* mutants having an average of 38 neutral red-positive cells. However, statistical analysis was not conducted due to a single biological replicate, low sample number and high variability within genotypes.

4.2.2.2.3 4c4 Wholemount Immunohistochemistry

Due to the high variability in neutral red staining between larvae, another method of analysing microglial number across the entire brain was utilised; 4c4 wholemount immunohistochemistry. This enabled a more reliable readout of microglial number as well as a comparison of microglial activation in the brains of *acmsd*$^{-/-}$ zebrafish larvae compared to their wildtype siblings.

4.2.2.2.3.1 Microglia Number

Immunohistochemistry against 4c4 was conducted on 5dpf zebrafish larvae. Decapitated heads were mounted in agarose whilst tails were used for genotyping. Fluorescently labelled microglia were imaged using the Opera Phenix and subjectively counted using ImageJ software. No differences were seen in the number of microglia (4c4+ cells) in the brains of *acmsd*$^{-/-}$ mutant zebrafish compared to their wildtype siblings ($p>0.9$ for each brain region, **figure 32**). Combining cell counts from the forebrain and midbrain gave an average of 65.59 4c4+ cells in wildtype larvae and 66.48 in *acmsd*$^{-/-}$ mutant larvae. Microglia did not appear to be differentially distributed between genotypes.

4.2.2.2.3.2 Microglia Activation

The activation state of the fluorescently labelled cells was determined based on morphology. Cells were assigned to one of two distinct groups; active (amoeboid morphology) or inactive (ramified with at least one visible process). This analysis found no difference in the percentage activation of microglia in *acmsd*$^{-/-}$ mutant zebrafish and their wildtype siblings ($p>0.6$ for each brain region, **figure 32**). Wildtype larvae had an average of 7.35% activated microglia in combined midbrain and forebrain regions, whilst *acmsd*$^{-/-}$ mutant larvae had an average of 8.31%.

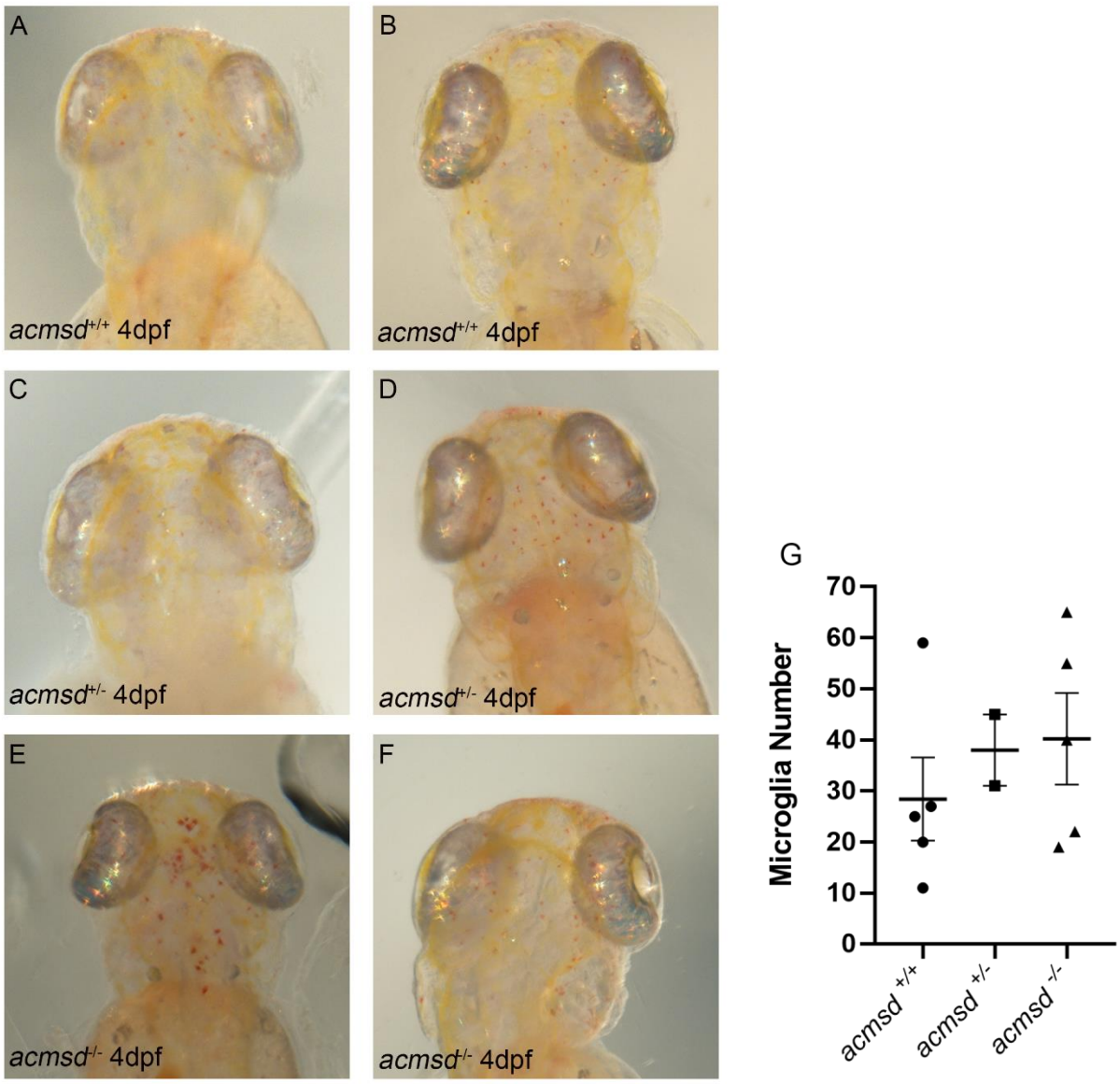

Figure 31. Neutral Red Staining of α-Amino-β-Carboxymuconate-ε-Semialdehyde Decarboxylase Homozygous and Heterozygous Mutants and Their Wildtype Siblings at 4-Days Post Fertilisation. *Representative brightfield images of microglial labelling of wildtype (acmsd$^{+/+}$ (**A, B**)), heterozygous (acmsd$^{+/-}$ (**C, D**)) and homozygous (acmsd$^{-/-}$ (**E, F**)) mutant zebrafish larvae using neutral red staining. Neutral red staining was achieved by incubating 4dpf zebrafish in 2.5µg of neutral red per mL of E3 media for 6 hours at 28°C. Anesthetised larvae were mounted in low melting point agarose and imaged immediately.* ***G.*** *Microglial number was assessed in ImageJ by subjectively counting the number of distinct red dots. Data represented as mean±SEM. n=5* acmsd$^{-/-}$*; 2* acmsd$^{+/-}$*; 5* acmsd$^{+/+}$ *from 1 biological replicate. acmsd, α-amino-β-carboxymuconate-ε-semialdehyde decarboxylase; dpf, days post fertilisation.*

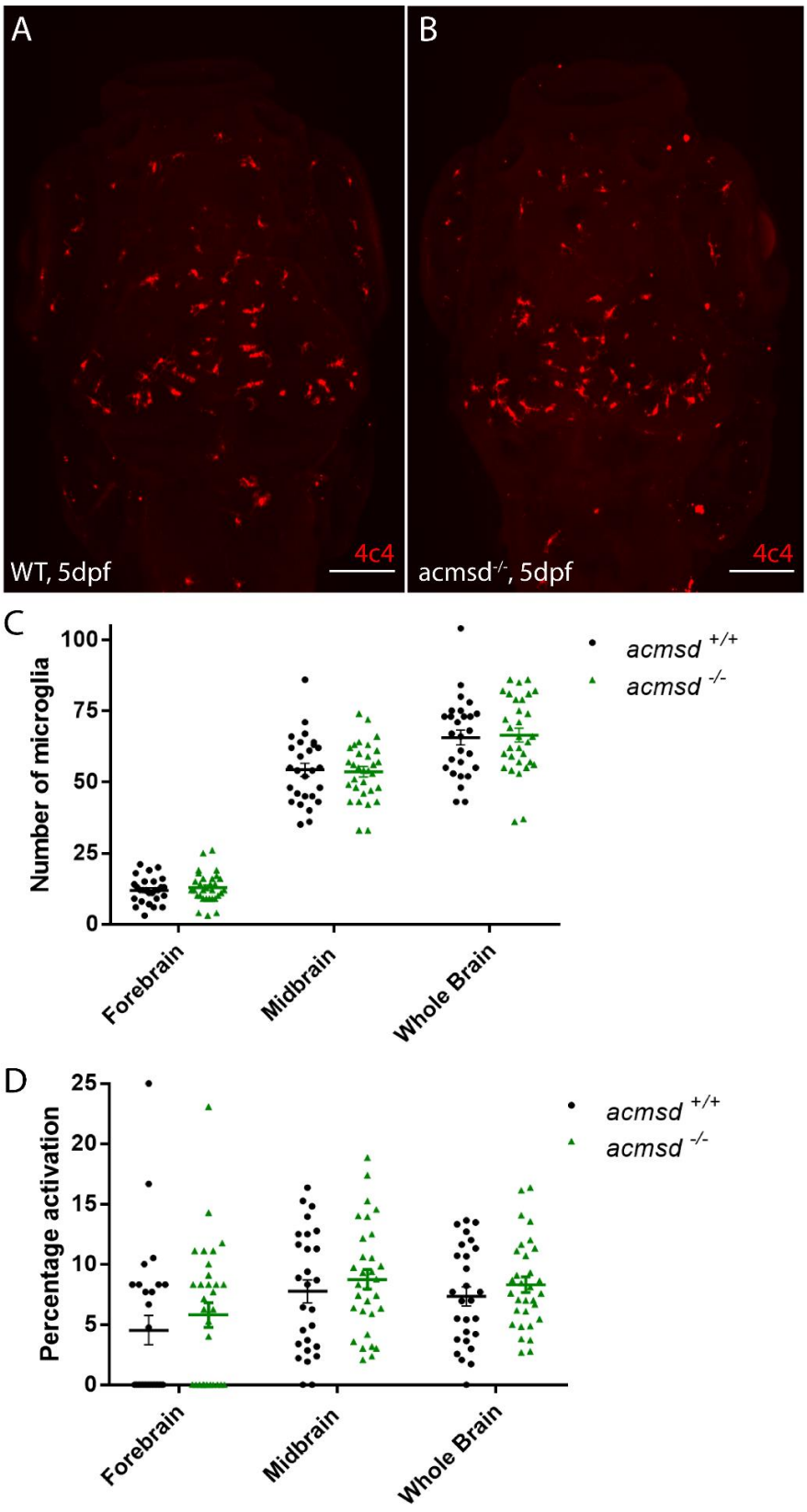

Figure 32. Microglial Analysis of α-Amino-β-Carboxymuconate-ε-Semialdehyde Decarboxylase Mutant Zebrafish Using 4c4. *Representative images from wholemount immunohistochemistry against 4c4 in wildtype (**A**) and acmsd$^{-/-}$ mutant (**B**) zebrafish at 5dpf (scale bar = 100μm).* ***C.*** *There is no difference in the number of 4c4+ cells (microglia) between wildtype (acmsd$^{+/+}$) and acmsd$^{-/-}$ mutant larvae in the forebrain, midbrain or these combined (whole brain) (p>0.9 for all brain regions).* ***D.*** *Microglial activation was determined using cell morphology, represented as the percentage of amoeboid cells out of the total 4c4+ cell count. No differences were identified between wildtype and acmsd$^{-/-}$ mutant activation levels in the forebrain, midbrain or these combined (whole brain) (p>0.6 for all brain regions). n=31 acmsd$^{-/-}$ and 27 acmsd$^{+/+}$ from 3 biological replicates. Data represented as mean±SEM. All individual groups were assessed for normality using Shapiro-Wilk test (all passed, except activation levels in forebrain). Statistics analysed by two-way ANOVA with post-hoc Sidak's multiple comparisons test between genotypes. 4c4, microglial marker; acmsd, α-amino-β-carboxymuconate-ε-semialdehyde decarboxylase; dpf, days post fertilisation.*

4.2.3 Susceptibility of *acmsd*$^{-/-}$ Mutant Zebrafish to Inflammation

acmsd$^{-/-}$ mutant fish were exposed to saponin from 3-5dpf to induce inflammation (see chapter 6, **section 6.2.6.2** for method optimisation). *acmsd*$^{-/-}$ mutants were obtained from an *acmsd*$^{-/-}$ incross and wildtype controls obtained from siblings of these adults (making experimental larvae cousins). Following exposure, larvae were culled using tricaine and RNA extracted from groups of 15 fish. cDNA was reverse transcribed and used in qPCR against markers of inflammation. As shown in *acmsd*$^{+/-}$ incross larvae (**section 4.2.2.1.1**), no differences in the expression of any marker was identified between *acmsd*$^{-/-}$ and *acmsd*$^{+/+}$ zebrafish (**figure 33**, p=0.6056 for *mmp9*; p=0.9993 for *il-1β*; p=0.7655 for *cxcl8*). Following exposure to 100µg/mL saponin for 48 hours, *acmsd*$^{+/+}$ larvae appeared to show an increased expression of these markers (**figure 33**). However, only the increase in *il-1β* reached significance (p=0.0189), although for other genes the significance was close to 0.05 (p=0.0831 for *mmp9*, p=0.0605 for *cxcl8*). A statistically significant increase in *mmp9* (p=0.0044), *il-1β* (p=0.0017) and *cxcl8* (p=0.0065) was seen following exposure of *acmsd*$^{-/-}$ larvae to 100µg/mL saponin (**figure 33**). Despite the difference in significance between genotypes, expression following exposure remained the same for *acmsd*$^{-/-}$ and *acmsd*$^{+/+}$ zebrafish (*mmp9*, p=0.9954; *il-1β, p*=0.9652; *cxcl8, p*=0.1648), suggesting there was no genotype effect on the response to saponin. To assess this further, the difference in expression per biological replicate was determined by calculating dddCt (ddCt after saponin – ddCt before saponin). Data was then converted to a fold change (2^(-dddCt)), making increases in expression after exposure denoted by values above 1 and decreases by values less than 1. Analysis of these datasets found that both wildtype and *acmsd*$^{-/-}$ mutant zebrafish larvae respond equally to saponin exposure (**figure 33**, *mmp9, p*=0.1774; *il-1β,* p=0.3675; *cxcl8,* p=0.1991).

4.2.1 NAD/NADH Assay

The data in this section (**section 4.2.1**) was collected and analysed by Mr Oluwaseyi Pearce, Bandmann Laboratory. Brains were extracted from 25mpf *acmsd*$^{-/-}$ mutant zebrafish and their wildtype siblings for colourimetric NAD assays. Three biological replicates (one pair per replicate) were conducted, with each replicate assessed on consecutive days. Total NAD (NADH and NAD+) levels in adult *acmsd*$^{-/-}$ mutant brain tissue remained unchanged from wildtype (p=0.2839, **figure 34A**). Individual levels of NADH and NAD+ also showed no significant difference to wildtype (p=0.2497 for NADH; p=0.4790 for NAD+, **figure 34B,C**). There was high variability between replicates for both genotypes and all three measurements. The ratio of NAD:NADH per replicate showed less variability and was no different in *acmsd*$^{-/-}$ mutant zebrafish compared to their wildtype siblings (p=0.5818, **figure 34D**).

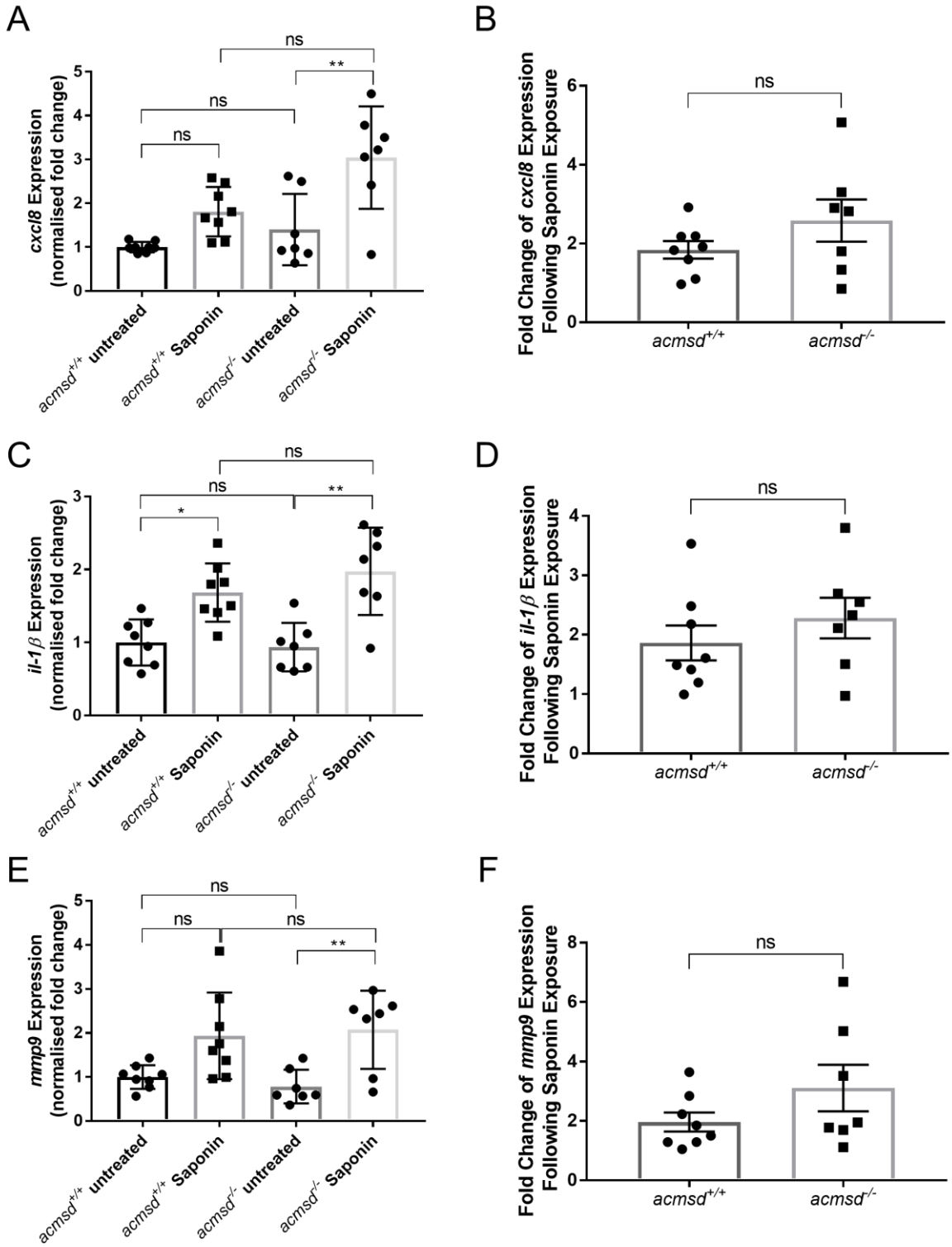

Figure 33. Susceptibility of α-Amino-β-Carboxymuconate-ε-Semialdehyde Decarboxylase Mutant Zebrafish to Saponin Exposure. *acmsd$^{-/-}$ and acmsd$^{+/+}$ zebrafish were exposed to 100µg/mL saponin from 3-5dpf. The expression of cxcl8 (**A, B**), il-1β (**B, C**) and mmp9 (**E, F**) were assessed using qPCR on RNA extracted at 5dpf. Graphs **A, C, E** show expression of inflammatory molecules relative to untreated wildtype samples. Statistical analysis using a two-way ANOVA with Tukey's multiple comparisons post hoc test (on ddCt data). Graphs **B, D, F** show the fold change of expression after exposure for each biological replicate. Statistical analysis using an unpaired t test (normality confirmed via Shapiro-Wilk test). All p values shown in main text. n=7 biological replicates for acmsd$^{-/-}$ and 8 biological replicates for acmsd$^{+/+}$(15 larvae combined per replicate). acmsd, α-amino-β-carboxymuconate-ε-semialdehyde decarboxylase; cxcl8, c-x-c motif chemokine ligand 8; dpf, days post fertilisation; il-1β, interleukin-1 beta; mmp9, matrix metalloproteinase 9.*

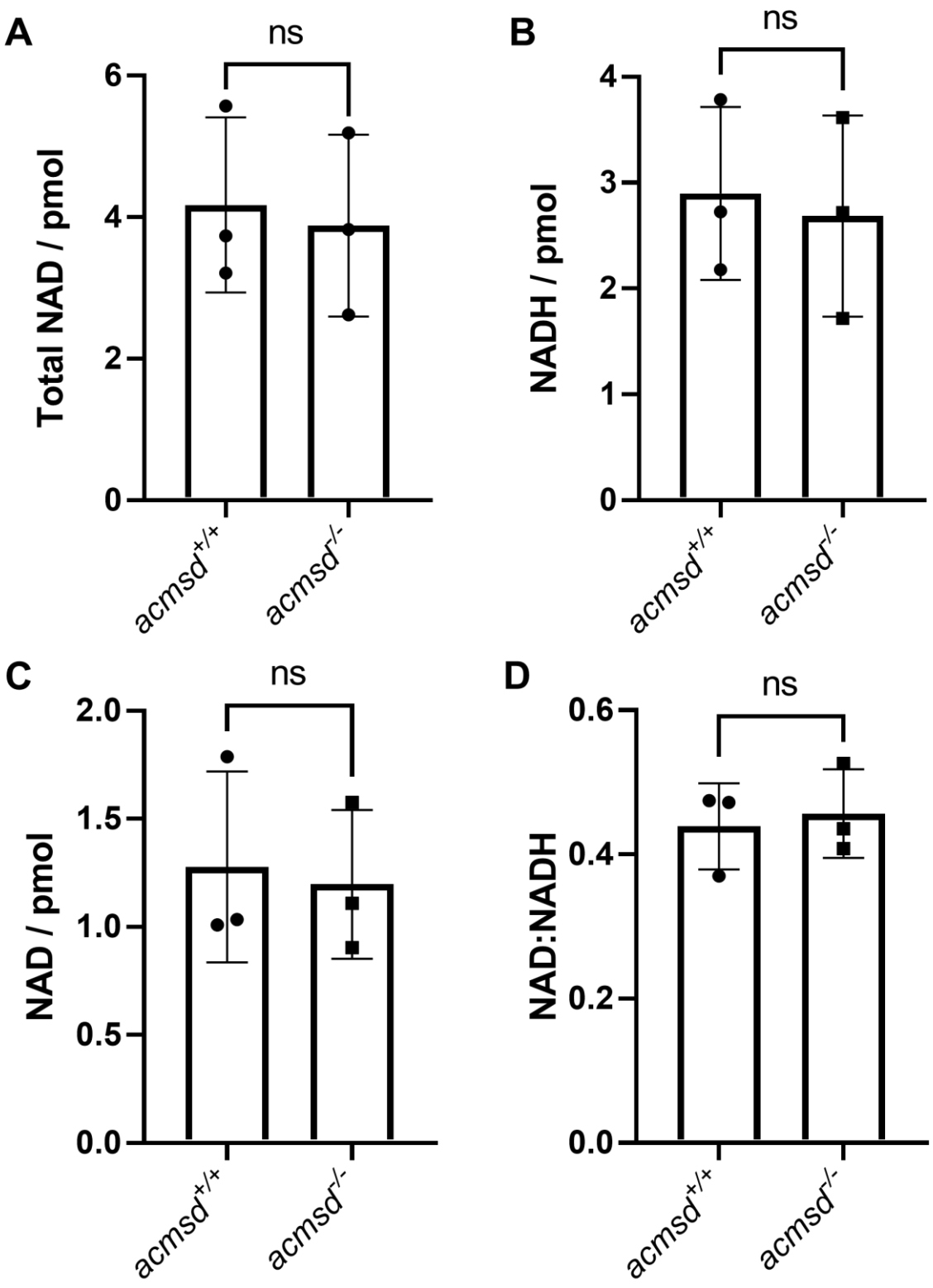

Figure 34. Nicotinamide Adenine Dinucleotide Levels Are Unchanged in α-Amino-β-Carboxymuconate-ε-Semialdehyde Decarboxylase Mutant Zebrafish. *Brain tissue from 25-months post fertilisation zebrafish of known genotype was assayed for NAD/NADH levels using a colourimetic assay. NAD levels were calculated from total NAD and NADH levels, which were measured directly. Data from 3 biological replicates (1 pair per replicate) with each replicate conducted on a different day. p=0.2839 (total); p=0.2497 (NADH); p=0.4790 (NAD); p=0.5818 (ratio). Statistical analysis conducted by two-way paired t test. acmsd, α-amino-β-carboxymuconate-ε-semialdehyde decarboxylase; NAD, nicotinamide adenine dinucleotide; NADH, reduced nicotinamide dinucleotide; ns, not significant; pmol, picomoles.*

4.2.2 Investigating the Liver of *acmsd*$^{-/-}$ Mutant Zebrafish Larvae

As *acmsd* was shown to be expressed primarily in the liver of both larval and adult zebrafish, *acmsd*$^{-/-}$ mutant larvae were assessed for changes in liver size and susceptibility to paracetamol, a compound known to cause hepatotoxicity, as discussed previously.

In situ hybridisation against *fabp10a* was able to specifically label the liver of larval zebrafish (**figure 35**). At 5dpf, there was no difference in the area of the liver between *acmsd*$^{-/-}$ mutant zebrafish and their wildtype siblings (**figure 35**), as analysed from *fabp10a* in situ hybridisation images.

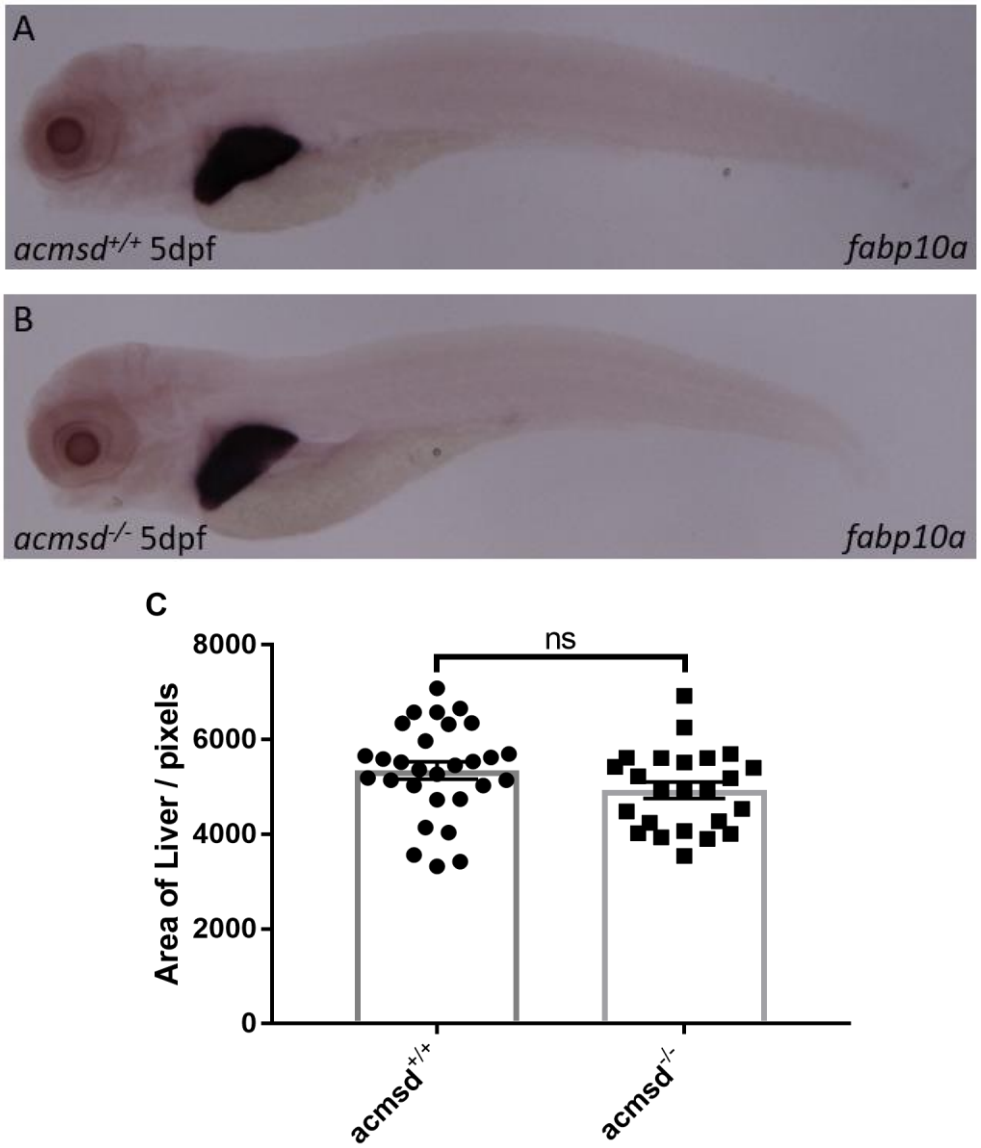

Figure 35. Comparison of Liver Size Between Larval α-Amino-β-Carboxymuconate-ε-Semialdehyde Decarboxylase Mutant Zebrafish and Their Wildtype Siblings. *Representative images from wholemount in situ hybridisation against fabp10a in wildtype (**A**) and acmsd*$^{-/-}$ *mutant (**B**) zebrafish at 5dpf. **C.** There is no difference in the area of the liver between wildtype (acmsd*$^{+/+}$*) and acmsd*$^{-/-}$ *mutant larvae (p=0.1058). n=24 acmsd*$^{-/-}$*, 29 acmsd*$^{+/+}$ *fish from 3 biological replicates. Larvae were genotyped following imaging. Data represented as mean±SEM. Data were assessed for normality using Shapiro-Wilk test (p=0.2518, acmsd*$^{+/+}$*; p=0.3797, acmsd*$^{-/-}$*) and then statistically analysed by an unpaired two-tailed t test. acmsd, α-amino-β-carboxymuconate-ε-semialdehyde decarboxylase; dpf, days post fertilisation; fabp10a, fatty acid-binding protein 10a.*

4.2.2.1 Susceptibility to Hepatotoxic Compounds

4.2.2.1.1 Method Development

Paracetamol exposure from 3dpf was used to induce hepatotoxicity in zebrafish larvae. Initially, toxicity trials were carried out in wildtype larvae, identifying 10mM as a lethal concentration where all larvae developed heart oedema and died by 5dpf (**figure 36**). Concentrations between 1mM and 10mM were then tested to identify the maximum tolerated concentration. However, in this trial fish survived in 10mM paracetamol to 5dpf, although larvae appeared unhealthy, developing severe heart oedema, lack of swim bladder and reduced swimming behaviour (**figure 36**). A darkened liver area was also seen in larvae treated with 10mM paracetamol from 3-5dpf (**figure 37**), indicative of liver damage. Wildtype zebrafish larvae were fixed for in situ hybridisation to assess liver area following treatment with various concentrations of paracetamol. Larvae were co-treated with phenylthiourea to ensure that fish remained transparent for staining; this did not affect paracetamol toxicity. Following in situ hybridisation against *fabp10a*, liver area was assessed using ImageJ. A dose-dependent decrease in liver size was seen in response to paracetamol exposure (**figure 38**). Exposure to 1mM, 3mM or 5mM paracetamol appeared to have no effect on liver area, whilst 7mM showed a moderate reduction in size (**figure 38**). Many fish in the 10mM treatment group had little or no staining of the liver so could not be measured (**figure 38G**). Therefore, this dose was not used in further experiments.

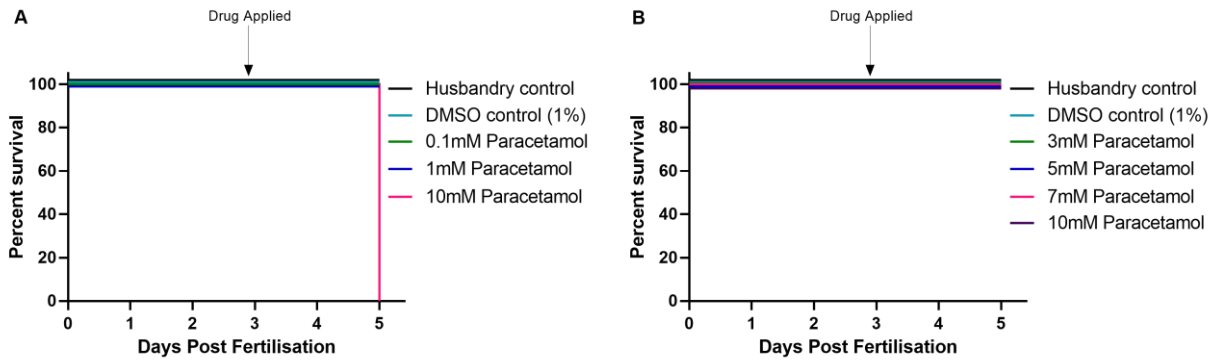

Untreated, 5dpf		Normal development
3mM paracetamol from 3-5dpf		Normal development
5mM paracetamol from 3-5dpf		Reduced swim bladder size in some fish
7mM paracetamol from 3-5dpf		Reduced or absent swim bladder in most fish
10mM paracetamol from 3-5dpf	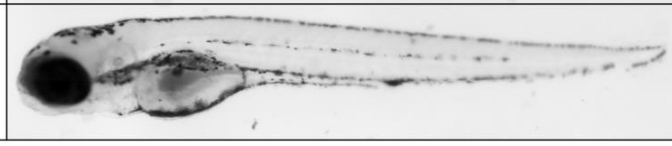	Absent / reduced swim bladder in most fish Darkened liver in all fish Cardiac oedema in some fish

Figure 36. Larval Zebrafish Can Tolerate Exposure to up to 10mM Paracetamol for 48 Hours. *Wildtype zebrafish larvae were exposed to various concentrations of paracetamol from 3dpf.* ***A.*** *Initial toxicity trials found 10mM to be toxic to larvae after 48-hours exposure, but larvae tolerated 0.1mM and 1mM with no impact on survival.* ***B.*** *A second toxicity trial was conducted based on the first trial with 10mM as a maximal dose. Here, larvae tolerated all doses tested, including 10mM.* ***C.*** *Representative images of 5dpf larvae treated with paracetamol from 3dpf. For all toxicity trials, n=20 wildtype larvae per group. DMSO, dimethyl sulfoxide; dpf, days post fertilisation; mM, millimolar.*

Figure 37. Liver Damage was Evident in Larval Zebrafish Exposed to 10mM Paracetamol from 3-5 Days Post Fertilisation*. Darkening of the liver can be seen in wildtype zebrafish larvae exposed to 10mM paracetamol (right) when compared to their untreated siblings (left).*

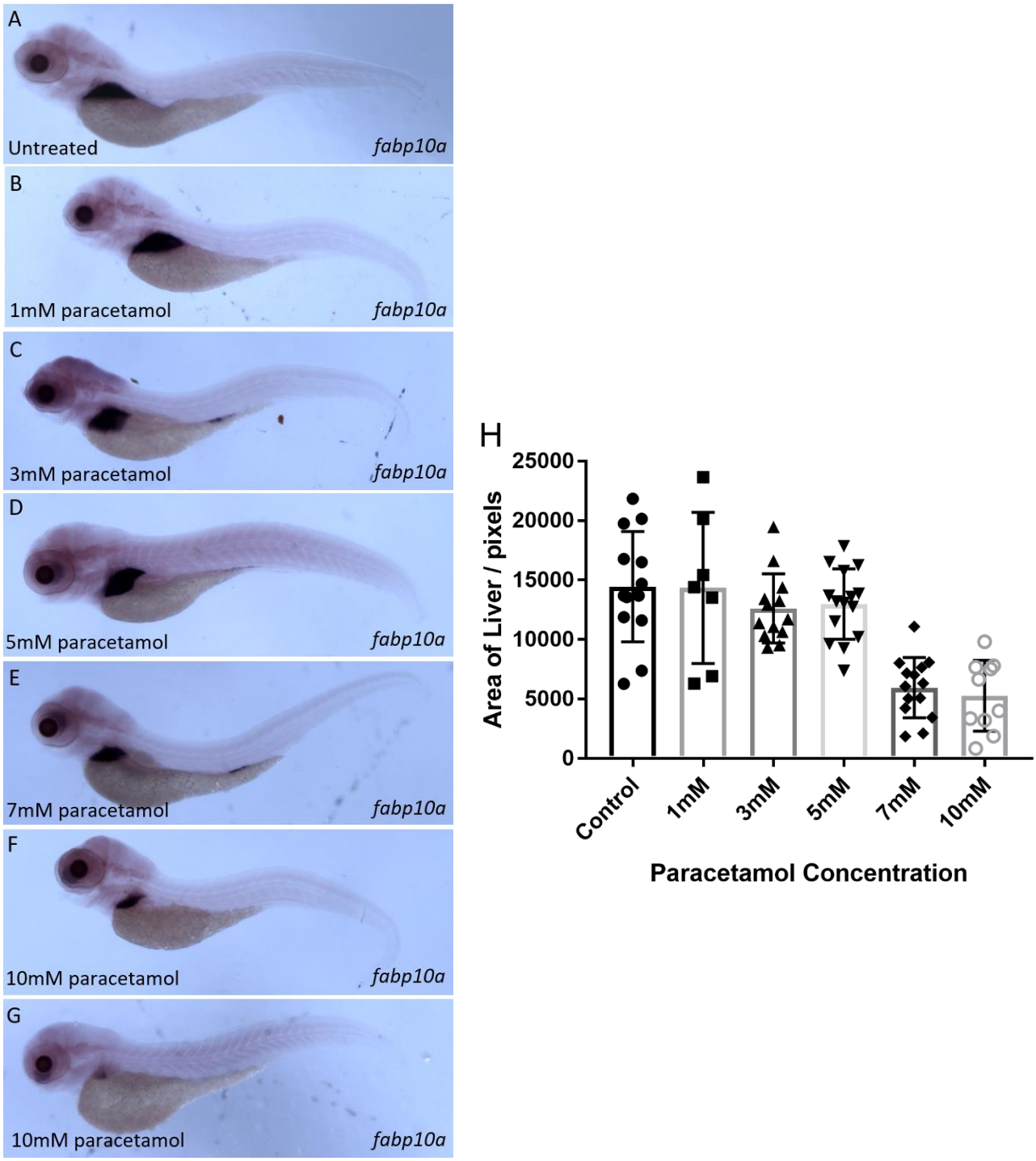

Figure 38. Liver Area of Zebrafish Larvae Exposed to Paracetamol. A-G. *Representative images of 5dpf zebrafish following in situ hybridisation against fabp10a after exposure to various concentrations of paracetamol from 3-5dpf.* ***G*** *shows example of low staining seen in many fish exposed to 10mM paracetamol.* ***H.*** *Liver area was measured from in situ hybridisation images using ImageJ software. A dose-dependent decrease in liver area in response to paracetamol is evident. Statistics were not conducted as only one biological replicate was included. dpf, days post fertilisation; fabp10a, fatty acid-binding protein 10a; mM, millimolar.*

4.2.2.1.2 Treatment of *acmsd*$^{-/-}$ Mutant Zebrafish

acmsd$^{-/-}$ mutant larvae were obtained from an incross of adult *acmsd*$^{-/-}$ homozygous zebrafish. Wildtype controls were obtained from the wildtype siblings of the adult *acmsd*$^{-/-}$ mutants, making experimental fish cousins. Survival analysis using concentrations of paracetamol between 1mM and 15mM found no difference in lethality between *acmsd*$^{-/-}$ mutant larvae and wildtype controls (**figure 39**). Whilst significant death, determined as a loss of heartbeat, was only seen in wildtype and not *acmsd*$^{-/-}$ mutant larvae treated with 15mM paracetamol, fish in both genotypes lost response to touch when exposed to concentrations above 10mM (**figure 39D**), suggesting paracetamol had negative effects on larval health independent of genotype. Based on the preliminary data obtained from treated wildtype larvae (above), 3mM and 7mM were selected for analysis of effect on liver area. As before, fish were exposed to paracetamol from 3-5dpf, as well as phenylthiourea. 1% DMSO was used as a carrier for paracetamol and therefore also as a control group. Three biological replicates of larvae were then fixed at 5dpf for in situ hybridisation against *fabp10a*. As shown previously, wildtype zebrafish demonstrated a dose-dependent decrease in liver size in response to paracetamol exposure (**figure 40**). This was also seen in *acmsd*$^{-/-}$ mutant zebrafish (**figure 40**). There was no difference in the response to paracetamol between *acmsd*$^{-/-}$ mutant and wildtype larvae when assessing liver area (**figure 40G**). 3mM paracetamol resulted in a significant decrease in liver area in both wildtype (19.96% decrease, $p=0.0004$) and *acmsd*$^{-/-}$ mutant larvae (21.26% decrease, $p<0.0001$). The effect of 3mM was more evident in this experiment compared to preliminary trials, where it appeared to have little effect on liver size. 7mM paracetamol exposure resulted in a larger significant decrease in liver area in both wildtype (59.62% decrease, $p<0.0001$) and *acmsd*$^{-/-}$ mutant larvae (63.37% decrease, $p<0.0001$). There was no significant difference in liver size between wildtype and *acmsd*$^{-/-}$ larvae in any treatment group ($p=0.8695$ for control, $p=0.9918$ for 3mM, $p=0.9990$ for 7mM), suggesting that wildtype and *acmsd*$^{-/-}$ mutant zebrafish are equally susceptible to paracetamol-induced hepatotoxicity.

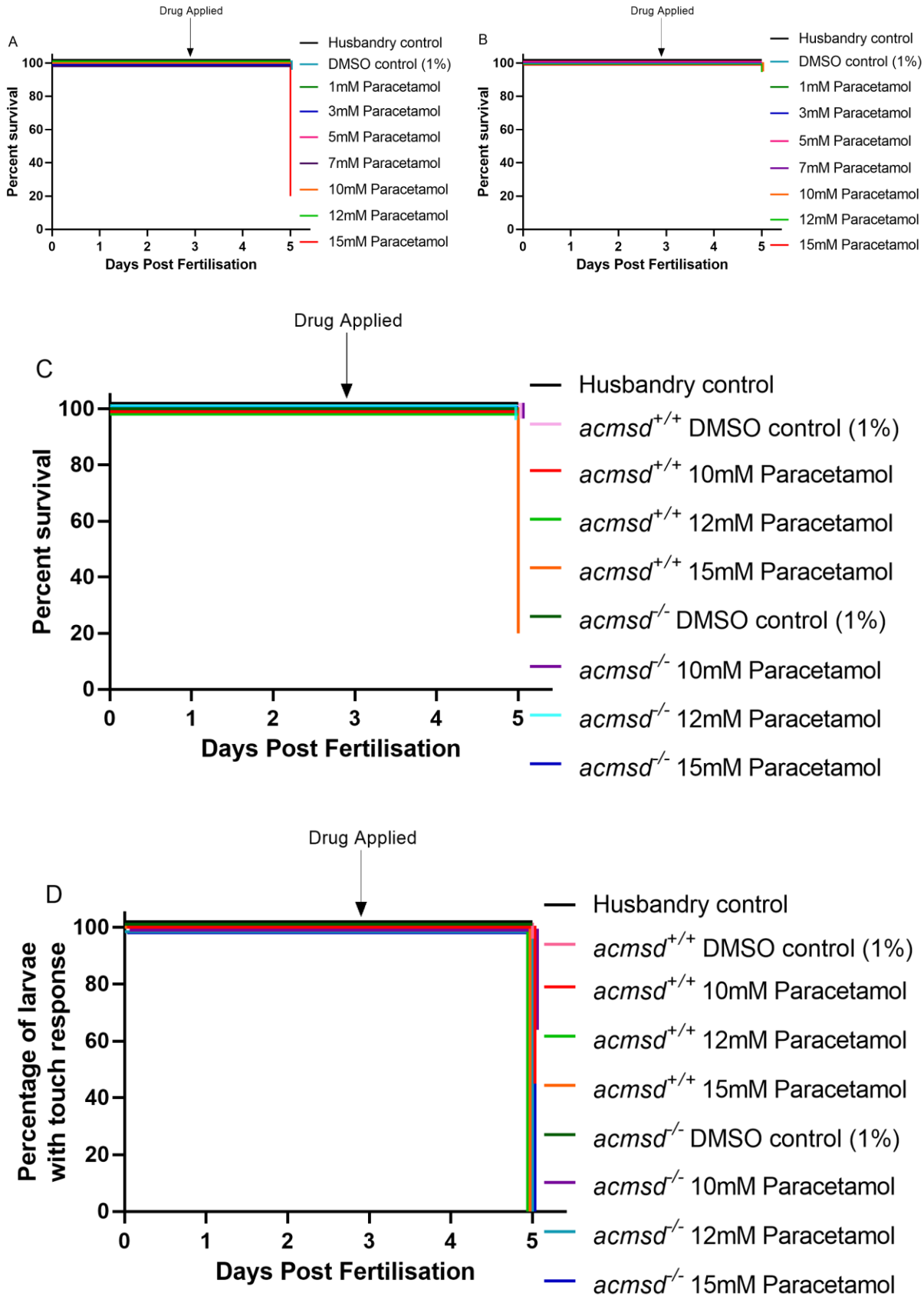

Figure 39. Paracetamol Appears Equally Toxic to α-Amino-β-Carboxymuconate-ε-Semialdehyde Decarboxylase Mutant and Wildtype Zebrafish Larvae. *3dpf zebrafish larvae were exposed to various concentrations of paracetamol for up to 48 hours. Paracetamol concentrations below 10mM had no effect on the survival of either wildtype* ***(A)*** *or mutant* ***(B)*** *larvae.* ***C*** *shows the survival of combined genotypes on one graph, for simplicity only concentrations above 10mM are shown. Whilst significant death was only seen in wildtype and not mutant larvae, fish in both genotypes lost response to touch* ***(D)****. n=20 per genotype from a single replicate. acmsd, α-amino-β-carboxymuconate-ε-semialdehyde decarboxylase; dpf, days post fertilisation; mM, millimolar.*

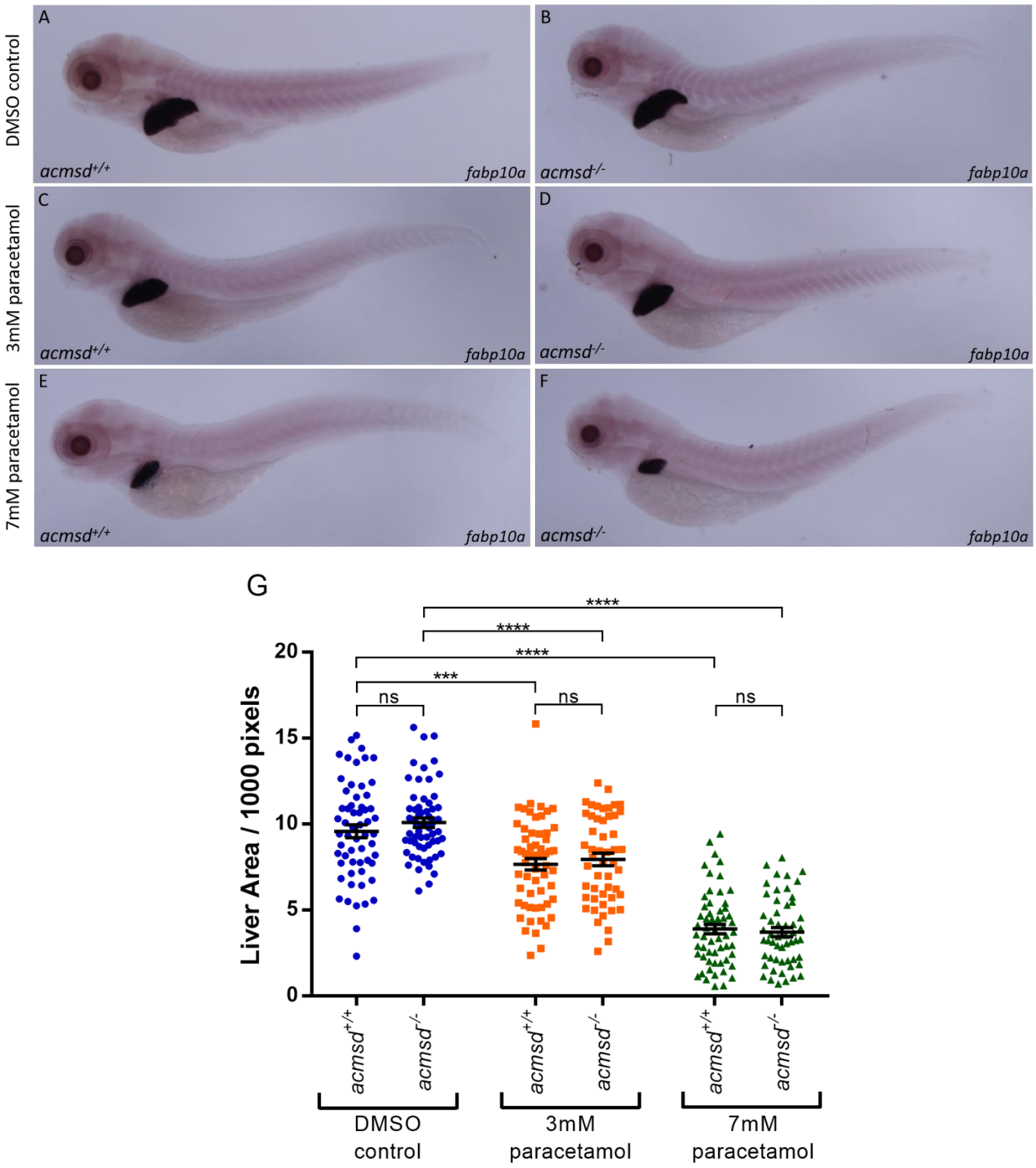

Figure 40. Wildtype and α-Amino-β-Carboxymuconate-ε-Semialdehyde Decarboxylase Mutant Zebrafish Larvae Are Equally Susceptible to Paracetamol Exposure. *3dpf zebrafish larvae were exposed to either 3mM or 7mM paracetamol for 48 hours. Following exposure, zebrafish were fixed and in situ hybridisation against fabp10a carried out (**A-F**, representative images). **G.** Graph showing liver area per genotype and treatment group as calculated using ImageJ following in situ hybridisation against fabp10a. Data points represent liver areas from individual fish with mean and SEM bars. 3mM paracetamol exposure resulted in a significant decrease in liver area in both wildtype (p=0.0003) and acmsd$^{-/-}$ mutant larvae (p<0.0001). 7mM paracetamol exposure also resulted in a significant decrease in liver area in both wildtype (p<0.0001) and acmsd$^{-/-}$ larvae (p<0.0001). There was no significant difference between wildtype and acmsd$^{-/-}$ larvae in any treatment group (p=0.8602 for control, p=0.9911 for 3mM, p=0.9990 for 7mM). Data from 3 biological replicates, n=51-59 per group. 1% DMSO was used as a carrier and therefore a control group. All statistical analyses from a two-way ANOVA following Shapiro-Wilk test for normality (all groups passed). acmsd, α-amino-β-carboxymuconate-ε-semialdehyde decarboxylase; dpf, days post fertilisation; fabp10a, fatty acid-binding protein 10a; mM, millimolar; ns, not significant.*

4.2.3 Kynurenine Pathway Metabolomics Analysis

4.2.3.1 Larvae

Larvae were obtained from an incross of *acmsd*$^{-/-}$ homozygous mutant parents or their wildtype siblings, making experimental fish cousins. Five 5dpf larvae were combined per replicate for analysis. Most kynurenine pathway metabolites were expressed in a concertation that was too low to detect in larvae (**table 15**). The only dataset that allowed for comparison between genotypes was 3-hydroxykynurenine expression, for which there was no significant difference between *acmsd*$^{+/+}$ and *acmsd*$^{-/-}$ zebrafish (**figure 41**, p=0.3232). The increase in QUIN in *acmsd*$^{-/-}$ mutant larvae was clear despite being undetectable in wildtype samples. The lower limit of quantification (LLOQ) for QUIN was 0.42ng/mL, suggesting that expression is at least 349.4 times higher in *acmsd*$^{-/-}$ mutant larvae. A Mann-Whitney statistical test between measured mutant values and the LLOQ suggested this minimum difference was statistically significant (p=0.0079).

Table 15. Kynurenine Pathway Metabolite Concentrations in Zebrafish Larvae

Sample	Kynurenine	Kynurenic Acid	3-Hydroxykinurenine	Quinolinic Acid
WT				
acmsd$^{+/+}$ 1	<LLOQ	<LLOQ	0.888	< LLOQ
acmsd$^{+/+}$ 2	3.81	<LLOQ	0.751	< LLOQ
acmsd$^{+/+}$ 3	2.89	<LLOQ	0.742	< LLOQ
acmsd$^{+/+}$ 4	2.12	<LLOQ	0.565	< LLOQ
acmsd$^{+/+}$ 5	<LLOQ	<LLOQ	0.502	< LLOQ
HOM				
acmsd$^{-/-}$ 1	<LLOQ	<LLOQ	0.478	91.9
acmsd$^{-/-}$ 2	<LLOQ	<LLOQ	0.552	129
acmsd$^{-/-}$ 3	<LLOQ	<LLOQ	0.300	197
acmsd$^{-/-}$ 4	3.31	<LLOQ	0.913	133
acmsd$^{-/-}$ 5	2.31	<LLOQ	0.565	183

Table outlining the measured concentration of kynurenine metabolites from 5dpf zebrafish larvae (5 fish per biological replicate, combined from a single larval clutch obtained from homozygous parents). Concentrations are given as ng/mL of extract. acmsd, α-amino-β-carboxymuconate-ε-semialdehyde decarboxylase; HOM, homozygous mutant; LLOQ, lower limit of quantification; WT, wildtype.

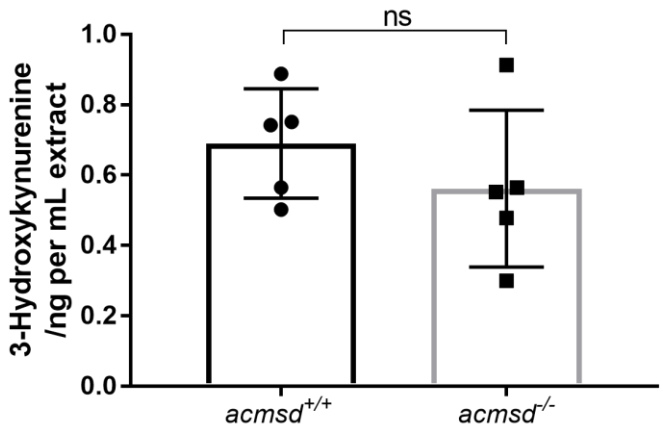

Figure 41. 3-Hydroxykynurenine Expression in α-Amino-β-Carboxymuconate-ε-Semialdehyde Decarboxylase Mutant Zebrafish Larvae. *The concentration of 3-hydroxykynurenine in the extract obtained from combining five 5dpf zebrafish larvae from a single clutch was determined in wildtype and acmsd mutant larvae. No significant difference was identified between genotypes (p=0.3232, unpaired, two-tailed t test). Both datasets passed Shapiro-Wilk test for normality. acmsd, α-amino-β-carboxymuconate-ε-semialdehyde decarboxylase; dpf, days post fertilisation; mL, millilitre; ng, nanograms.*

4.2.3.2 Adult Brain Tissue

Whole brains were extracted from 9-month old adult zebrafish for metabolite analysis, for which the data is summarised in **table 16**. Kynurenine and kynurenic acid were expressed in a concentration that was too low to detect in brain tissue so these could not be compared between genotypes. No significant difference in 3-hydroxykynurenine concentration was identified between *acmsd*$^{+/+}$ and *acmsd*$^{-/-}$ mutant zebrafish brains (**figure 42**, p=0.0827). There was a significant increase in QUIN expression in *acmsd*$^{-/-}$ mutant brains, with mutants possessing a 111.7 times greater average concentration than their wildtype siblings (**figure 42,** p=0.0002).

Table 16. Kynurenine Pathway Metabolite Concentrations in Adult Zebrafish Brain Tissue

Sample	Kynurenine	Kynurenic Acid	3-Hydroxykinurenine	Quinolinic Acid
WT				
acmsd$^{+/+}$ 1	< LLOQ	< LLOQ	14.6	23.2
acmsd$^{+/+}$ 2	< LLOQ	< LLOQ	10.6	18.8
acmsd$^{+/+}$ 3	< LLOQ	< LLOQ	8.06	17.0
acmsd$^{+/+}$ 4	< LLOQ	< LLOQ	7.39	11.1
acmsd$^{+/+}$ 5	< LLOQ	< LLOQ	9.74	13.7
HOM				
acmsd$^{-/-}$ 1	< LLOQ	< LLOQ	22.0	2030
acmsd$^{-/-}$ 2	< LLOQ	< LLOQ	14.5	1454
acmsd$^{-/-}$ 3	< LLOQ	< LLOQ	8.71	1220
acmsd$^{-/-}$ 4	< LLOQ	< LLOQ	17.9	1805
acmsd$^{-/-}$ 5	< LLOQ	< LLOQ	12.9	2858

Table outlining the measured concentration of kynurenine metabolites from whole brains extracted from 9-month old zebrafish. Concentrations are given as ng/gram of brain tissue. acmsd, α-amino-β-carboxymuconate-ε-semialdehyde decarboxylase; HOM, homozygous mutant, LLOQ, lower limit of quantification WT, wildtype.

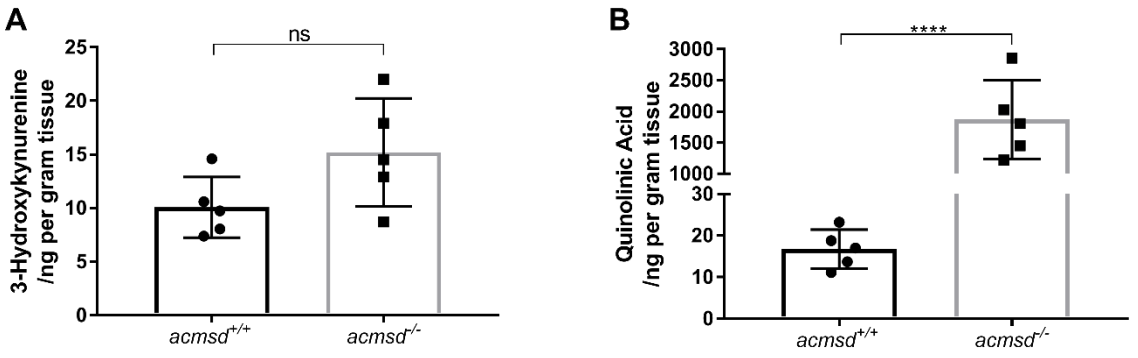

Figure 42. 3-Hydroxykynurenine and Quinolinic Acid Expression in Adult α-Amino-β-Carboxymuconate-ε-Semialdehyde Decarboxylase Mutant Zebrafish Brain Tissue. *The concentration of kynurenine metabolites was determined in brain tissue obtained from individual adult wildtype and acmsd mutant zebrafish. No significant difference was identified between genotypes in 3-hydroxykynurenine expression (**A**, p=0.0827, unpaired, two-tailed t test). Levels of quinolinic acid were found to be significantly increased in mutant zebrafish compared to controls (**B**, p=0.0002, unpaired, two-tailed t test). All datasets passed Shapiro-Wilk test for normality. acmsd, α-amino-β-carboxymuconate-ε-semialdehyde decarboxylase; ng, nanograms.*

4.2.3.3 Adult Liver Tissue

Liver samples were obtained from 9-month old adult zebrafish for metabolite analysis. As expected, high concentrations of kynurenine pathway metabolites were found in the liver (**table 17**), enabling a comparison of each metabolite between genotypes. Neither kynurenic acid (**figure 43B**, p=0.9125) or 3-hydroxykynurenine (**figure 43C**, p=0.0986) expression was found to vary between genotypes. However, kynurenine levels were significantly reduced in *acmsd*$^{-/-}$ mutant zebrafish liver tissue compared to controls (**figure 43A**, p=0.0079). QUIN in liver tissue obtained from *acmsd*$^{-/-}$ mutant zebrafish was found at levels averaging 715.4 times greater than those found in wildtype livers (**figure 43D**, p=0.0079).

Since no differences were found in kynurenic acid expression, but the levels of its precursor were significantly reduced, this suggested that this pathway may be upregulated in *acmsd*$^{-/-}$ mutant zebrafish. To explore this further, ratios of metabolites were calculated. The ratio of kynurenic acid to kynurenine was increased in homozygous mutants by an average of 2.53 times (**figure 43E**, p=0.0161), suggesting an upregulation of kynurenine aminotransferase. The ratio of 3-hydroxykynurenien to kynurenine was increased in homozygous mutants by an average of 1.92 times (**figure 43F**, p=0.0063), suggesting an upregulation of kynurenine-3-monooxygenase, but at a lower rate than kynurenine aminotransferase.

Table 17. Kynurenine Pathway Metabolite Concentrations in Adult Zebrafish Liver Tissue

Sample	Kynurenine	Kynurenic Acid	3-Hydroxykinurenine	Quinolinic Acid	Kynurenic Acid/Kynurenine	3-Hydroxykinurenine /Kynurenine
WT						
acmsd$^{+/+}$ 1	9234	9.84	161	111	0.001066	0.017436
acmsd$^{+/+}$ 2	8641	2.50	189	75.2	0.000289	0.021872
acmsd$^{+/+}$ 3	8453	10.6	117	80.0	0.001254	0.013841
acmsd$^{+/+}$ 4	8641	27.9	118	76.4	0.003229	0.013656
acmsd$^{+/+}$ 5	14575	16.4	254	123	0.001125	0.017427
HOM						
acmsd$^{-/-}$ 1	5112	21.7	136	57907	0.004245	0.026604
acmsd$^{-/-}$ 2	1301	2.30	61.8	52141	0.001768	0.047502
acmsd$^{-/-}$ 3	5611	21.4	146	61834	0.003814	0.02602
acmsd$^{-/-}$ 4	2322	10.7	75.7	60915	0.004608	0.032601
acmsd$^{-/-}$ 5	4529	14.3	132	100271	0.003157	0.029146

Table outlining the measured concentration of kynurenine metabolites from liver samples taken from 9-month old zebrafish. Concentrations are given as ng/gram of liver tissue. acmsd, α-amino-β-carboxymuconate-ε-semialdehyde decarboxylase; HOM, homozygous mutant, LLOQ, lower limit of quantification WT, wildtype.

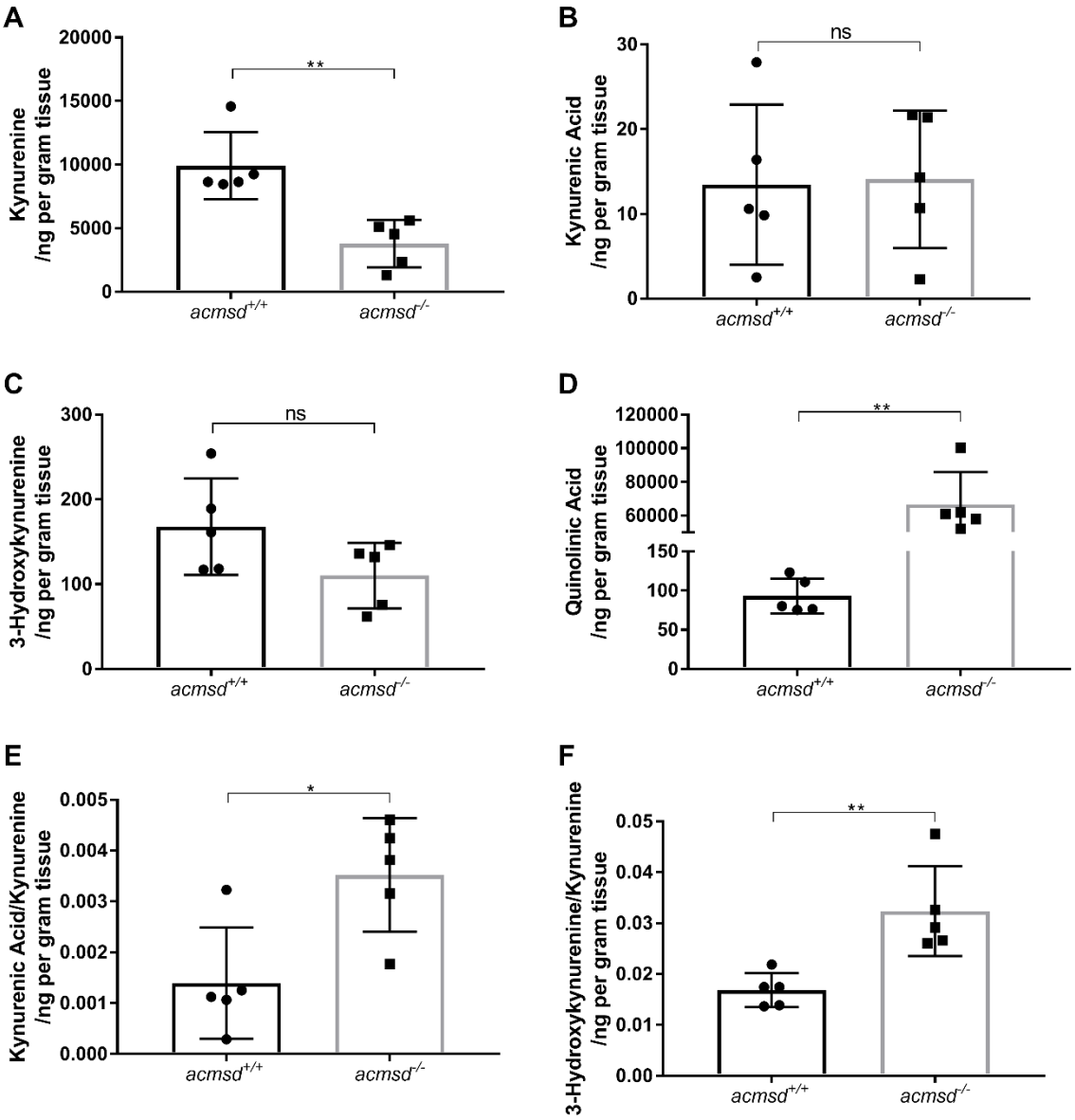

Figure 43. Kynurenine Pathway Metabolite Expression in Adult α-Amino-β-Carboxymuconate-ε-Semialdehyde Decarboxylase Mutant Zebrafish Liver Tissue. *The concentration of kynurenine metabolites was determined in liver tissue obtained from individual adult wildtype and acmsd mutant zebrafish. No significant difference was identified between genotypes in kynurenic acid (**B**, p=0.9125, unpaired, two-tailed t test) or 3-hydroxykynurenine (**C**, p=0.0986, unpaired, two-tailed t test) expression. Levels of kynurenine were significantly reduced in mutants compared to controls (**A**, p=0.0079, Mann-Whitney test), whilst quinolinic acid was significantly increased (**D**, p=0.0079, Mann-Whitney test). The ratio of kynurenic acid to kynurenine was increased in homozygous mutants (**E**, p=0.0161, unpaired t test) by an average of 2.53 times. The ratio of 3-hydroxykynurenine to kynurenine was increased in homozygous mutants (**F**, p=0.0063, unpaired t test) by an average of 1.92 times. All datasets passed Shapiro-Wilk test for normality except kynurenine and quinolinic acid; for these, nonparametric statistical tests were used. acmsd, α-amino-β-carboxymuconate-ε-semialdehyde decarboxylase; ng, nanograms.*

4.3 Discussion

Acmsd is expressed as two splice variants in humans, a 336aa protein and a 278aa protein, which is identical in the C-terminal but shorter than the full-length transcript. Previous reports have identified that whilst both variants are expressed in the kidney and liver, only ACMSD1, the longer transcript, is present in the human brain (Pucci et al., 2007). Since PD is a disease of the brain, the longer, brain-specific variant was used for *in silico* comparisons in this thesis.

In silico data strongly suggests that *acmsd* is the true and sole orthologue of the human *ACMSD* gene implicated as a risk gene for PD. High levels of similarity at both the DNA and protein level, as well as the conservation of synteny between comparable chromosome regions, suggest that these genes are indeed orthologous. The presence of a single *ACMSD* homologue, with only one protein product, indicates that zebrafish represent a good model system to study the biological role of Acmsd. By mutating a single gene, we can be sure that no other variants of the protein will provide compensation for this reduced function, a mechanism often seen when multiple homologues of the same gene are present, particularly where important domains are conserved. The high degree of similarity between zebrafish and human ACMSD also suggests that studying this protein in zebrafish is a valid means to study the role of this enzyme in humans. However, it is important to remember that, as mentioned in the chapter introduction, different organisms express differing levels of ACMSD as a trade-off between NAD+ production and the neurotoxic effects of QUIN. Where zebrafish lie on this opposing evolutionary solution has not been studied. Without directly comparing the expression and activity levels of Acmsd between organisms, we cannot be sure that any effects seen in zebrafish as a result of a loss-of-function of this enzyme recapitulate the effects that would occur in the human CNS.

RT-PCR data found that *acmsd* is expressed throughout development in zebrafish at seemingly increasing concentrations until 5dpf. This suggests that Acmsd likely plays a vital role at this time. Without measuring expression levels in unfertilised embryos, it is impossible to determine whether the *acmsd* expression in embryos occurs as a result of maternal contribution. However, maternal to zygotic transition, whereby maternal RNAs are degraded and zygotic transcription is activated, occurs after just 10 cell cycles (Harvey et al., 2013). This suggests that, at least from this point, *acmsd* is transcribed in the embryo itself, further supporting the notion that Acmsd is important during larval development. Interestingly, at a similar developmental age in chick embryos (based on the reliance of the yolk for energy), *ACMSD* decreases as development progresses (Cogburn et al., 2018), suggesting differences between organisms. However, this

assay only looked at transcript levels in the liver, whereas in zebrafish the whole larvae was used for analysis. RT-PCR also only represents a semi-quantitative means of assessing *acmsd* levels and small differences in band intensity do not always accurately represent changes in expression. In order to assess this in more detail, qPCR could be carried out throughout development.

In situ hybridisation identified that the *acmsd* expression in larval zebrafish was specific to the liver. Some fish also demonstrated low levels of staining in the intestines as well as the prominent liver staining, suggesting that *acmsd* may also be expressed in the gut of larval zebrafish. No staining was seen in the brain at this age. It may be that brain expression levels are much lower than in the liver, as is true in humans, and therefore the probe may need longer to stain (i.e. allowing the staining to over develop in the liver may result in staining appearing in the brain); this was not tested as part of this thesis. However, if the lack of staining indicates a true absence of expression in the brain of larval zebrafish, this may have implications on the relevance of larvae as a model for PD. The hallmark pathology of PD occurs within the brain and *ACMSD* is known to be expressed here in humans (Fukuoka et al., 2002). However, it is unclear whether changes to ACMSD within the brain itself is what alters the risk of PD in humans. The kynurenine pathway metabolites are altered not just in the brain and CSF, but also in the peripheral blood (see **table 18**), and these may originate from the liver or kidneys, the primary area of expression in humans. Since the liver is the primary area of expression in zebrafish larvae too, if the peripheral-origin theory is correct, then this model would still be relevant. Further research, both in humans and zebrafish, is needed to explore this further.

Within adult zebrafish, *acmsd* was found by RT-PCR to be expressed primarily in the liver and intestine, but also at lower levels in the brain, kidney, gonads and gall bladder. There appeared to be expression in the heart in females but not in males, although this may be due to contamination since this sex-dependent difference has no logical explanation. This suggests that as zebrafish develop, the expression of *acmsd*, which is primarily conserved to the liver at larval stages, spreads to other organs in the adult fish. The expression of *acmsd* in zebrafish imitates that of *ACMSD* in humans, where it is expressed in the kidney, liver and brain in adults (Fukuoka et al., 2002). As *acmsd* is expressed in both larval and adult zebrafish in a pattern similar to that seen in humans, the zebrafish appears to represent a good model system for assessing the role of this enzyme with relevance to human disease.

It is clear from the literature that kynurenine pathway metabolites are altered in people with PD (Hartai et al., 2005; Ogawa et al., 1992; Sorgdrager et al., 2019) and can even be used as a

biomarker for the disease (Klatt et al., 2021). However, the role of *ACMSD* within PD still represents an understudied area, possibly owing to the lack of vertebrate animal models.

The generation of a stable *acmsd*$^{-/-}$ mutant zebrafish line using CRISPR-Cas9 technology enabled the study of the role of this enzyme *in vivo*. qPCR analysis demonstrated that the mutation introduced into exon 6 of the gene resulted in nonsense-mediated decay of mutated *acmsd* mRNA in larvae. Brains dissected from adult zebrafish also demonstrated a reduced expression of *acmsd* mRNA; expression data for wildtype siblings in this experiment was highly variable affecting the significance level of this dataset, although the reduction in transcript level was still significant. This could be due to errors during experimentation or reflect the natural variation of expression seen across individuals. In situ hybridisation was used to confirm the loss of expression in larvae, which was clearly absent in homozygous mutants. The mixed phenotype of heterozygous mutants was unexpected. Most heterozygotes were indistinguishable from wildtype, suggesting haplosufficiency of *acmsd.* However, this hypothesis was challenged by the absence of staining in some lavae, indicative of a haploinsufficient gene. It is possible that the in situ had failed in these larvae, but this is unlikely as larvae of all genotypes were stained in a single eppendorf and an absence of staining was never seen in wildtype larvae. It is also possible that these larvae were misgenotyped or contaminated with wildtype DNA and were actually homozygous mutants. The expression of *acmsd* in *acmsd*$^{+/-}$ larvae could only be confirmed by qPCR, which was not conducted on heterozygotes during this project. However, it was clear that *acmsd*$^{-/-}$ mutant zebrafish larvae expressed very low levels of *acmsd* mRNA which remained reduced throughout adulthood, suggesting that very little protein would be made and a true knockout zebrafish had been created.

Despite finding a significant reduction in mRNA transcript levels, *acmsd*$^{-/-}$ mutant zebrafish did not demonstrate any obvious overt phenotypic changes. Homozygous mutant zebrafish were viable to adulthood and fed and bred normally. There were no changes to the overall size or shape of either adult or larval homozygous mutants, although this was not formally measured.

As primarily a movement disorder, mutations in PD risk genes may lead to alterations of movement within zebrafish. However, larval (5dpf) and adult (9mpf) *acmsd*$^{-/-}$ mutant zebrafish demonstrated swimming behaviour that was indistinguishable from their wildtype siblings, suggesting that the loss of *acmsd* did not have an effect on locomotion. It is important to take into consideration the aspects of movement assessed during this project. Swimming distance was measured over a pre-set time period in both adult and larval fish, whilst other aspects of

movement, such as direction, speed or stop-go behaviour was not assessed. Movement changes in PD are usually changes in gait, bradykinesia or akinesia (reviewed in Mazzoni et al. (2012)) and these were not assessed in the *acmsd*$^{-/-}$ mutant zebrafish. Such changes would likely result in an overall reduced distance travelled and as this also represented a relatively easy readout, swimming distance was initially assessed, with the plan of measuring other locomotive readouts if changes were seen.

To study the effect of an *acmsd* knockout in the context of PD, dopaminergic neurons, being the population of neurons specifically targeted in PD, were assessed. It was hypothesised that the mutation in *acmsd*, as a PD risk gene, would result in a reduction in the number of dopaminergic neurons, as is characteristic of human PD pathology. However, *acmsd*$^{-/-}$ mutant zebrafish larvae did not demonstrate changes in the number or positioning of their dopaminergic neurons at either 3dpf or 5dpf. There are three possible explanations for this. Firstly, it may be that Acmsd has no effect on the development or survival of dopaminergic neurons in zebrafish. Given that *ACMSD* is a risk gene and not linked to monogenic PD, it is unsurprising that *acmsd* mutations alone did not result in typical PD pathology. It is possible, however, that a knockout of *acmsd* could result in changes to dopaminergic neurons, even if less dramatic than seen in typical PD. PD is recognised as a disease of ageing with dopaminergic neuronal death usually occurring later in life, even in hereditary cases. Since this neuronal population was only studied at larval stages here, it cannot be ruled out that changes may occur in older *acmsd*$^{-/-}$ mutants. This is more difficult to assess due to the accessibility of neurons within the adult brain. Antibodies specific to tyrosine hydroxylase are available for use in zebrafish and could be used to look at these neuronal populations in sections, although this would only offer a 2D analysis and neuronal counting would not be possible. Large deviations from the norm would be able to be identified using this method, although it is unlikely that the *acmsd*$^{-/-}$ mutant zebrafish develop such changes given their seemingly healthy phenotype into late adulthood. Thirdly, Acmsd may be important in neuronal development/survival, even in larval zebrafish, but the upregulation of compensating proteins may act to preserve dopaminergic neuronal function in these mutants. With the lack of knowledge regarding this protein it is impossible to develop a hypothesis for which proteins may compensate for its loss. Only RNAseq would be able to identify such compensatory mechanisms.

In addition to the above suggestions, it is well established that SNPs in PD risk genes alter the chance of an individual developing PD, but do not directly cause or prevent the disease. Given this, it was hypothesised that *acmsd*$^{-/-}$ mutant zebrafish larvae would be more likely to develop

dopaminergic alterations in response to an additional trigger. To test this hypothesis, 1-3dpf larval zebrafish were exposed to MPP+, a well-studied PD neurotoxin that has been demonstrated to result in the death of dopaminergic neurons in the DC2 and DC4/5 populations in wildtype zebrafish (Lam et al., 2005). The treatment of wildtype larvae with MPP+ resulted in significant reductions in dopaminergic neuron number, recapitulating the data published in the literature. *acmsd*$^{-/-}$ mutant zebrafish larvae appeared no more or less susceptible to MPP+ than wildtype zebrafish, with both groups demonstrating similar reductions in neuronal numbers. This does not support the hypothesis that an additional PD trigger would have cumulative effects on dopaminergic neurons in these mutants. However, only one additional trigger was assessed during this project. Other factors, such as the intake of caffeine, smoking and exposure to other toxins have been demonstrated to alter PD risk in human and animal models. It is plausible that SNPs in risk genes interact specifically with other risk factors depending on the gene mutated. In a C.*elegans* knockdown model of acsd-1, the orthologue of *acmsd* in worms, mutants were less susceptible to paraquat exposure. They displayed reduced levels of ROS, an increase in activity and improved survival compared to their wildtype counterparts (Katsyuba et al., 2018), suggesting that a lack of Acmsd may indeed alter the sensitivity of zebrafish to PD risk factors. To fully explore this hypothesis, it would be necessary to treat the mutant zebrafish with further stressors.

The death of dopaminergic neurons in the substantia nigra is associated with the activation of microglia in the immediate area (McGeer et al., 1988). Gliosis is a neuropathological feature of many diseases, whereby the activation of glial cells, both macroglia (astrocytes and oligodendrocytes) and microglia, is observed. The presence of gliosis is often used as a readout of more general neuroinflammation. Since Acmsd can be thought of as an anti-inflammatory protein due to its ability to reduce the production of QUIN, a proinflammatory molecule, it was hypothesised that a loss-of-function of Acmsd would result in increased neuroinflammation, mostly likely resulting from increased levels of QUIN. To assess whether a loss of *acmsd* was indeed resulting in neuroinflammation in this zebrafish model, microglial number and activation levels were assessed in the brains of *acmsd*$^{-/-}$ larvae.

Initially this was attempted in sections using L-plastin immunoreactivity, a pan-leukocyte marker, which appeared increased in *acmsd* homozygous mutants compared to their heterozygous and wildtype siblings. It was difficult to make direct comparisons between genotype as obtaining high quality images of comparable brain regions proved difficult, despite the addition of a tyrosine

hydroxylase marker to assist with this. Furthermore, L-plastin has been described as highly expressed in monocytes and T cells in humans (Goldstein et al., 1985), but is not specific to microglia. Whilst this early stage of zebrafish development means that T cells are not yet present, as adaptive immunity is only activated after 3 weeks of age, monocytes other than microglia will also be L-plastin positive, a possible source of invalidity.

To provide a more representative readout of microglial number, neutral red staining of the entire larval brain was used. Whilst enabling visibility of the entire brain in one image, the staining obtained was unreliable, with some larvae staining better than others and some demonstrating no staining at all, even within genotypes. For this reason, quantification of microglial number by counting the neutral red stained dots in the larval brain was also unreliable. Additionally, neutral red acts by accumulating in the lysosomes of cells that directly phagocytose it, which also makes it imperfect for use as a microglia marker. Firstly, the dye will only label cells that are actively phagocytosing material so not all microglia will be labelled as some may be in an inactive, resting state. Secondly, the visible red dots are representative of lysosomes, not of the cell itself, so it is impossible to accurately determine the number of microglia as some cells may have more than one labelled lysosome. Finally, as with L-plastin staining, neutral red is not specific to microglia. The dye will be taken up by any cell able to carry out phagocytosis.

To overcome these issues, 4c4 wholemount immunohistochemistry was used to visualise microglia in the entire brain of fixed larvae at 5dpf. This method was the most reliable and therefore used for quantification. There was no difference in the number or activation level of microglia in the midbrain or forebrain of *acmsd*$^{-/-}$ mutant zebrafish larvae compared to their wildtype siblings. As discussed previously, there are multiple possible reasons for this; a genuine lack of effect of an absence of *acmsd*, 5dpf fish too young to observe a phenotype or the presence of compensatory mechanisms. There is also the possibility of subtle changes in *acmsd* mutant larvae being missed by using this method. A subjective measurement was used for both the counting and the activation of microglia. All microglial analysis was conducted by the same person to reduce issues of interrater reliability and had a difference been found, a second counter would have been used to confirm these changes. However, if changes in the number or activation level were small, a seemingly minor mistake in counting may have resulted in a false negative outcome. Additionally, static cell morphology, whilst offering a relatively quick assessment, may not be the most reliable way of measuring the activation state of microglia. Whilst it is widely accepted that microglia acquire an amoeboid morphology when activated, they

often develop new processes following activation (Stence et al., 2001). By using a binary method (cells with at least one process vs cells with no processes), not all active cells will be identified. Furthermore, by conducting experiments on fixed larvae, it is not possible to distinguish cells in an intermediate state, for example activated cells in the process of retracting their branches. This makes it nearly impossible to accurately determine the number of activated cells based on morphology alone. Thus, a new way of assessing neuroinflammation is desperately needed. The use of molecular markers enables a quantifiable readout of neuroinflammation, although no single marker has so-far been identified to provide such information.

Additionally, there is also a possibility that neuroinflammation is occurring via a mechanism that does not involve microglia. The activation of microglia represents only one part of the phenomenon of gliosis, which extends to other glial cells in the brain. However, oligodendrocytes have not been directly implicated in PD and astrocytes, for which their role in PD is debated, are not present in zebrafish (Liberatore et al., 1999; Qiao et al., 2016; Wu et al., 2002). Therefore, measuring microglial activation seems the most appropriate method of assessing neuroinflammation in zebrafish models.

Given that *acmsd* expression was not identified in the brain of zebrafish at this stage, the lack of a neuroinflammatory phenotype is not so surprising. Whilst there is a possibility that a lack of ACMSD in the periphery is responsible for altering the risk of PD, as discussed above, this is still an untested hypothesis. It would be interesting to assess neuroinflammation in adult *acmsd* mutant zebrafish, a stage when *acmsd* is normally expressed within the brain.

More global inflammation within the whole larvae was also assessed during this project, as peripheral inflammation has also been linked to PD (discussed in main introduction to this thesis). It was hypothesised that a reduction in Acmsd would lead to an increase in inflammation due to the subsequent increase of QUIN and other pro-inflammatory metabolites. qPCR analysis of three commonly studied markers of inflammation (*il-1β*, *mmp9* and *cxcl8*) was unable to find a difference in their expression between *acmsd*$^{-/-}$ mutant larvae and their wildtype siblings, suggesting that a heightened level of basal inflammation was not present in *acmsd* mutants. Transgenic reporter lines were also used to demonstrate this. No obvious difference was seen in neutrophil number / location or the expression of *tnf-α* in *acmsd* mutant larvae compared to their wildtype siblings, although these were not quantifiable due to low quality images. Using confocal microscopy for analysis of the fluorescent neutrophil line would have allowed for the counting of neutrophils within larvae, which may have shown small changes in the mutants.

Previous groups have suggested using spinning disc microscopy to assess neutrophils in this line due their constant movement making imaging difficult (Elks et al., 2011). Due to reduced access to training and the microscope facility during the coronavirus pandemic, such experiments were unable to be conducted as planned. Additionally, this line has been combined with the tailfin transection assay with consistent results (Elks et al., 2011). However, this assay is time consuming and an effect was unlikely given previous data so was not conducted in the present study. It could be interesting to combine these lines with exposure to inflammatory triggers, to assess whether *acmsd*$^{-/-}$ mutant zebrafish respond differently to this, although given their lack of an altered response to saponin, discussed below, this also seems unlikely.

The susceptibility of *acmsd*$^{-/-}$ mutant zebrafish to external inflammation was also assessed as it was hypothesised that a lack of *acmsd* may prime these larvae to react to inflammation in a heightened way. Multiple compounds were tested for use in this assay which are discussed in chapter 6. Saponin was chosen to induce inflammation as it was shown to result in an increase in inflammatory markers as assayed by qPCR (**section 6.2.6.2.2**). The increase in these markers in wildtype fish in this chapter did not reach significance, contrasting that which was found as part of the assay development in chapter 6. However, this likely reflects the power of the two-way ANOVA used for analysis in this chapter, opposed to the one-way ANOVA used during method development. To overcome this, data was also presented as a fold-change in expression following treatment per biological replicate, enabling a better comparison of the response to saponin exposure between genotypes. Importantly, using these readouts, *acmsd* mutant larvae were found to be no more or less susceptible to saponin exposure than wildtype larvae. Whilst this result cannot be generalised to conclude that an absence of *acmsd* does not increase the susceptibility of larval zebrafish to inflammation, this result was disappointing. It is clear that saponin is able to induce an inflammatory state in zebrafish, as was shown here and has been previously reported in the literature (López Nadal et al., 2018). However, whilst saponin is able to induce increases in inflammatory markers following qPCR, the effects of the compound may be specific to the gut. Neutrophil recruitment specifically to the intestines following immersion has been reported in zebrafish larvae (López Nadal et al., 2018), although the role of ingestion from the surrounding media during feeding cannot be ruled out. It would be interesting to challenge the *acmsd*$^{-/-}$ mutant larvae with other inflammation-inducing compounds that are known to act via a different mechanism. Unfortunately, these models could not be established during this project (see chapter 6 for further discussion).

QUIN is a known precursor for NAD+ synthesis in humans (**figure 44**). Therefore, a loss of *acmsd* may result in increased levels of QUIN in *acmsd*$^{-/-}$ mutant zebrafish which may subsequently increase the level of NAD+. To test this hypothesis, the levels of NAD+ and NADH were assessed in the brain tissue of adult *acmsd*$^{-/-}$ mutant zebrafish. Surprisingly, NAD+, NADH and the ratio of NAD:NADH were normal in *acmsd*$^{-/-}$ mutant zebrafish. As discussed in the introduction to this chapter, this expected increase in NAD+ has been seen in other cell and animal models of *acmsd* deficiency (Katsyuba et al., 2018). Why this expected change in NAD+ levels were not seen in *acmsd*$^{-/-}$ mutant zebrafish may be explained by examination of this pathway in humans. QUIN is initially converted to nicotinic acid mononucleotide via quinolinate phosphoribosyl transferase (QPRT) (**figure 44**). BLASTP of the human QPRT protein did not identify a homologue in zebrafish and this was supported by a search in Ensembl. This may explain why there is no change in NAD+ levels, even though QUIN was increased in these mutants. It is possible that another, unknown enzyme is responsible for the conversion of QUIN to NAD+ in zebrafish or that the kynurenine pathway does not lead to the production of NAD+ in zebrafish at all; as discussed in the introduction, this is a source of species variation (a trade-off between the production of a neurotoxic molecule but also a precursor to NAD+) (Palzer et al., 2018). Zebrafish do, however, have nicotinamide mononucleotide adenylyl transferase (NMNAT) and NAD synthetase 1 (NADSYN1) orthologues (**figure 44**) suggesting that NAD+ may be synthesised via the Preiss-Handler pathway in zebrafish, as this is where the pathways merge. If NAD+ production is substantially different in humans and zebrafish, fish may not represent the best model for *acmsd* deficiency as it may not recapitulate what is seen in human PD patients. If *ACMSD*-linked PD is the result of increased levels of QUIN, as is currently the consensus within the field, then this difference in NAD+ pathways may be irrelevant.

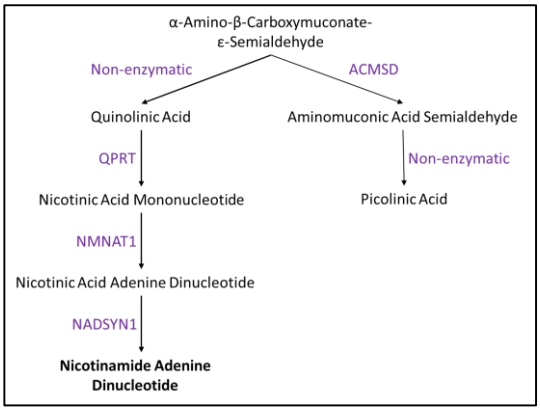

Figure 44. Nicotinamide Adenine Dinucleotide Synthesis from Quinolinic Acid. *Pathway of NAD synthesis via the kynurenine pathway. Enzymes in purple. Original image. ACMSD, α-amino-β-carboxymuconate-ε-semialdehyde decarboxylase; NADSYN1, NAD synthetase 1; NMNAT, nicotinamide mononucleotide adenylyl transferase; QPRT, quinolinate phosphoribosyl transferase.*

As *acmsd* was shown to be almost exclusively expressed in the liver of larval zebrafish and primarily in the liver in adults, a logical question to ask was whether the liver was abnormal in *acmsd*$^{-/-}$ mutant zebrafish. Fabp10a was used as a known liver marker in larval zebrafish, which was visualised using in situ hybridisation. No obvious differences were seen in the liver of *acmsd*$^{-}$

$^{/-}$ mutant zebrafish compared to controls. Liver area was measured using ImageJ software, calculating the area of staining as seen from the left side of the larvae (location of the largest lobe of the liver). Again, no difference was identified between *acmsd*$^{-/-}$ mutant zebrafish and the control larvae, suggesting that an absence of *acmsd* does not affect liver development in zebrafish. It may be more useful to look at liver volume as opposed to liver area, which may not be representative of the full liver and miss key changes occurring in other aspects. Whilst this is more difficult to do from in situ hybridisation stains, fluorescent lines that label the larval liver are available and could be crossed into the *acmsd* background to assess changes in the liver in a more reliable way. However, as demonstrated below with paracetamol, it is possible to detect changes to the size of the liver using this method so the conclusion that the liver is unaffected in larval *acmsd* mutants is likely correct.

To assess the effects of hepatotoxicity in *acmsd*$^{-/-}$ mutant zebrafish, paracetamol was chosen as it had been used extensively in zebrafish to induce liver damage (Cornet et al., 2017; He et al., 2013; M. Kim et al., 2018; Mesens et al., 2015; Nguyen et al., 2017; Yamashita et al., 2019; Zhang et al., 2014). Furthermore, paracetamol had been combined with phenylthiourea without affecting its ability to induce liver damage (M. Kim et al., 2018), which was important in the current study as treated larvae were to be used for in situ hybridisation experiments.

Paracetamol exposure had no effect on the survival of larval zebrafish under 10mM, with effects between 10 and 15mM being inconsistent between replicates. This is in agreement with others who found small effects on survival at 10mM, but large reductions in survival when larvae were immersed in 15mM for 3 days (Nguyen et al., 2017), although exposure in this study was for an additional 24 hours compared to the methodology used here. Importantly, however, no difference in survival was found between *acmsd*$^{-/-}$ mutants and wildtype controls exposed to various concentrations of paracetamol, suggesting that overall paracetamol toxicity was not enhanced in *acmsd* mutants.

Using in situ hybridisation against *fabp10a*, it was clear that exposure to paracetamol from 3-5dpf resulted in a decrease in the liver size of larval zebrafish, in concordance with published data (Cornet et al., 2017; He et al., 2013; M. Kim et al., 2018; Nguyen et al., 2017; Yamashita et al., 2019; Zhang et al., 2019). However, as with survival, *acmsd*$^{-/-}$ mutant zebrafish appeared equally susceptible to this damage, suggesting that a loss of *acmsd* does not make zebrafish more vulnerable to hepatotoxicity. The exposure via constant immersion, however, raises the question as to whether paracetamol was only having an effect on the liver. It may be that damage was

also being caused in other areas resulting in the observed toxicity. To achieve a more local effect, it was also considered to inject paracetamol directly into the yolk due to its close proximity to the larval liver. However, Nguyen et al. (2017) found that using this technique resulted in a reduced overall effect on the liver compared to immersion exposure and so immersion was used as the method of choice for inducing hepatotoxicity, despite its drawbacks.

It would be interesting to evaluate the effects of other hepatotoxic compounds within this line due to their different mechanisms of action. For example, tamoxifen is also commonly used to induce liver damage in zebrafish. Like paracetamol, larvae exposed to tamoxifen by immersion develop signs of hepatotoxicity including a decreased liver size, yolk retention and increased transaminase and lipids in the liver (Yu et al., 2020), ultimately resulting in liver-specific cell death (Nam et al., 2016). However, some groups have reported other toxicities, usually cardiac in nature, to occur in response to tamoxifen, often leading to the death of zebrafish larvae before effects on the liver can be measured (Mesens et al., 2015). Additionally, tamoxifen was shown to increase the expression of inflammatory cytokines (*tnf-α*, *il-1β* and *il-6*) in the whole larvae (Yu et al., 2020), which may add a confounding variable to experiments, particularly in lines like *acmsd*$^{-/-}$ where inflammation was hypothesised to be altered.

This is a common theme for compounds used to induce hepatotoxicity in zebrafish. For example, triptolide, which results in a reduced liver size, yolk retention, necrosis and the appearance of vacuoles in both larval and adult livers (Huo et al., 2019; Vliegenthart et al., 2017), can also induce heart oedema, notochord break, a missing swim bladder and an increase in inflammatory cytokines (Huo et al., 2019; Vliegenthart et al., 2017). Similarly, alcohol-induced liver toxicity also causes more widespread effects, including increased mortality, reduced hatching and a decreased somite number as well as a number of neural and cardiac defects (Cornet et al., 2017; Manjunatha et al., 2021; Zhang et al., 2014). Isoniazid, an anti-tuberculosis drug, has been reported to result in a reduced liver size, yolk retention and possible complete absence of the lateral liver lobes in exposed larvae (Jia et al., 2019; Zhang et al., 2014; Zhang et al., 2019). However, as seen with the other compounds, isoniazid has also been shown to have non-hepatic effects, including increased levels of *tnf-β* and *cox2* as well as an increase in the number of circulating myeloid cells (Zhang et al., 2019). This suggests that isoniazid may also induce widespread inflammation, supported by the finding that the effects of isoniazid are made worse if zebrafish are already challenged by inflammation, such as exposure to LPS (Zhang et al., 2019).

Exposure of zebrafish to monobutyl phthalate (MBP), an environmental pollutant, demonstrates an accumulation of MBP in the liver and subsequent hepatotoxicity including lesions and degeneration of hepatocytes (Jiao et al., 2020; Zhang et al., 2021). These studies suggested a liver-specific effect of exposure, primarily as a result of a decreased protection against oxidative stress due to the decreased expression and activity of antioxidant enzymes (Jiao et al., 2020). However, other studies have identified metabolic effects of MBP in additional areas of the zebrafish (Tao et al., 2020), suggesting that MBP toxicity is not specific to the liver. Similarly, macrolide antibiotics, whilst resulting in necrosis of the liver, changes in liver size, yolk retention and steatosis in zebrafish larvae, have also been shown to alter multiple pathways as identified by genetic analysis (KEGG) (He et al., 2013; Zhang et al., 2020). One pathway altered by exposure to a subset of macrolides was tryptophan metabolism (Zhang et al., 2020), which may be interesting within the context of *acmsd*, which is involved in the catabolism of tryptophan. However, these effects may also make results difficult to interpret in the context of hepatotoxicity.

Overall, it is difficult to select a compound to induce liver toxicity in zebrafish that is entirely specific to the liver without inducing more widespread effects that make data interpretation more difficult. Exposing zebrafish to a number of different hepatotoxic compounds would provide a more complete picture of their susceptibility to liver damage. However, such work is time consuming, particularly if in situ hybridisation is used to assay the effects of exposure.

The overarching hypothesis for the study of *ACMSD* as a risk gene for PD is that a loss of ACMSD function redirects ACMS towards the production of QUIN and away from the production of PIC at the final step in the kynurenine pathway. Since QUIN is a pro-inflammatory and neurotoxic molecule, able to activate microglia and cause direct neuronal excitotoxicity, it is attractive to hypothesise that an increase of this pathway metabolite could lead to neuroinflammation and the death of dopaminergic neurons seen in PD.

Metabolomics data supported this hypothesis by demonstrating a huge increase in QUIN concentration in *acmsd* mutant zebrafish, but the viability and lack of obvious phenotype was surprising if we consider the effect that increased QUIN could have on the brain and other tissues. Further analysis found that whilst the overall concentrations of 3-hydroxykynurenine and kynurenine were reduced, the activity of both branches of the pathway were upregulated (obtained from metabolite ratio data). The neuroprotective pathway (kynurenic acid production) was increased to a greater extent than the canonical pathway, suggesting a compensatory

upregulation of kynurenic acid. Kynurenic acid is an NMDA receptor antagonist, which may protect against QUIN-induced excitotoxicity and explain the lack of phenotype in *acmsd* mutant zebrafish. This conclusion is summarised in **figure 45**.

PIC was not directly measured during this study as it could not be separated from its isomer, nicotinic acid, during method development. However, the increase in QUIN strongly suggested that Acmsd function was indeed reduced in the *acmsd* mutant line, confirming a pathogenic mutation at the protein level. The only other vertebrate model of *ACMSD* deficiency has yet to be published, but a published abstract indicated that in mice, a loss of *ACMSD* at both the RNA and protein level resulted in up to 50X increased QUIN in the liver, kidney, brain and plasma, whilst levels of QPRT and kynurenine-3-monooxygenase were normal (Rajamani et al., 2017).

Kynurenine pathway metabolites in human PD vary by study; some of which mirror that seen in the *acmsd*$^{-/-}$ zebrafish model, some of which contrast it (summarised in **table 18**). Notably, whilst levels of QUIN have been shown to increase with age in the human brain (Heyes et al., 1992; Sorgdrager et al., 2019), these do not appear to be further increased in those with PD (Iwaoka et al., 2020; Sorgdrager et al., 2019). The patients in these studies did not, however, have identified SNPs in *ACMSD* and therefore the *ACMSD*-QUIN hypothesis in PD still remains unanswered. To fully assess this, PD patients identified as having SNPs in *ACMSD* would need to have kynurenine pathway metabolites measured. The protective mechanism against increased QUIN identified in zebrafish may not be present in other animals, so data obtained from this model may not be directly applicable to other models or human PD. In fact, in PD patients, the kynurenic acid:kynurenine ratio has been identified as unchanged or even decreased (**table 18**), although as mentioned above, these patients were not identified as having SNPs in *ACMSD*.

It is also possible that the increased level of QUIN did not have the expected effect in *acmsd* mutants due to the differing composition of the mammalian and zebrafish CNS. The mechanisms of QUIN-induced toxicity may not be fully conserved in the zebrafish.

The primary mechanism of neuronal death following exposure to QUIN is excitotoxicity conferred via NMDA receptors. As discussed in the chapter introduction, QUIN is differentially toxic depending on brain region which may be a result of the subunit composition of NMDA receptors in that area. QUIN is thought to act primarily on NMDA receptors with NR1, NR2A and NR2B subunits (de Carvalho et al., 1996), although this has been questioned by its inability to induce dopamine release from receptors with NR1/NR2B composition (Pittaluga et al., 2001). Zebrafish

NMDA receptors are comprised from the same subunits as those found in mammals, although zebrafish possess two copies of each gene (Cox et al., 2005). Both zebrafish NR1 paralogs are expressed throughout the larval brain, with NR1.1 expression from 24hpf and NR1.2 from 80hpf (Cox et al., 2005; Zoodsma et al., 2020). NR2A, however, is only expressed in the retina of the larval CNS and NR2B, whilst being expressed from 96hpf, does not appear to be expressed within the CNS during development (Cox et al., 2005). The expression of NMDA receptor subunits in adult zebrafish is not yet well determined.

The difference in subunit expression in the zebrafish CNS may explain the lack of excitotoxic effect in *acmsd*$^{-/-}$ mutant zebrafish, despite an increase in QUIN. However, the notion that QUIN is selective for only NR2A and NR2B subunits, which are not expressed in the larval brain, is not a fully accepted theory, possibly being disproved by the lack of effect of QUIN on neurons expressing NR1/NR2B NMDA receptors (Pittaluga et al., 2001). It is also important to consider that NMDA receptors are not only expressed in the CNS (see review by (Bozic & Valdivielso, 2015)). It is possible that QUIN may also have an NMDA receptor-induced excitotoxic effect in the periphery. This has not yet been studied.

As previously discussed, NMDA receptor-induced excitotoxicity is not the only way in which QUIN results in CNS damage. The increased availability of glutamate (Tavares et al., 2005; Tavares et al., 2002; Tavares et al., 2000) can also contribute to an enhanced calcium influx, a mechanism that is not receptor subunit dependent. It would be interesting to assess glutamate levels in *acmsd*$^{-/-}$ mutant zebrafish brains to establish whether this is indeed increased as a result of high levels of QUIN.

Microglial activation, oxidative stress and cytoskeletal disruption are also involved in QUIN-induced neurotoxicity and these processes occur independent of NMDA receptors (discussed in chapter introduction). Whilst the exact mechanisms of these processes are not fully understood, it is likely that at least some of these would be conserved within zebrafish. For example, microglia from larval zebrafish have an almost identical gene expression profile to those from adult mammals (Mazzolini et al., 2020), suggesting that functional processes are likely to be conserved.

Interestingly, kynurenic acid also offers protection from QUIN-induced toxicity via NMDA receptor-independent mechanisms. As an antagonist of all ionotropic glutamate receptors, kynurenic acid may protect against the increase in local glutamate concentrations. Kynurenic acid is also considered anti-oxidative, acting as a free radical scavenger (Lugo-Huitrón et al., 2011),

and can partially prevent QUIN-induced microglial activation, iNOS induction, TNFα release from astrocytes, and cytoskeletal changes in both neurons and astrocytes (Pierozan et al., 2018). Inhibition of the NMDA receptor was unable to prevent these protective effects (Pierozan et al., 2018), confirming that kynurenic acid protection is not only conferred via NMDA receptor antagonism.

Exogenous QUIN exposure in zebrafish does lead to phenotypic changes. In larvae, exposure via constant immersion results in stunted growth, cardiac oedema, seizures and a decreased heartrate (Cassar et al., 2017; Majewski et al., 2018). These data may not recapitulate the endogenous increased QUIN in *acmsd*$^{-/-}$ mutants since immersion exposure likely increases QUIN in the whole larvae rather than only in areas where the kynurenine pathway is active. However, in adult zebrafish, direct injection of QUIN into the telencephalon resulted in local cell death and microglial recruitment (Skaggs et al., 2014). Defects in swimming were also seen (Skaggs et al., 2014). These studies demonstrate that zebrafish are sensitive to QUIN, suggesting that high levels of QUIN, as demonstrated throughout life in *acmsd*$^{-/-}$ mutant zebrafish, would likely result in negative effects in the absence of additional protective mechanisms. This further supports the hypothesis that the increased activity of the neuroprotective branch of the kynurenine pathway may protect *acmsd*$^{-/-}$ mutants against toxic levels of QUIN.

Table 18. Summary of Altered Kynurenine Pathway Metabolites from Human Patients with Parkinson's Disease.

Sample and Reference	Tryptophan	Kynurenine	Kynurenic Acid	3-hydroxykynurenine	Quinolinic Acid	Kynurenic Acid/Kynurenine	3-hydroxykynurenine /Kynurenine
This thesis							
Adult zebrafish liver		↓	↔	↔	↑	↑	↑
Adult zebrafish brain		?	?	↔	↑	?	?
Whole zebrafish larvae		?	?	↔	↑	?	?
Serum							
Widner et al. (2002)	↓	↓					
Schulte et al. (2016)	↔	↔					
Han et al. (2017)	↓	↓		↑			
Oxenkrug et al. (2017)	↓	↑	↑				
Havelund et al. (2017)	↔	↔	↓*	↔		↔	↔↑*
Sorgdrager et al. (2019)	↓	↔	↓	↔	↔		
Heilman et al. (2020)	↔	↔	↔	↑	↔		
Klatt et al. (2021)		↓		↑			
Urine							
Luan et al. (2015)	↑	↑					
CSF							
Lewitt et al. (2013)				↑			
Havelund et al. (2017)	↔	↔	↔	↔		↔	↔↑*
Sorgdrager et al. (2019)	↔	↔	↓	↔	↔		
Iwaoka et al. (2020)	↔	↑	↔	↑	↔	↓	↑
Heilman et al. (2020)	↔	↔	↓	↔	↔	↓	
Brain							
Ogawa et al. (1992)		↓	↓	↑		↔	

*Changes in kynurenine pathway metabolites measured in human patients with Parkinson's disease as well as those measured as part of this thesis. Arrows represent changes from controls. * in this study, changes were only identified in patients on L-DOPA treatment who displayed signs of dyskinesia.*

The primary reason for studying PD risk genes is to better understand the pathology behind these genetic alterations to enable the development of more targeted, personalised medicine approaches. Pharmacological modulation of the kynurenine pathway has been suggested to have potential for PD treatment. The current zebrafish model suggests that an increase in kynurenic acid may have a therapeutic potential in PD cases where QUIN is increased. Indeed, kynurenic acid has been shown to reduce MPP+ toxicity in a human cell line (Lee et al., 2008), protect against QUIN damage to dopaminergic neurons in rats (Miranda et al., 1997) and reduce PD-like motor symptoms in primates exposed to MPTP (Graham et al., 1990). For this to be beneficial, kynurenic acid must be injected into the brain since it cannot cross the BBB, making it inappropriate as a real-world treatment strategy.

However, inhibiting the 3-hydroxykinurenine branch of the pathway could lead to subsequent increases in kynurenic acid as a secondary effect. Inhibition of kynurenine-3-monooxygenase using Ro-61-8048 or nicotinyalanine has been shown to result in increases in kynurenic acid in the brain and blood of rats and primates, protecting against the toxic effects of QUIN (Grégoire et al., 2008; Miranda et al., 1997). However, such modulation of the pathway in humans could result in decreased levels of QUIN and, therefore, NAD+. As discussed previously, humans rely less on this pathway for NAD+ production than other animals, although reducing the levels of all downstream kynurenine metabolites via the inhibition of kynurenine-3-monooxygenase would need careful consideration before its use in human disease.

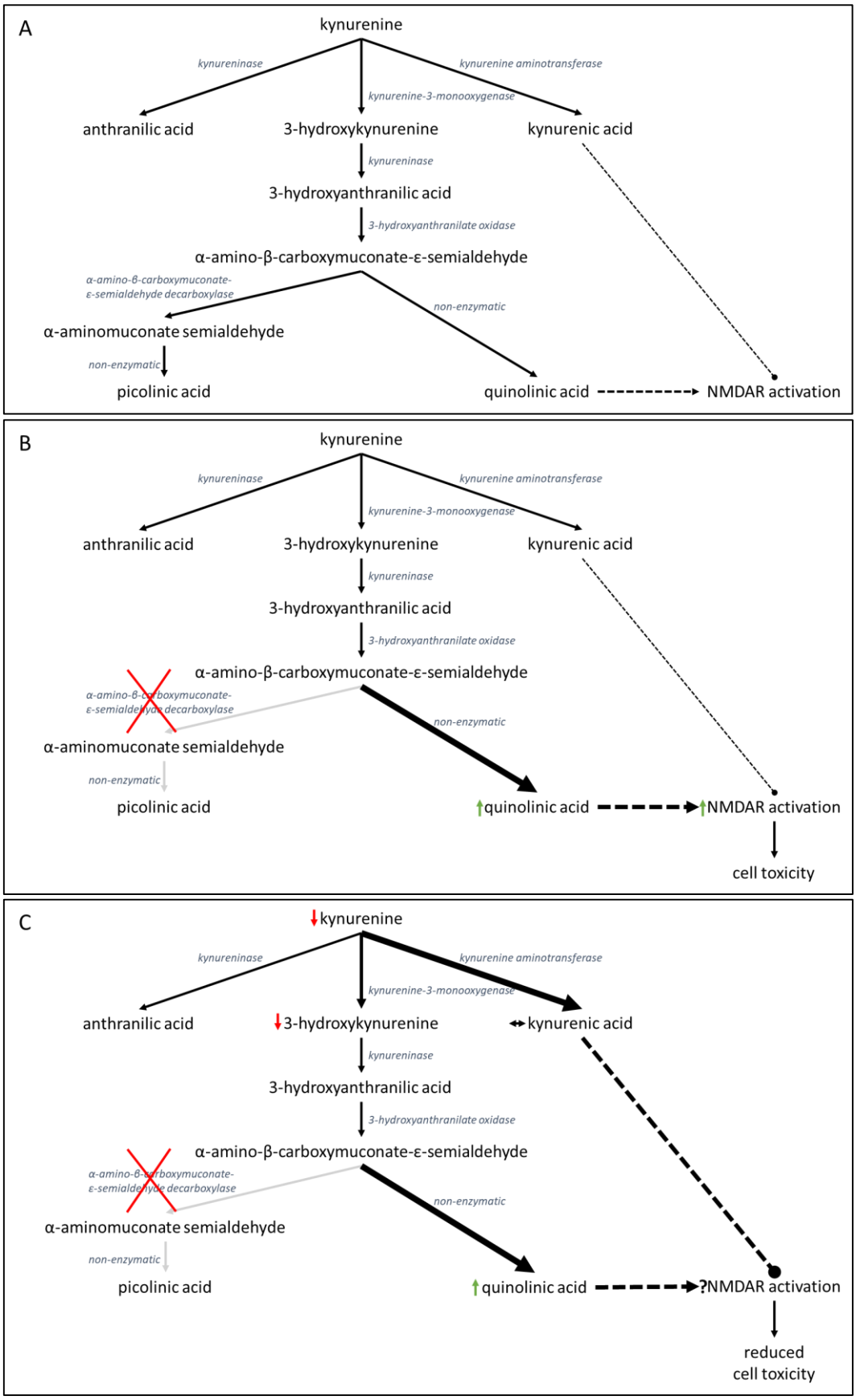

Figure 45. Summary of Kynurenine Pathway Metabolite Changes in α-Amino-β-Carboxymuconate-ε-Semialdehyde Decarboxylase Mutant Zebrafish. A. *The basic overall kynurenine pathway.* ***B.*** *Initial hypothesised result of a reduction in acmsd activity.* ***C.*** *Findings identified from metabolomics data. Green arrows show increases in metabolites in acmsd$^{-/-}$ mutant zebrafish compared to wildtype, red arrows show decreases. Arrow thickness represents enzyme activity. Round headed arrow depicts inhibition of target receptor. Original images.*

4.4 Conclusion

It is easy to hypothesise how a dysfunction of ACMSD may lead to vulnerability in the CNS; a decrease in activity would result in the build-up of neurotoxic QUIN and an increase in activity would result in a decrease of available NAD+. Zebrafish express a single orthologue of human *ACMSD*, which has been associated with altering the risk of a person developing PD. A loss-of-function *acmsd* mutant zebrafish was successfully created that demonstrated nonsense-mediated decay of mRNA at both the larval and adult stages, resulting in huge increases of toxic QUIN. Despite this, homozygous mutant zebrafish were indistinguishable from wildtype in all areas assessed during this project, even when the biological system was under stress.

Metabolomics suggested that this lack of phenotype may be explained by the compensatory upregulation neuroprotective kynurenic acid via increased kynurenine-3-monoxygenase activity. The upregulation of this enzyme in zebrafish, as well as the uncoupling to the NAD+ synthesis pathway, represents a key functional divergence from humans, which may have implications for applying results from this *in vivo* model to disease processes in humans. However, these findings support the literature in suggesting modulation of the pathway as a treatment option for PD.

The generation of this zebrafish represents the first vertebrate loss-of-function *acmsd* mutant, which has now been comprehensively characterised as a part of this thesis. Although no phenotype was identified, the system is now established for further experiments, including additional stressors or assessment of gene-gene interaction between PD risk genes.

5 Leucine-Rich Repeat Kinase 2 and Parkinson's Disease

5.1 Introduction

Leucine-rich repeat kinase 2 (*LRRK2*), also known as Dardarin, was identified as the gene responsible for PARK8-linked cases of autosomal dominant PD in 2004 and is now recognised as the most common Mendelian inherited, monogenic PD gene (Paisán-Ruíz et al., 2004; Zimprich et al., 2004). LRRK2 itself is an enzyme that possesses both kinase and GTPase activity, whilst also acting as a scaffolding protein (Li et al., 2007). It is primarily expressed in the lungs and kidneys, although lower levels have also been identified in the brain, and to an even lesser extent in the spleen and other tissues (Biskup et al., 2007; Li et al., 2007).

Within the brain itself, LRRK2 is observed in the cerebral cortex, amygdala, hippocampus, cerebellum, striatum and ventral tegmental area of mice, where expression levels appear to increase over time (Li et al., 2007; Melrose et al., 2007). Expression in the human brain is less well defined, but LRRK2 has been identified in the caudate and putamen (Galter et al., 2006; Higashi et al., 2007) as well as the cerebral cortex (Higashi et al., 2007). Of particular interest, *LRRK2* expression has been shown in the dopaminergic neurons of the substantia nigra in both mouse (Li et al., 2007; Melrose et al., 2007) and human (Greggio et al., 2006; Higashi et al., 2007) research; however, this is disputed amongst research groups where this was shown not to be the case (Galter et al., 2006), but where expression was identified in dopamine-receptive areas of the brain.

On a cellular level, LRRK2 is largely found in the cytoplasm but can also be seen on the cytosolic side of various cellular and organelle membranes (Biskup et al., 2006; Greggio et al., 2006; Li et al., 2007; West et al., 2005). Whilst the majority report *LRRK2* expression on the outer mitochondrial membrane (Biskup et al., 2006; West et al., 2005), some suggest it is not expressed in mitochondria as it does not co-localise with MitoTracker (Greggio et al., 2006). This may be due to the sub-organelle localisation of this marker, which is primarily inside, rather than at the membrane of, the mitochondrion.

LRRK2 forms a homodimer where cross phosphorylation at sites found in the activation loop is required for kinase activation (Luzón-Toro et al., 2007; West et al., 2007). The kinase and GTPase activities of LRRK2 can be linked; the kinase activity of LRRK2 is increased in the presence of GTP (Ito et al., 2007; West et al., 2007). Since GTPase activity converts GTP to GDP, a negative relationship between the activity of these two distinct domains is established. This relationship

is only maintained intracellularly and not seen with isolated LRRK2 in the presence of GTP (West et al., 2007), suggesting the involvement of other cofactors. This is imperative to remember when choosing models to study LRRK2 function, with *in vivo* models having a distinct advantage.

LRRK2 is implicated in many basic functions in the CNS including neurite outgrowth, cytoskeletal function, autophagy, phagocytosis and synaptic vesicle exocytosis (Alegre-Abarrategui et al., 2009; Gillardon, 2009; K. S. Kim et al., 2018; MacLeod et al., 2006; Parisiadou et al., 2009; Piccoli et al., 2011). Interestingly, LRRK2 isolated from brain tissue has been shown to have increased kinase and GTPase activity compared to that isolated from other tissues (Li et al., 2007), indicative of a more essential role in the CNS than elsewhere in the body. Co-immunoprecipitation studies suggest that LRRK2 directly interacts with other important PD-related proteins in the brain, including α-synuclein (Guerreiro et al., 2013) and parkin (Smith et al., 2005). However, despite the interaction between LRRK2 and α-synuclein, LRRK2 was shown not to phosphorylate it (Li et al., 2007), suggesting a separate purpose of this interaction.

Seven mutations in *LRRK2* (N1437H, R1441C, R1441G, R1441H, Y1699C, G2019S and I2020T) have so-far been confirmed as pathogenic causes of PD (Aasly et al., 2010; Di Fonzo et al., 2005; Nichols et al., 2005; Paisán-Ruíz et al., 2004; Zimprich et al., 2004). The majority of these result in gain-of-function mutations, usually increasing LRRK2 activity directly, by increasing kinase activity, or indirectly, by inhibiting GTPase activity; although the literature on the exact effect of each mutation is inconsistent (**table 19**).

In addition to its role in familial PD, *LRRK2* is also considered a PD risk gene (Chang et al., 2017; Nalls et al., 2019; Nalls et al., 2014), with 1-5% of sporadic PD patients identified as carrying *LRRK2* point mutations (Healy et al., 2008). By 2011, 121 exonic point mutations in *LRRK2* had been identified, although many of these were considered extremely rare (Ross et al., 2011). As with pathogenic *LRRK2* mutations identified in familial PD cases, the majority of SNPs at the *LRRK2* locus are predicted to result in increased LRRK2 function. Indeed, the most significant SNP, rs76904798 ($p=1.52\times10^{-28}$, (Nalls et al., 2019)), likely results in increased levels of *LRRK2* mRNA despite occurring at an intronic region (Ryan et al., 2017). Likewise, some SNPs in *LRRK2*, such as R1398H, which acts to reduce kinase activity (Nixon-Abell et al., 2016; Tan et al., 2010), are thought to be protective, reducing the overall risk of developing PD (Chen et al., 2011; Heckman et al., 2014).

Table 19. Mutations in Leucine-Rich Repeat Kinase 2 That Result in Monogenic Parkinson's Disease.

Mutation	Consequence of Mutation on LRRK2	Reference
N1437H	Decreased GTP binding affinity; Decreased GTPase activity	Huang et al. (2019)
	Increased kinase activity	Sheng et al. (2012)
R1441C	Increased kinase activity	West et al. (2005)
	Increased kinase activity	West et al. (2007)
	Increased kinase activity	Sheng et al. (2012)
	No change in kinase activity	Jaleel et al. (2007)
	Formation of cytoplasmic inclusion bodies and cellular toxicity, both dependent on kinase activity	Greggio et al. (2006)
	Increased GTP binding capabilities	West et al. (2007)
	Increased GTPase activity	Li et al. (2007)
R1441G	No change in kinase activity	Jaleel et al. (2007)
	Increased kinase activity; Increased GTP binding capabilities	West et al. (2007)
	Increased kinase activity; Increased ubiquitination	Zhao et al. (2015)
	Increased kinase activity	Sheng et al. (2012)
	Increased GTPase activity	Li et al. (2007)
R1441H	Reduced GTPase activity; Increased GTP affinity	Liao et al. (2014)
Y1699C	No change in kinase activity	Jaleel et al. (2007)
	No change in kinase activity	Luzón-Toro et al. (2007)
	Formation of cytoplasmic inclusion bodies and cellular toxicity, both dependent on kinase activity	Greggio et al. (2006)
	Increased GTP binding capabilities; Increased kinase activity; Increased neuronal toxicity; Increased susceptibility to hydrogen peroxide / oxidative stress	West et al. (2007)
	Increased kinase activity; Increased ubiquitination	Zhao et al. (2015)
G2019S	Increased kinase activity	West et al. (2005)
	Increased kinase activity	Sheng et al. (2012)
	Increased kinase activity	Luzón-Toro et al. (2007)
	Formation of cytoplasmic inclusion bodies, dependent on kinase activity	Greggio et al. (2006)
	No change in GTP binding capabilities; Increased kinase activity; Increased neuronal toxicity; Increased susceptibility to hydrogen peroxide / oxidative stress	West et al. (2007)
I2020T	Reduced kinase activity	Jaleel et al. (2007)
	Increased kinase activity	Sheng et al. (2012)
	Increased kinase activity	Gloeckner et al. (2006)
	No change in kinase activity	Luzón-Toro et al. (2007)
	Formation of cytoplasmic inclusion bodies, dependent on kinase activity	Greggio et al. (2006)
	No change in GTP binding capabilities; Increased kinase activity; Increased neuronal toxicity; Increased susceptibility to hydrogen peroxide / oxidative stress	West et al. (2007)
	Increased ubiquitination	Zhao et al. (2015)

Pathogenic mutations in leucine-rich repeat kinase 2 that have been shown to cause Parkinson's disease and the predicted effects of these mutations on the protein itself. GDP, guanosine diphosphate; GTP, guanosine triphosphate; LRRK2, leucine-rich repeat kinase 2.

Whilst most *LRRK2* SNPs and mutations that lead to PD likely result from an overall increase in kinase activity, this is not the case for them all. This alludes to a "homeostatic hypothesis" surrounding LRRK2, suggesting that dysfunction (either a gain or loss in activity) alters the risk of PD.

G2019S, a substitution of glycine for serine in the kinase domain of LRRK2, is the most common single genetic cause of PD. G2019S results in a gain-of-function mutation, whereby increased kinase activity (**table 19**) is conferred to LRRK2 via the addition of a novel autophosphorylation site and the continuous partial accessibility of an existing activation site, suggested to result from the increased size of serine compared to glycine (Kachergus et al., 2005; Luzón-Toro et al., 2007). This mutation has been linked to reduced striatal dopamine levels (Tozzi et al., 2018), increased neuronal toxicity (West et al., 2007) and decreased release of dopamine from striatal projection neurons, despite maintaining excitability (Xenias et al., 2020). However, there is a discrepancy between models, as younger mice harbouring this mutation show increased levels of dopamine (Volta et al., 2017). This could suggest an effect of age; PD is a disease of ageing and it is possible that such genetic alterations do not have their effects in model systems at a young age in the same way that symptoms are not apparent in humans until later in life, even in patients with defined causative PD mutations.

G2019S has been identified in 4% of familial PD cases, as well as in 1.6% of sporadic cases (Gilks et al., 2005). Some literature refers to these cases as "seemingly sporadic" as their sporadic nature may be due to the incomplete penetrance of the mutation, which is, on average, just 30% (Marder et al., 2015). G2019S has a penetrance that is age-, sex- and population-dependent, with ethnicity contributing the most to this inconsistency. G2019S accounts for 13.3% of PD cases in Ashkenazi Jews (Ozelius et al., 2006), 40.8% of cases in North African Arabs (Lesage et al., 2006), but only 0.7% of cases in the Russian population (Illarioshkin et al., 2007). This mutation is also more likely to affect women than men and, like most PD mutations, is more likely to be symptomatic in people over 60 years old (Kumari & Tan, 2009). Other mutations in *LRRK2* also demonstrate incomplete penetrance (Gosal et al., 2007; Ruiz-Martínez et al., 2010), which makes genetic data more difficult to interpret. However, there is no doubt that, even where mutations do not invariably lead to PD, certain missense alterations in *LRRK2* do have an impact on the risk of developing the disease.

LRRK2-associated PD is well documented to be a pleomorphic disease with a heterogeneous pathology (Zimprich et al., 2004). At the cellular level, pathological changes vary between

patients but are usually characteristic of sporadic PD, even when clearly identified as monogenic familial cases. For example, as with most sporadic cases, the primary site of dopaminergic neuronal damage in *LRRK2*-associated disease is the putamen and not the caudate nucleus usually seen in familial PD (Adams et al., 2005). Whilst the typical signs of PD are seen in the substantia nigra, namely the loss of dopamine and the death of dopaminergic neurons (Adams et al., 2005; Kalia et al., 2015; Takanashi et al., 2018), only half of PD patients with *LRRK2* mutations have been shown to have Lewy Body disease from post mortem brain analysis (Kalia et al., 2015), a sign that used to be required for a definitive PD diagnosis. Similar data was obtained from PET scans of patients with familial G2019S-linked PD (Adams et al., 2005). Whilst all seven participants had dopaminergic neuronal loss and gliosis in the substantia nigra, only two presented with Lewy Body pathology, of which one of these was isolated to the brainstem. Neurofibrillary tangles also represented an area of inconsistency between patients, with three demonstrating this pathology and four not.

Despite LRRK2-associated PD somewhat mimicking sporadic PD at a cellular level, at a clinical level *LRRK2* mutation carriers demonstrate differences to both sporadic and other monogenic cases of disease. Patients are more likely to experience tremor than those with sporadic PD and are less likely to suffer cognitive deficits or a loss of smell (Healy et al., 2008). Patients identified as *LRRK2* SNP carriers respond well to L-DOPA treatment, which is often required at a later stage compared to other subclasses of sporadic PD (Healy et al., 2008; Paisán-Ruíz et al., 2004; Puschmann et al., 2012; Zimprich et al., 2004). Furthermore, those treated with L-DOPA appear less likely to develop dyskinesia as a result of treatment (Healy et al., 2008).

As well as its relationship to PD as both a causative and risk gene, *LRRK2* can also be implicated in inflammation, creating a plausible hypothesis of how *LRRK2* may result in the disease phenotype; *LRRK2* SNPs may contribute to an inflammatory state in the CNS, which leads to the secondary development of PD symptoms.

LRRK2 expression has been demonstrated in immune cells. Although disagreement exists between research groups, *LRRK2* expression has been shown in B cells, CD14+ monocytes, T cells, microglia and astrocytes (Gardet et al., 2010; Hakimi et al., 2011; Miklossy et al., 2006; Moehle et al., 2012; Thévenet et al., 2011). Variations in expression data likely reflect differences between mRNA and protein levels as a result of post transcriptional regulation, as well as the possibility of inter-cellular transportation of LRRK2 protein. Additionally, multiple antibodies have been used by different research groups examining protein expression, creating a variable

that might result in unreliable data sets. Nevertheless, it is interesting to note that PD patients exhibit increased *LRRK2* expression in B cells, T cells, CD14+ monocytes and CD16+ monocytes compared to healthy controls (Bliederhaeuser et al., 2016; Cook et al., 2017).

The expression of *LRRK2* in these cells is increased during inflammation, strongly implicating *LRRK2* as a regulator of the inflammatory response. This has been intensely studied using the inflammation-inducing molecule IFN-γ. IFN-γ increases *LRRK2* mRNA and/or protein levels in monocytes, macrophages, T cells and B cells (Gardet et al., 2010; Kuss et al., 2014; Thévenet et al., 2011). Additionally, cell based models have shown other proinflammatory molecules, namely IFN-β, TNF-α and IL-6, to also increase *LRRK2* expression (Thévenet et al., 2011), although other cell models found TNF-α to have no effect (Gardet et al., 2010). Additionally, LPS, known to activate microglia, has also been shown to induce the expression of *LRRK2* in these cells (Moehle et al., 2012). However, in peripheral blood mononuclear cells, LPS actually resulted in a decreased expression of *LRRK2* (Thévenet et al., 2011).

Aside from expression data, LRRK2 can also be mechanistically linked to inflammation. The above mentioned increase in LRRK2 has been implicated in the intrinsic activation of immune cells. As monocytes mature from $CD14^{+}/CD16^{-}$ to $CD14^{+}/CD16^{+}$ cells, levels of LRRK2 increase and this maturation process can be prevented by pharmacologically inhibiting the kinase activity of LRRK2 (Thévenet et al., 2011), demonstrating its vital role in this process. In microglia, a knockdown of *LRRK2*, or its inhibition using small molecules, reduces the number of proinflammatory mediators, including IL-6, IL-1β, NO and TNF-α, expressed in response to LPS, as well as reducing the levels of iNOS (Kim et al., 2012; Moehle et al., 2012). Additionally, *in vitro*, microglia expressing a common mutant form of LRRK2 found in PD (R1441G) secrete more proinflammatory cytokines in response to LPS than control cells (Gillardon et al., 2012). Such data suggest that LRRK2 is required for the full response of microglia to immune insults. Indeed, transcriptome analysis of microglia activated using LPS or α-synuclein found that, although a knockout of *LRRK2* had little effect under basal conditions, microglia lacking LRRK2 demonstrated a reduced inflammatory phenotype, including less oxidative stress, in response to proinflammatory signals, most likely via alterations to the endolysosomal pathway (Russo et al., 2019).

Interestingly, LRRK2 has been shown to activate NFκB pathways, resulting in the expression of proinflammatory mediators, independent of kinase activity (Gardet et al., 2010). Therefore, even *LRRK2* mutations that result in decreased kinase activity may still be able to activate this pathway

and initiate neuroinflammation. This could, in part, explain the homeostatic hypothesis, whereby LRRK2 dysfunction, even if a loss of function, can result in PD.

This mechanistic link of increased LRRK2 activity resulting in inflammation is supported by animal models of the G2019S mutation. Rats or mice harbouring this *Lrrk2* mutation demonstrate increased activation of microglia and astrocytes in response to either LPS or an overexpression of α-synuclein compared to their wildtype littermates (Daher et al., 2015; Kozina et al., 2018; Lin et al., 2009; Schildt et al., 2019). This is further supported by *Lrrk2* knockout studies which prevent LPS or α-synuclein-induced neurodegeneration and neuroinflammation (Daher et al., 2014). Interestingly, the gliosis and neurodegeneration in the substantia nigra of the rat model in response to α-synuclein was abolished when the kinase activity of LRRK2 was inhibited (Daher et al., 2015). The neuroinflammation resulting from *Lrrk2* mutations has been suggested to be a consequence of increased LRRK2 activity in the periphery rather than the CNS, with the inflammatory state of the brain a secondary effect of this (Kozina et al., 2018).

To further link *LRRK2*-related PD to inflammation, proinflammatory cytokines have been found in the blood of PD patients carrying the G2019S mutation, even if they were asymptomatic (Dzamko et al., 2016). Furthermore, SNPs in *LRRK2* have also been found in other inflammatory diseases, where 17 loci overlap between PD and inflammatory diseases, including type 1 diabetes, Crohn's disease, ulcerative colitis, rheumatoid arthritis, celiac disease, psoriasis and multiple sclerosis (Witoelar et al., 2017). This is substantiated by multiple studies linking SNPs in *LRRK2* to the susceptibility of inflammatory diseases, including Crohn's disease, colitis, Leprosy, and cancer (Agalliu et al., 2015; Hui et al., 2018; Liu et al., 2015; Umeno et al., 2011; Younis et al., 2020; Zhang et al., 2009). In the periphery, LRRK2 has also been associated with the immune system where it appears to be protective against infections such as Listeria (Zhang et al., 2015) and Salmonella (Gardet et al., 2010; Shutinoski et al., 2019).

The above data suggest that mutations in *LRRK2* may enhance the immune response when inflammation is already present, such as during an infection. LRRK2 kinase activity appears to be required for the activation of immune cells, in particular those of monocyte origin, supporting the hypothesis that increased activity as a result of mutations or SNPs in *LRRK2* may result in detrimental levels of neuroinflammation during conditions where immune cells would normally act in a protective manner. This enhanced neuroinflammation may increase the susceptibility of developing PD by resulting in the death of dopaminergic neurons.

Currently used animal models of LRRK2 function are lacking. Drosophila and C.*elegans* models, whilst plentiful, must be carefully interpreted since neither of these have a true *LRRK2* orthologue. Mice, however, have proven a useful model regarding LRRK2. Knockout mouse models are able to recapitulate PD pathogenesis at the cellular level in the kidney, although were unable to demonstrate such changes in the brain (Hinkle et al., 2012). It has also been possible to induce the G2019S point mutation in transgenic mouse models, resulting in a hyperkinetic phenotype and less motor symptoms associated with the normal ageing process (Longo et al., 2014). However, this opposes what is usually seen in PD, where the primary motor symptom is bradykinesia. It is important to consider the differences between mouse and human LRRK2; the mouse protein is more stable, has less kinase activity, shows increased substrate binding and has higher expression levels under basal conditions (Langston et al., 2019).

In zebrafish, many groups have attempted to study Lrrk2 using a variety of approaches (discussed later in the chapter). Each model used has its drawbacks and data from different publications about the role of this protein in zebrafish appear contradictory. The relatively small toolbox available to reliably study Lrrk2 has meant that study of wildtype function is scarce. Since this protein is evolutionarily conserved and expressed throughout the human body, it is likely that LRRK2 has an important role across species.

5.1.1 Leucine-Rich Repeat Kinase 1

Leucine-Rich Repeat Kinase 1 (*LRRK1*) is the single paralogue of *LRRK2,* both of which evolved from a common ancestral gene (Marín, 2006). This was initially thought to be gene duplication (Marín, 2006), but was later discovered to be a more complex genetic event whereby three *LRRK* genes present in early organisms were lost in different branches of evolution; leaving deuterostomes with *LRRK1*/2 and protostomes with a single *LRRK* that differs from both deuterostome paralogues (Marín, 2008).

Structurally, both LRRK paralogues are very similar, with LRRK1 possessing five of the seven functional protein domains present in LRRK2 (Sejwal et al., 2017). However, differences between the proteins exist in the N and C terminals, where armadillo repeats and a WD40 domain present in LRRK2 are absent from LRRK1 (Civiero et al., 2012; Sejwal et al., 2017). Although the proteins are predicted to share only 26% identity and 45% similarity (Greggio et al., 2007), the important kinase domain is suggested to be 30-50% identical and 50-71% similar in its amino acid sequence, varying by publication (Civiero et al., 2012; Sejwal et al., 2017; Taylor et al., 2007).

Like LRRK2, LRRK1 also belongs to the ROCO family of proteins, possessing functional kinase and GTPase domains (Korr et al., 2006). Both proteins appear to have similar affinities for GTP (Civiero et al., 2012; Sejwal et al., 2017) and, as with LRRK2, the binding of GTP to the ROC domain increases LRRK1 kinase activity (Korr et al., 2006). Likewise, LRRK1 mutants unable to bind GTP demonstrate decreased kinase activity (Hanafusa et al., 2011).

Expression patterns of the *LRRK* paralogues largely overlap, but the levels of each vary and their profiles appear to diverge during adulthood. Throughout murine development, *Lrrk1* has similar but slightly more widespread expression than *Lrrk2* (Giesert et al., 2013). However, *Lrrk1* mRNA levels peak at E15.5 and later decline, remaining relatively low in the adult mouse, particularly in comparison to *Lrrk2* (Biskup et al., 2007; Giesert et al., 2013) although in some areas, namely the liver and gut, *Lrrk1* expression appears higher than *Lrrk2* throughout adulthood (Biskup et al., 2007). In humans, *LRRK1* expression is also described as ubiquitous and widespread (Korr et al., 2006). Very little data exists thus far for zebrafish *lrrk1*, although its expression during embryonic development has been demonstrated using in situ hybridisation (Suzzi, 2017; Suzzi et al., 2021). Expression was described as transient and tissue restricted, but included staining in the prechordal plate, polster, sensory organs and the proctodeum.

Within the brain, *LRRK1* expression has been confirmed in mice (Biskup et al., 2007; Giesert et al., 2013; Taylor et al., 2007), rats (Westerlund et al., 2008) and humans (Biskup et al., 2007; Greggio et al., 2007; Korr et al., 2006), but remains far lower than that of *LRRK2* (Biskup et al., 2007). In the human brain, *LRRK1,* as demonstrated with *LRRK2,* is most highly expressed in the frontal cortex (Greggio et al., 2007). However, in the adult mouse brain *Lrrk1* is expressed only in the olfactory bulb, which, interestingly, is the sole region devoid of *Lrrk2* (Giesert et al., 2013). When analysing brain tissue, *LRRK1* appears restricted to the deep cell layers, in contrast to the diffuse expression of *LRRK2* (Westerlund et al., 2008). The expression of *lrrk1* in the zebrafish brain remains inconclusive. *lrrk1* mRNA has been identified in the telencephalon and ventral hindbrain at 24hpf, but its expression throughout the CNS appears to be transient and absent after this time point (Suzzi, 2017; Suzzi et al., 2021). In adults, whilst qPCR data suggests *lrrk1* is expressed in the brain, in situ hybridization in adult brain sections was unable to confirm this (Suzzi, 2017).

At the cellular level, LRRK1 is a cytoplasmic protein (Greggio et al., 2007; Korr et al., 2006), existing primarily as anti-parallel homodimers (Civiero et al., 2012; Klein et al., 2009; Sejwal et al., 2017). These dimers have been shown to undergo autophosphorylation (Greggio et al., 2007;

Korr et al., 2006), although this has been debated using pure protein preparations (Civiero et al., 2012). Given the important role of autophosphorylation in LRRK2 regulation, it is highly plausible that LRRK1 is indeed also phosphorylated by other LRRK1 proteins. The tertiary and quaternary structures of the LRRK paralogues are very similar, except for the smaller size of LRRK1 and its subsequently narrower binding pocket (Civiero et al., 2012; Sejwal et al., 2017). Despite this similarity, autophosphorylation assays have suggested that the LRRK1 protein may not be as enzymatically active as LRRK2 (Greggio et al., 2007). Interestingly, both LRRK paralogues have been shown to interact *in vitro* (Dachsel et al., 2010; Klein et al., 2009), which may have functional implications where their expression overlaps, such as during early development.

Functionally, LRRK1 has been shown to promote cell proliferation (Harada et al., 2005), regulate exocytosis (Wang et al., 2018) and play a role in the cell stress response pathway, acting as part of the BCR-ABL1 network (Titz et al., 2010). Additionally, LRRK1 acts in the endolysosomal pathway, in particular during autophagosome-lysosome fusion (Toyofuku et al., 2015). Its role in this pathway has primarily been described for EGF signalling, where LRRK1, via interactions with GRB2, ensures proper endosomal trafficking of EGFR (Hanafusa et al., 2011; Ishikawa et al., 2012). Furthermore, *Lrrk1* knockout mice develop lysosomal dysfunction (Toyofuku et al., 2015), supporting an important role for LRRK1 in this pathway.

Functional enrichment analysis suggests that LRRK1 is also likely involved in neurogenesis, cell development and neuron projection development (Tomkins et al., 2018). The role of LRRK1 in the nervous system is supported by Onishi et al. (2020), who identified that LRRK1 is crucial to axon pathfinding. LRRK1 acts as a scaffolding protein within the growth cone, bringing additional kinases into close proximity of Frizzled3 at the plasma membrane, a requirement for correct pathfinding in a Wnt gradient (Onishi et al., 2020). The group created three knockout mouse lines using CRISPR-Cas9; *Lrrk1*$^{-/-}$, *Lrrk2*$^{-/-}$ *and Lrrk1/2*$^{-/-}$. All three mouse lines demonstrated disorganised pathfinding of spinal cord commissural axons and midbrain dopaminergic neurons during development. A loss of both *Lrrk* paralogues resulted in a more severe phenotype than either single knockout, although the loss of *Lrrk2* appeared more detrimental than *Lrrk1*. Interestingly, G2019S mutants had a similar phenotype, suggesting that a dysregulation, rather than a loss, of *Lrrk* is responsible for the dysregulated pathfinding phenotype.

However, the most commonly reported function of LRRK1 is within osteoclasts. Mice carrying homozygous knockout mutations of *Lrrk1* have a shorter body length due to decreased bone length and develop osteopetrosis, although heterozygotes remain unaffected (Brommage et al.,

2014; Xing et al., 2013). To study this phenotype further, osteoclasts from *Lrrk1* knockout mice have been studied ex vivo and found to possess a disrupted cytoskeletal arrangement, including the dephosphorylation of L-plastin (Si et al., 2018). *In vitro* research has also discovered that INO4, a compound that prevents the binding of ATP to LRRK1, disrupts the function of osteoclasts (Si et al., 2019).

Pathologically, multiple mutations in *LRRK1* have been directly linked to osteosclerotic metaphyseal dysplasia (Guo et al., 2017; Howaldt et al., 2020; Iida et al., 2016; Miryounesi et al., 2020), a disease primarily affecting the bones but also resulting in developmental delay, hypotonia and spastic paraplegia (Nishimura & Kozlowski, 1993). This complements data from knockout studies (discussed above and in the discussion of this chapter), where LRRK1 is suggested to play a vital role in bone development. Additionally, *LRRK1* has also been identified as a risk gene for central corneal thickness (Cornes et al., 2011; Guo et al., 2017) and Crohn's disease (Hong et al., 2018) and suggested to act as a prognostic biomarker for lung adenocarcinoma (Zhao et al., 2020) and acute myeloid leukaemia, where increased expression is associated with a worse outcome (Lv et al., 2018).

LRRK1 is particularly relevant to this project because of its links to immunity and inflammation. As mentioned above, *LRRK1* is a risk gene for Crohn's disease (Hong et al., 2018), an inflammatory bowel disease associated with increased levels of inflammation in the intestines. *LRRK1* is also upregulated in blood samples taken from patients with T cell acute lymphoblastic leukaemia (Li et al., 2020), suggesting a role within T cell development. *LRRK1* has also been shown to be expressed in B cells from both mice (Morimoto et al., 2016) and humans (Thévenet et al., 2011). In mice, this is responsible for B cell development, namely in response to NFκB activation, and immunoglobulin production (Morimoto et al., 2016), affording LRRK1 a role in humoral immunity.

The aim of this chapter is to explore the biological role of Lrrk2 *in vivo* by creating a loss-of-function mutation in the zebrafish gene using CRISPR-Cas9. The role of this protein in the development of PD will be explored by assessing alterations in dopaminergic neurons in *lrrk2* mutant larvae, as well as a basic characterisation of the overall phenotype. Additionally, neuroinflammatory phenotypes will be explored using microglial analysis. Lrrk1 will also be assessed as a possible compensating protein. Finally, methods to develop new zebrafish lines harbouring equivalent mutations to confirmed pathogenic human *LRRK2* mutations will be discussed.

5.2 Results

5.2.1 In Silico Research

The Ensembl database was used to explore basic features of human *LRRK2*. *LRRK2* (ENSG00000188906.16), found on chromosome 12, has nine splice variants; four of these are protein coding, resulting in proteins of 454, 521, 1271 or 2527 amino acids in length (**table 20**). Previous research has concluded that the full length (2527aa) protein is most dominant in humans (Vlachakis et al., 2018), so this isoform was used for further *in silico* analysis. Inputting this amino acid sequence into InterPro software enabled the identification of seven protein domains within full-length LRRK2; an armadillo domain, an ankyrin repeat domain, a leucine-rich repeat (LRR) domain, a Ras of complex protein (Roc) domain, a C-terminal of Roc domain, a mitogen-activated protein kinase kinase kinase (MAPKKK) domain and a WD40-repeat-containing domain (**figure 46**).

To identify the zebrafish orthologue of *LRRK2*, the human LRRK2 protein sequence was aligned to the zebrafish proteome using BLASTP software. The top hit resulting from this alignment was Lrrk2 on chromosome 25, which had 47.61% identity to the human protein. When this protein sequence was aligned to the human proteome, similarly LRRK2 was the top hit, with 47.66% identity to the zebrafish amino acid sequence. At the DNA level, Ensembl also identified *lrrk2* as the single orthologue to human *LRRK2*, possessing 47.76% identity. Lrrk2 exists as a single 2523 amino acid protein in zebrafish with no splice variants, unlike its human orthologue. InterPro domain analysis identified all seven domains present in human LRRK2 to be conserved in zebrafish (**figure 46**). Each domain was then compared individually between species using BLASTP software and subrange selection based on InterPro data. Protein domain identity is described in **figure 46**; notably, the kinase domain, which confers most of LRRK2's activity, is highly conserved between human and zebrafish, sharing 72.03% amino acid sequence identity.

A comparison of genome synteny between the human and zebrafish *lrrk2* loci found only one common gene between organisms, *SLC2A13 /slc2a13b* (**figure 47**), although it should be noted that only four other protein-coding genes lie within 1Mb of the *LRRK2* gene in humans. SLC2A13 lies upstream of *LRRK2* on human chromosome 12, whilst *slc2a13b* lies downstream of *lrrk2* on chromosome 25 in zebrafish.

The *in silico* research conducted on Lrrk2 strongly suggests that this is the true orthologue of human LRRK2.

Table 20. Comparison of Human and Zebrafish Leucine-Rich Repeat Kinase 2.

	Human	Zebrafish
Transcript Base Pairs	9239	8042
Amino Acids	2527	2532
Exons	51	51
Protein Coding Splice Variants	4	1
Chromosome	12	25

A table outlining the basic features of the leucine-rich repeat kinase 2 protein and gene and comparing these between human and zebrafish. The full length human transcript was used for comparison.

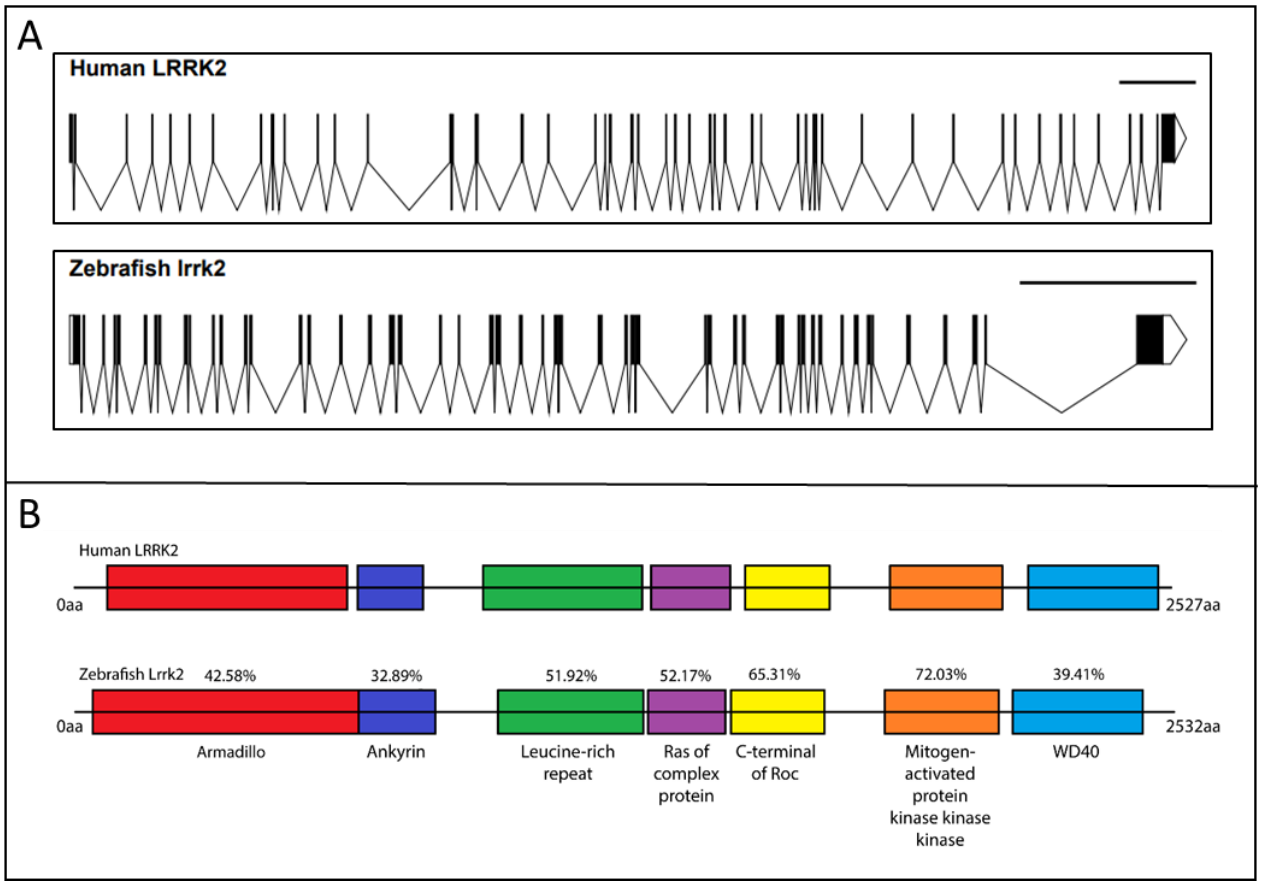

Figure 46. Comparison of Leucine-Rich Repeat Kinase 2 Structure Between Human and Zebrafish. A. *Schematic comparison of the LRRK2 gene at the DNA level. Human LRRK2 is made up of 51 exons, whilst zebrafish lrrk2 is comprised of 51. Scale bar represents 10kb.* ***B.*** *Comparison of LRRK2 protein structure between human and zebrafish finds that both proteins are comprised of the same 7 conserved domains. Percentage values represent sequence identity specifically between protein domains. Graphic is drawn to scale by equating 1 pixel to 1 amino acid. aa, amino acids; LRRK2, leucine-rich repeat kinase 2.*

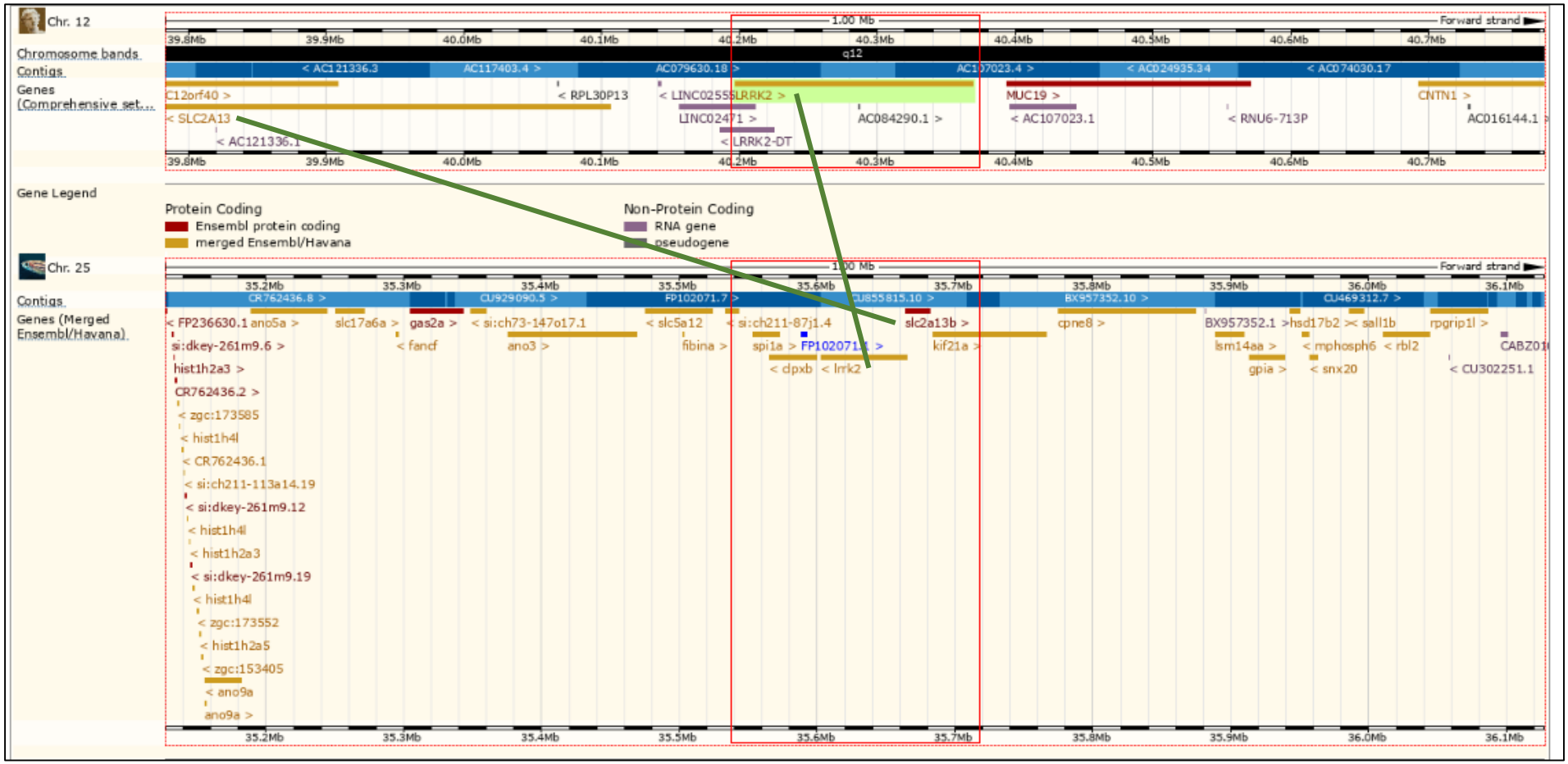

Figure 47. Synteny Around Leucine-Rich Repeat Kinase 2 is Maintained Between Human and Zebrafish. *Screenshot of the results of the region comparison feature from Ensembl comparing 1Mb around the LRRK2 gene on human chromosome 12 and zebrafish chromosome 25. Genes labelled in red or yellow were used for synteny comparison. Green lines depict orthologous genes.*

5.2.2 Expression of *lrrk2* in Wildtype Zebrafish

5.2.2.1 Reverse Transcriptase Polymerase Chain Reaction (RT-PCR)

RT-PCR was completed in our laboratory by Dr Sarah Brown prior to the commencement of this project. It demonstrated that *lrrk2* was expressed throughout development in whole zebrafish larvae (from 1-5dpf) as well as throughout adulthood (from 3-24mpf) specifically in the brain (**figure 48**). Expression levels remained constant regardless of age.

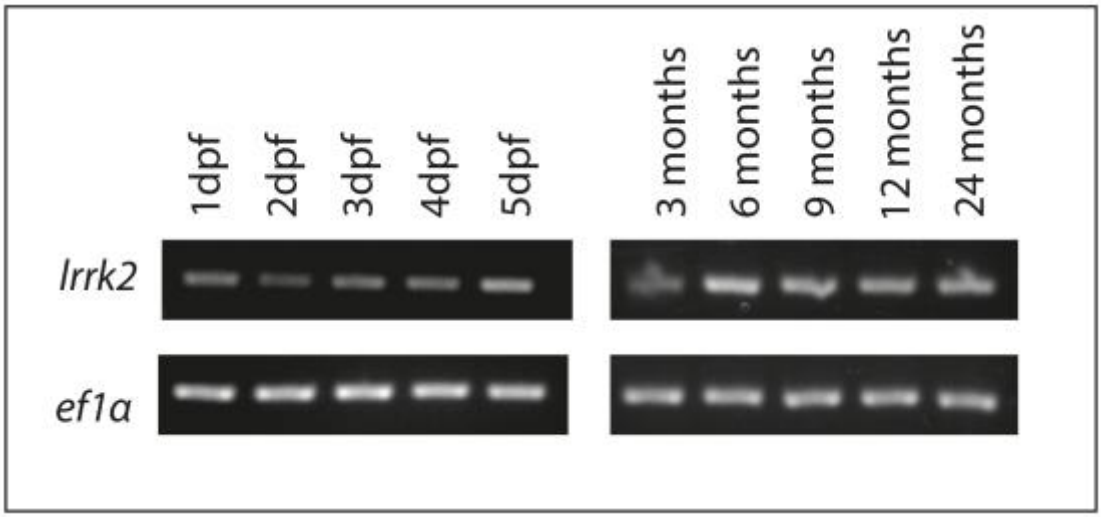

Figure 48. The Expression of Leucine-Rich Repeat Kinase 2 in Larval and Adult Zebrafish. *RT-PCR shows that lrrk2 is expressed at a constant level during zebrafish development from 1-5dpf as well as during adulthood. Whole zebrafish larvae were used up to 5dpf. Whole brains were used for expression analysis in adult zebrafish. ef1α was used as a loading control. dpf, days post fertilisation; lrrk2, leucine-rich repeat kinase 2; ef1α, eukaryotic translation elongation factor 1 alpha 1. Experiment and figure by Dr Sarah Brown (Bandmann Laboratory).*

5.2.2.2 In Situ Hybridisation

Two in situ hybridisation probes were designed to target zebrafish *lrrk2*. Probe 1 primer sequences were taken from published work by Sheng et al. (2010) and probe 2 sequences were designed using Primer3 software. Both primer pairs produced single, clean bands when PCR amplified using wildtype cDNA as a template, suggesting that both amplified *lrrk2* specifically and would produce *lrrk2*-specific staining during in situ hybridisation.

To create riboprobes for in situ hybridisation, wildtype cDNA was initially amplified using the probe primer pairs. For probe 2, the antisense primers inadequately amplified the cDNA, resulting in weak bands when visualised by gel electrophoresis. For this reason, only probe 1 was completed and taken forward in experiments.

In situ hybridisation was conducted on wildtype 5dpf zebrafish larvae to determine the expression pattern of *lrrk2* under basal conditions. Two time points were used to analyse *lrrk2* staining. After 45 minutes of staining, fish incubated with antisense *lrrk2* probe appeared to have

slightly increased staining, particularly in the head region (**figure 49**). Staining could be seen in 'tracts' within the brain (**figure 49F**), which was not evident in larvae incubated with the sense control (**figure 49C**).

However, after 1hour 45minutes of staining, the expression pattern of *lrrk2* appeared different (**figure 50**). Although similar, albeit stronger, staining was seen in larvae incubated with the antisense probe (**figure 50D-F**), there was now very little difference between this and the staining pattern in larvae incubated with the sense probe. What appeared as specific tract staining in the brains of larvae incubated with the antisense probe after 45 minutes, was now also clearly visible in control larvae (**figure 50C**).

The experiment was repeated using 3dpf wildtype larvae. Clear differences in staining between sense and antisense probes were now evident (**figure 51**). The staining pattern in 3dpf larvae suggested that *lrrk2* is expressed diffusely in the head region of wildtype larvae. Staining appeared darker in clusters (**figure 51G**), possibly representing *lrrk2* expression specifically within microglia or other cell bodies within the brain.

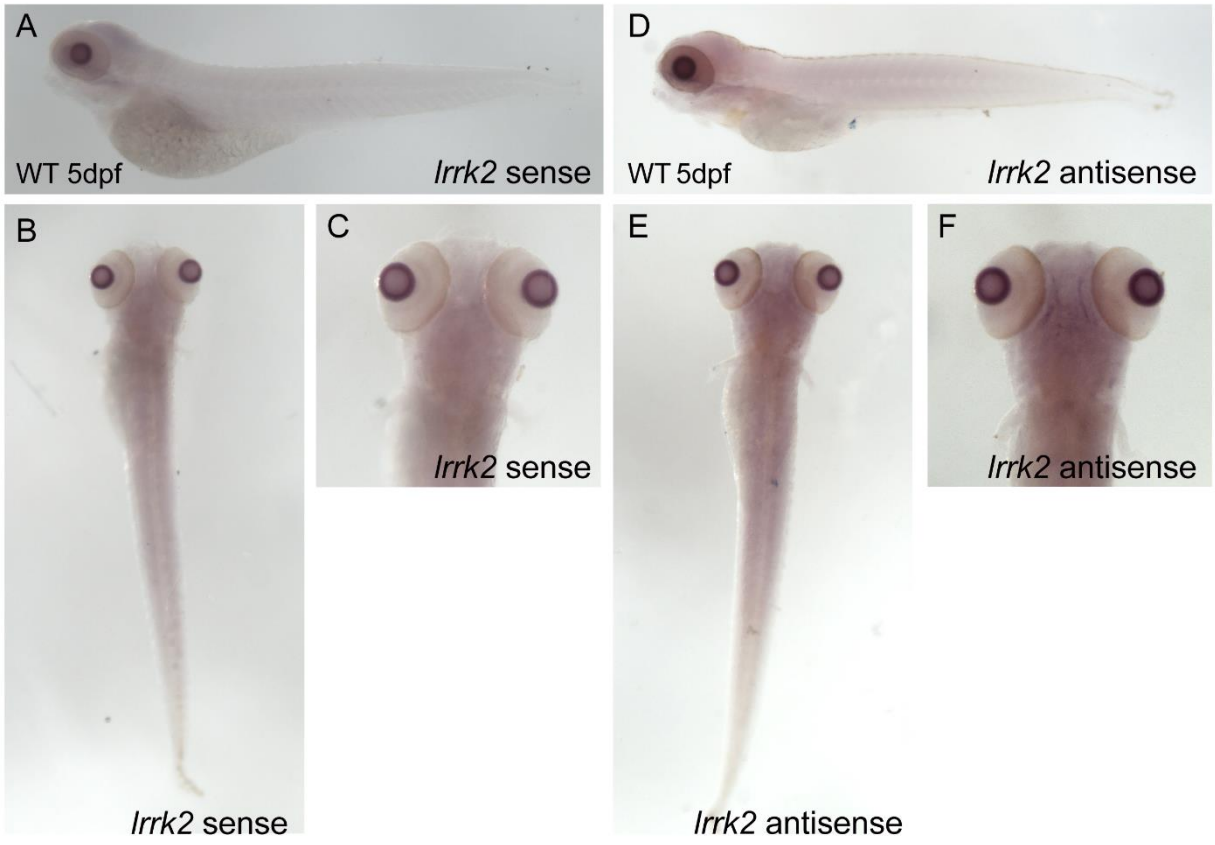

Figure 49. In Situ Hybridisation of Leucine-Rich Repeat Kinase 2 in Wildtype Zebrafish at 5-Days Post Fertilisation, 45 Minute Staining. *Representative brightfield images of staining patterns obtained after 45 minutes of staining in wildtype larvae incubated with either sense (**A-C**) or antisense (**D-F**) lrrk2 probes. Images show staining patterns seen from lateral (**A, D**), dorsal (**B, E**) and dorsal head (**C, F**) regions. dpf, days post fertilisation; lrrk2, leucine-rich repeat kinase 2; WT, wildtype.*

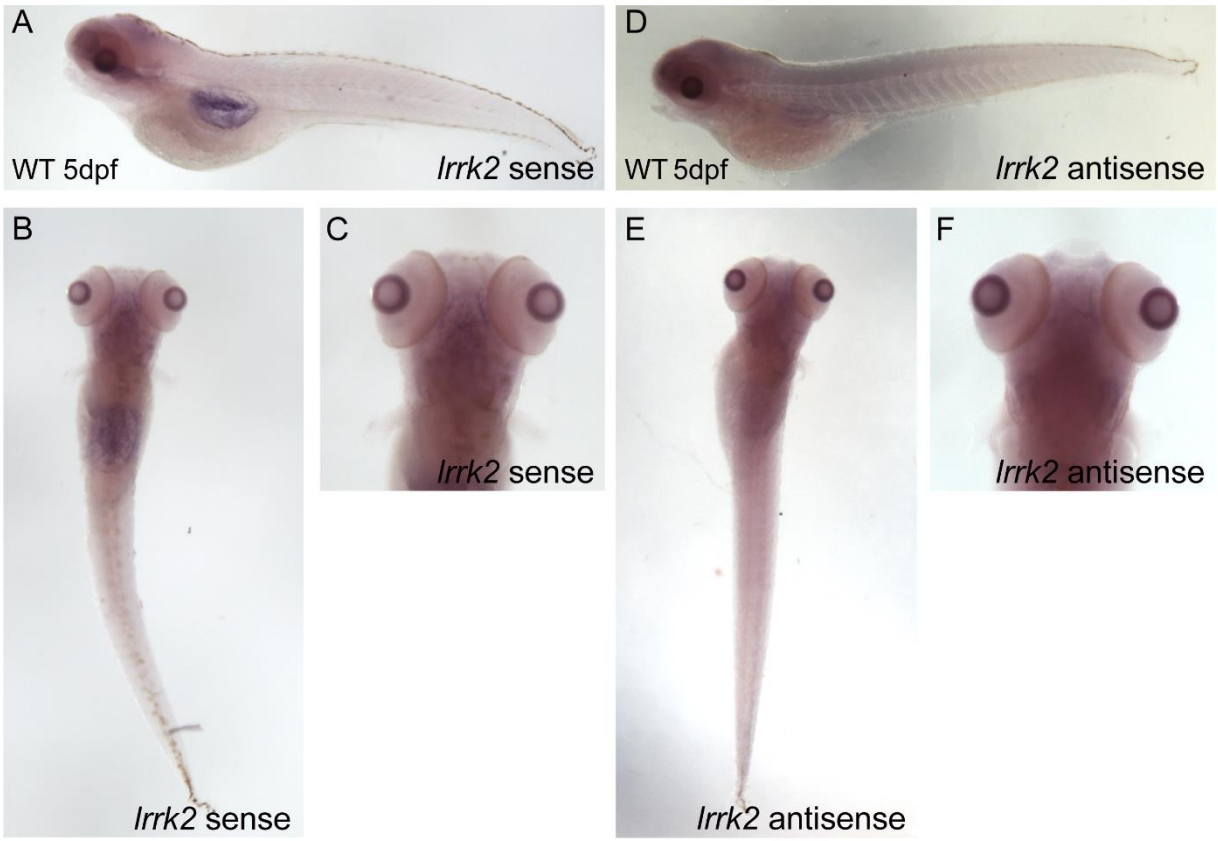

Figure 50. In Situ Hybridisation of Leucine-Rich Repeat Kinase 2 in Wildtype Zebrafish at 5-Days Post Fertilisation, 1 Hour 45 Minute Staining. *Representative brightfield images of staining patterns obtained after 1 hour 45 minutes of staining in wildtype larvae incubated with either sense (**A-C**) or antisense (**D-F**) lrrk2 probes. Images show staining patterns seen from lateral (**A, D**), dorsal (**B, E**) and dorsal head (**C, F**) regions. dpf, days post fertilisation; lrrk2, leucine-rich repeat kinase 2; WT, wildtype.*

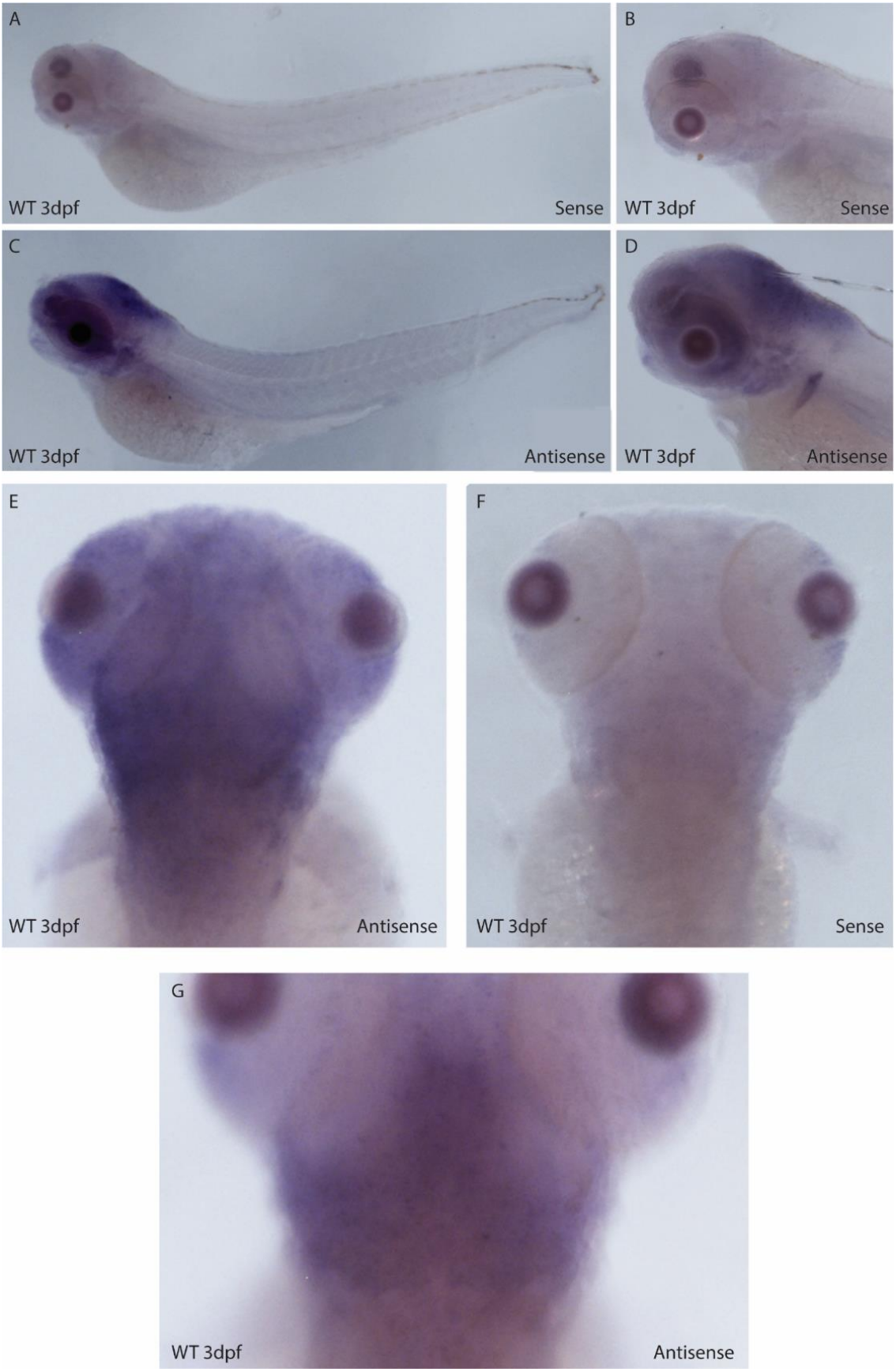

Figure 51. In Situ Hybridisation of Leucine-Rich Repeat Kinase 2 in Wildtype Zebrafish at 3-Days Post Fertilisation. *Representative brightfield images of staining patterns obtained in wildtype larvae incubated with either sense (**A, B, F**) or antisense (**C, D, E, G**) lrrk2 probes. Images show staining patterns seen from lateral (**A-D**) and dorsal head (**E-G**) regions. lrrk2 appears to be expressed diffusely in the head of 3dpf larvae. **G.** Within the head, staining can be seen in clusters, possibly representing cell bodies or microglia. dpf, days post fertilisation; lrrk2, leucine-rich repeat kinase 2; WT, wildtype.*

5.2.3 Generation of a *lrrk2* Knockout Mutant Zebrafish

A *lrrk2* loss-of-function mutant zebrafish was created prior to the commencement of this project by Dr Marcus Keatinge and Dr Sarah Brown, but all data reported, except initial adult qPCR analysis, was collected by the author as part of this PhD. Using CRISPR-Cas9 technology, a frameshift mutation was introduced into the ankyrin repeat domain via a 5bp insertion into exon 19 of *lrrk2*. The likely outcome of this mutation at the protein level was predicted using EMBOSS Transeq software, where it was predicted to result in the introduction of a premature stop codon at position 796, in theory creating a truncated protein beyond this point (**figure 52B**). Using the Needleman–Wunsch algorithm in SnapGene, the protein sequences for exon 19 were compared (**figure 52C**). This predicted an additional amino acid to be present in the mutated protein, as well as numerous dissimilar amino acids prior to the newly generated STOP codon (represented as a star). Due to the small (5bp) overall change in DNA length, mutant zebrafish could not be identified by PCR alone. However, this mutation resulted in the disruption of a restriction enzyme (Bsl1) site, enabling mutants to be easily identified following a Bsl1 digest (**figure 52A**).

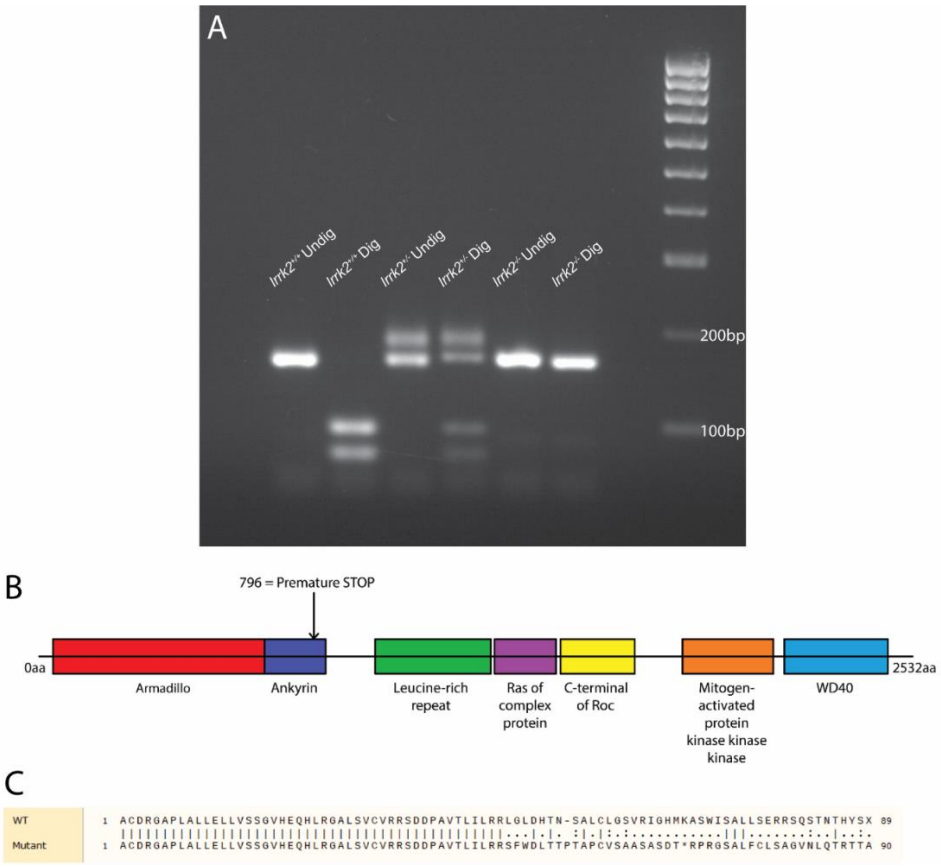

Figure 52. CRISPR-generated Knockout Mutation of lrrk2 in Zebrafish. A. *The resulting mutation is visible by digest with Bsl1. Wildtype zebrafish (left) are identified by a single 161bp band which is completely digested by Bsl1 to give fragments of 92bp and 69bp. Heterozygous mutants (centre) have 2 bands, the longer representing a heteroduplex, which undergo partial digestion by Bsl1. Homozygous mutants (right) appear as a single 166bp band which is not digested by Bsl1.* ***B.*** *Schematic representation of the mutation induced by CRISPR-Cas9 targeting exon 19 of the zebrafish lrrk2 gene. The protein created by this mutation has a premature stop codon at position 796 in the ankyrin repeat domain.* ***C.*** *Comparison of exon 19 amino acid sequence resulting from the mutation. A line represents identical amino acids, two pluses (+) represent amino acids that are similar and a single plus represents positions where amino acids are not similar. The asterisk (*) represents a STOP codon. Image taken from SnapGene. aa, amino acids; bp, basepairs; Dig, DNA digested with Bsl1; lrrk2, leucine-rich repeat kinase 2; Undig, undigested DNA.*

5.2.1 Confirmation of a Pathogenic Mutation

5.2.1.1 Quantitative Polymerase Chain Reaction (qPCR)

qPCR analysis of mRNA transcripts in adult (3mpf) brain tissue identified that *lrrk2*$^{-/-}$ mutant zebrafish demonstrated a 95% decrease in *lrrk2* transcript levels compared to their wildtype counterparts (p=0.0111, **figure 53**). This suggested that the CRISPR-Cas9 induced mutation in *lrrk2* led to nonsense-mediated decay of the resulting mRNA (data and figure by Dr Sarah Brown, Bandmann Laboratory). Access to the original raw data was not available during this project, so individual values are not known.

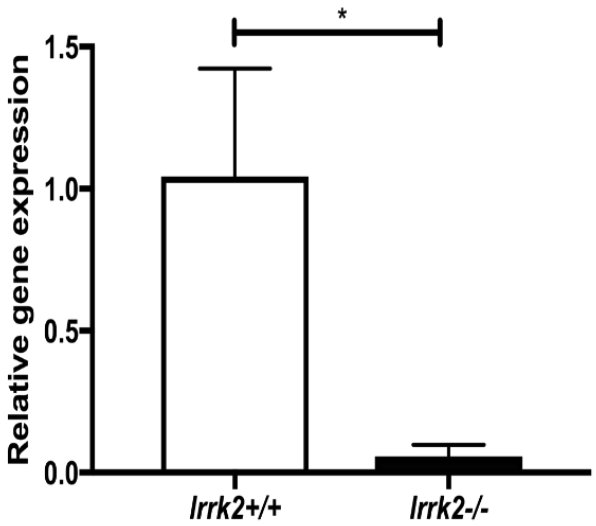

Figure 53. Quantitative Polymerase Chain Reaction of Leucine-Rich Repeat Kinase 2 Transcript Levels Demonstrates Nonsense-Mediated Decay of mRNA in Homozygous Mutant Knockout Zebrafish. *Transcript levels in lrrk2 homozygous mutant zebrafish (lrrk2-/-) are expressed as a percentage of wildtype (lrrk2+/+) (one-tailed t test, n=3 biological replicates (cDNA extracted from adult (3 months old) brain tissue), p=0.0110). Expression was normalised to elongation factor 1 alpha 1 (ef1α). Data and graph created by Dr Sarah Brown.*

5.2.1.2 In Situ Hybridisation

In situ hybridisation was conducted in *lrrk2*$^{-/-}$ mutant zebrafish larvae at 3dpf using the *lrrk2* probe discussed above. For this experiment, larvae were obtained by incrossing homozygous mutant parents and control larvae from the wildtype siblings of these adults, making experimental fish cousins. As seen previously, wildtype zebrafish demonstrated widespread staining in the head region (**figure 54A-C**). *lrrk2*$^{-/-}$ mutant zebrafish expressed two distinct staining patterns; almost half of the fish (12/30) demonstrated staining identical to wildtype larvae (**figure 54D-F**) whilst the other half (18/30) had clearly reduced staining, although demonstrated the same pattern as wildtype (**figure 54G-I**).

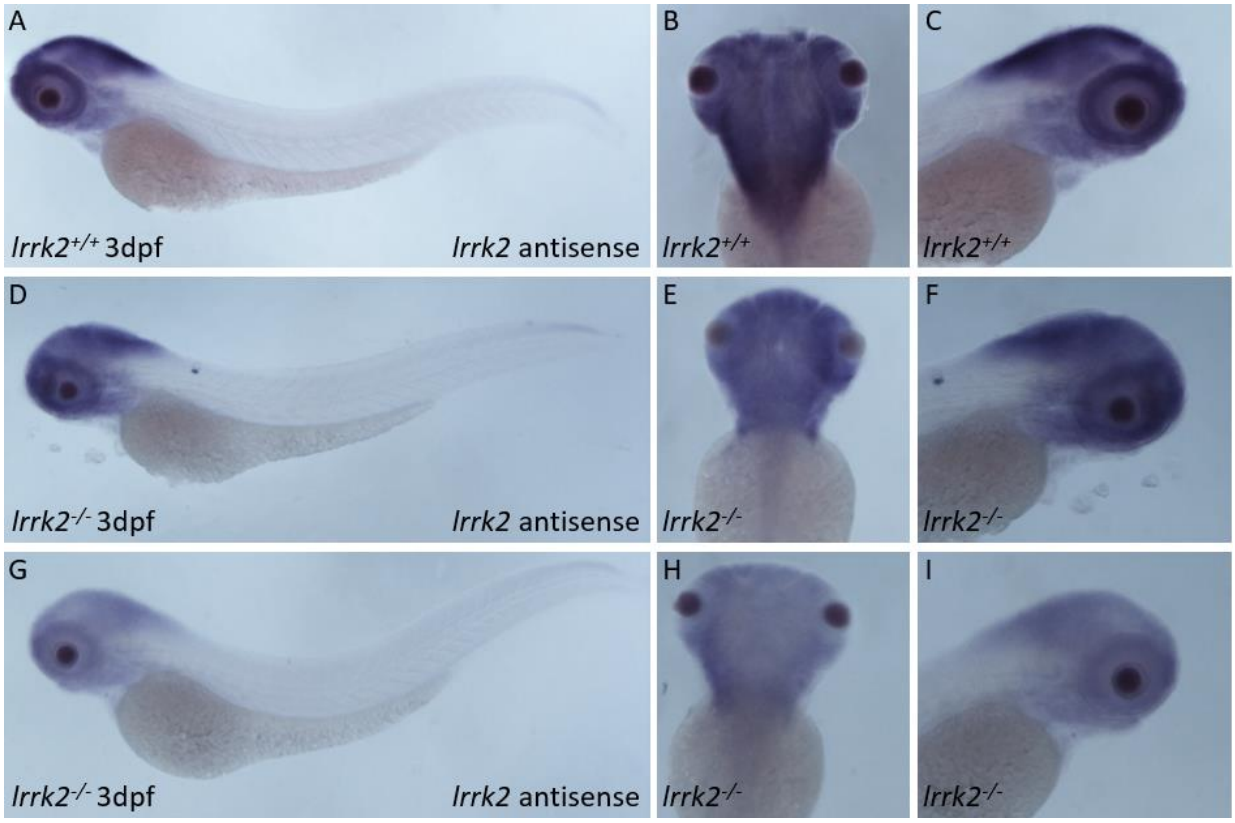

Figure 54. In Situ Hybridisation of Homozygous Leucine-Rich Repeat Kinase 2 Mutant Larvae at 3-Days Post Fertilisation Demonstrates Two Distinct Staining Patterns. A, B, C. *Staining in wildtype zebrafish larvae demonstrates expression of lrrk2 mRNA in the head.* ***D, E, F.*** *12 out of 30 lrrk2$^{-/-}$ mutant larvae demonstrated a staining pattern indistinguishable from wildtype.* ***G, H, I.*** *18 out of 30 lrrk2$^{-/-}$ larvae showed reduced staining. All larvae obtained from a homozygous adult incross. dpf, days post fertilisation; lrrk2, leucine-rich repeat kinase 2.*

5.2.2 Assessing Leucine-Rich Repeat Kinase 1 Compensation

Due to the similarities between *LRRK2* and its paralogue, *LRRK1*, expression levels of *lrrk1* were assessed in *lrrk2*$^{-/-}$ mutant zebrafish to check for a compensatory upregulation following a loss of *lrrk2* mRNA.

Ensembl states that zebrafish possess a single copy of *lrrk1,* found as three protein coding splice variants; a 1377aa protein, a 585aa protein and a 444aa protein. However, on closer examination of the RNA sequences for these variants, it is clear that there are, in fact, only two protein-coding variants, as one of the variants suggested by Ensembl is actually a continuation of another, possessing no ATG. This means there are actually two *lrrk1* splice variants in zebrafish, a 444aa protein and a 1962aa protein. The 444aa variant, hereafter referred to as “short variant” is identical to the 1962aa variant, hereafter referred to as “long variant”, but shorter in both the N and C terminal (**figure 55A**). Since there is no unique sequence in the short variant, a single set of primers alone could not be used to detect its levels. To overcome this issue, primers specific to the long variant and primers common to both variants were designed to distinguish between transcript levels of each variant (**figure 55**). Eight primer pairs were designed using Primer3 and checked for specificity using primerBLAST software. Primers were tested using a gradient PCR

(55-65°C) using wildtype cDNA to ensure specificity and select the most appropriate to take forward in qPCR experiments (**figure 55**). From this, pair 1 was selected to amplify the long transcript and pair 7 for amplification of both transcripts. Both sets of primers were optimised for qPCR using wildtype cDNA as described previously (see section 4 for details).

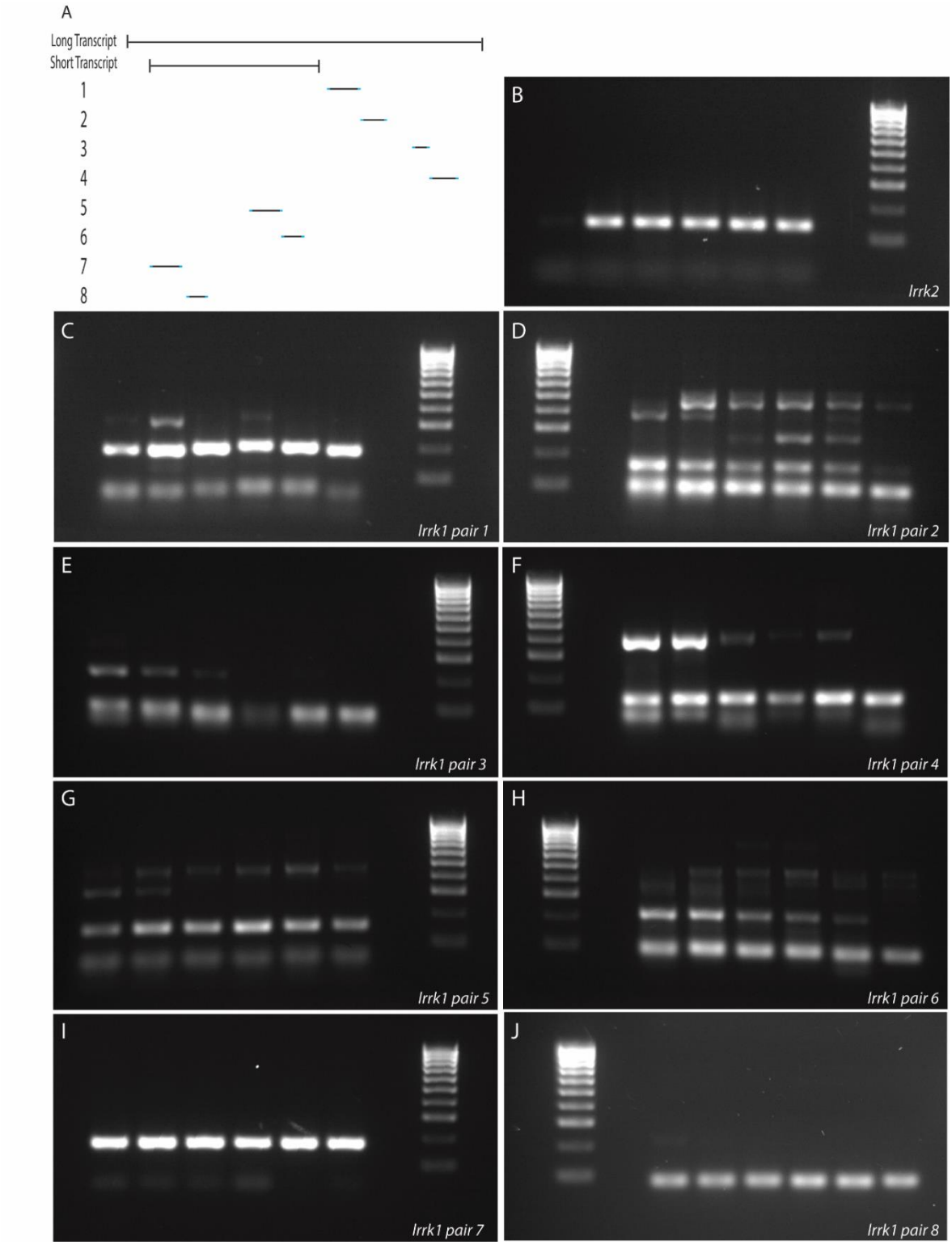

Figure 55. Designing Leucine-Rich Repeat Kinase 1 Quantitative Polymerase Chain Reaction Primers. A. *Schematic of both lrrk1 transcripts and the approximate region amplified by each primer pair.* ***B-J.*** *Gradient PCR from 55(left)-65(right)°C using wildtype larval cDNA. lrrk1, leucine-rich repeat kinase 1; lrrk2, leucine-rich repeat kinase 2.*

To obtain cDNA for qPCR, adult *lrrk2* heterozygous mutants were incrossed and single clutches of larvae collected. At 3dpf, larvae were finclipped and genotyped and then allowed to develop until 5dpf. 15 larvae were combined per genotype from the same biological replicate for RNA extraction and cDNA synthesis.

No significant difference in expression of *lrrk1*, either the long transcript (p=0.8021) or both transcripts combined (p=0.5384), was identified between *lrrk2*$^{-/-}$ mutant zebrafish and their wildtype siblings (**figure 56**). Large variations in expression were seen within genotypes.

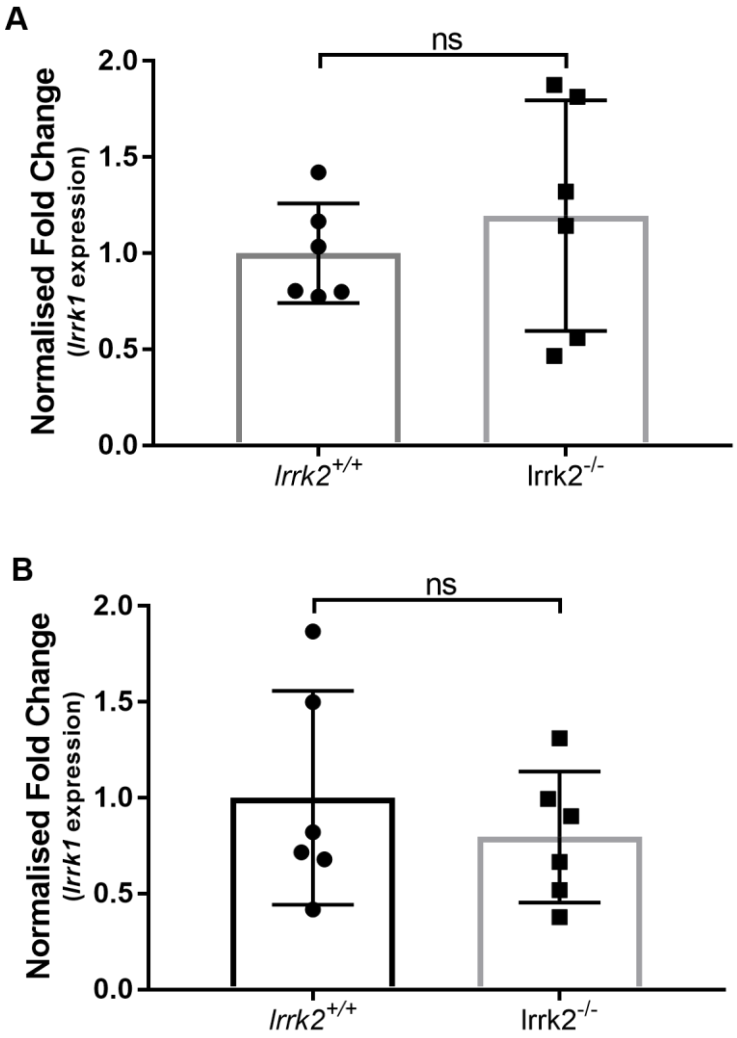

Figure 56. Quantitative Polymerase Chain Reaction Assessment of Leucine-Rich Repeat Kinase 1 Expression in Leucine-Rich Repeat Kinase 2 Mutant Zebrafish. *qPCR analysis of lrrk1 expression in lrrk2*$^{-/-}$ *mutant larvae at 5dpf. Larvae were obtained from a heterozygous incross and genotyped by finclipping at 3dpf.* ***A.*** *When assessing just the long transcript of lrrk1, there was no difference in expression between mutant and wildtype larvae (p=0.8021).* ***B.*** *Using primers that amplify both variants, no significant difference in overall lrrk1 expression was identified between lrrk2*$^{-/-}$ *mutant larvae and their wildtype siblings (p=0.5384). rps29 was used as a reference gene for both experiments. n=3 biological replicates (15 larvae per replicate). Statistics from an unpaired, two-tailed t test following Shapiro-Wilk test for normality (all groups passed) on ddCt values. dpf, days post fertilisation; lrrk1, leucine-rich repeat kinase 1; lrrk2, leucine-rich repeat kinase 2; ns, not significant.*

5.2.1 Overall Morphological Phenotype

Despite *lrrk2* expression identified throughout early zebrafish development as well as during adulthood, *lrrk2*$^{-/-}$ mutant zebrafish were viable, bred well and appeared phenotypically normal at both larval (**figure 57**) and adult stages (data not shown).

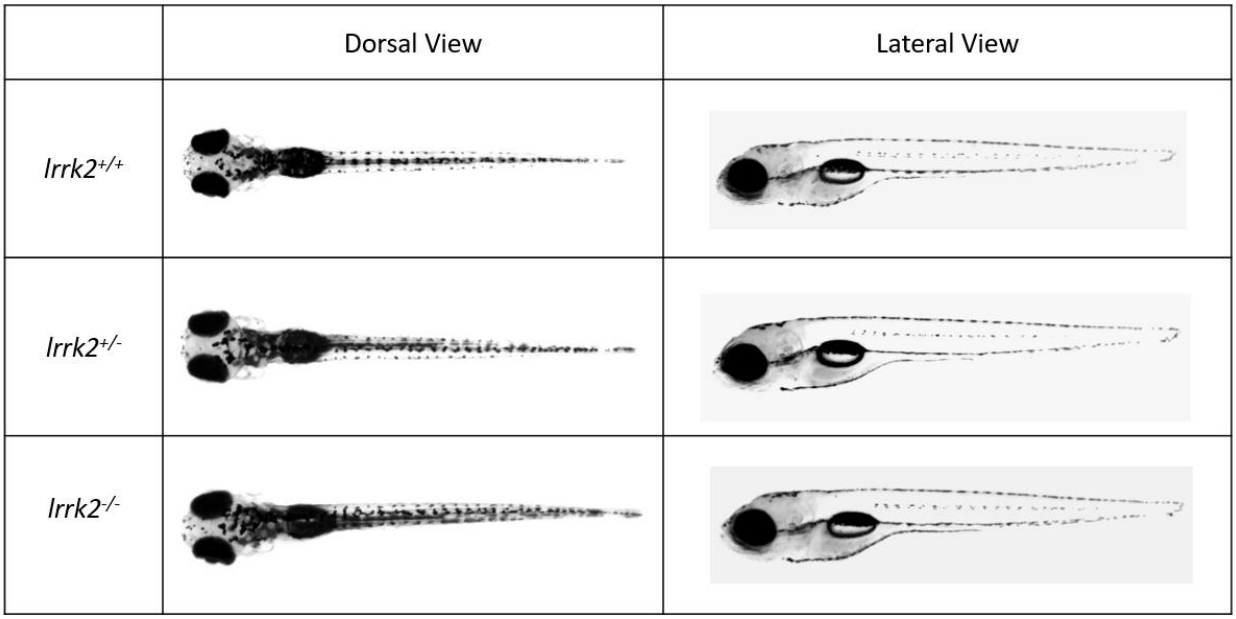

Figure 57. Gross Morphology of Leucine-Rich Repeat Kinase 2 Wildtype, Heterozygous and Homozygous Knockout Sibling Zebrafish at 5-Days Post Fertilisation. *Brightfield images of 5dpf zebrafish showing normal gross morphology between genotypes. Larvae were anaesthetised using 4.2% tricaine for imaging. Fish were genotyped following imaging. dpf, days post fertilisation; lrrk2, leucine-rich repeat kinase 2.*

5.2.2 Movement Analysis

5.2.2.1 Larval (5dpf) Movement Analysis

Tracking the distance travelled by larvae under a series of light/dark cycles found no significant difference in the behaviour of *lrrk2*$^{-/-}$ mutant zebrafish and their wildtype siblings (**figure 58**). Movement was recorded over a 1-hour time period; following an unrecorded habituation period, larvae were maintained in light conditions for 30 minutes prior to alternating 5-minute dark-light cycles for 30 minutes. From initial data it appeared that *lrrk2*$^{-/-}$ larvae moved more during dark periods (**figure 58**), so the total distance travelled in each of these phases was also quantified. No differences were found between *lrrk2*$^{+/+}$, *lrrk2*$^{+/-}$ and *lrrk2*$^{-/-}$ zebrafish during the initial 30-minute light period, the combined light phases, the combined dark phases or over the entire 1-hour recording period ($p<0.05$ for each period, **figure 58B-E**).

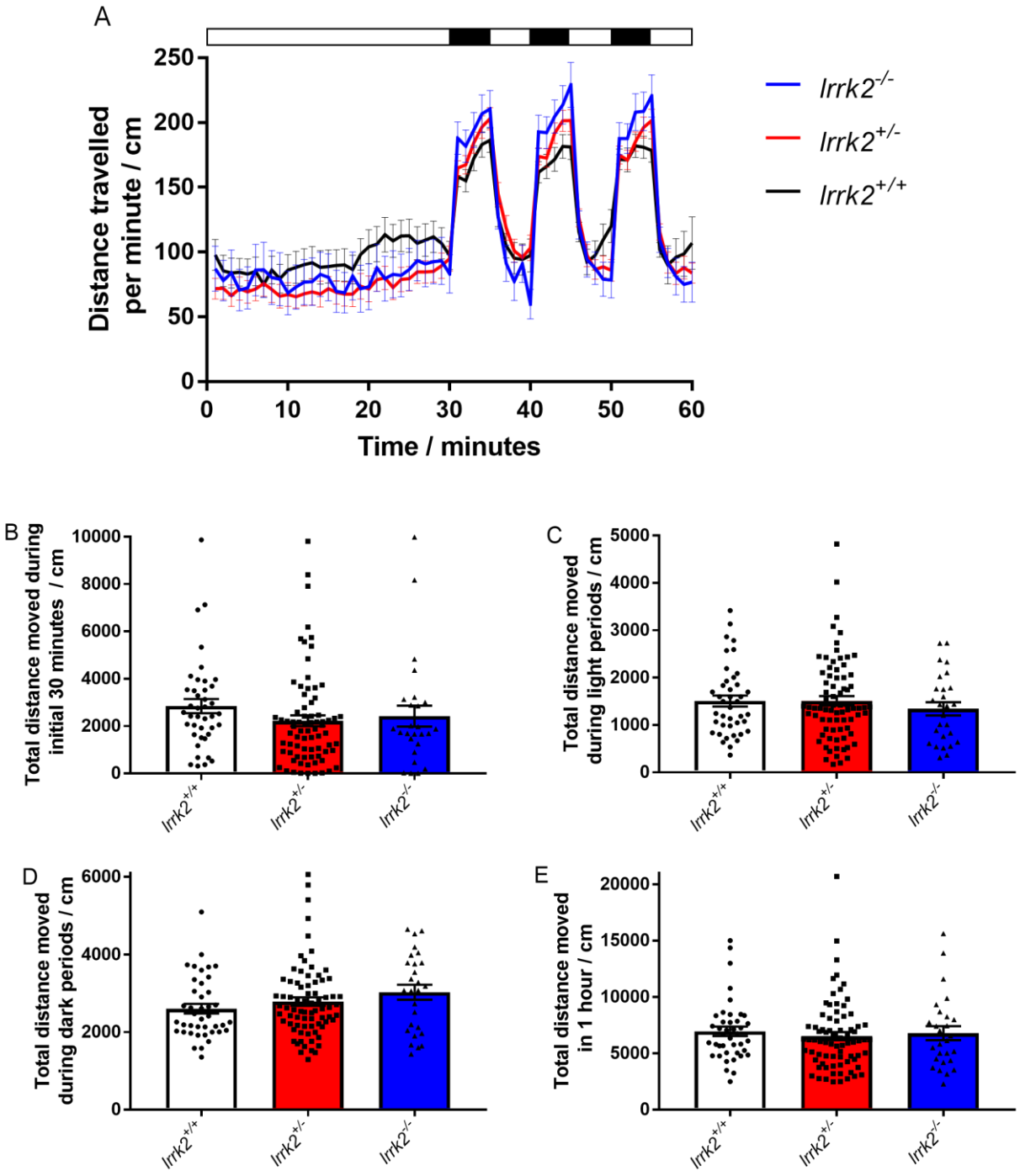

Figure 58. Leucine-Rich Repeat Kinase 2 Knockout Zebrafish Larvae Demonstrate Normal Swimming Behaviour. *Larval zebrafish movement was recorded over a 1-hour time period at 5dpf. Following habituation, larvae were maintained in light conditions for 30 minutes prior to alternating dark-light cycles for 30 minutes. Fish were genotyped after the experiment.* ***A.*** *Distance over time analysis between* lrrk2$^{-/-}$, lrrk2$^{+/-}$ *or their wildtype siblings. Horizontal white bar represents time zebrafish were in light conditions, black bar represents time in dark conditions.* ***B-E.*** *Comparing the distance travelled in each phase of the experiment found no differences between genotypes during (**B**) the initial 30-minute period (p=0.2876), (**C**) during the combined light phases (p=0.6234), (**D**) during the combined dark phases (p=0.1750), or (**E**) over the entire 1-hour recording period (p=0.7490). Note different axis scales between graphs. Data from 3 biological replicates. n=41 lrrk2$^{+/+}$; 76 lrrk2$^{+/-}$; 27 lrrk2$^{-/-}$. All statistics analysed using a one-way ANOVA following Shapiro-Wilk test for normality. lrrk2, leucine-rich repeat kinase; cm, centimetre.*

5.2.2.2 Adult (12 months) Movement Analysis

Movement was also assessed in adult zebrafish at 12 months of age. Zebrafish, held in single tanks, were maintained in light conditions at 28°C and swimming distance recorded over 7 hours. The first hour was used as the habituation period so not included in further analysis. No significant difference in the distance moved over the 6-hour experimental period was identified between *lrrk2*$^{-/-}$ mutant zebrafish and their wildtype siblings (p=0.6254, **figure 59**).

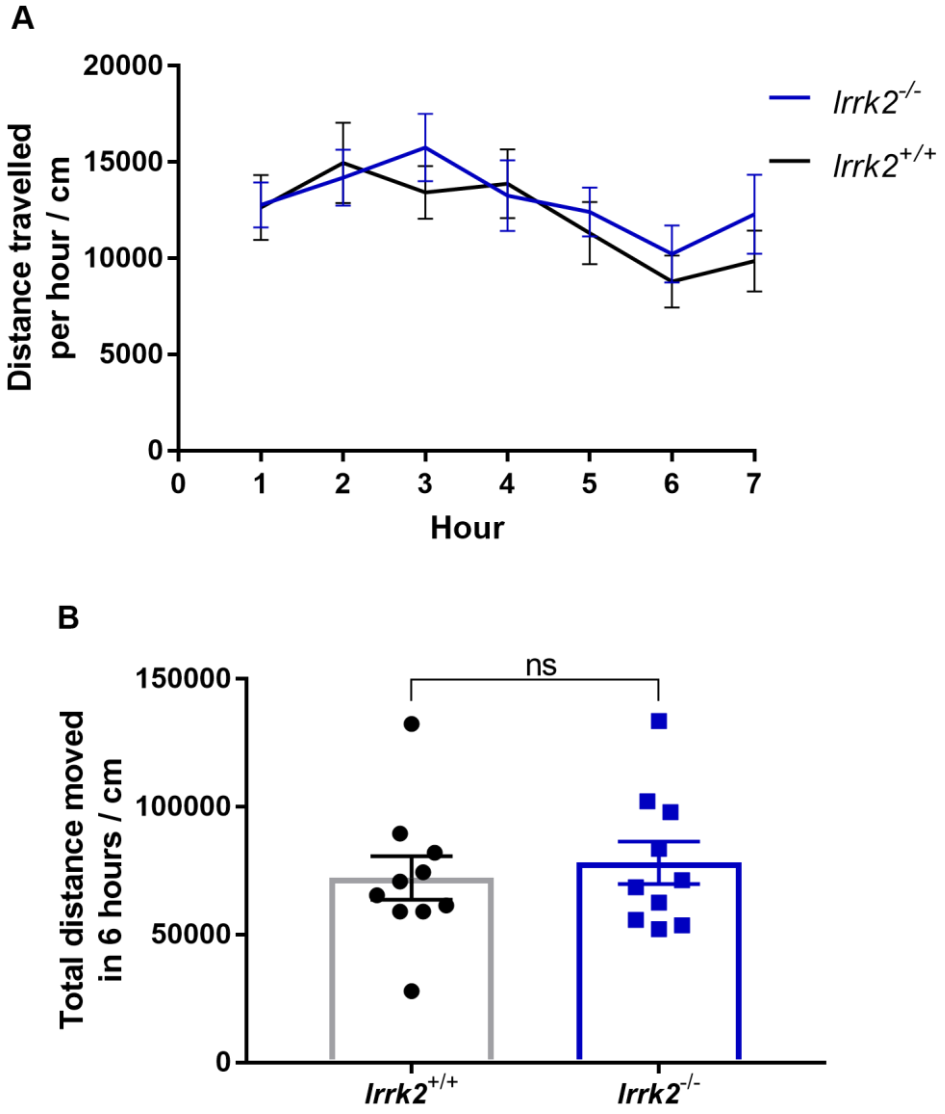

Figure 59. Distance Travelled by 12-Month Old Adult Leucine-Rich Repeat Kinase 2 Homozygous Mutant Knockout Zebrafish Over 7 Hours Compared to their Wildtype Siblings. A*. Distance travelled per hour by 12-month old lrrk2*$^{-/-}$ *mutant zebrafish (blue) compared to their wildtype (lrrk2*$^{+/+}$*) siblings (black). Adult fish were maintained in single tanks and light conditions throughout.* ***B.*** *Taking the first hour as a habituation period, the total distance moved over the entire 6-hour recording period was measured, showing no difference between genotypes (p=0.6254, two-tailed t test following Shapiro-Wilk test for normality). n=10 lrrk2*$^{+/+}$*; 10 lrrk2*$^{-/-}$ *(equal male: female ratio) taken at two separate time points. lrrk2, leucine-rich repeat kinase; cm, centimetre.*

5.2.1 Dopaminergic Neuron Quantification

5.2.1.1 th1+ Cell Counts

In situ hybridisation against tyrosine hydroxylase *(th1*, marker of dopaminergic neurons) was used to assess changes in dopaminergic neuron number in 3dpf *lrrk2*$^{-/-}$ mutant zebrafish. On average, wildtype larvae had 19.13 *th1+* cells in neuronal populations DC2 and DC4/5 in the ventral diencephalon (**figure 60**). No significant difference in the number of *th1*+ cells was found in *lrrk2*$^{-/-}$ mutant zebrafish, who had, on average, 18.13 cells (p=0.5674, **figure 60**).

5.2.1.2 Methyl-4-phenylpyridinium (MPP+) Toxin Exposure

As described in chapter 4, the neurotoxin MPP+ results in a decrease of *th1*+ cells in zebrafish and other animal models. *lrrk2*$^{-/-}$ mutant zebrafish and their wildtype siblings were exposed to 3mM MPP+ from 1-3dpf via constant immersion. This resulted in a significant 25.87% reduction of *th1*+ cells, to an average of 14.18 cells, in wildtype zebrafish (p<0.0001, **figure 60**) and a significant 22.79% reduction, to an average of 14.00 cells, in *lrrk2*$^{-/-}$ mutant zebrafish (p=0.0003, **figure 60**). No significant difference in the number of *th1*+ cells was seen between genotypes following MPP+ treatment (p=0.9977, **figure 60**), suggesting that the mutation in *lrrk2* did not alter the susceptibility of larvae to MPP+.

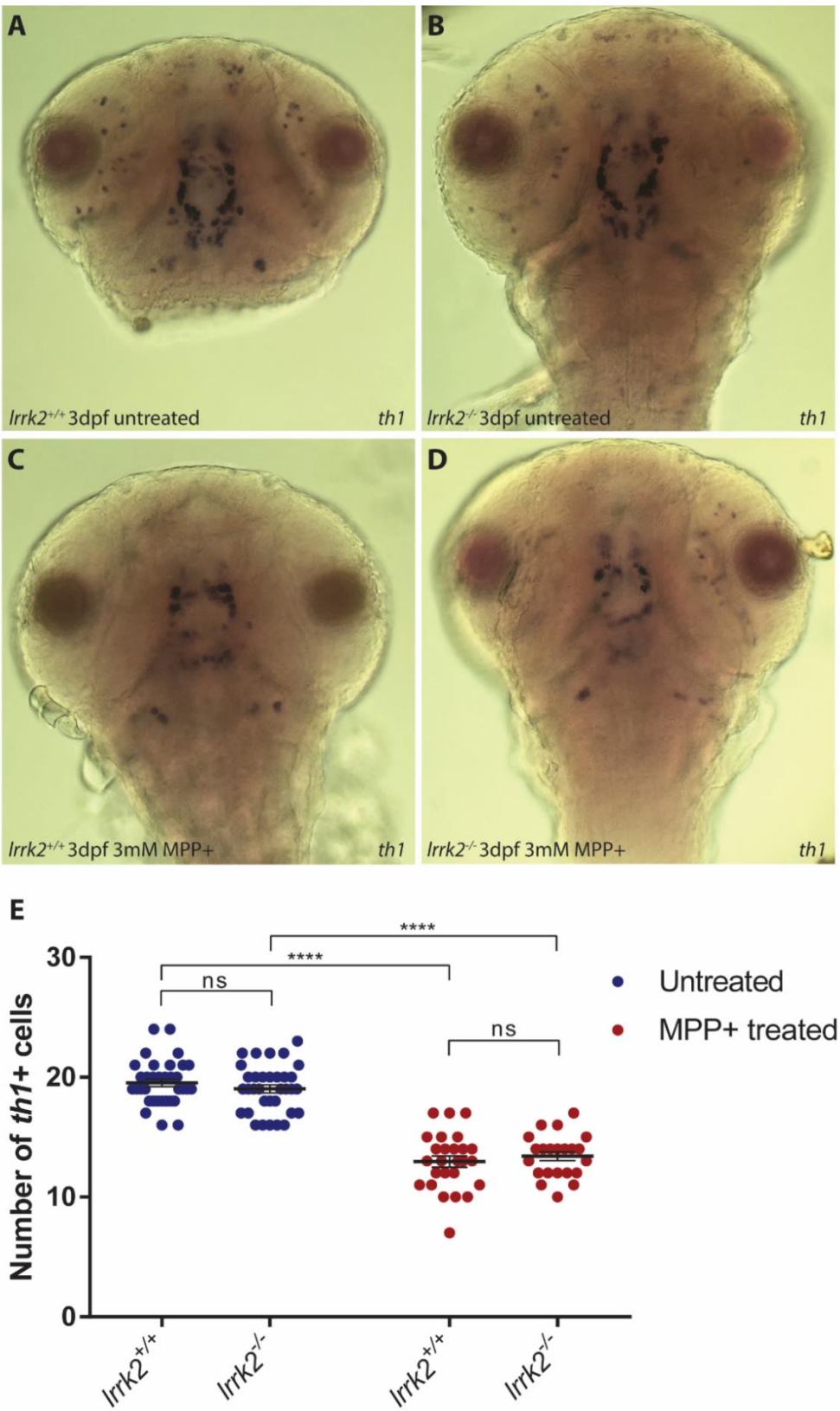

Figure 60. Leucine-Rich Repeat Kinase 2 Mutant Zebrafish Retain Normal Dopaminergic Neuron Numbers and Susceptibility to 1-methyl-4-phenylpyridinium. *In situ hybridisation against th1 shows no change in staining pattern between wildtype (**A**) and lrrk2$^{-/-}$ mutant (**B**) zebrafish. MPP+ exposure resulted in clear reductions in th1+ cells in both wildtype (**C**) and lrrk2$^{-/-}$ mutant (**D**) zebrafish. **D**. th1+ neuron numbers in the ventral diencephalon show no difference between wildtype and lrrk2$^{-/-}$ mutant zebrafish (p=0.5674). MPP+ treatment resulted in significant reductions in th1+ cells irrespective of genotype (25.87% in wildtype, p=0.0001; 22.79% in lrrk2$^{-/-}$ mutant larvae, p=0.0003). Total cell counts between groups following MPP+ treatment remained indistinguishable (p=0.9977). Data represented as mean±SEM. n=22-35 per group, from 3 biological replicates. Data were assessed for normality using Shapiro-Wilk test (all groups passed) and then statistically analysed using a two-way ANOVA with Tukey's multiple comparisons post-hoc test. MPP+, 1-methyl-4-phenylpyridinium; dpf, days post fertilisation; lrrk2, leucine-rich repeat kinase 2; th1, tyrosine hydroxylase 1.*

5.2.2 Microglial Characterisation

5.2.2.1 Neutral Red Staining

Microglia number in *lrrk2*$^{-/-}$ mutant zebrafish was initially assessed using neutral red staining in live 4dpf larvae (**figure 61**). Larvae were incubated in neutral red stain for 6 hours, anaesthetised using 4.2% tricaine and mounted in agarose for brightfield imaging. Larvae were genotyped following imaging. Microglia number was estimated by counting the number of distinct red dots in brightfield images using ImageJ (**figure 61**). *lrrk2*$^{-/-}$ mutant larvae demonstrated an increased mean microglial number from 38.50 in wildtype siblings to 61.67 in homozygous mutants. Heterozygous *lrrk2* mutant larvae demonstrated an intermediate number of microglia in their brains, with an average of 44.00. The low sample size, single replicate and high variability within genotypes meant that these differences were not statistically analysed.

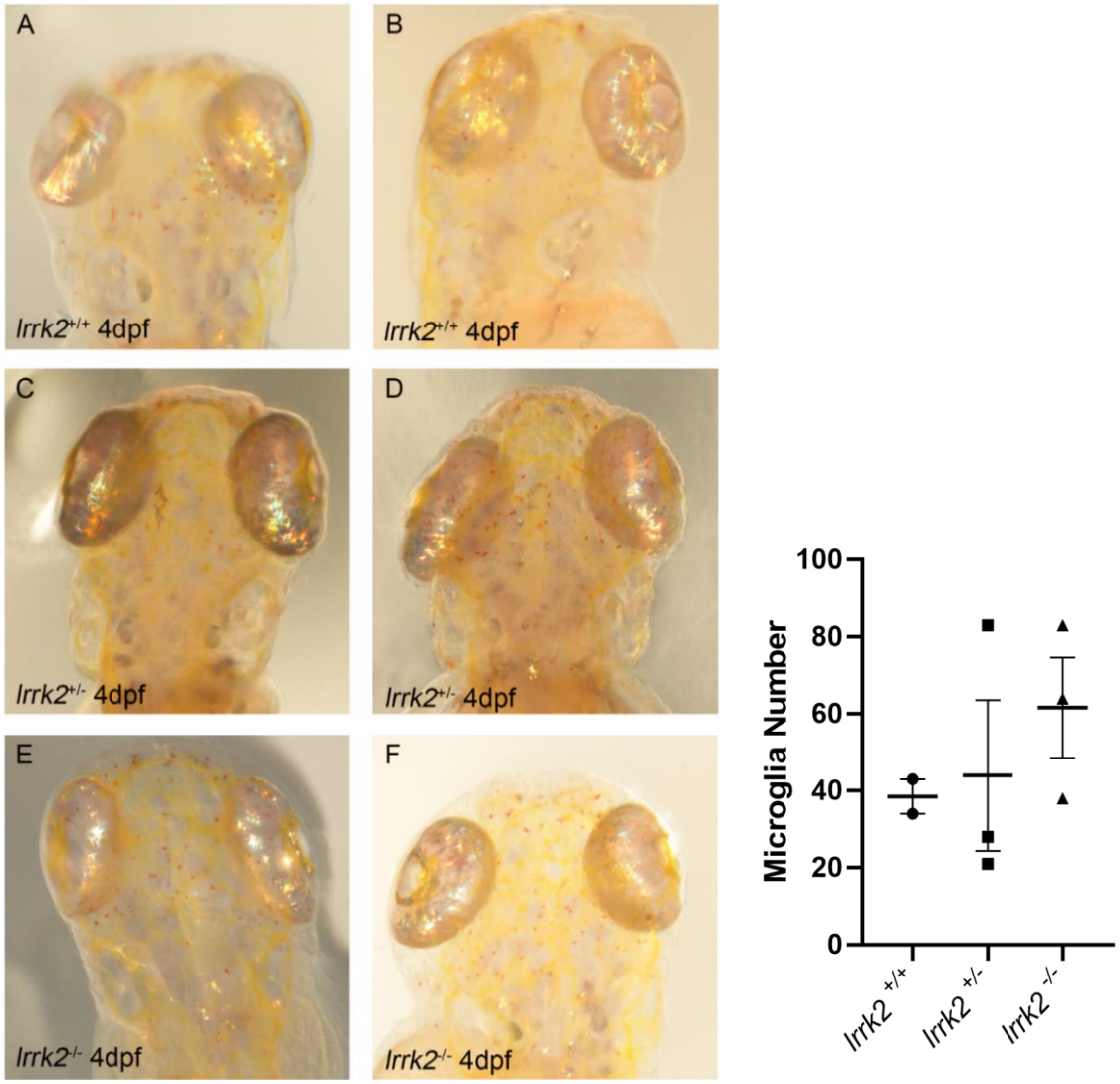

Figure 61. Neutral Red Staining of Leucine-Rich Repeat Kinase 2 Homozygous and Heterozygous Mutants and Their Wildtype Siblings at 4-Days Post Fertilisation. *Representative brightfield images of microglial labelling of wildtype (lrrk2*$^{+/+}$ *(**A, B**)), heterozygous (lrrk2*$^{+/-}$ *(**C, D**)) and homozygous (lrrk2*$^{-/-}$ *(**E, F**)) leucine-rich repeat kinase 2 mutant zebrafish larvae using neutral red staining. Neutral red staining was achieved by incubating 4dpf zebrafish in 2.5µg of neutral red per mL of E3 media for 6 hours at 28°C. Larvae were mounted in low melting point agarose and imaged immediately**. G.** Microglial number was assessed in ImageJ by subjectively counting the number of distinct red dots. Data represented as mean±SEM. n=3 lrrk2*$^{-/-}$*; 3 lrrk2*$^{+/-}$*; 2 lrrk2*$^{+/+}$ *from 1 biological replicate. lrrk2, leucine-rich repeat kinase 2; dpf, days post fertilisation.*

5.2.2.2 4c4 Wholemount Immunohistochemistry

As found in previous chapters, large variations in microglial number estimated from neutral red staining was evident within genotypes. For a more reliable method of microglia counting in larval zebrafish, 4c4 immunohistochemistry was used, which also enabled a comparison of microglial activation levels in the brains of *lrrk2*$^{-/-}$ zebrafish larvae and their wildtype siblings.

5.2.2.2.1 Microglia Number

Immunohistochemistry against 4c4 was conducted on 5dpf fixed zebrafish larvae. Decapitated heads were mounted in low melting point agarose whilst tails were used for genotyping. Fluorescently labelled microglia were imaged using the Opera Phenix and manually counted using ImageJ software. No significant difference in the number of microglia (4c4+ cells) was found between *lrrk2*$^{+/+}$ and *lrrk2*$^{-/-}$ larval zebrafish (p=0.9458, **figure 62**). Combining cell counts from the forebrain and midbrain gave an average of 54.00 cells in wildtype larvae and 55.42 in *lrrk2*$^{-/-}$ mutant larvae. Microglia did not appear to be differentially distributed in the brain between genotypes.

5.2.2.2.2 Microglia Activation

The activation state of 4c4+ cells was determined based upon morphology. As previously described, each cell was classed as either active (amoeboid) or inactive (ramified with at least one visible process). This analysis found no difference in the percentage activation of microglia in the brains of *lrrk2*$^{-/-}$ mutant zebrafish compared to their wildtype siblings; wildtype larvae had an average of 6.29% activated microglia in the midbrain and forebrain, whilst *lrrk2*$^{-/-}$ mutant larvae had an average of 6.90% (p=0.2121, **figure 62**).

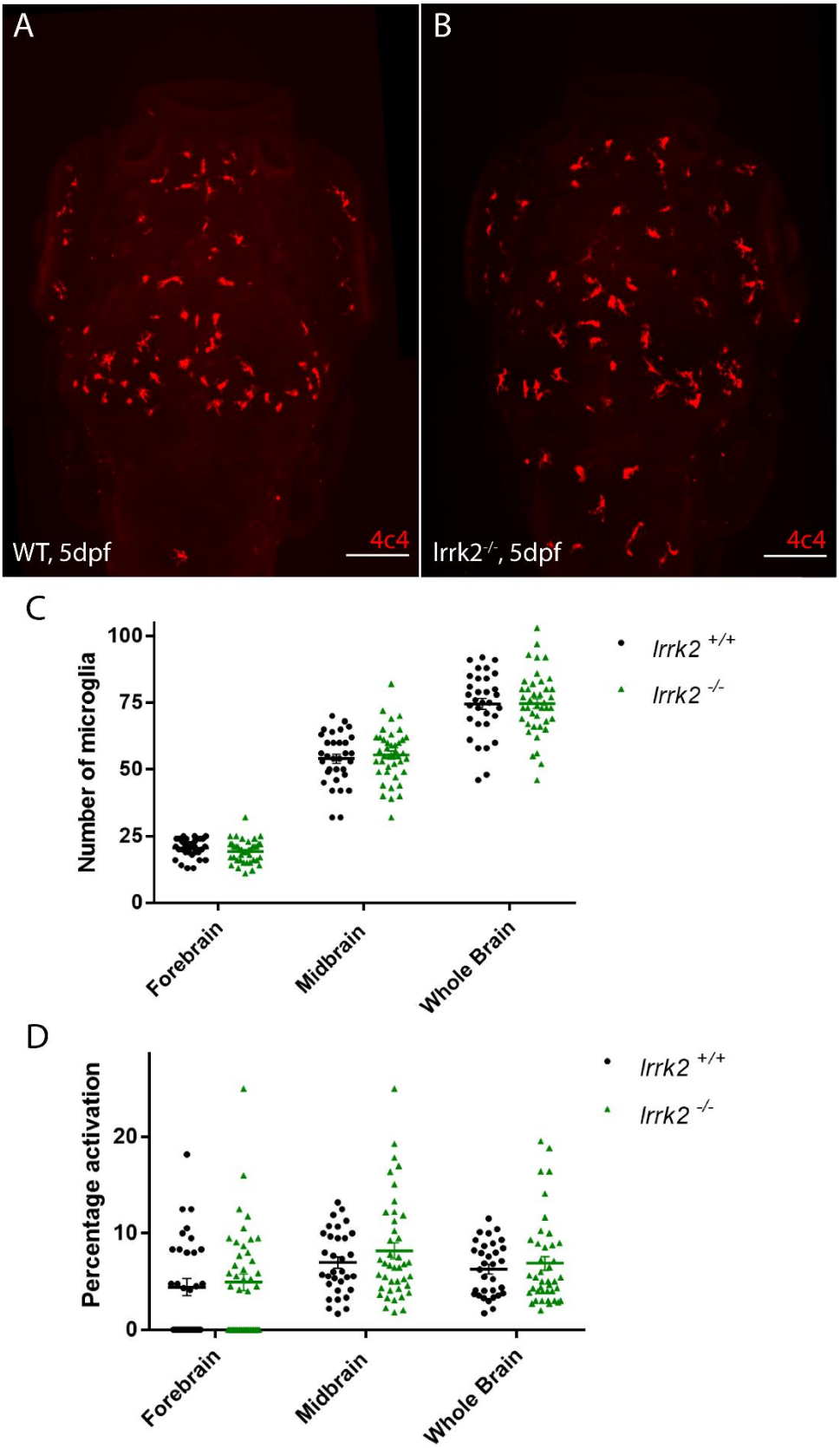

Figure 62. Microglial Analysis of Leucine-Rich Repeat Kinase 2 Mutant Zebrafish. *Representative images from wholemount immunohistochemistry against 4c4 in wildtype (**A**) and lrrk2$^{-/-}$ mutant (**B**) zebrafish at 5dpf (scale bar = 100µm). **C.** There is no difference in the number of 4c4+ cells (microglia) between wildtype and lrrk2$^{-/-}$ mutant larvae in the forebrain, midbrain or these combined (whole brain) (p>0.9000 for all brain regions). **D.** Microglial activation was determined using cell morphology, represented as the percentage of amoeboid cells out of the total 4c4+ cell count. No differences were identified between lrrk2$^{-/-}$ mutant larvae and their wildtype siblings in activation levels in the forebrain, midbrain or these combined (whole brain) (p>0.8000 for all brain regions). n=41 lrrk2$^{-/-}$, 32, lrrk2$^{+/+}$, from 3 biological replicates. Data represented as mean±SEM. Statistics analysed by two-way ANOVA with post hoc Tukey's multiple comparisons test between genotypes. 4c4, microglial marker; dpf, days post fertilisation; lrrk2, leucine-rich repeat kinase 2; WT, wildtype.*

5.2.3 Homozygous Mutants from Homozygous Parents

lrrk2$^{-/-}$ mutant zebrafish are viable to adulthood and can breed to produce homozygous offspring. Larvae obtained from an incross of homozygous parents appeared morphologically normal (data not shown). To assess their phenotype with a relevance to PD, *th1+* cells were counted with and without prior exposure to MPP+, as above. Wildtype control larvae were obtained from an incross of the wildtype siblings of the *lrrk2* homozygous mutant parents, making experimental larvae cousins. No difference was seen in the number of dopaminergic neurons between *lrrk2*$^{-/-}$ mutant larvae (average 19.69 cells) and wildtype control larvae (average 19.3 cells, **figure 63,** p=0.8381). As with previous experiments, exposure to 3mM MPP+ from 1-3dpf resulted in significant reductions in *th1+* cells in the ventral diencephalon in wildtype larvae (39.95%, p<0.0001), and this was also true for *lrrk2*$^{-/-}$ mutant larvae (42.31%, p<0.0001, **figure 63**). No difference in *th1+* cell counts was seen between genotypes after MPP+ exposure (p=0.9653).

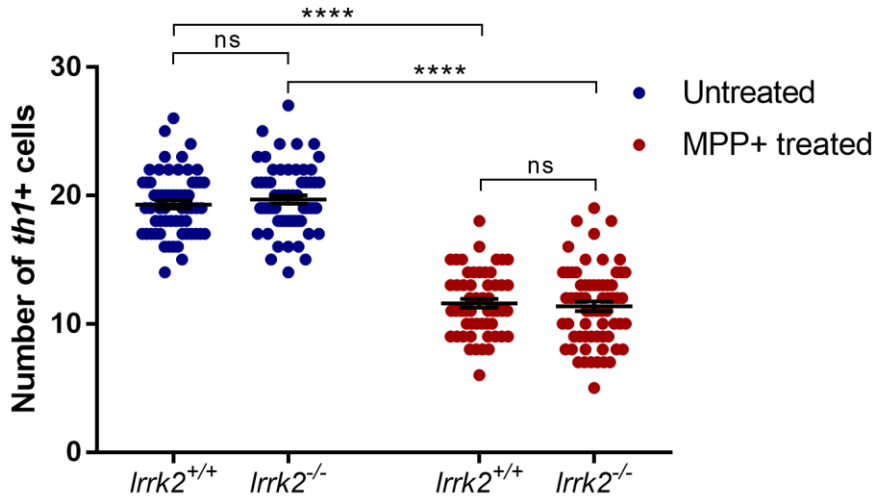

Figure 63. Leucine-Rich Repeat Kinase 2 Homozygous Mutants from Homozygous Parents Retain Normal Dopaminergic Neuron Numbers and Susceptibility to 1-methyl-4-phenylpyridinium. *Dopaminergic neuron numbers in the ventral diencephalon were counted following in situ hybridisation against tyrosine hydroxylase 1 (th1). No difference was seen between wildtype and lrrk2*$^{-/-}$ *mutant zebrafish (p=0.8381). 1-methyl-4-phenylpyridinium (MPP+) exposure resulted in significant reductions in th1+ cells irrespective of genotype (39.95% in wildtype, p<0.0001 and 42.31% in lrrk2*$^{-/-}$ *mutants, p<0.0001). Total cell counts between groups following MPP+ treatment remained indistinguishable (p=0.9653). Data represented as mean±SEM. n=54-66 per group, from 3 biological replicates. Statistics from a two-way ANOVA with Tukey's multiple comparisons post-hoc test. lrrk2, leucine-rich repeat kinase 2; MPP+, 1-methyl-4-phenylpyridinium; ns, not significant.*

5.2.4 Mutation Effect on Protein Function

To assess the effect of the *lrrk2* mutation at the protein level, phopsho-Rab assays were conducted via western blotting. These assays assess the phosphorylation of Rab8A and Rab10 proteins (known targets of *lrrk2* kinase activity (Steger et al., 2017; Steger et al., 2016)). An increase in the phosphorylation of these Rab proteins would suggest an increase in Lrrk2 function, whilst a decrease in phosphorylation would suggest a decrease in kinase function. Sample preparation was carried out by the author, western blots and image generation were conducted by Dr Pawel Lis in the Laboratory of Dr Dario Alessi (University of Dundee).

For optimisation assays, whole wildtype 5dpf larvae (20 per Eppendorf) or dissected wildtype brain tissue was snap frozen and sent to Dundee on dry ice. Samples were homogenised and resuspended in lysis buffer. Although large quantities of protein (~2mg) were obtained from larval samples resuspended in 300µL of lysis buffer, western blots using 30µg lysate from these samples were unsuccessful, despite no detection of protein degradation via Ponceau S staining (**figure 64**). Brain tissue, however, gave more robust staining for some of the proteins of interest (**figure 64**). Therefore, brain tissue was used for the analysis of mutant larvae, for which assays had already been established and optimised in the Alessi group. For all blots, human A549 cells were used as positive controls, as each antibody was known to work on these samples. Membranes were also stained with Ponceau S to assess the quality of lysates.

Whole brains were dissected from adult zebrafish of known genotype, snap frozen and sent to Dundee on dry ice. Two separate blots were performed using three biological replicates of *lrrk2*$^{-/-}$ mutant brain tissue, as well as age-matched control tissue, although these were not siblings. A phosphorylated Rab10 signal was readily detected in the brain samples, although there was no obvious difference in band intensity between mutant and control samples (**figure 65**). Although two of the LRRK2 antibodies did not work (one that recognises autophosphorylated LRRK2 and one that recognises LRRK2 c-terminal), even in wildtype tissue, the UDD3 LRRK2 antibody gave a correct band size following immunoblotting. However, this antibody suggested equal levels of Lrrk2 protein were present in *lrrk2*$^{-/-}$ mutant brains and wildtype controls (**figure 65**). A pan-phosphoT-Rab antibody, able to recognise various Thr-phosphorylated Rab proteins, was also tested, although again no differences were seen between controls and *lrrk2*$^{-/-}$ mutant samples (**figure 65**). Levels of Protein Phosphatase, Mg2+/Mn2+ Dependent 1H (PPM1H), a phosphatase that opposes LRRK2 activity by dephosphorylating Rab proteins (Berndsen et al., 2019), were also assessed in the brain samples, but staining was the same between genotypes (**figure 65**).

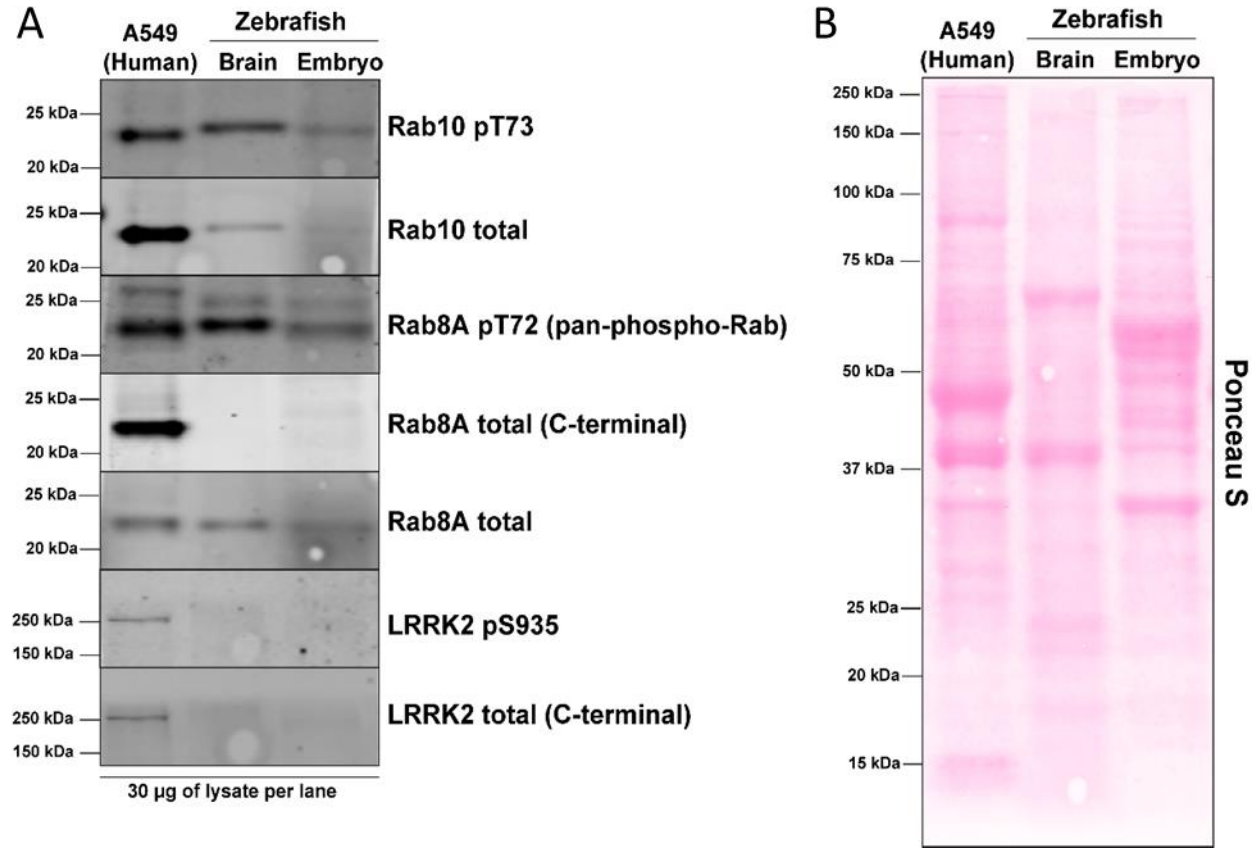

Figure 64. Phospho-Rab Assay Optimisation Using Wildtype Zebrafish Tissues. A. *Western blot using adult brain (centre) or 5dpf embryo (right) lysates against a number of proteins.* ***B.*** *Ponceau S blot using brain (centre) or embryo (right) lysates. In both cases, human A549 cell lysates were used as positive controls for the antibodies. Experiments and figure kindly produced by Dr Pawel Lis (University of Dundee). kDa, kilodaltons; lrrk2, leucine-rich repeat kinase 2; µg, micrograms.*

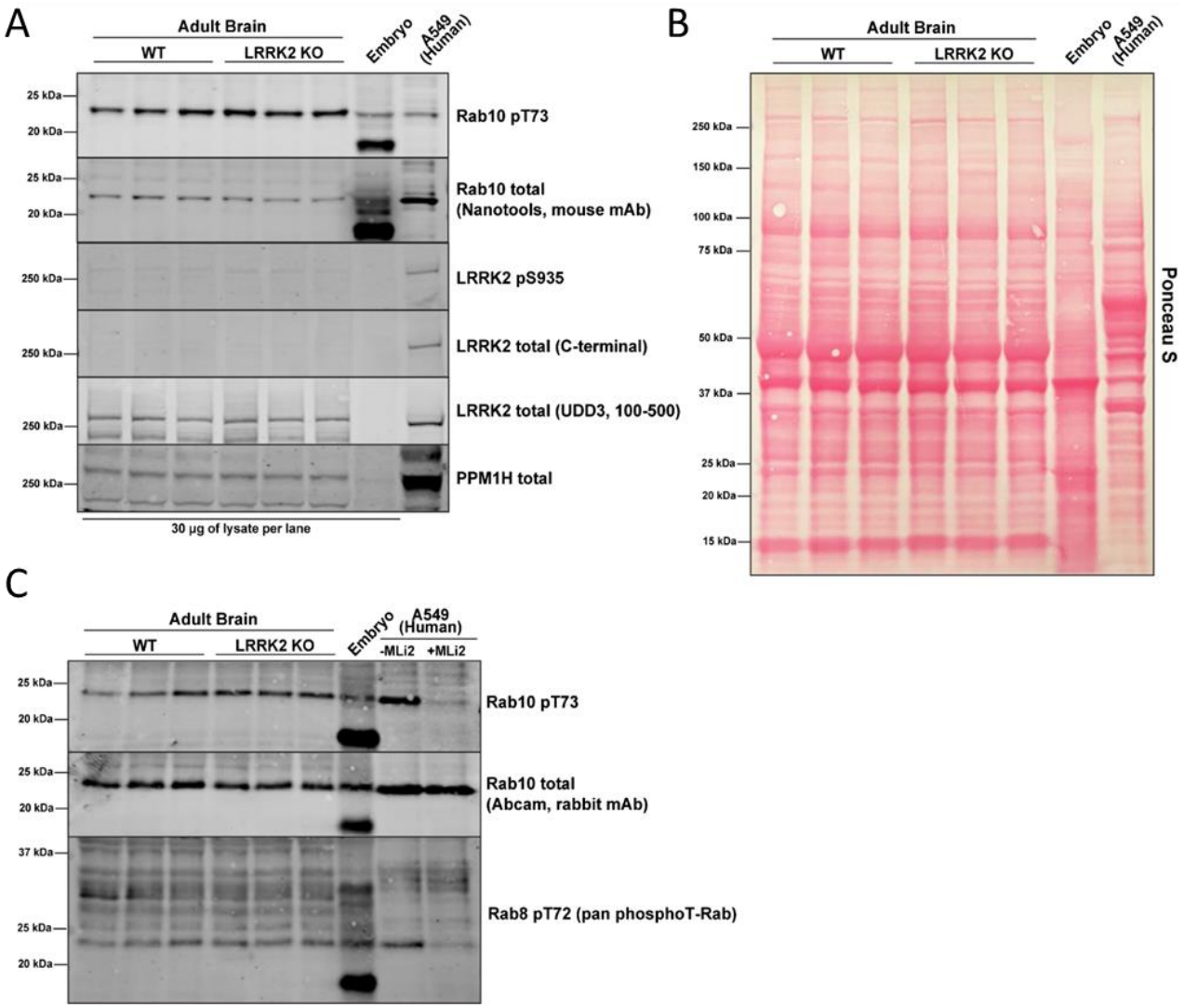

Figure 65. Leucine-Rich Repeat Kinase 2 Protein Function Assay using Phospho-Rab Western Blotting. A. *Western blot showing levels of Rab10 phosphorylated on tyrosine 73 (row 1), total Rab10 protein (row 2), LRRK2 protein (rows 3, 4, 5) and PPM1H (row 6) in adult zebrafish brain tissue from lrrk2 homozygous mutants (LRRK2 KO) or their wildtype siblings (WT).* ***B.*** *Western blot with ponceau S staining to assess protein quality in brain samples.* ***C.*** *Western blot showing levels of Rab10 phosphorylated on tyrosine 73 (row 1), total Rab10 protein (row 2) and Rab8 phosphorylated on tyrosine 72 (this antibody recognises multiple phosphorylated Rab proteins). For all blots, each column represents a single adult zebrafish brain. All embryo samples refer to wildtype embryos. A549 cells were used as a positive control. Experiments and figure kindly produced by Dr Pawel Lis (University of Dundee). kDa, kilodaltons; lrrk2, leucine-rich repeat kinase 2; MLi2, lrrk2 inhibitor; PPM1H, Protein Phosphatase, Mg2+/Mn2+ Dependent 1H; µg, micrograms.*

5.2.5 Further Analysis of mRNA

Following the disappointing western blot data, *lrrk2* mRNA levels were re-tested in *lrrk2*$^{-/-}$ mutant larvae. Larvae were finclipped and genotyped at 3dpf and allowed to develop until 5dpf. Fifteen larvae per genotype per replicate were then combined for RNA extraction and cDNA synthesis. The primer pair initially designed and tested by Dr Sarah Brown was also used for these experiments to maintain consistency. This primer pair was tested for specificity in a gradient PCR using wildtype cDNA (**figure 55B**) and optimised for qPCR as described previously.

In contrast to the previous data obtained by Dr Brown (**section 5.2.9.8**), there was no significant difference in *lrrk2* mRNA levels between *lrrk2*$^{-/-}$ *mutant zebrafish* and their wildtype siblings in this generation of mutants (**figure 66**). The initial qPCR by Dr Brown was conducted using adult brain samples. Therefore, the qPCR was repeated using adult brain RNA; this also showed no significant difference in expression levels of *lrrk2* mRNA between wildtype and *lrrk2*$^{-/-}$ mutant zebrafish (**figure 66**). Repeating the larval experiment using *lrrk2*$^{-/-}$ mutant larvae from *lrrk2*$^{-/-}$ parents (homozygous incross), also did not demonstrate a significant reduction in mRNA levels, although there did seem to be a trend of reduced expression (**figure 66**). For this experiment, wildtype control larvae were cousins as opposed to siblings of the *lrrk2*$^{-/-}$ mutant larvae.

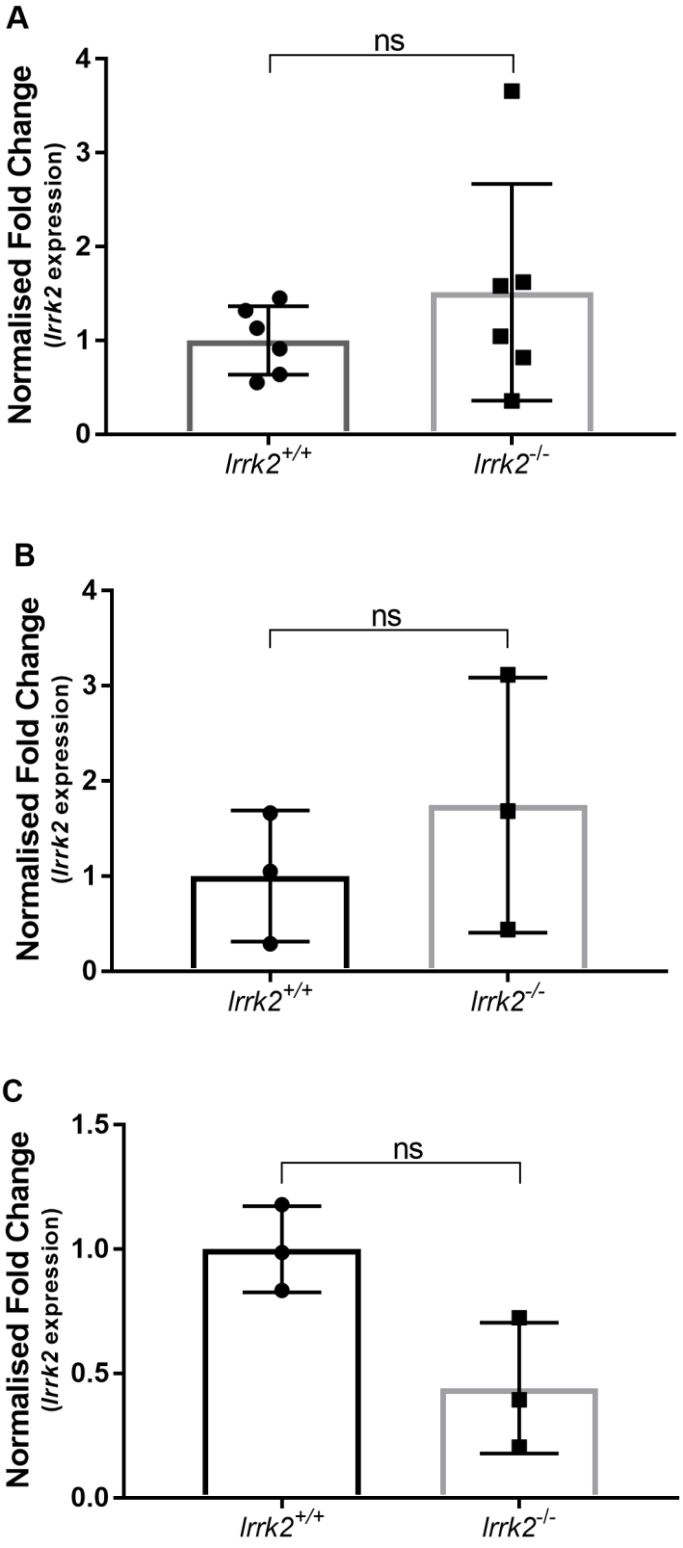

Figure 66. Quantitative Polymerase Chain Reaction of Leucine-Rich Repeat Kinase 2 Transcript Levels Demonstrates the Nonsense-Mediated Decay of mRNA is Lost. A. *No significant difference was seen in expression levels of lrrk2 mRNA between wildtype and lrrk2$^{-/-}$ mutant larvae at 5dpf (p=0.5233). n=6 biological replicates (15 larvae per replicate)* ***B.*** *No significant difference was seen in expression levels of lrrk2 mRNA between wildtype and lrrk2$^{-/-}$ mutant zebrafish when assessing expression in brain tissue (p=0.5537). n=3 biological replicates (1 brain per replicate)* ***C.*** *No significant difference was seen in expression levels of lrrk2 mRNA between wildtype and lrrk2$^{-/-}$ mutant larvae (5dpf) obtained from a homozygous incross (p=0.0685). n=3 biological replicates (15 larvae per replicate). Wildtype control larvae were obtained from the siblings of the lrrk2$^{-/-}$ mutant adult zebrafish, making experimental larvae cousins. In all datasets, transcript levels of lrrk2$^{-/-}$ mutant zebrafish are expressed as a percentage of wildtype. Expression was normalised to rps29. All groups passed Shapiro-Wilk test for normality and were statistically analysed using an unpaired, two-tailed t test on ddCt values. lrrk2, leucine-rich repeat kinase 2; ns, not significant; rps29, ribosomal protein S29.*

5.2.6 Using The CRISPant Approach to Assess Leucine-Rich Repeat Kinase 2 Function

5.2.6.1 Creating lrrk2 CRISPants

Due to the absence of a measurable functional kinase deficit and the loss of nonsense-mediated decay in the stable *lrrk2* mutant line, additional experiments using the CRISPant method were designed to continue assessing the effect of a loss of *lrrk2* in zebrafish. Guides targeting *lrrk2* were designed by Dr Deepak Ailani (Bandmann group), but all future work including testing the primers and guides was done as part of this thesis by the author.

Firstly, primer pairs flanking the guide target site were tested on wildtype genomic DNA. A gradient PCR before and after digestion with appropriate restriction enzymes (those that would be disrupted following Cas9 cleavage) was conducted to ensure primer specificity and detectable digestion. All four pairs were able to recognise altered DNA length following digestion at all temperatures tested (**figure 67**). Therefore, corresponding guides were ordered and underwent efficiency testing in wildtype embryos (for experimental details, see methods). Two HAGs were identified with an almost complete loss of corresponding restriction sites, one targeting exon 1 and another targeting exon 6 (**figure 68**). These were combined and co-injected into single-celled embryos to create *lrrk2* CRISPants.

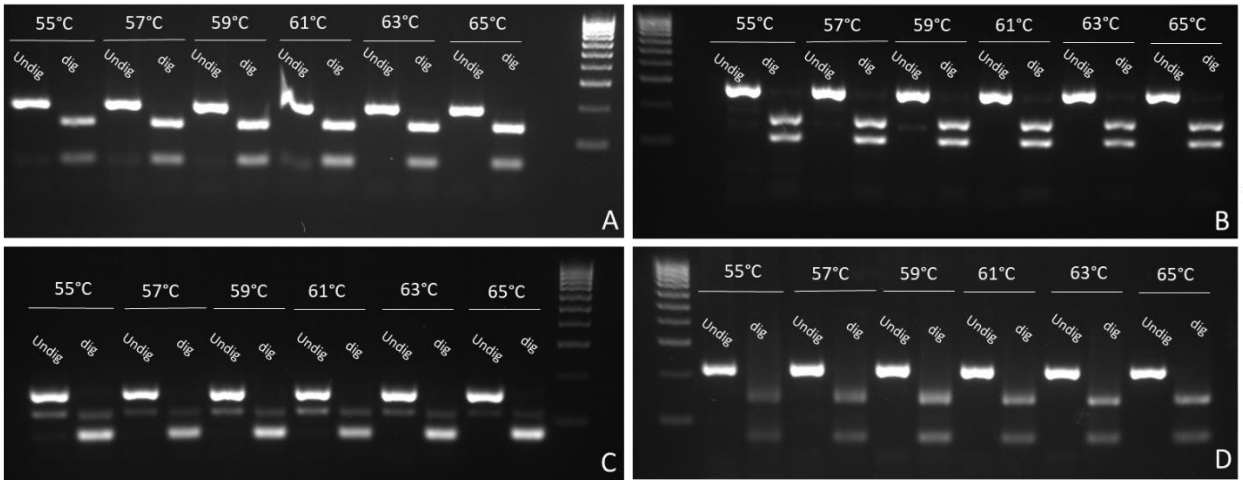

Figure 67. Electrophoresis Gel Following a Gradient Polymerase Chain Reaction Experiment and Subsequent 2-Hour Digest with Restriction Enzymes to Assess Suitability for Leucine-Rich Repeat Kinase 2 CRISPant Work. A. *Primer pair flanking guide RNA targeting exon 1 of lrrk2, digested with BsrI.* ***B.*** *Primer pair flanking guide RNA targeting exon 5 of lrrk2, digested with AlwNI.* ***C.*** *Primer pair flanking guide RNA targeting exon 6 of lrrk2, digested with BslI. Non-specific band can be seen at ~110bp, although this does not affect ability to detect efficient digestion.* ***D.*** *Primer pair flanking guide RNA targeting exon 9 of lrrk2, digested with MwoI. Ladder is 100bp [Bioline]. Temperatures above represent the annealing temperature used for each PCR. dig, digested PCR product with appropriate restriction enzyme; Undig, undigested PCR product.*

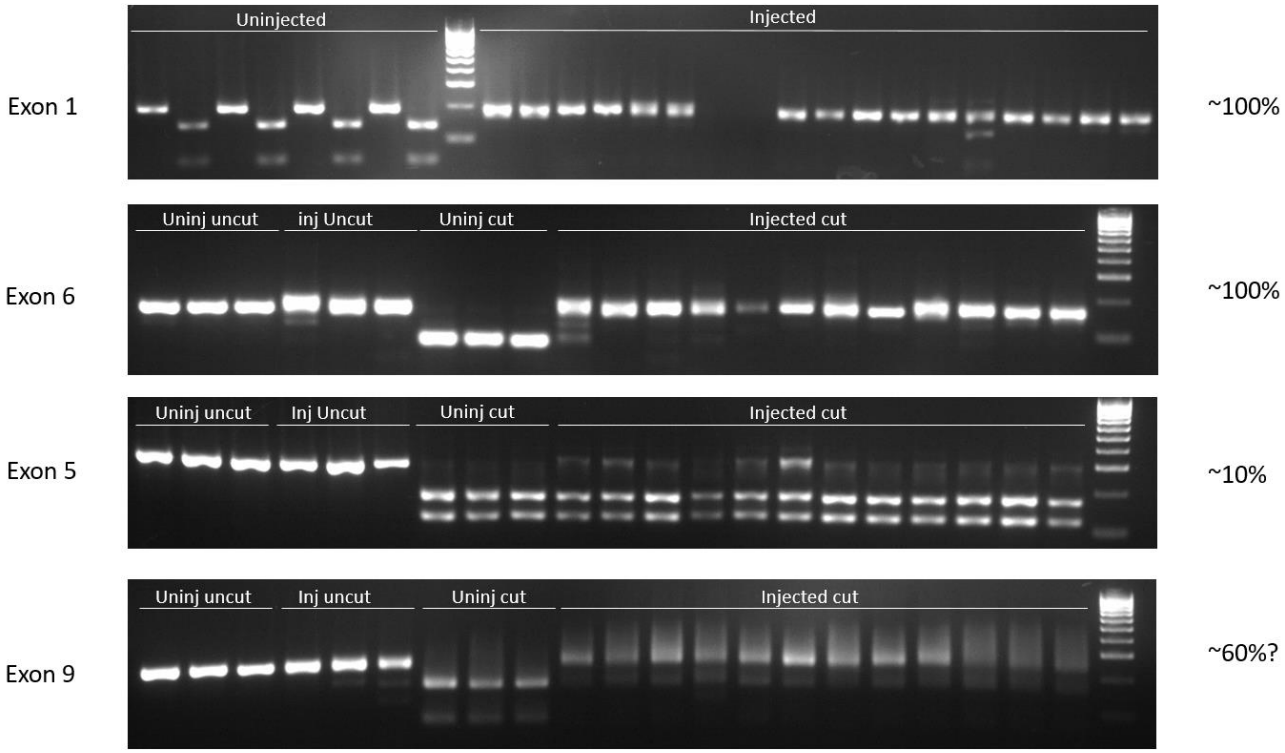

Figure 68. Efficiency Testing of Guides That Target Leucine-Rich Repeat Kinase 2. *DNA was extracted from injected 1dpf embryos and amplified by PCR. Following digest with respective restriction enzymes, samples were run on 2% gel. For exon 1 (top lane) samples are shown as undigested (PCR product) followed by digested result of the same sample in adjacent lane. For all other target exons, gels are laid out as 3 uninjected, undigested samples (Uninj uncut), 3 injected undigested samples (Inj Uncut), 3 uninjected digested samples (Uninj cut) and 12 injected digested samples (Injected cut). Ladder is 100bp [Bioline]. Percentages represent estimates of guide efficiency based on the reduction in digested products.*

5.2.6.2 Analysis of the lrrk2 CRISPant

Following injection, fish were raised to assess effects on their phenotype. *lrrk2* CRISPants were viable and appeared morphologically normal up to 5dpf (**figure 69**). Fish were not raised beyond this point.

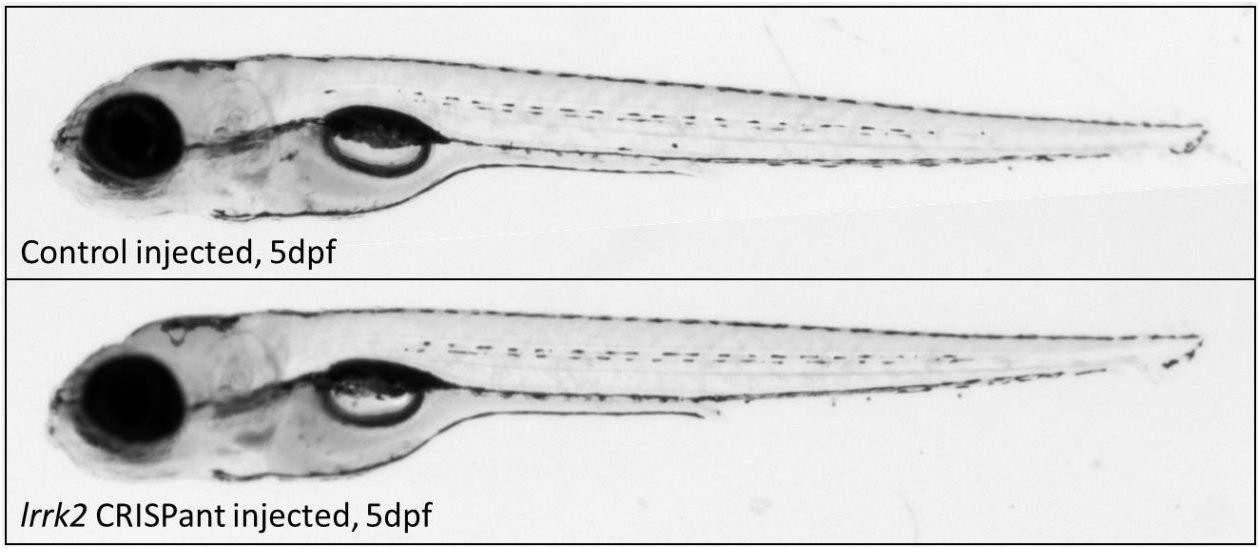

Figure 69. Leucine-Rich Repeat Kinase 2 CRISPants Appear Morphologically Normal at 5-Days Post Fertilisation. *Representative brightfield images of lrrk2 CRISPant and control injected wildtype sibling at 5dpf. dpf, days post fertilisation; lrrk2, leucine-rich repeat kinase 2.*

5.2.6.2.1 Quantitative PCR

RNA was extracted from 5dpf *lrrk2* CRISPants or control larvae (injected with Cas9 and tracrRNA only). Following cDNA production, levels of *lrrk2* and *lrrk1* were assessed using qPCR. *lrrk2* mRNA levels appeared reduced in *lrrk2* CRISPants compared to controls, although this was not significant due to the large variability in control-injected larvae (p=0.0809, **figure 70**). l*rrk1* mRNA levels were measured in *lrrk2* CRISPants to assess *lrrk1* compensation. Unexpectedly, levels of *lrrk1* were found to be reduced in *lrrk2* CRISPants, although as with *lrrk2* this was not significant, likely owing to the high variability in wildtype samples (p=0.1960 and 0.1626, **figure 70**). Of note, control samples with high levels of *lrrk2* also demonstrated high levels of *lrrk1*, and vice versa. However, analysis of *rps29* levels, as well as an additional qPCR against another gene (*acmsd*) using the same cDNA samples (data not shown), suggested that this was real and specific as variations in control samples were not seen for these additional genes. Furthermore, primer specificity was checked using Primer-BLAST software, which suggested that each primer pair was specific for only one *lrrk* paralog. The gRNAs used should also only target *lrrk2*, having no recognition sites in *lrrk1* DNA.

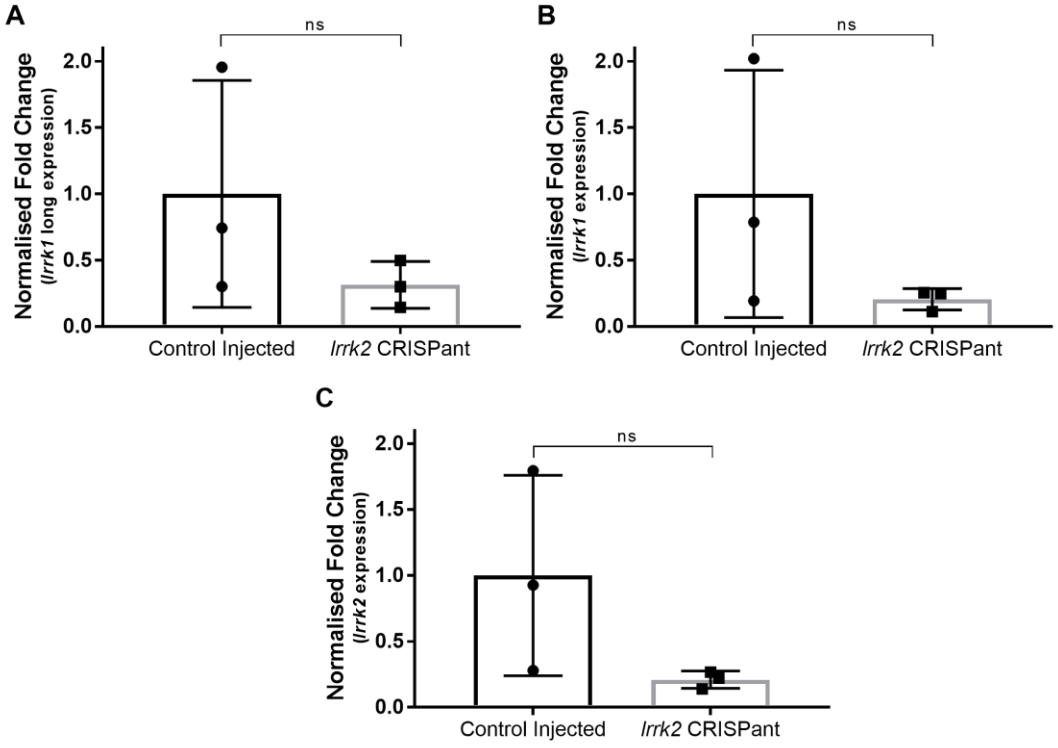

Figure 70. mRNA Levels of Both Leucine-Rich Repeat Kinase Paralogues in Leucine-Rich Repeat Kinase 2 CRISPants. *Quantitative PCR found no significant differences in expression between lrrk2 CRISPants and control-injected larvae of either the long transcript of lrrk1 (**A**, p=0.1960), the combined expression of both lrrk1 splice variants (**B**, p=0.1626) or lrrk2 (**C**, p=0.0809). For all experiments, RNA was pooled from 15 5dpf larvae. Control larvae were injected with tracrRNA and Cas9 only. rps29 was used as a reference gene and all data is expressed as a change to control levels. Each group passed a Shapiro-Wilk test for normality, so were statistically analysed using an unpaired, two-tailed t test on ddCt values (note fold change is displayed on graph). dpf, days post fertilisation; lrrk1, leucine-rich repeat kinase 1; lrrk2, leucine-rich repeat kinase 2; ns, not significant; rps29, ribosomal protein S29.*

5.2.6.2.2 Dopaminergic Neuron Number and Susceptibility to MPP+

lrrk2 CRISPants were assessed for their dopaminergic neuron count and response to MPP+. Injected larvae were treated with phenylthiourea and raised to 3dpf, either being exposed to MPP+ from 1-3dpf or a MilliQ control. Fixed larvae underwent *th1* in situ hybridisation and t*h1+* cells were counted from three biological replicates. *lrrk2* CRISPants did not show significant differences in the number of dopaminergic neurons compared to control injected larvae (**figure 71**, p=0.0512). MPP+ treatment resulted in significant reductions in *th1+* cells in both groups (**figure 71,** 35.51% in *lrrk2* CRISPants, p<0.0001; 37.90% in controls, p<0.0001). Total cell counts between groups following MPP+ treatment remained indistinguishable (**figure 71,** p=0.8874).

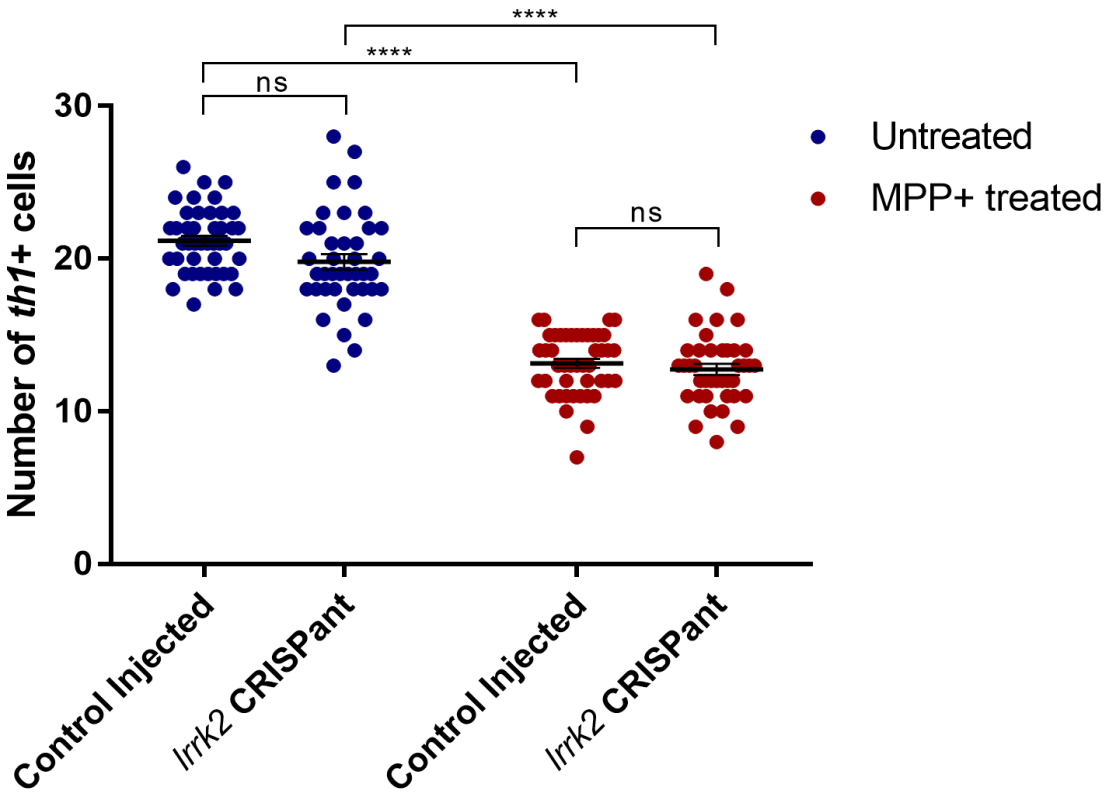

Figure 71. Leucine-Rich Repeat Kinase 2 CRISPants Have Normal Dopaminergic Neuron Numbers and Susceptibility to 1-methyl-4-phenylpyridinium. *Dopaminergic neuron numbers in the ventral diencephalon, counted following in situ hybridisation against tyrosine hydroxylase 1 (th1), show no difference between lrrk2 CRISPants and control injected larvae (p=0.0512). 1-methyl-4-phenylpyridinium (MPP+) treatment resulted in significant reductions in th1+ cells in both groups (35.51% in lrrk2 CRISPants, p<0.0001; 37.90% in controls, p<0.0001). Total cell counts between groups following MPP+ treatment remained indistinguishable (p=0.8874). Data represented as mean±SEM. n=39-45 per group, from 3 biological replicates. Statistics from a two-way ANOVA with Tukey's multiple comparisons post-hoc test. th1, tyrosine hydroxylase; lrrk2, leucine-rich repeat kinase 2; MPP+, 1-methyl-4-phenylpyridinium; ns, not significant.*

5.2.7 Leucine-Rich Repeat Kinase 1 CRISPants

lrrk1 CRISPants were also developed as a part of this thesis with the aim of combining their use with *lrrk2*$^{-/-}$ mutant zebrafish or *lrrk2* CRISPants, effectively creating a zebrafish devoid of all *lrrk* paralogues.

5.2.7.1 Creating lrrk1 CRISPants

Guides were designed to target regions of *lrrk1* present in both spice variants of the gene to reduce the likelihood of either variant being part-translated. This was done manually by assessing the presence of Cas9 recognition sites (NGG/CCN) in the cDNA of the shorter *lrrk1* variant. Initially, primer pairs were tested using a gradient PCR on wildtype genomic DNA to ensure they were specific and could recognise changes in DNA length following digestion with the appropriate restriction enzymes (**figure 72**). All four primer pairs were successful, so guides were ordered and tested by injecting into wildtype embryos (for details, see methods). Problems occurred with the PCRs for some of these samples, which was later revealed as an issue with the NaOH used for DNA extraction. However, guide efficiencies could still be estimated from the remaining samples, by assessing alterations to the digest following injection (**figure 73**). Only one guide, targeting exon 1, appeared to have a high efficiency and so four new guides were designed and tested in the same way. Primers were initially tested in wildtype genomic DNA (**figure 74**). The primer pair flanking gRNA targeting exon 7 demonstrated non-specific amplification (**figure 74D**), so new primers were designed and found to be specific (**figure 74E**). These four new guides underwent efficiency testing, which identified two guides that were approximately 70% active (**figure 75**). The gRNA targeting exon 1 from the initial set and the gRNA targeting exon 5 from new set were combined to create *lrrk1* CRISPants.

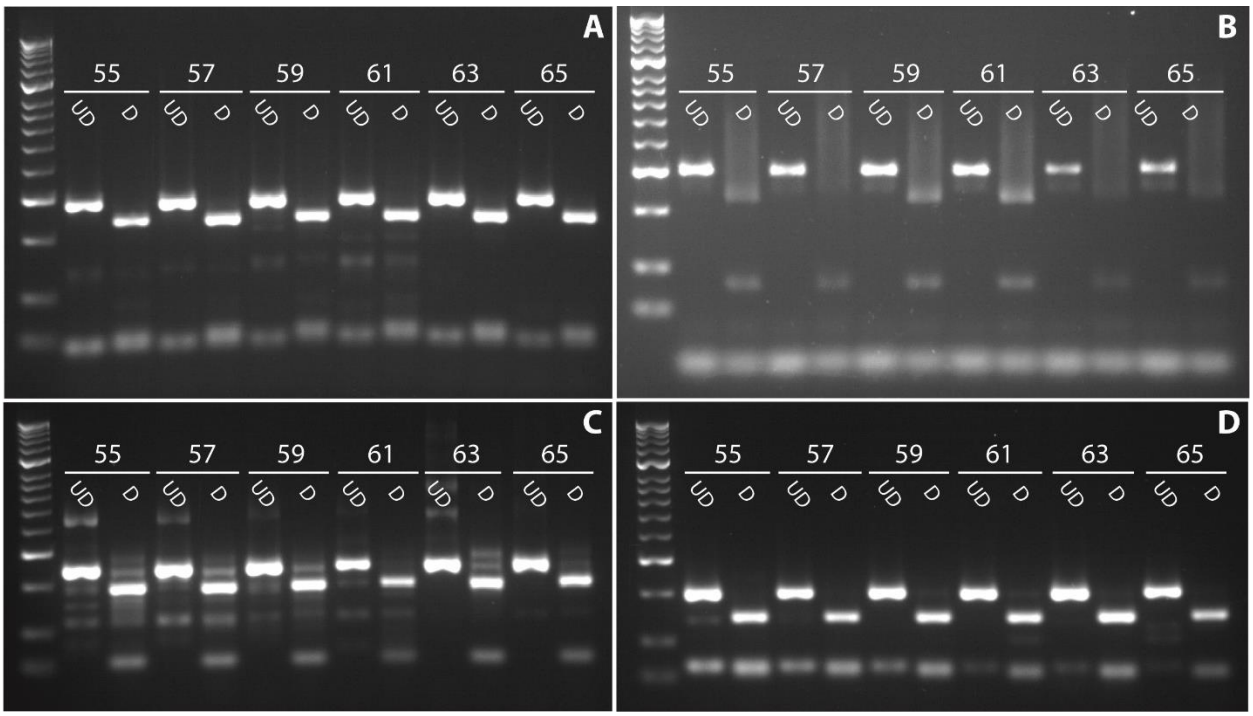

Figure 72. Electrophoresis Gel Following a Gradient Polymerase Chain Reaction Experiment and Subsequent 2-Hour Digest with Restriction Enzymes to Assess Suitability for Leucine-Rich Repeat Kinase 1 CRISPant Work. A. *Primer pair flanking guide RNA targeting exon 1 of lrrk1, digested with AvaII.* ***B.*** *Primer pair flanking guide RNA targeting exon 2 of lrrk1, digested with MwoI.* ***C.*** *Primer pair flanking guide RNA targeting exon 3 of lrrk1, digested with AluI.* ***D.*** *Primer pair flanking guide RNA targeting exon 4 of lrrk1, digested with MslI. Ladder is 50bp [Meridian Bioscience]. The numbers above represent the annealing temperature used for each PCR. D, digested PCR product with appropriate restriction enzyme; UD, undigested PCR product.*

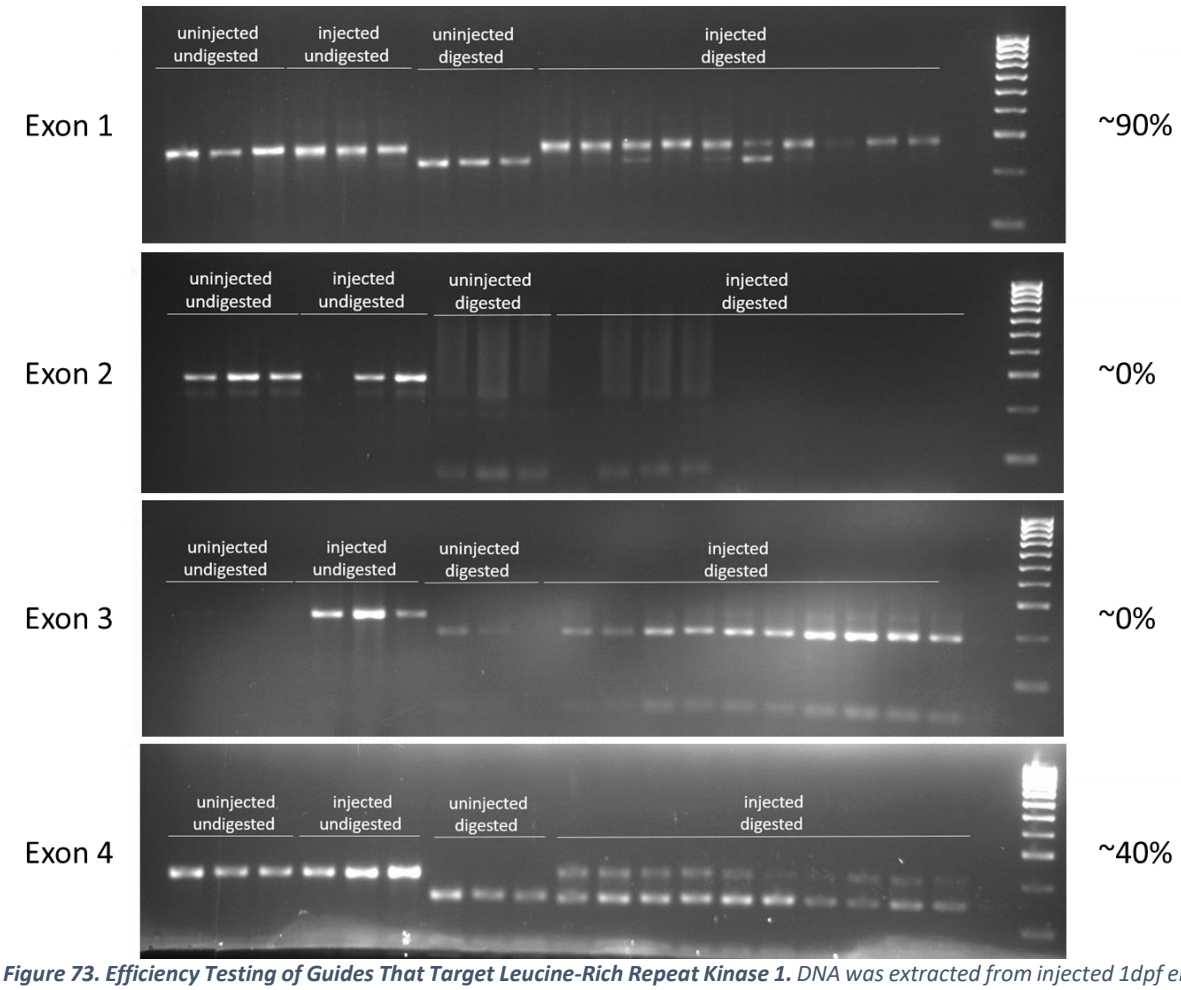

Figure 73. Efficiency Testing of Guides That Target Leucine-Rich Repeat Kinase 1. *DNA was extracted from injected 1dpf embryos and amplified by PCR. Following digest with respective restriction enzymes, samples were run on 2% gel. For all target exons, gels are laid out as 3 uninjected, undigested samples, 3 injected undigested samples, 3 uninjected digested samples and 10 injected digested samples. Ladder is 100bp [Bioline]. Percentages represent estimates of guide efficiency based on reduction in digest efficiency.*

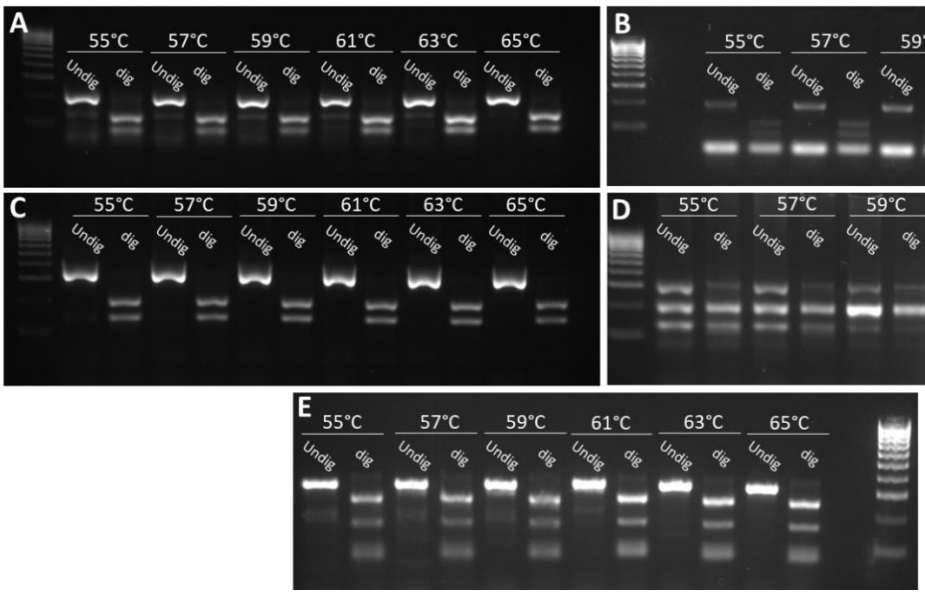

Figure 74. New Electrophoresis Gel Following a Gradient Polymerase Chain Reaction Experiment and Subsequent 2-Hour Digest with Restriction Enzymes to Assess Suitability for Leucine-Rich Repeat Kinase 1 CRISPant Work. A. *Primer pair flanking guide RNA targeting exon 2 of lrrk1, digested with BslI.* ***B.*** *Primer pair flanking guide RNA targeting exon 3 of lrrk1, digested with DdeI.* ***C.*** *Primer pair flanking guide RNA targeting exon 5 of lrrk1, digested with BtgI.* ***D.*** *Primer pair flanking guide RNA targeting exon 7 of lrrk1, digested with AlwNI.* ***E.*** *New primer pair flanking guide RNA targeting exon 7 of lrrk1, digested with AlwNI. Ladder is 100bp [Bioline]. Temperatures above represent the annealing temperature used for each PCR. dig, digested PCR product with appropriate restriction enzyme; Undig, undigested PCR product.*

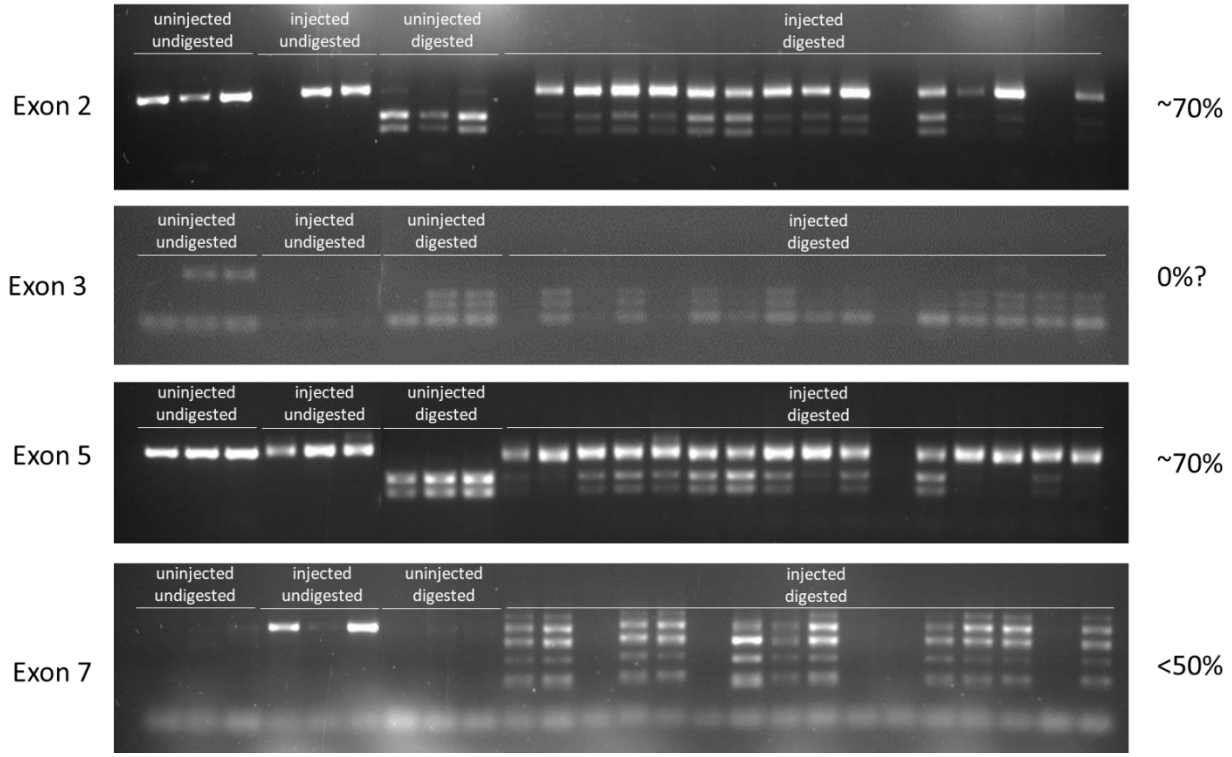

Figure 75. Efficiency Testing of New Guides That Target Leucine-Rich Repeat Kinase 1. *DNA was extracted from injected 1dpf embryos and amplified by PCR. Following digest with respective restriction enzymes, samples were run on a 2% gel. For all target exons, gels are laid out as 3 uninjected, undigested samples, 3 injected undigested samples, 3 uninjected digested samples and 16 injected digested samples. Ladder is 100bp [Bioline]. Percentages represent estimates of guide efficiency based on the reduction of digested products.*

5.2.7.2 Analysis of lrrk1 CRISPants

lrrk1 CRISPants were generated by injecting these two HAGs into single-cell stage wildtype zebrafish embryos. Resulting CRISPants were viable and appeared morphologically identical to their control injected (tracrRNA and Cas9 only) siblings until 5dpf (**figure 76**). Larvae were not raised beyond this point.

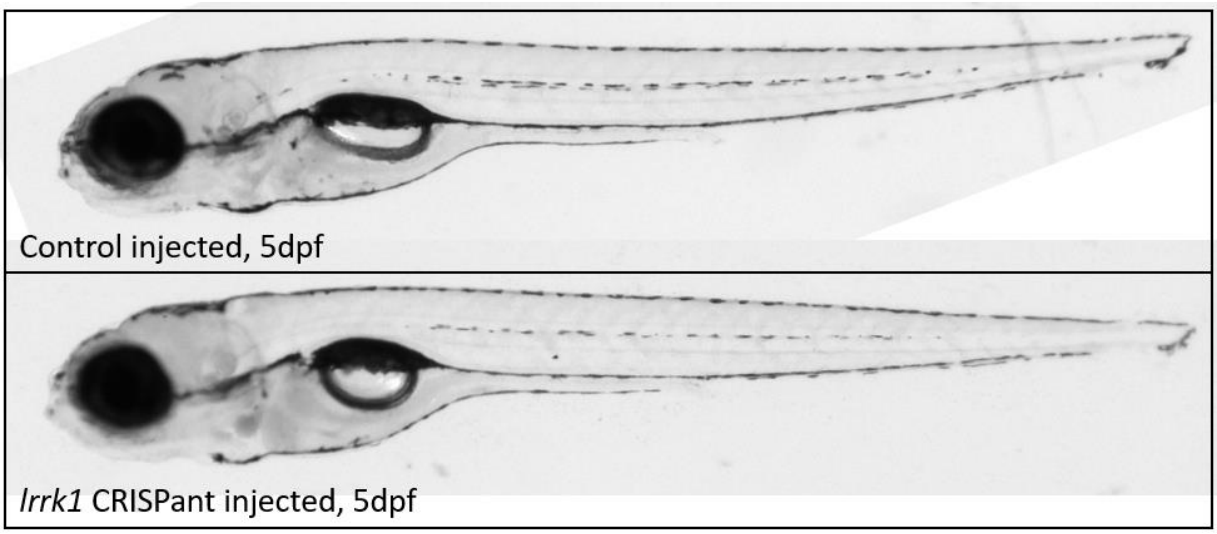

Figure 76. Leucine-Rich Repeat Kinase 1 CRISPants Appear Morphologically Normal at 5-Days Post Fertilisation. *Brightfield images of a lrrk1 CRISPant and control injected wildtype sibling at 5-dpf. dpf, days post fertilisation; lrrk1, leucine-rich repeat kinase 1.*

5.2.7.2.1 Quantitative PCR

qPCR was used to assess the effect of *lrrk1* gRNA injections on the expression of the target gene, *lrrk1*, and for compensatory up-regulation of *lrrk2*. No significant difference was found in the expression of either transcript of *lrrk1* in the *lrrk1* CRISPants compared to controls (**figure 77**). *lrrk2* mRNA levels were also assessed, demonstrating *lrrk2* expression to show a trend of increasing in *lrrk1* CRISPants, although no significant differences were found (**figure 77**).

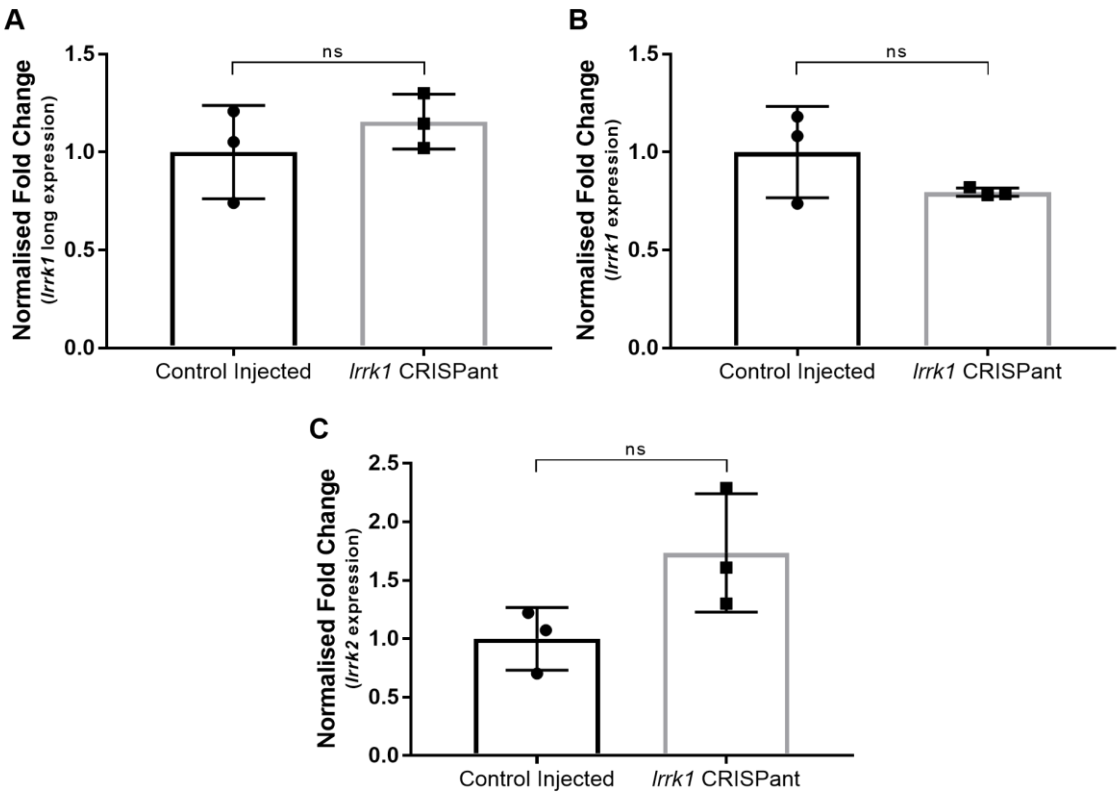

Figure 77. mRNA Levels of Both Leucine-Rich Repeat Kinase Paralogues in Leucine-Rich Repeat Kinase 1 CRISPants. *Quantitative PCR found no significant differences in expression between lrrk1 CRISPants and control-injected larvae of either the long transcript of lrrk1 (**A**, p=0.3781), the combined expression of both lrrk1 splice variants (**B**, p=0.2247) or lrrk2 (**C**, p=0.0794). Note different axis between lrrk1 and lrrk2 data. For all experiments, RNA was pooled from 15 5dpf larvae. Control larvae were injected with tracrRNA and Cas9 only. rps29 was used as a reference gene and all data is expressed as a change to control levels. Each group passed a Shapiro-Wilk test for normality, so were statistically analysed using an unpaired, two-tailed t test on ddCt values. dpf, days post fertilisation; lrrk1, leucine-rich repeat kinase 1; lrrk2, leucine-rich repeat kinase 2; ns, not significant; rps29, ribosomal protein S29.*

5.2.7.2.2 Dopaminergic Neuron Counting and Susceptibility to MPP+

As before, dopaminergic neurons were assessed following in situ hybridisation against *th1*. No difference was seen in the number of *th1+* cells between *lrrk1* CRISPants and control injected larvae (**figure 78**, p=0.9996). MPP+ exposure resulted in significant reductions in *th1+* cells in both *lrrk1* CRISPants (39.30% reduction, p<0.0001) and controls (39.34% reduction, p<0.0001), although total cell counts between groups following exposure remained indistinguishable (**figure 78**, p>0.9990).

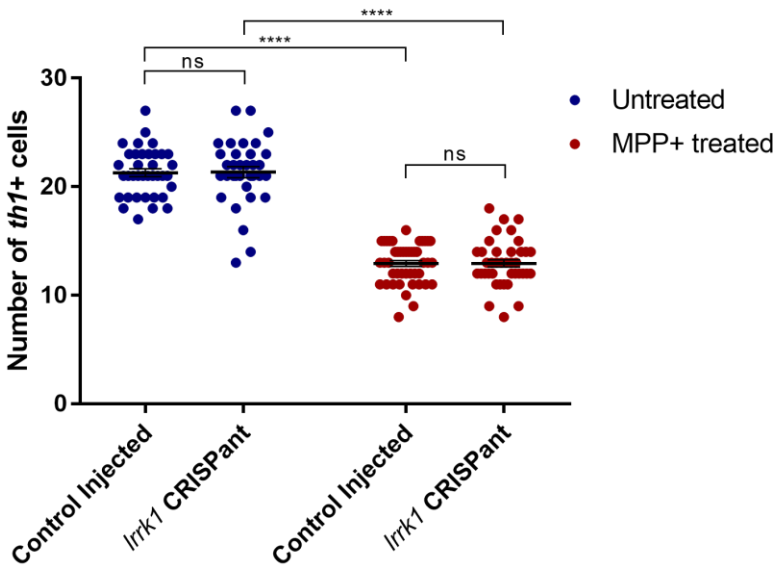

Figure 78. Leucine-Rich Repeat Kinase 1 CRISPants Have Normal Dopaminergic Neuron Numbers and Susceptibility to 1-methyl-4-phenylpyridinium. *Dopaminergic neuron numbers in the ventral diencephalon, counted following in situ hybridisation against tyrosine hydroxylase 1 (th1), show no difference between lrrk1 CRISPants and control injected larvae (p=0.9996). MPP+ treatment resulted in significant reductions in th1+ cells in both groups (39.30% in lrrk1 CRISPants, p<0.0001; 39.34% in controls, p<0.0001). Total cell counts between groups following MPP+ treatment remained indistinguishable (p>0.9990). Data represented as mean±SEM. n=34-44 per group, from 3 biological replicates. Statistics from a two-way ANOVA with Tukey's multiple comparisons post-hoc test. lrrk1, leucine-rich repeat kinase 1; MPP+, 1-methyl-4-phenylpyridinium; ns, not significant; th1, tyrosine hydroxylase.*

5.2.8 Leucine-Rich Repeat Kinase Double Mutants

To generate *lrrk1/2* double mutants, the CRISPant techniques used to create the single *lrrk* CRISPants were combined. Two guides targeting each gene (described above) were simultaneously injected into single-cell stage wildtype embryos. Briefly, 1µL of each 20µM gRNA, 1µL 20µM tracrRNA, 1µL Cas9 and 1µL water were combined and 2nL of this mixture injected. The resulting double CRISPants were viable and appeared morphologically normal up to 5dpf (**figure 79**). As before, controls were injected with tracrRNA and Cas9 only.

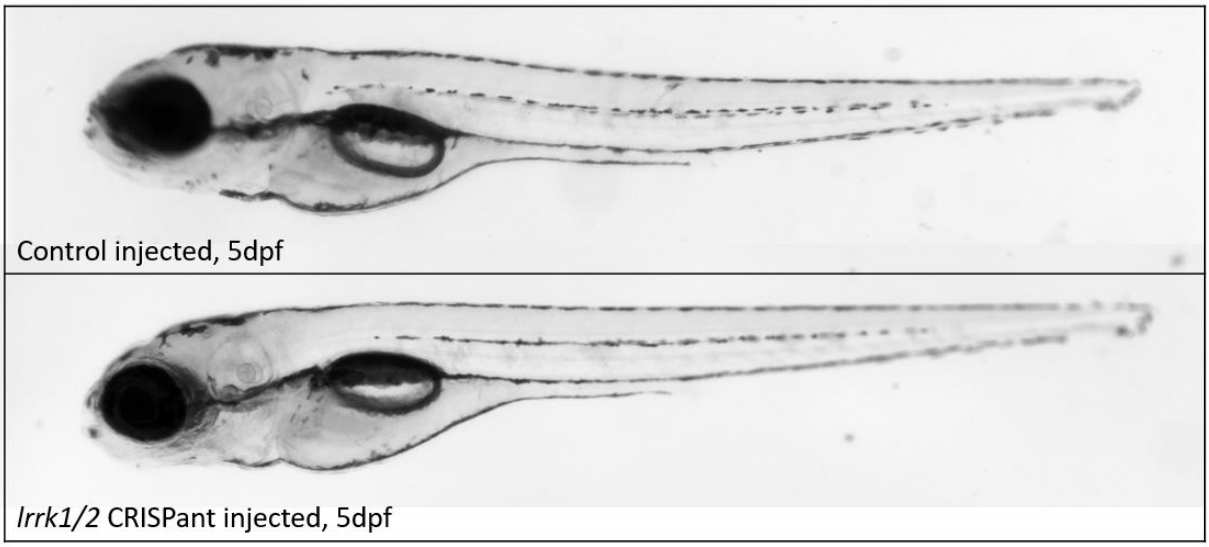

Figure 79. Leucine-Rich Repeat Kinase 1/2 Double CRISPants Appear Morphologically Normal at 5-Days Post Fertilisation. *Brightfield images of a lrrk1/2 double CRISPant and control injected wildtype sibling at 5dpf. dpf, days post fertilisation; lrrk, leucine-rich repeat kinase.*

5.2.8.1 Quantitative PCR

As before, levels of *lrrk1* and *lrrk2* were assessed in double CRISPants using qPCR. However, some samples during this experiment did not amplify (**figure 80**). Therefore, no statistical analysis could be applied to these data and no conclusions can be drawn about expression levels in double CRISPants without repeating this experiment. This repeat was not conducted as the study focus had shifted towards the generation of new stable mutant lines (**section 80**).

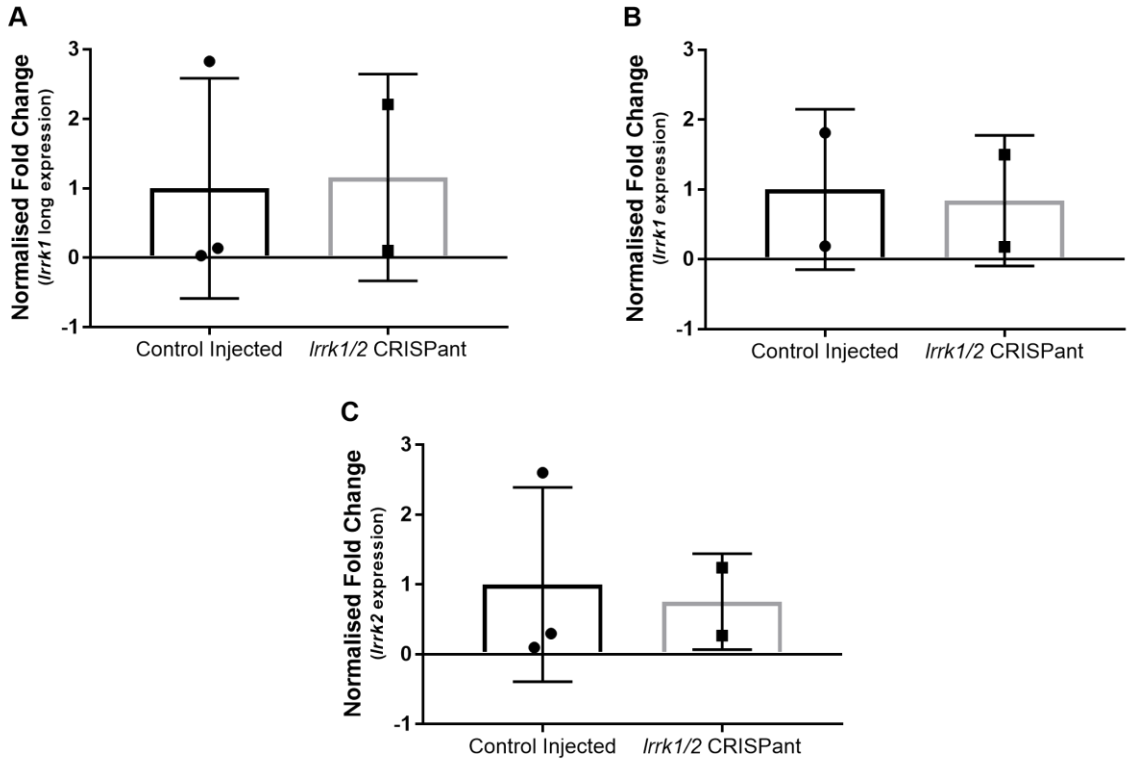

Figure 80. mRNA Levels of Both Leucine-Rich Repeat Kinase Paralogues in Leucine-Rich Repeat Kinase 1/2 Double CRISPants. *Quantitative PCR assessment of the expression of either the long transcript of lrrk1 (**A**), the combined expression of both lrrk1 splice variants (**B**) or lrrk2 (**C**). No statistical analysis was conducted due to the small number of replicates. For all experiments, RNA was pooled from 15 5dpf larvae. Control larvae were injected with tracrRNA and Cas9 only. rps29 was used as a reference gene and all data is expressed as a change to control levels. dpf, days post fertilisation; lrrk1, leucine-rich repeat kinase 1; lrrk1/2, leucine-rich repeat kinase 1 and 2; lrrk2, leucine-rich repeat kinase 2; rps29, ribosomal protein S29.*

5.2.8.2 Dopaminergic Neuron Counting and Susceptibility to MPP+

Dopaminergic neuron numbers in the ventral diencephalon were found to be no different between *lrrk1/2* CRISPants and control injected larvae (**figure 81**, p=0.8010). However, *lrrk1/2* double CRISPants appeared to be more susceptible to MPP+ exposure, which resulted in a larger reduction in *th1+* cells in *lrrk1/2* CRISPants (42.19%, p<0.0001) compared to controls (34.85%, p<0.0001). Subsequently, total cell counts following exposure to MPP+ were significantly lower in *lrrk1/2* CRISPants compared to controls (**figure 81**, p=0.0361), although the actual difference in cell number was small (2 cells).

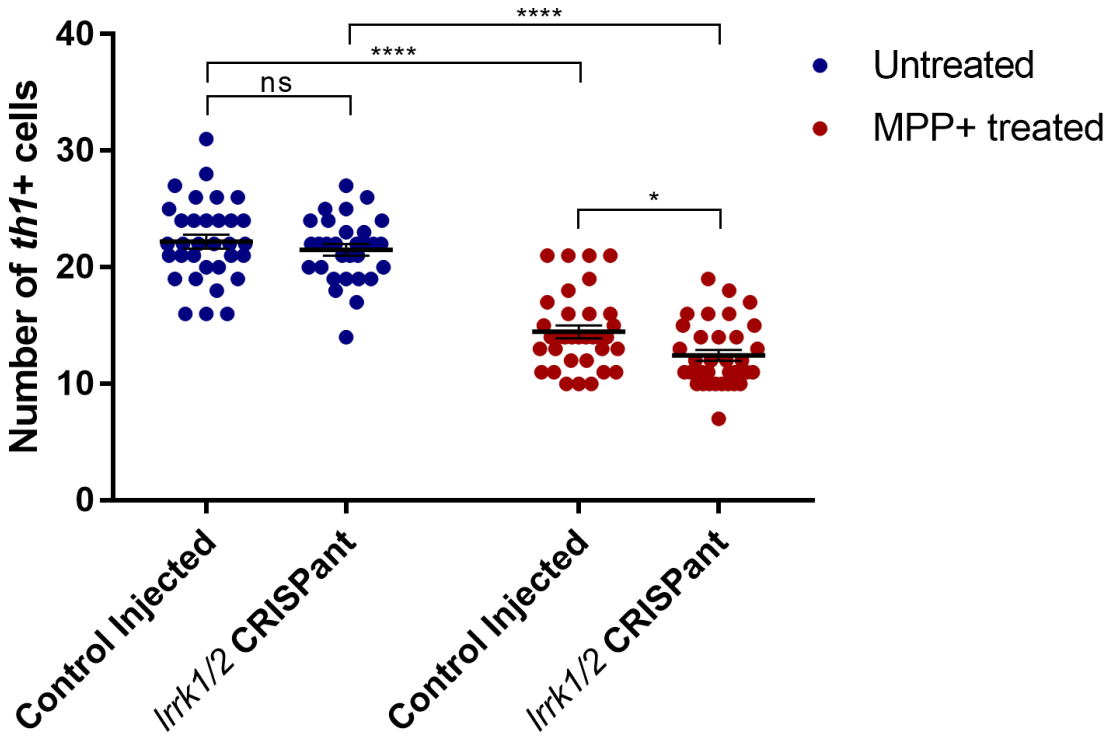

Figure 81. Leucine-Rich Repeat Kinase 1/2 Double CRISPants Have Normal Dopaminergic Neuron Numbers but Increased Susceptibility to 1-Methyl-4-Phenylpyridinium. *Dopaminergic neuron numbers in the ventral diencephalon, counted following in situ hybridisation against tyrosine hydroxylase 1 (th1), show no difference between lrrk1/2 CRISPants and control injected larvae (p=0.8010). MPP+ exposure from 1-3dpf resulted in significant reductions in th1+ cells in both groups, with a larger reduction seen in lrrk1/2 CRISPants (42.19% in lrrk1/2 CRISPants, p<0.0001; 34.85% in controls, p<0.0001). Subsequently, total cell counts following MPP+ treatment were lower in lrrk1/2 CRISPants compared to controls (p=0.0361). Data represented as mean±SEM. n=31-34 per group, from 3 biological replicates. Statistics from a two-way ANOVA with Tukey's multiple comparisons post-hoc test. lrrk1/2, leucine-rich repeat kinase 1 and 2; MPP+, 1-methyl-4-phenylpyridinium; th1, tyrosine hydroxylase.*

5.2.9 Generation of New Stable Mutant Lines

Seven mutations in *LRRK2* have been confirmed as pathological causes of familial PD with a variable penetrance (discussed in the introduction to chapter 5). The generation of stable zebrafish lines carrying equivalent single amino acid changes was attempted using CRISPR/Cas9 technology. For the following section, all proteins and DNA alignments were conducted in SnapGene and guides identified manually by the presence of NGG / CCN (see methods for further details).

5.2.9.1 G2019S

Protein alignments in SnapGene found that glycine at position 2019 in human *LRRK2* is equivalent to glycine at position 2009 in zebrafish *lrrk2* (**figure 82A**). *In silico* transcription of the *lrrk2* DNA sequence found that this glycine was coded for by the codon "GGC" in zebrafish (**figure 82**). gRNA was designed to target this region of the gene, where the Cas9 cut site was 4bps upstream of the target codon, and primers either side of this were designed using Primer3 (for guide and primer sequences, see methods). This gRNA was tested by injecting into the yolk of single-celled wildtype zebrafish embryos and analysed at 1dpf using the flanking primer pair. The smearing of injected samples on a high percentage gel, which was not seen in uninjected samples, suggested that this guide was active and could create dsDNA breaks (**figure 82**). Therefore, a single-stranded donor oligonucleotide (ssODN) to act as a template for HDR was designed.

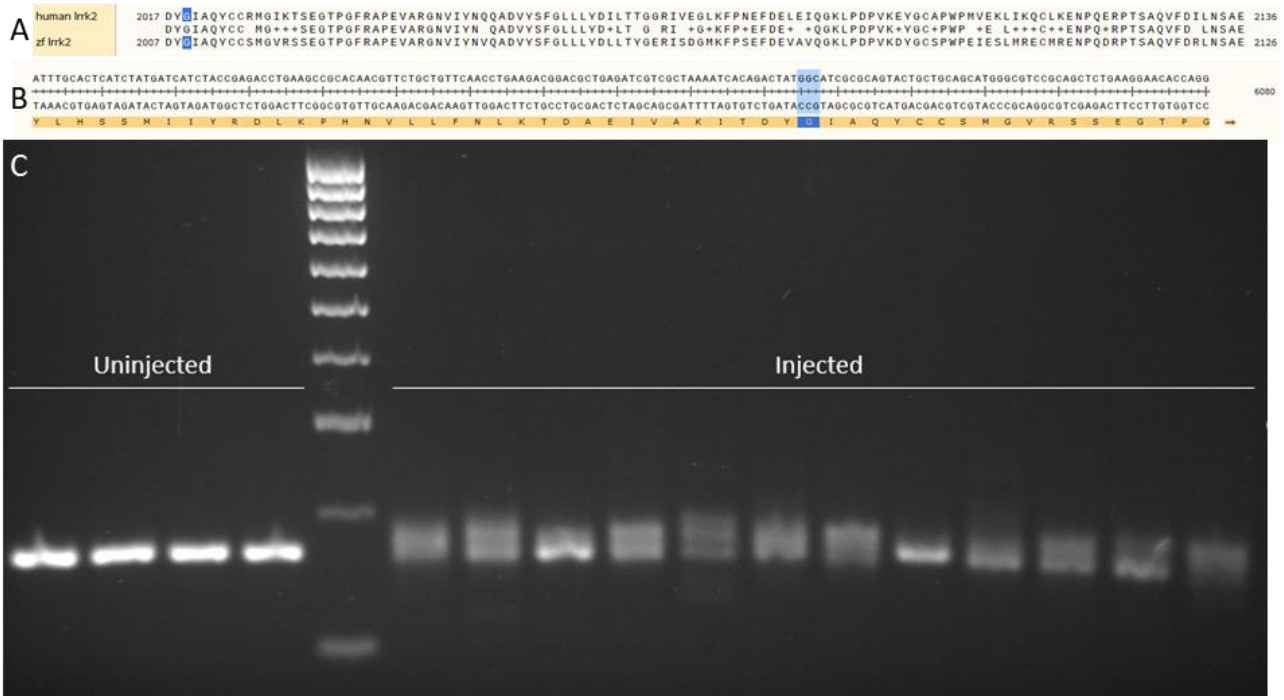

Figure 82. Designing Guide RNA to Target the Zebrafish Equivalent of G2019. A. *Protein-protein alignment of human and zebrafish Lrrk2, demonstrating glycine 2009 to be the zebrafish equivalent of human glycine 2019.* ***B.*** *DNA sequence and in silico transcription of zebrafish lrrk2, demonstrating that the target glycine (highlighted in blue) is coded for by GGC.* ***C.*** *Electrophoresis gel (3%) of PCR amplified DNA extracted from 1dpf zebrafish embryos either injected with G2019 guide RNA, tracrRNA and Cas9 or uninjected. Ladder is 100bp [Bioline]. dpf, days post fertilisation; lrrk2, leucine-rich repeat kinase 2; zf, zebrafish.*

Serine can be coded for by multiple codons (**table 21**). Each codon was looked up in a zebrafish codon usage table to exclude the use of any rare codons in the ssODN design, as these may be less likely to be transcribed by the transcription machinery. From this, UCG was excluded due to its low frequency of use in the zebrafish genome (5.6 per 1000 codons). Each codon was also assessed for the induction of novel restriction enzyme sites using SnapGene; UCU and UCA did not add any restriction sites so were not used. AGC was selected to take forward since it had the highest codon use frequency and resulted in the addition of an SfcI restriction site (**figure 83**). However, an SfcI restriction site was also present 21bps downstream, which needed to be taken into account when analysing gels following digest; *in silico* electrophoresis was conducted to assist with gel interpretation (**figure 86B**).

Table 21. Possible Codons for Serine to Use in the Design of the G2009S Donor Oligonucleotide

Possible Codon	Frequency (per thousand)	Enzyme site added?
UCU	16.9	None
UCC	15.2	BccI
UCG	5.6	TaqI, BfuCI, MboI, DpnII, Sau3AI, PvuI, BsiEI
UCA	13.2	None
AGU	13.2	HgaI, BaeI, SfcI
AGC	18.4	SfcI

Table showing codons that are translated into the amino acid serine and their frequency in the zebrafish genome. Final column describes restriction enzyme sites that are added into the DNA following mutation of the wildtype codon to each of the possible serine codons. For more information, see methods section.

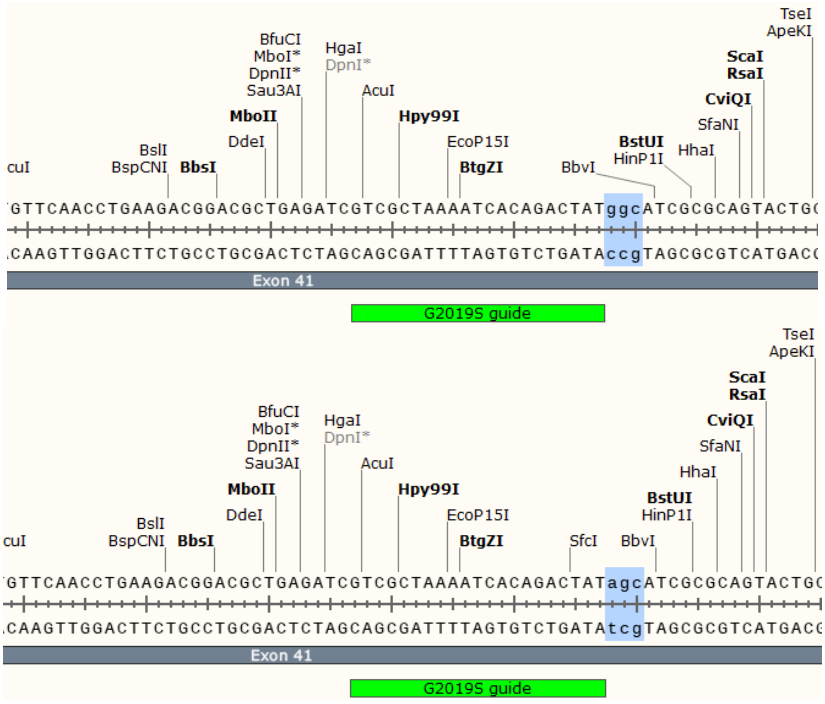

Figure 83. Restriction Enzyme Sites in Zebrafish Leucine-Rich Repeat Kinase 2 Before and After G2009S Mutation. *Screenshots taken from SnapGene showing the position of the G2019 guide in green, target codon in blue and restriction enzyme sites above. An SfcI site is added following mutation of GGC (top) to AGC (bottom).*

An oligonucleotide of 127bps and an oligonucleotide-specific primer were then designed around this region. To achieve this, the 127bp region and 300bps before or after were copied into Primer3 and wobble bases altered until a primer pair was generated with the lowest penalty (**figure 84A**). A forward primer in the intron before the exon of interest and a reverse primer that covered the new codon plus two additional wobble bases (ACA -> ACG; ATC -> ATT) were chosen as the best primer pair. These were assessed using Primer-BLAST, which suggested that this pair should not amplify zebrafish DNA unless mutated and had no ectopic binding sites (**figure 84B**). The ssODN sequence was reverse complemented and ordered from IDT (**table 22**). The oligonucleotide-specific primers were tested on wildtype DNA using a gradient PCR, with no amplification of the correct product size seen at any temperature tested (**figure 84C,D**).

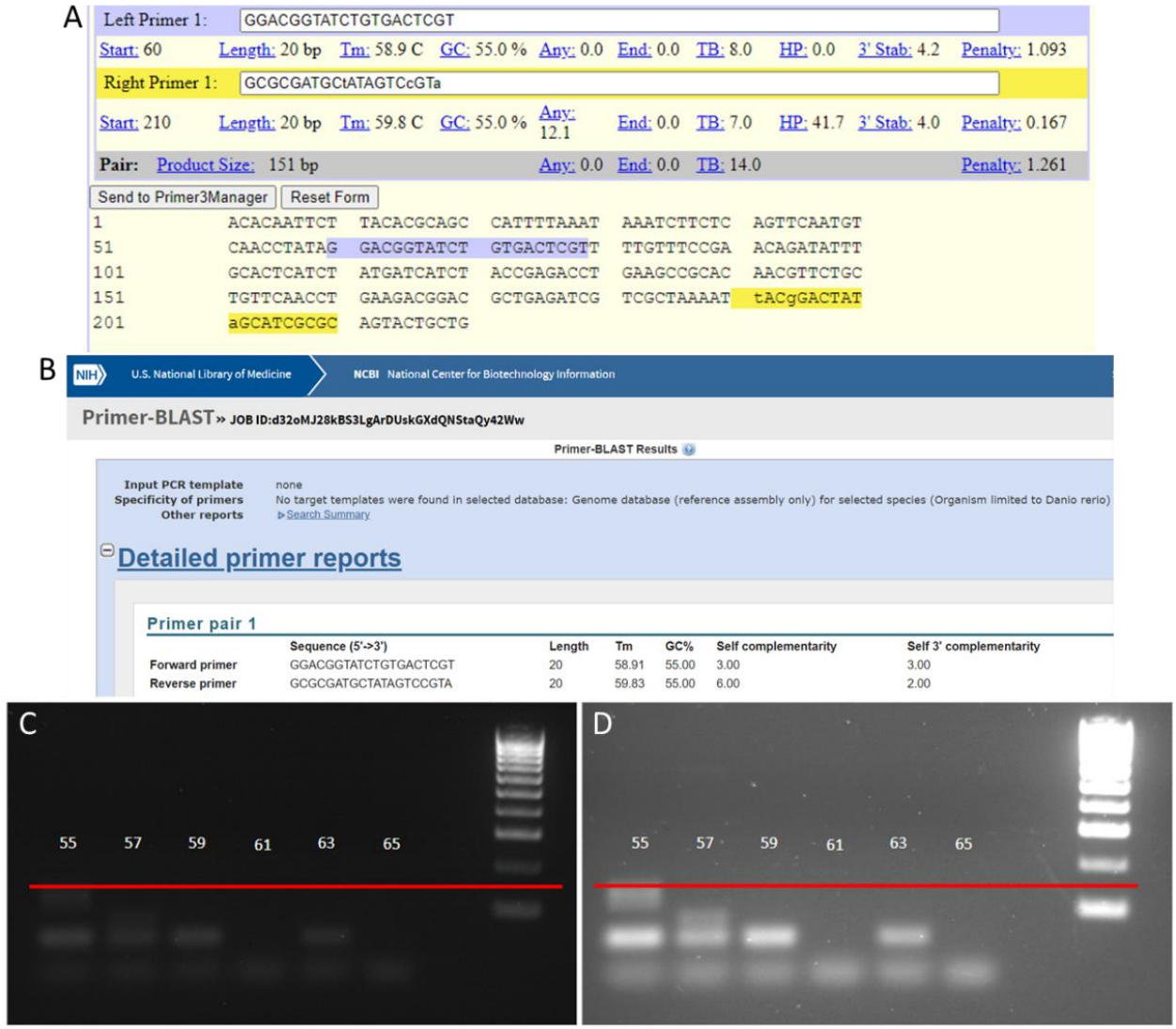

Figure 84. Designing Oligonucleotide-Specific Primers for G2009S. A. *Screenshot from Primer3 software showing the final chosen primer pair with the lowest penalty of 1.261. Lower case letters represent bases that differ from the wildtype sequence.* ***B.*** *Screenshot from NCBI Primer-BLAST software demonstrating that the chosen primer pair has no target templates in the zebrafish genome.* ***C.*** *Electrophoresis gel showing the chosen primer pair does not amplify the correct size product (red line) in wildtype zebrafish DNA. Numbers represent the annealing temperature of the PCR protocol.* ***D.*** *Over-exposed gel to check for weak bands. Ladder is 100bp [Bioline].*

Table 22. G2009S Oligonucleotide Development

A. Original DNA	GAAGACGGACGCTGAGATCGTCGCTAAAATCACAGACTATGGCATCGCGCAGTACTGCTGCAGCATGG GCGTCCGCAGCTCTGAAGGAACACCAGGTCTCGCTCATTTACCCATAATCCTCCTTTAA
B. Mutated DNA	GAAGACGGACGCTGAGATCGTCGCTAAAATtACgGACTATaGCATCGCGCAGTACTGCTGCAGCATGG GCGTCCGCAGCTCTGAAGGAACACCAGGTCTCGCTCATTTACCCATAATCCTCCTTTAA
C. ssODN	T*T*AAAGGAGGATTATGGGTAAATGAGCGAGACCTGGTGTTCCTTCAGAGCTGCGGACGCCCATGCT GCAGCAGTACTGCGCGATGCtATAGTCcGTaATTTTAGCGACGATCTCAGCGTCCGTCT*T*C

*Table showing the stages of oligonucleotide development for the induction of G2009S mutation in zebrafish. **A.** Original 127bp DNA sequence with the guide sequence shown in yellow, the PAM site underlined and the target codon in red. **B.** The 127bp sequence following mutation (new codon plus wobble bases). The novel primer (reverse) is shown in blue, PAM site underlined and target codon in red. **C.** The ssODN that was ordered from IDT. It is a reverse complemented version of the sequence in B. Stars represent bases that have been phosphorothioated.*

Next, the ssODN was co-injected with the G2009 gRNA to assess HDR. Oligonucleotide-only controls were used to check for toxicity induced by the direct injection of DNA and to ensure the oligonucleotide itself was not affecting subsequent PCRs. Using the oligonucleotide-specific primer pair, it appeared that approximately 1/3 of embryos had successfully incorporated the new DNA sequence into at least some of their cells (**figure 85**). Whilst clear differences were also seen between injected and control samples following restriction digest (**figure 86**), an SfcI restriction site present in wildtype DNA should have been evident in all samples but was missing from controls. Additionally, the bands present in injected samples represent the predicted band sizes for wildtype DNA following SfcI digestion (**figure 86**). This is unsurprising due to the expected low rate of successful HDR; the oligonucleotide-specific primers, being highly specific, are likely to reflect the real picture. The reason for the absence of digested products in uninjected samples is unclear.

100 injected embryos were raised to adulthood and screened at 3-months of age to assess germline transmission. Here, individual injected zebrafish were crossed to wildtype zebrafish and DNA extracted from their offspring at 24hpf. DNA from 24 individual embryos was amplified using the oligonucleotide-specific primers to assess whether they carried the G2009S mutation. For the majority of the screened fish none of the 24 embryos produced a band following this PCR. Any embryos that produced bands of the correct size were then sequenced by running an additional PCR using the primer pair that flanked the mutation site and sending cleaned-up DNA to Genewiz for sequencing. Some embryos produced the correct bands following PCR, but after sequencing turned out to not have the correct DNA sequence. After screening 71 injected adult fish, two males were identified that produced embryos carrying the correct DNA sequence (**figure 87**). Each of these was then outcrossed to wildtype and 60 of their offspring raised. When these fish reach 3mpf, they will be finclipped to check for successful insertion of the correct DNA sequence. Those that do not have this will be culled and the remainder of the fish will be outcrossed to wildtype to generate a heterozygous stock.

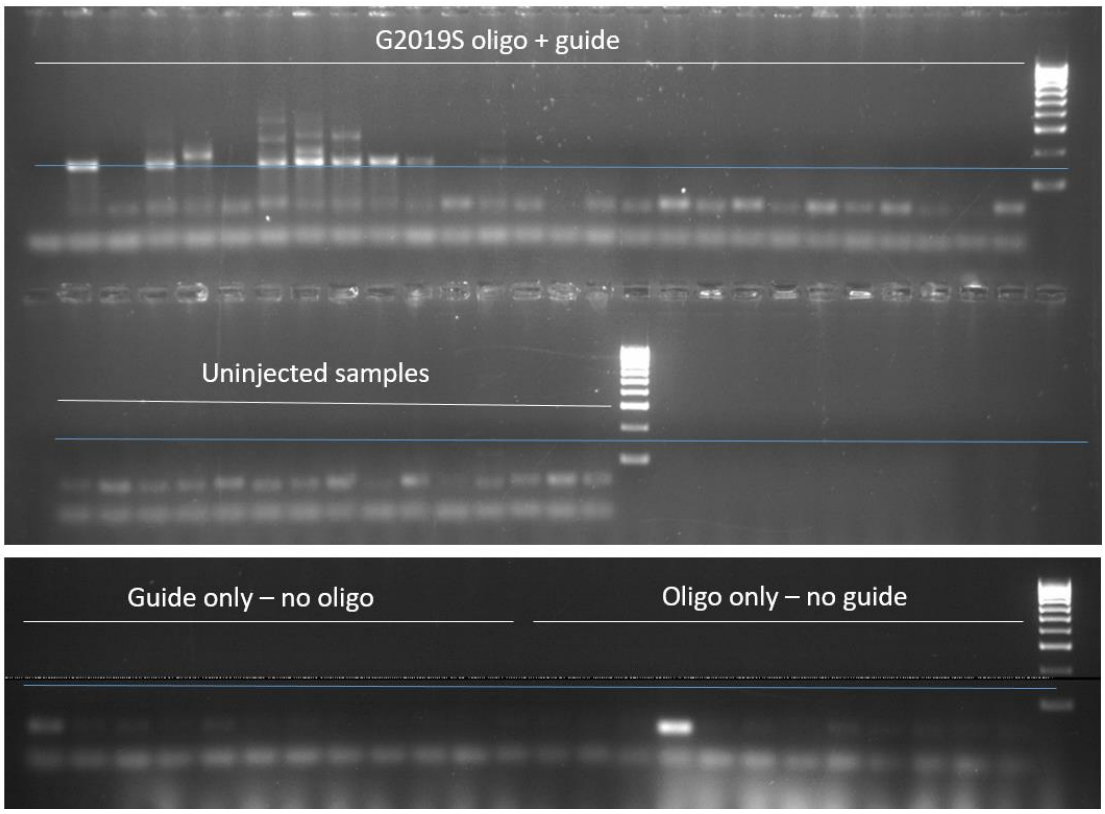

Figure 85. Electrophoresis Gel Showing Successful Insertion of the G2019S Mutation. *DNA samples were collected at 1dpf from embryos injected with the G2019S oligonucleotide, guide RNA, tracrRNA and Cas9 (top row); guide RNA, tracrRNA and Cas9 only (bottom left); oligonucleotide only (bottom right) or uninjected samples (middle row). Samples were run using an oligonucleotide-specific primer pair at 65°C. Blue line represents expected product size after successful insertion. Ladder is 100bp [Bioline].*

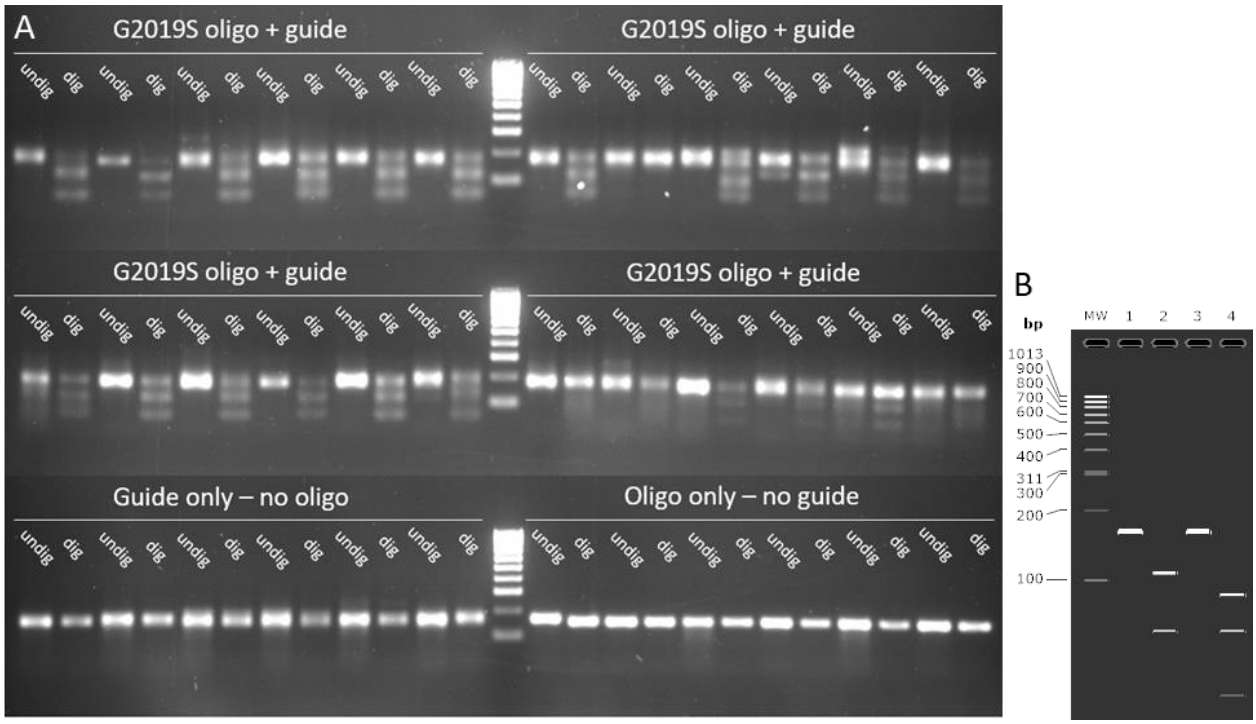

Figure 86. Electrophoresis Gel Showing SfcI Digest of G2019S Injected Samples and Controls. A. *DNA samples were collected at 1dpf from embryos injected with G2019S oligonucleotide, guide RNA, tracrRNA and Cas9 (top 2 rows), guide RNA, tracrRNA and Cas9 only (bottom left) or oligonucleotide only (bottom right). Samples were run by PCR using primers flanking the target region and then digested with SfcI for 2 hours. 100bp ladder [Bioline].* ***B.*** *Screenshot from SnapGene of an in silico PCR and SfcI digest. Lane 1 shows amplified wildtype DNA, lane 2 shows wildtype DNA digested with SfcI, lane 3 shows amplified mutated DNA, lane 4 shows mutated DNA following SfcI digest. dig, digested samples; dpf, days post fertilisation; undig, undigested samples.*

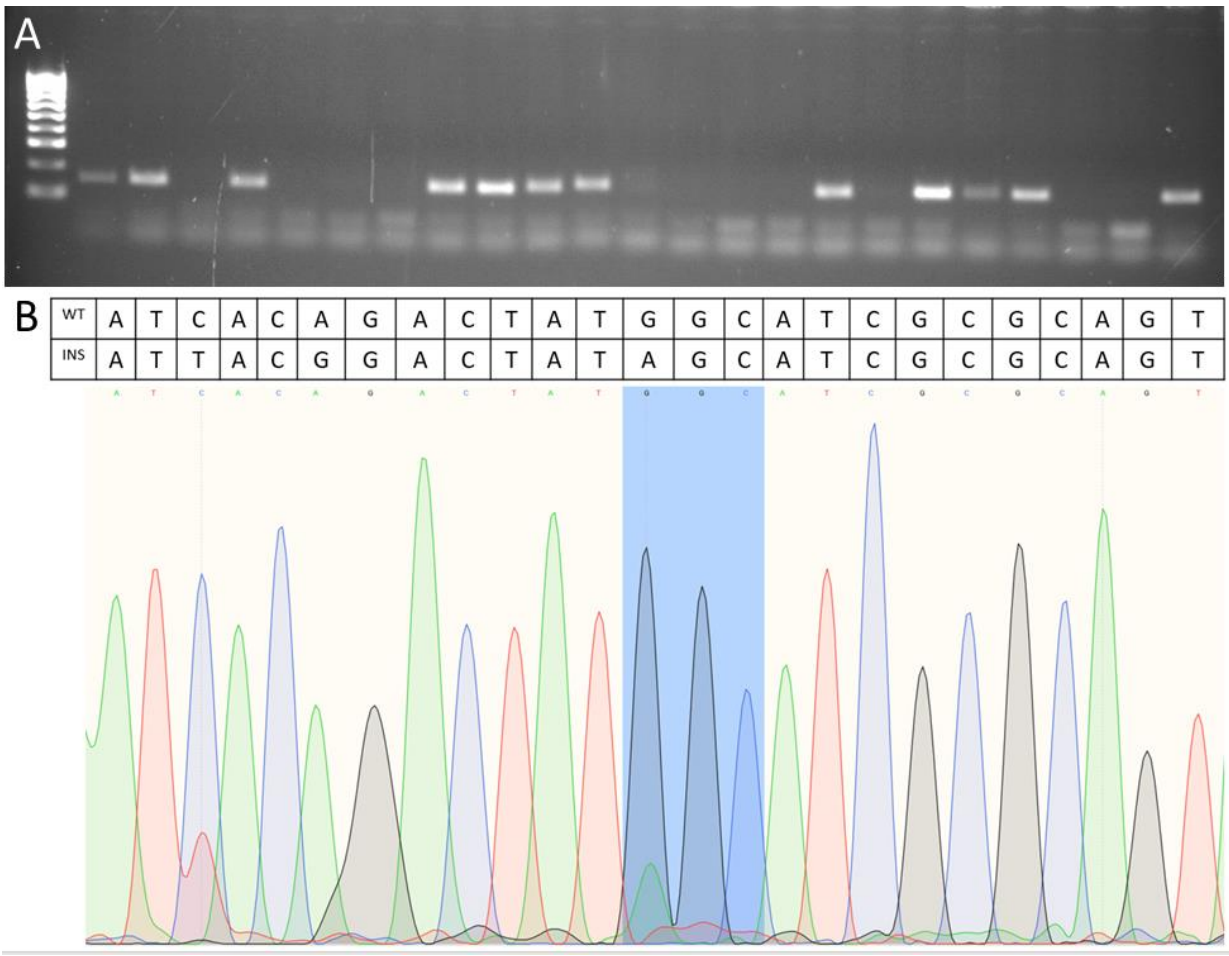

Figure 87. Germline Transmission of the G2009S Mutation was Identified in Adult Zebrafish by Assessment of Their Offspring. ***A.*** *PCR using oligonucleotide-specific primers on the offspring obtained by crossing a zebrafish injected with the G2009S construct with a wildtype zebrafish. Each lane represents a single embryo. Ladder is 100bp [Bioline].* ***B.*** *Chromatogram following sequencing of the DNA from a single embryo obtained from this cross. The table above shows the expected DNA sequence of the region in wildtype zebrafish and in zebrafish following successful insertion of the construct. The embryo had both sequences, as expected.*

5.2.9.2 R1441C/G/H

Protein-protein alignment in SnapGene identified arginine at position 1441 in human *LRRK2* to be equivalent to valine at position 1428 in zebrafish *lrrk2* (**figure 88A**). Valine 1428 was found to be coded for by the codon "GTA" following *in silico* transcription of the *lrrk2* DNA sequence (**figure 88**). There were two possible guide choices in this region, differing by a single base. These were inputted into the ChopChop online software, which identified one guide as slightly more active than the other (50.6% vs 50.0%) which was therefore selected for use. The Cas9 cut site of this gRNA directly disrupts the codon of interest as well as an SfcI restriction site. Primers flanking this region were designed using Primer3 (for guide and primer sequences, see methods). Guide activity was assessed by injecting into the yolk of single-celled wildtype zebrafish embryos and analysed at 1dpf using the flanking primer pair and a digest with SfcI. Injected embryos demonstrated a successful loss of the SfcI restriction site, suggesting that this guide is highly active (**figure 88**). Therefore, ssODNs to act as templates for HDR for all three mutations in this region were designed.

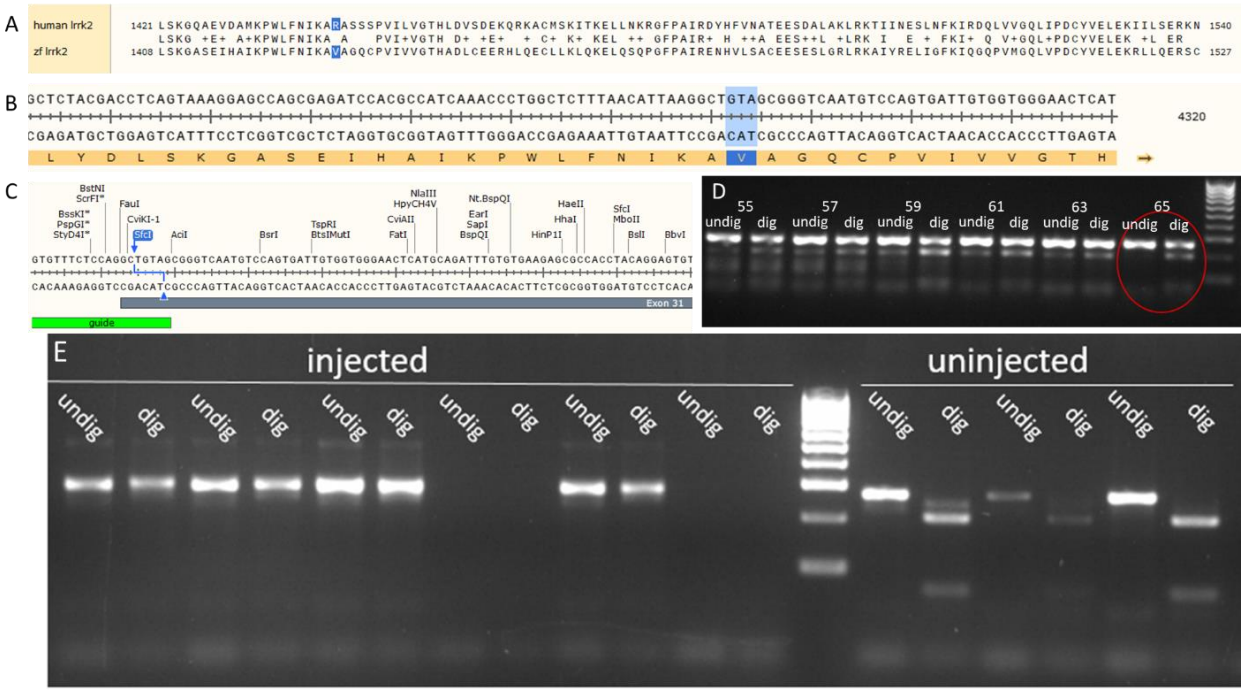

Figure 88. Designing Guide RNA to Target the Zebrafish Equivalent of R1441. A. *Protein-protein alignment of human and zebrafish Lrrk2 in SnapGene, demonstrating valine 1428 to be the zebrafish equivalent of human arginine 1441.* ***B.*** *DNA sequence and in silico transcription of zebrafish lrrk2, with target valine highlighted in blue. This shows that this is coded for by "GTA"* ***C.*** *Screenshot from SnapGene demonstrating the guide design for targeting this region, showing the disruption of an SfcI site.* ***D.*** *A gradient PCR identified 65°C as the most appropriate annealing temperature for this primer pair and demonstrated wildtype DNA would be digested with SfcI at this site.* ***E.*** *Electrophoresis gel (3%) of PCR amplified DNA extracted from 1dpf zebrafish embryos either injected with R1441 guide RNA, tracrRNA and Cas9 or uninjected. Some DNA samples did not amplify. Ladder is 100bp [Bioline]. dig, DNA digested with SfcI; dpf, days post fertilisation; lrrk2, leucine-rich repeat kinase 2; undig, undigested DNA; zf, zebrafish.*

5.2.9.3 R1441C

One amino acid variant found in this region is the substitution of arginine for cysteine. Two codons result in translation to cysteine, and these were assessed for their codon usage in zebrafish (**table 23**). Whilst both codons had equal frequency in the zebrafish genome, only TGC resulted in the addition of restriction enzyme sites and was therefore chosen for HDR.

Table 23. Possible Codons for Cysteine to Use in the Design of the V1428C Donor Oligonucleotide

Possible Codon	Frequency (per thousand)	Enzyme site added?
TGT	11.3	None
TGC	11.2	Cac8I, HinP1I, HhaI, BstUI

Table showing codons that are translated into the amino acid cysteine and their frequency in the zebrafish genome. Final column describes restriction enzyme sites that are added into the DNA following mutation of the wildtype codon to each of the possible cysteine codons. For more information, see methods section.

A 127bp ssODN and oligonucleotide-specific primers were then designed around this region, as described previously. The PAM was mutated at the wobble base to ensure that gRNA would not cleave DNA that had undergone successful HDR. The CGG PAM site was made up by two codons; GCG (Ala / GCN) and GGT (Gly / GGN). Each potential PAM mutation was tested in Primer3, with GCG -> GCA resulting in the best possible oligonucleotide-specific primer pair (**figure 89**). Following alteration of the PAM site, the newly-added BstUI restriction enzyme site was lost, although HhaI, Cac8I, and HinP1I were still present. A forward primer in the exon before the exon

of interest and a reverse primer that targeted the new codon plus the mutated PAM site (GTA -> TGC; CGG -> GCA) were designed and checked using Primer-BLAST (**figure 89D**). Whilst some ectopic binding sites were identified, all products produced were over 2000bps which would be unlikely to amplify during a PCR with an extension time of 30 seconds.

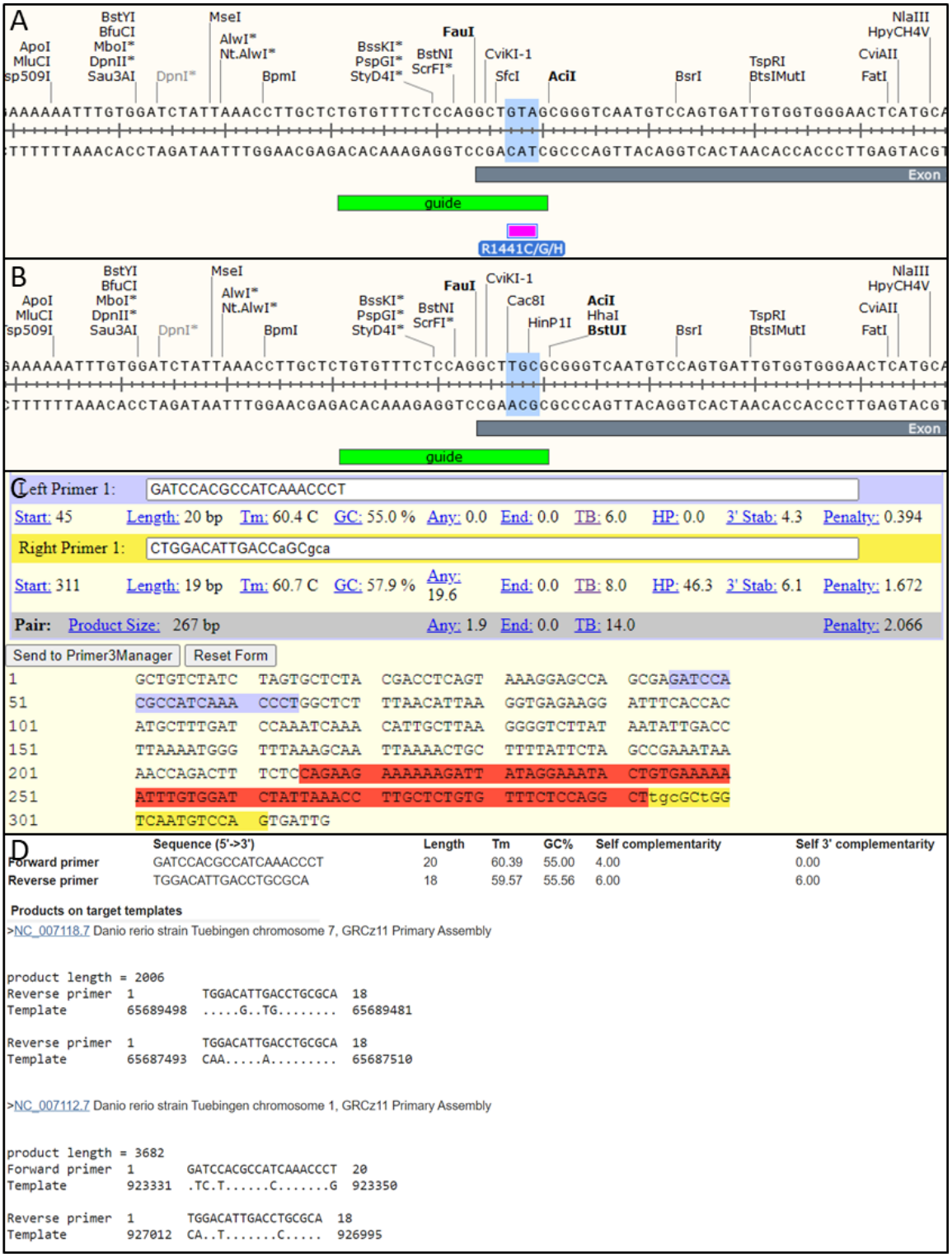

Figure 89. Designing Oligonucleotide-Specific Primers for V1428C. A. *Original DNA sequence and restriction enzyme sites, with R1441 guide RNA shown in green and the codon for the target arginine in pink / blue highlighted.* ***B.*** *DNA sequence and restriction enzyme sites following the mutation of GTA to TGC.* ***C.*** *Screenshot from Primer3 software showing final chosen primer pair with lowest penalty of 2.066. Lower case letters represent bases that differ from wildtype sequence* ***D.*** *Screenshot from NCBI Primer-BLAST software demonstrating that the chosen primer pair only has targets in the zebrafish genome that are over 2000bps in length and therefore will not amplify by standard PCR.*

Oligonucleotide-specific primers were initially tested on wildtype DNA, finding no amplification of products of the correct length (**figure 90A**). Wildtype embryos were then injected at the one-cell stage with the ssODN and gRNA. DNA was extracted at 24hpf and amplified using the oligonucleotide-specific primers (**figure 90B**). Following electrophoresis, bands of the correct size were present in the control samples as well as the injected samples, although the intensity was drastically reduced. The PCR was run again with an increased annealing temperature of 65°C to improve discrimination between the wildtype and mutant sequence. Bands were now only present in samples injected with both the ssODN and gRNA (**figure 90C**).

100 injected embryos were raised to adulthood and screened at 3 months of age to assess germline transmission, as described previously. As seen with other mutations, some samples that produced the correct bands following oligonucleotide-specific PCR did not possess the correct DNA sequence. After screening 45 injected adult fish, two males were identified that produced embryos with the correct DNA sequence (**figure 91**). Each of these was then outcrossed to wildtype and 60 of their offspring raised.

Table 24. V1428C Oligonucleotide Development

A. Original DNA	GATCTATTAAACCTTGCTCTGTGTTTCTCCAGGCTGTAGCGGGTCAATGTCCAGTGATTGTGGTGGGAAC TCATGCAGATTTGTGTGAAGAGCGCCACCTACAGGAGTGTTTGCTGAAGCTGCAGAA
B. Mutated DNA	GATCTATTAAACCTTGCTCTGTGTTTCTCCAGGCTtgcGCaGGTCAATGTCCAGTGATTGTGGTGGGAACTC ATGCAGATTTGTGTGAAGAGCGCCACCTACAGGAGTGTTTGCTGAAGCTGCAGAA
C. ssODN	T*T*CTGCAGCTTCAGCAAACACTCCTGTAGGTGGCGCTCTTCACACAAATCTGCATGAGTTCCCACCACA ATCACTGGACATTGACCtGCgcaAGCCTGGAGAAACACAGAGCAAGGTTTAATAGA*T*C

*Table showing the stages of oligonucleotide development for the induction of V1428C mutation in zebrafish. **A.** Original 127bp DNA sequence with the guide sequence shown in yellow, the PAM site underlined and the target codon in red. **B.** The 127bp sequence following mutation (new codon plus wobble bases). The novel primer (reverse) is shown in blue, PAM site underlined and target codon in red. Lower case letters represent base changes from wildtype. **C.** The ssODN that was ordered from IDT. It is a reverse complemented version of the sequence in B. Stars represent bases that have been phosphorothioated.*

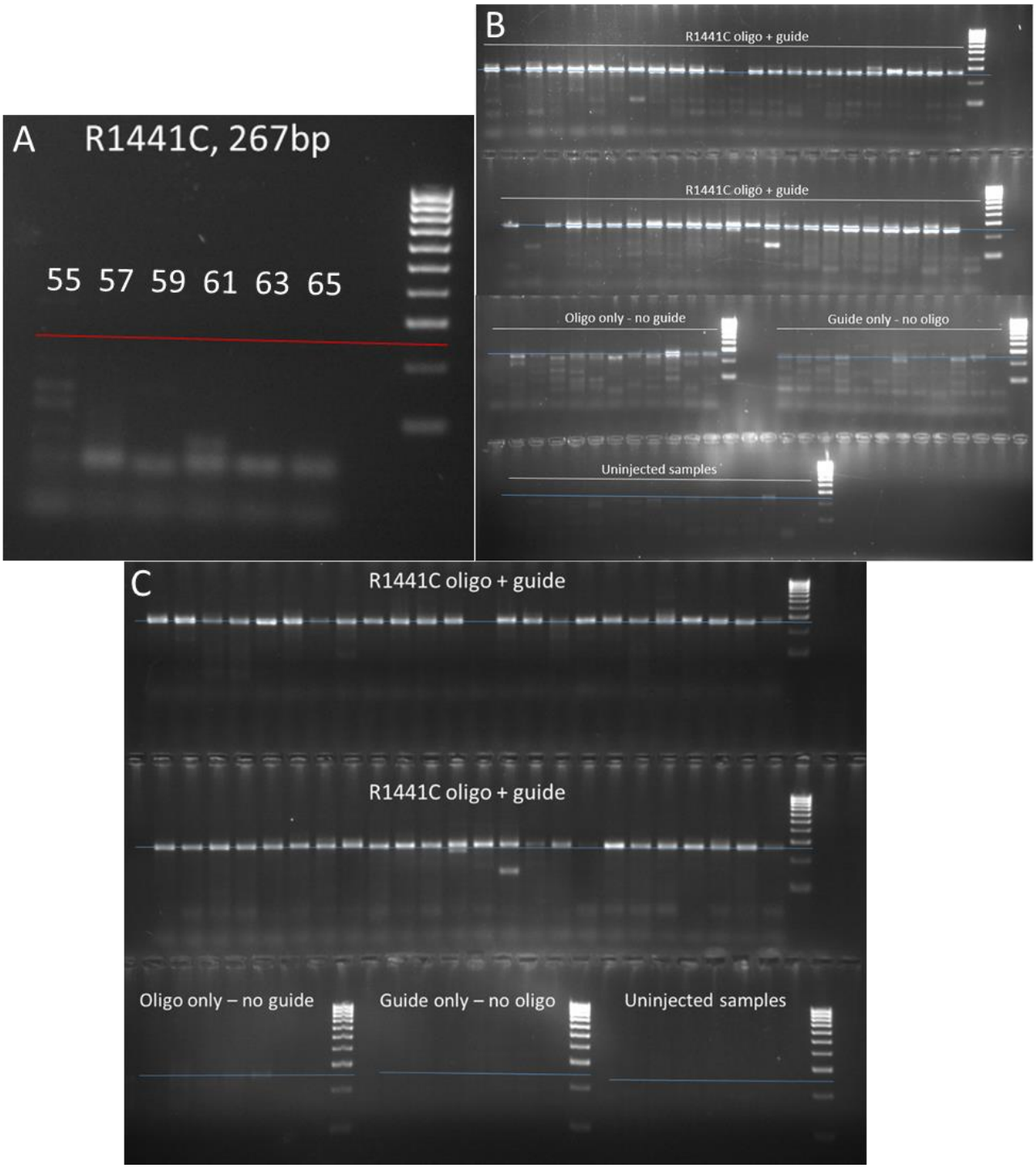

Figure 90. Assessment of the Zebrafish Equivalent of the R1441C Oligonucleotide. A. *The R1441C oligonucleotide-specific primer pair was used to amplify wildtype zebrafish DNA in a gradient PCR, demonstrating that the correct sized product (267bp, red line) was not produced at any temperature. Numbers represent annealing temperature.* ***B.*** *DNA was extracted from 1dpf zebrafish injected with R1441C oligonucleotide, guide RNA, tracrRNA and Cas9 (top two rows) or controls (oligonucleotide only (bottom left), guide RNA, tracrRNA and Cas9 (bottom middle) or uninjected (bottom right)) and amplified using oligonucleotide-specific primers at 60°C.* ***C.*** *The same DNA samples were run again with the PCR annealing temperature increased to 65°C. Ladder for all gels is 100bp [Bioline].*

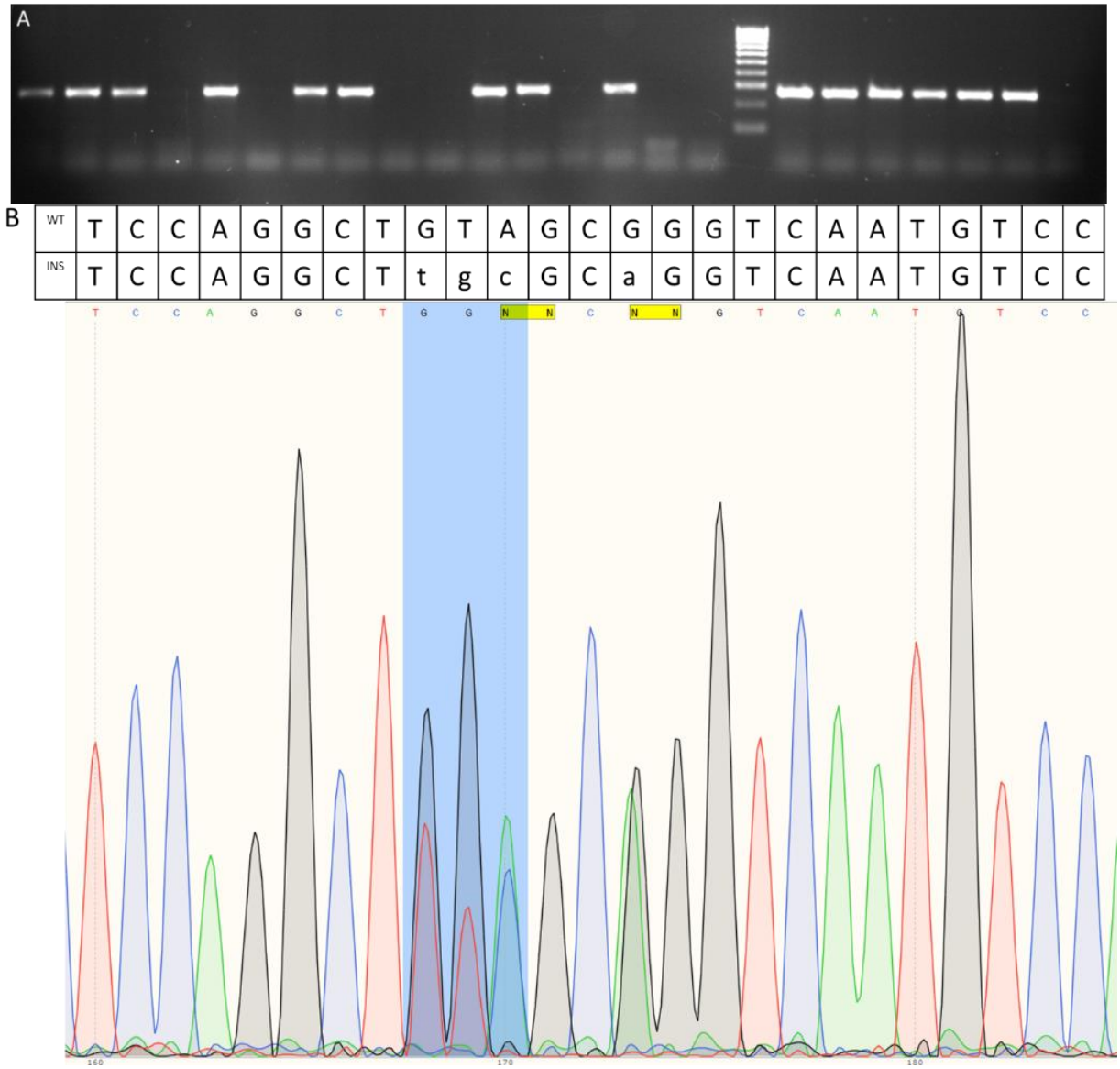

Figure 91. Germline Transmission of the V1428C Mutation was Identified in Adult Zebrafish by Assessment of Their Offspring. ***A.*** *PCR using oligonucleotide-specific primers on the offspring obtained by crossing a zebrafish injected with the V1428C construct with a wildtype zebrafish. Each lane represents a single embryo. Ladder is 100bp [Bioline].* ***B.*** *Chromatogram following sequencing of the DNA from a single embryo obtained from this cross. The table above shows the expected DNA sequence of the region in wildtype zebrafish and in zebrafish following successful insertion of the construct. The embryo had both sequences, as expected.*

5.2.9.4 R1441G

The second substitution at this position is arginine to glycine. Glycine has four possible codons which were all checked against the zebrafish codon usage table and SnapGene was used to check for restriction enzyme sites that would be added after each codon change (**table 25**).

Table 25. Possible Codons for Glycine to Use in the Design of the V1428G Donor Oligonucleotide

Possible Codon	Frequency (per thousand)	Enzyme site added?
GGT	13.7	None
GGC	17.2	Cac8I, HinP1I, HhaI, BstUI
GGA	21.5	BsrBI, BpmI
GGG	10.0	BseYI, BslI

Table showing the possible codons that are translated into the amino acid glycine and their frequency in the zebrafish genome. Final column describes restriction enzyme sites that are added into the DNA following mutation of wildtype codon to each of the glycine codons. For more information, see methods section.

A 127bp oligonucleotide (**table 27**) and oligonucleotide-specific primers were then designed around this region. The PAM site (CGG) was mutated to ensure gRNA would not re-cleave DNA that had been successfully mutated. The PAM was made up of two codons; GCG (Ala / GCN) and GGT (Gly / GGN), each of which could be altered at the wobble base. All combinations of glycine and PAM codons were inputted to Primer3 to identify the combination that produced the lowest primer pair penalty (summarised in **table 26**). The lowest penalty was achieved with a combination of GGA and GCC. However, this combination, or indeed any PAM option with GGA, removed the BsrBI restriction site. The remaining novel BpmI site would be difficult to work with due to other nearby sites making it difficult to see changes on a gel (**figure 92A**). The second choice option for primer design was GGG with GCA. However, as with the BpmI site, using a BslI digest would not be appropriate due to nearby restriction sites (**figure 92B**). The other novel site, BseyI, whilst giving differing digest patterns (**figure 92C**), is not a good enzyme to work as it is able to stay bound to DNA following cleavage which can change how it runs on a gel. Therefore, a final option was assessed, GGC with GCA. Following this mutation combination, the BstUI site was lost but all three additional novel sites remained and provided good discrimination between mutants and controls (**figure 92D-F**).

Table 26. Assessment of Glycine and PAM Codon Combinations.

Codon change	PAM change	Penalty with best primers	Comments
GGC	GCT	3.576	
GGC	GCC	3.894	
GGC	GCA	2.067	Removes BstUI site
GGA (best codon choice)	GCT	1.841 (hairpin stability high)	Removes BsrBI site
GGA (best codon choice)	GCC	1.691	Removes BsrBI site
GGA (best codon choice)	GCA	1.841	Removes BsrBI site
GGG	GCT	1.357 (hairpin stability high)	
GGG	GCC	2.833	
GGG	GCA	1.775	

Each combination of glycine codon and PAM change at the wobble base was assessed using Primer3 software. Both forward and reverse primers in the region were tested and the primer pairs that gave the lowest penalty score are reported in the table. Rows highlighted in red represent those that were assessed further, discussed in the main text.

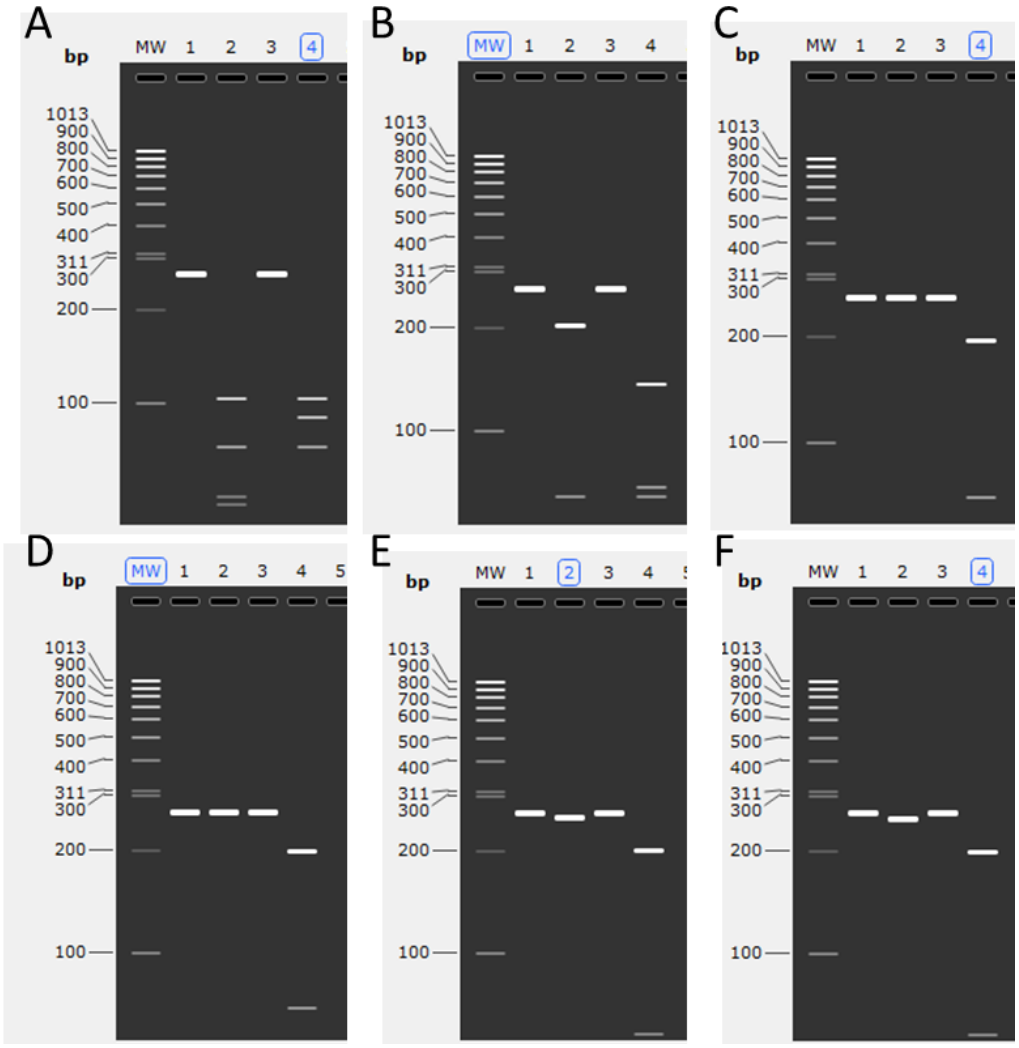

Figure 92. In Silico Gel Electrophoresis Images Assessing Restriction Enzyme Choices Following V1428G Mutation. A. *The oligonucleotide-specific primer pair that resulted in the lowest penalty gave very little discrimination following digest with BpmI.* ***B.*** *The second choice combination of mutations also resulted in difficult discrimination between wildtype and mutant following digest with BslI.* ***C.*** *This combination was successful following BseyI digest, but was not used due to this enzymes properties. The third choice of codon combinations enabled easy identification of mutants following restriction digest with either Cac8I (**D**), HhaI (**E**) or HinpI (**F**). In all images, row 1 represents wildtype DNA amplified with flanking primers, row 2 represents this product following restriction digest with appropriate enzyme, row 3 represents mutated DNA amplified with flanking primers and row 4 represents mutated DNA digested with appropriate enzymes.*

Table 27. R1441G Oligonucleotide Development

A. Original DNA	GATCTATTAAACCTTGCTCTGTGTTTCTCCAGGCTGTAGCGGGTCAATGTCCAGTGATTGTGGTGGGA ACTCATGCAGATTTGTGTGAAGAGCGCCACCTACAGGAGTGTTTGCTGAAGCTGCAGAA
B. Mutated DNA	GATCTATTAAACCTTGCTCTGTGTTTCTCCAGGCTGgcGCaGGTCAATGTCCAGTGATTGTGGTGGGAA CTCATGCAGATTTGTGTGAAGAGCGCCACCTACAGGAGTGTTTGCTGAAGCTGCAGAA
C. ssODN	T*T*CTGCAGCTTCAGCAAACACTCCTGTAGGTGGCGCTCTTCACACAAATCTGCATGAGTTCCCACCA CAATCACTGGACATTGACCtGCgcCAGCCTGGAGAAACACAGAGCAAGGTTTAATAGA*T*C

Table showing the stages of oligonucleotide development for the induction of V1428G mutation in zebrafish. ***A.*** *Original 127bp DNA sequence with the guide sequence shown in yellow, the PAM site underlined and the target codon in red.* ***B.*** *The 127bp sequence following mutation (new codon plus wobble bases). The novel primer (reverse) is shown in blue, PAM site underlined and target codon in red. Lower case letters represent bases that differ from wildtype.* ***C.*** *The ssODN that was ordered from IDT. It is a reverse complemented version of the sequence in B. Stars represent bases that have been phosphorothioated.*

The oligonucleotide-specific primer pair chosen was made up of a forward primer in the exon before the exon of interest and a reverse primer that covered the new codon plus the mutated PAM site (GTA -> GGC and GCG -> GCA). The primers were assessed using Primer-BLAST software which found that although ectopic binding sites exist in wildtype zebrafish DNA, the resulting products would be over 1kb and, therefore, unlikely to amplify in a PCR with a 30-second annealing time (**figure 93**). Thus, this primer pair should not amplify zebrafish DNA unless successfully mutated.

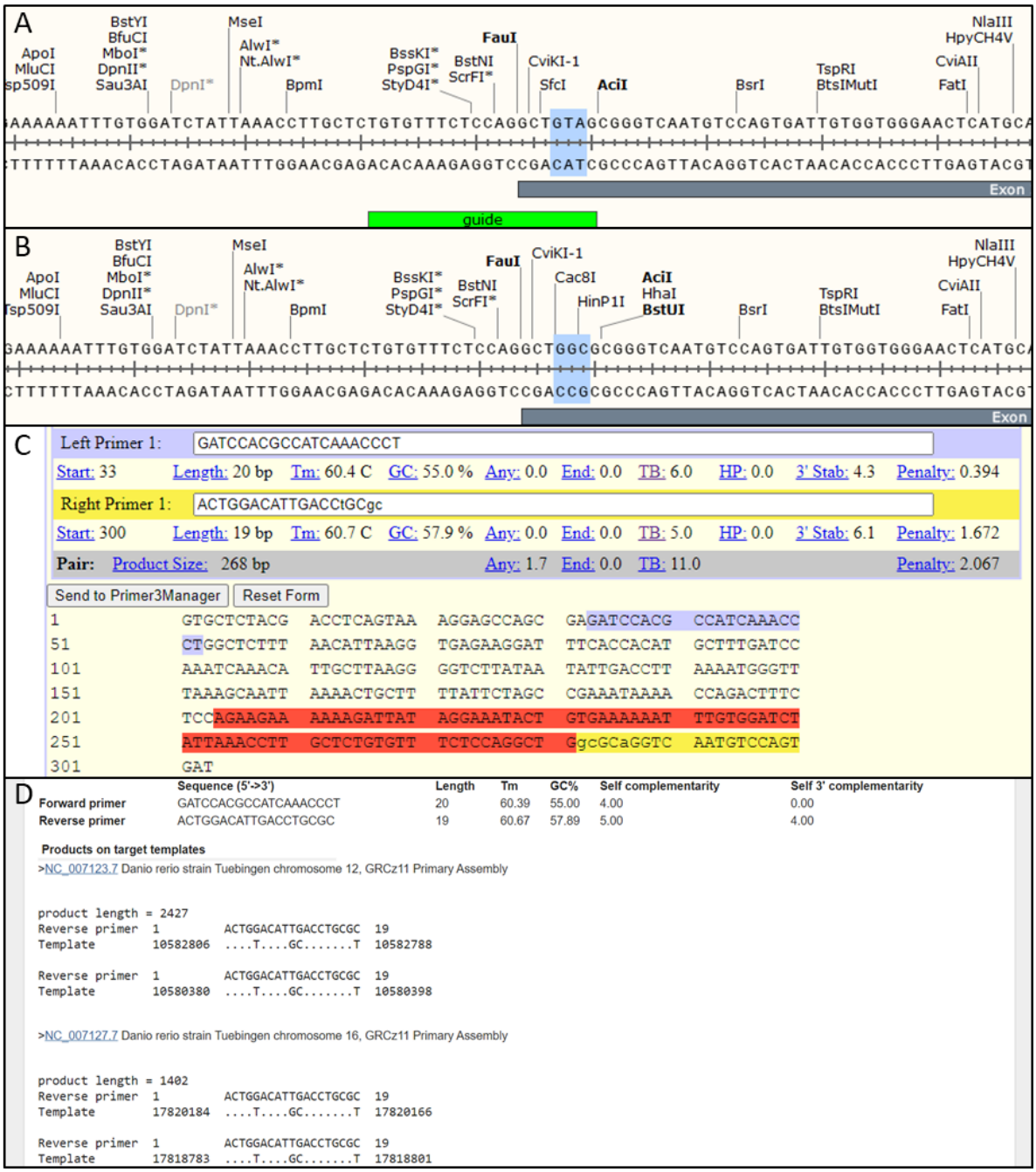

Figure 93. Design of Oligonucleotide-Specific Primers for the V1428G Mutation. A. *DNA sequence and restriction enzyme sites in the target region of wildtype leucine-rich repeat kinase 2. Target codon shown in blue. Region of guide binding shown by green bar.* ***B.*** *DNA sequence and restriction enzyme sites following mutation of the codon of interest.* ***C.*** *Screenshot from Primer3 software showing the design of the chosen oligonucleotide-specific primers.* ***D.*** *Screenshot from NCBI Primer-BLAST software demonstrating that the chosen primer pair only has targets in the zebrafish genome that are over 1kb in length and therefore will not amplify by standard PCR.*

The oligonucleotide-specific primer pair was first assessed in a gradient PCR on wildtype zebrafish DNA to ensure no products of expected size were amplified (**figure 94A**). Following confirmation, HDR using this construct was determined by injecting the gRNA, tracrRNA, Cas9 and the ssODN into wildtype embryos at the one-cell stage. DNA was extracted at 24hpf and amplified using the oligonucleotide-specific primers. Whilst products of the correct size seemed to be evident in all conditions, those amplified from DNA extracted from embryos injected with the ssODN were considerably brighter, suggesting successful insertion of the mutation of interest (**figure 94B**).

100 injected embryos were raised to adulthood and screened at 3 months of age to assess germline transmission, as described previously. After screening 12 injected adult fish, two males were identified that produced embryos carrying the correct DNA sequence (**figure 95**). Each of these was then outcrossed to wildtype and 60 of their offspring raised.

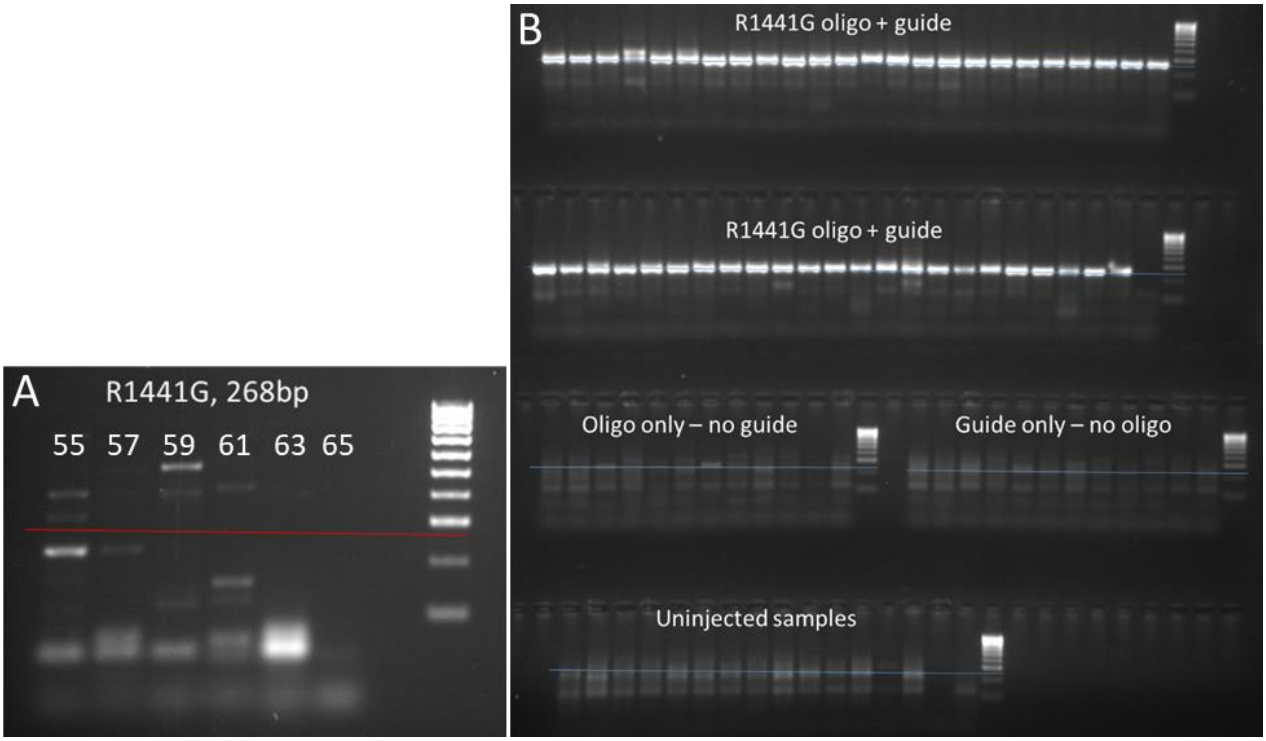

Figure 94. Electrophoresis Gel Showing Successful Insertion of the Zebrafish Equivalent of the R1441G Mutation. A. *Assessment of the oligonucleotide-specific primer pair found it was unable to amplify products of the correct length (268bp, red line) in wildtype DNA.* ***B.*** *DNA samples were collected at 1dpf from embryos injected with the R1441G oligonucleotide, guide RNA, tracrRNA and Cas9 (top 2 rows); oligonucleotide only (middle left); guide RNA, tracrRNA and Cas9 only (middle right) or uninjected samples (bottom row). Samples were amplified using the oligonucleotide-specific primer pair at 65°C. Blue line represents expected product size after successful insertion. Ladder is 100bp [Bioline].*

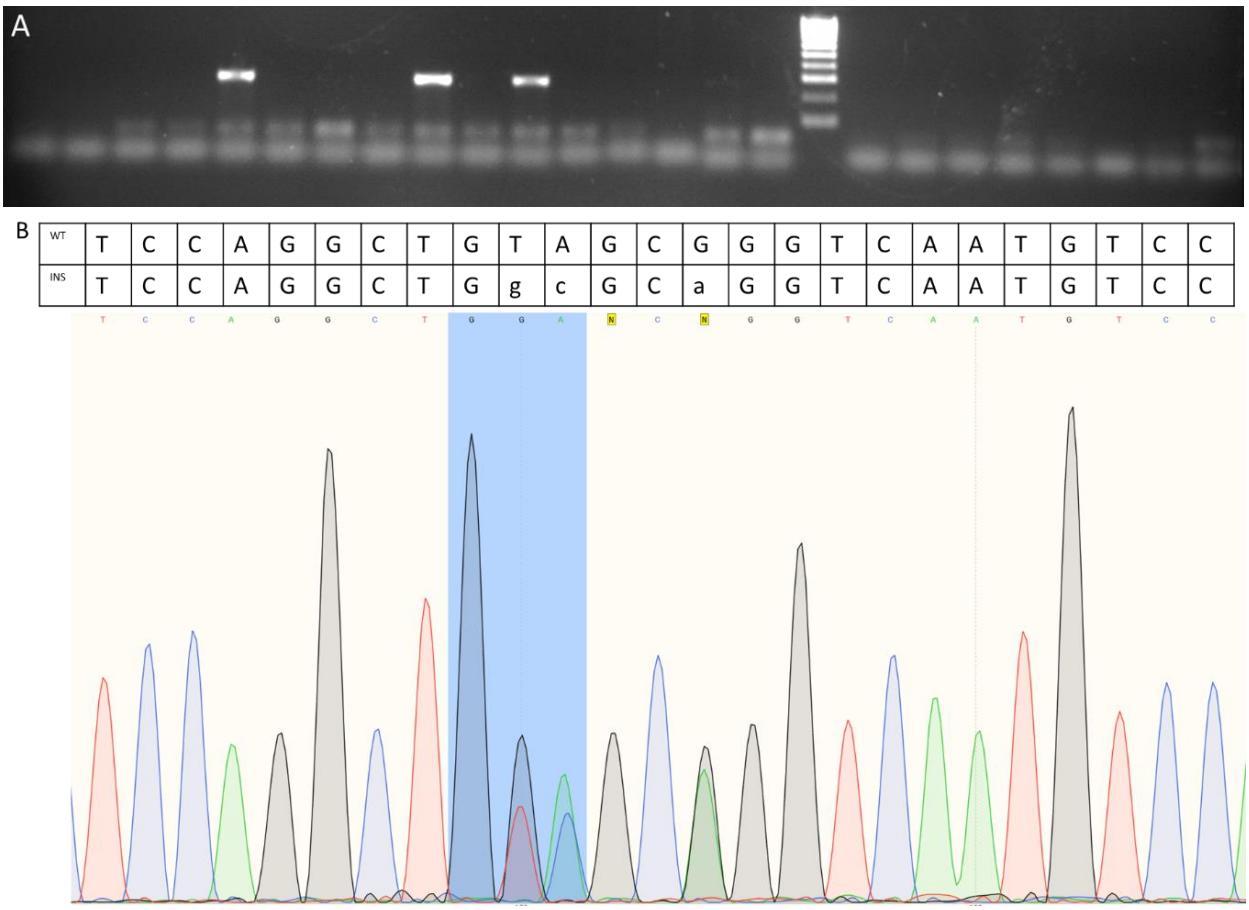

Figure 95. Germline Transmission of the V1428C Mutation was Identified in Adult Zebrafish by Assessment of Their Offspring. ***A.*** *PCR using oligonucleotide-specific primers on the offspring obtained by crossing a zebrafish injected with the V1428C construct with a wildtype zebrafish. Each lane represents a single embryo. Ladder is 100bp [Bioline].* ***B.*** *Chromatogram following sequencing of the DNA from a single embryo obtained from this cross. The table above shows the expected DNA sequence of the region in wildtype zebrafish and in zebrafish following successful insertion of the construct. The embryo had both sequences, as expected.*

5.2.9.5 R1441H

The final amino acid change at this region was arginine to histidine, which is coded for by two possible codons (**table 28**). Whilst CAC had the highest frequency of use in the zebrafish genome, the only additional restriction enzyme site, BstUI, was lost when the PAM was mutated at wobble bases (to inhibit additional cleavage, as discussed above). Therefore, CAT was used as the codon for histidine, which resulted in the addition of three restriction enzyme sites 30-40bps downstream of the codon of interest. The PAM was altered at wobble bases, chosen by trial and error using Primer3, identifying GCG - > GCC to give the best possible oligonucleotide-specific primer (**figure 96**). The forward primer was designed in the intron before exon of interest and the reverse primer spanning the new codon plus the mutated PAM site (GTA -> CAT and GCG -> GCC). When choosing the best restriction enzyme for use here, it was realised that digestion by FatI, CviAII or NlaIII would be difficult to see on a gel due to the small additional band added following mutation (**figure 96**); CviAII and NlaIII are also unstable enzymes and therefore difficult to work with. However, following mutation of the PAM as well as the codon of interest, additional

restriction sites were induced (BsrFi, MspI and HpaII). MspI appeared to enable discrimination of wildtype and mutant DNA using *in silico* restriction digest so was chosen for use.

Table 28. Possible Codons for Histidine to Use in the Design of the V1428H Donor Oligonucleotide

Possible Codon	Frequency (per thousand)	Enzyme site added?
CAT	10.9	FatI, CviAII, NlaIII
CAC	14.8	BstUI

Table showing the possible codons that are translated into the amino acid histidine and their frequency in the zebrafish genome. Final column describes restriction enzyme sites that are added into the DNA following mutation of wildtype codon to each of the histidine codons. For more information, see methods section.

Figure 96. Designing Oligonucleotide-Specific Primers for the V1428H Mutation. A. *Screenshot from SnapGene showing the DNA sequence and restriction enzyme sites of the region prior to mutation. The codon of interest is highlighted in blue. The target region of the R1441 guide is depicted by the green bar.* ***B.*** *Screenshot from SnapGene showing the DNA sequence and restriction enzyme sites of the region following mutation of the codon of interest to CAT.* ***C.*** *The oligonucleotide-specific primers designed using Primer3 software. Lower case letters represent bases that differ from wildtype.* ***D.*** *In silico electrophoresis of PCR amplification of the region using flanking primers in wildtype (row 1) or mutated DNA (row 3) samples. A digest following PCR using one of the initially selected enzymes resulted in a small additional band in mutated DNA (row 4) compared to wildtype DNA (row 2).* ***E.*** *Samples were then digested with MspI in silico, which resulted in digested products in only the mutated DNA (row 4).* ***F.*** *Screenshot from SnapGene showing the DNA sequence and restriction enzyme sites of the region following mutation of the codon of interest as well as the additional wobble bases. The novel MspI site can be seen.*

The 127bp oligonucleotide (**table 29**) was then co-injected with the R1441 gRNA into wildtype zebrafish at the single-celled stage to assess HDR using the oligonucleotide-specific primer pair, as described previously. However, no difference was seen between injected fish and controls at 24hpf, with no DNA being amplified using the oligonucleotide-specific primers in any condition (**figure 97**). However, this was also the case for N1437H (discussed below, **section 5.2.9.8**) which was injected and assessed on the same day as the V1428H construct. To determine whether the lack of PCR product was reproducible or the result of a poor injecting session or DNA analysis, the V1428H construct was tested again in wildtype larvae. This time, bands of expected size were present following PCR, but their pattern (present in every other embryo) seemed unlikely (**figure 98**). This may be due to contamination and the presence of some bands at this length does suggest that this mutation is inducible in zebrafish. As this re-test was conducted late into the current project, there would not have been time to raise and genotype these larvae before completion so these fish were not taken to adulthood and assessed for successful DNA insertion.

Table 29. V1428H Oligonucleotide Development

A. Original DNA	GATCTATTAAACCTTGCTCTGTGTTTCTCCAGGCTGTAGCGGGTCAATGTCCAGTGATTGTGGTGGGA ACTCATGCAGATTTGTGTGAAGAGCGCCACCTACAGGAGTGTTTGCTGAAGCTGCAGAA
B. Mutated DNA	GATCTATTAAACCTTGCTCTGTGTTTCTCCAGGCTcatGCcGGTCAATGTCCAGTGATTGTGGTGGGAA CTCATGCAGATTTGTGTGAAGAGCGCCACCTACAGGAGTGTTTGCTGAAGCTGCAGAA
C. ssODN	T*T*CTGCAGCTTCAGCAAACACTCCTGTAGGTGGCGCTCTTCACACAAATCTGCATGAGTTCCCACCA CAATCACTGGACATTGACCgGCatgAGCCTGGAGAAACACAGAGCAAGGTTTAATAGA*T*C

*Table showing the stages of oligonucleotide development for the induction of V1428H mutation in zebrafish. **A.** Original 127bp DNA sequence with the guide sequence shown in yellow, the PAM site underlined and the target codon in red. **B.** The 127bp sequence following mutation (new codon plus wobble bases). The novel primer (reverse) is shown in blue, PAM site underlined and target codon in red. Lower case letters represent bases that differ from wildtype. **C.** The ssODN that was ordered from IDT. It is a reverse complemented version of the sequence in B. Stars represent bases that have been phosphorothioated.*

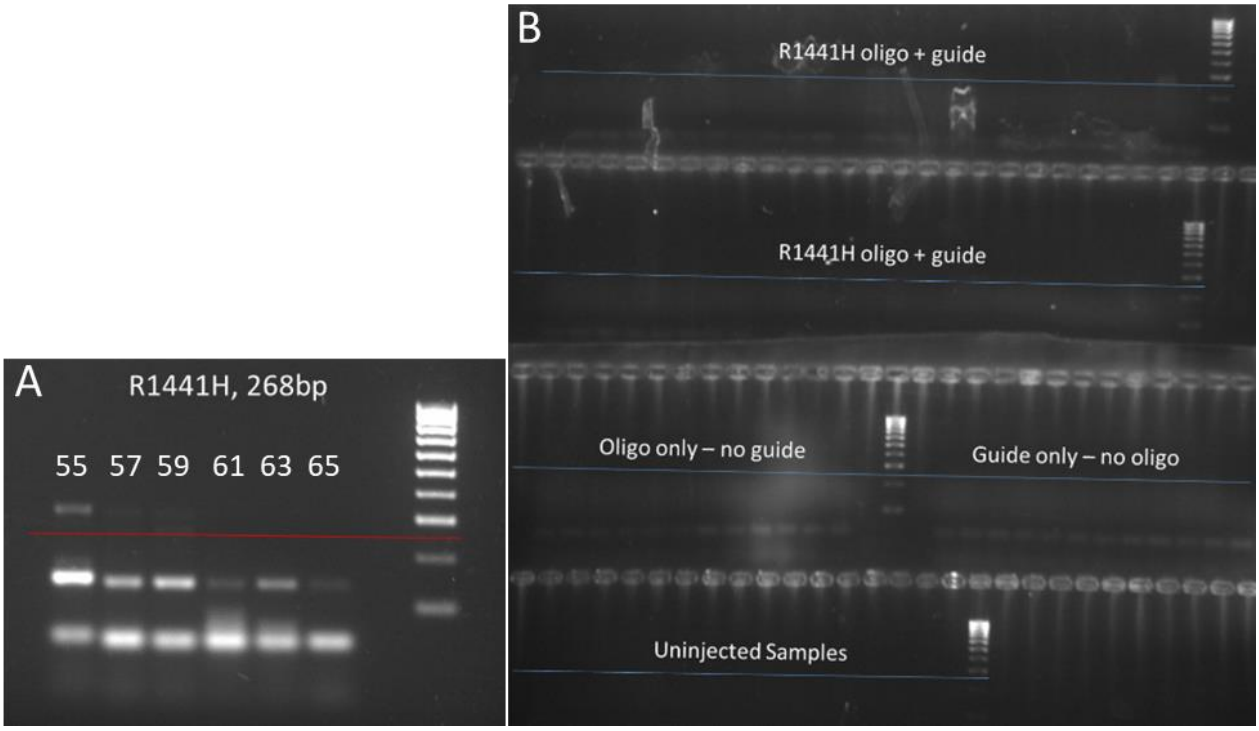

Figure 97. Electrophoresis Gel Showing No Successful Insertion of the R1441H Mutation. A. *Assessment of the oligonucleotide-specific primer pair found it was unable to amplify products of the correct length (red line) in wildtype DNA.* ***B.*** *DNA samples were collected at 1dpf from embryos injected with the R1441H oligonucleotide, guide RNA, tracrRNA and Cas9 (top 2 rows); oligonucleotide only (middle left); guide RNA, tracrRNA and Cas9 only (middle right) or uninjected samples (bottom row). Samples were run using the oligonucleotide-specific primer pair at 65°C. Blue line represents expected product size following successful insertion. Ladder is 100bp [Bioline].*

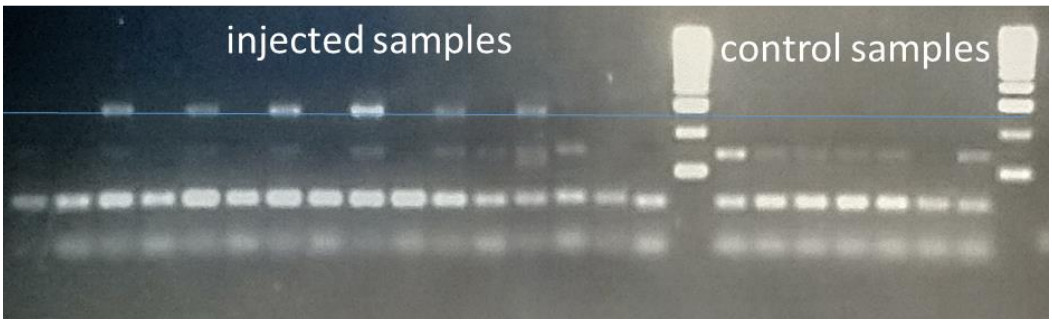

Figure 98. Re-testing the V1428H Construct in Wildtype Zebrafish. *Wildtype zebrafish were injected with V1428H oligonucleotide, guide RNA, tracrRNA and Cas9 and DNA extracted from these embryos at 24hpf. For control samples, DNA from uninjected siblings was used. DNA was amplified by PCR using the oligonucleotide-specific primer pair and run by gel electrophoresis. Blue line represents expected product size following successful insertion of the new DNA sequence.*

5.2.9.6 Y1699C

Another pathogenic mutation in *LRRK2* is the substitution of tyrosine for cysteine at 1699. Protein alignment in SnapGene identified this tyrosine in human *LRRK2* to be equivalent to tyrosine at position 1684 in zebrafish *lrrk2,* encoded by the codon TAT (**figure 99**). There were three possible guide choices in this region. However, one of these had two target sites in the *lrrk2* gene, as shown using ChopChop software, and one demonstrated a predicted low efficiency of 32%. The guide chosen had a predicted efficiency of 54% and resulted in the disruption of a Hpy188I

restriction site. Primers flanking this region were designed in Primer3 and tested using wildtype DNA. Amplification using a gradient PCR and Hpy188I digest found that this primer pair produced a single product that was digested as expected at all annealing temperatures (**figure 99**). To assess the activity of this guide, it was injected into single-cell stage wildtype embryos and subject to PCR amplification and Hpy188I digest at 24hpf. However, this guide did not appear to disrupt the Hpy188I site as predicted (**figure 99**). It is possible that this was due to a poor injecting session or this guide may truly be inactive. Re-testing this guide or testing one of the other available guides in the region may have provided success, but to enable focus on those that were working well, the Y1699C mutant was not taken any further during this project.

Figure 99. Development of the Y1684C Guide. A. *Protein-protein alignment in SnapGene identified tyrosine (Y) at position 1699 in human LRRK2 to be equivalent to tyrosine at position 1684 in zebrafish lrrk2, highlighted in blue.* ***B.*** *In silico transcription of the lrrk2 gene found this tyrosine to be coded for by TAT, highlighted in blue.* ***C.*** *The guide designed in this region disrupted a Hpy188I restriction site. Green shows the target region of the guide RNA and pink represents the codon of interest.* ***D.*** *Gradient PCR test of the primers designed around this region and digest with Hpy188I. Numbers represent annealing temperatures used.* ***E.*** *The guide was tested for efficiency by injecting into single-celled wildtype embryos and assessing DNA at 24hpf. No difference was seen following digest with Hpy188I, suggesting the guide was not active. Ladder is 100bp [Bioline]. dig, DNA samples digested with Hpy188I; lrrk2, leucine-rich repeat kinase 2; undig, undigested PCR product; zf, zebrafish.*

5.2.9.7 I2020T

A further LRRK2 mutation (I2020T) was also created in zebrafish. Protein-protein alignment in SnapGene identified isoleucine at position 2020 in human LRRK2 to be equivalent to isoleucine at position 2010 in zebrafish (**figure 100A**). This isoleucine was found to be coded for by ATC using *in silico* transcription (**figure 100B**). Due to its proximity to G2019S(human)/G2010S(zf), the G2019 guide discussed in **section 5.2.9.1** was also used for creating the dsDNA break needed for HDR to achieve I2010T. Four codons are known to be translated to threonine, with ACA being the most commonly used in the zebrafish genome (**table 30**).

Table 30. Possible Codons for Threonine to Use in the Design of the I2010T Donor Oligonucleotide

Possible Codon	Frequency (per thousand)	Enzyme site added?
ACT	14.5	BtsaI, Nb.BtsI, BtsIMutI, TspRI (multiple nearby sites so not good), FspI
ACC	16.2	BanI, NlaIV, AciI (multiple nearby sites so not good)
ACA	17.0	None
ACG	7.4	BceAI (14bps downstream)

Table showing the possible codons that are translated into the amino acid glycine and their frequency in the zebrafish genome. Final column describes restriction enzyme sites that are added into the DNA following mutation of wildtype codon to each of the glycine codons. For more information, see methods section.

The PAM site for this guide (TGG) was made up of two codons: TAT/GGC. All combinations of wobble bases in both codons still resulted in the presence of an NGG recognition sequence in the DNA as glycine (GGC) can only be coded for by GGN. Consequently, using the method of mutating the PAM to inhibit re-cleavage of the DNA was unfeasible. Therefore, the guide sequence was heavily mutated to prevent binding of the gRNA to DNA that had successfully undergone HDR. Wobble bases for five codons 5' of the I2010 site were altered, creating five bases that differed from wildtype and therefore the gRNA recognition site (**table 31**). Following this mutation, novel restriction enzyme sites were induced: Tsp5091, MluCI, FspI and BsmFI (**figure 100D**).

Table 31. Codon Combinations to Create the I2010T Oligonucleotide.

ATC	ACA	GAC	TAT	GGC	ATC (I2010)
ATt	ACt	GAt	TAc	GGa	Act
	ACg			GGt	Acc
	ACc			GGg	Aca

Bases in bold represent the wildtype DNA sequence of this region. Bases below each column show the possible codons that could replace the wildtype sequence without altering the final amino acid sequence. The final codon is isoleucine at position 2010, the target codon for this oligonucleotide. The codons below this are those which code for tyrosine. Lower case letters represent bases that differ from the wildtype sequence. All combinations were tested using Primer3 software. For the optimal primer design, the sequence in red was used: ATtACtGAtTAcGGgAct.

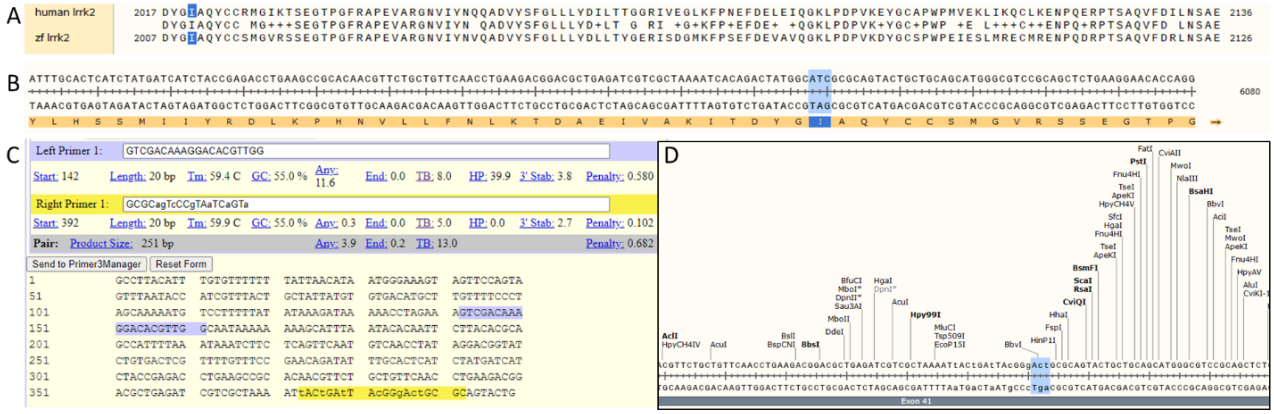

Figure 100. Designing Primers for the I2010T Mutation in Zebrafish Leucine-Rich Repeat Kinase 2. A. *Protein-protein alignment in SnapGene found that isoleucine in position 2020 in human LRRK2 was equivalent to isoleucine at position 2010 in zebrafish lrrk2 (blue).* ***B.*** *In silico transcription identified ATC as the codon for this isoleucine (blue).* ***C.*** *The oligonucleotide-specific primers designed using Primer3 software. Lower case letters represent bases that differ from wildtype.* ***D.*** *Restriction enzyme sites following the mutation of the codon of interest and five wobble bases.*

The oligonucleotide-specific primer pair (**figure 100C**) was then assessed to ensure no amplification of the wildtype DNA sequence occurs (**figure 101A**). The 127bp oligonucleotide (**table 32**) was ordered from IDT and co-injected with the G2009 gRNA into wildtype zebrafish at the single-celled stage. HDR was assessed using the oligonucleotide-specific primer pair, as described previously, identifying a high rate of insertion (**figure 101B**). 100 injected embryos were raised to adulthood and screened for germline transmission. Due to time constraints, only one transmitter was identified for this line, after screening 32 adults. This male produced offspring that carried the correct DNA sequence when outcrossed to wildtype (**figure 102**); 60 of these were then raised to adulthood.

Table 32. I2010T Oligonucleotide Development

A. Original DNA	GAAGACGGACGCTGAGATCGTCGCTAAAATCACAGACTATGGCATCGCGCAGTACTGCTGCAGC ATGGGCGTCCGCAGCTCTGAAGGAACACCAGGTCTCGCTCATTTACCCATAATCCTCCTTTAA
B. Mutated DNA	GAAGACGGACGCTGAGATCGTCGCTAAAATtACtGAtTAcGGgActGCGCAGTACTGCTGCAGCAT GGGCGTCCGCAGCTCTGAAGGAACACCAGGTCTCGCTCATTTACCCATAATCCTCCTTTAA
C. ssODN	T*T*AAAGGAGGATTATGGGTAAATGAGCGAGACCTGGTGTTCCTTCAGAGCTGCGGACGCCCA TGCTGCAGCAGTACTGCGCagTcCCgTAaTCaGTaATTTTAGCGACGATCTCAGCGTCCGTCT*T*C

*Table showing the stages of oligonucleotide development for the induction of I2010T mutation in zebrafish. **A.** Original 127bp DNA sequence with the guide sequence shown in yellow, the PAM site underlined and the target codon in red. **B.** The 127bp sequence following mutation (new codon plus wobble bases). The novel primer (reverse) is shown in blue, PAM site underlined and target codon in red. Lower case letters represent base changes from wildtype. **C.** The ssODN that was ordered from IDT. It is a reverse complemented version of the sequence in **B**. Stars represent bases that have been phosphorothioated.*

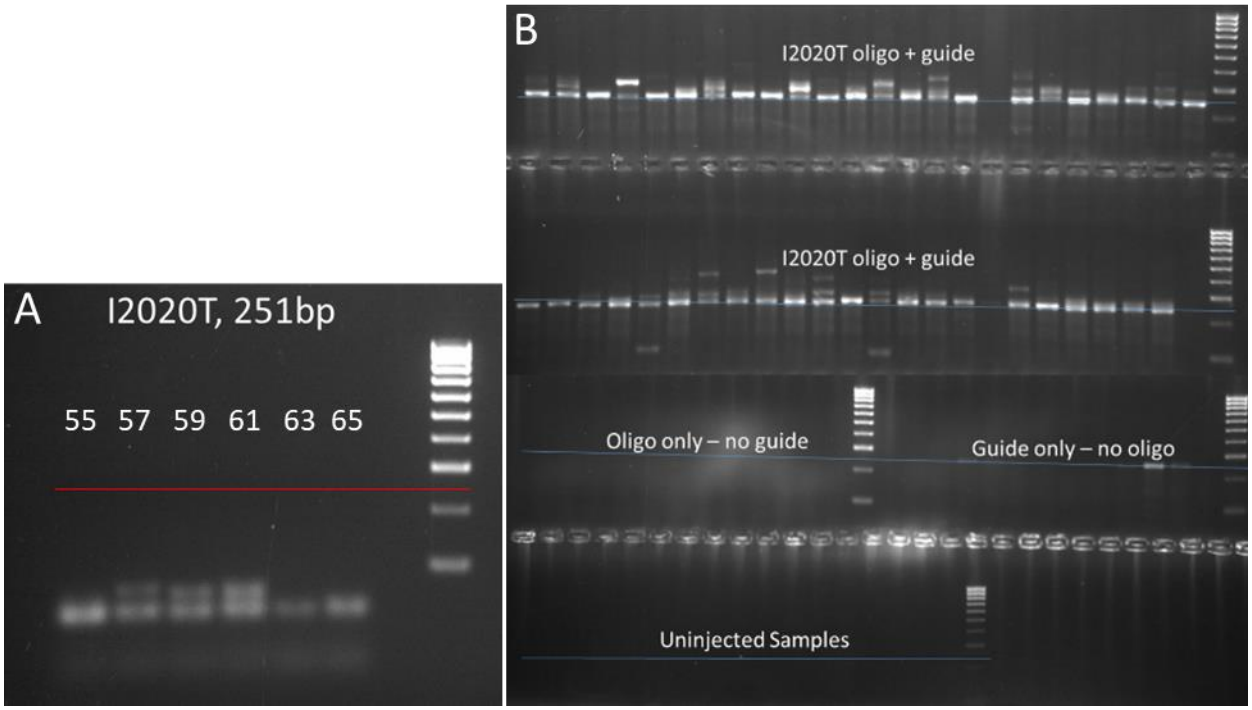

***Figure 101. Electrophoresis Gel Showing Successful Insertion of the Zebrafish Equivalent of the I2020T Mutation. A.** Assessment of the oligonucleotide-specific primer pair found it was unable to amplify products of the correct length (red line, 251bp) in wildtype DNA. **B.** DNA samples were collected at 1dpf from embryos injected with the R1441G oligonucleotide, guide RNA, tracrRNA and Cas9 (top 2 rows); oligonucleotide only (middle left); guide RNA, tracrRNA and Cas9 only (middle right) or uninjected samples (bottom row). Samples were run using the oligonucleotide-specific primer pair at 65°C. Blue line represents expected product size after successful insertion. Ladder is 100bp [Bioline].*

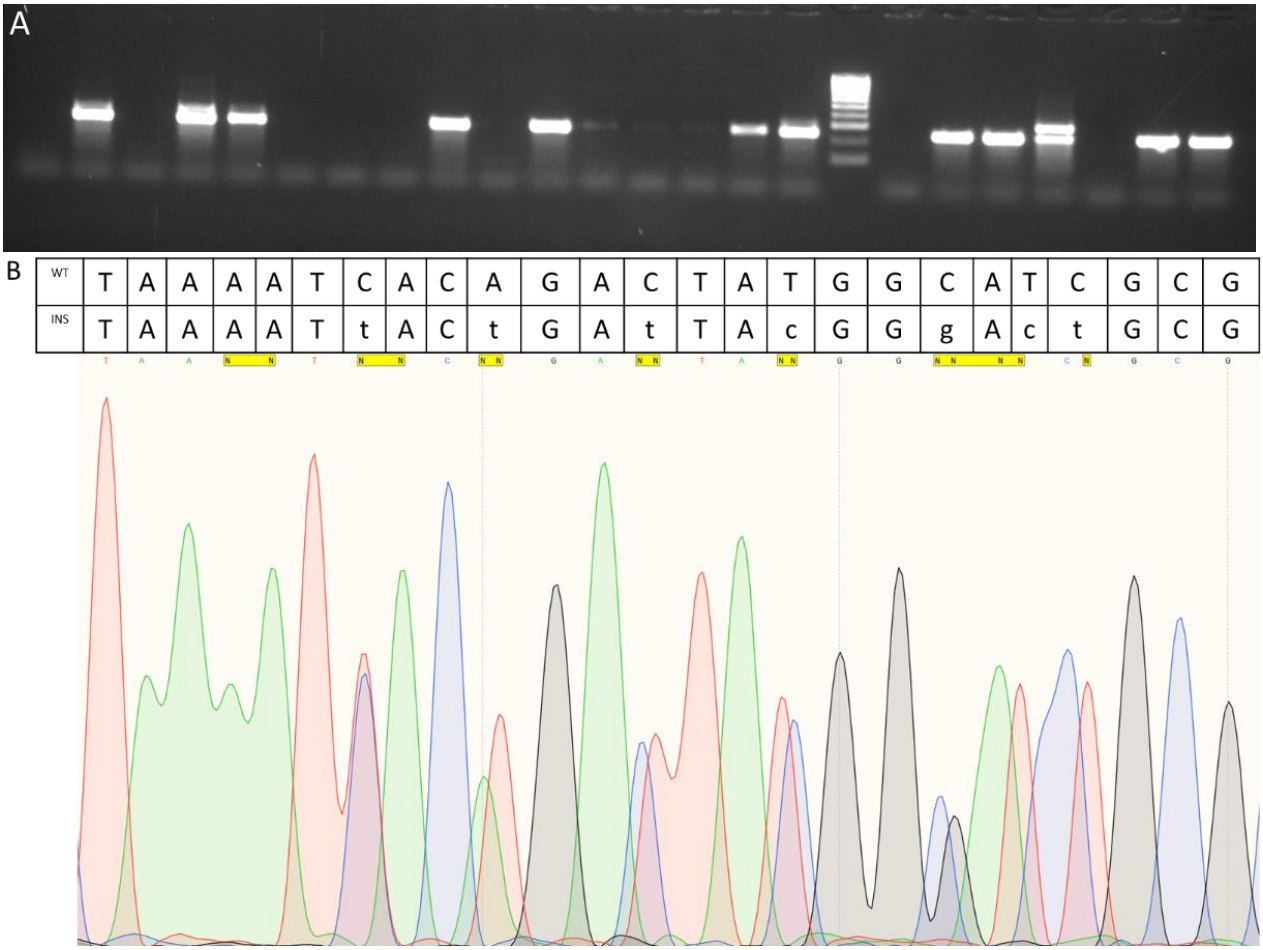

Figure 102. Germline Transmission of the I2010T Mutation was Identified in Adult Zebrafish by Assessment of Their Offspring. ***A.*** *PCR using oligonucleotide-specific primers on the offspring obtained by crossing a zebrafish injected with the I2010T construct with a wildtype zebrafish. Each lane represents a single embryo. Ladder is 100bp [Bioline].* ***B.*** *Chromatogram following sequencing of the DNA from a single embryo obtained from this cross. The table above shows the expected DNA sequence of the region in wildtype zebrafish and in zebrafish following successful insertion of the construct. The embryo had both sequences, as expected.*

5.2.9.8 N1437H

The final pathogenic *LRRK2* mutation is the substitution of asparagine for histidine at position 1437. The zebrafish equivalent to this is asparagine at position 1424, coded for by AAC (**figure 103A,B**). A guide was designed in this region, with a cut site 1bp downstream of the codon of interest, resulting in the disruption of an MslI restriction site. Primers flanking this region were designed and tested using wildtype zebrafish DNA in a gradient PCR and MslI digest (**figure 103D**). At an annealing temperature of 65°C, this primer pair produced a single product that was completely digested following incubation with MslI for 2 hours. The gRNA for this region was tested in wildtype embryos (described previously) and found to be approximately 60% efficient based on the loss of the MslI site (**figure 103E**). A 127bp ssODN was then designed to target this region. First, redundant codons for histidine were assessed for their usage in the zebrafish genome, finding both to be common (**table 34**).

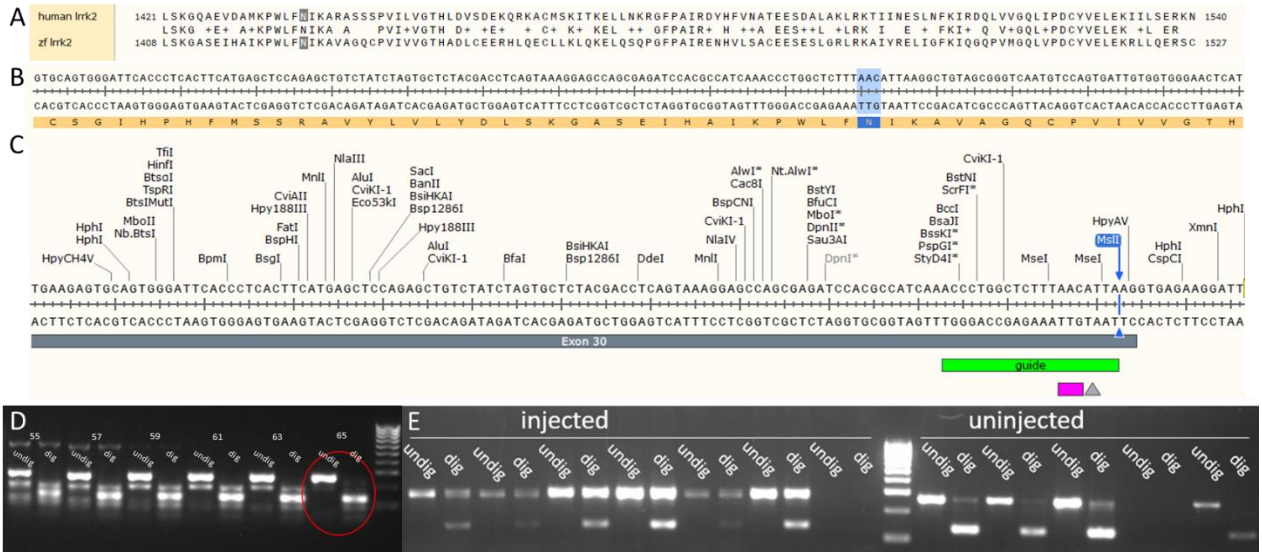

Figure 103. Designing A Guide RNA to Target N1424. A. *Protein-protein alignment of human and zebrafish Lrrk2 in SnapGene shows asparagine at position 1437 in human LRRK2 to be equivalent to asparagine at position 1424 in zebrafish lrrk2* ***B.*** *In silico transcription identifies the codon for this asparagine as AAC.* ***C.*** *Restriction enzyme sites nearby the guide cut site (grey arrow), highlighting the MslI cut site (blue). Green bar shows the region of the guide RNA and the pink bar shows the codon of interest.* ***D.*** *Gradient PCR using primers flanking the target region followed by digest with MslI identified 65°C as the optimum annealing temperature. Numbers represent annealing temperature used.* ***E.*** *Electrophoresis gel of DNA obtained at 24hpf from wildtype embryos injected with the N1424 guide RNA, tracrRNA and Cas9 and amplified using the flanking primers. Samples were the digested with MslI. Less digestion can be seen in injected samples compared to uninjected controls. Ladder is 100bp [Bioline]. dig, digested with mslI for 2 hours; lrrk2, leucine-rich repeat kinase 2; undig, DNA from PCR reaction.*

Table 34. Possible Codons for Histidine to Use in the Design of the N1424H Donor Oligonucleotide

Possible Codon	Frequency (per thousand)	Enzyme site added?
CAT	10.9	None
CAC	14.8	None

Table showing the possible codons that are translated into the amino acid histidine and their frequency in the zebrafish genome. Final column describes restriction enzyme sites that are added into the DNA following mutation of wildtype codon to each of the glycine codons. For more information, see methods section.

However, mutating the zebrafish DNA to either codon would not induce any novel restriction enzyme sites. However, as the PAM also needed to be mutated, restriction sites could be created from altering wobble bases in the PAM. The PAM site was made up of two codons; AAG/GTG. GTG (valine) could only be altered in the third position which would not affect the PAM. Therefore, AAG (lysine) was mutated to the only other codon, AAA. After mutating both the codon of interest and the PAM, five new restriction sites were induced: MboII, EarI, SapI, **BspQI**, Nt. BspQI. Further wobble bases were altered by trial and error in Primer3 to identify oligonucleotide-specific primers with the lowest penalty (**figure 104**). ssODN development is summarised in **table 35**. Oligonucleotide-specific primers were tested using a gradient PCR on wildtype zebrafish DNA, showing that no products of the correct size are amplified (**figure 104**). The ssODN was then co-injected with the N1437 gRNA into wildtype zebrafish at the single-celled stage to assess HDR using the oligonucleotide-specific primer pair, as described previously.

However, no difference was seen between injected fish and controls at 24hpf, with no DNA being amplified using the oligonucleotide-specific primers in any condition (**figure 104**). As mentioned previously, HDR for N1424H was assessed at the same time as V1428H, which was also seen to be unsuccessful. To determine whether the lack of PCR product was reproducible or the result of a poor injecting session or DNA analysis, the N1424H construct was tested again in wildtype larvae. Again, no bands of expected size were present following PCR (**figure 105**), suggesting that this construct is unable to induce HDR in zebrafish *lrrk2*.

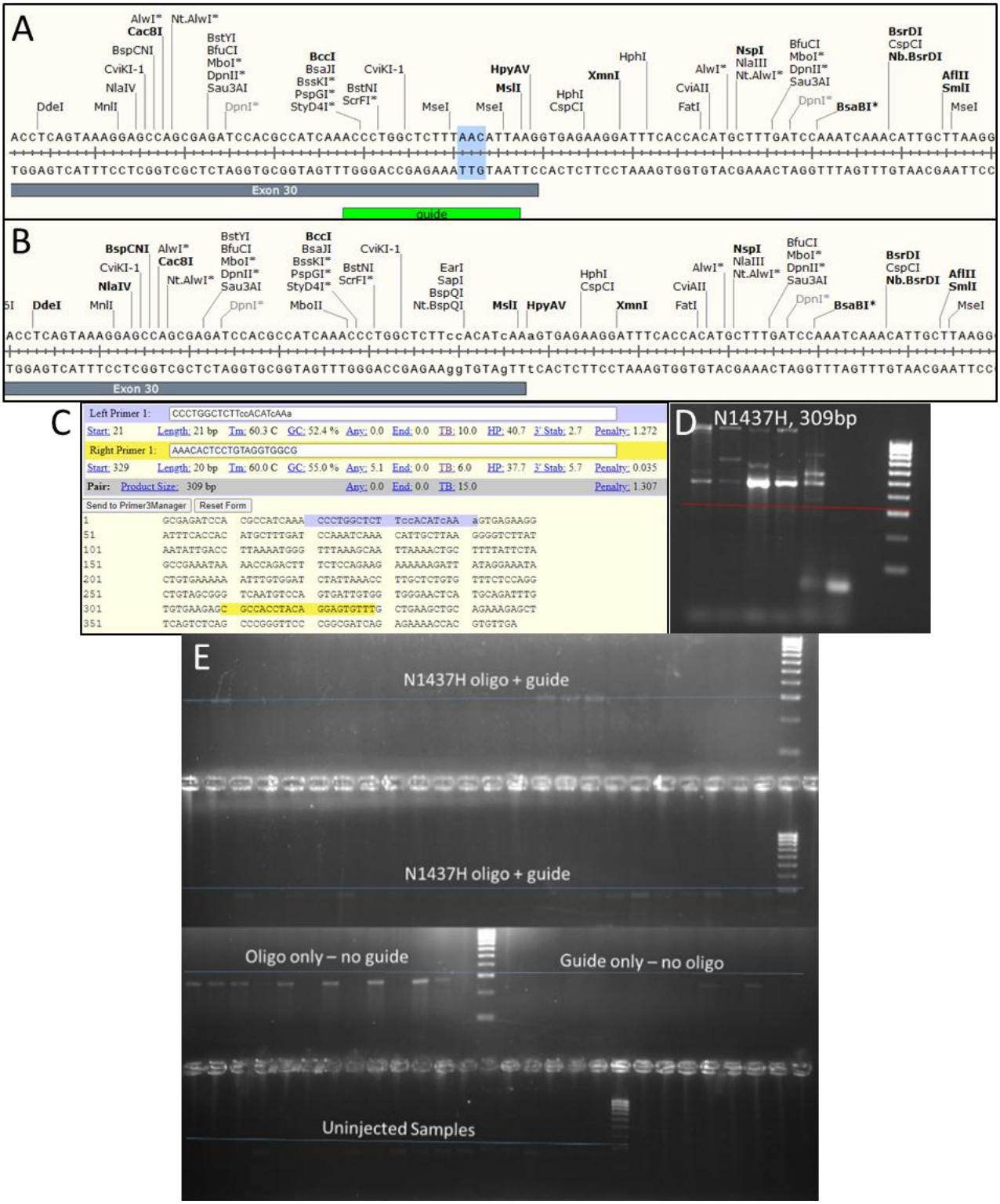

Figure 104. Oligonucleotide Development to Induce a Zebrafish Equivalent of the N1437H Mutation into Leucine-Rich Repeat Kinase 2. A. *Screenshot taken from SnapGene showing the position of the N1437 guide in green, target codon in blue and restriction enzyme sites above in wildtype zebrafish DNA.* ***B.*** *DNA sequence and restriction enzyme site following the mutation of the target codon AAC to CAC as well as additional wobble bases.* ***C.*** *Design of the oligonucleotide-specific primer using Primer3 software.* ***D.*** *Testing the oligonucleotide-specific primer pair in wildtype zebrafish DNA demonstrated that this primer pair did not amplify any products of the correct size.* ***E.*** *DNA samples were collected at 1dpf from embryos injected with the N1437H oligonucleotide, guide RNA, tracrRNA and Cas9 (top 2 rows); oligonucleotide only (middle left); guide RNA, tracrRNA and Cas9 only (middle right) or uninjected samples (bottom row). Samples were run using the oligonucleotide-specific primer pair at 65°C. Blue line represents expected product size after successful insertion. Ladder is 100bp [Bioline].*

Table 35. N1424H Oligonucleotide Development

A. Original DNA	GCGAGATCCACGCCATCAAACCCTGGCTCTTTAACATTAAGGTGAGAAGGATTTCACCACATGCTTTGAT CCAAATCAAACATTGCTTAAGGGGTCTTATAATATTGACCTTAAAATGGGTTTAAAG
B. Mutated DNA	GCGAGATCCACGCCATCAAACCCTGGCTCTTccACATcAAaGTGAGAAGGATTTCACCACATGCTTTGATC CAAATCAAACATTGCTTAAGGGGTCTTATAATATTGACCTTAAAATGGGTTTAAAG
C. ssODN	C*T*TTAAACCCATTTTAAGGTCAATATTATAAGACCCCTTAAGCAATGTTTGATTTGGATCAAAGCATGT GGTGAAATCCTTCTCACtTTgATGTggAAGAGCCAGGGTTTGATGGCGTGGATCTC*G*C

Table showing the stages of oligonucleotide development for the induction of N1424H mutation in zebrafish. ***A.*** *Original 127bp DNA sequence with the guide sequence shown in yellow, the PAM site underlined and the target codon in red.* ***B.*** *The 127bp sequence following mutation (new codon plus wobble bases). The novel primer (reverse) is shown in blue, PAM site underlined and target codon in red. Lower case letters represent base changes from wildtype.* ***C.*** *The ssODN that was ordered from IDT. It is a reverse complemented version of the sequence in B. Stars represent bases that have been phosphorothioated.*

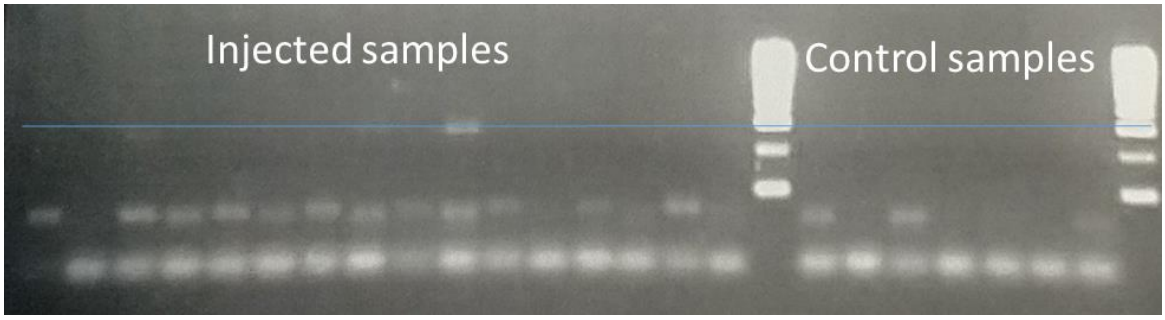

Figure 105. Re-testing the N1424H Construct in Wildtype Zebrafish. *Wildtype zebrafish were injected with N1424H oligonucleotide, guide RNA, tracrRNA and Cas9 and DNA extracted from these embryos at 24hpf. For control samples, DNA from uninjected siblings was used. DNA was amplified by PCR using the oligonucleotide-specific primer pair and run by gel electrophoresis. Blue line represents expected product size following successful insertion of the new DNA sequence.*

5.3 Discussion

The aim of chapter two of this thesis was to explore the function of Lrrk2 in zebrafish, with a particular focus on its role in PD and inflammation. To ensure that studying this protein in zebrafish had relevance to human PD, where *LRRK2* mutations and SNPs have been implicated in disease processes, genetic comparisons between organisms were initially conducted.

In silico data supported Lrrk2 as the zebrafish orthologue of human LRRK2, having a conserved protein domain structure and both amino acid and DNA similarity. Although the overall identity between organisms was less than 50% at both the DNA and amino acid level, a comparison of each protein domain independently found high levels of similarity. Of particular importance, the kinase domain demonstrated over 70% identity between organisms, suggesting that the most important functional domain represents an evolutionarily conserved region of the protein. It was difficult to compare chromosomal synteny between organisms as human *LRRK2* had only four other genes within a 1Mb region. Nevertheless, of these, one gene was also found in the same size region surrounding *lrrk2* in the zebrafish genome, indicating some level of conserved synteny. It is important to remember, however, that this conservation does not necessarily equate to conserved protein properties. For example, in mice, *Lrrk2* shares 88% identity to human *LRRK2* and yet the biochemical properties, including stability, expression levels and activity, differ significantly (Langston et al., 2019). Despite this, the presence of a true *LRRK2* orthologue in zebrafish suggests that this model may be a useful tool to assess the role of this protein in an *in vivo* system. The lack of multiple *lrrk2* splice variants, or paralogues resulting from genome duplication, reduces the likelihood of compensation mechanisms occurring. It is possible, however, that Lrrk1, a structurally similar protein, may compensate for a loss of Lrrk2 function. It has been suggested that LRRK1 and LRRK2 may have redundant functions in mammals (Biskup et al., 2007), although expression patterns of each paralogue in zebrafish differ considerably, overlapping only in distinct areas (Suzzi, 2017; Suzzi et al., 2021). This is discussed in further detail below.

In wildtype zebrafish, *lrrk2* mRNA was found to be expressed throughout development from 1-5dpf. This supports existing literature where *lrrk2* transcript levels have been shown to gradually increase throughout larval development (Sheng et al., 2010). To further explore the spatial expression of *lrrk2*, in situ hybridisation was conducted in wildtype 5dpf larvae. The results from this experiment were inconclusive, as the staining pattern observed following different staining times were markedly different. Initially, it appeared that *lrrk2* mRNA was upregulated in specific

tracts of the zebrafish brain. However, this pattern was also seen in control larvae following a longer incubation with the staining buffer, suggesting that this was nonspecific. The absence of specific staining with the antisense probe may be a result of using older larvae, preventing penetrance of the probe into their more developed tissues. The experiment was repeated using 3dpf larvae, which resulted in staining in the head region from the antisense probe that was not seen in the sense probe. This expression pattern mimics that seen in another study published this year, where *lrrk2* expression was ubiquitous before 24hpf but became restricted to the head during development (Suzzi et al., 2021). Previous literature, from which the riboprobe sequences were acquired, also report ubiquitous brain expression at both 24hpf and 6dpf (Sheng et al., 2010). Immunohistochemistry against the Lrrk2 protein has also identified Lrrk2 in the CNS, as well as in the heart and kidney, of wildtype larvae (Prabhudesai et al., 2016).

In this project, RT-PCR also identified *lrrk2* mRNA in adult brain tissue, which has also been found at the protein level (Sheng et al., 2010). This implies a role of Lrrk2 in the function of the zebrafish CNS under basal conditions. This is unsurprising since LRRK2 is reported to have a wide variety of functions in vital cellular pathways, particularly in CNS immune cells and during neuronal development (See review by Harvey and Outeiro (2019)).

The expression profile of *lrrk2* suggests a continued, important role throughout life, potentially being required during zebrafish patterning and also for normal functioning in adulthood. The staining patterns obtained mimic the expression data demonstrated for human LRRK2 as discussed in the chapter introduction. To explore this protein further, a *lrrk2* knockout line was created using CRISPR/Cas9 targeting exon 19 of zebrafish *lrrk2*. The mutation induced led to the introduction of a premature stop codon and resulted in nonsense-mediated decay of the resulting mRNA, as shown by qPCR.

Whilst studying a loss-of-function mutation may seem counterintuitive in a gene that usually shows gain-of-function pathogenesis, there are many benefits. Loss-of-function models enable study of the biological role of proteins. By understanding the effects of an absence of a particular protein, inferences can be made about its role under basal conditions. Whilst LRRK2 function has been studied in detail in mammalian systems, its role in zebrafish has not been fully determined as currently available zebrafish models have important limitations (discussed in detail below).

Furthermore, as a risk gene, *LRRK2* SNPs are plentiful and some may confer reduced activity rather than result in the usual gain-of-function seen in LRRK2 Mendelian cases. For example,

G2385R has been described as a loss-of-function SNP in LRRK2 (Carrion et al., 2017) and both G2385R and R1941H have been demonstrated to result in reduced kinase activity (Jaleel et al., 2007). Similarly, I2020T presents as a dominant negative mutation that increases the degradation of wildtype LRRK2 with which it forms heterodimers (Ohta et al., 2013) and is also associated with reduced kinase activity (Jaleel et al., 2007). However, recent genetic studies have concluded that loss-of-function mutations in *LRRK2* are not associated with disease, Parkinson's or otherwise (Whiffin et al., 2020).

Finally, since *LRRK2* mutations are primarily gain-of-function, future personalised therapy is likely to target LRRK2 activity. This option also offers therapeutic use more broadly in idiopathic PD because LRRK2 kinase activity has been identified as increased in dopaminergic neurons in idiopathic cases where *LRRK2* mutations were not identified (Di Maio et al., 2018). Likewise, inhibiting LRRK2 kinase activity using a brain-penetrant compound was able to protect rats against the endolysosomal impairment, α-synuclein accumulation and nigrostriatal dopaminergic neuron degeneration in response to rotenone (Rocha et al., 2020). Using LRRK2 inhibitors in cases where LRRK2 hyper-activity is not thought to be the main the cause of pathogenesis would likely result in decreasing LRRK2 function to below basal conditions. The effect of this remains relatively unknown at this time. By studying the effect of a complete loss of *lrrk2* function in zebrafish, it may be possible to predict potential side effects that may occur with such interventions in humans. It is especially important to study this in an *in vivo* system as LRRK2 appears to have conflicting roles in different regions. In the periphery, for example, LRRK2 appears to be protective against infections, such as Listeria (Zhang et al., 2015) and Salmonella (Gardet et al., 2010; Shutinoski et al., 2019). Therefore, inhibiting LRRK2 in the entire body may present problems with an increased risk of infection.

The resulting *lrrk2*$^{-/-}$ mutant zebrafish were viable, fertile and appeared morphologically identical to their wildtype siblings. Given the involvement of Lrrk2 in many cell-critical pathways, the lack of a severe phenotype was somewhat surprising. Indeed, previous morpholino zebrafish studies report a complete loss of *lrrk2* as an embryonic lethal mutation (Sheng et al., 2010), although this has not been supported in later morpholino study (Suzzi et al., 2021). Zebrafish lacking the entire *lrrk2* locus are also viable (Suzzi, 2017; Suzzi et al., 2021) and *LRRK2* knockout in other animals, including mice (Hinkle et al., 2012; Lin et al., 2009; Pellegrini et al., 2018; Tong et al., 2010), rats (Baptista et al., 2013; Ness et al., 2013) and drosophila (Lee et al., 2007; D. Wang et al., 2008) also report viability, usually without any obvious phenotype. This suggests that the role of LRRK2

in seemingly vital cell survival pathways may have a redundant role that can be compensated for by other proteins, a capacity that seems evolutionarily conserved across organisms.

Due to the similarity in structure between LRRK1 and LRRK2, it is reasonable to question whether these proteins are functionally redundant and a reason for the absence of an obvious phenotype in these animal models. Attempts to associate *LRRK1* with PD have been unsuccessful. The sequencing of people with PD has, on multiple occasions, found no segregating amino acid substitutions (Haugarvoll et al., 2007; Taylor et al., 2007). Likewise, the probing of specific *LRRK1* variants in PD patient populations also concluded that there were no associations with disease (Chung et al., 2011; Dachsel et al., 2010). Additionally, *LRRK1* loss-of-function variants have been identified in PD patients at the same frequency as the general population (Blauwendraat et al., 2018), suggesting they have no impact on the risk of disease. Furthermore, LRRK1 proteins carrying corresponding amino acid substitutions to well-known *LRRK2* mutations appear less toxic than their LRRK2 counterparts and result in less inclusions in cell-based, *in vitro* assays (Greggio et al., 2007).

However, one *LRRK1* variant (p.L416M SNP) has been suggested to lower the age of onset in PD patients carrying the G2019S *LRRK2* mutation (Dachsel et al., 2010). p.L416M is also thought to act as a protective variant in other cases of PD (Dachsel et al., 2010). Despite these data not being conclusive, it is possible that *LRRK1* may be a disease modifying gene, having a modulatory role in PD resulting from other causal mutations, rather than directly causing the disease itself.

Research also suggests that LRRK1 and LRRK2 have distinct biological roles and both paralogues have been shown to interact with different proteins on multiple occasions. A dual-method protein-protein interaction screen, whilst identifying some common interactors, primarily concluded that each paralogue has its own distinct interactome (Reyniers et al., 2014). The authors admit to having false positives and negatives within their dataset, as borne out by other research, and more recent reports have found that only low numbers of previously published LRRK1 and LRRK2 interactors are replicated across studies (Tomkins et al., 2018). Nevertheless, specific examples, such as the ability of LRRK1 but not LRRK2 to interact with GRB2 during EGFR signalling (Hanafusa et al., 2011), have been separately researched and verified. From an inflammatory standpoint there are also differences between the *LRRK* paralogues. Whilst *LRRK2* expression is increased in hPBMCs in response to inflammatory stressors, including IFN-γ, IL-6 and TNF-α, this is not the case for *LRRK1*, whose expression remains constant when exposed to these cytokines (Thévenet et al., 2011). To further support the diverging roles of the *LRRK*

paralogues, LRRK2 inhibitors appear to have no effect on LRRK1 (Li et al., 2014), suggesting that their structure and/or functions differ. Additionally, Lrrk1 is unable to compensate for Lrrk2 during synaptic transmission and vesicle release, demonstrated in mouse hippocampal slices (Maas et al., 2017).

Whilst structurally LRRK1 and LRRK2 appear to have a high degree of homology, most research suggests that these paralogues are not functionally redundant. Each protein appears to have overlapping but distinct expression patterns, binding partners, kinase targets and regulation. However, these diverging functions do not mean that under pathological conditions there is no interplay between the *LRRK* paralogues and that in the complete absence of *LRRK2*, *LRRK1* is unable to partially compensate. Given this, it is still important to determine the effect of *LRRK1* in *LRRK2* knockout models. *lrrk1* expression was assessed in the *lrrk2*$^{-/-}$ mutant zebrafish during this project, where an upregulation was not identified, suggesting that this was not the reason behind the absence of phenotype seen in these mutants.

PD is primarily recognised as a movement disorder and bradykinesia is described in *LRRK2*-associated cases, where tremor is also more commonly reported than in idiopathic PD (Healy et al., 2008). To determine whether disruptions to movement were seen in zebrafish with a reduced expression of *lrrk2,* behavioural analysis was conducted on larval (5dpf) and adult (12-month old) zebrafish using the ZebraBox and Viewpoint software.

No significant differences in movement were identified between *lrrk2*$^{-/-}$ mutant zebrafish and their wildtype siblings at 5dpf. This replicates other zebrafish loss-of-function mutants, both knockdown (Ren et al., 2011) and knockout (Suzzi, 2017; Suzzi et al., 2021) models, where no defects in swimming behaviour were identified at 5-6dpf. However, Sheng et al. (2010) reported a reduced distance travelled by larvae when the WD40 domain was disrupted using morpholinos, which was rescued by human *LRRK2* expression and L-dopa treatment. Furthermore, the whole locus deletion reported by Suzzi (2017) developed swimming defects (stop-go behaviour) by 10dpf, which were absent at 5dpf. These inconsistencies could reflect differences in the model used or in the methodology of assessing movement, both of which varied by study.

Despite the loss of *lrrk2* having no effect on movement at 5dpf, it is possible that *lrrk2*$^{-/-}$ zebrafish develop changes to their movement later in life. PD is a disease of aging, with signs and symptoms appearing during late adulthood in patients and so movement was also assessed in adult zebrafish. Sheng et al. (2018) also reported varied movement data depending on batch in larval

zebrafish, as was also seen during the current project, but were able to demonstrate significant differences in adulthood in *lrrk2* loss-of-function mutants.

However, no differences were identified in the movement of *lrrk2*$^{-/-}$ zebrafish at 12mpf in this project. Previously reported *lrrk2* mutations have been shown to result in hyperactivity of adult (8-22mpf) zebrafish (Sheng et al., 2018). However, this mutation occurred only in the final WD40 domain of *lrrk2*; when analysing complete loss-of-function mutants, such as the whole locus deletion reported by Suzzi (2017), the differences in adult movement at 6mpf were minimal and when reported in publication were said to be absent (Suzzi et al., 2021). Mouse knockout models also report no changes in movement (Herzig et al., 2011; Lin et al., 2009), although this is not supported by all research groups (Hinkle et al., 2012). The effect of a loss of LRRK2 on movement *in vivo* appears to be inconclusive, even within organisms. Logically, if pathogenic mutations in *LRRK2* are primarily gain-of-function, then movement abnormalities associated with PD would be unlikely to occur in knockout models. However, the involvement of LRRK2 in multiple cellular pathways could suggest substantial changes to cell function that leads to a nonspecific effect on movement as well as other areas.

A hallmark of PD pathology is the loss of dopaminergic neurons in the SNpc. This has been demonstrated in the brains of patients with *LRRK2* mutations, where the substantia nigra appeared depigmented on post mortem analysis, supported by reduced TH staining (Takanashi et al., 2018). Gain-of-function mutations resulting in increased LRRK2 activity have been suggested to result in this neuronal loss due to the toxicity of increased kinase activity, as kinase-dead LRRK2 was unable to cause neuronal death (West et al., 2007). This would suggest that the current zebrafish model, which in theory possessed reduced/absent kinase activity due to low expression levels of a truncated mRNA, would not result in dopaminergic neuronal toxicity. However, cell culture studies have suggested that a loss of *LRRK2* can prevent the differentiation of dopaminergic neurons (Milosevic et al., 2009). Since this zebrafish was a stable mutant, Lrrk2 should have been absent from fertilisation, including during the development of the nervous system. Therefore, dopaminergic neurons in *lrrk2*$^{-/-}$ larvae were assessed, with the hypothesis that mutants would demonstrate reduced numbers in DC2 and DC4/5 due to possible inhibition of differentiation during early development.

lrrk2$^{-/-}$ mutant zebrafish did not demonstrate any changes to the number of dopaminergic neurons at 3dpf. Whilst not supporting the current hypothesis, this data corroborates other zebrafish models where morpholinos targeting *lrrk2* also failed to alter mRNA levels of the

dopamine transporter (*dat*) or tyrosine hydroxylase (*th*) at 3dpf (Ren et al., 2011). However, other zebrafish *lrrk2* morpholino models do report reduced *th* or *dat* levels in larvae (Prabhudesai et al., 2016; Sheng et al., 2010). The model most similar to the present *lrrk2*$^{-/-}$ mutant, the entire locus deletion, reported varying levels of *th* mRNA depending on age; reduced at 5dpf, normal at 10dpf and normal at 6 months (Suzzi, 2017). In agreement with this RNA data, a reduction in Th1+ cells was observed in multiple brain regions, including the diencephalic populations, using a Th1 antibody in this mutant at 5dpf, a phenotype that was not evident at 6mpf (Suzzi et al., 2021). Mouse models with *LRRK2* knockout mutations also report no changes to dopaminergic neurons (Andres-Mateos et al., 2009; Giaime et al., 2017; Herzig et al., 2011; Hinkle et al., 2012; Lin et al., 2009; Tong et al., 2010) and this is also seen in most drosophila models (Imai et al., 2008; D. Wang et al., 2008), although reduced *th* was reported in one mutant (Lee et al., 2007). Given the previous literature, the lack of a neuronal phenotype in the *lrrk2*$^{-/-}$ mutant is not unexpected.

Mice harbouring the G2019S mutation display a mild phenotype that is exacerbated by exposure to MPTP, including selective dopaminergic neuronal death (Arbez et al., 2020). Importantly, this enhanced neuronal death was not seen when mice were treated with a kinase inhibitor, suggesting that the gain of kinase function resulting from the G2019S substitution was responsible for the increased susceptibility to this toxin. Therefore, the hypothesis that *lrrk2*$^{-/-}$ zebrafish, as a loss-of-function mutant, would be less severely affected by MPP+ than wildtype fish seemed logical. However, treatment of *lrrk2*$^{-/-}$ mutant larvae with MPP+ from 1-3dpf did not result in a more or less severe loss of dopaminergic neurons compared to their wildtype siblings. However, although an increase in Lrrk2 activity appears to lead to an increased susceptibility to MPTP, this does not necessarily mean that the opposite is true and basing a hypothesis on this may have been naïve. An absence of *lrrk2* in larval zebrafish appears to have no effect on dopaminergic neuronal number or their susceptibility to MPP+.

As discussed in the introduction to this chapter, LRRK2 positively regulates inflammation via microglia and is required for their full response. LRRK2 has been demonstrated to be upregulated at the protein level in activated microglia in both mouse and cell-based models (Moehle et al., 2012). Furthermore, studies on manganese exposure, which activates LRRK2, have shown that this results in the apoptosis of microglia and macrophage cell lines, effects not seen when LRRK2 was inhibited (Kim et al., 2019). This literature suggests that an absence of *lrrk2* may lead to a reduced inflammatory state in the CNS, but may increase overall microglial numbers due to the reduction in apoptosis.

To assess the inflammatory phenotype of *lrrk2*$^{-/-}$ zebrafish, microglial number and activation was initially assessed in 5dpf larvae, finding no change in either parameter compared to their wildtype siblings. *In vitro*, microglia exposed to LRRK2 kinase inhibitors were unable to undergo morphological remodelling to become amoeboid in response to LPS (Moehle et al., 2012). Therefore, using morphological changes as a readout for microglial activation may not be valid in this genetic model; cells that are activated may be unable to display the usual morphology due to the loss of Lrrk2. However, some microglia were identified as amoeboid during image analysis, suggesting that the effects seen *in vitro* may not be present to the same extent *in vivo*, at least in the zebrafish. Previous animal models of *LRRK2* knockout differ in their findings regarding microglia. Mice lacking *LRRK2* have been shown to have both increases (Lin et al., 2009) and no changes (Tong et al., 2010) in microglia number depending on publication. In zebrafish, the whole locus deletion of *lrrk2* was reported to result in a reduced number of microglia that appeared larger and more ramified at 5dpf, but were indistinguishable from wildtype at 10dpf and in adults (Suzzi, 2017; Suzzi et al., 2021). This increase in ramification could corroborate results from cell-based models suggesting an inability to develop an amoeboid morphology, although the loss of this effect at later stages is unclear. It is relevant to mention that this analysis was on L-plastin labelled cells, whereas the current mutant was assessed using 4c4 immunolabelling, which could potentially mean that different cell populations were assessed between models.

The phenotypes seen in mouse and cell models discussed above were only evident following exposure to microglial-activating compounds or toxins. Therefore, the absence of a microglial phenotype under basal conditions is unsurprising. It is plausible that following stimulation of the system, a phenotype may become evident. The Bandmann Laboratory had previously established a technique to assess microglial response involving the injection of zymosan directly into larval zebrafish brains (Larbalestier et al., 2021). Using this methodology on the *lrrk2*$^{-/-}$ mutant may have revealed a microglial phenotype but due to issues with this line, discussed below, these experiments were not completed.

It may also be more relevant to study other aspects of inflammation besides microglial activation in *lrrk2*$^{-/-}$ zebrafish. The brain pathology of patients carrying *LRRK2* mutations do not always demonstrate activated microglia, but neuroinflammation, including the activation of astrocytes, is usually reported (Takanashi et al., 2018). In zebrafish *lrrk2* mutants, evidence of altered inflammation elsewhere in the fish has been shown in multiple models, including ZFN-induced mutants, CRISPR- induced mutants and morpholino knockdowns (Prabhudesai et al., 2016; Sheng

et al., 2018; Suzzi, 2017). Phenotypes included a weakened anti-bacterial response, reduced leucocyte response to external inflammation and an increase in ROS in the tail. Furthermore, RNAseq pathway analysis using the ZFN-induced 5bp deletion in the WD40 domain identified "infectious disease" and "immunological disease" as altered groups alongside the expected "neurological function" (Sheng et al., 2018). To assess inflammation more broadly in this line, *lrrk2*$^{-/-}$ mutants had been crossed into fluorescent reporter lines and qPCR against inflammatory mediators was planned, as reported for *acmsd* in chapter 4, but due to issues with this line, discussed below, these experiments were also not completed.

There are a number of *lrrk2* loss-of-function zebrafish models currently available, but each is not without limitation. The majority of published models were created using morpholinos targeted to either prevent translation or splicing of *lrrk2* mRNA (Prabhudesai et al., 2016; Ren et al., 2011; Sheng et al., 2010). These knockdown models present a number of widely accepted issues including the inability to determine knockdown effectiveness and the differences in genetic compensation between stable mutants and mophants, creating phenotypes that are often more severe. Additionally, the effects of a morpholino are usually transient, lasting for around four days in zebrafish. Perhaps the most concerning issue with morpholino models are the off-target effects, particularly that resulting from cell death via activation of p53, which can result in a number of phenotypes unrelated to the gene of interest (Robu et al., 2007).

Stable mutants are often more reliable when studying the effects of a loss-of-function. One reported *lrrk2* stable zebrafish line was created using zinc finger nucleases (Sheng et al., 2018). Whilst overcoming the issues of morpholino knockdown models, this mutation targeted the WD40 domain of the protein, creating an expressed but truncated version of Lrrk2. Since this is the final domain of Lrrk2, the truncated protein likely retains at least some of its activity due to the presence of both catalytic domains and almost all of its amino acid sequence, which may assist in secondary structure formation and binding to its usual targets. It is unlikely that this line represents a true loss-of-function phenotype because of this.

The *lrrk2*$^{-/-}$ mutant created in the current project presents a stable mutant line that resulted in reduced expression levels of mutated *lrrk2* mRNA. Furthermore, due to the formation of a premature stop codon, translation of any remaining mRNA would result in a truncated protein lacking five of the seven Lrrk2 protein domains, including both enzymatic domains. This would result in a protein without kinase or GTPase activity. The amorphic model, created using CRISPR-Cas9 to delete the entire *lrrk2* locus (Suzzi, 2017; Suzzi et al., 2021), may be a superior model to

the one used during this project since no truncated protein can be produced. However, the low levels of mRNA and early stop codon in the current mutant would mean that any potential protein translated would be minimal and almost certainly non-functional, suggesting that this mutant was equally valid.

Unfortunately, following full characterisation of the stable *lrrk2*$^{-/-}$ mutant, qPCR data revealed that this line no longer showed the reduction in *lrrk2* mRNA that was detected when it was first created. Levels were assessed alongside *lrrk1* during compensation experiments and the results were unexpected. This may explain the absence of a phenotype in this line and why functional assays carried out by external collaborators did not see a reduction in Lrrk2 kinase activity of the *lrrk2*$^{-/-}$ homozygous mutant, as expected. Due to these findings, this line was culled and no future experiments were carried out as planned.

Whilst it is impossible to know why this loss of nonsense-mediated decay occurred, re-sequencing of new DNA confirmed that it was not due to a change in DNA sequence at the initial mutation site; the 5bp deletion was still present in the *lrrk2* gene. The initial qPCR was conducted prior to the start of this project and access to the original data was not possible. The expression of *lrrk2* in the wildtype samples from this initial dataset demonstrated a large variance that was not seen in the *lrrk2*$^{-/-}$ samples. It is possible that outliers in the initial dataset gave the impression of a loss of RNA expression, but without knowing the individual values for each replicate it is impossible to evaluate. Nevertheless, the loss of expression was suggested to be significant, although the use of a one-tailed (as opposed to the two-tailed) t test in this case may have afforded less power to the statistics, making the difference appear significant even if this was not the case. Again, without accessing the raw data, it is impossible to conclude such possibilities. It is important to note that an absence of nonsense-mediated decay does not mean that a mutation is not pathogenic, but the loss of this phenotype between generations was concerning. If the loss of nonsense-mediated decay is real, one explanation may be that additional compensatory mutations may have been introduced throughout the generations. For example, the introduction of a novel splice site may have resulted in the induced mutation being skipped and therefore no longer resulting in a premature stop codon and the subsequent degradation of mRNA. This possibility, whilst unlikely, would also explain the lack of difference found in functional assays. Without sequencing the entire *lrrk2* locus any suggestions are speculative and whilst it would be interesting to explore such compensatory mechanisms, this was beyond the scope of the current project.

To enable the continued research into the effect of a loss of *lrrk2* function in zebrafish, another method was employed, the CRISPant technique. Using two highly active guides that targeted the *lrrk2* gene, zebrafish with a predicted loss-of-function mutation were generated. Only basic overall larval morphology, *th1+* cells and response to MPP+ were assessed in the *lrrk2* CRISPants, all of which were found to be indistinguishable from wildtype. The data from these experiments supported that collected from the stable mutant line, suggesting that mutations in *lrrk2* have no effect in zebrafish larvae. However, whilst the guides were highly active at inducing indels in the zebrafish DNA, the effect of these mutations or the percentage of cells carrying them remains unknown using this technique. Therefore, data from CRISPant work alone should be interpreted with this in mind.

The CRISPant approach was also used to explore the gene-gene interaction between *lrrk1* and *lrrk2*. *lrrk1* CRISPants were intended to be combined with the stable *lrrk2*$^{-/-}$ mutant. However, as this line appeared to have no loss-of-function, it was decided to combine *lrrk1* and *lrrk2* CRISPants together to assess a possible effect of mutating both paralogous genes.

Initially *lrrk1* CRISPants were assessed alone, identifying no changes to larval survival, overall morphology, *th1+* cell counts or susceptibility to MPP+. This is in concordance with mouse models, where a knockout of *Lrrk1* also had no effect on survival or *th+* cells (Giaime et al., 2017). The only effect observed in this knockout mouse was an age-dependent reduction in body weight compared to their littermates. However, other groups have found that mice lacking *Lrrk1*, whilst displaying no developmental defects at birth, possess a vulnerability to starvation and lysosomal dysfunction that resulted in half of the homozygous mutants dying by 1 day old (Toyofuku et al., 2015). This is in contrast to that seen in mice reported by Giaime et al. (2017) and in zebrafish reported in this thesis.

Interestingly, with relevance to inflammation, a mouse *Lrrk1* knockout model was also found to have an increased number of B cells in the spleen and altered immunoglobulins in the blood, despite a normal response to LPS (Morimoto et al., 2016). Inflammation was not assessed in the CRISPants created as a part of this project, but this data suggests that exploring inflammatory phenotypes in *lrrk1* CRISPants may be relevant.

The primary effect of a loss of *Lrrk1* appears to be on osteoclasts, as discussed in the introduction to this chapter. Mice with homozygous *Lrrk1* loss-of-function mutations appear healthy during the 1st year of life but develop osteopetrosis as they age (Brommage et al., 2014; Xing et al.,

2013). This suggests that whilst appearing healthy at the larval stage, there may be abnormalities in the *lrrk1* CRISPants that are not yet evident, particularly with respect to bone health. Further experiments would be needed to assess this. However, as this project was primarily interested in its interaction with *lrrk2* and relevance to PD, no additional experiments were conducted on the *lrrk1* CRISPants.

In mouse models, it has been shown that a loss of both *Lrrk* paralogues results in the emergence of phenotypes that are not present in either mutant alone (Giaime et al., 2017; Onishi et al., 2020). To assess whether this may also be the case for zebrafish, *lrrk1* and *lrrk2* CRISPant approaches were combined to create *lrrk1/2* double CRISPants, with mutations in both *lrrk* paralogues. As before, no changes to the overall phenotype or *th1+* cell number was observed in the double CRISPants. A reduction in *th+* cells was seen in double *Lrrk* mouse mutants, but only from 14 months of age (Giaime et al., 2017), so the assessment at 3dpf may be too early a time point to observe any differences. In fact, most of the phenotypic changes identified in double knockout mice were age-dependent, including a reduction in body weight, reduction in striatal dopamine, and an increase of α-synuclein in the brain. These mice also demonstrated a reduced overall survival, suggesting that the *lrrk1/2* double CRISPants may need to be assessed into adulthood to observe a phenotype.

However, this project did identify that the *lrrk1/2* double CRISPants appeared more susceptible to the effects of MPP+, having less *th1+* cells following exposure compared to controls. This would suggest that whilst the loss of either paralogue alone has no effect on dopaminergic neurons, the loss of both *lrrk* paralogues may make this neuronal population more susceptible to external damage. However, despite being significant, the actual difference in cell number was minimal (a mean decrease of 2 cells) and, therefore, unlikely to be biologically relevant. The use of a subjective measurement for this also creates the possibility of this result being inaccurate; because the absolute difference in cell number was small, even slight miscounts of cells could have resulted in this significant difference. To confirm this result, the experiment should be repeated with a second counter or the loss of dopaminergic neurons explored using a different method, such as the *ETvmat2*:GFP transgenic line or by *th1* RNA analysis. It is also important to confirm such findings in a stable mutant line. This was not explored during this project due to the minimal effect seen and to allocate additional time to the creation of more biologically relevant *lrrk2* lines.

It is important to note that no changes in RNA of either *lrrk* paralogue was seen in any CRISPant created as part of this thesis. However, conclusions in the double CRISPant cannot be drawn due to issues with one replicate of the qPCR. It is also important to note the implicit limitations of the CRISPant technique resulting from specificity. CRISPR can result in the induction of large deletions and off-target mutations (Adikusuma et al., 2018), predicted to occur in up to 2.5% of cases (Hruscha et al., 2013). These are usually removed by outcrossing during the generation of a new stable mutant line. However, this does not occur when using CRISPants, as experiments are conducted directly on the injected embryos. Variants of Cas9 known to have increased specificity could be used to reduce the likelihood of these off-target effects occurring, but these variants often also result in reduced DNA cleavage at the target site (Jamal et al., 2018). Whilst this may be less important in the creation of a stable mutant line, when using the CRISPant approach it is paramount that guide activity is high to ensure larvae have significant reductions in expressed genes.

The final aim of this chapter was to generate new stable mutant zebrafish lines with targeted mutations in *lrrk2*. Single amino acid changes in the LRRK2 protein sequence have been identified to result in a number of familial PD cases. Therefore, studying zebrafish harbouring equivalent mutations may better recapitulate patient pathology, creating a more relevant *in vivo* model to study PD. CRISPR was used to induce specific mutations via the co-injection of gRNA, tracrRNA and Cas9, and a single-stranded DNA oligonucleotide that acted as a template for HDR.

The technique of using CRISPR technology to induce specific amino acid changes is a relatively new technique that has been scarcely utilised in zebrafish. Whilst CRISPR has been used to induce knock-ins for many years, the first report of germline transmission of a specific edit to the zebrafish genome was in 2016 (Armstrong et al., 2016). It was quickly demonstrated that 127bp asymmetrical ssODNs afford an increased efficiency at successful editing compared to symmetrical ssODNs in cells (Liang et al., 2017; Richardson et al., 2016) and later in zebrafish (Prykhozhij et al., 2018). Likewise, ssODNs complementary to the target strand are also thought to increase the efficiency of gene editing (Prykhozhij et al., 2018; Richardson et al., 2016). Although this is not supported in other studies (Liang et al., 2017) and has been suggested to be locus dependent (Hwang et al., 2013), there are no reports of such a design resulting in less efficient editing. Therefore, all oligonucleotides used in the current project to create the novel *lrrk2* lines were designed as antisense, asymmetrical ssODNs. Additionally, the Cas9 cleavage site was designed as close as possible to the intended base changes, since an inverse relationship

between this distance and editing success has been identified in all previous studies (Liang et al., 2017; Paquet et al., 2016; Prykhozhij et al., 2018). Finally, phosphothioate was incorporated into the ssODNs during this project, as this had also been shown to improve efficiency (Liang et al., 2017; Prykhozhij et al., 2018). Whilst not effecting the number of positive founders, phosphothioate addition is thought to result in a higher number of offspring from positive founders with the correct edit (Prykhozhij et al., 2018).

The founders for these lines were screened by outcrossing and analysis of their offspring. Whilst it may have been quicker to finclip these injected fish, a positive result would not necessarily mean that the mutation would show germline transmission. It has also been shown that some positive transmitters can be missed using the finclipping technique (Zhang, Zhang, et al., 2018). During screening, it was common to identify larvae that consistently generated positive bands via the oligonucleotide-specific PCR, but when sequenced would show only the wildtype DNA sequence. The reason for this is unclear, but this anomaly was observed in all four lines. Furthermore, some of the founders, when screened by sequencing, were found to have the correct sequence as well as additional indels. The addition of mutations at wobble bases in the PAM site was included to reduce the likelihood of Cas9 re-cutting correctly edited DNA and resulting in additional indels. However, it is possible that additional mutations could be introduced during the repair process. Furthermore, altering wobble bases within the PAM site rather than elsewhere in the guide recognition sequence has been shown to result in less indels (Paquet et al., 2016), but this was not possible for some of the PAM sites during this project due to their spanning of multiple codons. Conversely, there was no difference in the number of offspring that demonstrated successful editing without further mutations between R1441C/G, which had the PAM site altered, and I2020T which had the guide sequence altered. It is possible, however, that some were missed due to a lack of amplification by the oligonucleotide-specific primers due to the potential alteration of DNA.

The success of HDR in the new *lrrk2* lines differed depending on region and base change. For example, attempts to induce the zebrafish equivalent of the N1437H mutation were completely unsuccessful, despite the high activity of the gRNA. Likewise, at the R1441 locus, analysis of injected fish found that almost all fish had at least some cells with the correct DNA alteration, shown by oligonucleotide-specific PCR. However, the rate for the G2019S mutation was considerably lower, at approximately 30%. However, in all lines made during this project, the success rate was much higher than previously reported (3.8-21.4%) (Tessadori et al 2018). In

some PCRs, the mismatch of bases between DNA and primer was ignored and the oligonucleotide-specific primers amplified the wildtype DNA sequence. The increased intensity of bands from samples injected with both oligonucleotide and gRNA, and the disappearance of bands when annealing temperatures were increased, suggested that there had been insertion of the correct sequence in these cases. This was later confirmed when sequencing offspring from these adults.

One way to increase the success rate even further would be the addition of an NHEJ inhibitor, such as SCR7, which has been shown to increase edit efficiency in zebrafish (Zhang, Zhang, et al., 2018). Likewise, ssODNs have been shown to interfere with guide efficiency (Hwang et al., 2013) and the use of dsDNA or plasmids have been shown to offer improved genome editing (Zhang, Zhang, et al., 2018). Furthermore, it has been suggested that sequential application of the gRNA and ssODN results in enhanced editing efficiency compared to co-injection (Liang et al., 2017). However, this is impractical in zebrafish due to the time constraints around injecting. There are also other methods to induce gene edits. For example, by using a deactivated version of Cas9 (dCas9) and tethered enzymes that convert single bases, less indels are created since no DNA cleavage occurs (Gaudelli et al., 2017; Komor et al., 2016).

The most recent technology to increase efficiency has been demonstrated using a prime editing-ribonucleoprotein, with the ability to induce base substitutions with an increased efficacy compared to HDR in cells (Petri et al., 2021). This involves the injection of a single construct consisting of a partially deactivated Cas9 able to induce single-stranded breaks, a gRNA for gene targeting that also acts as a template for repair, and reverse transcriptase. In zebrafish, this technique increased the efficiency when used to induce insertion or deletion mutations, although for substitutions the efficiency was equal to that of the HDR technique used in this project. However, using an editing-ribonucleoprotein did have the advantage of resulting in significantly less unintended gene edits / off-target effects.

The demonstrated success of this new genetic editing technique via the creation of four new stable mutant lines during this project offers a new technique to the zebrafish field. Previously thought to be a lengthy and difficult process, site-directed mutagenesis in zebrafish has been scarcely utilised despite its obvious advantages. This thesis demonstrates the reliable success of this methodology in generating transmissible mutations at a number of different loci in the zebrafish genome. Not only does this provide new disease models for PD, but this technique

could also now be applied to additional genes, generating more disease-relevant zebrafish lines in other research areas throughout the field.

5.4 Conclusion

Zebrafish carrying a CRISPR-induced knockout mutation in *lrrk2* displayed no phenotypic changes from their wildtype siblings. Whilst this is surprising given the known important biological function of LRRK2, these data were supported by the assessment of an additional CRISPant model and also by much of the literature. These mutants appeared to lose the nonsense-mediated decay of *lrrk2* RNA observed when this line was generated, resulting in no effect of this DNA mutation at the functional level in later generations. Whilst it was impossible to say at which point this occurred, further experiments using this line were discontinued.

Studying a loss-of-function mutant may not be the most relevant to PD anyway, since most pathogenic PD mutations result in the gain of LRRK2 function. Therefore, new *lrrk2* zebrafish lines with equivalent mutations to human cases of familial PD were generated to provide more relevant vertebrate models of PD. Whilst these could not be characterised during this project, the production of these stable mutant zebrafish lines will be useful to the field for future work into *lrrk2*-linked PD and the demonstrated ease-of-use of this novel methodology can be translated into other areas of research.

6 Resolving Inflammation in Zebrafish Models of Parkinson's Disease

6.1 Introduction

This thesis has so far explored the possible role of inflammation in PD by evaluating inflammation-linked PD risk genes. The large body of evidence suggesting that neuroinflammation contributes to the development of PD suggests that its resolution may represent a disease-modifying treatment option, a currently unmet clinical need. Chapter 6 of this thesis will explore how the modulation of inflammation in zebrafish, using both genetic and pharmacological approaches, may be beneficial within the context of PD.

6.1.1 Targeting Inflammation Pharmacologically

Currently available treatments for PD are symptomatic only, of limited number, demonstrate decreased efficacy over time and are responsible for a number of side effects (Thanvi et al., 2007). Given the likely role of neuroinflammation in PD neurodegeneration, targeting the immune system is a promising approach for a disease-modifying treatment that may prevent disease progression. Dopaminergic neurons are reported to be essentially absent by four years after diagnosis (Kordower et al., 2013), therefore, any therapy aimed at neuroprotection must be given early in the disease process. There are two ways in which to establish new treatment strategies for PD, but neither are without their limitations. Creating entirely new compounds is a timely, costly and complex method, whilst the repurposing of existing drugs affords its own challenges of requiring altered bioavailability and obstacles surrounding existing patents.

6.1.1.1 Targeting Microglia

Given the vital role of microglia in establishing neuroinflammation, as discussed previously, these cells represent an obvious target for pharmacological intervention. Indeed, inhibiting microglial activation has been suggested to be neuroprotective in PD, initially demonstrated using the antibiotic minocycline (Wu et al., 2002). Minocycline, which inhibits the activation of microglia, significantly reduced dopaminergic neuronal death by more than 90% in an MPTP mouse model of PD. However, this neuroprotection did not translate into symptom reduction in a small scale clinical trial of the antibiotic (The NINDS NET-PD Investigators, 2008), though it is impossible to conclude whether further neuronal death occurred in patients during this study.

Microglia express both β1- and β2-adrenergic receptors, able to increase the levels of intracellular cyclic adenosine monophosphate (cAMP) in response to β-agonists (Tanaka et al., 2002). β2 receptors inhibit microglial proliferation and therefore β-agonists, including

adrenaline, isoproterenol and terbutaline, act to prevent increases in microglial cell number (Fujita et al., 1998), reducing the number of cells able to induce neuroinflammation. In addition to cell proliferation, β2 adrenergic receptors are also involved in cytokine production in microglia. Salmeterol has been identified as one drug that acts on microglial β2 receptors to significantly reduce the production of TNF-α, proving to be neuroprotective to dopaminergic neurons treated with LPS or MPTP both *in vitro* and *in vivo* (Qian et al., 2011). Salbutamol use has been associated with a reduced risk of developing PD in a Norwegian study involving over four million participants, whilst β2 antagonists were associated with an increased risk of the disease (Mittal et al., 2017). This is likely due to their effects on neuroinflammation, although this cannot be confirmed from such correlative data. These data suggest that the activation of β2 adrenergic receptors on microglia, and thus the prevention of cytokine production and cell proliferation, are protective in PD, possibly offering a disease-modifying treatment option via the inhibition of neuroinflammtion.

Other compounds that target microglia have been identified that may be beneficial in neurodegenerative disease. Tacrolimus, an immunophilin ligand, is a clinically available drug able to decrease the number of microglia in the substantia nigra, leading to reduced levels of TNF-α and IL-2 (Brecht et al., 2009). Although initially demonstrated in ischemia, this data has been replicated in a rat model of PD, where tacrolimus was also found to afford dopaminergic neuroprotection (Van der Perren et al., 2015). Epigallocatechin gallate, a monomer from green tea polyphenols, is able to prevent the death of neurons and primary mesencephalic cultured cells by regulating the activation of microglia in response to LPS. Epigallocatechin gallate inhibited NO production from microglia by over 70% and TNF-α by 67% (Li et al., 2004), preventing the build-up of proinflammatory molecules surrounding the neurons and the subsequent toxicity.

The most recently identified microglia-mediating pharmacological agents for possible PD treatment are idebenone and tubeimoside. Idebenone, an antioxidant, decreases the production of IL-6, IL-1β, TNF-α, and NO from microglia and induces their switching away from the proinflammatory M1 phenotype towards a protective M2 phenotype (Yan et al., 2018). *In vivo*, idebenone reduced neurodegeneration in the substantia nigra and protected against motor deficits in a model of PD (Yan et al., 2018). The reduced levels of proinflammatory cytokines may be responsible for this neuroprotection and rescue of motor symptoms, which suggests that modulating the neuroinflammatory state in PD could potentially prevent the development of these symptoms in humans. Similarly, tubeimoside, an anti-inflammatory drug, is able to

suppress microglial activation and the degeneration of dopaminergic neurons, at least in a rat model of PD (He et al., 2018). A natural alternative, salidroside, was recently identified to have similar effects, demonstrated in an MPP+-induced cell model of PD to reduce the levels of inflammatory cytokines, ROS and oxidative stress, consequently improving cell survival (F. Zhou et al., 2019). It will be interesting to see whether future research is able to recapitulate the effects of these newly identified compounds in PD patients.

Vaccines against PD have also been developed that target microglia, including AFFITOPE which has successfully completed phase 1 trials (McFarthing & Simuni, 2019). This involves injecting short fragments of α-synuclein that result in the generation of anti-α-synuclein antibodies, which have been shown to enter the brain and prevent the degeneration of dopaminergic neurons in animal models of PD (Mandler et al., 2014). This approach induces microglia to phagocytose excess α-synuclein and increase their production of anti-inflammatory cytokines which, alongside the long-term reduction in microglial reactivity, results in a decreased inflammatory state of the CNS (Mandler et al., 2014). Promisingly, an immune response against α-synuclein, including in the CSF, was seen during the clinical trial (McFarthing & Simuni, 2019). The results of this trial could be a game changer in PD research, creating the ability to prevent those with genetic predispositions from ever developing the disease.

Given the availability of compounds that modulate glial responses and provide neuroprotection in PD models, further study into developing similar drugs that are more specific, more potent and more efficacious may be the key to the early treatment and prevention of PD.

6.1.1.2 Non-Steroidal Anti-Inflammatory Drugs

Non-Steroidal Anti-Inflammatory Drugs (NSAIDs) are the obvious class of drugs for reducing inflammation. Correlations between the use of NSAIDs and PD have been identified (Bower et al., 2006), with some studies suggesting a 45% lower risk of PD among regular users of non-aspirin NSAIDs compared to non-users (Chen et al., 2003). However, such correlations do not demonstrate causality. There may have been other, uncontrolled factors affecting the risk of developing PD and these interesting data were not supported in later studies (Hancock et al., 2007). A meta-analysis of NSAID use, however, did associate the use of non-aspirin NSAIDs with a reduced risk of developing PD, which reduced further with long-term treatment (Gagne & Power, 2010). Interestingly, this effect was not seen in users of aspirin in either study. A previous meta-analysis concluded that there was no association between NSAIDs and PD (Samii et al., 2009), although these authors did not separate aspirin from other NSAIDs. It appears evident

that NSAIDs, beside aspirin, are able to reduce the likelihood of developing PD, though more research is required to conclude that this is due to their anti-inflammatory properties.

6.1.1.3 Bile Acids and Zebrafish

If found to be efficacious, bile acids represent a useful treatment option for PD due to their previous regulatory approval and demonstrated ability to penetrate the BBB when administered orally (Parry et al., 2010). Ursodeoxycholic acid (UDCA), an FDA-approved hepatic and liver-disease drug, and its taurine conjugate tauroursodeoxycholic acid (TUDCA) have recently been identified as having neuroprotective effects in PD (Mortiboys et al., 2015) and other neurodegenerative diseases (Elia et al., 2016; Keene et al., 2002; Nunes et al., 2012).

Bile acids have previously been recognised as having a marked anti-inflammatory effect. In animal models, rotenone-induced increases in striatal proinflammatory molecules, including TNF-α and IL-1β, were halved by the addition of UDCA (Abdelkader et al., 2016). TUDCA has been shown to exert its anti-inflammatory effect via the bile salt receptor GPBAR1/TGR5 which increases intracellular cAMP (Yanguas-Casás et al., 2017). This induces the anti-inflammatory TGFβ pathway (Yanguas-Casás et al., 2017) and prevents NFκB activation (Joo et al., 2004), leading to increases in anti-inflammatory mediators (Yanguas-Casás et al., 2017), decreases in proinflammatory mediators (Joo et al., 2004) and overall reductions in microglial activation (Yanguas-Casás et al., 2014).

Bile acids and bile alcohols, collectively known as cholanoids, are metabolic products of cholesterol. In mammals, the main cholanoids are C_{24} bile acids, whilst in other vertebrates, like amphibians and jawless fish, the main cholanoids are C_{27} bile alcohols. In zebrafish, like other cypriniform fish, C_{27} alcohols, namely 5α-cyprinol, predominate (Hagey et al., 2010; Haslewood, 1967). Cholanoids facilitate the digestion and absorption of dietary fat and vitamins, transport cholesterol, stimulate bile flow and aid mucin secretion (de Aguiar Vallim et al., 2013). The conjugation of bile acids to taurine or glycine, or bile alcohols to sulfate, enhances their solubility, making them impermeable to cell membranes (Russell, 2003). Secondary bile acids are bacteria-modified versions of bile acids, where deconjugation occurs to remove the amino acid moieties, allowing them to be absorbed into the intestines. However, zebrafish bile alcohols are not found in secondary forms, since 5α-cyprinol is unlikely to be absorbed even post-deconjugation due to its large number of hydroxy groups and limited solubility (Goto et al., 2003).

6.1.1 Targeting Inflammation Genetically

Zebrafish are a genetically tractable model organism, meaning that inflammatory pathways can be modulated using genetic approaches. Creating knockout or knockdown models of inflammation-relevant genes allows the effects of pathway disruption to be identified without the need to develop compounds that target these specifically and with high potency, which can be a costly and time-demanding task. Such modulation represents a useful initial experiment in the identification of disease-modifying treatments, as pathways identified as critical to pathology can then be targeted pharmacologically in human patients.

6.1.1.1 Interferon Regulatory Factor 8

As described in the introduction to this thesis, microglia are central to inflammatory processes. As zebrafish do not possess astrocytes, microglia may be even more relevant to inflammation in the CNS in these models.

Interferon regulatory factor 8 (IRF8), also known as interferon consensus sequence binding protein (ICSBP), is a nuclear transcription factor required for myeloid cell differentiation (Tamura et al., 2000). *IRF8* was first discovered in mice by Driggers et al. (1990), with a predominant expression in lymphoid tissue. *IRF8* is primarily expressed in hematopoietic cells, including constitutively in B cells (H. Wang et al., 2008) and monocytes (Hagemeyer et al., 2016; Kierdorf et al., 2013; Minten et al., 2012). *IRF8* is also expressed in T cells, where it is involved in the response to infections and in the development of effector T cells via the activation of TGFβ (Giese et al., 1997; Yoshida et al., 2014). The identification of this transcription factor primarily in immune cells suggests its role in the immune response and inflammation. This is supported by its ability to protect against bacterial and viral infections (Giese et al., 1997; Holtschke et al., 1996; Masud et al., 2019). Additionally, IFNγ increases *IRF8* expression in microglia (Minten et al., 2012) and macrophages (Driggers et al., 1990; Hagemeyer et al., 2016), further suggesting its expression is linked to the immune response.

IRF8 belongs to the interferon regulatory factor (IRF) family of transcription factors, characterised by an N-terminal DNA binding domain and a C-terminal IRF association motif. The latter is responsible for dimerisation with other transcription factors, including other IRF family members and PU.1, an important factor discussed below. IRF8 can act as an activator or repressor of transcription (Masuda et al., 2014), partly depending on the dimer made, and regulates many genes, with 851 IRF8 target sites identified in the mouse genome (N. Zhou et al., 2019). IRF8 target sites include cytokines which further links IRF8 to the immune response. The expression

of *IRF8* in microglia is usually associated with inflammation, in part due to the ability of IRF8 to induce *IRF1* expression, resulting in downstream *IL-1β* expression (Masuda et al., 2015). IRF8 induces transcription in microglia of mediators required for their activation (Masuda et al., 2014) and has been shown to increase the production of cytokines, particularly IL-12 and IFNγ (Giese et al., 1997; Turcotte et al., 2005).

PU.1 is a critical transcription factor also required for the differentiation of myeloid cells, governing a broader range of cell fates than IRF8. Inhibition of PU.1 has been demonstrated to result in the absence of macrophages, microglia and neutrophils from animal models (Kierdorf et al., 2013; Rhodes et al., 2005; Yu et al., 2017). Further study revealed IRF8 to act downstream of PU.1 to regulate myeloid cell differentiation (Kierdorf et al., 2013; Li et al., 2011; N. Zhou et al., 2019). Interestingly, IRF8 can also directly regulate PU.1 expression, creating a feedback loop that is potentially relevant to cell fate decisions (H. Wang et al., 2008; N. Zhou et al., 2019).

Mouse models with a loss of IRF8 function are found to have increased granulocytes, increased macrophages, immunodeficiency and a downregulation of immune-related genes (Giese et al., 1997; Hagemeyer et al., 2016; Holtschke et al., 1996; Turcotte et al., 2005). Of particular interest, these knockout mice demonstrated changes in microglia, including an increase in microglial number and the development of less developed / more amoeboid cells (Hagemeyer et al., 2016; Horiuchi et al., 2012; Minten et al., 2012). These microglia were described as having a reduced ability to become activated; defective chemotaxis, proliferation and phagocytosis; altered transcriptional responses to LPS and IFNγ; and a delayed response to tissue damage (Akagi et al., 2014; Horiuchi et al., 2012; Masuda et al., 2014). However, not all research groups reported this increase in microglial number; reduced numbers were demonstrated in the midbrain of embryonic and adult mice lacking *Irf8* in one publication (Kierdorf et al., 2013).

Ten common IRF family members have been identified in vertebrates and all ten, plus an additional member not recognised in other vertebrates, are found in zebrafish (Huang et al., 2010). Zebrafish *irf8* has 55% sequence identity to mammalian *IRF8*, with conserved DNA binding and IRF domains (Li et al., 2011). *irf8* is first seen in the rostral blood island at 16hpf, in the yolk sac a few hours later and finally in the tail region by 30hpf (Li et al., 2011). It was found to be expressed in myeloid cells during development, specifically those of macrophage, and not neutrophil, linage (Li et al., 2011). *irf8* is expressed in the zebrafish brain by 2dpf, becoming restricted to microglia in 3-7dpf larvae, but with its highest expression level at 3dpf (Li et al., 2011; Mazzolini et al., 2020).

A loss of Irf8 function in zebrafish appears to cause a fate transition of myeloid progenitor cells, resulting in a lack of macrophage and microglia development (Earley et al., 2018; Li et al., 2011; Prajsnar et al., 2021; Shiau et al., 2015; Tsarouchas et al., 2018; Yu et al., 2017; Zhao et al., 2018). *irf8* knockout is also associated with an increase in neutrophil number (Li et al., 2011; Prajsnar et al., 2021; Shiau et al., 2015; Zhao et al., 2018). These cell changes oppose the changes seen in mouse models, possibly owing to a difference in compensation mechanisms between organisms. However, the lack of macrophages and microglia in these zebrafish enable their use as a genetic model of reduced inflammation. The absence of these crucial cell populations results in fish with a reduced ability to mount an immune response.

6.1.1 Zebrafish Lines Used in Chapter 6

6.1.1.1 Cyclin G Associated Kinase

Cyclin G Associated Kinase (GAK), known for its vital role in clathrin-mediated intracellular transport (C. X. Zhang et al., 2005), has been suggested as a candidate gene associated with the risk of developing PD (Nalls et al., 2014). GAK interacts with the IL-12 receptor β on T cells, where it prevents the production of IFN-γ (Lin et al., 2007). It is clear that GAK is involved in immunity and inflammation in the periphery, suggesting that a direct link to neuroinflammation may also be present. GAK can also be indirectly linked to neuroinflammation via its ability to alter α-synuclein expression. A knockdown of *GAK in vitro* induced an accumulation of α-synuclein (Dumitriu et al., 2011), a process known to lead to neuroinflammation, as discussed previously. Furthermore one *GAK* SNP, rs1564282, is associated with an increased expression of α-synuclein in human PD brains (Dumitriu et al., 2011), which, as well as demonstrating a link between α-synuclein regulation and *GAK*, suggests that the loci identified by GWAS is likely to be *GAK* indeed.

In zebrafish, the single *gak* gene (ENSDARG00000090654) demonstrates 62.94% sequence and 62% protein identity to the human orthologue (ENSG00000178950, based on CLUSTAL W v1.81 data). Zebrafish models with homozygous *gak* knockout mutations demonstrate a severe phenotype (death by 5dpf) and were available in the Bandmann Laboratory.

6.1.1.2 GTP Cyclohydrolase 1

GTP Cyclohydrolase 1 (GCH1) mutations are usually associated with dopamine responsive dystonia, although SNPs lying close to this gene have also been associated with PD (Nalls et al., 2019; Nalls et al., 2014). Whole exome sequencing identified certain alleles to increase the risk of developing PD by seven times (Mencacci et al., 2014). *GCH1* encodes the rate-limiting enzyme needed for tetrahydrobiopterin (BH4) biosynthesis and, therefore, dopamine production (Werner et al., 2011).

GCH1 is expressed in activated microglia (Thomas et al., 2006), strongly suggesting a role for the enzyme in neuroinflammatory pathways. A further link between GCH1 and neuroinflammation can be made by evaluating how the expression of *GCH1* is regulated. Proinflammatory cytokines, namely IL-1, IFN-γ, TNF-α, increase *GCH1* expression whilst, conversely, anti-inflammatory cytokines, namely IL-4, IL-10 and TGF-β, reduce its expression (Shi et al., 2004). Given the involvement of GCH1 in inflammatory pathways, the increased risk of PD may arise from the effects that GCH1 deficiency may have on inflammation in the CNS.

Independent of GWAS, pathogenic *GCH1* mutations have been identified in 0.57% of patients with PD (Guella et al., 2014), further demonstrating the importance of this gene in PD. Given this, a zebrafish mutant line has been created by knocking out the single *gch1* zebrafish orthologue (ENSDARG00000070453) which possesses 72.51% sequence homology and 72% protein identity to human *GCH1* (ENSG00000131979, based on CLUSTAL W v1.81 data). This homozygous deletion leads to death by 10-12dpf, as well as other phenotypic changes including a lack of swim bladder inflation, movement abnormalities and neuroinflammation (Larbalestier et al., 2021).

6.1.1.3 Chemically-Induced Models of Inflammation

Inducing inflammation pharmacologically in zebrafish serves two purposes. Wildtype zebrafish exposed to such compounds provide a useful model for drug efficacy experiments. Phenotypes resulting from exposure may be rescued by the addition of secondary compounds, suggesting an anti-inflammatory activity of the rescue drug. Secondly, these models can be combined with existing zebrafish mutants to assess their susceptibility to external inflammatory factors.

A number of compounds have been used in zebrafish to induce inflammation. For example, trinitrobenzene sulfonic acid (TNBS), a hapten primarily used in murine models of colitis, has been demonstrated to increase proinflammatory mediators in zebrafish larvae (Oehlers et al., 2011; Oehlers et al., 2010). A hapten is a molecule that, only once bound to larger proteins, can act as an antigen to ilicit immune responses. Most research evaluates the effect of TNBS in the GI tract, although the increase in proinflammatory mediators in exposed zebrafish has been seen in the whole larvae.

Dextran sodium sulfate (DSS) is another compound commonly used as a murine colitis model that, when added directly to E3 media, results in zebrafish larvae developing inflammation, including recruitment of macrophages and neutrophils (Oehlers et al., 2012). DSS causes

inflammation via epithelial damage as it is toxic to colonic epithelial cells causing reduced mucosal barrier functioning (Wang et al., 2021).

Saponin is a naturally occurring compound that has been associated with a number of health benefits in humans, including reports of reducing inflammation (Hassan et al., 2012; Jang et al., 2013). However, it was discovered that feeding food high in saponins to farmed fish could result in intestinal inflammation (Gu et al., 2018; Krogdahl et al., 2015), suggesting the use of this model for zebrafish research. Indeed, saponin has been demonstrated to cause recruitment of neutrophils and dose-dependent increases in *il-1β*, *mmp9*, *il-10* and *tnf-α* in zebrafish larvae (López Nadal et al., 2018).

6.2 Results

6.2.1 Developing a Method of Microglial Knockout

6.2.1.1 Pre-Existing Interferon Regulatory Factor 8 CRISPR

Research groups in the zebrafish field have targeted *irf8* using CRISPR to create zebrafish with an absence of microglia. Initially, a single gRNA provided by Dr Daniel Lysko was assessed for its ability to inhibit microglia development in G0 larvae. Injecting gRNA against *irf8* into the yolk of single-cell stage zebrafish embryos was successful in preventing the development of microglia, demonstrated by a lack of neutral red staining (**figure 106**). The efficiency of this guide at resulting in a complete loss of neutral red staining was 66.7% when 2nL of the maximum gRNA concentration was injected (**table 36**).

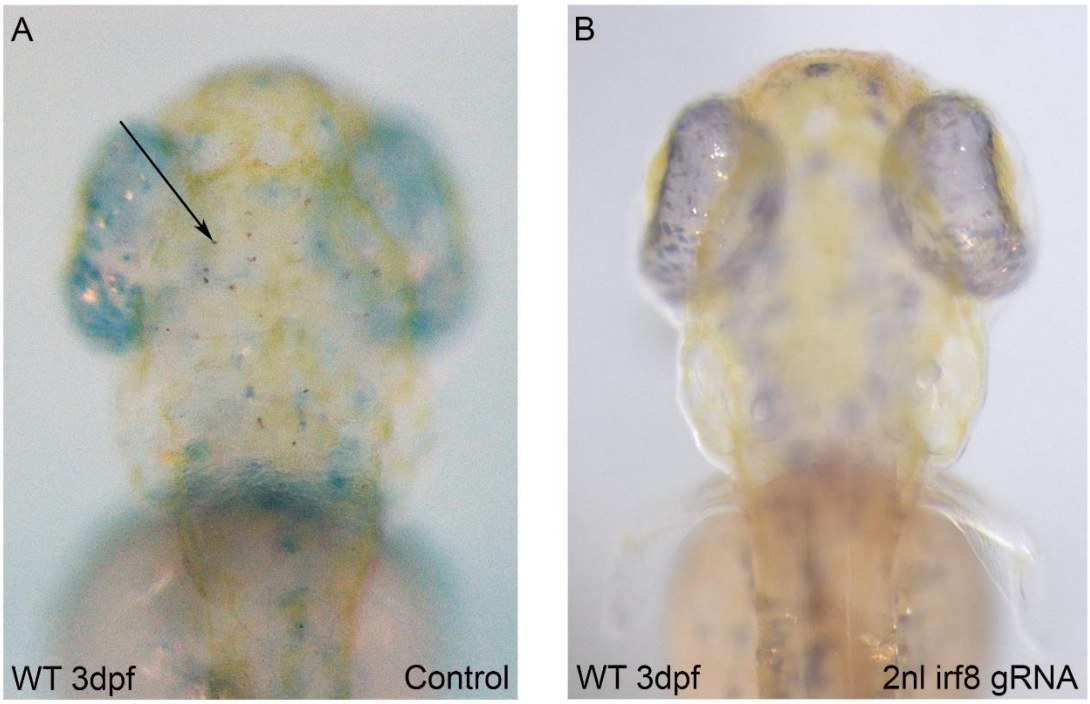

Figure 106. Knockout of Microglia Using CRISPR-Cas9 Technology Against Interferon Regulatory Factor 8. *Neutral red staining of microglia in control injected (tracrRNA and Cas9 only) zebrafish (**A**) and following injection of 2nL 50µM irf8 gRNA (**B**). Arrow highlights neutral red staining of microglia in the midbrain. dpf; days post fertilisation; irf8, interferon regulatory factor 8; gRNA, guide RNA; WT, wildtype.*

Table 36. Efficiency of irf8 Guide RNA at Inhibiting Microglia Development in Zebrafish Larvae.

Injection Group	No. with microglia	No. without microglia	n	% efficiency
2nl 50µM *irf8* gRNA	3	6	9	**66.7%**
1nl 50µM *irf8* gRNA	10	10	20	**50%**
Control	20	0	20	n/a

Efficiency of the irf8 guide RNA was assessed by calculating the percentage of fish with a complete loss of microglia as determined by neutral red staining. Guide RNA was injected along with Cas9 and tracrRNA into the yolk of one-cell stage wildtype zebrafish. Control larvae were injected with tracrRNA and Cas9 only. Neutral red staining was conducted at 4dpf. dpf, days post fertilisation; irf8, interferon regulatory factor 8; gRNA, guide RNA; µM, micromolar.

6.2.1.2 Generation of a Novel irf8 CRISPR Triple gRNA

To increase the efficiency of microglia depletion, three gRNAs, each targeting a different region of the *irf8* gene, were combined in a single injection mix. Injection of this triple gRNA was demonstrated to result in successful microglia depletion (**figure 107**) with a higher efficiency (87.5%) than the single gRNA (**table 37**). Unfortunately, fish injected with 1nL of this injection mix developed too much pigment during development for accurate assessment of microglial number. Microglia depletion was confirmed using immunohistochemistry against 4c4 in 5dpf larvae (**figure 107C,D**).

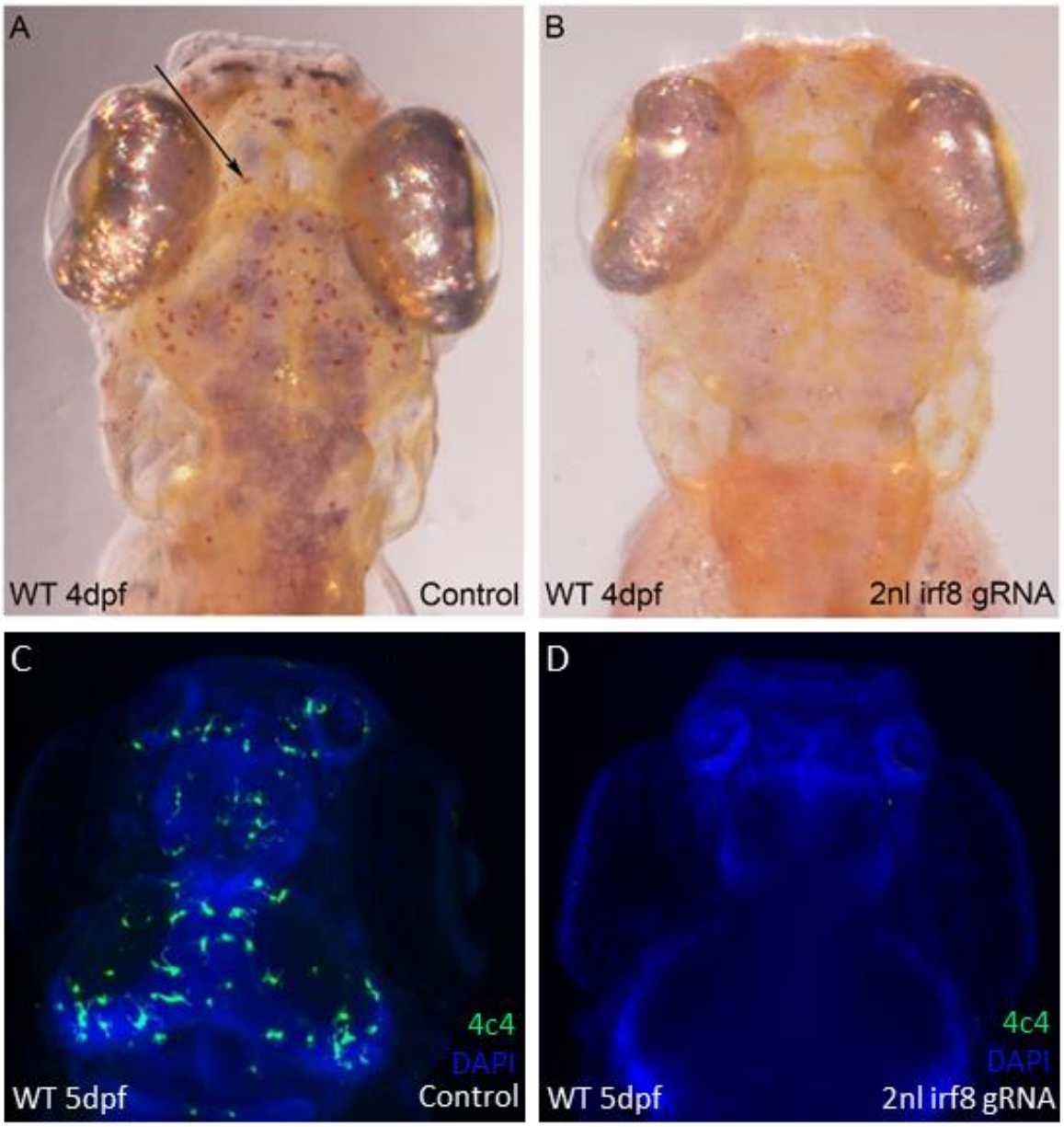

Figure 107. Microglial Depletion Using CRISPR-Cas9 Technology Against Interferon Regulatory Factor 8. *Neutral red staining of microglia in control injected (tracrRNA and Cas9 only) zebrafish (**A**) and 2nL 50µM triple irf8 gRNA (**B**). Arrow highlighting neutral red staining of microglia in the brain. This was confirmed in wholemount immunohistochemistry against 4c4 in 5dpf larvae. 4c4+ cells were seen in control injected larvae (**C**) but were absent in larvae injected with 2nL 50µM triple irf8 gRNA (**D**). DAPI, 4',6-diamidino-2-phenylindole; dpf, days post fertilisation; irf8, interferon regulatory factor 8; gRNA, guide RNA; WT, wildtype.*

Table 37. Efficiency of the Triple irf8 Guide RNA at Inhibiting Microglia Development in Zebrafish Larvae.

Injection Group	No. with microglia	No. without microglia	n	% efficiency
Control	20	0	20	**n/a**
1nL triple gRNA (each at 50µM)			Fish were too pigmented	**?**
2nL triple gRNA (each at 50µM)	3	21	24	**87.5%**

The efficiency of the triple irf8 guide RNA was assessed by calculating the percentage of fish with a complete loss of microglia as determined by neutral red staining. Three guide RNAs were injected along with Cas9 and tracrRNA into the yolk of one-cell stage wildtype zebrafish. Control larvae were injected with tracrRNA and Cas9 only. Neutral red staining was conducted at 4dpf. dpf, days post fertilisation; irf8, interferon regulatory factor 8; gRNA, guide RNA; µM, micromolar.

6.2.2 Microglial Inactivation in *gch1*$^{-/-}$ Mutant Zebrafish

gch1$^{-/-}$ mutant zebrafish have been shown to demonstrate increased microglial activity (Larbalestier et al., 2021). It was, therefore, hypothesised that preventing microglial development, and hence activation of these immune cells, could positively impact their phenotype.

Heterozygous *gch1*$^{+/-}$ zebrafish were incrossed to obtain homozygous mutant larvae and wildtype siblings. Half of the offspring were injected with the *irf8* triple gRNA at the one-cell stage and half were injected with a control mixture (tracrRNA and Cas9 only). The efficiency of microglial depletion was determined by neutral red staining on 10% of injected larvae at 4dpf. This was shown to be 77.3%. The remaining larvae were allowed to develop until 11dpf and assessed for their survival and swim bladder inflation, a known defect in *gch1*$^{-/-}$ mutants. Larvae were genotyped once they had reached their end-point or at the end of the experiment.

Despite an estimated 77.3% of *gch1*$^{-/-}$ larvae having no microglia, there was no significant difference in the survival of these zebrafish compared to control injected homozygous mutants (p=0.7817, **figure 108A**). Additionally, analysis of swim bladder inflation found no significant differences between treatment groups (p=0.1790, **figure 108B**). This experiment was stopped one day early due to high death rates in the husbandry control group between days 10 and 11.

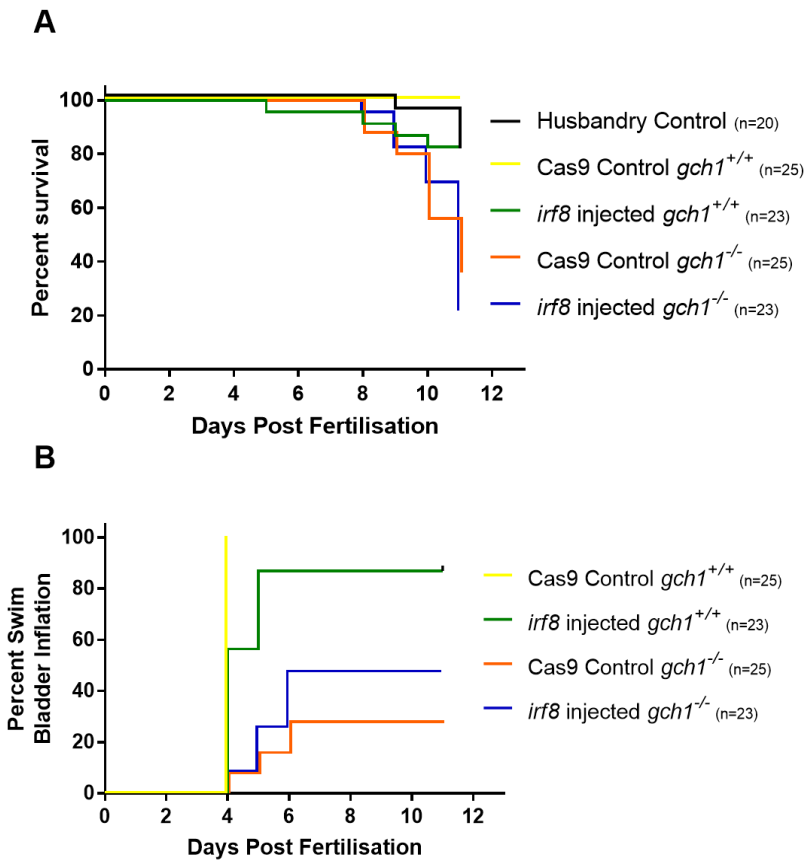

Figure 108. Microglial Inactivation in GTP Cyclohydrolase 1 Homozygous Mutant Zebrafish. A. *Survival analysis demonstrates no difference between control injected gch1$^{-/-}$ mutant larvae and irf8 injected gch1$^{-/-}$ mutant larvae (p=0.7817).* ***B.*** *No difference was identified in swim bladder inflation between control injected gch1$^{-/-}$ mutant larvae and irf8 injected gch1$^{-/-}$ mutant larvae (p=0.1790). Fish were genotyped following the experiment and the numbers for each group are specified in the graph legend. All statistics were analysed using a Mantel-Cox log rank test. gch1, GTP cyclohydrolase 1; irf8, interferon regulatory factor 8.*

6.2.3 Microglial Development at Later Larval Stages

To assess the prolonged effects of *irf8* CRISPants, wholemount immunohistochemistry against 4c4 was conducted on larval zebrafish at 5, 8 and 10dpf. Half of those imaged had been injected with the triple *irf8* gRNA, whilst the others were injected with tracrRNA and Cas9 only. This revealed that although microglia were absent in *irf8* injected larvae at 5dpf, by 8dpf microglia had repopulated the brain and by 10dpf microglia numbers appeared to be at wildtype levels (**figure 109**). Exact microglia number in each case was not quantified due to less than perfect images and low sample size per group, but are broadly summarised in **table 38**.

Table 38. The Number of Zebrafish Larvae with More Than or Less Than One 4c4+ Cell.

dpf	Control injected with >1 microglia	Control injected with <1 microglia	%	*irf8* injected with >1 microglia	*irf8* injected with <1 microglia	%
5	5	0	**100**	0	5	**0**
8	5	0	**100**	6	0	**100**
10	6	0	**100**	3	0	**100**

The number of microglia in the brains of larval zebrafish was determined by 4c4 immunohistochemistry. Larvae were classified into two groups; those with one or less microglia and those with more than one microglia. irf8 CRISPants were created by co-injecting three gRNAs against the irf8 gene. Control larvae were injected with Cas9 and tracrRNA only. dpf, days post fertilisation; irf8, interferon regulatory factor 8.

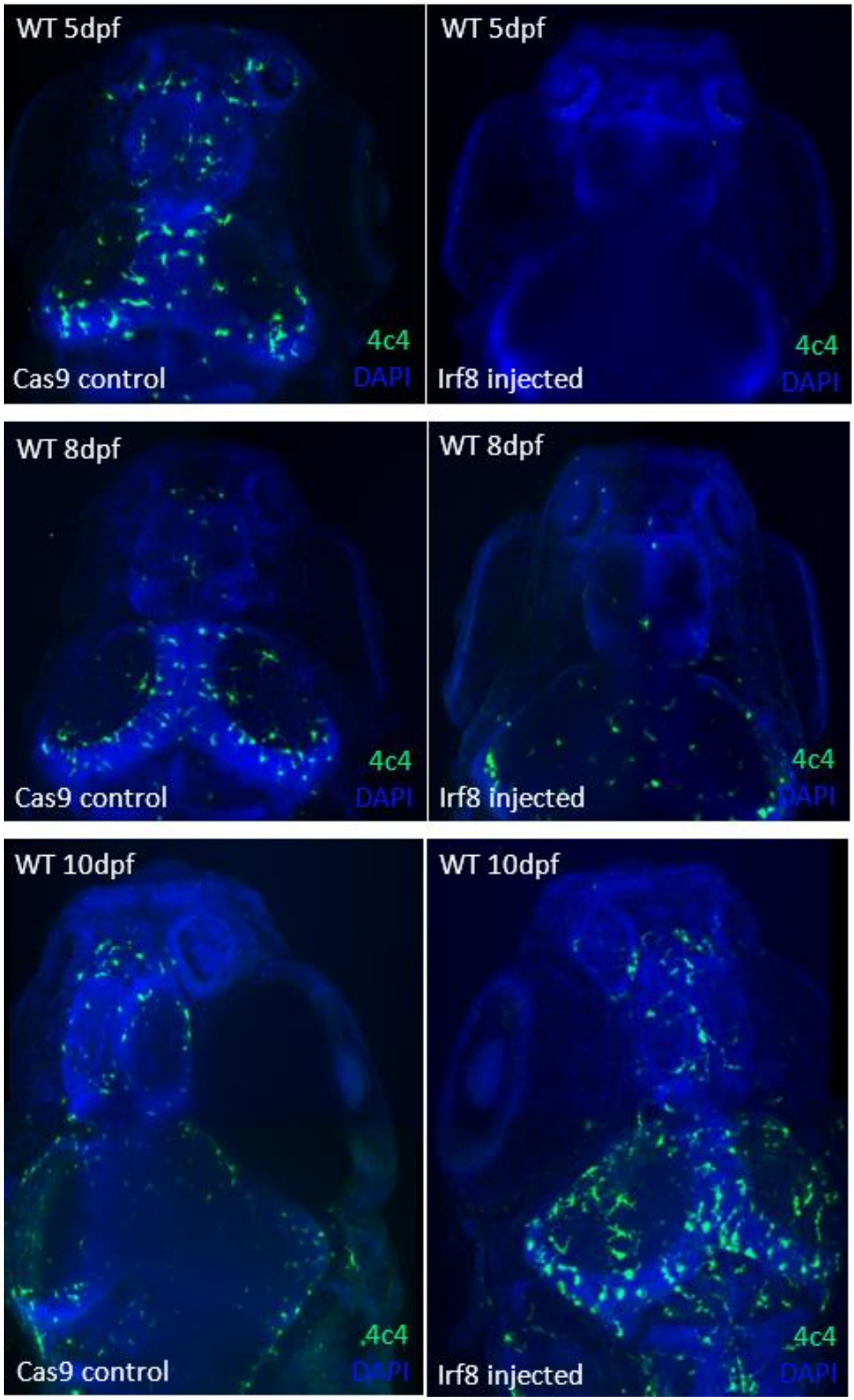

Figure 109. Microglia Repopulate in Interferon Regulatory Factor-8 CRISPants by 8-Days Post Fertilisation. *4c4 immunohistochemistry revealed that microglia are absent in irf8 CRISPants at 5dpf (top) but repopulate the brain at 8dpf (middle). irf8 CRISPants were created using three guide RNAs targeting the gene. Control larvae were injected with Cas9 and tracr RNA only. 4c4, microglial marker; DAPI, 4',6-diamidino-2-phenylindole; dpf, days post fertilisation; irf8, interferon regulatory factor 8; WT, wildtype.*

6.2.4 Pharmacological Ablation of Microglia

Due to the microglial repopulation evident in *irf8* CRISPants, this technique was combined with a pharmacological approach. Ki20227 was used as an inhibitor of microglial proliferation in zebrafish.

Toxicity trials were initially conducted in wildtype larvae finding no effect of survival in concentrations of up to 50µM (**figure 110A**). However, 50µM resulted in oedema that was evident around the eyes at 5dpf (**figure 111**) so this concentration was not used in further experiments. Toxicity trials were then conducted up to 12dpf, which suggested that Ki20227 was well tolerated (**figure 110B**).

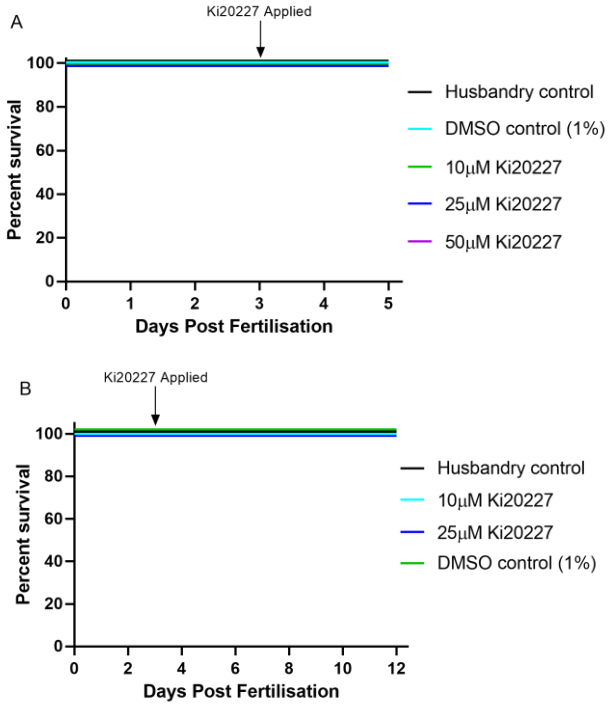

Figure 110. Toxicity Trials of Ki20227 in Wildtype Zebrafish. *All tested concentrations had no effect on the survival of zebrafish up to 5dpf (**A**) or up to 12dpf (**B**). For toxicity trials, 20 wildtype larvae were exposed to Ki20227 via constant immersion in E3 media with 1% DMSO. DMSO, dimethyl sulfoxide; dpf; days post fertilisation; µM, micromolar.*

To assess the effect of Ki20227 treatment on microglia, neutral red staining was conducted on larvae following exposure from 3-5dpf. This was assessed using nacre larvae as well as combining AB larvae with phenylthiourea, in case the phenylthiourea interacted with the Ki20227. Neutral red staining suggested a slight reduction of microglia following exposure, although staining was still clearly evident in some larvae (**figure 111**). To explore this in more detail, 5dpf wildtype larvae were fixed following treatment with Ki20227 and used for 4c4 immunohistochemistry. This demonstrated that whilst this compound was able to induce a marked reduction in microglial cells, the cells that remained demonstrated an amoeboid morphology (**figure 112**).

Treatment with Ki20227 was combined with *irf8* CRISPants in the *gch1*$^{-/-}$ mutants. For this, *gch1* heterozygous adults were incrossed and larvae injected with *irf8* CRISPants at the one-cell stage. Ki20227 treatment was then started at 3dpf and fish were exposed via constant immersion. Larvae were genotyped at the end of the experiment. No difference in survival was seen between *gch1* homozygous mutant zebrafish in any experimental arm (**figure 113**). The median survival of *gch1*$^{-/-}$ mutant larvae was 10dpf in the untreated group, which remained true for the Ki20227 treated group (p=0.6516) and reduced, not significantly, to 9dpf for both the *irf8* CRISPant alone (p=0.2552) and the combined treatment group (p=0.1549).

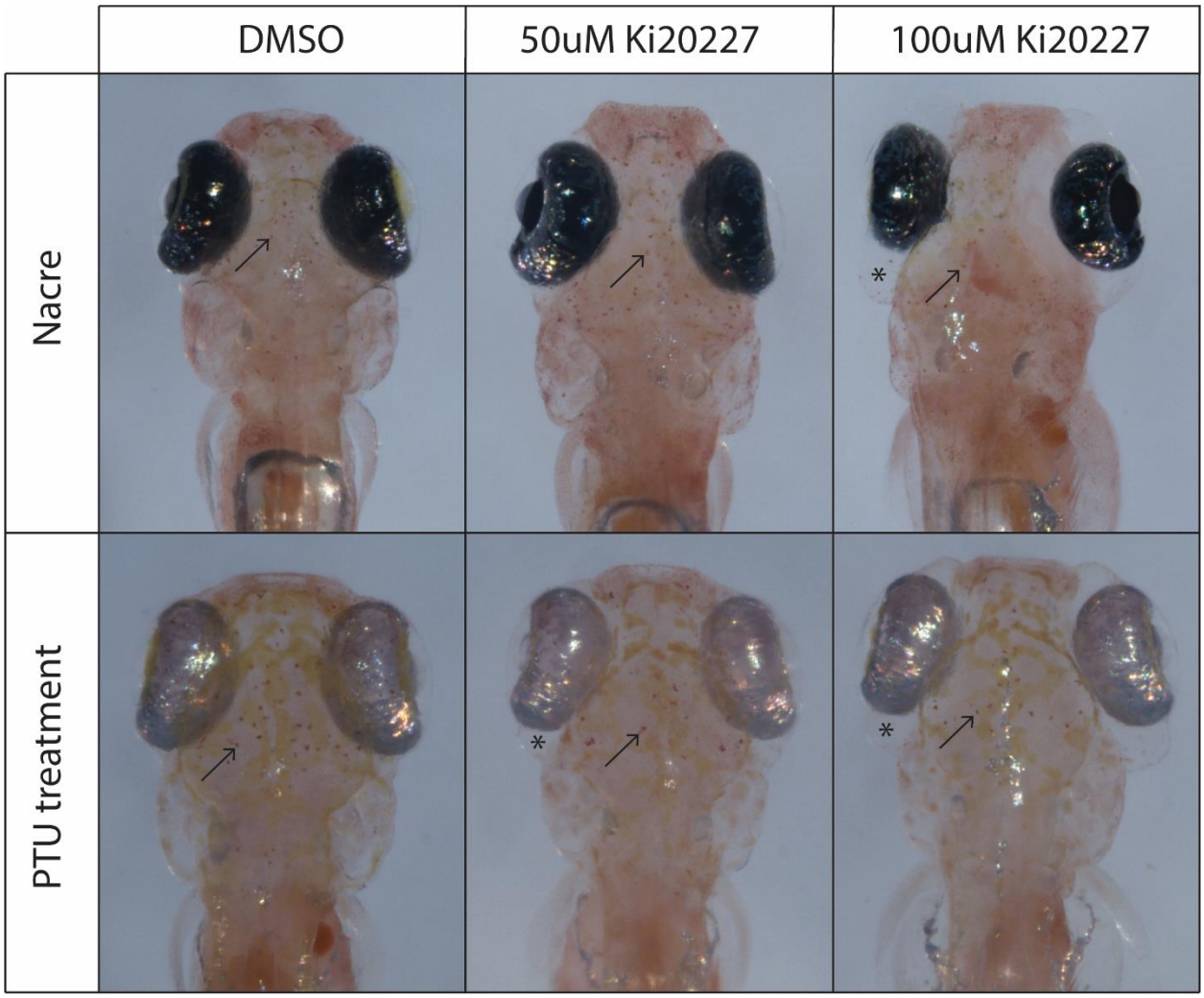

Figure 111. Neutral Red Staining Following Exposure to Ki20227. *Representative brightfield images of 5dpf larvae exposed to Ki20227 from 3dpf. Neutral red staining was achieved by incubating 5dpf zebrafish in 2.5µg of neutral red per mL of E3 media for 6 hours at 28°C. Anesthetised larvae were mounted in low melting point agarose and imaged immediately. Experiment was conducted using nacre larvae (top) and AB wildtype larvae treated with PTU (bottom). Star highlights oedema. Arrow highlights microglia. DMSO, dimethyl sulfoxide; dpf, days post fertilisation; PTU, phenylthiourea; uM, micromolar.*

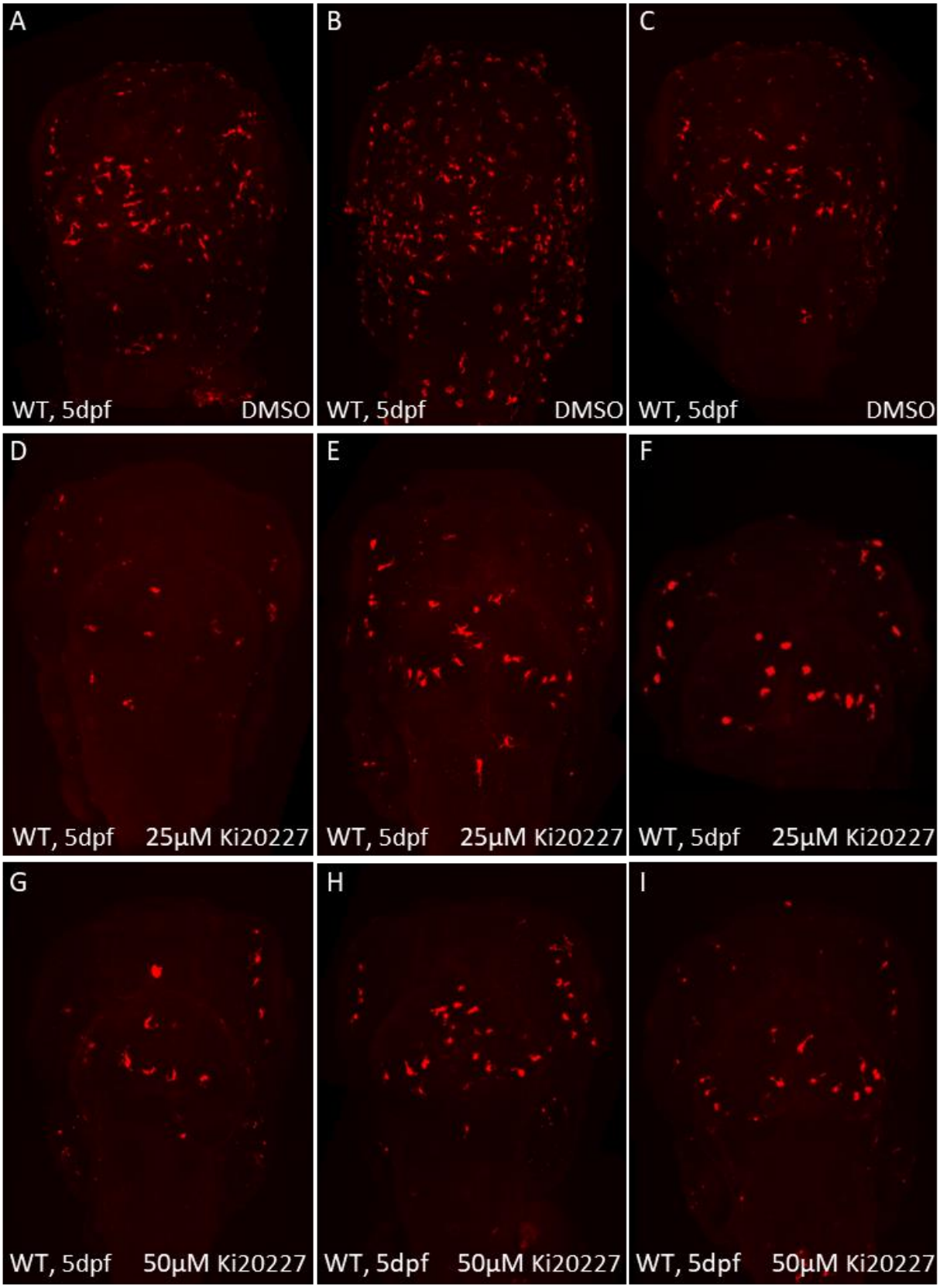

Figure 112. Assessment of Ki20227 Effect on Microglia Using 4c4 Immunohistochemistry. *Following exposure to Ki20227 via constant immersion from 3-5dpf, larvae were fixed and used in immunohistochemistry against 4c4. Whilst normal numbers of 4c4+ cells were evident in larvae exposed to DMSO (**A-C**), larvae exposed to either 25µM (**D-F**) or 50µM (**G-I**) Ki20227 demonstrated a reduced number of cells. The cells remaining appeared to have a more amoeboid morphology compared to untreated fish. DMSO, dimethyl sulfoxide; dpf, days post fertilisation; µM, micromolar; WT, wildtype.*

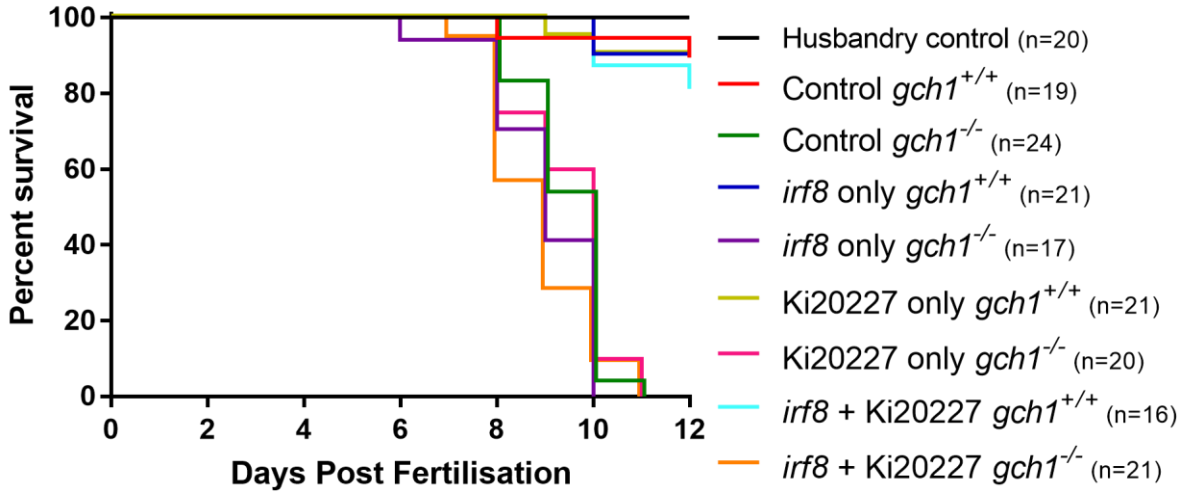

Figure 113. GTP Cyclohydrolase 1 Mutant Zebrafish Larvae Were Unaffected by the Combined Treatment of irf8 CRISPants and Ki20227. *Offspring were obtained from a heterozygous gch1 incross and split into groups. Embryos were injected with either combined irf8 guide RNAs or control mixture (Cas9 and tracrRNA only) at the one-cell stage. Some larvae were then exposed to 25μM Ki20227 from 3dpf via constant immersion. 1% DMSO was used in groups not treated with Ki20227. Mantel-Cox log rank test found no significant differences in survival between untreated gch1$^{-/-}$ larvae and gch1$^{-/-}$ larvae treated with Ki20227 (p=0.6516), irf8 CRISPant (p=0.2552) or these combined (p=0.1549). DMSO, dimethyl sulfoxide; dpf, days post fertilisation; gch1, GTP cyclohydrolase 1; irf8, interferon regulatory factor 8.*

6.2.5 Drug Treatments of Parkinson's Disease Mutant Zebrafish

A primary focus of this project was inflammation in PD. This section focuses on whether anti-inflammatory pharmacological treatments could be useful in disease modulation. Whilst no inflammatory phenotype was identified in the two lines assessed in chapters one and two as hoped, other PD mutant zebrafish created in the Bandmann laboratory are known to develop inflammatory phenotypes. These lines were therefore used in this section.

6.2.5.1 Dexamethasone

Dexamethasone has been used extensively in zebrafish with proven anti-inflammatory effects, making it an obvious choice for use as a positive control in the following experiments.

6.2.5.1.1 Toxicity Trials

Wildtype zebrafish larvae were exposed to dexamethasone from 3dpf via constant immersion. No effect on survival was seen in larvae treated with up to 100μM dexamethasone from 3-5dpf, but toxicity was evident in older larvae when treated from either 1dpf or 5dpf (**figure 114**). These toxicity trials were terminated early due to this toxicity. Larvae exposed to dexamethasone demonstrated a wider spacing of their melanophores (**figure 114**), indicative of glucocorticoid activity.

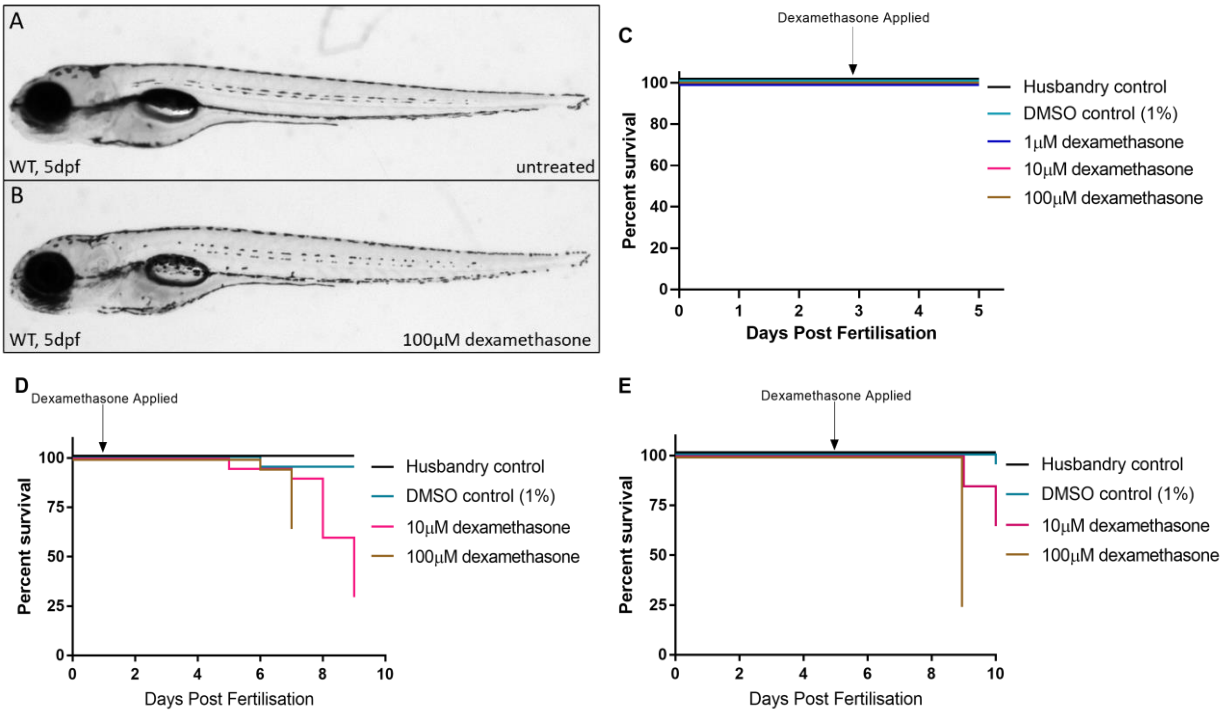

Figure 114. Toxicity Trials of Dexamethasone in Wildtype Zebrafish. A-B. *Representative brightfield images of 5dpf larvae following exposure to either 1% DMSO (**A**) or 100µM dexamethasone (**B**) from 3-5dpf. **C.** Survival analysis of fish treated from 3-dpf demonstrated that dexamethasone was well tolerated up to 5dpf. **D.** Survival analysis of fish treated from 1dpf shows toxicity of all concentrations from 7dpf. **E.** Survival analysis of fish treated from 5dpf shows toxicity from 9dpf. n=20 wildtype fish per group. DMSO, dimethyl sulfoxide; dpf, day post fertilisation; µM, micromolar; WT, wildtype.*

6.2.5.1.2 Treatment of gch1$^{-/-}$ Mutant Zebrafish

gch1$^{+/-}$ mutant zebrafish were incrossed and their larvae exposed to 10µM dexamethasone via constant immersion from 5-8dpf. Larvae were washed out of the drug after this time point due to the toxicity seen in the above trials. Larvae exposed to dexamethasone showed significant toxicity by 9dpf, although unexplained toxicity was also seen in the control (**figure 115A**). These fish were not genotyped as it was clear that this effect was unrelated to genotype based on the number of deaths. Following additional toxicity trials (data not shown), this experiment was repeated using a lower concentration of dexamethasone (1µM) and exposure from 5dpf with no wash out. Larvae were culled and genotyped once they had reached their endpoint or at the end of the experiment. Dexamethasone had no effect on the survival of *gch1*$^{-/-}$ mutant zebrafish; all larvae had reached their endpoint by 10dpf regardless of treatment group (p=0.0528, **figure 115B**). It should be noted that larvae were fed powdered food during this experiment due to the unavailability of rotifers during the coronavirus pandemic.

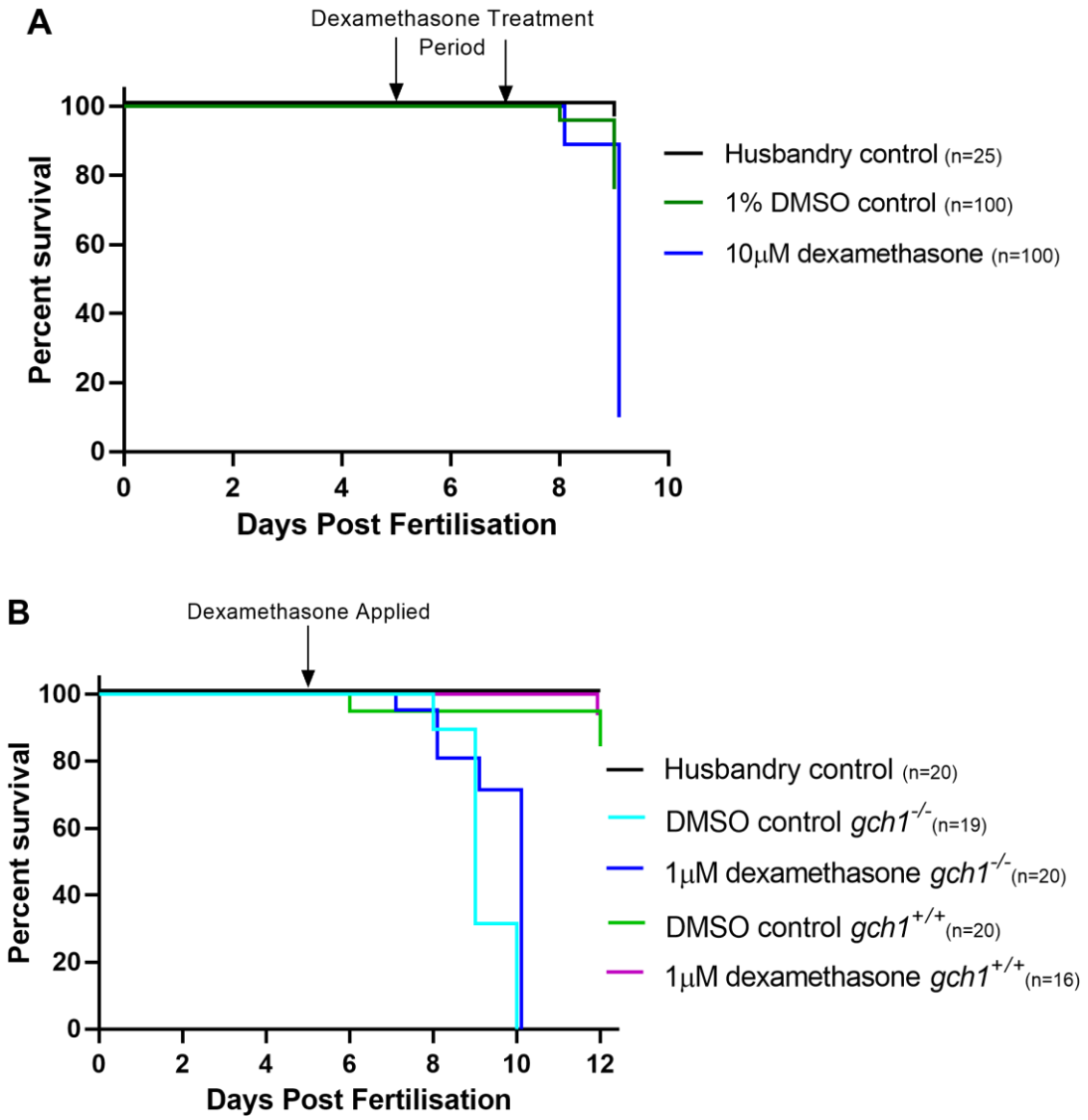

Figure 115. Dexamethasone Treatment of GTP Cyclohydrolase 1 Homozygous Mutant Zebrafish Had No Effect On Survival. A. *gch1 heterozygous mutant adults were incrossed and 100 larvae exposed to either DMSO or 10μM dexamethasone from 5-8dpf. Larvae were then washed into E3 for the remainder of the experiment. The experiment was terminated early and larvae were not genotyped due to toxicity.* ***B.*** *The experiment was repeated using 1μM dexamethasone with no wash out period. Fish were genotyped following the experiment and numbers per group are given in the figure legend. No difference was seen in the survival of gch1$^{-/-}$ larvae (p=0.0528, Mantel-Cox log rank test). DMSO, dimethyl sulfoxide; gch1, GTP cyclohydrolase 1; μM, micromolar.*

6.2.5.2 Quinacrine Dihydrochloride

RNAseq data collected by Dr Hannah Larbalestier (Bandmann Laboratory) was used by Dr Katjuša Koler (University of Sheffield) to identify compounds *in silico* that may have a modulatory effect in *gch1*$^{-/-}$ mutant zebrafish. For this data, four biological replicates of RNA were collected from brains extracted from *gch1*$^{-/-}$ mutant larvae and their wildtype siblings at 8dpf (this data can be found in Larbalestier et al. (2021)). Following analysis, a number of compounds were suggested to have an effect in this line. Quinacrine hydrochloride (mepacrine) was chosen for *in vivo* study in this project because of its links to inflammation.

6.2.5.2.1 Toxicity Trials

Quinacrine use in zebrafish has only been reported in one published paper (Cosme et al., 2015), where adult zebrafish exposed to 100µg/L (equivalent to 211.47nM) exhibited signs of infertility. Using this concentration as a starting point, toxicity trials were conducted in wildtype zebrafish from 1-5dpf with no effect on survival or phenotype (**figure 116**). A further trial was conducted with increased concentrations to find the maximum tolerated dose; toxicity trials up to 12dpf identified 2µM as the maximum tolerated concentration of quinacrine at this age (**figure 116**). 2µM was therefore used to treat *gch1*$^{-/-}$ mutant larvae.

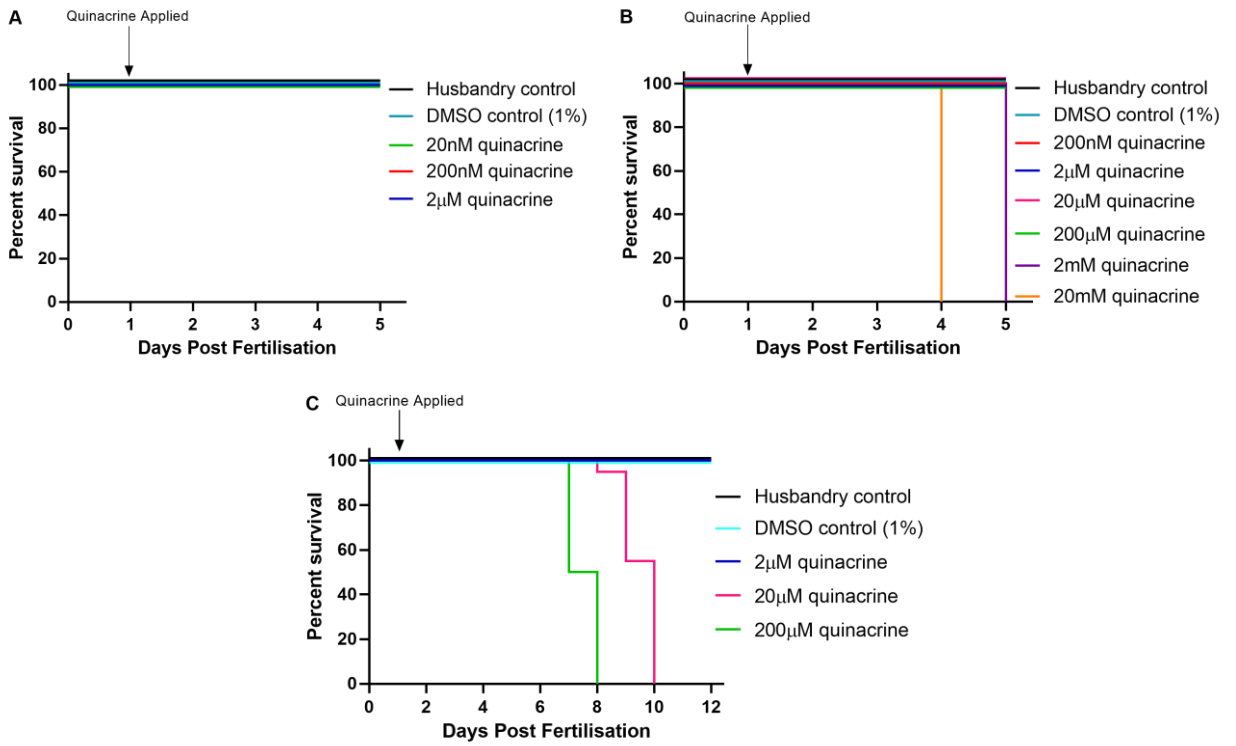

Figure 116. Toxicity Trials of Quinacrine Exposure in Wildtype Zebrafish. *Wildtype zebrafish larvae were exposed to quinacrine via constant immersion from 1dpf. Initial trials found that concentrations up to 2µM had no effect on survival (**A**), but concentrations over 2mM were toxic to larvae by 5dpf (**B**). A toxicity trial in older fish identified 2µM as the only concentration to be tolerated in larvae up to 12dpf (**C**). n=20 wildtype fish per group. 1% DMSO was used as a carrier and control group for these experiments. Media and drug were replenished daily. DMSO, dimethyl sulfoxide; dpf, days post fertilisation; µM, micromolar.*

6.2.5.2.2 Treatment of GTP Cyclohydrolase 1 Mutant Zebrafish

As before, *gch1*$^{+/-}$ zebrafish were incrossed and their offspring divided into two groups; 100 larvae were exposed to 2µM quinacrine from 1dpf via constant immersion and 100 larvae were exposed to 1% DMSO. Fish were genotyped at the end of the experiment. Exposure of *gch1*$^{-/-}$ mutant zebrafish to quinacrine did not result in a rescue effect on survival (p=0.5091, **figure 117**).

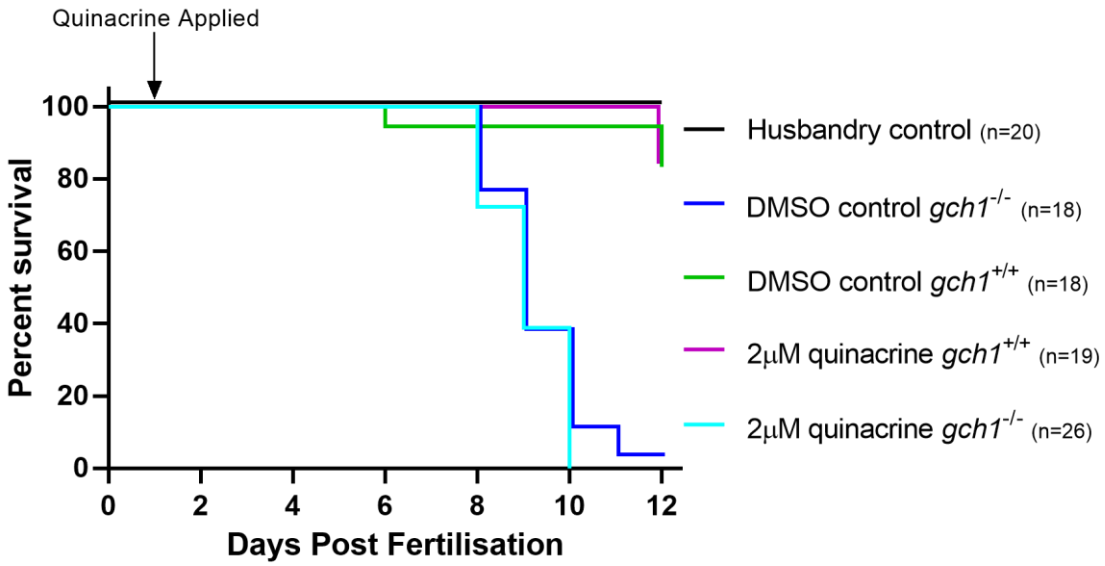

Figure 117. Quinacrine Treatment of GTP Cyclohydrolase 1 Homozygous Mutant Zebrafish Did Not Result in a Rescue Effect. *Zebrafish larvae obtained from a gch1$^{+/-}$ incross were exposed to either 2μM quinacrine or a DMSO control from 1dpf via constant immersion. Larvae were genotyped following exposure and numbers per group are given in the figure legend. The endpoint for this experiment was the loss of response to touch. No difference in survival was seen between gch1$^{-/-}$ larvae exposed to quinacrine or DMSO (p=0.5091, Mantel-Cox log rank test). DMSO, dimethyl sulfoxide; gch1, GTP cyclohydrolase 1; μM, micromolar.*

6.2.5.3 Ursodeoxycholic Acid (UDCA)

Ursodeoxycholic acid (UDCA) and its common conjugates are an active research area within PD treatment and are a particular focus within The University of Sheffield. Since they can also be associated with anti-inflammatory activity, these compounds were candidates for phenotype modulation of PD mutant zebrafish during this project.

6.2.5.3.1 Toxicity Trials

UDCA toxicity was assessed by treating wildtype larvae from 1dpf via constant immersion. Exposure to concentrations over 10μM caused significant toxicity ($p<0.0001$), reducing the median survival to 4dpf or 2dpf when treated with 10μM or 100μM, respectively (**figure 118**). Phenotypically, zebrafish exposed to UDCA demonstrated heart and yolk-sac oedema 24-hours prior to their death (**figure 118**). No further experiments were conducted using UDCA due to the tolerability of TUDCA, a more relevant compound, discussed below.

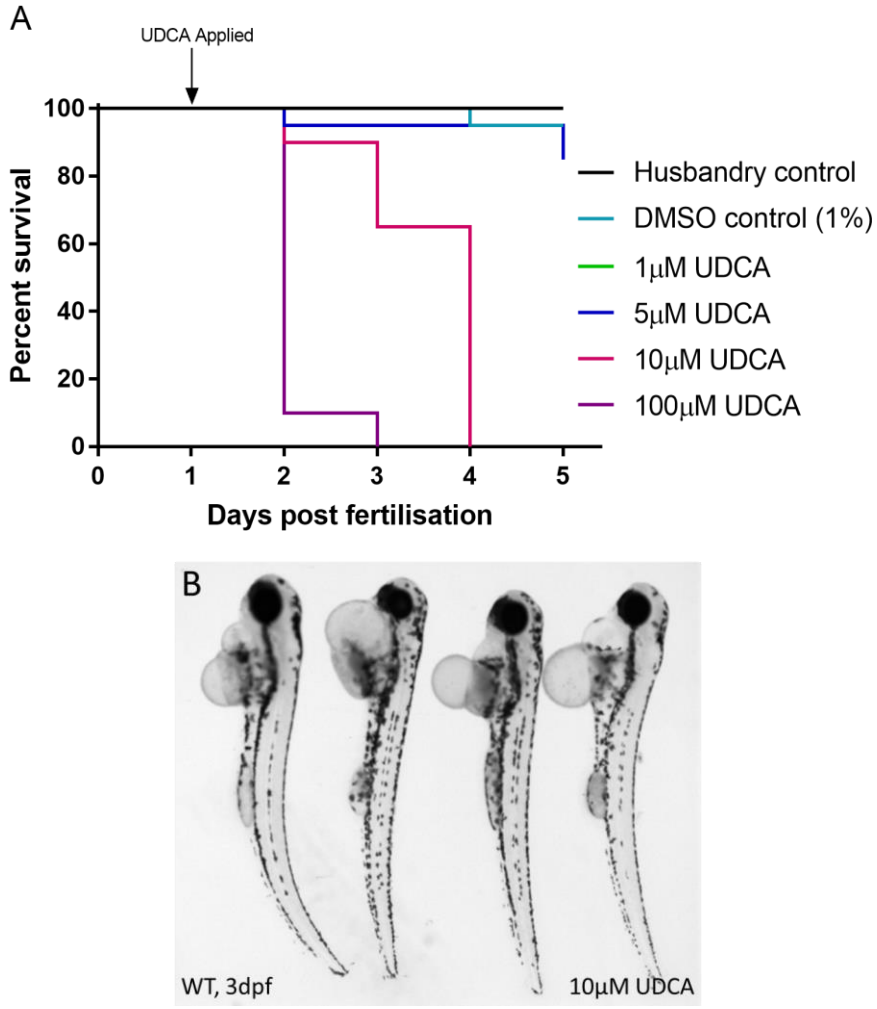

Figure 118. Survival Analysis of Wildtype Zebrafish Treated with Ursodeoxycholic Acid from 1-Day Post Fertilisation. A. *The effect of UDCA on the survival of wildtype zebrafish up to 5dpf when treated from 1dpf. Fish were treated via constant immersion in UDCA and 1% DMSO with daily media changes. n=20 wildtype fish per group. p<0.0001 for 10μM or 100μM compared to control (Mantel-Cox log rank test).* ***B.*** *Representative brightfield image of 3dpf larvae following a 24-hour exposure to 10μM UDCA. dpf, days post fertilisation; DMSO, dimethyl sulfoxide; UDCA, ursodeoxycholic acid; μM, micromolar.*

6.2.5.4 Tauroursodeoxycholic Acid (TUDCA)

6.2.5.4.1 Toxicity Trials

Toxicity trials of TUDCA in wildtype zebrafish up to 5dpf found no significant effects of the compound on survival or phenotype, even at the maximum concentration tested (p=0.1295, **figure 119A**). However, when the same concentrations were tested in zebrafish up to 10dpf, 100μM became toxic, significantly reducing the survival of larvae from 8dpf (p=0.0182, **figure 119B**). To establish the highest maximum tolerable dose, toxicity trials were repeated using concentrations between 10μM and 100μM. When treated from 5dpf, concentrations up to 75μM were not toxic (**figure 119C**), however, when treated from 1dpf, 75μM appeared to cause the death of fish at 10dpf (**figure 119D**). Although the difference in survival was not statistically significant (p=0.3202), the remaining larvae also appeared unhealthy (heart and yolk sac oedema and reduced movement), prompting the use of 50μM TUDCA for future experiments.

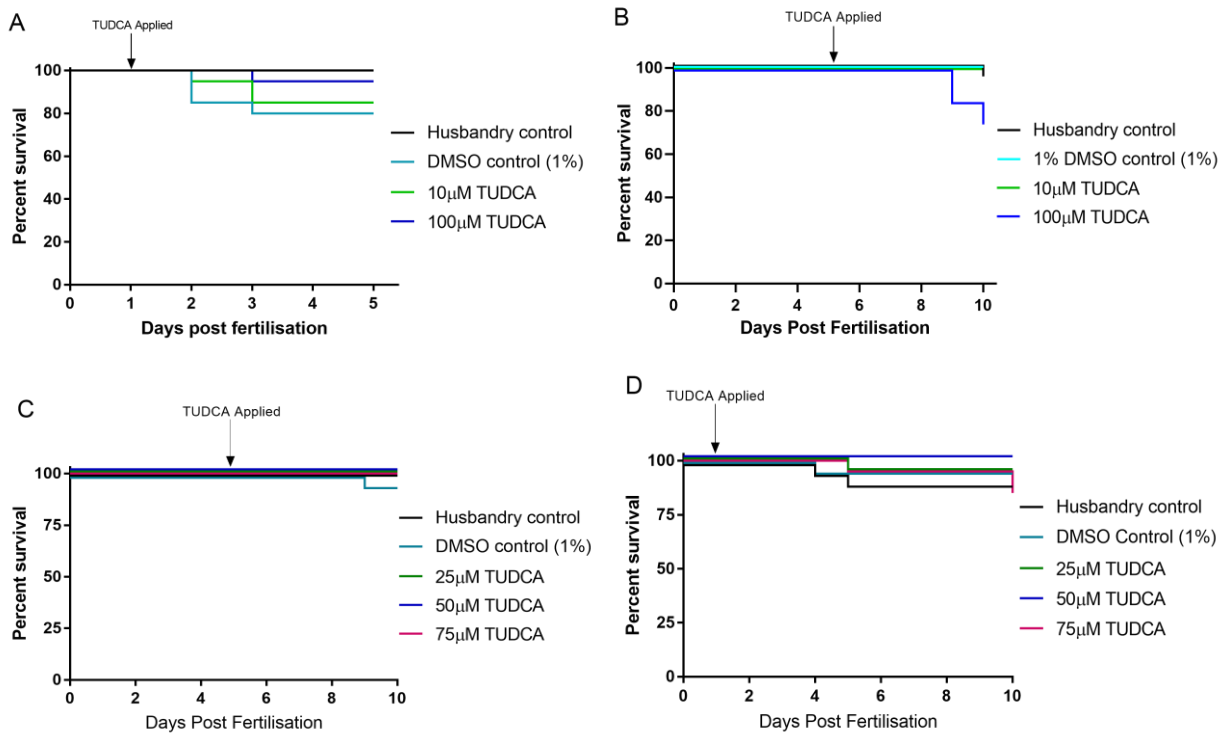

Figure 119. Survival Analysis of Wildtype Zebrafish Treated with Tauroursodeoxycholic Acid. A. *The effect of TUDCA on the survival of wildtype zebrafish up to 5dpf when treated from 1dpf. p=0.1295, Mantel-Cox log rank test.* ***B.*** *100µM TUDCA reduced the survival of wildtype zebrafish when treated from 5dpf (p=0.0182, Mantel-Cox log rank test, comparing 100µM TUDCA to DMSO control).* ***C.*** *25-75µM TUDCA had no effect on the survival of wildtype zebrafish when treated from 5dpf (p=0.4060, Mantel-Cox log rank test).* ***D.*** *25-75µM TUDCA had minimal effect on the survival of wildtype zebrafish when treated from 1dpf (p=0.4336, Mantel-Cox log rank test). For all experiments, fish were treated via constant submersion with daily media changes. n=20 wildtype fish per group. DMSO, dimethyl sulfoxide; dpf, days post fertilisation; TUDCA, tauroursodeoxycholic acid; µM, micromolar.*

6.2.5.4.2 Treatment of Cyclin G-Associated Kinase Mutant Zebrafish

gak$^{-/-}$ zebrafish were treated from 1dpf with 10µM TUDCA to establish whether this could rescue the survival of this mutant line. This experiment was conducted prior to the establishment of a new higher tolerable dose (50µM). TUDCA was unable to rescue the survival of *gak*$^{-/-}$ zebrafish (**figure 120**), with no significant difference in survival between treated and untreated homozygous mutants (p=0.3232). After the new tolerable dose of 50µM was established, the experiment was repeated. This new dose made no difference to the impact of TUDCA on survival of *gak*$^{-/-}$, with the median survival remaining at 5dpf for both treated and untreated groups (**figure 120**).

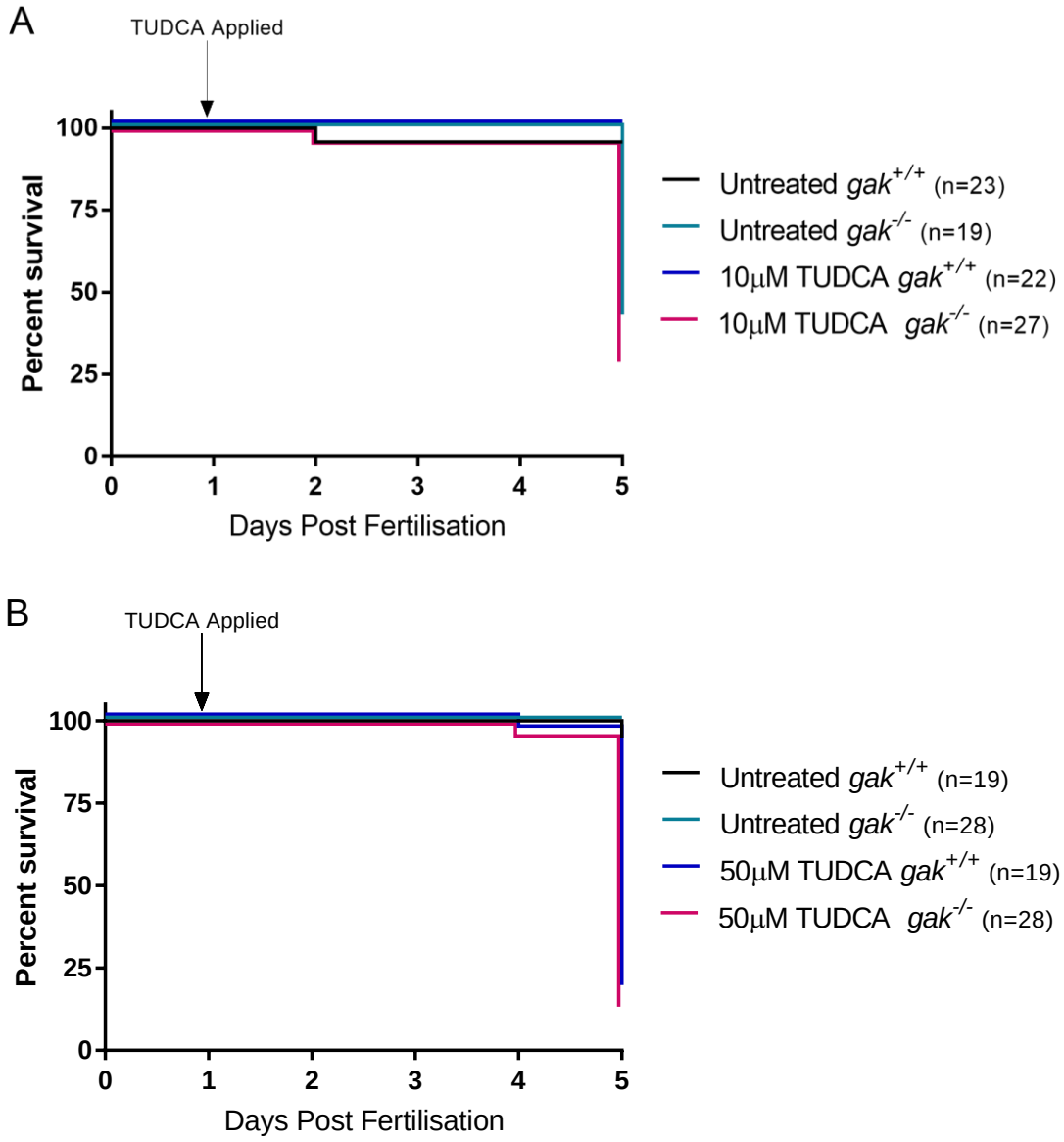

Figure 120. Survival Analysis of Cyclin G-associated Kinase Homozygous Mutant Zebrafish and Their Wildtype Siblings When Treated with Tauroursodeoxycholic Acid from 1-Day Post Fertilisation. *The effect of 10µM (**A**) or 50 µM (**B**) TUDCA on the survival of gak homozygous mutant zebrafish and their wildtype siblings when treated from 1dpf. Fish were treated daily via constant submersion with daily media changes. p=0.3232 for 10µM and p=0.7470 for 50µM (Mantel-Cox log rank test, comparison between treated and untreated homozygous mutants). DMSO, dimethyl sulfoxide; gak, cyclin g-associated kinase; TUDCA, tauroursodeoxycholic acid; µM, micromolar.*

6.2.5.4.3 Treatment of GTP Cyclohydrolase 1 Mutant Zebrafish

gch1$^{+/-}$ zebrafish were incrossed and their offspring divided into two groups; 100 larvae were exposed to 50µM TUDCA from 1dpf via constant immersion and 100 larvae were exposed to 1% DMSO. Fish were genotyped at the end of the experiment. Exposure of *gch1*$^{-/-}$ mutant zebrafish to TUDCA increased the median survival from 10 to 11dpf, although differences in survival curves were not significant (p=0.1150, **figure 121**). The effect of TUDCA on swim bladder inflation was also assessed; TUDCA appeared to increase the percentage of fish inflating their swim bladder by 6dpf, however, statistical analysis of these curves found no significant differences between treated and untreated *gch1*$^{-/-}$ mutants (p=0.2198).

This experiment was repeated with treatment starting at 5dpf to avoid any effects that TUDCA may have on early development. As before, no difference in the survival of homozygous mutants was identified (p=0.3751, **figure 121**). Swim bladder inflation was not assessed in this trial because separating fish by swim bladder inflation at 5dpf prior to treatment would result in the almost certain separation of *gch1*$^{-/-}$ and wildtype fish between plates, creating an extraneous variable in the experiment.

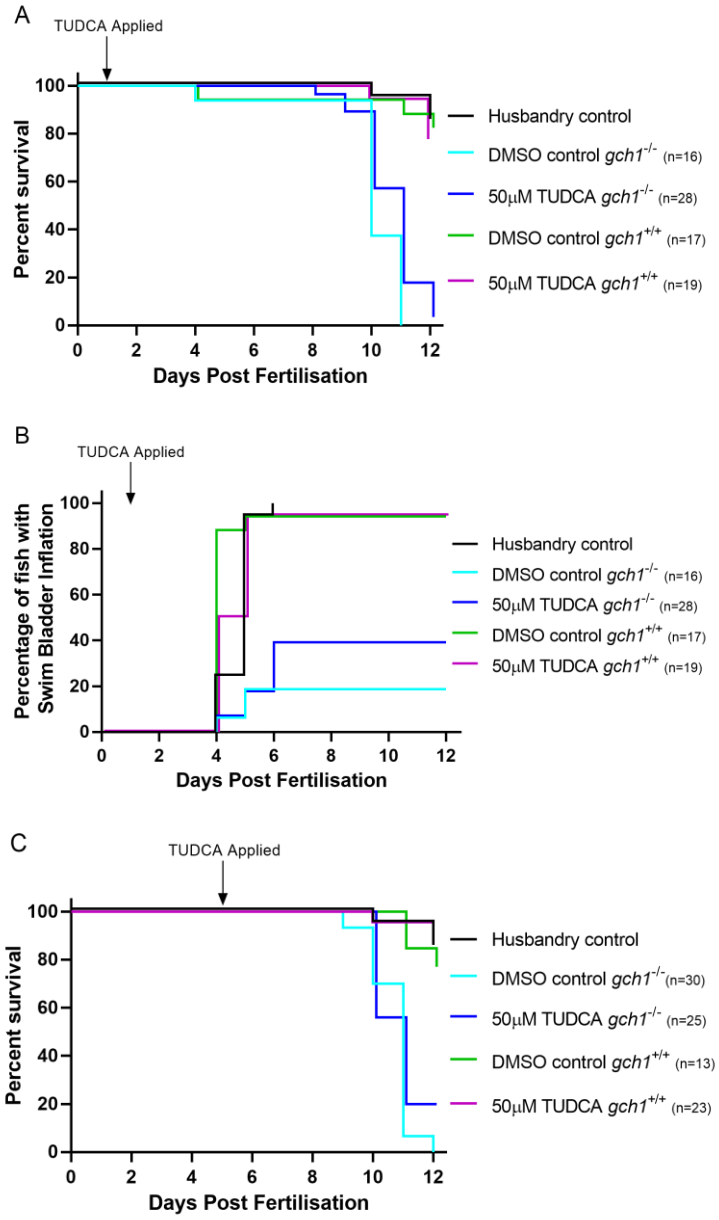

Figure 121. Analysis of GTP Cyclohydrolase 1 Homozygous Mutant Zebrafish and Their Wildtype Siblings When Treated with Tauroursodeoxycholic Acid. *When exposed from 1dpf, 50μM TUDCA had no effect on the survival of gch1*$^{-/-}$ *mutant zebrafish (**A**, p=0.1150) or their ability to inflate their swim bladder (**B**, p=0.2198). Exposure from 5dpf also had no effect on the survival of gch1*$^{-/-}$ *mutant zebrafish (**C**, p=0.3751). Fish were treated via constant submersion with daily media changes. All statistics were calculated using a Mantel-Cox log rank test between TUDCA treated and DMSO control treated gch1*$^{-/-}$ *fish. DMSO, dimethyl sulfoxide; dpf, days post fertilisation; gch1, GTP cyclohydrolase 1; TUDCA, tauroursodeoxycholic acid; μM, micromolar.*

6.2.5.5 Glycoursodeoxycholic Acid (GUDCA)

Glycine conjugated UDCA (GUDCA) is another commercially available version of this compound. Toxicity trials in zebrafish up to 5dpf (data not shown) were inconclusive due to the crystallisation of the drug in E3 media. To establish at which concentration GUDCA is unable to remain in solution, various concentrations were left at 28°C overnight and observed for crystal formation. There was no clear link between the concentration of GUDCA and the formation of crystals (**table 39**). This compound was not taken any further in this study for this reason.

Table 39. Solubility of Glycoursodeoxycholic Acid in E3 Media

Final concentration of GUDCA / µM	Overnight crystal formation?
100	Yes
75	No
50	Yes
25	No

Various concentrations of glycoursodeoxycholic acid were added to 3mL E3 media with 1% dimethyl sulfoxide and left at 28°C overnight. Crystallisation visible under a microscope was used as a readout of solubility. GUDCA, glycoursodeoxycholic acid; DMSO, dimethyl sulfoxide; µM, micromolar.

6.2.5.6 Compound X1

The names of the following compounds have been redacted for reasons of confidentiality. They were tested as part of this project due to their relationship to the bile acid compounds discussed above and synthesis by the sponsor. The effect of these compounds on inflammation is unknown.

6.2.5.6.1 Solubility Testing

The first novel compound testing during this project was compound X1. An initial solubility assay found that X1 was insoluble in E3 media with 1% DMSO (**table 40**). Since long-term treatment with DMSO at concentrations higher than 1% can cause toxicity issues in zebrafish, X1 was not taken forward for toxicity trials or application to PD mutants.

Table 40. Solubility of X1 in E3 Media.

Final concentration of X1 / µM	Final percentage of DMSO	Overnight crystal formation?
100	1%	Yes
50	1%	Yes
50	0.5%	Yes

Compound X1 was added to 3mL E3 media with dimethyl sulfoxide and left at 28°C overnight. Crystallisation visible under a microscope was used as a readout of solubility.

6.2.5.7 Compound X2

6.2.5.7.1 Solubility Testing

Another novel compound used in this project was compound X2. Solubility testing found that X2 was soluble in E3 media (**table 41**).

Table 41. Solubility of X2 in E3 Media.

Final concentration of X2 / µM	Final percentage of DMSO	Overnight crystal formation?
100	1%	No
50	1%	No
50	0.5%	No

Compound X2 was added to 3mL E3 media with dimethyl sulfoxide and left at 28°C overnight. Crystallisation visible under a microscope was used as a readout of solubility. DMSO, dimethyl sulfoxide; µM, micromolar.

6.2.5.7.2 Toxicity Trials

Initial toxicity trials using compound X2 found that 100µM was well tolerated by zebrafish larvae up to 5dpf (data not shown) and later up to 10dpf when treating from either 1dpf or 5dpf (**figure 122**). When treating from 1dpf, larvae exposed to 1µM died at 10dpf. Since these fish displayed no signs of toxicity before this time point and larvae exposed to higher concentrations did not develop toxicity, this was assumed to be unrelated to compound exposure.

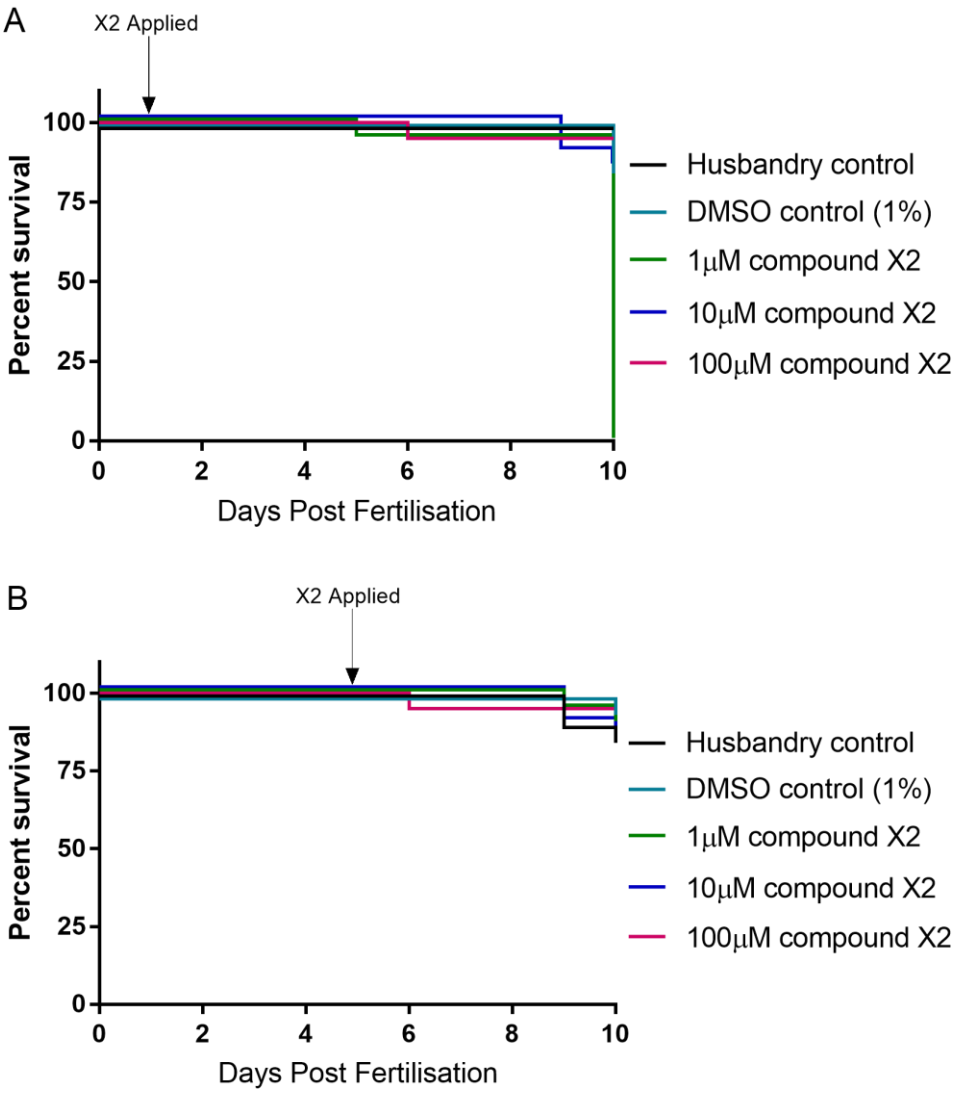

Figure 122. Survival Analysis of Wildtype Zebrafish Treated with Compound X2. *Toxicity trials of compound X2 demonstrated that it was well tolerated in wildtype zebrafish up to 10dpf when treated from either 1dpf (**A**, p=0.2591) or 5dpf (**B**, p=0.7070). For all experiments, fish were treated via constant submersion in compound X2 and 1% DMSO with daily media changes. n=20 wildtype fish per group. Data were statistically analysed using Mantel-Cox log rank test (for **A**, 1µM was omitted from analysis). DMSO, dimethyl sulfoxide; dpf, days post fertilisation; µM, micromolar.*

6.2.5.7.3 Treatment of GTP Cyclohydrolase 1 Mutant Zebrafish

gch1$^{+/-}$ zebrafish were incrossed and their offspring exposed to either 100µM compound X2 or DMSO from 1dpf. Compound X2 had no effect on the survival of *gch1*$^{-/-}$ mutant zebrafish (**figure 123**, p=0.4571), with the median survival in either group remaining at 10dpf. Fish were not treated from 5dpf with compound X2 due to the limited availability of this compound and its unlikely effect in older larvae.

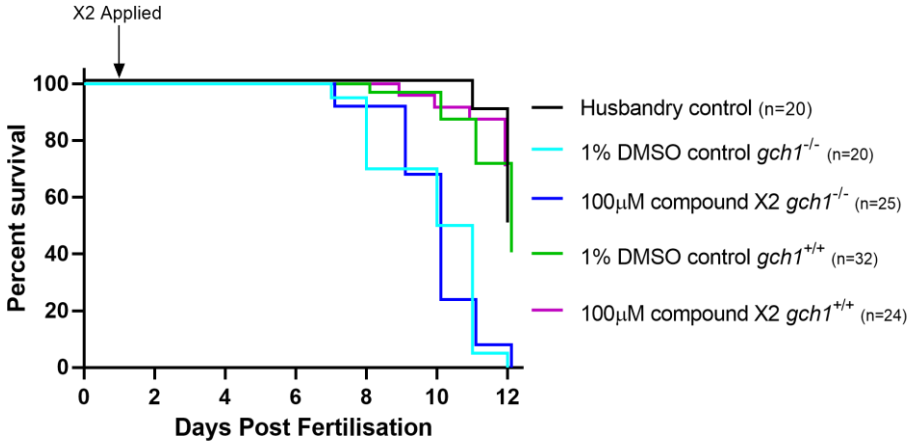

Figure 123. Treatment of GTP Cyclohydrolase 1 Homozygous Mutant Zebrafish with Compound X2. *Larvae were obtained from a heterozygous incross and split into two groups. Fish were treated via constant submersion in compound X2 with 1% DMSO and media changed daily. Larvae were genotyped at the end of the experiment and numbers per each genotype are given in the legend. p=0.4571, Mantel-Cox log rank test (comparison between compound X2 treated and DMSO control treated gch1*$^{-/-}$ *fish). DMSO, dimethyl sulfoxide; gch1, GTP cyclohydrolase 1; µM, micromolar.*

6.2.6 Pharmacological Induction of Inflammation in Zebrafish Larvae

In wildtype zebrafish a number of techniques were tested to establish a method of inducing inflammation in otherwise healthy fish. The techniques developed were aimed for use in the mutants discussed in previous chapters and also as a system for the assessment of the novel compounds discussed above. This latter aim was not achieved due to restrictions generated by the coronavirus pandemic.

6.2.6.1 Lipopolysaccharide

Lipopolysaccharide (LPS) was injected directly into the yolk of 3dpf zebrafish. Zebrafish were then incubated in neutral red solution to stain microglia and macrophages, and larvae imaged using brightfield microscopy. Successful neutral red staining was confirmed by the presence of microglia in the brain, as staining is obvious here. Neutral red staining was evident in the head, caudal hematopoietic tissue (CHT) and yolk of larvae (**figure 124**). Puncta staining in the yolk appeared to only be seen in LPS injected fish, although this staining was difficult to see or quantify. No differences in survival were seen between LPS injected larvae and controls (data not shown).

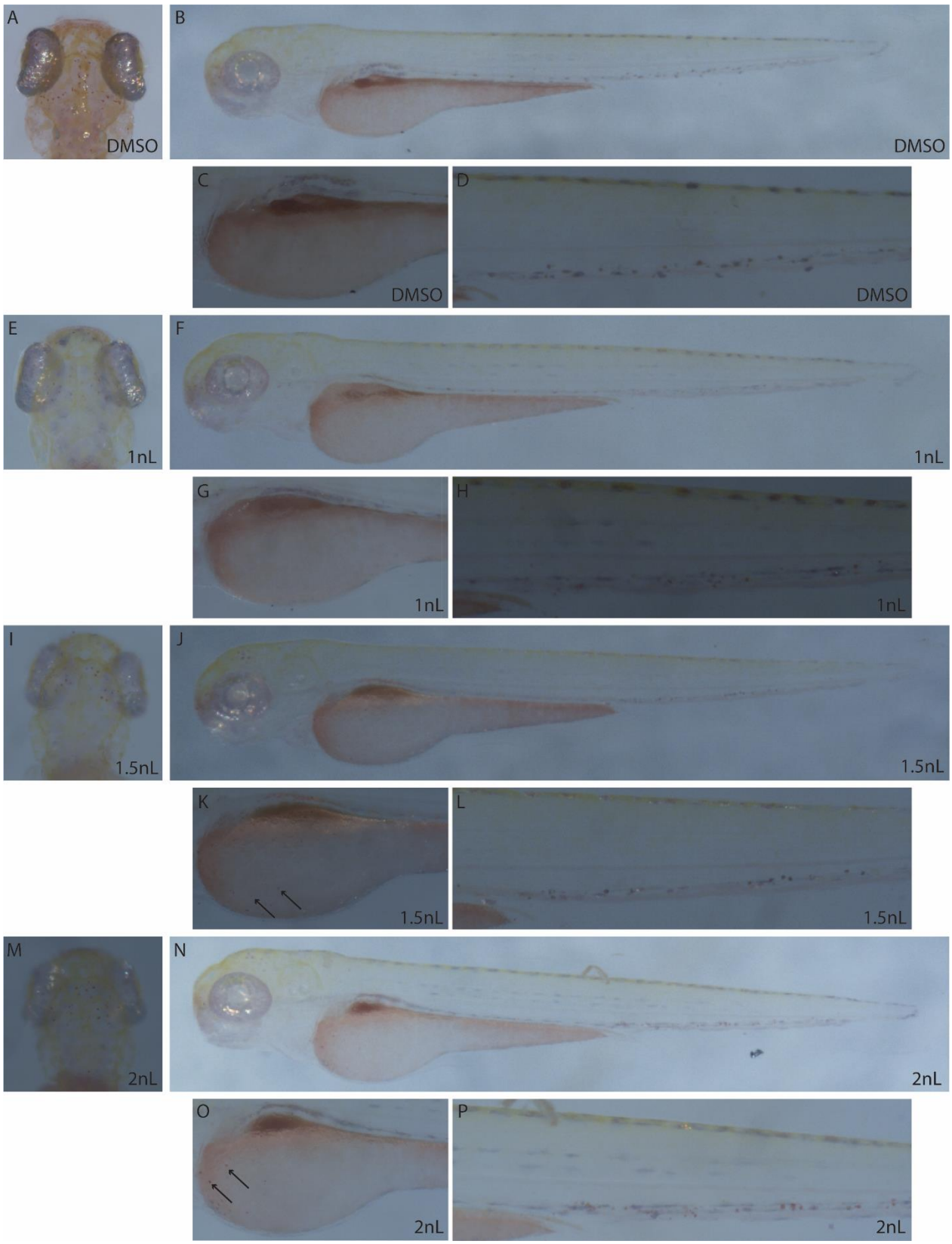

Figure 124. Neutral Red Staining in Wildtype Zebrafish Injected with Lipopolysaccharide. *Neutral red staining of 3dpf zebrafish larvae following injection into the yolk with DMSO (**A-D**), 1nL LPS (**E-H**), 1.5nL LPS (**I-L**) or 2nL LPS (**M-P**). Successful neutral red staining was confirmed by imaging the head (**A, E, I, M**) and was then assessed in the whole larvae, focussing on the yolk (**C, G, K, O**) and caudal hematopoietic tissue (**D, H, L, P**). Arrows show puncta staining in the yolk. DMSO, dimethyl sulfoxide; dpf, days post fertilisation; LPS, lipopolysaccharide; nL, nanolitre.*

6.2.6.2 Saponin

6.2.6.2.1 Toxicity Trials

Toxicity trials were conducted on wildtype larvae. Initially, larvae were exposed to 0.5mg/mL, the concentration suggested for use by Dr Sylvia Brugman. However, this concentration resulted in the death of all exposed larvae within 24 hours (data not shown). Therefore, a toxicity trial of lower concentrations was conducted, finding that larval zebrafish could tolerate up to 40µg/mL saponin, but 400µg/mL resulted in significant death within 24-72 hours (**figure 125**). Intermediate concentrations were therefore assessed, identifying 100µg/mL as the maximum tolerable concentration (**figure 125**).

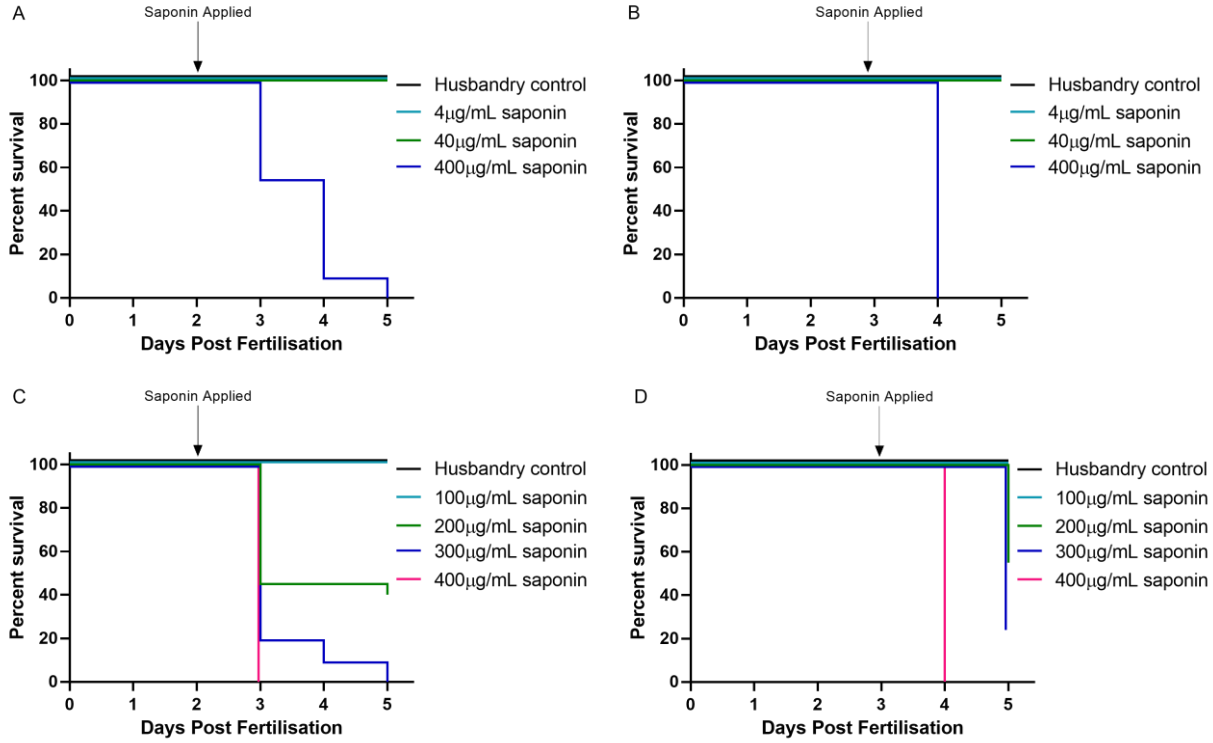

Figure 125. Toxicity Trials of Saponin Exposure in Wildtype Larval Zebrafish. *Larvae were exposed to saponin via constant immersion from either 2-(**A, C**) or 3-(**B, D**) dpf. Survival was assessed every 24 hours. n=20 wildtype fish per group. dpf, days post fertilisation; µg, micrograms.*

6.2.6.2.2 Induction of Inflammation using Saponin

For the assessment of the induction of inflammation, wildtype larvae were exposed to concentrations up to 100µg/mL saponin from 3-5dpf. RNA was then extracted from groups of 15 larvae, cDNA created and qPCRs conducted to assess the levels of three inflammatory mediators. 100µg/mL saponin significantly increased the expression of *il-1β* (**figure 126A**, p<0.0001), *mmp9* (**figure 126B**, p=0.0053) and *cxcl8* (**figure 126C**, p=0.0008). Concentrations below 100µg/mL had no effect on expression.

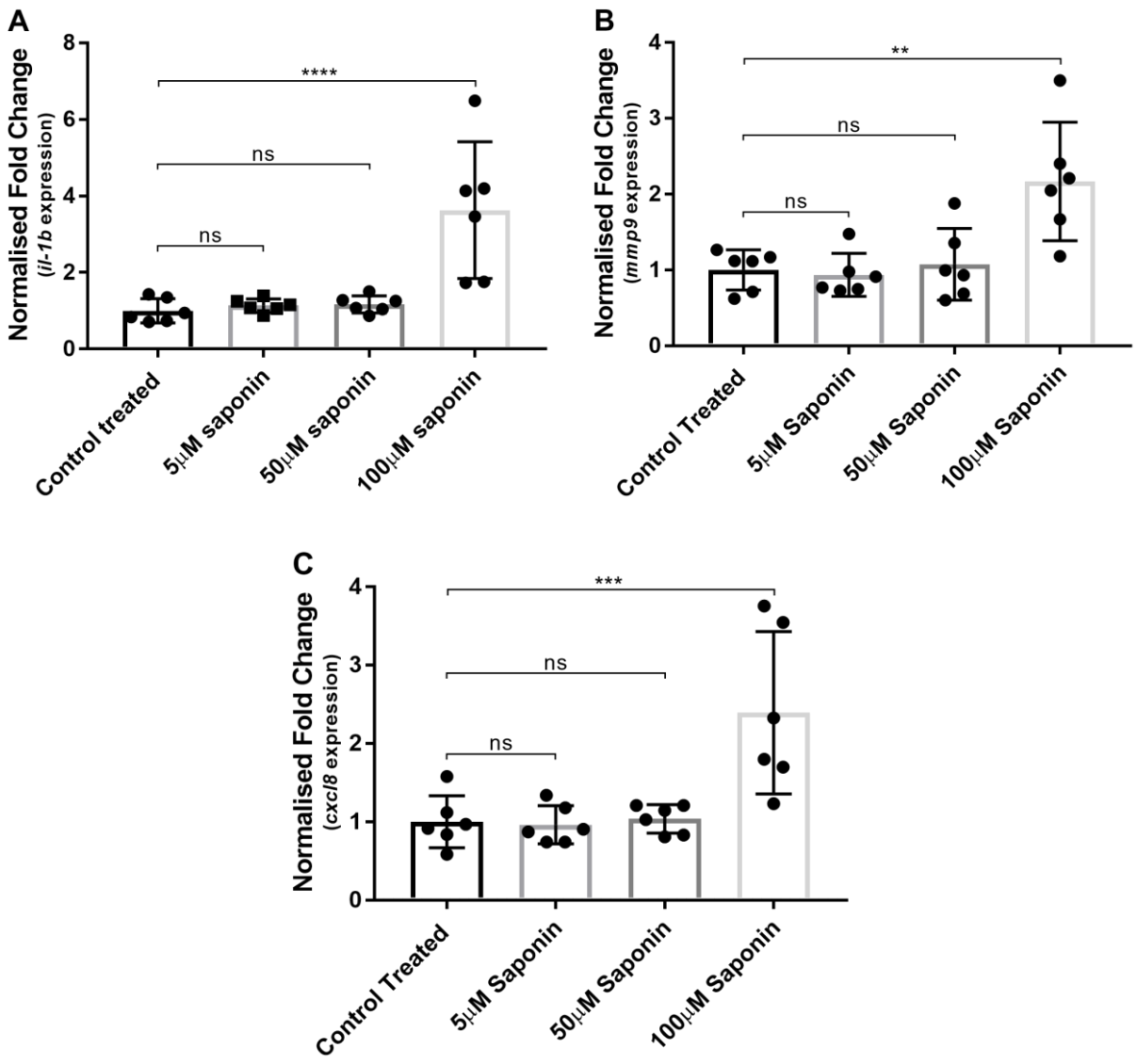

Figure 126. Expression of Inflammatory Mediators in Wildtype Larvae Exposed to Saponin for 72 Hours. *Wildtype zebrafish were exposed to saponin from 3-5dpf via constant immersion. Significant increases in the expression of il-1β (p<0.0001, **A**), mmp9 (p=0.0053, **B**) and cxcl8 (p=0.0008, **C**) were identified using qPCR on RNA extracted at 5dpf. Expression is shown relative to control samples. Statistical analysis conducted on ddCt data, using a one-way ANOVA (all datasets passed Shapiro-Wilk test for normality). n=6 biological replicates (15 larvae combined per replicate). rps29 was used as a loading control for all qPCRs. cxcl8, c-x-c motif chemokine ligand 8; dpf, days post fertilisation; il-1β, interleukin-1 beta; mmp9, matrix metalloproteinase 9; µg, micrograms.*

6.2.6.3 Dextran Sodium Sulfate (DSS)

6.2.6.3.1 Toxicity Trials

Three concentrations of DSS were selected for use based on previous publications and discussions with Dr Sylvia Brugman. No toxicity was seen with any concentration when wildtype larvae were treated from either 2dpf or 3dpf (**figure 127**).

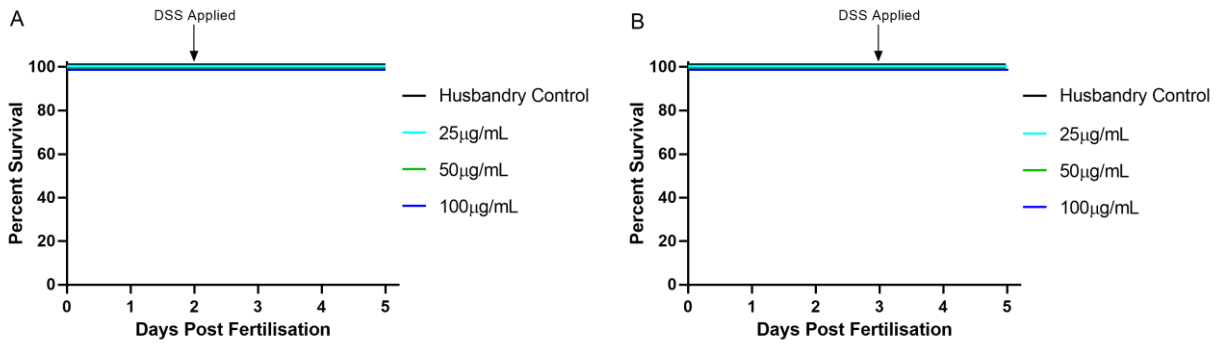

Figure 127. Toxicity Trials of Dextran Sodium Sulfate using Wildtype Zebrafish Larvae. *No toxicity of DSS was seen when wildtype larvae were exposed from either 2-5dpf (**A**) or 3-5dpf (**B**) with any of the concentrations tested. n=20 wildtype larvae per group. dpf, days post fertilisation; µg, microgram. DSS, dextran sodium sulfate.*

6.2.6.3.2 Induction of Inflammation using DSS

All three concentrations were then used in triplicate to obtain RNA post-treatment, which was used for qPCR against three inflammatory mediators, as for saponin above. The results from these qPCRs were inconsistent between replicates (**table 42**) and opposite to the expected results; the data suggested a dose-dependent decrease in *il-1β* and *mmp9* expression and an increase in *cxcl8* expression following exposure to DSS (**figure 128**). No *mmp9* amplification was seen in larvae exposed to 100µg/mL and in some replicates no amplification was seen for *il-1β* or *mmp9* in larvae exposed to 50µg/mL or 100µg/mL. Based on the trend of these datasets, it is likely that expression was too low to detect above background using qPCR.

These results were unexpected. However, the same trend was identified following exposure from 2-5dpf, although this was only conducted using one biological replicate (**figure 128**). The lack of amplification following exposure to 100µg/mL was also replicated in this dataset.

Table 42. Summary of Quantitative PCR Data Following Exposure to Dextran Sodium Sulfate

	il-1β	*cxcl8*	*mmp9*
Rep 1	Linear dose-dependent **decrease**	Linear dose-dependent **increase**, plateaus at high dose	Dramatic dose-dependent **decrease**, no expression detected in high dose
Rep 2	Dose-dependent **decrease**, almost linear	No pattern seen	Dramatic dose-dependent **decrease**, no expression detected in high dose
Rep 3	Biological effect? Starting expression lower so after initial **decrease**, no expression detected	Linear dose-dependent **increase**, less dramatic than rep1	Dramatic **decrease** with initial dose, no expression detected in higher doses

Table outlining the trend in expression of interleukin-1 beta (il-1β), C-X-C motif chemokine ligand 8 (cxcl8) and matrix metalloproteinase 9 (mmp9) following treatment of wildtype zebrafish larvae with dextran sodium sulfate from 3-5dpf. Colours relate to biological replicates (rep) and match those shown in figure 128 below.

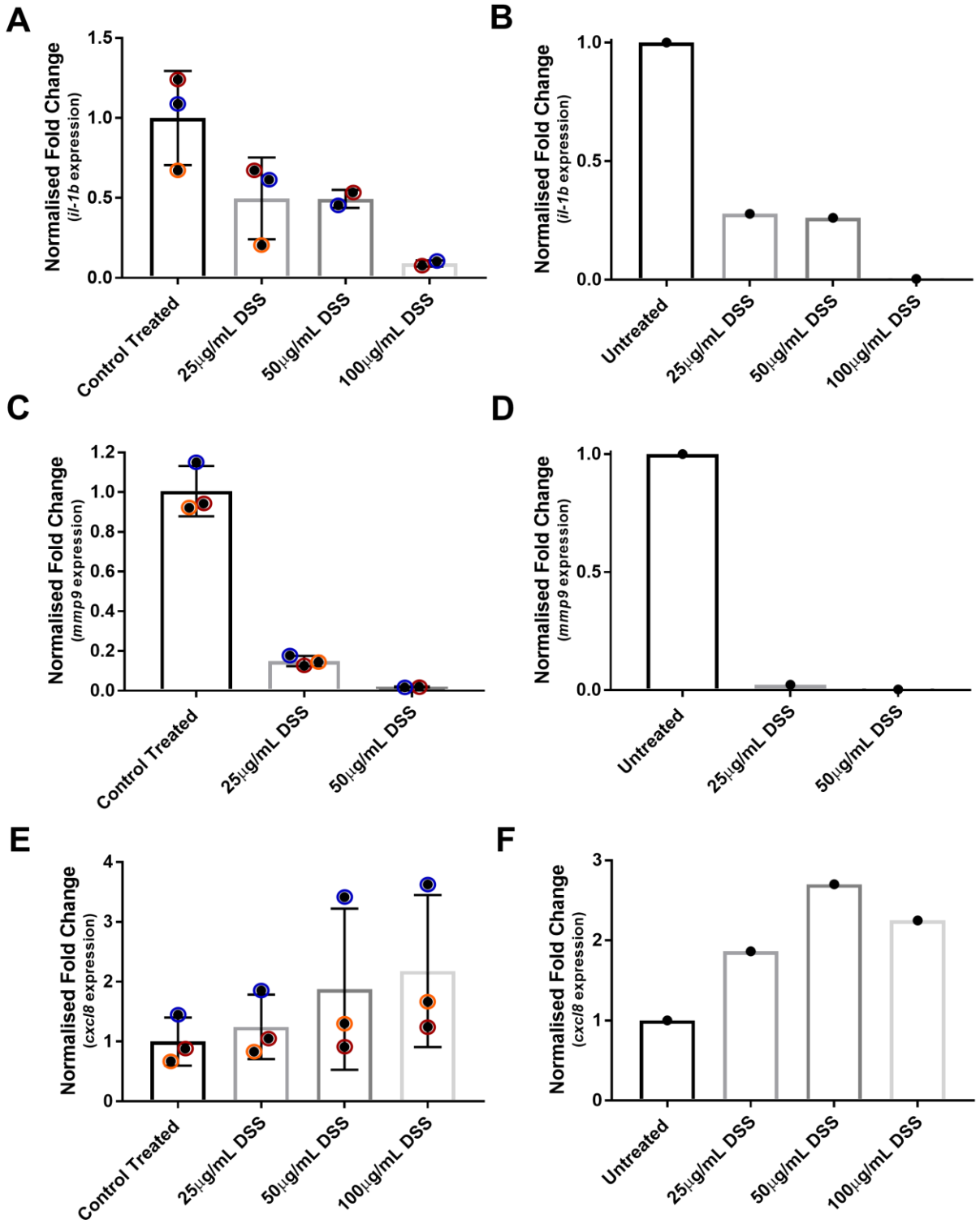

Figure 128. Dextran Sodium Sulfate Resulted in Inconsistent Changes in the Expression of Inflammatory Mediators. *Expression of il-1β (**A, B**), mmp9 (**C, D**) and cxcl8 (**E, F**) in wildtype larvae following exposure to DSS. **A, C, E** data from 3 biological replicates (15 larvae per replicate), treated from 3-5dpf, colour-coded to replicate. **B, D, F** from a single replicate, treated from 2-5dpf. All data was normalised to rps29 and shown relative to control expression levels. cxcl8, C-X-C motif chemokine ligand 8; dpf, days post fertilisation; dss, dextran sodium sulfate; il-1β, interleukin 1-beta; mmp9, matrix metalloproteinase 9; µg, micrograms.*

6.2.6.4 Trinitrobenzene Sulfonic Acid (TNBS)

6.2.6.4.1 Toxicity Trials

The final compound assessed for the induction of inflammation was TNBS. Toxicity trials on wildtype larvae identified 75µg/mL to result in oedema of the heart and yolk sac as well as body curvature at 4dpf, preceding larval death (**figure 129**). 50µg/mL TNBS also caused milder heart and yolk sac oedema by 4dpf but resulted in less death than 75µg/mL. Due to the high toxicity, 75µg/mL was not included in further experiments.

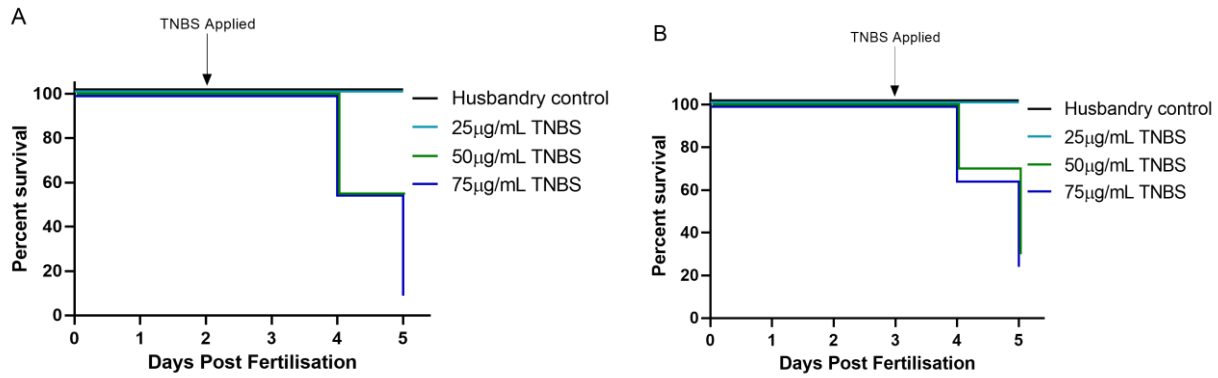

Figure 129. Toxicity Trials of Trinitrobenzene Sulfonic Acid using Wildtype Zebrafish Larvae. *Survival curves of wildtype larvae exposed to TNBS from either 2-5dpf (**A**) or 3-5dpf (**B**). n=20 wildtype larvae per group. dpf, days post fertilisation; TNBS, trinitrobenzene sulfonic acid; µg, microgram.*

6.2.6.4.2 Induction of Inflammation using TNBS

Treatment with 25µg/mL and 50µg/mL TNBS was repeated in triplicate and RNA extracted at 5dpf. Slight variations in survival were seen between replicates but most larvae survived, even when exposed to 50µg/mL, which was less well tolerated in toxicity trials. The expression of inflammatory mediators was assessed as before (**table 43**). Whilst it appeared that TNBS was increasing the expression of these inflammatory mediators, closer examination identified this was likely due to an outlier in the 50µg/mL treated group (orange, **figure 130**). Changes in expression were not significant for either *il-1β* (p=0.0753) or *cxcl8* (p=0.0666), but a significant increase was seen in *mmp9* expression when larvae were exposed to 50µg/mL (p=0.0268). As this concentration resulted in oedema, TNBS was not used for inducing inflammation as effects would be difficult to distinguish from nonspecific toxicity.

Table 43. Summary of Quantitative PCR Data Following Exposure to Trinitrobenzene Sulfonic Acid

	il-1β	*cxcl8*	*mmp9*
Rep 1	Effect only seen with 50µg/mL, **increased** expression	Effect only seen with 50µg/mL, **increased** expression	Dramatic dose-dependent **increased** expression
Rep 2	Dose-dependent **increase**, more evident with 50µg/mL (outlier?)	Effect only seen with 50µg/mL, **increased** expression (outlier)	Dose-dependent **increase**, more evident with 50µg/mL (outlier?)
Rep 3	Both doses saw moderate **increase**, but no further effect of increasing concentration	Small dose-dependent **increased** expression	Moderate dose-dependent **increased** expression

Table outlining the trend in expression of interleukin-1 beta (il-1β), C-X-C motif chemokine ligand 8 (cxcl8) and matrix metalloproteinase 9 (mmp9) following treatment of wildtype zebrafish larvae with TNBS from 3-5dpf. Colours relate to biological replicates (rep) and match those shown in figure 130 below.

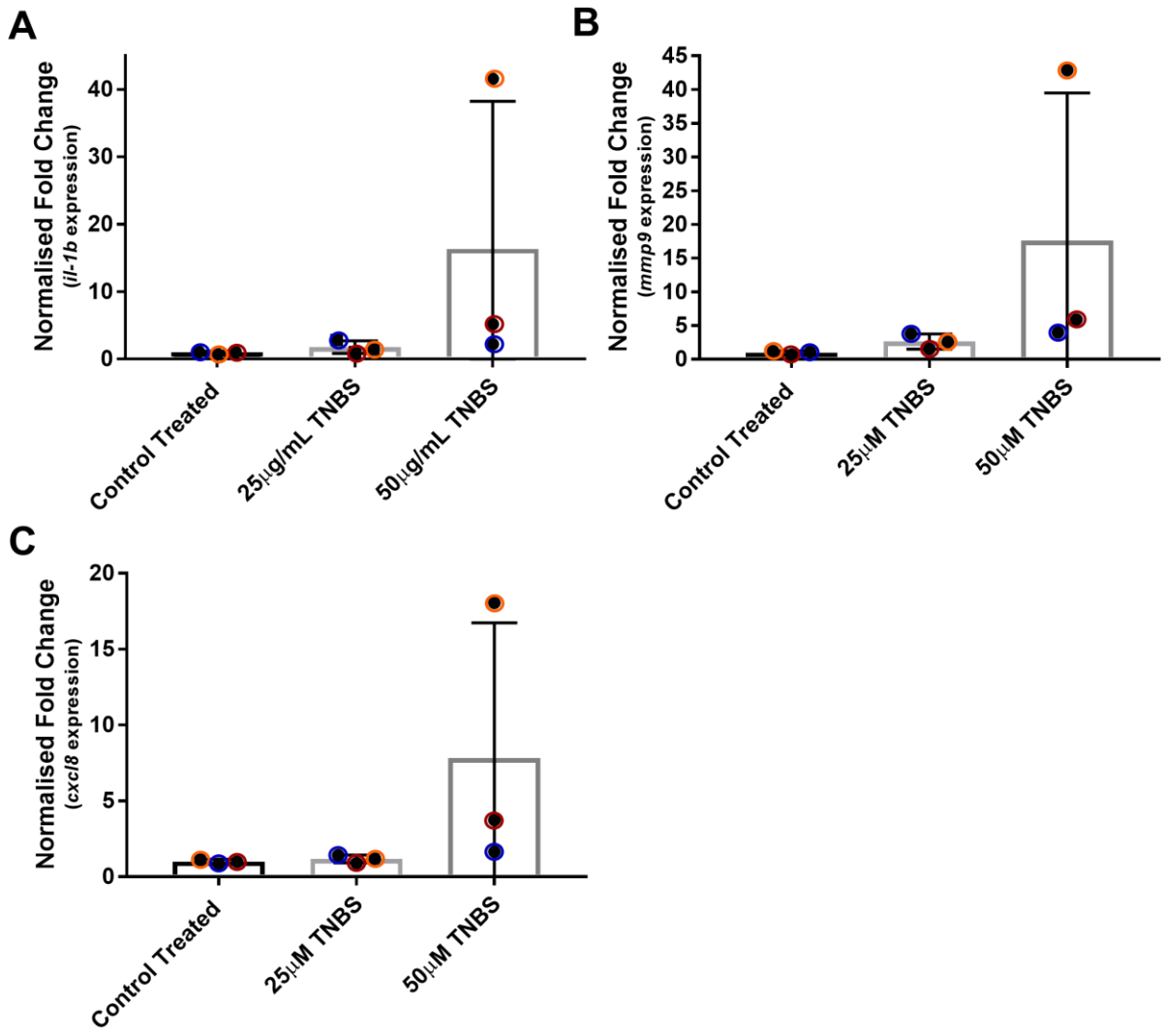

Figure 130. Trinitrobenzene Sulfonic Acid Resulted in Inconsistent Changes in the Expression of Inflammatory Mediators. *Expression of il-1β (**A**), mmp9 (**B**) and cxcl8 (**C**) in wildtype larvae following exposure to TNBS. Data from 3 biological replicates (15 larvae per replicate), treated from 3-5dpf, colour-coded to replicate. No statistical difference was found between treatment groups for il-1β (p=0.0753) or cxcl8 (p=0.0666). A significant increase in mmp9 expression was found following exposure to 50µg/mL (p=0.0268). All data was normalised to rps29 and shown relative to control expression levels. Statistics were analysed using a one-way ANOVA on ddCt values following Shapiro-Wilk test for normality. For mmp9 data, Tukey's post-hoc multiple comparisons test was used following ANOVA. cxcl8, C-X-C motif chemokine ligand 8; dpf, days post fertilisation; TNBS, trinitrobenzene sulfonic acid; il-1β, interleukin 1-beta; mmp9, matrix metalloproteinase 9; µg, micrograms.*

6.3 Discussion

There were two aims of chapter 6 of this thesis; to explore the option of inflammatory modulation in PD mutant zebrafish and to develop methodology to induce inflammation in otherwise healthy larvae.

To reduce neuroinflammation, a genetic approach was developed to inhibit the development of microglia in the brains of larval zebrafish. Zebrafish microglia are derived from primitive macrophages that infiltrate the brain and differentiate within the tissue to become CNS-resident microglia. During this process, cells develop new sets of gene expression and alter their morphology. A subpopulation of primitive macrophages / erythromyeloid progenitors, which develop not from hematopoietic stem cells but from the rostral blood island (RBI) of the yolk sac, initially colonise the brain to become embryonic microglia (Bertrand et al., 2007). The number of microglia from this initial wave decreases over time, becoming completely absent by one year (Xu et al., 2015). A second wave, cells originating from hematopoietic stem cells on the ventral wall of the dorsal aorta (VDA), infiltrate the brain from 15dpf becoming the most dominant population by 3 months of age (Xu et al., 2015). The gene expression profile of larval microglia demonstrates their similarity to adult zebrafish populations and those found in other animals (Mazzolini et al., 2020), suggesting that zebrafish larvae are a good model of microglial function.

irf8 has been used to genetically target microglia in zebrafish. As discussed in the chapter introduction, *irf8* is expressed in myeloid cells during development, becoming restricted to microglia in 3-7dpf larvae (Li et al., 2011; Mazzolini et al., 2020). Unlike in mouse models, a loss of *irf8* in zebrafish results in a lack of macrophages and microglia (Earley et al., 2018; Li et al., 2011; Prajsnar et al., 2021; Shiau et al., 2015; Tsarouchas et al., 2018; Yu et al., 2017; Zhao et al., 2018), enabling their use a genetic model of reduced inflammation. Larvae without microglia would have a reduced ability to mount an immune response within the brain.

Commonly, a single gRNA targeting exon 1 of *irf8* is used to create CRISPants with reduced microglia in zebrafish larvae, and this was used as standard in the department. Whilst this thesis showed that this method was able to achieve microglial depletion, the addition of two additional novel gRNAs, also targeting exon 1, was able to further increase the success of microglia knockout in zebrafish larvae. This is likely due to the increased double-stranded DNA breaks and the insertion of further deleterious indels in the gene. This triple gRNA was used for further experiments and has also now been used by other research groups at The University of Sheffield.

gch1$^{-/-}$ mutant zebrafish develop an inflammatory phenotype by 8dpf, characterised by hyperactive microglia and increases in proinflammatory cytokine production (Larbalestier et al., 2021). These larvae also fail to inflate their swim bladders and have a reduced survival, with most larvae dying by 10dpf. Microglia in *gch1*$^{-/-}$ mutants have been shown to have increased rates of phagocytosis compared to their wildtype siblings, indicative of increased activity. Not only does a reduced expression of *irf8* significantly reduce the number of microglia in zebrafish, it has also been demonstrated to inhibit the ability of these cells to phagocytose (Li et al., 2011) and prevent proinflammatory gene induction (Das et al., 2017). Therefore, it was hypothesised that a lack of microglia in *gch1*$^{-/-}$ mutant larvae using *irf8* CRISPants would reduce their neuroinflammatory phenotype and, at least partially, rescue their reduced survival.

Whilst *irf8* CRISPR was successful in reducing the number of microglia in *gch1*$^{-/-}$ mutant zebrafish, this was unable to rescue the survival or lack of swim bladder inflation in these mutants. The effect on specific readouts of inflammation was not conducted. Performing microglial counting and activation studies, the methodology initially used to show an inflammatory phenotype, would be impractical in larvae with depleted microglia and RNAseq analysis would be costly and time consuming. Furthermore, additional study found that *irf8* CRISPR was unable to prevent microglia development at later time points. This is particularly relevant since *gch1*$^{-/-}$ larvae only develop inflammatory phenotypes from 8dpf, a stage at which microglial repopulation was found in *irf8* CRISPants.

The *irf8* CRISPants created during this project lacked microglia up to 5dpf, but 4c4+ cells appeared to repopulate the brain by 8dpf, becoming fully repopulated by 10dpf. The lack of microglia at this early stage is in agreement with other zebrafish models of *irf8* deficiency (Earley et al., 2018; Shiau et al., 2015; Tsarouchas et al., 2018; Yu et al., 2017). These models also identified reductions in peripheral macrophages and an increase in peripheral neutrophils (Prajsnar et al., 2021; Shiau et al., 2015; Tsarouchas et al., 2018; Yu et al., 2017; Zhao et al., 2018), an effect that has been confirmed in overexpression studies (Li et al., 2011).

From the data presented in this chapter, it appears that *irf8* CRISPants have a depletion of only microglia derived from the first wave of development. This has also been shown in other zebrafish *irf8* mutants, where a partial recovery of macrophages during adulthood suggests that some VDA-derived macrophages develop independent of *irf8* (Yu et al., 2017). In TALEN-generated mutants and morphants, microglia and macrophages have been shown to be absent in larval zebrafish but macrophages reappeared slowly from 7dpf (Shiau et al., 2015).

Pu.1 mutants can also be used to illustrate this. As mentioned in the introduction, Pu.1 acts upstream of *irf8* in zebrafish myeloid development (Li et al., 2011; Yu et al., 2017). The loss of macrophages and microglia in young amorphic Pu.1 mutant zebrafish larvae has been shown to recover by 5dpf (Yu et al., 2017). The repopulated microglia were functional, able to phagocytose and had normal branched morphology. These data suggest that Pu.1 is required for RBI-derived, but not VDA-derived cells, which may also be the case for downstream *irf8*.

Whilst the above data support the hypothesis that the repopulation of microglia in the *irf8* CRISPants in this thesis are VDA-derived peripheral macrophages that infiltrate the brain and differentiate into microglia, other data suggests this is not the case. In the mutants and morphants published by Shiau et al. (2015), whilst peripheral macrophages repopulated in older larvae, no microglia were evident even by 31dpf. Likewise, in *irf8* null adult zebrafish, whilst peripheral macrophages appear normal, microglia remain absent throughout life (Earley et al., 2018). If peripheral macrophages in *irf8* mutant larvae were able to differentiate into microglia and repopulate the brain, these would be expected to be present in the adult *irf8* nulls. The cells found to peripherally repopulate *irf8* mutants have been suggested to be a population of B cells rather than true macrophages (Ferrero et al., 2020), which may explain why their differentiation into microglia is not seen in these mutants.

As discussed previously in this thesis, CRISPR mutagenesis results in mosaic animals, with some cell populations having no mutations. The addition of two gRNAs in this project is likely to reduce the number of cells without mutations, as multiple guides targeting a single gene has been shown to reduce mosaicism (Wu et al., 2018). However, even a small subset of cells able to express *irf8* could repopulate over time and explain the short lasting depletion of microglia in these CRISPants.

Due to this repopulation, an additional method to prevent microglia development was sought. Pharmacological depletion of microglia has been shown to occur in zebrafish exposed to Ki20227 (Chia et al., 2018). In this project, 4c4 immunohistochemistry revealed that although the number of microglia was reduced in larvae exposed to Ki20227, the remaining cells possessed an amoeboid morphology, indicative of activated cells. As *gch1*$^{-/-}$ mutant zebrafish are known to already have increased activation of their microglial cells, treatment with Ki20227 may not be appropriate, although exposure did not increase the mortality of these mutants.

A combination of *irf8* CRISPants and Ki20227 was used as a double knockout method to prevent microglial development in *gch1*$^{-/-}$ mutant zebrafish. Immunohistochemistry was not conducted on *irf8* CRISPants that had been exposed to Ki20227 due to a lack of available 4c4, so the effect of this combined treatment is largely unknown. It was hypothesised that the initial absence of microglia evident in *irf8* CRISPants is maintained by exposure to Ki20227, as this is a microglial proliferation inhibitor and the increased activation state would in this case be negligible. Combined treatment of the *gch1*$^{-/-}$ mutant zebrafish larvae had no effect on their survival, although conclusions about the reason for this cannot be fully drawn without assessment of the microglia.

The absence of a rescue effect in these microglial experiments suggests that the *gch1* phenotype may not be driven by the perceived microglial abnormalities. In other models of neurodegeneration, for example LPS exposure in rats, the inhibition of microglia has been shown to result in a phenotypic rescue (Tomás-Camardiel et al., 2004), suggesting that microglia are a key driving force in the pathological process. It is likely that more widespread effects are occurring that result in the premature death of the *gch1*$^{-/-}$ mutant zebrafish, and reducing the activity of microglial cells is not enough the rescue this.

More global inflammation was also targeted in the *gch1*$^{-/-}$ mutant zebrafish using a number of commonly used and novel anti-inflammatory compounds. Dexamethasone was used as a positive control during this project since its anti-inflammatory properties are well characterised and it has been widely used in zebrafish. Dexamethasone was unable to rescue the survival of *gch1*$^{-/-}$ mutant zebrafish although additional readouts were not assessed during this project. The lack of effect suggests that the pharmacological inhibition of inflammation is unlikely to rescue this mutant and helps explain the absence of effect of the following compounds.

Analysis of RNAseq data obtained directly from *gch1*$^{-/-}$ mutant zebrafish brains suggested that quinacrine, along with a number of other compounds, could have a rescue effect in this line. Quinacrine, an outdated antimalarial drug, acts via a number of mechanisms, one being anti-inflammatory activity primarily via phospholipase A2 and NF-κB inhibition (Vigo et al., 1980). A reduction in TNF-α-induced iNOS expression in macrophages, as well as their apoptosis, has been demonstrated in cells exposed to quinacrine *in vitro* (Chumanevich et al., 2016). Additionally, two models of colitis have demonstrated that quinacrine protects against inflammation and ulceration, with reductions in COX2, iNOS and p53 identified in the colon of mice exposed to DSS (Chumanevich et al., 2016). Relevant to PD, quinacrine can partially rescue the depletion of

dopamine and prevent the degeneration of dopaminergic neurons in MPTP and 6-OHDA mouse, rat and cell-based models (Goulding et al., 2021; Tariq et al., 2001). Its use in zebrafish has not been widely published, although a link has been found between exposure and reduced ovulation in adult females (Cosme et al., 2015).

Exposure of *gch1*$^{-/-}$ mutant zebrafish larvae to the maximum tolerated concentration of quinacrine was unable to rescue the survival of these mutants, further suggesting that inflammatory modulation is not sufficient for *gch1*$^{-/-}$ phenotype rescue. Quinacrine is not a purely anti-inflammatory compound and has additional actions, including as an antioxidant (Struhar et al., 1992; Turnbull et al., 2003). It could be proposed that modulation of these other pathways is also not relevant in the *gch1*$^{-/-}$ mutant zebrafish. However, readouts directly relating to these pathways were not assessed, so the effect of quinacrine in these experiments, or indeed in the zebrafish at all, cannot be confirmed.

The final set of compounds assessed in this line were bile acids. Whilst UDCA toxicity trials suggested that the compound was having an effect in zebrafish exposed via immersion, conjugated bile acids were of more relevance and therefore established as a treatment. GUDCA was unable to remain in solution in E3 media, so was not used for experiments. TUDCA was therefore used for the treatment of *gch1*$^{-/-}$ mutant zebrafish, although this was unable to rescue the survival of these mutants. Once again, this supports the conclusion that anti-inflammatory compounds may not be useful in the *gch1*$^{-/-}$ line.

However, since no toxicity was seen following TUDCA exposure in zebrafish, it cannot be confirmed that the compound was having a biological effect. In humans, bile acids bind to three receptors; the farnesoid X receptor (FXR) (Makishima et al., 1999), the pregnane X receptor (PXR) (Staudinger et al., 2001) and the vitamin D receptor (VDR) (Makishima et al., 2002). Non-mammalian receptors demonstrate large differences in protein sequence and ligand binding. For example, zebrafish FXRs and PXRs bind nearly exclusively 5α-bile alcohols, resulting from differences in the shape of the ligand-binding pockets (Reschly et al., 2008), suggesting that the results of zebrafish drug treatments could hinge largely on whether the zebrafish ligand binding domains are structurally able to accommodate the bile acid derivatives used. However, the positive benefits of bile acids in neurodegenerative disease have been suggested to result from binding to sites other than the canonical binding pocket and to other receptors entirely, such as the GPBAR1/TGR5 receptor (Yanguas-Casás et al., 2017). An Ensembl search of GPBAR1 found that zebrafish do not possess an orthologue of this receptor, which may further indicate that

zebrafish are not a good model for the assessment of bile acid compounds for anti-inflammatory actions in neurodegenerative disease. Further research into the actions of these compounds in zebrafish is needed to explore this and draw reliable conclusions from data presented in this thesis.

All of the above data suggest that inflammation is not driving the phenotype of the *gch1*$^{-/-}$ mutant zebrafish. Inflammation is likely only one aspect of the phenotype and its treatment alone is therefore not enough to rescue these mutants. A primary motive for the pharmacological treatment of this line with known anti-inflammatory compounds was to assess whether the novel compound, X2, used during this project possessed anti-inflammatory properties. Exposure of *gch1*$^{-/-}$ mutant zebrafish to compound X2 was unable to rescue their survival or swim bladder inflation defect. Since the positive control, dexamethasone, was also unable to achieve this, no conclusions can be drawn about the anti-inflammatory properties compound X2 as hoped. Therefore, a new methodology was established to reassess this compound - the pharmacological induction of inflammation in wildtype zebrafish larvae. Inducing inflammation pharmacologically in zebrafish has two uses. Wildtype zebrafish exposed to such compounds provide a useful model for drug efficacy experiments. Phenotypes resulting from exposure may be rescued by the addition of secondary compounds, suggesting an anti-inflammatory activity of the rescue drug. Secondly, these models can be combined with existing zebrafish mutants to assess their susceptibility to external inflammatory factors.

LPS is a well-known inducer of inflammation and is widely used in animal models. Numerous attempts in zebrafish to induce inflammation by immersing larvae in LPS have been unsuccessful. Yang et al (2014) published a novel technique for using LPS to stimulate an inflammatory phenotype in zebrafish larvae. Injecting 2nL of 0.5mg/mL LPS directly into the yolk of 3dpf larvae was able to induce morphological changes, yolk necrosis and 100% mortality within 32 hours. An inflammatory phenotype was identified by the recruitment of macrophages and neutrophils to the yolk sac within 4 hours and a significant upregulation of *tnf-α*, *il-1β* and *il-6*. Furthermore, dexamethasone was able to significantly reduce the mortality associated with LPS injection.

Attempts to recreate this data during this project were unsuccessful. Despite following the published methodology, including the purchasing of LPS from the same supplier, no effect on the survival of LPS injected larvae was seen and neutral red staining was unremarkable. Whilst there were small areas of staining in the yolk of LPS-injected larvae, indicative of a few macrophages, this was much lower than that seen by Yang et al (2014), where huge numbers of macrophages

were recruited to the yolk. More recent zebrafish papers have altered this technique to inject much larger quantities, 10nL of 10mg/mL LPS (Zhang, Yuan, et al., 2018; J. Zhou et al., 2019). The 50X increase in total LPS injected and a volume of 10nL seemed like a large volume for the yolk to tolerate, however, this new methodology was trialled. Even at this high dose, LPS had no effect on the survival or neutral red staining of injected larvae.

As this method could not be established, a number of other compounds previously used in zebrafish to induce inflammation were then tested in parallel. All three compounds were assessed in the same way; their ability to affect larval expression of three inflammatory mediators, *mmp9*, *il-1β* and *cxcl8*.

DSS exposure resulted in changes in expression that directly opposed the published data, in which an increased expression of all three inflammatory mediators was reported (Oehlers et al., 2012). These qPCRs were repeated to ensure this was not human error. The data collected suggested that DSS reduced inflammation in exposed larvae, demonstrated by dose-dependent decreases in *il-1β* and *cxcl8* expression. A possible explanation for this unexpected result is DSS toxicity. If cell death had occurred in DSS-exposed larvae, then lower expression levels could be expected. However, *rps29* expression was as expected and fish appeared healthy following DSS exposure. Additionally, *mmp9* demonstrated a dose-dependent increase in expression in the same larvae, as expected given the previous literature. This was not explored as part of this project as the primary aim was to establish a proinflammatory model for use in other experiments.

The second compound used to induce inflammation in this project was TNBS. In previous publications, TNBS has been demonstrated to increase all three of the inflammatory mediators assessed, as well as others (Oehlers et al., 2011; Oehlers et al., 2010). In the current project, TNBS was able to induce a proinflammatory effect in larvae, although this differed substantially between replicates. Furthermore, the only concentration able to induce these increases also resulted in toxicity, primarily evidenced by heart and yolk sac oedema. The inconsistency and toxicity associated with TNBS therefore prevented the use of this compound in further experiments.

The final compound, saponin, was used successfully to induce a reliable, significant inflammatory effect with a measurable readout. The expression of *mmp9*, *il-1β* and *cxcl8* were significantly upregulated in larvae exposed to the maximum tolerable concentration of saponin for 48-hours.

This data aligns with previous publications, where increases in *il-1β* and *mmp9* have also been reported (López Nadal et al., 2018). The doses used in this paper were much higher than those used in this thesis; these doses resulted in the death of zebrafish during this project. Furthermore, no change in *cxcl8* expression in response to saponin was reported by López Nadal et al (2018), an effect that was seen in the current project. This model was hoped to be used as a readout for the anti-inflammatory activity of the novel compounds tested as a part of this project. However, compound availability and the coronavirus pandemic meant that this did not go ahead as planned. The second reason for developing such methodology was to assess the susceptibility of PD mutant zebrafish to external inflammatory stress. This was successfully done in *acmsd*$^{-/-}$ mutant larvae, which can be found in chapter 4.

6.4 Conclusion

Targeting inflammation in *gch1*$^{-/-}$ mutant zebrafish both genetically and pharmacologically was unable to rescue the phenotype of these fish, suggesting that their ultimate premature death is the result of more than just inflammation alone. Whilst these mutants display an inflammatory phenotype, including microglial-specific effects, reducing the number of these inflammatory cells had no effect in these larvae.

Since these mutants were unaffected by known anti-inflammatory compounds, they were not a good model for assessing the anti-inflammatory effect of novel compounds as planned. New method development lead to the identification of saponin as a reliable inducer of inflammation in larvae. Zebrafish exposed to saponin developed an inflammatory phenotype with a simple qPCR readout, enabling this model to be used in further study. Whilst this was never combined with novel compound testing, this model was successfully used in other PD mutant zebrafish to gain more information about their overall phenotype.

7 Concluding Remarks, Limitations and Future Work

This thesis has explored the role of two Parkinson's disease risk genes that also have a role in inflammation using the zebrafish as a model system. Whilst zebrafish *lrrk2* mutants have been published previously, the characterisation of the *acmsd* mutant in this thesis represents the first loss-of-function *acmsd* vertebrate model in the field. Interestingly, a loss of either *lrrk2* or *acmsd* did not result in phenotypic changes in the zebrafish, contrasting what was expected given their key biological roles. Despite stressing both mutants with external triggers, including neurotoxic, inflammatory and hepatotoxic compounds, the induction of a phenotype in either knockout was not observed. Whilst a possible explanation for this in *acmsd* mutants was identified, the upregulation of a compensatory pathway, the absence of effect in *lrrk2* mutants was not explored. This thesis also outlined how targeting inflammation in PD-relevant zebrafish mutants that are known to possess an inflammatory phenotype was unable to rescue their phenotype.

An exciting outcome of this thesis was the development of novel *lrrk2* lines that recapitulate mutations seen in human cases of *LRRK2*-linked PD. Whilst these were unable to be characterised during the time restraints of this PhD, these new lines afford an opportunity to potentially build a new PhD project and study PD in zebrafish in a more relevant way.

The work presented here alongside that published in the literature leaves a number of key unanswered questions. Is the upregulation of the neuroprotective pathway observed in *acmsd* mutant zebrafish also upregulated in other animal models of *acmsd* deficiency, or indeed in humans with SNPs in *ACMSD*? What additional stressors may be required in this line to induce a phenotype or are zebrafish able to indefinitely compensate via this mechanism? Why do small changes in *acmsd* in humans alter the risk of PD but relatively huge changes (i.e. a complete loss of activity) seem to have no effect in zebrafish? What is happening in the *lrrk2*$^{-/-}$ mutant line to overcome the effect of the DNA mutation? Do the newly generated *lrrk2* lines recapitulate human PD? What is driving the phenotype of the *gch1* line, if not inflammation?

Whilst the data presented in this thesis may suggest that inflammation is not relevant in *acmsd*, *lrrk2* or *gch1* – linked PD, it more likely reflects the downfalls of zebrafish as a model or the limited methodologies used. Further stressors may be able to induce a phenotype in *acmsd* and *lrrk2* mutant zebrafish, identifying their "second hit" required for disease. Compounds used for external stimulation of these lines were chosen using knowledge of gene function, expression information and their relevance to PD, however, the number of possible stressors is endless.

Similarly, whilst the anti-inflammatory compounds assessed in the *gch1* line suggest that inflammation is unlikely to be the key driving force of their phenotype, only a handful of compounds were tested and only gross phenotypes used as a readout. It would be interesting to establish specific inflammatory readouts in this line to use to assess the effect of these compounds. This was attempted using immunohistochemistry during the first year of this project, although no successful targets were identified (data not presented). Research using an *in vivo* model enables the best representation of the human condition. Zebrafish, despite their limitations, are useful in that they are an easily manipulatable whole animal system. However, zebrafish have a number of key differences to humans in both their genetics and interplay between biological systems. For example, the compensatory upregulation of kynurenic acid seen in the *acmsd* mutant zebrafish may not occur in humans with reduced ACMSD activity. Furthermore, whilst loss-of-function mutants are useful in understanding the basic biology of gene function, they do not represent the human condition, where a complete loss of gene function is rare. It will, therefore, be interesting to see the results of the new zebrafish lines that are more relevant to disease.

It is also imperative to remember that each variant typically exerts only a small effect on the overall risk of developing PD. Additional triggers or combinations of genetic variants are often required for PD to manifest and identification of these would be useful in identifying those most at risk of disease. Studying each gene independently has limitations in this. However, further research into *ACMSD* and *LRRK2* will hopefully identify specific pathology resulting from alterations to these enzymes, leading to targeted treatment that is more likely to work on an individual basis. For this personalised approach, genetic testing would need to be conducted, possibly before the development of PD symptoms, an unrealistic task at present.

The overarching hypotheses tested during this project are outlined below, along with justification of their acceptance / rejection based on the data presented in this thesis.

1. Zebrafish carrying functionally inactivating mutations in PD risk genes that can also be linked to inflammation will display a PD-relevant phenotype.

Rejected: Neither *acmsd*$^{-/-}$ or *lrrk2*$^{-/-}$ mutant zebrafish demonstrated a PD-relevant phenotype in terms of abnormalities of movement, changes to dopaminergic neurons or susceptibility to neurotoxic compounds.

2. Zebrafish carrying functionally inactivating mutations in PD risk genes that can also be linked to inflammation will display an inflammatory phenotype.

Rejected: Neither *acmsd*$^{-/-}$ or *lrrk2*$^{-/-}$ mutant zebrafish displayed an inflammatory phenotype. This was studied more in-depth in *acmsd*$^{-/-}$ mutants.

3. Zebrafish carrying functionally inactivating mutations in PD risk genes will be more susceptible to additional, external triggers.

Rejected: *acmsd*$^{-/-}$ mutant zebrafish were no more susceptible to neurotoxicity (MPP+), inflammation (saponin) or hepatotoxicity (paracetamol) than wildtype zebrafish. *lrrk2*$^{-/-}$ mutant zebrafish were no more susceptible to MPP+.

4. Inhibiting neuroinflammation, either pharmacologically or otherwise, will be able to, at least partially, rescue the phenotype of PD mutant zebrafish.

Rejected: g*ch1*$^{-/-}$ mutant zebrafish were primarily used to test this hypothesis due to their known inflammatory phenotype. However, treatment with anti-inflammatory compounds (known and novel) or inhibition of the primary inflammatory cells of the brain was unable to rescue the mutant phenotype.

Despite rejecting all of the proposed hypotheses outlined at the start of this thesis based only on the data presented, further experiments are necessary to fully and confidently reject these. Only some avenues for each question were explored, as discussed elsewhere. However, all aims of this thesis were achieved:

Objective 1: To characterise novel zebrafish models of PD. Aim one of this thesis was achieved by the full characterisation of two zebrafish lines with knockout mutations in PD relevant genes*; lrrk2*$^{-/-}$ and *acmsd*$^{-/-}$. The *acmsd* line underwent a more in-depth characterisation than *lrrk2* due to issues identified with the *lrrk2* line during this project. New, PD-relevant *lrrk2* lines were also created as a part of this project, although these have not yet been characterised due to their young age.

Objective 2: To determine whether inflammation, particularly that mediated by microglia, drives the phenotype of these models. Aim two of this thesis was partially achieved during this project. Microglial characterisation in both mutants was assessed, and baseline inflammation and susceptibility to external inflammation was also evaluated in the *acmsd* line. Microglial contribution to phenotype was explored using the *gch1* mutant, although some issues were identified with the methodology used to inhibit microglia in this model.

Objective 3: To target inflammation pharmacologically using known anti-inflammatory drugs, bile-acids and novel compounds. Aim three was achieved by exposing zebrafish mutants to a number of anti-inflammatory compounds, primarily in the *gch1* line. None of the tested compounds were seen to have an effect on the overall survival of this line.

Objective 4: Develop new, more relevant PD zebrafish lines. Aim four of this project was achieved by the creation of four new *lrrk2* zebrafish lines that harbour mutations in the *lrrk2* gene that recapitulate pathogenic mutations identified in human PD.

8 References

Aasly, J. O., Vilariño-Güell, C., Dachsel, J. C., Webber, P. J., West, A. B., Haugarvoll, K., Johansen, K. K., Toft, M., Nutt, J. G., Payami, H., Kachergus, J. M., Lincoln, S. J., Felic, A., Wider, C., Soto-Ortolaza, A. I., Cobb, S. A., White, L. R., Ross, O. A., & Farrer, M. J. (2010). Novel pathogenic LRRK2 p.Asn1437His substitution in familial Parkinson's disease. *Mov Disord*, *25*(13), 2156-2163. https://doi.org/10.1002/mds.23265

Abdelkader, N. F., Safar, M. M., & Salem, H. A. (2016). Ursodeoxycholic Acid Ameliorates Apoptotic Cascade in the Rotenone Model of Parkinson's Disease: Modulation of Mitochondrial Perturbations. *Mol Neurobiol*, *53*(2), 810-817. https://doi.org/10.1007/s12035-014-9043-8

Adams-Carr, K. L., Bestwick, J. P., Shribman, S., Lees, A., Schrag, A., & Noyce, A. J. (2016). Constipation preceding Parkinson's disease: a systematic review and meta-analysis. *Journal of Neurology, Neurosurgery & Psychiatry*, *87*(7), 710-716. https://doi.org/10.1136/jnnp-2015-311680

Adams, J. R., van Netten, H., Schulzer, M., Mak, E., McKenzie, J., Strongosky, A., Sossi, V., Ruth, T. J., Lee, C. S., Farrer, M., Gasser, T., Uitti, R. J., Calne, D. B., Wszolek, Z. K., & Stoessl, A. J. (2005). PET in LRRK2 mutations: comparison to sporadic Parkinson's disease and evidence for presymptomatic compensation. *Brain*, *128*(Pt 12), 2777-2785. https://doi.org/10.1093/brain/awh607

Adikusuma, F., Piltz, S., Corbett, M. A., Turvey, M., McColl, S. R., Helbig, K. J., Beard, M. R., Hughes, J., Pomerantz, R. T., & Thomas, P. Q. (2018). Large deletions induced by Cas9 cleavage. *Nature*, *560*(7717), E8-E9. https://doi.org/10.1038/s41586-018-0380-z

Agalliu, I., San Luciano, M., Mirelman, A., Giladi, N., Waro, B., Aasly, J., Inzelberg, R., Hassin-Baer, S., Friedman, E., Ruiz-Martinez, J., Marti-Masso, J. F., Orr-Urtreger, A., Bressman, S., & Saunders-Pullman, R. (2015). Higher frequency of certain cancers in LRRK2 G2019S mutation carriers with Parkinson disease: a pooled analysis. *JAMA Neurol*, *72*(1), 58-65. https://doi.org/10.1001/jamaneurol.2014.1973

Airas, L., Nylund, M., & Rissanen, E. (2018). Evaluation of Microglial Activation in Multiple Sclerosis Patients Using Positron Emission Tomography [Mini Review]. *Frontiers in Neurology*, *9*(181). https://doi.org/10.3389/fneur.2018.00181

Akagi, T., Matsumura, Y., Yasui, M., Minami, E., Inoue, H., Masuda, T., Tozaki-Saitoh, H., Tamura, T., Mizumura, K., Tsuda, M., Kiyama, H., & Inoue, K. (2014). Interferon regulatory factor 8 expressed in microglia contributes to tactile allodynia induced by repeated cold stress in rodents. *J Pharmacol Sci*, *126*(2), 172-176. https://doi.org/10.1254/jphs.14143sc

Akundi, R. S., Huang, Z., Eason, J., Pandya, J. D., Zhi, L., Cass, W. A., Sullivan, P. G., & Büeler, H. (2011). Increased Mitochondrial Calcium Sensitivity and Abnormal Expression of Innate Immunity Genes Precede Dopaminergic Defects in Pink1-Deficient Mice. *PLoS ONE*, *6*(1), e16038. https://doi.org/10.1371/journal.pone.0016038

Alegre-Abarrategui, J., Christian, H., Lufino, M. M., Mutihac, R., Venda, L. L., Ansorge, O., & Wade-Martins, R. (2009). LRRK2 regulates autophagic activity and localizes to specific membrane microdomains in a novel human genomic reporter cellular model. *Hum Mol Genet*, *18*(21), 4022-4034. https://doi.org/10.1093/hmg/ddp346

Andres-Mateos, E., Mejias, R., Sasaki, M., Li, X., Lin, B. M., Biskup, S., Zhang, L., Banerjee, R., Thomas, B., Yang, L., Liu, G., Beal, M. F., Huso, D. L., Dawson, T. M., & Dawson, V. L. (2009). Unexpected lack of hypersensitivity in LRRK2 knock-out mice to MPTP (1-methyl-4-phenyl-1,2,3,6-tetrahydropyridine). *J Neurosci*, *29*(50), 15846-15850. https://doi.org/10.1523/jneurosci.4357-09.2009

Arbez, N., He, X., Huang, Y., Ren, M., Liang, Y., Nucifora, F. C., Wang, X., Pei, Z., Tessarolo, L., Smith, W. W., & Ross, C. A. (2020). G2019S-LRRK2 mutation enhances MPTP-linked Parkinsonism in mice. *Hum Mol Genet*, *29*(4), 580-590. https://doi.org/10.1093/hmg/ddz271

Armstrong, G. A. B., Liao, M., You, Z., Lissouba, A., Chen, B. E., & Drapeau, P. (2016). Homology Directed Knockin of Point Mutations in the Zebrafish tardbp and fus Genes in ALS Using the CRISPR/Cas9 System. *PLoS ONE*, *11*(3), e0150188. https://doi.org/10.1371/journal.pone.0150188

Ashley, A. K., Hinds, A. I., Hanneman, W. H., Tjalkens, R. B., & Legare, M. E. (2016). DJ-1 mutation decreases astroglial release of inflammatory mediators. *NeuroToxicology*, *52*, 198-203. https://doi.org/https://doi.org/10.1016/j.neuro.2015.12.007

Bandrés-Ciga, S., Price, T. R., Barrero, F. J., Escamilla-Sevilla, F., Pelegrina, J., Arepalli, S., Hernández, D., Gutiérrez, B., Cervilla, J., Rivera, M., Rivera, A., Ding, J. H., Vives, F., Nalls, M., Singleton, A., & Durán, R. (2016). Genome-wide assessment of Parkinson's disease in a Southern Spanish population. *Neurobiol Aging*, *45*, 213.e213-213.e219. https://doi.org/10.1016/j.neurobiolaging.2016.06.001

Baptista, M. A., Dave, K. D., Frasier, M. A., Sherer, T. B., Greeley, M., Beck, M. J., Varsho, J. S., Parker, G. A., Moore, C., Churchill, M. J., Meshul, C. K., & Fiske, B. K. (2013). Loss of leucine-rich repeat kinase 2 (LRRK2) in rats leads to progressive abnormal phenotypes in peripheral organs. *PLoS ONE*, *8*(11), e80705. https://doi.org/10.1371/journal.pone.0080705

Berndsen, K., Lis, P., Yeshaw, W. M., Wawro, P. S., Nirujogi, R. S., Wightman, M., Macartney, T., Dorward, M., Knebel, A., Tonelli, F., Pfeffer, S. R., & Alessi, D. R. (2019). PPM1H phosphatase counteracts LRRK2 signaling by selectively dephosphorylating Rab proteins. *Elife*, *8*. https://doi.org/10.7554/eLife.50416

Bertrand, J. Y., Kim, A. D., Violette, E. P., Stachura, D. L., Cisson, J. L., & Traver, D. (2007). Definitive hematopoiesis initiates through a committed erythromyeloid progenitor in the zebrafish embryo. *Development*, *134*(23), 4147-4156. https://doi.org/10.1242/dev.012385

Biskup, S., Moore, D. J., Celsi, F., Higashi, S., West, A. B., Andrabi, S. A., Kurkinen, K., Yu, S. W., Savitt, J. M., Waldvogel, H. J., Faull, R. L., Emson, P. C., Torp, R., Ottersen, O. P., Dawson, T. M., & Dawson, V. L. (2006). Localization of LRRK2 to membranous and vesicular structures in mammalian brain. *Ann Neurol*, *60*(5), 557-569. https://doi.org/10.1002/ana.21019

Biskup, S., Moore, D. J., Rea, A., Lorenz-Deperieux, B., Coombes, C. E., Dawson, V. L., Dawson, T. M., & West, A. B. (2007). Dynamic and redundant regulation of LRRK2 and LRRK1 expression. *BMC Neurosci*, *8*, 102. https://doi.org/10.1186/1471-2202-8-102

Blauwendraat, C., Reed, X., Kia, D. A., Gan-Or, Z., Lesage, S., Pihlstrøm, L., Guerreiro, R., Gibbs, J. R., Sabir, M., Ahmed, S., Ding, J., Alcalay, R. N., Hassin-Baer, S., Pittman, A. M., Brooks, J., Edsall, C., Hernandez, D. G., Chung, S. J., Goldwurm, S., Toft, M., Schulte, C., Bras, J., Wood, N. W., Brice, A., Morris, H. R., Scholz, S. W., Nalls, M. A., Singleton, A. B., & Cookson, M. R. (2018). Frequency of Loss of Function Variants in LRRK2 in Parkinson Disease. *JAMA Neurol*, *75*(11), 1416-1422. https://doi.org/10.1001/jamaneurol.2018.1885

Bliederhaeuser, C., Zondler, L., Grozdanov, V., Ruf, W. P., Brenner, D., Melrose, H. L., Bauer, P., Ludolph, A. C., Gillardon, F., Kassubek, J., Weishaupt, J. H., & Danzer, K. M. (2016). LRRK2 contributes to monocyte dysregulation in Parkinson's disease. *Acta Neuropathol Commun*, *4*(1), 123. https://doi.org/10.1186/s40478-016-0396-2

Block, M. L., & Hong, J. S. (2005). Microglia and inflammation-mediated neurodegeneration: multiple triggers with a common mechanism. *Prog Neurobiol*, *76*(2), 77-98. https://doi.org/10.1016/j.pneurobio.2005.06.004

Bonifati, V., Oostra, B. A., & Heutink, P. (2004). Linking DJ-1 to neurodegeneration offers novel insights for understanding the pathogenesis of Parkinson's disease. *Journal of Molecular Medicine*, *82*(3), 163-174. https://doi.org/10.1007/s00109-003-0512-1

Bonifati, V., Rizzu, P., van Baren, M. J., Schaap, O., Breedveld, G. J., Krieger, E., Dekker, M. C. J., Squitieri, F., Ibanez, P., Joosse, M., van Dongen, J. W., Vanacore, N., van Swieten, J. C., Brice, A., Meco, G., van Duijn, C. M., Oostra, B. A., & Heutink, P. (2003). Mutations in the DJ-1 Gene Associated with Autosomal Recessive Early-Onset Parkinsonism. *Science*, *299*(5604), 256-259. https://doi.org/10.1126/science.1077209

Bower, J. H., Maraganore, D. M., Peterson, B. J., Ahlskog, J. E., & Rocca, W. A. (2006). Immunologic diseases, anti-inflammatory drugs, and Parkinson disease: A case-control study. *Neurology*, *67*(3), 494-496. https://doi.org/10.1212/01.wnl.0000227906.99570.cc

Bozic, M., & Valdivielso, J. M. (2015). The potential of targeting NMDA receptors outside the CNS. *Expert Opin Ther Targets*, *19*(3), 399-413. https://doi.org/10.1517/14728222.2014.983900

Braak, H., de Vos, R. A., Bohl, J., & Del Tredici, K. (2006). Gastric alpha-synuclein immunoreactive inclusions in Meissner's and Auerbach's plexuses in cases staged for Parkinson's disease-related brain pathology. *Neurosci Lett*, *396*(1), 67-72. https://doi.org/10.1016/j.neulet.2005.11.012

Braak, H., Ghebremedhin, E., Rub, U., Bratzke, H., & Del Tredici, K. (2004). Stages in the development of Parkinson's disease-related pathology. *Cell Tissue Res*, *318*(1), 121-134. https://doi.org/10.1007/s00441-004-0956-9

Braidy, N., Grant, R., Adams, S., Brew, B. J., & Guillemin, G. J. (2009). Mechanism for quinolinic acid cytotoxicity in human astrocytes and neurons. *Neurotox Res*, *16*(1), 77-86. https://doi.org/10.1007/s12640-009-9051-z

Brecht, S., Waetzig, V., Hidding, U., Hanisch, U. K., Walther, M., Herdegen, T., & Neiss, W. F. (2009). FK506 protects against various immune responses and secondary degeneration following cerebral ischemia. *Anat Rec (Hoboken)*, *292*(12), 1993-2001. https://doi.org/10.1002/ar.20994

Brodacki, B., Staszewski, J., Toczylowska, B., Kozlowska, E., Drela, N., Chalimoniuk, M., & Stepien, A. (2008). Serum interleukin (IL-2, IL-10, IL-6, IL-4), TNFalpha, and INFgamma concentrations are elevated in patients with atypical and idiopathic parkinsonism. *Neurosci Lett*, *441*(2), 158-162. https://doi.org/10.1016/j.neulet.2008.06.040

Brommage, R., Liu, J., Hansen, G. M., Kirkpatrick, L. L., Potter, D. G., Sands, A. T., Zambrowicz, B., Powell, D. R., & Vogel, P. (2014). High-throughput screening of mouse gene knockouts identifies established and novel skeletal phenotypes. *Bone Res*, *2*, 14034. https://doi.org/10.1038/boneres.2014.34

Camacho-Soto, A., Gross, A., Searles Nielsen, S., Dey, N., & Racette, B. A. (2018). Inflammatory bowel disease and risk of Parkinson's disease in Medicare beneficiaries. *Parkinsonism Relat Disord*, *50*, 23-28. https://doi.org/10.1016/j.parkreldis.2018.02.008

Cang, C., Aranda, K., Seo, Y. J., Gasnier, B., & Ren, D. (2015). TMEM175 Is an Organelle K(+) Channel Regulating Lysosomal Function. *Cell*, *162*(5), 1101-1112. https://doi.org/10.1016/j.cell.2015.08.002

Cao, Z., Xia, Z., Zhou, Y., Yang, X., Hao, H., Peng, N., Liu, S., & Zhu, Y. (2016). Methylcrotonoyl-CoA carboxylase 1 potentiates RLR-induced NF-κB signaling by targeting MAVS complex. *Scientific Reports*, *6*(1), 33557. https://doi.org/10.1038/srep33557

Cardoso, F. L., Kittel, A., Veszelka, S., Palmela, I., Tóth, A., Brites, D., Deli, M. A., & Brito, M. A. (2012). Exposure to lipopolysaccharide and/or unconjugated bilirubin impair the integrity and function of brain microvascular endothelial cells. *PLoS ONE*, *7*(5), e35919. https://doi.org/10.1371/journal.pone.0035919

Carrion, M. D. P., Marsicano, S., Daniele, F., Marte, A., Pischedda, F., Di Cairano, E., Piovesana, E., von Zweydorf, F., Kremmer, E., Gloeckner, C. J., Onofri, F., Perego, C., & Piccoli, G. (2017). The LRRK2 G2385R variant is a partial loss-of-function mutation that affects synaptic vesicle trafficking through altered protein interactions. *Sci Rep*, *7*(1), 5377. https://doi.org/10.1038/s41598-017-05760-9

Cassar, S., Breidenbach, L., Olson, A., Huang, X., Britton, H., Woody, C., Sancheti, P., Stolarik, D., Wicke, K., Hempel, K., & LeRoy, B. (2017). Measuring drug absorption improves interpretation of behavioral responses in a larval zebrafish locomotor assay for predicting seizure liability. *J Pharmacol Toxicol Methods*, *88*(Pt 1), 56-63. https://doi.org/10.1016/j.vascn.2017.07.002

Castaño, A., Herrera, A. J., Cano, J., & Machado, A. (1998). Lipopolysaccharide intranigral injection induces inflammatory reaction and damage in nigrostriatal dopaminergic system. *J Neurochem*, *70*(4), 1584-1592. https://doi.org/10.1046/j.1471-4159.1998.70041584.x

Chang, D., Nalls, M. A., Hallgrímsdóttir, I. B., Hunkapiller, J., van der Brug, M., Cai, F., Kerchner, G. A., Ayalon, G., Bingol, B., Sheng, M., Hinds, D., Behrens, T. W., Singleton, A. B., Bhangale, T. R., Graham, R. R., International Parkinson's Disease Genomics, C., & andMe Research, T. (2017). A meta-analysis of genome-wide association studies identifies 17 new Parkinson's disease risk loci. *Nature Genetics*, *49*(10), 1511-1516. https://doi.org/10.1038/ng.3955

Chang, K.-H., Chen, C.-M., Chen, Y.-C., Fung, H.-C., & Wu, Y.-R. (2019). Polymorphisms of ACMSD-TMEM163, MCCC1, and BCKDK-STX1B Are Not Associated with

Parkinson’s Disease in Taiwan. *Parkinson’s Disease*, *2019*, 3489638. https://doi.org/10.1155/2019/3489638

Chen, H., Zhang, S. M., Hernán, M. A., Schwarzschild, M. A., Willett, W. C., Colditz, G. A., Speizer, F. E., & Ascherio, A. (2003). Nonsteroidal anti-inflammatory drugs and the risk of Parkinson disease. *Arch Neurol*, *60*(8), 1059-1064. https://doi.org/10.1001/archneur.60.8.1059

Chen, H., Zhao, E. J., Zhang, W., Lu, Y., Liu, R., Huang, X., Ciesielski-Jones, A. J., Justice, M. A., Cousins, D. S., & Peddada, S. (2015). Meta-analyses on prevalence of selected Parkinson’s nonmotor symptoms before and after diagnosis. *Translational Neurodegeneration*, *4*(1), 1. https://doi.org/10.1186/2047-9158-4-1

Chen, L., Zhang, S., Liu, Y., Hong, H., Wang, H., Zheng, Y., Zhou, H., Chen, J., Xian, W., He, Y., Li, J., Liu, Z., Pei, Z., & Zeng, J. (2011). LRRK2 R1398H polymorphism is associated with decreased risk of Parkinson's disease in a Han Chinese population. *Parkinsonism Relat Disord*, *17*(4), 291-292. https://doi.org/10.1016/j.parkreldis.2010.11.012

Chia, K., Mazzolini, J., Mione, M., & Sieger, D. (2018). Tumor initiating cells induce Cxcr4-mediated infiltration of pro-tumoral macrophages into the brain. *Elife*, *7*. https://doi.org/10.7554/eLife.31918

Chumanevich, A. A., Witalison, E. E., Chaparala, A., Chumanevich, A., Nagarkatti, P., Nagarkatti, M., & Hofseth, L. J. (2016). Repurposing the anti-malarial drug, quinacrine: new anti-colitis properties. *Oncotarget*, *7*(33), 52928-52939. https://doi.org/10.18632/oncotarget.10608

Chung, S. J., Armasu, S. M., Biernacka, J. M., Lesnick, T. G., Rider, D. N., Lincoln, S. J., Ortolaza, A. I., Farrer, M. J., Cunningham, J. M., Rocca, W. A., & Maraganore, D. M. (2011). Common variants in PARK loci and related genes and Parkinson's disease. *Mov Disord*, *26*(2), 280-288. https://doi.org/10.1002/mds.23376

Cicchetti, F., Brownell, A. L., Williams, K., Chen, Y. I., Livni, E., & Isacson, O. (2002). Neuroinflammation of the nigrostriatal pathway during progressive 6-OHDA dopamine degeneration in rats monitored by immunohistochemistry and PET imaging. *Eur J Neurosci*, *15*(6), 991-998. https://doi.org/10.1046/j.1460-9568.2002.01938.x

Civiero, L., Vancraenenbroeck, R., Belluzzi, E., Beilina, A., Lobbestael, E., Reyniers, L., Gao, F., Micetic, I., De Maeyer, M., Bubacco, L., Baekelandt, V., Cookson, M. R., Greggio, E., & Taymans, J. M. (2012). Biochemical characterization of highly purified leucine-rich repeat kinases 1 and 2 demonstrates formation of homodimers. *PLoS ONE*, *7*(8), e43472. https://doi.org/10.1371/journal.pone.0043472

Cogburn, L. A., Trakooljul, N., Chen, C., Huang, H., Wu, C. H., Carré, W., Wang, X., & White, H. B., 3rd. (2018). Transcriptional profiling of liver during the critical embryo-to-hatchling transition period in the chicken (Gallus gallus). *BMC Genomics*, *19*(1), 695. https://doi.org/10.1186/s12864-018-5080-4

Cook, D. A., Kannarkat, G. T., Cintron, A. F., Butkovich, L. M., Fraser, K. B., Chang, J., Grigoryan, N., Factor, S. A., West, A. B., Boss, J. M., & Tansey, M. G. (2017). LRRK2 levels in immune cells are increased in Parkinson's disease. *NPJ Parkinsons Dis*, *3*, 11. https://doi.org/10.1038/s41531-017-0010-8

Cornes, B. K., Khor, C. C., Nongpiur, M. E., Xu, L., Tay, W.-T., Zheng, Y., Lavanya, R., Li, Y., Wu, R., Sim, X., Wang, Y.-X., Chen, P., Teo, Y. Y., Chia, K.-S., Seielstad, M., Liu, J., Hibberd, M. L., Cheng, C.-Y., Saw, S.-M., Tai, E.-S., Jonas, J. B., Vithana, E. N., Wong, T. Y., & Aung, T. (2011). Identification of four novel variants that influence central corneal thickness in multi-ethnic Asian populations. *Human Molecular Genetics*, *21*(2), 437-445. https://doi.org/10.1093/hmg/ddr463

Cornet, C., Calzolari, S., Miñana-Prieto, R., Dyballa, S., van Doornmalen, E., Rutjes, H., Savy, T., D'Amico, D., & Terriente, J. (2017). ZeGlobalTox: An Innovative Approach to Address Organ Drug Toxicity Using Zebrafish. *Int J Mol Sci*, *18*(4). https://doi.org/10.3390/ijms18040864

Cosme, M. M., Lister, A. L., & Van Der Kraak, G. (2015). Inhibition of spawning in zebrafish (Danio rerio): Adverse outcome pathways of quinacrine and ethinylestradiol. *Gen Comp Endocrinol*, *219*, 89-101. https://doi.org/10.1016/j.ygcen.2015.01.013

Cox, J. A., Kucenas, S., & Voigt, M. M. (2005). Molecular characterization and embryonic expression of the family of N-methyl-D-aspartate receptor subunit genes in the zebrafish. *Dev Dyn*, *234*(3), 756-766. https://doi.org/10.1002/dvdy.20532

Croisier, E., Moran, L. B., Dexter, D. T., Pearce, R. K. B., & Graeber, M. B. (2005). Microglial inflammation in the parkinsonian substantia nigra: relationship to alpha-synuclein deposition. *Journal of Neuroinflammation*, *2*(1), 14. https://doi.org/10.1186/1742-2094-2-14

Cunningham, C., Campion, S., Lunnon, K., Murray, C. L., Woods, J. F., Deacon, R. M., Rawlins, J. N., & Perry, V. H. (2009). Systemic inflammation induces acute behavioral and cognitive changes and accelerates neurodegenerative disease. *Biol Psychiatry*, *65*(4), 304-312. https://doi.org/10.1016/j.biopsych.2008.07.024

da Cunha, A., Jefferson, J. A., Jackson, R. W., & Vitković, L. (1993). Glial cell-specific mechanisms of TGF-beta 1 induction by IL-1 in cerebral cortex. *J Neuroimmunol*, *42*(1), 71-85. https://doi.org/10.1016/0165-5728(93)90214-j

Dachsel, J. C., Nishioka, K., Vilariño-Güell, C., Lincoln, S. J., Soto-Ortolaza, A. I., Kachergus, J., Hinkle, K. M., Heckman, M. G., Jasinska-Myga, B., Taylor, J. P., Dickson, D. W., Gibson, R. A., Hentati, F., Ross, O. A., & Farrer, M. J. (2010). Heterodimerization of Lrrk1-Lrrk2: Implications for LRRK2-associated Parkinson disease. *Mech Ageing Dev*, *131*(3), 210-214. https://doi.org/10.1016/j.mad.2010.01.009

Daher, J. P., Abdelmotilib, H. A., Hu, X., Volpicelli-Daley, L. A., Moehle, M. S., Fraser, K. B., Needle, E., Chen, Y., Steyn, S. J., Galatsis, P., Hirst, W. D., & West, A. B. (2015). Leucine-rich Repeat Kinase 2 (LRRK2) Pharmacological Inhibition Abates α-Synuclein Gene-induced Neurodegeneration. *J Biol Chem*, *290*(32), 19433-19444. https://doi.org/10.1074/jbc.M115.660001

Daher, J. P., Volpicelli-Daley, L. A., Blackburn, J. P., Moehle, M. S., & West, A. B. (2014). Abrogation of α-synuclein-mediated dopaminergic neurodegeneration in LRRK2-deficient rats. *Proc Natl Acad Sci U S A*, *111*(25), 9289-9294. https://doi.org/10.1073/pnas.1403215111

Das, A., Arifuzzaman, S., Kim, S. H., Lee, Y. S., Jung, K. H., & Chai, Y. G. (2017). FTY720 (fingolimod) regulates key target genes essential for inflammation in microglial cells as defined by high-resolution mRNA sequencing. *Neuropharmacology*, *119*, 1-14. https://doi.org/10.1016/j.neuropharm.2017.03.034

de Aguiar Vallim, T. Q., Tarling, E. J., & Edwards, P. A. (2013). Pleiotropic roles of bile acids in metabolism. *Cell Metab*, *17*(5), 657-669. https://doi.org/10.1016/j.cmet.2013.03.013

de Carvalho, L. P., Bochet, P., & Rossier, J. (1996). The endogenous agonist quinolinic acid and the non endogenous homoquinolinic acid discriminate between NMDAR2 receptor subunits. *Neurochem Int*, *28*(4), 445-452. https://doi.org/10.1016/0197-0186(95)00091-7

de Leseleuc, L., Orlova, M., Cobat, A., Girard, M., Huong, N. T., Ba, N. N., Thuc, N. V., Truman, R., Spencer, J. S., Adams, L., Thai, V. H., Alcais, A., & Schurr, E. (2013). PARK2 mediates interleukin 6 and monocyte chemoattractant protein 1 production by human macrophages. *PLoS Negl Trop Dis*, *7*(1), e2015. https://doi.org/10.1371/journal.pntd.0002015

Denovan-Wright, E. M., Pierce, M., Sharma, M. K., & Wright, J. M. (2000). cDNA sequence and tissue-specific expression of a basic liver-type fatty acid binding protein in adult zebrafish (Danio rerio)11Genbank Accession number: AF254642. *Biochimica et Biophysica Acta (BBA) - Gene Structure and Expression*, *1492*(1), 227-232. https://doi.org/https://doi.org/10.1016/S0167-4781(00)00102-0

Devos, D., Lebouvier, T., Lardeux, B., Biraud, M., Rouaud, T., Pouclet, H., Coron, E., Bruley des Varannes, S., Naveilhan, P., Nguyen, J.-M., Neunlist, M., & Derkinderen, P. (2013). Colonic inflammation in Parkinson's disease. *Neurobiology of Disease*, *50*, 42-48. https://doi.org/https://doi.org/10.1016/j.nbd.2012.09.007

Di Fonzo, A., Rohé, C. F., Ferreira, J., Chien, H. F., Vacca, L., Stocchi, F., Guedes, L., Fabrizio, E., Manfredi, M., Vanacore, N., Goldwurm, S., Breedveld, G., Sampaio, C., Meco, G., Barbosa, E., Oostra, B. A., & Bonifati, V. (2005). A frequent LRRK2 gene mutation associated with autosomal dominant Parkinson's disease. *Lancet*, *365*(9457), 412-415. https://doi.org/10.1016/s0140-6736(05)17829-5

Di Maio, R., Hoffman, E. K., Rocha, E. M., Keeney, M. T., Sanders, L. H., De Miranda, B. R., Zharikov, A., Van Laar, A., Stepan, A. F., Lanz, T. A., Kofler, J. K., Burton, E. A., Alessi, D. R., Hastings, T. G., & Greenamyre, J. T. (2018). LRRK2 activation in idiopathic Parkinson's disease. *Sci Transl Med*, *10*(451). https://doi.org/10.1126/scitranslmed.aar5429

Diao, J., Burre, J., Vivona, S., Cipriano, D. J., Sharma, M., Kyoung, M., Sudhof, T. C., & Brunger, A. T. (2013). Native alpha-synuclein induces clustering of synaptic-vesicle mimics via binding to phospholipids and synaptobrevin-2/VAMP2. *Elife*, *2*, e00592. https://doi.org/10.7554/eLife.00592

Dionísio, P. E. A., Oliveira, S. R., Amaral, J. S. J. D., & Rodrigues, C. M. P. (2019). Loss of Microglial Parkin Inhibits Necroptosis and Contributes to Neuroinflammation. *Molecular Neurobiology*, *56*(4), 2990-3004. https://doi.org/10.1007/s12035-018-1264-9

Dorsey, E. R., Constantinescu, R., Thompson, J. P., Biglan, K. M., Holloway, R. G., Kieburtz, K., Marshall, F. J., Ravina, B. M., Schifitto, G., Siderowf, A., & Tanner, C. M. (2007). Projected number of people with Parkinson disease in the most populous nations, 2005 through 2030. *Neurology*, *68*(5), 384-386. https://doi.org/10.1212/01.wnl.0000247740.47667.03

Driggers, P. H., Ennist, D. L., Gleason, S. L., Mak, W. H., Marks, M. S., Levi, B. Z., Flanagan, J. R., Appella, E., & Ozato, K. (1990). An interferon gamma-regulated protein that binds the interferon-inducible enhancer element of major histocompatibility complex class I genes. *Proc Natl Acad Sci U S A*, *87*(10), 3743-3747. https://doi.org/10.1073/pnas.87.10.3743

Du, T.-T., Wang, L., Duan, C.-L., Lu, L.-L., Zhang, J.-L., Gao, G., Qiu, X.-B., Wang, X.-M., & Yang, H. (2015). GBA deficiency promotes SNCA/α-synuclein accumulation through autophagic inhibition by inactivated PPP2A. *Autophagy*, *11*(10), 1803-1820. https://doi.org/10.1080/15548627.2015.1086055

Du, Y., Guo, Q., Shan, M., Wu, Y., Huang, S., Zhao, H., Hong, H., Yang, M., Yang, X., Ren, L., Peng, J., Sun, J., Zhou, H., Li, S., & Su, B. (2016). Spatial and Temporal Distribution of Dopaminergic Neurons during Development in Zebrafish. *Front Neuroanat*, *10*, 115. https://doi.org/10.3389/fnana.2016.00115

Duchen, M. R. (2012). Mitochondria, calcium-dependent neuronal death and neurodegenerative disease. *Pflugers Arch*, *464*(1), 111-121. https://doi.org/10.1007/s00424-012-1112-0

Dumitriu, A., Pacheco, C. D., Wilk, J. B., Strathearn, K. E., Latourelle, J. C., Goldwurm, S., Pezzoli, G., Rochet, J.-C., Lindquist, S., & Myers, R. H. (2011). Cyclin-G-associated kinase modifies α-synuclein expression levels and toxicity in Parkinson's disease: results from the GenePD Study. *Human Molecular Genetics*, *20*(8), 1478-1487. https://doi.org/10.1093/hmg/ddr026

Dzamko, N., Rowe, D. B., & Halliday, G. M. (2016). Increased peripheral inflammation in asymptomatic leucine-rich repeat kinase 2 mutation carriers. *Mov Disord*, *31*(6), 889-897. https://doi.org/10.1002/mds.26529

Earley, A. M., Graves, C. L., & Shiau, C. E. (2018). Critical Role for a Subset of Intestinal Macrophages in Shaping Gut Microbiota in Adult Zebrafish. *Cell Rep*, *25*(2), 424-436. https://doi.org/10.1016/j.celrep.2018.09.025

Ehrlich, J., Sankoff, D., & Nadeau, J. H. (1997). Synteny conservation and chromosome rearrangements during mammalian evolution. *Genetics*, *147*(1), 289-296. https://pubmed.ncbi.nlm.nih.gov/9286688

https://www.ncbi.nlm.nih.gov/pmc/articles/PMC1208112/

Elia, A. E., Lalli, S., Monsurrò, M. R., Sagnelli, A., Taiello, A. C., Reggiori, B., La Bella, V., Tedeschi, G., & Albanese, A. (2016). Tauroursodeoxycholic acid in the treatment of patients with amyotrophic lateral sclerosis. *Eur J Neurol*, *23*(1), 45-52. https://doi.org/10.1111/ene.12664

Elkabes, S., DiCicco-Bloom, E. M., & Black, I. B. (1996). Brain microglia/macrophages express neurotrophins that selectively regulate microglial proliferation and function. *J Neurosci*, *16*(8), 2508-2521. https://www.ncbi.nlm.nih.gov/pubmed/8786427

Elks, P. M., Loynes, C. A., & Renshaw, S. A. (2011). Measuring inflammatory cell migration in the zebrafish. *Methods Mol Biol*, *769*, 261-275. https://doi.org/10.1007/978-1-61779-207-6_18

Ellis, G. I., Zhi, L., Akundi, R., Büeler, H., & Marti, F. (2013). Mitochondrial and cytosolic roles of PINK1 shape induced regulatory T-cell development and function. *European Journal of Immunology*, *43*(12), 3355-3360. https://doi.org/https://doi.org/10.1002/eji.201343571

Emmrich, J. V., Hornik, T. C., Neher, J. J., & Brown, G. C. (2013). Rotenone induces neuronal death by microglial phagocytosis of neurons. *The FEBS Journal*, *280*(20), 5030-5038. https://doi.org/https://doi.org/10.1111/febs.12401

Erickson, M. A., Hansen, K., & Banks, W. A. (2012). Inflammation-induced dysfunction of the low-density lipoprotein receptor-related protein-1 at the blood–brain barrier: Protection by the antioxidant N-acetylcysteine. *Brain, Behavior, and Immunity*, *26*(7), 1085-1094. https://doi.org/https://doi.org/10.1016/j.bbi.2012.07.003

Farfel-Becker, T., Vitner, E. B., Pressey, S. N. R., Eilam, R., Cooper, J. D., & Futerman, A. H. (2011). Spatial and temporal correlation between neuron loss and neuroinflammation in a mouse model of neuronopathic Gaucher disease. *Human Molecular Genetics*, *20*(7), 1375-1386. https://doi.org/10.1093/hmg/ddr019

Feng, W., Wang, Y., Liu, Z. Q., Zhang, X., Han, R., Miao, Y. Z., & Qin, Z. H. (2017). Microglia activation contributes to quinolinic acid-induced neuronal excitotoxicity through TNF-α. *Apoptosis*, *22*(5), 696-709. https://doi.org/10.1007/s10495-017-1363-5

Ferrero, G., Gomez, E., Lyer, S., Rovira, M., Miserocchi, M., Langenau, D. M., Bertrand, J. Y., & Wittamer, V. (2020). The macrophage-expressed gene (mpeg) 1 identifies a subpopulation of B cells in the adult zebrafish. *J Leukoc Biol*, *107*(3), 431-443. https://doi.org/10.1002/jlb.1a1119-223r

Field, H. A., Ober, E. A., Roeser, T., & Stainier, D. Y. R. (2003). Formation of the digestive system in zebrafish. I. liver morphogenesis. *Developmental Biology*, *253*(2), 279-290. https://doi.org/https://doi.org/10.1016/S0012-1606(02)00017-9

Fujioka, S., Curry, S. E., Kennelly, K. D., Tacik, P., Heckman, M. G., Tsuboi, Y., Strongosky, A. J., van Gerpen, J. A., Uitti, R. J., Ross, O. A., Ikezu, T., & Wszolek, Z. K. (2017). Occurrence of Crohn's disease with Parkinson's disease. *Parkinsonism Relat Disord*, *37*, 116-117. https://doi.org/10.1016/j.parkreldis.2017.01.013

Fujita, H., Tanaka, J., Maeda, N., & Sakanaka, M. (1998). Adrenergic agonists suppress the proliferation of microglia through beta 2-adrenergic receptor. *Neurosci Lett*, *242*(1), 37-40. https://doi.org/10.1016/s0304-3940(98)00003-2

Fukuoka, S., Ishiguro, K., Yanagihara, K., Tanabe, A., Egashira, Y., Sanada, H., & Shibata, K. (2002). Identification and expression of a cDNA encoding human alpha-amino-beta-carboxymuconate-epsilon-semialdehyde decarboxylase (ACMSD). A key enzyme for the tryptophan-niacine pathway and "quinolinate hypothesis". *J Biol Chem*, *277*(38), 35162-35167. https://doi.org/10.1074/jbc.M200819200

Gagne, J. J., & Power, M. C. (2010). Anti-inflammatory drugs and risk of Parkinson disease: a meta-analysis. *Neurology*, *74*(12), 995-1002. https://doi.org/10.1212/WNL.0b013e3181d5a4a3

Galter, D., Westerlund, M., Carmine, A., Lindqvist, E., Sydow, O., & Olson, L. (2006). LRRK2 expression linked to dopamine-innervated areas. *Ann Neurol*, *59*(4), 714-719. https://doi.org/10.1002/ana.20808

Gao, H. M., Hong, J. S., Zhang, W., & Liu, B. (2003). Synergistic dopaminergic neurotoxicity of the pesticide rotenone and inflammogen lipopolysaccharide: relevance to the etiology of Parkinson's disease. *J Neurosci*, *23*(4), 1228-1236. https://doi.org/10.1523/jneurosci.23-04-01228.2003

Gao, H. M., Zhang, F., Zhou, H., Kam, W., Wilson, B., & Hong, J. S. (2011). Neuroinflammation and α-synuclein dysfunction potentiate each other, driving chronic progression of neurodegeneration in a mouse model of Parkinson's disease. *Environ Health Perspect*, *119*(6), 807-814. https://doi.org/10.1289/ehp.1003013

García-Domínguez, I., Veselá, K., García-Revilla, J., Carrillo-Jiménez, A., Roca-Ceballos, M. A., Santiago, M., de Pablos, R. M., & Venero, J. L. (2018). Peripheral Inflammation Enhances Microglia Response and Nigral Dopaminergic Cell Death in an in vivo MPTP Model of Parkinson's Disease [Original Research]. *Frontiers in Cellular Neuroscience*, *12*(398). https://doi.org/10.3389/fncel.2018.00398

Gardet, A., Benita, Y., Li, C., Sands, B. E., Ballester, I., Stevens, C., Korzenik, J. R., Rioux, J. D., Daly, M. J., Xavier, R. J., & Podolsky, D. K. (2010). LRRK2 is involved in the IFN-gamma response and host response to pathogens. *J Immunol*, *185*(9), 5577-5585. https://doi.org/10.4049/jimmunol.1000548

Gasiunas, G., Barrangou, R., Horvath, P., & Siksnys, V. (2012). Cas9-crRNA ribonucleoprotein complex mediates specific DNA cleavage for adaptive immunity in bacteria. *Proc Natl Acad Sci U S A*, *109*(39), E2579-2586. https://doi.org/10.1073/pnas.1208507109

Gaudelli, N. M., Komor, A. C., Rees, H. A., Packer, M. S., Badran, A. H., Bryson, D. I., & Liu, D. R. (2017). Programmable base editing of A•T to G•C in genomic DNA without DNA cleavage. *Nature*, *551*(7681), 464-471. https://doi.org/10.1038/nature24644

Gerber, S. H., Rah, J.-C., Min, S.-W., Liu, X., de Wit, H., Dulubova, I., Meyer, A. C., Rizo, J., Arancillo, M., Hammer, R. E., Verhage, M., Rosenmund, C., & Südhof, T. C. (2008). Conformational Switch of Syntaxin-1 Controls Synaptic Vesicle Fusion. *Science*, *321*(5895), 1507-1510. https://doi.org/10.1126/science.1163174

Gerhard, A., Pavese, N., Hotton, G., Turkheimer, F., Es, M., Hammers, A., Eggert, K., Oertel, W., Banati, R. B., & Brooks, D. J. (2006). In vivo imaging of microglial activation with [11C](R)-PK11195 PET in idiopathic Parkinson's disease. *Neurobiol Dis*, *21*(2), 404-412. https://doi.org/10.1016/j.nbd.2005.08.002

Giaime, E., Tong, Y., Wagner, L. K., Yuan, Y., Huang, G., & Shen, J. (2017). Age-Dependent Dopaminergic Neurodegeneration and Impairment of the Autophagy-Lysosomal Pathway in LRRK-Deficient Mice. *Neuron*, *96*(4), 796-807.e796. https://doi.org/10.1016/j.neuron.2017.09.036

Giese, N. A., Gabriele, L., Doherty, T. M., Klinman, D. M., Tadesse-Heath, L., Contursi, C., Epstein, S. L., & Morse, H. C., 3rd. (1997). Interferon (IFN) consensus sequence-binding protein, a transcription factor of the IFN regulatory factor family, regulates immune responses in vivo through control of interleukin 12 expression. *J Exp Med*, *186*(9), 1535-1546. https://doi.org/10.1084/jem.186.9.1535

Giesert, F., Hofmann, A., Bürger, A., Zerle, J., Kloos, K., Hafen, U., Ernst, L., Zhang, J., Vogt-Weisenhorn, D. M., & Wurst, W. (2013). Expression analysis of Lrrk1, Lrrk2 and Lrrk2 splice variants in mice. *PLoS ONE*, *8*(5), e63778. https://doi.org/10.1371/journal.pone.0063778

Gilks, W. P., Abou-Sleiman, P. M., Gandhi, S., Jain, S., Singleton, A., Lees, A. J., Shaw, K., Bhatia, K. P., Bonifati, V., Quinn, N. P., Lynch, J., Healy, D. G., Holton, J. L., Revesz, T., & Wood, N. W. (2005). A common LRRK2 mutation in idiopathic Parkinson's disease. *Lancet*, *365*(9457), 415-416. https://doi.org/10.1016/s0140-6736(05)17830-1

Gillardon, F. (2009). Interaction of elongation factor 1-alpha with leucine-rich repeat kinase 2 impairs kinase activity and microtubule bundling in vitro. *Neuroscience*, *163*(2), 533-539. https://doi.org/10.1016/j.neuroscience.2009.06.051

Gillardon, F., Schmid, R., & Draheim, H. (2012). Parkinson's disease-linked leucine-rich repeat kinase 2(R1441G) mutation increases proinflammatory cytokine release from activated primary microglial cells and resultant neurotoxicity. *Neuroscience*, *208*, 41-48. https://doi.org/10.1016/j.neuroscience.2012.02.001

Gloeckner, C. J., Kinkl, N., Schumacher, A., Braun, R. J., O'Neill, E., Meitinger, T., Kolch, W., Prokisch, H., & Ueffing, M. (2006). The Parkinson disease causing LRRK2 mutation I2020T is associated with increased kinase activity. *Hum Mol Genet*, *15*(2), 223-232. https://doi.org/10.1093/hmg/ddi439

Goldstein, D., Djeu, J., Latter, G., Burbeck, S., & Leavitt, J. (1985). Abundant synthesis of the transformation-induced protein of neoplastic human fibroblasts, plastin, in normal lymphocytes. *Cancer Res*, *45*(11 Pt 2), 5643-5647.

Gosal, D., Lynch, T., Ross, O. A., Haugarvoll, K., Farrer, M. J., & Gibson, J. M. (2007). Global distribution and reduced penetrance: Lrrk2 R1441C in an Irish Parkinson's disease kindred. *Mov Disord*, *22*(2), 291-292. https://doi.org/10.1002/mds.21200

Goto, T., Holzinger, F., Hagey, L. R., Cerrè, C., Ton-Nu, H. T., Schteingart, C. D., Steinbach, J. H., Shneider, B. L., & Hofmann, A. F. (2003). Physicochemical and physiological properties of 5alpha-cyprinol sulfate, the toxic bile salt of cyprinid fish. *J Lipid Res*, *44*(9), 1643-1651. https://doi.org/10.1194/jlr.M300155-JLR200

Goulding, S. R., Lévesque, M., Sullivan, A. M., Collins, L. M., & O'Keeffe, G. W. (2021). Quinacrine and Niclosamide Promote Neurite Growth in Midbrain Dopaminergic Neurons Through the Canonical BMP-Smad Pathway and Protect Against Neurotoxin and α-Synuclein-Induced Neurodegeneration. *Mol Neurobiol*, *58*(7), 3405-3416. https://doi.org/10.1007/s12035-021-02351-8

Graham, W. C., Robertson, R. G., Sambrook, M. A., & Crossman, A. R. (1990). Injection of excitatory amino acid antagonists into the medial pallidal segment of a 1-methyl-4-phenyl-1,2,3,6-tetrahydropyridine (MPTP) treated primate reverses motor symptoms of parkinsonism. *Life Sciences*, *47*(18), PL91-PL97. https://doi.org/https://doi.org/10.1016/0024-3205(90)90376-3

Gray, M. T., & Woulfe, J. M. (2015). Striatal blood-brain barrier permeability in Parkinson's disease. *J Cereb Blood Flow Metab*, *35*(5), 747-750. https://doi.org/10.1038/jcbfm.2015.32

Greggio, E., Jain, S., Kingsbury, A., Bandopadhyay, R., Lewis, P., Kaganovich, A., van der Brug, M. P., Beilina, A., Blackinton, J., Thomas, K. J., Ahmad, R., Miller, D. W., Kesavapany, S., Singleton, A., Lees, A., Harvey, R. J., Harvey, K., & Cookson, M. R. (2006). Kinase activity is required for the toxic effects of mutant LRRK2/dardarin. *Neurobiol Dis*, *23*(2), 329-341. https://doi.org/10.1016/j.nbd.2006.04.001

Greggio, E., Lewis, P. A., van der Brug, M. P., Ahmad, R., Kaganovich, A., Ding, J., Beilina, A., Baker, A. K., & Cookson, M. R. (2007). Mutations in LRRK2/dardarin associated with Parkinson disease are more toxic than equivalent mutations in the homologous kinase LRRK1. *J Neurochem*, *102*(1), 93-102. https://doi.org/10.1111/j.1471-4159.2007.04523.x

Grégoire, L., Rassoulpour, A., Guidetti, P., Samadi, P., Bédard, P. J., Izzo, E., Schwarcz, R., & Di Paolo, T. (2008). Prolonged kynurenine 3-hydroxylase inhibition reduces development of levodopa-induced dyskinesias in parkinsonian monkeys. *Behav Brain Res*, *186*(2), 161-167. https://doi.org/10.1016/j.bbr.2007.08.007

Grozdanov, V., Bliederhaeuser, C., Ruf, W. P., Roth, V., Fundel-Clemens, K., Zondler, L., Brenner, D., Martin-Villalba, A., Hengerer, B., Kassubek, J., Ludolph, A. C., Weishaupt, J. H., & Danzer, K. M. (2014). Inflammatory dysregulation of blood monocytes in Parkinson's disease patients. *Acta Neuropathologica*, *128*(5), 651-663. https://doi.org/10.1007/s00401-014-1345-4

Gu, M., Jia, Q., Zhang, Z., Bai, N., Xu, X., & Xu, B. (2018). Soya-saponins induce intestinal inflammation and barrier dysfunction in juvenile turbot (Scophthalmus maximus). *Fish Shellfish Immunol*, *77*, 264-272. https://doi.org/10.1016/j.fsi.2018.04.004

Guella, I., Sherman, H. E., Appel-Cresswell, S., Rajput, A., Rajput, A. H., & Farrer, M. J. (2014). Parkinsonism in GTP cyclohydrolase 1 mutation carriers. *Brain*, *138*(5), e349-e349. https://doi.org/10.1093/brain/awu341

Guerreiro, P. S., Huang, Y., Gysbers, A., Cheng, D., Gai, W. P., Outeiro, T. F., & Halliday, G. M. (2013). LRRK2 interactions with α-synuclein in Parkinson's disease brains and in cell models. *J Mol Med (Berl)*, *91*(4), 513-522. https://doi.org/10.1007/s00109-012-0984-y

Guillemin, G. J., Croitoru-Lamoury, J., Dormont, D., Armati, P. J., & Brew, B. J. (2003). Quinolinic acid upregulates chemokine production and chemokine receptor expression in astrocytes. *Glia*, *41*(4), 371-381. https://doi.org/10.1002/glia.10175

Guillemin, G. J., Kerr, S. J., Smythe, G. A., Smith, D. G., Kapoor, V., Armati, P. J., Croitoru, J., & Brew, B. J. (2001). Kynurenine pathway metabolism in human astrocytes: a paradox for neuronal protection. *J Neurochem*, *78*(4), 842-853. https://doi.org/10.1046/j.1471-4159.2001.00498.x

Guo, L., Girisha, K. M., Iida, A., Hebbar, M., Shukla, A., Shah, H., Nishimura, G., Matsumoto, N., Nismath, S., Miyake, N., & Ikegawa, S. (2017). Identification of a novel LRRK1 mutation in a family with osteosclerotic metaphyseal dysplasia. *J Hum Genet*, *62*(3), 437-441. https://doi.org/10.1038/jhg.2016.136

Hagemeyer, N., Kierdorf, K., Frenzel, K., Xue, J., Ringelhan, M., Abdullah, Z., Godin, I., Wieghofer, P., Costa Jordão, M. J., Ulas, T., Yorgancioglu, G., Rosenbauer, F., Knolle, P. A., Heikenwalder, M., Schultze, J. L., & Prinz, M. (2016). Transcriptome-based profiling of yolk sac-derived macrophages reveals a role for Irf8 in macrophage maturation. *Embo j*, *35*(16), 1730-1744. https://doi.org/10.15252/embj.201693801

Hagey, L. R., Møller, P. R., Hofmann, A. F., & Krasowski, M. D. (2010). Diversity of bile salts in fish and amphibians: evolution of a complex biochemical pathway. *Physiol Biochem Zool*, *83*(2), 308-321. https://doi.org/10.1086/649966

Hakimi, M., Selvanantham, T., Swinton, E., Padmore, R. F., Tong, Y., Kabbach, G., Venderova, K., Girardin, S. E., Bulman, D. E., Scherzer, C. R., LaVoie, M. J., Gris, D., Park, D. S., Angel, J. B., Shen, J., Philpott, D. J., & Schlossmacher, M. G. (2011). Parkinson's disease-linked LRRK2 is expressed in circulating and tissue immune cells and upregulated following recognition of microbial structures. *J Neural Transm (Vienna)*, *118*(5), 795-808. https://doi.org/10.1007/s00702-011-0653-2

Han, W., Sapkota, S., Camicioli, R., Dixon, R. A., & Li, L. (2017). Profiling novel metabolic biomarkers for Parkinson's disease using in-depth metabolomic analysis. *Mov Disord*, *32*(12), 1720-1728. https://doi.org/10.1002/mds.27173

Hanafusa, H., Ishikawa, K., Kedashiro, S., Saigo, T., Iemura, S., Natsume, T., Komada, M., Shibuya, H., Nara, A., & Matsumoto, K. (2011). Leucine-rich repeat kinase LRRK1 regulates endosomal trafficking of the EGF receptor. *Nat Commun*, *2*, 158. https://doi.org/10.1038/ncomms1161

Hancock, D. B., Martin, E. R., Stajich, J. M., Jewett, R., Stacy, M. A., Scott, B. L., Vance, J. M., & Scott, W. K. (2007). Smoking, caffeine, and nonsteroidal anti-inflammatory drugs in families with Parkinson disease. *Arch Neurol*, *64*(4), 576-580. https://doi.org/10.1001/archneur.64.4.576

Harada, J. N., Bower, K. E., Orth, A. P., Callaway, S., Nelson, C. G., Laris, C., Hogenesch, J. B., Vogt, P. K., & Chanda, S. K. (2005). Identification of novel mammalian growth regulatory factors by genome-scale quantitative image analysis. *Genome Res*, *15*(8), 1136-1144. https://doi.org/10.1101/gr.3889305

Harris, M. A., Tsui, J. K., Marion, S. A., Shen, H., & Teschke, K. (2012). Association of Parkinson's disease with infections and occupational exposure to possible vectors. *Movement Disorders*, *27*(9), 1111-1117. https://doi.org/https://doi.org/10.1002/mds.25077

Hartai, Z., Klivenyi, P., Janaky, T., Penke, B., Dux, L., & Vecsei, L. (2005). Kynurenine metabolism in plasma and in red blood cells in Parkinson's disease. *J Neurol Sci*, *239*(1), 31-35. https://doi.org/10.1016/j.jns.2005.07.006

Harvey, K., & Outeiro, T. F. (2019). The role of LRRK2 in cell signalling. *Biochem Soc Trans*, *47*(1), 197-207. https://doi.org/10.1042/bst20180464

Harvey, S. A., Sealy, I., Kettleborough, R., Fenyes, F., White, R., Stemple, D., & Smith, J. C. (2013). Identification of the zebrafish maternal and paternal transcriptomes. *Development*, *140*(13), 2703-2710. https://doi.org/10.1242/dev.095091

Haslewood, G. A. (1967). Bile salt evolution. *J Lipid Res*, *8*(6), 535-550.

Hassan, H. S., Sule, M. I., Musa, A. M., Musa, K. Y., Abubakar, M. S., & Hassan, A. S. (2012). Anti-inflammatory activity of crude saponin extracts from five Nigerian medicinal plants. *Afr J Tradit Complement Altern Med*, *9*(2), 250-255. https://doi.org/10.4314/ajtcam.v9i2.10

Haugarvoll, K., Toft, M., Ross, O. A., White, L. R., Aasly, J. O., & Farrer, M. J. (2007). Variants in the LRRK1 gene and susceptibility to Parkinson's disease in Norway. *Neurosci Lett*, *416*(3), 299-301. https://doi.org/10.1016/j.neulet.2007.02.020

Havelund, J. F., Andersen, A. D., Binzer, M., Blaabjerg, M., Heegaard, N. H. H., Stenager, E., Faergeman, N. J., & Gramsbergen, J. B. (2017). Changes in kynurenine pathway metabolism in Parkinson patients with L-DOPA-induced dyskinesia. *J Neurochem*, *142*(5), 756-766. https://doi.org/10.1111/jnc.14104

He, D., Huang, B., Fu, S., Li, Y., Ran, X., Liu, Y., Chen, G., Liu, J., & Liu, D. (2018). Tubeimoside I Protects Dopaminergic Neurons Against Inflammation-Mediated Damage in Lipopolysaccharide (LPS)-Evoked Model of Parkinson's Disease in Rats. *Int J Mol Sci*, *19*(8). https://doi.org/10.3390/ijms19082242

He, J.-H., Guo, S.-Y., Zhu, F., Zhu, J.-J., Chen, Y.-X., Huang, C.-J., Gao, J.-M., Dong, Q.-X., Xuan, Y.-X., & Li, C.-Q. (2013). A zebrafish phenotypic assay for assessing drug-induced hepatotoxicity. *Journal of Pharmacological and Toxicological Methods*, *67*(1), 25-32. https://doi.org/https://doi.org/10.1016/j.vascn.2012.10.003

Healy, D. G., Falchi, M., O'Sullivan, S. S., Bonifati, V., Durr, A., Bressman, S., Brice, A., Aasly, J., Zabetian, C. P., Goldwurm, S., Ferreira, J. J., Tolosa, E., Kay, D. M., Klein, C., Williams, D. R., Marras, C., Lang, A. E., Wszolek, Z. K., Berciano, J., Schapira, A. H., Lynch, T., Bhatia, K. P., Gasser, T., Lees, A. J., & Wood, N. W. (2008). Phenotype, genotype, and worldwide genetic penetrance of LRRK2-associated Parkinson's disease: a case-control study. *Lancet Neurol*, *7*(7), 583-590. https://doi.org/10.1016/s1474-4422(08)70117-0

Heckman, M. G., Elbaz, A., Soto-Ortolaza, A. I., Serie, D. J., Aasly, J. O., Annesi, G., Auburger, G., Bacon, J. A., Boczarska-Jedynak, M., Bozi, M., Brighina, L., Chartier-Harlin, M. C., Dardiotis, E., Destée, A., Ferrarese, C., Ferraris, A., Fiske, B., Gispert, S., Hadjigeorgiou, G. M., Hattori, N., Ioannidis, J. P., Jasinska-Myga, B., Jeon, B. S., Kim, Y. J., Klein, C., Kruger, R., Kyratzi, E., Lin, C. H., Lohmann, K., Loriot, M. A., Lynch, T., Mellick, G. D., Mutez, E., Opala, G., Park, S. S., Petrucci, S., Quattrone, A., Sharma, M., Silburn, P. A., Sohn, Y. H., Stefanis, L., Tadic, V., Tomiyama, H., Uitti, R. J., Valente, E. M., Vassilatis, D. K., Vilariño-Güell, C., White, L. R., Wirdefeldt, K., Wszolek, Z. K., Wu, R. M., Xiromerisiou, G., Maraganore, D. M., Farrer, M. J., & Ross, O. A. (2014). Protective effect of LRRK2 p.R1398H on risk of Parkinson's disease is independent of MAPT and SNCA variants. *Neurobiol Aging*, *35*(1), 266.e265-214. https://doi.org/10.1016/j.neurobiolaging.2013.07.013

Heeman, B., Van den Haute, C., Aelvoet, S.-A., Valsecchi, F., Rodenburg, R. J., Reumers, V., Debyser, Z., Callewaert, G., Koopman, W. J. H., Willems, P. H. G. M., & Baekelandt, V. (2011). Depletion of PINK1 affects mitochondrial metabolism, calcium homeostasis and energy maintenance. *Journal of Cell Science*, *124*(7), 1115-1125. https://doi.org/10.1242/jcs.078303

Heilman, P. L., Wang, E. W., Lewis, M. M., Krzyzanowski, S., Capan, C. D., Burmeister, A. R., Du, G., Escobar Galvis, M. L., Brundin, P., Huang, X., & Brundin, L. (2020). Tryptophan Metabolites Are Associated With Symptoms and Nigral Pathology in Parkinson's Disease. *Movement Disorders*, *35*(11), 2028-2037. https://doi.org/https://doi.org/10.1002/mds.28202

Herbomel, P., Thisse, B., & Thisse, C. (2001). Zebrafish early macrophages colonize cephalic mesenchyme and developing brain, retina, and epidermis through a M-CSF receptor-dependent invasive process. *Dev Biol*, *238*(2), 274-288. https://doi.org/10.1006/dbio.2001.0393

Herlofson, K., Heijnen, C. J., Lange, J., Alves, G., Tysnes, O.-B., Friedman, J. H., & Fagundes, C. P. (2018). Inflammation and fatigue in early, untreated Parkinson's Disease. *Acta Neurologica Scandinavica*, *138*(5), 394-399. https://doi.org/https://doi.org/10.1111/ane.12977

Herzig, M. C., Kolly, C., Persohn, E., Theil, D., Schweizer, T., Hafner, T., Stemmelen, C., Troxler, T. J., Schmid, P., Danner, S., Schnell, C. R., Mueller, M., Kinzel, B., Grevot, A., Bolognani, F., Stirn, M., Kuhn, R. R., Kaupmann, K., van der Putten, P. H., Rovelli, G., & Shimshek, D. R. (2011). LRRK2 protein levels are determined by kinase function and are crucial for kidney and lung homeostasis in mice. *Hum Mol Genet*, *20*(21), 4209-4223. https://doi.org/10.1093/hmg/ddr348

Heyes, M. P., Saito, K., Crowley, J. S., Davis, L. E., Demitrack, M. A., Der, M., Dilling, L. A., Elia, J., Kruesi, M. J., Lackner, A., & et al. (1992). Quinolinic acid and kynurenine pathway metabolism in inflammatory and non-inflammatory neurological disease. *Brain*, *115 (Pt 5)*, 1249-1273. https://doi.org/10.1093/brain/115.5.1249

Higashi, S., Biskup, S., West, A. B., Trinkaus, D., Dawson, V. L., Faull, R. L., Waldvogel, H. J., Arai, H., Dawson, T. M., Moore, D. J., & Emson, P. C. (2007). Localization of Parkinson's disease-associated LRRK2 in normal and pathological human brain. *Brain Res*, *1155*, 208-219. https://doi.org/10.1016/j.brainres.2007.04.034

Hinkle, K. M., Yue, M., Behrouz, B., Dächsel, J. C., Lincoln, S. J., Bowles, E. E., Beevers, J. E., Dugger, B., Winner, B., Prots, I., Kent, C. B., Nishioka, K., Lin, W. L., Dickson, D. W., Janus, C. J., Farrer, M. J., & Melrose, H. L. (2012). LRRK2 knockout mice have an intact dopaminergic system but display alterations in exploratory and motor co-ordination behaviors. *Mol Neurodegener*, *7*, 25. https://doi.org/10.1186/1750-1326-7-25

Hirsch, L., Jette, N., Frolkis, A., Steeves, T., & Pringsheim, T. (2016). The Incidence of Parkinson's Disease: A Systematic Review and Meta-Analysis. *Neuroepidemiology*, *46*(4), 292-300. https://doi.org/10.1159/000445751

Holmqvist, S., Chutna, O., Bousset, L., Aldrin-Kirk, P., Li, W., Björklund, T., Wang, Z.-Y., Roybon, L., Melki, R., & Li, J.-Y. (2014). Direct evidence of Parkinson pathology spread from the gastrointestinal

tract to the brain in rats. *Acta Neuropathologica*, *128*(6), 805-820. https://doi.org/10.1007/s00401-014-1343-6

Holtschke, T., Löhler, J., Kanno, Y., Fehr, T., Giese, N., Rosenbauer, F., Lou, J., Knobeloch, K. P., Gabriele, L., Waring, J. F., Bachmann, M. F., Zinkernagel, R. M., Morse, H. C., 3rd, Ozato, K., & Horak, I. (1996). Immunodeficiency and chronic myelogenous leukemia-like syndrome in mice with a targeted mutation of the ICSBP gene. *Cell*, *87*(2), 307-317. https://doi.org/10.1016/s0092-8674(00)81348-3

Holzschuh, J., Ryu, S., Aberger, F., & Driever, W. (2001). Dopamine transporter expression distinguishes dopaminergic neurons from other catecholaminergic neurons in the developing zebrafish embryo. *Mech Dev*, *101*(1-2), 237-243. https://doi.org/10.1016/s0925-4773(01)00287-8

Hong, M., Ye, B. D., Yang, S. K., Jung, S., Lee, H. S., Kim, B. M., Lee, S. B., Hong, J., Baek, J., Park, S. H., Han, B., Li, Y., Liu, W., Haritunians, T., Taylor, K. D., Rotter, J. I., Bang, S. Y., Kim, T. H., McGovern, D. P. B., Liu, J., & Song, K. (2018). Immunochip Meta-Analysis of Inflammatory Bowel Disease Identifies Three Novel Loci and Four Novel Associations in Previously Reported Loci. *J Crohns Colitis*, *12*(6), 730-741. https://doi.org/10.1093/ecco-jcc/jjy002

Horiuchi, M., Wakayama, K., Itoh, A., Kawai, K., Pleasure, D., Ozato, K., & Itoh, T. (2012). Interferon regulatory factor 8/interferon consensus sequence binding protein is a critical transcription factor for the physiological phenotype of microglia. *J Neuroinflammation*, *9*, 227. https://doi.org/10.1186/1742-2094-9-227

Hosoi, R., Fujii, Y., Hiroyuki, O., Shukuri, M., Nishiyama, S., Kanazawa, M., Todoroki, K., Arano, Y., Sakai, T., Tsukada, H., & Inoue, O. (2021). Evaluation of intracellular processes in quinolinic acid-induced brain damage by imaging reactive oxygen species generation and mitochondrial complex I activity. *EJNMMI Res*, *11*(1), 99. https://doi.org/10.1186/s13550-021-00841-3

Houser, M. C., Chang, J., Factor, S. A., Molho, E. S., Zabetian, C. P., Hill-Burns, E. M., Payami, H., Hertzberg, V. S., & Tansey, M. G. (2018). Stool Immune Profiles Evince Gastrointestinal Inflammation in Parkinson's Disease. *Movement Disorders*, *33*(5), 793-804. https://doi.org/https://doi.org/10.1002/mds.27326

Houser, M. C., & Tansey, M. G. (2017). The gut-brain axis: is intestinal inflammation a silent driver of Parkinson's disease pathogenesis? *npj Parkinson's Disease*, *3*(1), 3. https://doi.org/10.1038/s41531-016-0002-0

Howaldt, A., Hennig, A. F., Rolvien, T., Rössler, U., Stelzer, N., Knaus, A., Böttger, S., Zustin, J., Geißler, S., Oheim, R., Amling, M., Howaldt, H. P., & Kornak, U. (2020). Adult Osteosclerotic Metaphyseal Dysplasia With Progressive Osteonecrosis of the Jaws and Abnormal Bone Resorption Pattern Due to a LRRK1 Splice Site Mutation. *J Bone Miner Res*, *35*(7), 1322-1332. https://doi.org/10.1002/jbmr.3995

Howe, K., Clark, M. D., Torroja, C. F., Torrance, J., Berthelot, C., Muffato, M., Collins, J. E., Humphray, S., McLaren, K., Matthews, L., McLaren, S., Sealy, I., Caccamo, M., Churcher, C., Scott, C., Barrett, J. C., Koch, R., Rauch, G. J., White, S., Chow, W., Kilian, B., Quintais, L. T., Guerra-Assunção, J. A., Zhou, Y., Gu, Y., Yen, J., Vogel, J. H., Eyre, T., Redmond, S., Banerjee, R., Chi, J., Fu, B., Langley, E., Maguire, S. F., Laird, G. K., Lloyd, D., Kenyon, E., Donaldson, S., Sehra, H., Almeida-King, J., Loveland, J., Trevanion, S., Jones, M., Quail, M., Willey, D., Hunt, A., Burton, J., Sims, S., McLay, K., Plumb, B., Davis, J., Clee, C., Oliver, K., Clark, R., Riddle, C., Elliot, D., Threadgold, G., Harden, G., Ware, D., Begum, S., Mortimore, B., Kerry, G., Heath, P., Phillimore, B., Tracey, A., Corby, N., Dunn, M., Johnson, C., Wood, J., Clark, S., Pelan, S., Griffiths, G., Smith, M., Glithero, R., Howden, P., Barker, N., Lloyd, C., Stevens, C., Harley, J., Holt, K., Panagiotidis, G., Lovell, J., Beasley, H., Henderson, C., Gordon, D., Auger, K., Wright, D., Collins, J., Raisen, C., Dyer, L., Leung, K., Robertson, L., Ambridge, K., Leongamornlert, D., McGuire, S., Gilderthorp, R., Griffiths, C., Manthravadi, D., Nichol, S., Barker, G., Whitehead, S., Kay, M., Brown, J., Murnane, C., Gray, E., Humphries, M., Sycamore, N., Barker, D., Saunders, D., Wallis, J., Babbage, A., Hammond, S., Mashreghi-Mohammadi, M., Barr, L., Martin, S., Wray, P., Ellington, A., Matthews, N., Ellwood, M., Woodmansey, R., Clark, G., Cooper, J., Tromans, A., Grafham, D., Skuce, C., Pandian, R., Andrews, R., Harrison, E., Kimberley, A., Garnett, J., Fosker, N., Hall, R., Garner, P., Kelly, D., Bird, C., Palmer, S., Gehring, I., Berger, A., Dooley, C. M., Ersan-Ürün, Z., Eser, C., Geiger, H., Geisler,

M., Karotki, L., Kirn, A., Konantz, J., Konantz, M., Oberländer, M., Rudolph-Geiger, S., Teucke, M., Lanz, C., Raddatz, G., Osoegawa, K., Zhu, B., Rapp, A., Widaa, S., Langford, C., Yang, F., Schuster, S. C., Carter, N. P., Harrow, J., Ning, Z., Herrero, J., Searle, S. M., Enright, A., Geisler, R., Plasterk, R. H., Lee, C., Westerfield, M., de Jong, P. J., Zon, L. I., Postlethwait, J. H., Nüsslein-Volhard, C., Hubbard, T. J., Roest Crollius, H., Rogers, J., & Stemple, D. L. (2013). The zebrafish reference genome sequence and its relationship to the human genome. *Nature*, *496*(7446), 498-503. https://doi.org/10.1038/nature12111

Hruscha, A., Krawitz, P., Rechenberg, A., Heinrich, V., Hecht, J., Haass, C., & Schmid, B. (2013). Efficient CRISPR/Cas9 genome editing with low off-target effects in zebrafish. *Development*, *140*(24), 4982-4987. https://doi.org/10.1242/dev.099085

Huang, B., Qi, Z. T., Xu, Z., & Nie, P. (2010). Global characterization of interferon regulatory factor (IRF) genes in vertebrates: glimpse of the diversification in evolution. *BMC Immunol*, *11*, 22. https://doi.org/10.1186/1471-2172-11-22

Huang, X., Wu, C., Park, Y., Long, X., Hoang, Q. Q., & Liao, J. (2019). The Parkinson's disease-associated mutation N1437H impairs conformational dynamics in the G domain of LRRK2. *Faseb j*, *33*(4), 4814-4823. https://doi.org/10.1096/fj.201802031R

Hui, K. Y., Fernandez-Hernandez, H., Hu, J., Schaffner, A., Pankratz, N., Hsu, N. Y., Chuang, L. S., Carmi, S., Villaverde, N., Li, X., Rivas, M., Levine, A. P., Bao, X., Labrias, P. R., Haritunians, T., Ruane, D., Gettler, K., Chen, E., Li, D., Schiff, E. R., Pontikos, N., Barzilai, N., Brant, S. R., Bressman, S., Cheifetz, A. S., Clark, L. N., Daly, M. J., Desnick, R. J., Duerr, R. H., Katz, S., Lencz, T., Myers, R. H., Ostrer, H., Ozelius, L., Payami, H., Peter, Y., Rioux, J. D., Segal, A. W., Scott, W. K., Silverberg, M. S., Vance, J. M., Ubarretxena-Belandia, I., Foroud, T., Atzmon, G., Pe'er, I., Ioannou, Y., McGovern, D. P. B., Yue, Z., Schadt, E. E., Cho, J. H., & Peter, I. (2018). Functional variants in the LRRK2 gene confer shared effects on risk for Crohn's disease and Parkinson's disease. *Sci Transl Med*, *10*(423). https://doi.org/10.1126/scitranslmed.aai7795

Huo, J., Yu, Q., Zhang, Y., Liu, K., Hsiao, C. D., Jiang, Z., & Zhang, L. (2019). Triptolide-induced hepatotoxicity via apoptosis and autophagy in zebrafish. *J Appl Toxicol*, *39*(11), 1532-1540. https://doi.org/10.1002/jat.3837

Huo, L., Davis, I., Chen, L., & Liu, A. (2013). The power of two: arginine 51 and arginine 239* from a neighboring subunit are essential for catalysis in α-amino-β-carboxymuconate-epsilon-semialdehyde decarboxylase. *J Biol Chem*, *288*(43), 30862-30871. https://doi.org/10.1074/jbc.M113.496869

Hwang, W. Y., Fu, Y., Reyon, D., Maeder, M. L., Kaini, P., Sander, J. D., Joung, J. K., Peterson, R. T., & Yeh, J.-R. J. (2013). Heritable and Precise Zebrafish Genome Editing Using a CRISPR-Cas System. *PLoS ONE*, *8*(7), e68708. https://doi.org/10.1371/journal.pone.0068708

Iida, A., Xing, W., Docx, M. K., Nakashima, T., Wang, Z., Kimizuka, M., Van Hul, W., Rating, D., Spranger, J., Ohashi, H., Miyake, N., Matsumoto, N., Mohan, S., Nishimura, G., Mortier, G., & Ikegawa, S. (2016). Identification of biallelic LRRK1 mutations in osteosclerotic metaphyseal dysplasia and evidence for locus heterogeneity. *J Med Genet*, *53*(8), 568-574. https://doi.org/10.1136/jmedgenet-2016-103756

Ilin, V. A., Bai, Q., Watson, A. M., Volgushev, M., & Burton, E. A. (2021). Mechanism of Pacemaker Activity in Zebrafish DC2/4 Dopaminergic Neurons. *J Neurosci*, *41*(18), 4141-4157. https://doi.org/10.1523/jneurosci.2124-20.2021

Illarioshkin, S. N., Shadrina, M. I., Slominsky, P. A., Bespalova, E. V., Zagorovskaya, T. B., Bagyeva, G., Markova, E. D., Limborska, S. A., & Ivanova-Smolenskaya, I. A. (2007). A common leucine-rich repeat kinase 2 gene mutation in familial and sporadic Parkinson's disease in Russia. *Eur J Neurol*, *14*(4), 413-417. https://doi.org/10.1111/j.1468-1331.2007.01685.x

Imai, Y., Gehrke, S., Wang, H. Q., Takahashi, R., Hasegawa, K., Oota, E., & Lu, B. (2008). Phosphorylation of 4E-BP by LRRK2 affects the maintenance of dopaminergic neurons in Drosophila. *Embo j*, *27*(18), 2432-2443. https://doi.org/10.1038/emboj.2008.163

Imamura, K., Hishikawa, N., Sawada, M., Nagatsu, T., Yoshida, M., & Hashizume, Y. (2003). Distribution of major histocompatibility complex class II-positive microglia and cytokine profile of Parkinson's

disease brains. *Acta Neuropathologica*, *106*(6), 518-526. https://doi.org/10.1007/s00401-003-0766-2
Inoue, D., & Wittbrodt, J. (2011). One for all--a highly efficient and versatile method for fluorescent immunostaining in fish embryos. *PLoS ONE*, *6*(5), e19713. https://doi.org/10.1371/journal.pone.0019713
Ishikawa, K., Nara, A., Matsumoto, K., & Hanafusa, H. (2012). EGFR-dependent phosphorylation of leucine-rich repeat kinase LRRK1 is important for proper endosomal trafficking of EGFR. *Mol Biol Cell*, *23*(7), 1294-1306. https://doi.org/10.1091/mbc.E11-09-0780
Ito, G., Okai, T., Fujino, G., Takeda, K., Ichijo, H., Katada, T., & Iwatsubo, T. (2007). GTP binding is essential to the protein kinase activity of LRRK2, a causative gene product for familial Parkinson's disease. *Biochemistry*, *46*(5), 1380-1388. https://doi.org/10.1021/bi061960m
Iwaoka, K., Otsuka, C., Maeda, T., Yamahara, K., Kato, K., Takahashi, K., Takahashi, K., & Terayama, Y. (2020). Impaired metabolism of kynurenine and its metabolites in CSF of parkinson's disease. *Neurosci Lett*, *714*, 134576. https://doi.org/10.1016/j.neulet.2019.134576
Jaleel, M., Nichols, R. J., Deak, M., Campbell, D. G., Gillardon, F., Knebel, A., & Alessi, D. R. (2007). LRRK2 phosphorylates moesin at threonine-558: characterization of how Parkinson's disease mutants affect kinase activity. *Biochem J*, *405*(2), 307-317. https://doi.org/10.1042/bj20070209
Jamal, M., Ullah, A., Ahsan, M., Tyagi, R., Habib, Z., & Rehman, K. (2018). Improving CRISPR-Cas9 On-Target Specificity. *Curr Issues Mol Biol*, *26*, 65-80. https://doi.org/10.21775/cimb.026.065
Jang, K.-J., Kim, H. K., Han, M. H., Oh, Y. N., Yoon, H.-M., Chung, Y. H., Kim, G. Y., Hwang, H. J., Kim, B. W., & Choi, Y. H. (2013). Anti-inflammatory effects of saponins derived from the roots of Platycodon grandiflorus in lipopolysaccharide-stimulated BV2 microglial cells. *Int J Mol Med*, *31*(6), 1357-1366. https://doi.org/10.3892/ijmm.2013.1330
Jao, L. E., Wente, S. R., & Chen, W. (2013). Efficient multiplex biallelic zebrafish genome editing using a CRISPR nuclease system. *Proc Natl Acad Sci U S A*, *110*(34), 13904-13909. https://doi.org/10.1073/pnas.1308335110
Jay, M., De Faveri, F., & McDearmid, J. R. (2015). Firing dynamics and modulatory actions of supraspinal dopaminergic neurons during zebrafish locomotor behavior. *Curr Biol*, *25*(4), 435-444. https://doi.org/10.1016/j.cub.2014.12.033
Jia, Z.-l., Cen, J., Wang, J.-b., Zhang, F., Xia, Q., Wang, X., Chen, X.-q., Wang, R.-c., Hsiao, C.-d., Liu, K.-c., & Zhang, Y. (2019). Mechanism of isoniazid-induced hepatotoxicity in zebrafish larvae: Activation of ROS-mediated ERS, apoptosis and the Nrf2 pathway. *Chemosphere*, *227*, 541-550. https://doi.org/https://doi.org/10.1016/j.chemosphere.2019.04.026
Jiao, Y., Tao, Y., Yang, Y., Diogene, T., Yu, H., He, Z., Han, W., Chen, Z., Wu, P., & Zhang, Y. (2020). Monobutyl phthalate (MBP) can dysregulate the antioxidant system and induce apoptosis of zebrafish liver. *Environmental Pollution*, *257*, 113517. https://doi.org/https://doi.org/10.1016/j.envpol.2019.113517
Jinek, M., Chylinski, K., Fonfara, I., Hauer, M., Doudna, J. A., & Charpentier, E. (2012). A programmable dual-RNA-guided DNA endonuclease in adaptive bacterial immunity. *Science*, *337*(6096), 816-821. https://doi.org/10.1126/science.1225829
Jinn, S., Drolet, R. E., Cramer, P. E., Wong, A. H.-K., Toolan, D. M., Gretzula, C. A., Voleti, B., Vassileva, G., Disa, J., Tadin-Strapps, M., & Stone, D. J. (2017). TMEM175 deficiency impairs lysosomal and mitochondrial function and increases α-synuclein aggregation. *Proceedings of the National Academy of Sciences*, *114*(9), 2389-2394. https://doi.org/10.1073/pnas.1616332114
Jones, S., & Gibb, A. J. (2005). Functional NR2B- and NR2D-containing NMDA receptor channels in rat substantia nigra dopaminergic neurones. *J Physiol*, *569*(Pt 1), 209-221. https://doi.org/10.1113/jphysiol.2005.095554
Joo, S. S., Won, T. J., & Lee, D. I. (2004). Potential role of ursodeoxycholic acid in suppression of nuclear factor kappa B in microglial cell line (BV-2). *Arch Pharm Res*, *27*(9), 954-960. https://doi.org/10.1007/bf02975850
Kachergus, J., Mata, I. F., Hulihan, M., Taylor, J. P., Lincoln, S., Aasly, J., Gibson, J. M., Ross, O. A., Lynch, T., Wiley, J., Payami, H., Nutt, J., Maraganore, D. M., Czyzewski, K., Styczynska, M., Wszolek, Z. K., Farrer, M. J., & Toft, M. (2005). Identification of a novel LRRK2 mutation linked to autosomal

dominant parkinsonism: evidence of a common founder across European populations. *Am J Hum Genet*, *76*(4), 672-680. https://doi.org/10.1086/429256

Kalia, L. V., Lang, A. E., Hazrati, L. N., Fujioka, S., Wszolek, Z. K., Dickson, D. W., Ross, O. A., Van Deerlin, V. M., Trojanowski, J. Q., Hurtig, H. I., Alcalay, R. N., Marder, K. S., Clark, L. N., Gaig, C., Tolosa, E., Ruiz-Martínez, J., Marti-Masso, J. F., Ferrer, I., López de Munain, A., Goldman, S. M., Schüle, B., Langston, J. W., Aasly, J. O., Giordana, M. T., Bonifati, V., Puschmann, A., Canesi, M., Pezzoli, G., Maues De Paula, A., Hasegawa, K., Duyckaerts, C., Brice, A., Stoessl, A. J., & Marras, C. (2015). Clinical correlations with Lewy body pathology in LRRK2-related Parkinson disease. *JAMA Neurol*, *72*(1), 100-105. https://doi.org/10.1001/jamaneurol.2014.2704

Kalkonde, Y. V., Morgan, W. W., Sigala, J., Maffi, S. K., Condello, C., Kuziel, W., Ahuja, S. S., & Ahuja, S. K. (2007). Chemokines in the MPTP model of Parkinson's disease: Absence of CCL2 and its receptor CCR2 does not protect against striatal neurodegeneration. *Brain Research*, *1128*, 1-11. https://doi.org/https://doi.org/10.1016/j.brainres.2006.08.041

Karperien, A., Ahammer, H., & Jelinek, H. (2013). Quantitating the subtleties of microglial morphology with fractal analysis [Review]. *Frontiers in Cellular Neuroscience*, *7*(3). https://doi.org/10.3389/fncel.2013.00003

Karperien, A., Ahammer, H., & Jelinek, H. F. (2013). Quantitating the subtleties of microglial morphology with fractal analysis. *Front Cell Neurosci*, *7*, 3. https://doi.org/10.3389/fncel.2013.00003

Katsyuba, E., Mottis, A., Zietak, M., De Franco, F., van der Velpen, V., Gariani, K., Ryu, D., Cialabrini, L., Matilainen, O., Liscio, P., Giacchè, N., Stokar-Regenscheit, N., Legouis, D., de Seigneux, S., Ivanisevic, J., Raffaelli, N., Schoonjans, K., Pellicciari, R., & Auwerx, J. (2018). De novo NAD(+) synthesis enhances mitochondrial function and improves health. *Nature*, *563*(7731), 354-359. https://doi.org/10.1038/s41586-018-0645-6

Keatinge, M., Bui, H., Menke, A., Chen, Y.-C., Sokol, A. M., Bai, Q., Ellett, F., Da Costa, M., Burke, D., Gegg, M., Trollope, L., Payne, T., McTighe, A., Mortiboys, H., de Jager, S., Nuthall, H., Kuo, M.-S., Fleming, A., Schapira, A. H. V., Renshaw, S. A., Highley, J. R., Chacinska, A., Panula, P., Burton, E. A., O'Neill, M. J., & Bandmann, O. (2015). Glucocerebrosidase 1 deficient Danio rerio mirror key pathological aspects of human Gaucher disease and provide evidence of early microglial activation preceding alpha-synuclein-independent neuronal cell death. *Human Molecular Genetics*, *24*(23), 6640-6652. https://doi.org/10.1093/hmg/ddv369

Keene, C. D., Rodrigues, C. M., Eich, T., Chhabra, M. S., Steer, C. J., & Low, W. C. (2002). Tauroursodeoxycholic acid, a bile acid, is neuroprotective in a transgenic animal model of Huntington's disease. *Proc Natl Acad Sci U S A*, *99*(16), 10671-10676. https://doi.org/10.1073/pnas.162362299

Keshavarzian, A., Green, S. J., Engen, P. A., Voigt, R. M., Naqib, A., Forsyth, C. B., Mutlu, E., & Shannon, K. M. (2015). Colonic bacterial composition in Parkinson's disease. *Movement Disorders*, *30*(10), 1351-1360. https://doi.org/https://doi.org/10.1002/mds.26307

Kierdorf, K., Erny, D., Goldmann, T., Sander, V., Schulz, C., Perdiguero, E. G., Wieghofer, P., Heinrich, A., Riemke, P., Hölscher, C., Müller, D. N., Luckow, B., Brocker, T., Debowski, K., Fritz, G., Opdenakker, G., Diefenbach, A., Biber, K., Heikenwalder, M., Geissmann, F., Rosenbauer, F., & Prinz, M. (2013). Microglia emerge from erythromyeloid precursors via Pu.1- and Irf8-dependent pathways. *Nat Neurosci*, *16*(3), 273-280. https://doi.org/10.1038/nn.3318

Kim, B., Yang, M. S., Choi, D., Kim, J. H., Kim, H. S., Seol, W., Choi, S., Jou, I., Kim, E. Y., & Joe, E. H. (2012). Impaired inflammatory responses in murine Lrrk2-knockdown brain microglia. *PLoS ONE*, *7*(4), e34693. https://doi.org/10.1371/journal.pone.0034693

Kim, C., Cho, E.-D., Kim, H.-K., You, S., Lee, H.-J., Hwang, D., & Lee, S.-J. (2014). β1-integrin-dependent migration of microglia in response to neuron-released α-synuclein. *Experimental & Molecular Medicine*, *46*(4), e91-e91. https://doi.org/10.1038/emm.2014.6

Kim, J., Pajarillo, E., Rizor, A., Son, D. S., Lee, J., Aschner, M., & Lee, E. (2019). LRRK2 kinase plays a critical role in manganese-induced inflammation and apoptosis in microglia. *PLoS ONE*, *14*(1), e0210248. https://doi.org/10.1371/journal.pone.0210248

Kim, K. S., Marcogliese, P. C., Yang, J., Callaghan, S. M., Resende, V., Abdel-Messih, E., Marras, C., Visanji, N. P., Huang, J., Schlossmacher, M. G., Trinkle-Mulcahy, L., Slack, R. S., Lang, A. E., & Park, D. S.

(2018). Regulation of myeloid cell phagocytosis by LRRK2 via WAVE2 complex stabilization is altered in Parkinson's disease. *Proceedings of the National Academy of Sciences*, *115*(22), E5164. https://doi.org/10.1073/pnas.1718946115

Kim, M., Gu, G. J., Koh, Y. S., Lee, S. H., Na, Y. R., Seok, S. H., & Lim, K. M. (2018). Fasiglifam (TAK-875), a G Protein-Coupled Receptor 40 (GPR40) Agonist, May Induce Hepatotoxicity through Reactive Oxygen Species Generation in a GPR40-Dependent Manner. *Biomol Ther (Seoul)*, *26*(6), 599-607. https://doi.org/10.4062/biomolther.2017.225

Kim, W.-G., Mohney, R. P., Wilson, B., Jeohn, G.-H., Liu, B., & Hong, J.-S. (2000). Regional Difference in Susceptibility to Lipopolysaccharide-Induced Neurotoxicity in the Rat Brain: Role of Microglia. *The Journal of Neuroscience*, *20*(16), 6309-6316. https://doi.org/10.1523/jneurosci.20-16-06309.2000

Kimmel, C. B., Ballard, W. W., Kimmel, S. R., Ullmann, B., & Schilling, T. F. (1995). Stages of embryonic development of the zebrafish. *Dev Dyn*, *203*(3), 253-310. https://doi.org/10.1002/aja.1002030302

Kipnis, J., & Filiano, A. J. (2018). The central nervous system: privileged by immune connections. *Nature Reviews Immunology*, *18*(2), 83-84. https://doi.org/10.1038/nri.2017.152

Kitada, T., Asakawa, S., Hattori, N., Matsumine, H., Yamamura, Y., Minoshima, S., Yokochi, M., Mizuno, Y., & Shimizu, N. (1998). Mutations in the parkin gene cause autosomal recessive juvenile parkinsonism. *Nature*, *392*(6676), 605-608. https://doi.org/10.1038/33416

Klatt, S., Doecke, J. D., Roberts, A., Boughton, B. A., Masters, C. L., Horne, M., & Roberts, B. R. (2021). A six-metabolite panel as potential blood-based biomarkers for Parkinson's disease. *NPJ Parkinsons Dis*, *7*(1), 94. https://doi.org/10.1038/s41531-021-00239-x

Klein, C. L., Rovelli, G., Springer, W., Schall, C., Gasser, T., & Kahle, P. J. (2009). Homo- and heterodimerization of ROCO kinases: LRRK2 kinase inhibition by the LRRK2 ROCO fragment. *J Neurochem*, *111*(3), 703-715. https://doi.org/10.1111/j.1471-4159.2009.06358.x

Knyihár-Csillik, E., Csillik, B., Pákáski, M., Krisztin-Péva, B., Dobó, E., Okuno, E., & Vécsei, L. (2004). Decreased expression of kynurenine aminotransferase-I (KAT-I) in the substantia nigra of mice after 1-methyl-4-phenyl-1,2,3,6-tetrahydropyridine (MPTP) treatment. *Neuroscience*, *126*(4), 899-914. https://doi.org/10.1016/j.neuroscience.2004.04.043

Koblinger, K., Jean-Xavier, C., Sharma, S., Füzesi, T., Young, L., Eaton, S. E. A., Kwok, C. H. T., Bains, J. S., & Whelan, P. J. (2018). Optogenetic Activation of A11 Region Increases Motor Activity [Original Research]. *Frontiers in Neural Circuits*, *12*(86). https://doi.org/10.3389/fncir.2018.00086

Kofuji, T., Fujiwara, T., Sanada, M., Mishima, T., & Akagawa, K. (2014). HPC-1/syntaxin 1A and syntaxin 1B play distinct roles in neuronal survival. *Journal of Neurochemistry*, *130*(4), 514-525. https://doi.org/https://doi.org/10.1111/jnc.12722

Komor, A. C., Kim, Y. B., Packer, M. S., Zuris, J. A., & Liu, D. R. (2016). Programmable editing of a target base in genomic DNA without double-stranded DNA cleavage. *Nature*, *533*(7603), 420-424. https://doi.org/10.1038/nature17946

Kordower, J. H., Olanow, C. W., Dodiya, H. B., Chu, Y., Beach, T. G., Adler, C. H., Halliday, G. M., & Bartus, R. T. (2013). Disease duration and the integrity of the nigrostriatal system in Parkinson's disease. *Brain*, *136*(Pt 8), 2419-2431. https://doi.org/10.1093/brain/awt192

Korr, D., Toschi, L., Donner, P., Pohlenz, H. D., Kreft, B., & Weiss, B. (2006). LRRK1 protein kinase activity is stimulated upon binding of GTP to its Roc domain. *Cell Signal*, *18*(6), 910-920. https://doi.org/10.1016/j.cellsig.2005.08.015

Kozina, E., Sadasivan, S., Jiao, Y., Dou, Y., Ma, Z., Tan, H., Kodali, K., Shaw, T., Peng, J., & Smeyne, R. J. (2018). Mutant LRRK2 mediates peripheral and central immune responses leading to neurodegeneration in vivo. *Brain*, *141*(6), 1753-1769. https://doi.org/10.1093/brain/awy077

Krogdahl, Å., Gajardo, K., Kortner, T. M., Penn, M., Gu, M., Berge, G. M., & Bakke, A. M. (2015). Soya Saponins Induce Enteritis in Atlantic Salmon (Salmo salar L.). *Journal of Agricultural and Food Chemistry*, *63*(15), 3887-3902. https://doi.org/10.1021/jf506242t

Kumar, N., Leonzino, M., Hancock-Cerutti, W., Horenkamp, F. A., Li, P., Lees, J. A., Wheeler, H., Reinisch, K. M., & De Camilli, P. (2018). VPS13A and VPS13C are lipid transport proteins differentially

localized at ER contact sites. *Journal of Cell Biology*, *217*(10), 3625-3639. https://doi.org/10.1083/jcb.201807019
Kumari, U., & Tan, E. K. (2009). LRRK2 in Parkinson's disease: genetic and clinical studies from patients. *Febs j*, *276*(22), 6455-6463. https://doi.org/10.1111/j.1742-4658.2009.07344.x
Kuss, M., Adamopoulou, E., & Kahle, P. J. (2014). Interferon-γ induces leucine-rich repeat kinase LRRK2 via extracellular signal-regulated kinase ERK5 in macrophages. *J Neurochem*, *129*(6), 980-987. https://doi.org/10.1111/jnc.12668
Lam, C. S., Korzh, V., & Strahle, U. (2005). Zebrafish embryos are susceptible to the dopaminergic neurotoxin MPTP. *Eur J Neurosci*, *21*(6), 1758-1762. https://doi.org/10.1111/j.1460-9568.2005.03988.x
Langston, R. G., Rudenko, I. N., Kumaran, R., Hauser, D. N., Kaganovich, A., Ponce, L. B., Mamais, A., Ndukwe, K., Dillman, A. A., Al-Saif, A. M., Beilina, A., & Cookson, M. R. (2019). Differences in Stability, Activity and Mutation Effects Between Human and Mouse Leucine-Rich Repeat Kinase 2. *Neurochem Res*, *44*(6), 1446-1459. https://doi.org/10.1007/s11064-018-2650-4
Larbalestier, H., Keatinge, M., Watson, L., White, E., Gowda, S., Wei, W., Koler, K., Semenova, S. A., Elkin, A. M., Rimmer, N., Sweeney, S. T., Mazzolini, J., Sieger, D., Hide, W., McDearmid, J., Panula, P., MacDonald, R. B., & Bandmann, O. (2021). GCH1 deficiency activates brain innate immune response and impairs tyrosine hydroxylase homeostasis. *The Journal of Neuroscience*, JN-RM-0653-0621. https://doi.org/10.1523/jneurosci.0653-21.2021
Larochelle, C., Alvarez, J. I., & Prat, A. (2011). How do immune cells overcome the blood-brain barrier in multiple sclerosis? *FEBS Lett*, *585*(23), 3770-3780. https://doi.org/10.1016/j.febslet.2011.04.066
Lee, D. Y., Lee, K.-S., Lee, H. J., Noh, Y. H., Kim, D. H., Lee, J. Y., Cho, S. H., Yoon, O. J., Lee, W. B., Kim, K. Y., Chung, Y. H., & Kim, S. S. (2008). Kynurenic acid attenuates MPP+-induced dopaminergic neuronal cell death via a Bax-mediated mitochondrial pathway. *European Journal of Cell Biology*, *87*(6), 389-397. https://doi.org/https://doi.org/10.1016/j.ejcb.2008.03.003
Lee, H. J., & Chung, K. C. (2012). PINK1 positively regulates IL-1β-mediated signaling through Tollip and IRAK1 modulation. *Journal of Neuroinflammation*, *9*(1), 271. https://doi.org/10.1186/1742-2094-9-271
Lee, M. C., Ting, K. K., Adams, S., Brew, B. J., Chung, R., & Guillemin, G. J. (2010). Characterisation of the expression of NMDA receptors in human astrocytes. *PLoS ONE*, *5*(11), e14123. https://doi.org/10.1371/journal.pone.0014123
Lee, S. B., Kim, W., Lee, S., & Chung, J. (2007). Loss of LRRK2/PARK8 induces degeneration of dopaminergic neurons in Drosophila. *Biochem Biophys Res Commun*, *358*(2), 534-539. https://doi.org/10.1016/j.bbrc.2007.04.156
Lesage, S., Dürr, A., Tazir, M., Lohmann, E., Leutenegger, A. L., Janin, S., Pollak, P., & Brice, A. (2006). LRRK2 G2019S as a cause of Parkinson's disease in North African Arabs. *N Engl J Med*, *354*(4), 422-423. https://doi.org/10.1056/NEJMc055540
Letsiou, E., Sammani, S., Wang, H., Belvitch, P., & Dudek, S. M. (2017). Parkin regulates lipopolysaccharide-induced proinflammatory responses in acute lung injury. *Transl Res*, *181*, 71-82. https://doi.org/10.1016/j.trsl.2016.09.002
Lewis, A., & Elks, P. M. (2019). Hypoxia Induces Macrophage tnfa Expression via Cyclooxygenase and Prostaglandin E2 in vivo [Original Research]. *Frontiers in Immunology*, *10*(2321). https://doi.org/10.3389/fimmu.2019.02321
Lewitt, P. A., Li, J., Lu, M., Beach, T. G., Adler, C. H., & Guo, L. (2013). 3-hydroxykynurenine and other Parkinson's disease biomarkers discovered by metabolomic analysis. *Mov Disord*, *28*(12), 1653-1660. https://doi.org/10.1002/mds.25555
Li, J.-Q., Tan, L., & Yu, J.-T. (2014). The role of the LRRK2 gene in Parkinsonism. *Molecular Neurodegeneration*, *9*(1), 47. https://doi.org/10.1186/1750-1326-9-47
Li, L., Jin, H., Xu, J., Shi, Y., & Wen, Z. (2011). Irf8 regulates macrophage versus neutrophil fate during zebrafish primitive myelopoiesis. *Blood*, *117*(4), 1359-1369. https://doi.org/10.1182/blood-2010-06-290700
Li, R., Huang, Y.-G., Fang, D., & Le, W.-D. (2004). (−)-Epigallocatechin gallate inhibits lipopolysaccharide-induced microglial activation and protects against inflammation-mediated dopaminergic

neuronal injury. *Journal of Neuroscience Research*, *78*(5), 723-731. https://doi.org/https://doi.org/10.1002/jnr.20315

Li, S., Guo, W., Geng, H., Wang, C., Yang, S., & Xu, X. (2020). LINC00511 exacerbated T-cell acute lymphoblastic leukemia via miR-195-5p/LRRK1 axis. *Biosci Rep*, *40*(5). https://doi.org/10.1042/bsr20193631

Li, X., Tan, Y. C., Poulose, S., Olanow, C. W., Huang, X. Y., & Yue, Z. (2007). Leucine-rich repeat kinase 2 (LRRK2)/PARK8 possesses GTPase activity that is altered in familial Parkinson's disease R1441C/G mutants. *J Neurochem*, *103*(1), 238-247. https://doi.org/10.1111/j.1471-4159.2007.04743.x

Liang, X., Potter, J., Kumar, S., Ravinder, N., & Chesnut, J. D. (2017). Enhanced CRISPR/Cas9-mediated precise genome editing by improved design and delivery of gRNA, Cas9 nuclease, and donor DNA. *Journal of Biotechnology*, *241*, 136-146. https://doi.org/https://doi.org/10.1016/j.jbiotec.2016.11.011

Liao, J., Wu, C. X., Burlak, C., Zhang, S., Sahm, H., Wang, M., Zhang, Z. Y., Vogel, K. W., Federici, M., Riddle, S. M., Nichols, R. J., Liu, D., Cookson, M. R., Stone, T. A., & Hoang, Q. Q. (2014). Parkinson disease-associated mutation R1441H in LRRK2 prolongs the "active state" of its GTPase domain. *Proc Natl Acad Sci U S A*, *111*(11), 4055-4060. https://doi.org/10.1073/pnas.1323285111

Liberatore, G. T., Jackson-Lewis, V., Vukosavic, S., Mandir, A. S., Vila, M., McAuliffe, W. G., Dawson, V. L., Dawson, T. M., & Przedborski, S. (1999). Inducible nitric oxide synthase stimulates dopaminergic neurodegeneration in the MPTP model of Parkinson disease. *Nature Medicine*, *5*(12), 1403-1409. https://doi.org/10.1038/70978

Lill, C. M., Roehr, J. T., McQueen, M. B., Kavvoura, F. K., Bagade, S., Schjeide, B. M., Schjeide, L. M., Meissner, E., Zauft, U., Allen, N. C., Liu, T., Schilling, M., Anderson, K. J., Beecham, G., Berg, D., Biernacka, J. M., Brice, A., DeStefano, A. L., Do, C. B., Eriksson, N., Factor, S. A., Farrer, M. J., Foroud, T., Gasser, T., Hamza, T., Hardy, J. A., Heutink, P., Hill-Burns, E. M., Klein, C., Latourelle, J. C., Maraganore, D. M., Martin, E. R., Martinez, M., Myers, R. H., Nalls, M. A., Pankratz, N., Payami, H., Satake, W., Scott, W. K., Sharma, M., Singleton, A. B., Stefansson, K., Toda, T., Tung, J. Y., Vance, J., Wood, N. W., Zabetian, C. P., Young, P., Tanzi, R. E., Khoury, M. J., Zipp, F., Lehrach, H., Ioannidis, J. P., & Bertram, L. (2012). Comprehensive research synopsis and systematic meta-analyses in Parkinson's disease genetics: The PDGene database. *PLoS Genet*, *8*(3), e1002548. https://doi.org/10.1371/journal.pgen.1002548

Lin, X., Parisiadou, L., Gu, X. L., Wang, L., Shim, H., Sun, L., Xie, C., Long, C. X., Yang, W. J., Ding, J., Chen, Z. Z., Gallant, P. E., Tao-Cheng, J. H., Rudow, G., Troncoso, J. C., Liu, Z., Li, Z., & Cai, H. (2009). Leucine-rich repeat kinase 2 regulates the progression of neuropathology induced by Parkinson's-disease-related mutant alpha-synuclein. *Neuron*, *64*(6), 807-827. https://doi.org/10.1016/j.neuron.2009.11.006

Lin, Y., Tang, Y. J., Zong, H. L., Gu, J. X., Deng, W. W., Wang, C., & Sun, B. (2007). Cyclin G associated kinase interacts with interleukin 12 receptor β2 and suppresses interleukin 12 induced IFN-γ production. *FEBS Letters*, *581*(26), 5151-5157. https://doi.org/https://doi.org/10.1016/j.febslet.2007.09.056

Liu, B., Fang, F., Pedersen, N. L., Tillander, A., Ludvigsson, J. F., Ekbom, A., Svenningsson, P., Chen, H., & Wirdefeldt, K. (2017). Vagotomy and Parkinson disease. *A Swedish register–based matched-cohort study*, *88*(21), 1996-2002. https://doi.org/10.1212/wnl.0000000000003961

Liu, J. Z., van Sommeren, S., Huang, H., Ng, S. C., Alberts, R., Takahashi, A., Ripke, S., Lee, J. C., Jostins, L., Shah, T., Abedian, S., Cheon, J. H., Cho, J., Dayani, N. E., Franke, L., Fuyuno, Y., Hart, A., Juyal, R. C., Juyal, G., Kim, W. H., Morris, A. P., Poustchi, H., Newman, W. G., Midha, V., Orchard, T. R., Vahedi, H., Sood, A., Sung, J. Y., Malekzadeh, R., Westra, H. J., Yamazaki, K., Yang, S. K., Barrett, J. C., Alizadeh, B. Z., Parkes, M., Bk, T., Daly, M. J., Kubo, M., Anderson, C. A., & Weersma, R. K. (2015). Association analyses identify 38 susceptibility loci for inflammatory bowel disease and highlight shared genetic risk across populations. *Nat Genet*, *47*(9), 979-986. https://doi.org/10.1038/ng.3359

Liu, W., Vives-Bauza, C., Acín-Peréz, R., Yamamoto, A., Tan, Y., Li, Y., Magrané, J., Stavarache, M. A., Shaffer, S., Chang, S., Kaplitt, M. G., Huang, X.-Y., Beal, M. F., Manfredi, G., & Li, C. (2009). PINK1

Defect Causes Mitochondrial Dysfunction, Proteasomal Deficit and α-Synuclein Aggregation in Cell Culture Models of Parkinson's Disease. *PLoS ONE*, *4*(2), e4597. https://doi.org/10.1371/journal.pone.0004597

Longo, F., Russo, I., Shimshek, D. R., Greggio, E., & Morari, M. (2014). Genetic and pharmacological evidence that G2019S LRRK2 confers a hyperkinetic phenotype, resistant to motor decline associated with aging. *Neurobiol Dis*, *71*, 62-73. https://doi.org/10.1016/j.nbd.2014.07.013

López Nadal, A., Peggs, D., Wiegertjes, G. F., & Brugman, S. (2018). Exposure to Antibiotics Affects Saponin Immersion-Induced Immune Stimulation and Shift in Microbial Composition in Zebrafish Larvae. *Front Microbiol*, *9*, 2588. https://doi.org/10.3389/fmicb.2018.02588

Luan, H., Liu, L. F., Meng, N., Tang, Z., Chua, K. K., Chen, L. L., Song, J. X., Mok, V. C., Xie, L. X., Li, M., & Cai, Z. (2015). LC-MS-based urinary metabolite signatures in idiopathic Parkinson's disease. *J Proteome Res*, *14*(1), 467-478. https://doi.org/10.1021/pr500807t

Lücking, C. B., Dürr, A., Bonifati, V., Vaughan, J., De Michele, G., Gasser, T., Harhangi, B. S., Meco, G., Denèfle, P., Wood, N. W., Agid, Y., Nicholl, D., Breteler, M. M. B., Oostra, B. A., De Mari, M., Marconi, R., Filla, A., Bonnet, A.-M., Broussolle, E., Pollak, P., Rascol, O., Rosier, M., Arnould, A., & Brice, A. (2000). Association between Early-Onset Parkinson's Disease and Mutations in the Parkin Gene. *New England Journal of Medicine*, *342*(21), 1560-1567. https://doi.org/10.1056/nejm200005253422103

Lugo-Huitrón, R., Blanco-Ayala, T., Ugalde-Muñiz, P., Carrillo-Mora, P., Pedraza-Chaverrí, J., Silva-Adaya, D., Maldonado, P. D., Torres, I., Pinzón, E., Ortiz-Islas, E., López, T., García, E., Pineda, B., Torres-Ramos, M., Santamaría, A., & La Cruz, V. P. (2011). On the antioxidant properties of kynurenic acid: free radical scavenging activity and inhibition of oxidative stress. *Neurotoxicol Teratol*, *33*(5), 538-547. https://doi.org/10.1016/j.ntt.2011.07.002

Luzón-Toro, B., Rubio de la Torre, E., Delgado, A., Pérez-Tur, J., & Hilfiker, S. (2007). Mechanistic insight into the dominant mode of the Parkinson's disease-associated G2019S LRRK2 mutation. *Hum Mol Genet*, *16*(17), 2031-2039. https://doi.org/10.1093/hmg/ddm151

Lv, C., Sun, L., Guo, Z., Li, H., Kong, D., Xu, B., Lin, L., Liu, T., Guo, D., Zhou, J., & Li, Y. (2018). Circular RNA regulatory network reveals cell-cell crosstalk in acute myeloid leukemia extramedullary infiltration. *J Transl Med*, *16*(1), 361. https://doi.org/10.1186/s12967-018-1726-x

Maas, J. W., Yang, J., & Edwards, R. H. (2017). Endogenous Leucine-Rich Repeat Kinase 2 Slows Synaptic Vesicle Recycling in Striatal Neurons. *Front Synaptic Neurosci*, *9*, 5. https://doi.org/10.3389/fnsyn.2017.00005

MacLeod, D., Dowman, J., Hammond, R., Leete, T., Inoue, K., & Abeliovich, A. (2006). The familial Parkinsonism gene LRRK2 regulates neurite process morphology. *Neuron*, *52*(4), 587-593. https://doi.org/10.1016/j.neuron.2006.10.008

Madeira, F., Park, Y. M., Lee, J., Buso, N., Gur, T., Madhusoodanan, N., Basutkar, P., Tivey, A. R. N., Potter, S. C., Finn, R. D., & Lopez, R. (2019). The EMBL-EBI search and sequence analysis tools APIs in 2019. *Nucleic Acids Research*, *47*(W1), W636-W641. https://doi.org/10.1093/nar/gkz268

Majewski, M., Kasica, N., Jakimiuk, A., & Podlasz, P. (2018). Toxicity and cardiac effects of acute exposure to tryptophan metabolites on the kynurenine pathway in early developing zebrafish (Danio rerio) embryos. *Toxicol Appl Pharmacol*, *341*, 16-29. https://doi.org/10.1016/j.taap.2018.01.004

Makishima, M., Lu, T. T., Xie, W., Whitfield, G. K., Domoto, H., Evans, R. M., Haussler, M. R., & Mangelsdorf, D. J. (2002). Vitamin D receptor as an intestinal bile acid sensor. *Science*, *296*(5571), 1313-1316. https://doi.org/10.1126/science.1070477

Makishima, M., Okamoto, A. Y., Repa, J. J., Tu, H., Learned, R. M., Luk, A., Hull, M. V., Lustig, K. D., Mangelsdorf, D. J., & Shan, B. (1999). Identification of a nuclear receptor for bile acids. *Science*, *284*(5418), 1362-1365. https://doi.org/10.1126/science.284.5418.1362

Mandler, M., Valera, E., Rockenstein, E., Weninger, H., Patrick, C., Adame, A., Santic, R., Meindl, S., Vigl, B., Smrzka, O., Schneeberger, A., Mattner, F., & Masliah, E. (2014). Next-generation active immunization approach for synucleinopathies: implications for Parkinson's disease clinical trials. *Acta Neuropathol*, *127*(6), 861-879. https://doi.org/10.1007/s00401-014-1256-4

Mangano, E. N., Litteljohn, D., So, R., Nelson, E., Peters, S., Bethune, C., Bobyn, J., & Hayley, S. (2012). Interferon-γ plays a role in paraquat-induced neurodegeneration involving oxidative and proinflammatory pathways. *Neurobiology of Aging*, *33*(7), 1411-1426. https://doi.org/https://doi.org/10.1016/j.neurobiolaging.2011.02.016

Manjunatha, B., Sreevidya, B., & Lee, S. J. (2021). Developmental toxicity triggered by benzyl alcohol in the early stage of zebrafish embryos: Cardiovascular defects with inhibited liver formation and degenerated neurogenesis. *Sci Total Environ*, *752*, 141631. https://doi.org/10.1016/j.scitotenv.2020.141631

Marder, K., Wang, Y., Alcalay, R. N., Mejia-Santana, H., Tang, M. X., Lee, A., Raymond, D., Mirelman, A., Saunders-Pullman, R., Clark, L., Ozelius, L., Orr-Urtreger, A., Giladi, N., & Bressman, S. (2015). Age-specific penetrance of LRRK2 G2019S in the Michael J. Fox Ashkenazi Jewish LRRK2 Consortium. *Neurology*, *85*(1), 89-95. https://doi.org/10.1212/wnl.0000000000001708

Marín, I. (2006). The Parkinson disease gene LRRK2: evolutionary and structural insights. *Mol Biol Evol*, *23*(12), 2423-2433. https://doi.org/10.1093/molbev/msl114

Marín, I. (2008). Ancient origin of the Parkinson disease gene LRRK2. *J Mol Evol*, *67*(1), 41-50. https://doi.org/10.1007/s00239-008-9122-4

Marjoram, L., Alvers, A., Deerhake, M. E., Bagwell, J., Mankiewicz, J., Cocchiaro, J. L., Beerman, R. W., Willer, J., Sumigray, K. D., Katsanis, N., Tobin, D. M., Rawls, J. F., Goll, M. G., & Bagnat, M. (2015). Epigenetic control of intestinal barrier function and inflammation in zebrafish. *Proc Natl Acad Sci U S A*, *112*(9), 2770-2775. https://doi.org/10.1073/pnas.1424089112

Martí-Massó, J. F., Bergareche, A., Makarov, V., Ruiz-Martinez, J., Gorostidi, A., López de Munain, A., Poza, J. J., Striano, P., Buxbaum, J. D., & Paisán-Ruiz, C. (2013). The ACMSD gene, involved in tryptophan metabolism, is mutated in a family with cortical myoclonus, epilepsy, and parkinsonism. *J Mol Med (Berl)*, *91*(12), 1399-1406. https://doi.org/10.1007/s00109-013-1075-4

Martinou, J. C., Le Van Thai, A., Valette, A., & Weber, M. J. (1990). Transforming growth factor beta 1 is a potent survival factor for rat embryo motoneurons in culture. *Brain Res Dev Brain Res*, *52*(1-2), 175-181. https://doi.org/10.1016/0165-3806(90)90233-o

Masud, S., Prajsnar, T. K., Torraca, V., Lamers, G. E. M., Benning, M., Van Der Vaart, M., & Meijer, A. H. (2019). Macrophages target Salmonella by Lc3-associated phagocytosis in a systemic infection model. *Autophagy*, *15*(5), 796-812. https://doi.org/10.1080/15548627.2019.1569297

Masuda, T., Iwamoto, S., Mikuriya, S., Tozaki-Saitoh, H., Tamura, T., Tsuda, M., & Inoue, K. (2015). Transcription factor IRF1 is responsible for IRF8-mediated IL-1β expression in reactive microglia. *J Pharmacol Sci*, *128*(4), 216-220. https://doi.org/10.1016/j.jphs.2015.08.002

Masuda, T., Nishimoto, N., Tomiyama, D., Matsuda, T., Tozaki-Saitoh, H., Tamura, T., Kohsaka, S., Tsuda, M., & Inoue, K. (2014). IRF8 is a transcriptional determinant for microglial motility. *Purinergic Signal*, *10*(3), 515-521. https://doi.org/10.1007/s11302-014-9413-8

Matsumoto, H., Sengoku, R., Saito, Y., Kakuta, Y., Murayama, S., & Imafuku, I. (2014). Sudden death in Parkinson's disease: a retrospective autopsy study. *J Neurol Sci*, *343*(1-2), 149-152. https://doi.org/10.1016/j.jns.2014.05.060

Mazzolini, J., Le Clerc, S., Morisse, G., Coulonges, C., Kuil, L. E., van Ham, T. J., Zagury, J.-F., & Sieger, D. (2020). Gene expression profiling reveals a conserved microglia signature in larval zebrafish. *Glia*, *68*(2), 298-315. https://doi.org/https://doi.org/10.1002/glia.23717

Mazzoni, P., Shabbott, B., & Cortés, J. C. (2012). Motor control abnormalities in Parkinson's disease. *Cold Spring Harb Perspect Med*, *2*(6), a009282. https://doi.org/10.1101/cshperspect.a009282

McFarthing, K., & Simuni, T. (2019). Clinical Trial Highlights: Targeting Alpha-Synuclein. *Journal of Parkinson's Disease*, *9*, 5-16. https://doi.org/10.3233/JPD-189004

McGeer, P. L., Itagaki, S., Boyes, B. E., & McGeer, E. G. (1988). Reactive microglia are positive for HLA-DR in the substantia nigra of Parkinson's and Alzheimer's disease brains. *Neurology*, *38*(8), 1285-1291. https://doi.org/10.1212/wnl.38.8.1285

Melrose, H. L., Kent, C. B., Taylor, J. P., Dachsel, J. C., Hinkle, K. M., Lincoln, S. J., Mok, S. S., Culvenor, J. G., Masters, C. L., Tyndall, G. M., Bass, D. I., Ahmed, Z., Andorfer, C. A., Ross, O. A., Wszolek, Z. K., Delldonne, A., Dickson, D. W., & Farrer, M. J. (2007). A comparative analysis of leucine-rich

repeat kinase 2 (Lrrk2) expression in mouse brain and Lewy body disease. *Neuroscience*, *147*(4), 1047-1058. https://doi.org/10.1016/j.neuroscience.2007.05.027

Mencacci, N. E., Isaias, I. U., Reich, M. M., Ganos, C., Plagnol, V., Polke, J. M., Bras, J., Hersheson, J., Stamelou, M., Pittman, A. M., Noyce, A. J., Mok, K. Y., Opladen, T., Kunstmann, E., Hodecker, S., Münchau, A., Volkmann, J., Samnick, S., Sidle, K., Nanji, T., Sweeney, M. G., Houlden, H., Batla, A., Zecchinelli, A. L., Pezzoli, G., Marotta, G., Lees, A., Alegria, P., Krack, P., Cormier-Dequaire, F., Lesage, S., Brice, A., Heutink, P., Gasser, T., Lubbe, S. J., Morris, H. R., Taba, P., Koks, S., Majounie, E., Raphael Gibbs, J., Singleton, A., Hardy, J., Klebe, S., Bhatia, K. P., Wood, N. W., Consortium, o. b. o. t. I. P. s. D. G., & consortium, U.-e. (2014). Parkinson's disease in GTP cyclohydrolase 1 mutation carriers. *Brain*, *137*(9), 2480-2492. https://doi.org/10.1093/brain/awu179

Mesens, N., Crawford, A. D., Menke, A., Hung, P. D., Van Goethem, F., Nuyts, R., Hansen, E., Wolterbeek, A., Van Gompel, J., De Witte, P., & Esguerra, C. V. (2015). Are zebrafish larvae suitable for assessing the hepatotoxicity potential of drug candidates? *J Appl Toxicol*, *35*(9), 1017-1029. https://doi.org/10.1002/jat.3091

Miklossy, J., Arai, T., Guo, J. P., Klegeris, A., Yu, S., McGeer, E. G., & McGeer, P. L. (2006). LRRK2 expression in normal and pathologic human brain and in human cell lines. *J Neuropathol Exp Neurol*, *65*(10), 953-963. https://doi.org/10.1097/01.jnen.0000235121.98052.54

Milosevic, J., Schwarz, S. C., Ogunlade, V., Meyer, A. K., Storch, A., & Schwarz, J. (2009). Emerging role of LRRK2 in human neural progenitor cell cycle progression, survival and differentiation. *Mol Neurodegener*, *4*, 25. https://doi.org/10.1186/1750-1326-4-25

Minghetti, L., Greco, A., Potenza, R. L., Pezzola, A., Blum, D., Bantubungi, K., & Popoli, P. (2007). Effects of the adenosine A2A receptor antagonist SCH 58621 on cyclooxygenase-2 expression, glial activation, and brain-derived neurotrophic factor availability in a rat model of striatal neurodegeneration. *J Neuropathol Exp Neurol*, *66*(5), 363-371. https://doi.org/10.1097/nen.0b013e3180517477

Minten, C., Terry, R., Deffrasnes, C., King, N. J., & Campbell, I. L. (2012). IFN regulatory factor 8 is a key constitutive determinant of the morphological and molecular properties of microglia in the CNS. *PLoS ONE*, *7*(11), e49851. https://doi.org/10.1371/journal.pone.0049851

Miranda, A. F., Boegman, R. J., Beninger, R. J., & Jhamandas, K. (1997). Protection against quinolinic acid-mediated excitotoxicity in nigrostriatal dopaminergic neurons by endogenous kynurenic acid. *Neuroscience*, *78*(4), 967-975. https://doi.org/https://doi.org/10.1016/S0306-4522(96)00655-0

Miryounesi, M., Nikfar, A., Changi-Ashtiani, M., Shahrooei, M., Dinmohammadi, H., Shahani, T., Zarvandi, S., Bahrami, T., Momenilandi, M., & Rokni-Zadeh, H. (2020). A novel homozygous LRRK1 stop gain mutation in a patient suspected with osteosclerotic metaphyseal dysplasia. *Ann Hum Genet*, *84*(1), 102-106. https://doi.org/10.1111/ahg.12352

Mitchell, A. L., Attwood, T. K., Babbitt, P. C., Blum, M., Bork, P., Bridge, A., Brown, S. D., Chang, H. Y., El-Gebali, S., Fraser, M. I., Gough, J., Haft, D. R., Huang, H., Letunic, I., Lopez, R., Luciani, A., Madeira, F., Marchler-Bauer, A., Mi, H., Natale, D. A., Necci, M., Nuka, G., Orengo, C., Pandurangan, A. P., Paysan-Lafosse, T., Pesseat, S., Potter, S. C., Qureshi, M. A., Rawlings, N. D., Redaschi, N., Richardson, L. J., Rivoire, C., Salazar, G. A., Sangrador-Vegas, A., Sigrist, C. J. A., Sillitoe, I., Sutton, G. G., Thanki, N., Thomas, P. D., Tosatto, S. C. E., Yong, S. Y., & Finn, R. D. (2019). InterPro in 2019: improving coverage, classification and access to protein sequence annotations. *Nucleic Acids Res*, *47*(D1), D351-d360. https://doi.org/10.1093/nar/gky1100

Mittal, S., Bjørnevik, K., Im, D. S., Flierl, A., Dong, X., Locascio, J. J., Abo, K. M., Long, E., Jin, M., Xu, B., Xiang, Y. K., Rochet, J. C., Engeland, A., Rizzu, P., Heutink, P., Bartels, T., Selkoe, D. J., Caldarone, B. J., Glicksman, M. A., Khurana, V., Schüle, B., Park, D. S., Riise, T., & Scherzer, C. R. (2017). β2-Adrenoreceptor is a regulator of the α-synuclein gene driving risk of Parkinson's disease. *Science*, *357*(6354), 891-898. https://doi.org/10.1126/science.aaf3934

Moehle, M. S., Webber, P. J., Tse, T., Sukar, N., Standaert, D. G., DeSilva, T. M., Cowell, R. M., & West, A. B. (2012). LRRK2 inhibition attenuates microglial inflammatory responses. *J Neurosci*, *32*(5), 1602-1611. https://doi.org/10.1523/jneurosci.5601-11.2012

Mogi, M., Harada, M., Kondo, T., Narabayashi, H., Riederer, P., & Nagatsu, T. (1995). Transforming growth factor-beta 1 levels are elevated in the striatum and in ventricular cerebrospinal fluid in Parkinson's disease. *Neurosci Lett*, *193*(2), 129-132. https://doi.org/10.1016/0304-3940(95)11686-q

Mogi, M., Harada, M., Kondo, T., Riederer, P., Inagaki, H., Minami, M., & Nagatsu, T. (1994). Interleukin-1 beta, interleukin-6, epidermal growth factor and transforming growth factor-alpha are elevated in the brain from parkinsonian patients. *Neurosci Lett*, *180*(2), 147-150. https://doi.org/10.1016/0304-3940(94)90508-8

Mogi, M., Harada, M., Narabayashi, H., Inagaki, H., Minami, M., & Nagatsu, T. (1996). Interleukin (IL)-1 beta, IL-2, IL-4, IL-6 and transforming growth factor-alpha levels are elevated in ventricular cerebrospinal fluid in juvenile parkinsonism and Parkinson's disease. *Neurosci Lett*, *211*(1), 13-16. https://doi.org/10.1016/0304-3940(96)12706-3

Mogi, M., Harada, M., Riederer, P., Narabayashi, H., Fujita, K., & Nagatsu, T. (1994). Tumor necrosis factor-alpha (TNF-alpha) increases both in the brain and in the cerebrospinal fluid from parkinsonian patients. *Neurosci Lett*, *165*(1-2), 208-210. https://doi.org/10.1016/0304-3940(94)90746-3

Montague, T. G., Cruz, J. M., Gagnon, J. A., Church, G. M., & Valen, E. (2014). CHOPCHOP: a CRISPR/Cas9 and TALEN web tool for genome editing. *Nucleic Acids Res*, *42*(Web Server issue), W401-407. https://doi.org/10.1093/nar/gku410

Moresco, R. M., Lavazza, T., Belloli, S., Lecchi, M., Pezzola, A., Todde, S., Matarrese, M., Carpinelli, A., Turolla, E., Zimarino, V., Popoli, P., Malgaroli, A., & Fazio, F. (2008). Quinolinic acid induced neurodegeneration in the striatum: a combined in vivo and in vitro analysis of receptor changes and microglia activation. *Eur J Nucl Med Mol Imaging*, *35*(4), 704-715. https://doi.org/10.1007/s00259-007-0651-7

Morimoto, K., Baba, Y., Shinohara, H., Kang, S., Nojima, S., Kimura, T., Ito, D., Yoshida, Y., Maeda, Y., Sarashina-Kida, H., Nishide, M., Hosokawa, T., Kato, Y., Hayama, Y., Kinehara, Y., Okuno, T., Takamatsu, H., Hirano, T., Shima, Y., Narazaki, M., Kurosaki, T., Toyofuku, T., & Kumanogoh, A. (2016). LRRK1 is critical in the regulation of B-cell responses and CARMA1-dependent NF-κB activation. *Sci Rep*, *6*, 25738. https://doi.org/10.1038/srep25738

Morris, M. C., Evans, D. A., Bienias, J. L., Scherr, P. A., Tangney, C. C., Hebert, L. E., Bennett, D. A., Wilson, R. S., & Aggarwal, N. (2004). Dietary niacin and the risk of incident Alzheimer's disease and of cognitive decline. *Journal of Neurology, Neurosurgery & Psychiatry*, *75*(8), 1093-1099. https://doi.org/10.1136/jnnp.2003.025858

Mortiboys, H., Furmston, R., Bronstad, G., Aasly, J., Elliott, C., & Bandmann, O. (2015). UDCA exerts beneficial effect on mitochondrial dysfunction in LRRK2(G2019S) carriers and in vivo. *Neurology*, *85*(10), 846-852. https://doi.org/10.1212/wnl.0000000000001905

Murín, R., Verleysdonk, S., Rapp, M., & Hamprecht, B. (2006). Immunocytochemical localization of 3-methylcrotonyl-CoA carboxylase in cultured ependymal, microglial and oligodendroglial cells. *Journal of Neurochemistry*, *97*(5), 1393-1402. https://doi.org/https://doi.org/10.1111/j.1471-4159.2006.03819.x

Nakatsu, F., Messa, M., Nández, R., Czapla, H., Zou, Y., Strittmatter, S. M., & De Camilli, P. (2015). Sac2/INPP5F is an inositol 4-phosphatase that functions in the endocytic pathway. *Journal of Cell Biology*, *209*(1), 85-95. https://doi.org/10.1083/jcb.201409064

Nalls, M. A., Blauwendraat, C., Vallerga, C. L., Heilbron, K., Bandres-Ciga, S., Chang, D., Tan, M., Kia, D. A., Noyce, A. J., Xue, A., Bras, J., Young, E., von Coelln, R., Simón-Sánchez, J., Schulte, C., Sharma, M., Krohn, L., Pihlstrom, L., Siitonen, A., Iwaki, H., Leonard, H., Faghri, F., Raphael Gibbs, J., Hernandez, D. G., Scholz, S. W., Botia, J. A., Martinez, M., Corvol, J.-C., Lesage, S., Jankovic, J., Shulman, L. M., Sutherland, M., Tienari, P., Majamaa, K., Toft, M., Andreassen, O. A., Bangale, T., Brice, A., Yang, J., Gan-Or, Z., Gasser, T., Heutink, P., Shulman, J. M., Wood, N., Hinds, D. A., Hardy, J. A., Morris, H. R., Gratten, J., Visscher, P. M., Graham, R. R., & Singleton, A. B. (2019). Expanding Parkinson's disease genetics: novel risk loci, genomic context, causal insights and heritable risk. *bioRxiv*, 388165. https://doi.org/10.1101/388165

Nalls, M. A., Pankratz, N., Lill, C. M., Do, C. B., Hernandez, D. G., Saad, M., DeStefano, A. L., Kara, E., Bras, J., Sharma, M., Schulte, C., Keller, M. F., Arepalli, S., Letson, C., Edsall, C., Stefansson, H., Liu, X., Pliner, H., Lee, J. H., Cheng, R., Ikram, M. A., Ioannidis, J. P. A., Hadjigeorgiou, G. M., Bis, J. C., Martinez, M., Perlmutter, J. S., Goate, A., Marder, K., Fiske, B., Sutherland, M., Xiromerisiou, G., Myers, R. H., Clark, L. N., Stefansson, K., Hardy, J. A., Heutink, P., Chen, H., Wood, N. W., Houlden, H., Payami, H., Brice, A., Scott, W. K., Gasser, T., Bertram, L., Eriksson, N., Foroud, T., Singleton, A. B., International Parkinson's Disease Genomics, C., Parkinson's Study Group Parkinson's Research: The Organized, G. I., andMe, GenePd, NeuroGenetics Research, C., Hussman Institute of Human, G., The Ashkenazi Jewish Dataset, I., Cohorts for, H., Aging Research in Genetic, E., North American Brain Expression, C., United Kingdom Brain Expression, C., Greek Parkinson's Disease, C., & Alzheimer Genetic Analysis, G. (2014). Large-scale meta-analysis of genome-wide association data identifies six new risk loci for Parkinson's disease. *Nature Genetics*, *46*(9), 989-993. https://doi.org/10.1038/ng.3043

Nalls, M. A., Plagnol, V., Hernandez, D. G., Sharma, M., Sheerin, U. M., Saad, M., Simón-Sánchez, J., Schulte, C., Lesage, S., Sveinbjörnsdóttir, S., Stefánsson, K., Martinez, M., Hardy, J., Heutink, P., Brice, A., Gasser, T., Singleton, A. B., & Wood, N. W. (2011). Imputation of sequence variants for identification of genetic risks for Parkinson's disease: a meta-analysis of genome-wide association studies. *Lancet*, *377*(9766), 641-649. https://doi.org/10.1016/s0140-6736(10)62345-8

Nam, H. S., Hwang, K. S., Jeong, Y. M., Ryu, J. I., Choi, T. Y., Bae, M. A., Son, W. C., You, K. H., Son, H. Y., & Kim, C. H. (2016). Expression of miRNA-122 Induced by Liver Toxicants in Zebrafish. *Biomed Res Int*, *2016*, 1473578. https://doi.org/10.1155/2016/1473578

Ness, D., Ren, Z., Gardai, S., Sharpnack, D., Johnson, V. J., Brennan, R. J., Brigham, E. F., & Olaharski, A. J. (2013). Leucine-rich repeat kinase 2 (LRRK2)-deficient rats exhibit renal tubule injury and perturbations in metabolic and immunological homeostasis. *PLoS ONE*, *8*(6), e66164. https://doi.org/10.1371/journal.pone.0066164

Nguyen, X. B., Kislyuk, S., Pham, D. H., Kecskés, A., Maes, J., Cabooter, D., Annaert, P., De Witte, P., & Ny, A. (2017). Cell Imaging Counting as a Novel Ex Vivo Approach for Investigating Drug-Induced Hepatotoxicity in Zebrafish Larvae. *Int J Mol Sci*, *18*(2). https://doi.org/10.3390/ijms18020356

Nichols, W. C., Pankratz, N., Hernandez, D., Paisán-Ruíz, C., Jain, S., Halter, C. A., Michaels, V. E., Reed, T., Rudolph, A., Shults, C. W., Singleton, A., & Foroud, T. (2005). Genetic screening for a single common LRRK2 mutation in familial Parkinson's disease. *Lancet*, *365*(9457), 410-412. https://doi.org/10.1016/s0140-6736(05)17828-3

Nishimura, G., & Kozlowski, K. (1993). Osteosclerotic metaphyseal dysplasia. *Pediatr Radiol*, *23*(6), 450-452. https://doi.org/10.1007/bf02012448

Nixon-Abell, J., Berwick, D. C., Grannó, S., Spain, V. A., Blackstone, C., & Harvey, K. (2016). Protective LRRK2 R1398H Variant Enhances GTPase and Wnt Signaling Activity [Original Research]. *Frontiers in Molecular Neuroscience*, *9*(18). https://doi.org/10.3389/fnmol.2016.00018

Nunes, A. F., Amaral, J. D., Lo, A. C., Fonseca, M. B., Viana, R. J., Callaerts-Vegh, Z., D'Hooge, R., & Rodrigues, C. M. (2012). TUDCA, a bile acid, attenuates amyloid precursor protein processing and amyloid-β deposition in APP/PS1 mice. *Mol Neurobiol*, *45*(3), 440-454. https://doi.org/10.1007/s12035-012-8256-y

Obata, K., Fukuda, T., Morishita, R., Abe, S., Asakawa, S., Yamaguchi, S., Yoshino, M., Ihara, K., Murayama, K., Shigemoto, K., Shimizu, N., & Kondo, I. (2001). Human Biotin-Containing Subunit of 3-Methylcrotonyl-CoA Carboxylase Gene (MCCA): cDNA Sequence, Genomic Organization, Localization to Chromosomal Band 3q27, and Expression. *Genomics*, *72*(2), 145-152. https://doi.org/https://doi.org/10.1006/geno.2000.6366

Oehlers, S. H., Flores, M. V., Hall, C. J., Crosier, K. E., & Crosier, P. S. (2012). Retinoic acid suppresses intestinal mucus production and exacerbates experimental enterocolitis. *Dis Model Mech*, *5*(4), 457-467. https://doi.org/10.1242/dmm.009365

Oehlers, S. H., Flores, M. V., Hall, C. J., Okuda, K. S., Sison, J. O., Crosier, K. E., & Crosier, P. S. (2013). Chemically induced intestinal damage models in zebrafish larvae. *Zebrafish*, *10*(2), 184-193. https://doi.org/10.1089/zeb.2012.0824

Oehlers, S. H., Flores, M. V., Okuda, K. S., Hall, C. J., Crosier, K. E., & Crosier, P. S. (2011). A chemical enterocolitis model in zebrafish larvae that is dependent on microbiota and responsive to pharmacological agents. *Dev Dyn*, *240*(1), 288-298. https://doi.org/10.1002/dvdy.22519

Oehlers, S. H. B., Flores, M. V., Hall, C. J., O'Toole, R., Swift, S., Crosier, K. E., & Crosier, P. S. (2010). Expression of zebrafish cxcl8 (interleukin-8) and its receptors during development and in response to immune stimulation. *Developmental & Comparative Immunology*, *34*(3), 352-359. https://doi.org/https://doi.org/10.1016/j.dci.2009.11.007

Ogawa, T., Matson, W. R., Beal, M. F., Myers, R. H., Bird, E. D., Milbury, P., & Saso, S. (1992). Kynurenine pathway abnormalities in Parkinson's disease. *Neurology*, *42*(9), 1702-1706. https://doi.org/10.1212/wnl.42.9.1702

Ohta, E., Kawakami, F., Kubo, M., & Obata, F. (2013). Dominant-negative effects of LRRK2 heterodimers: a possible mechanism of neurodegeneration in Parkinson's disease caused by LRRK2 I2020T mutation. *Biochem Biophys Res Commun*, *430*(2), 560-566. https://doi.org/10.1016/j.bbrc.2012.11.113

Onishi, K., Tian, R., Feng, B., Liu, Y., Wang, J., Li, Y., & Zou, Y. (2020). LRRK2 mediates axon development by regulating Frizzled3 phosphorylation and growth cone-growth cone communication. *Proc Natl Acad Sci U S A*, *117*(30), 18037-18048. https://doi.org/10.1073/pnas.1921878117

Oosterhof, N., Holtman, I. R., Kuil, L. E., van der Linde, H. C., Boddeke, E. W. G. M., Eggen, B. J. L., & van Ham, T. J. (2017). Identification of a conserved and acute neurodegeneration-specific microglial transcriptome in the zebrafish. *Glia*, *65*(1), 138-149. https://doi.org/https://doi.org/10.1002/glia.23083

Ouchi, Y., Yoshikawa, E., Sekine, Y., Futatsubashi, M., Kanno, T., Ogusu, T., & Torizuka, T. (2005). Microglial activation and dopamine terminal loss in early Parkinson's disease. *Annals of Neurology*, *57*(2), 168-175. https://doi.org/https://doi.org/10.1002/ana.20338

Oxenkrug, G., van der Hart, M., Roeser, J., & Summergrad, P. (2017). Peripheral Tryptophan - Kynurenine Metabolism Associated with Metabolic Syndrome is Different in Parkinson's and Alzheimer's Diseases. *Endocrinol Diabetes Metab J*, *1*(4).

Ozelius, L. J., Senthil, G., Saunders-Pullman, R., Ohmann, E., Deligtisch, A., Tagliati, M., Hunt, A. L., Klein, C., Henick, B., Hailpern, S. M., Lipton, R. B., Soto-Valencia, J., Risch, N., & Bressman, S. B. (2006). LRRK2 G2019S as a cause of Parkinson's disease in Ashkenazi Jews. *N Engl J Med*, *354*(4), 424-425. https://doi.org/10.1056/NEJMc055509

Paisán-Ruíz, C., Jain, S., Evans, E. W., Gilks, W. P., Simón, J., van der Brug, M., López de Munain, A., Aparicio, S., Gil, A. M., Khan, N., Johnson, J., Martinez, J. R., Nicholl, D., Martí Carrera, I., Pena, A. S., de Silva, R., Lees, A., Martí-Massó, J. F., Pérez-Tur, J., Wood, N. W., & Singleton, A. B. (2004). Cloning of the gene containing mutations that cause PARK8-linked Parkinson's disease. *Neuron*, *44*(4), 595-600. https://doi.org/10.1016/j.neuron.2004.10.023

Palacios, E. H., & Weiss, A. (2004). Function of the Src-family kinases, Lck and Fyn, in T-cell development and activation. *Oncogene*, *23*(48), 7990-8000. https://doi.org/10.1038/sj.onc.1208074

Palzer, L., Bader, J. J., Angel, F., Witzel, M., Blaser, S., McNeil, A., Wandersee, M. K., Leu, N. A., Lengner, C. J., Cho, C. E., Welch, K. D., Kirkland, J. B., Meyer, R. G., & Meyer-Ficca, M. L. (2018). Alpha-Amino-Beta-Carboxy-Muconate-Semialdehyde Decarboxylase Controls Dietary Niacin Requirements for NAD(+) Synthesis. *Cell Rep*, *25*(5), 1359-1370.e1354. https://doi.org/10.1016/j.celrep.2018.09.091

Panicker, N., Saminathan, H., Jin, H., Neal, M., Harischandra, D. S., Gordon, R., Kanthasamy, K., Lawana, V., Sarkar, S., Luo, J., Anantharam, V., Kanthasamy, A. G., & Kanthasamy, A. (2015). Fyn Kinase Regulates Microglial Neuroinflammatory Responses in Cell Culture and Animal Models of Parkinson's Disease. *J Neurosci*, *35*(27), 10058-10077. https://doi.org/10.1523/jneurosci.0302-15.2015

Paquet, D., Kwart, D., Chen, A., Sproul, A., Jacob, S., Teo, S., Olsen, K. M., Gregg, A., Noggle, S., & Tessier-Lavigne, M. (2016). Efficient introduction of specific homozygous and heterozygous mutations using CRISPR/Cas9. *Nature*, *533*(7601), 125-129. https://doi.org/10.1038/nature17664

Parisiadou, L., Xie, C., Cho, H. J., Lin, X., Gu, X. L., Long, C. X., Lobbestael, E., Baekelandt, V., Taymans, J. M., Sun, L., & Cai, H. (2009). Phosphorylation of ezrin/radixin/moesin proteins by LRRK2

promotes the rearrangement of actin cytoskeleton in neuronal morphogenesis. *J Neurosci*, *29*(44), 13971-13980. https://doi.org/10.1523/jneurosci.3799-09.2009

Parkinson Study Group. (2000). Pramipexole vs levodopa as initial treatment for Parkinson disease: A randomized controlled trial. . *Jama*, *284*(15), 1931-1938. https://doi.org/10.1001/jama.284.15.1931

Parry, G. J., Rodrigues, C. M., Aranha, M. M., Hilbert, S. J., Davey, C., Kelkar, P., Low, W. C., & Steer, C. J. (2010). Safety, tolerability, and cerebrospinal fluid penetration of ursodeoxycholic Acid in patients with amyotrophic lateral sclerosis. *Clin Neuropharmacol*, *33*(1), 17-21. https://doi.org/10.1097/WNF.0b013e3181c47569

Pellegrini, L., Hauser, D. N., Li, Y., Mamais, A., Beilina, A., Kumaran, R., Wetzel, A., Nixon-Abell, J., Heaton, G., Rudenko, I., Alkaslasi, M., Ivanina, N., Melrose, H. L., Cookson, M. R., & Harvey, K. (2018). Proteomic analysis reveals co-ordinated alterations in protein synthesis and degradation pathways in LRRK2 knockout mice. *Hum Mol Genet*, *27*(18), 3257-3271. https://doi.org/10.1093/hmg/ddy232

Peter, I., Dubinsky, M., Bressman, S., Park, A., Lu, C., Chen, N., & Wang, A. (2018). Anti–Tumor Necrosis Factor Therapy and Incidence of Parkinson Disease Among Patients With Inflammatory Bowel Disease. *JAMA Neurology*, *75*(8), 939-946. https://doi.org/10.1001/jamaneurol.2018.0605

Petri, K., Zhang, W., Ma, J., Schmidts, A., Lee, H., Horng, J. E., Kim, D. Y., Kurt, I. C., Clement, K., Hsu, J. Y., Pinello, L., Maus, M. V., Joung, J. K., & Yeh, J.-R. J. (2021). CRISPR prime editing with ribonucleoprotein complexes in zebrafish and primary human cells. *Nature Biotechnology*. https://doi.org/10.1038/s41587-021-00901-y

Piccoli, G., Condliffe, S. B., Bauer, M., Giesert, F., Boldt, K., De Astis, S., Meixner, A., Sarioglu, H., Vogt-Weisenhorn, D. M., Wurst, W., Gloeckner, C. J., Matteoli, M., Sala, C., & Ueffing, M. (2011). LRRK2 controls synaptic vesicle storage and mobilization within the recycling pool. *J Neurosci*, *31*(6), 2225-2237. https://doi.org/10.1523/jneurosci.3730-10.2011

Pierozan, P., Biasibetti-Brendler, H., Schmitz, F., Ferreira, F., Pessoa-Pureur, R., & Wyse, A. T. S. (2018). Kynurenic Acid Prevents Cytoskeletal Disorganization Induced by Quinolinic Acid in Mixed Cultures of Rat Striatum. *Mol Neurobiol*, *55*(6), 5111-5124. https://doi.org/10.1007/s12035-017-0749-2

Pierozan, P., Zamoner, A., Soska Â, K., de Lima, B. O., Reis, K. P., Zamboni, F., Wajner, M., & Pessoa-Pureur, R. (2012). Signaling mechanisms downstream of quinolinic acid targeting the cytoskeleton of rat striatal neurons and astrocytes. *Exp Neurol*, *233*(1), 391-399. https://doi.org/10.1016/j.expneurol.2011.11.005

Pihlstrøm, L., Axelsson, G., Bjørnarå, K. A., Dizdar, N., Fardell, C., Forsgren, L., Holmberg, B., Larsen, J. P., Linder, J., Nissbrandt, H., Tysnes, O. B., Ohman, E., Dietrichs, E., & Toft, M. (2013). Supportive evidence for 11 loci from genome-wide association studies in Parkinson's disease. *Neurobiol Aging*, *34*(6), 1708.e1707-1713. https://doi.org/10.1016/j.neurobiolaging.2012.10.019

Pittaluga, A., Pattarini, R., Feligioni, M., & Raiteri, M. (2001). N-methyl-D-aspartate receptors mediating hippocampal noradrenaline and striatal dopamine release display differential sensitivity to quinolinic acid, the HIV-1 envelope protein gp120, external pH and protein kinase C inhibition. *J Neurochem*, *76*(1), 139-148. https://doi.org/10.1046/j.1471-4159.2001.00057.x

Pláteník, J., Stopka, P., Vejražka, M., & Štípek, S. (2001). Quinolinic acid — Iron(II) complexes: Slow autoxidation, but enhanced hydroxyl radical production in the Fenton reaction. *Free Radical Research*, *34*(5), 445-459. https://doi.org/10.1080/10715760100300391

Polymeropoulos, M. H., Lavedan, C., Leroy, E., Ide, S. E., Dehejia, A., Dutra, A., Pike, B., Root, H., Rubenstein, J., Boyer, R., Stenroos, E. S., Chandrasekharappa, S., Athanassiadou, A., Papapetropoulos, T., Johnson, W. G., Lazzarini, A. M., Duvoisin, R. C., Di Iorio, G., Golbe, L. I., & Nussbaum, R. L. (1997). Mutation in the α-Synuclein Gene Identified in Families with Parkinson's Disease. *Science*, *276*(5321), 2045-2047. https://doi.org/10.1126/science.276.5321.2045

Postlethwait, J. H., Woods, I. G., Ngo-Hazelett, P., Yan, Y. L., Kelly, P. D., Chu, F., Huang, H., Hill-Force, A., & Talbot, W. S. (2000). Zebrafish comparative genomics and the origins of vertebrate chromosomes. *Genome Res*, *10*(12), 1890-1902. https://doi.org/10.1101/gr.164800

Postuma, R. B., Berg, D., Stern, M., Poewe, W., Olanow, C. W., Oertel, W., Obeso, J., Marek, K., Litvan, I., Lang, A. E., Halliday, G., Goetz, C. G., Gasser, T., Dubois, B., Chan, P., Bloem, B. R., Adler, C. H., & Deuschl, G. (2015). MDS clinical diagnostic criteria for Parkinson's disease. *Mov Disord*, *30*(12), 1591-1601. https://doi.org/10.1002/mds.26424

Prabhudesai, S., Bensabeur, F. Z., Abdullah, R., Basak, I., Baez, S., Alves, G., Holtzman, N. G., Larsen, J. P., & Møller, S. G. (2016). LRRK2 knockdown in zebrafish causes developmental defects, neuronal loss, and synuclein aggregation. *J Neurosci Res*, *94*(8), 717-735. https://doi.org/10.1002/jnr.23754

Prajsnar, T. K., Serba, J. J., Dekker, B. M., Gibson, J. F., Masud, S., Fleming, A., Johnston, S. A., Renshaw, S. A., & Meijer, A. H. (2021). The autophagic response to Staphylococcus aureus provides an intracellular niche in neutrophils. *Autophagy*, *17*(4), 888-902. https://doi.org/10.1080/15548627.2020.1739443

Prykhozhij, S. V., Fuller, C., Steele, S. L., Veinotte, C. J., Razaghi, B., Robitaille, J. M., McMaster, C. R., Shlien, A., Malkin, D., & Berman, J. N. (2018). Optimized knock-in of point mutations in zebrafish using CRISPR/Cas9. *Nucleic Acids Research*, *46*(17), e102-e102. https://doi.org/10.1093/nar/gky512

Pucci, L., Perozzi, S., Cimadamore, F., Orsomando, G., & Raffaelli, N. (2007). Tissue expression and biochemical characterization of human 2-amino 3-carboxymuconate 6-semialdehyde decarboxylase, a key enzyme in tryptophan catabolism. *The FEBS Journal*, *274*(3), 827-840. https://doi.org/https://doi.org/10.1111/j.1742-4658.2007.05635.x

Puschmann, A., Englund, E., Ross, O. A., Vilariño-Güell, C., Lincoln, S. J., Kachergus, J. M., Cobb, S. A., Törnqvist, A. L., Rehncrona, S., Widner, H., Wszolek, Z. K., Farrer, M. J., & Nilsson, C. (2012). First neuropathological description of a patient with Parkinson's disease and LRRK2 p.N1437H mutation. *Parkinsonism Relat Disord*, *18*(4), 332-338. https://doi.org/10.1016/j.parkreldis.2011.11.019

Qian, L., Wu, H. M., Chen, S. H., Zhang, D., Ali, S. F., Peterson, L., Wilson, B., Lu, R. B., Hong, J. S., & Flood, P. M. (2011). β2-adrenergic receptor activation prevents rodent dopaminergic neurotoxicity by inhibiting microglia via a novel signaling pathway. *J Immunol*, *186*(7), 4443-4454. https://doi.org/10.4049/jimmunol.1002449

Qiao, C., Yin, N., Gu, H.-Y., Zhu, J.-L., Ding, J.-H., Lu, M., & Hu, G. (2016). Atp13a2 Deficiency Aggravates Astrocyte-Mediated Neuroinflammation via NLRP3 Inflammasome Activation. *CNS Neuroscience & Therapeutics*, *22*(6), 451-460. https://doi.org/https://doi.org/10.1111/cns.12514

Qiao, C., Zhang, Q., Jiang, Q., Zhang, T., Chen, M., Fan, Y., Ding, J., Lu, M., & Hu, G. (2018). Inhibition of the hepatic Nlrp3 protects dopaminergic neurons via attenuating systemic inflammation in a MPTP/p mouse model of Parkinson's disease. *Journal of Neuroinflammation*, *15*(1), 193. https://doi.org/10.1186/s12974-018-1236-z

Rajamani, K. T., Krzyzanowski, S., Escobar Galvis, M. L., Brundin, P., & Brundin, L. (2017). 840. Developing a Rodent Model of Depression and Neurodegenerative Disease by Targeting ACMSD, a Key Enzyme in the Kynurenine Pathway. *Biological Psychiatry*, *81*(10, Supplement), S340. https://doi.org/https://doi.org/10.1016/j.biopsych.2017.02.565

Rajput, A. H., Fenton, M. E., Birdi, S., Macaulay, R., George, D., Rozdilsky, B., Ang, L. C., Senthilselvan, A., & Hornykiewicz, O. (2002). Clinical-pathological study of levodopa complications. *Mov Disord*, *17*(2), 289-296. https://doi.org/10.1002/mds.10031

Ramirez, A., Heimbach, A., Gründemann, J., Stiller, B., Hampshire, D., Cid, L. P., Goebel, I., Mubaidin, A. F., Wriekat, A.-L., Roeper, J., Al-Din, A., Hillmer, A. M., Karsak, M., Liss, B., Woods, C. G., Behrens, M. I., & Kubisch, C. (2006). Hereditary parkinsonism with dementia is caused by mutations in ATP13A2, encoding a lysosomal type 5 P-type ATPase. *Nature Genetics*, *38*(10), 1184-1191. https://doi.org/10.1038/ng1884

Ramonet, D., Podhajska, A., Stafa, K., Sonnay, S., Trancikova, A., Tsika, E., Pletnikova, O., Troncoso, J. C., Glauser, L., & Moore, D. J. (2011). PARK9-associated ATP13A2 localizes to intracellular acidic vesicles and regulates cation homeostasis and neuronal integrity. *Human Molecular Genetics*, *21*(8), 1725-1743. https://doi.org/10.1093/hmg/ddr606

Ren, G., Xin, S., Li, S., Zhong, H., & Lin, S. (2011). Disruption of LRRK2 does not cause specific loss of dopaminergic neurons in zebrafish. *PLoS ONE*, *6*(6), e20630. https://doi.org/10.1371/journal.pone.0020630

Renshaw, S. A., Loynes, C. A., Trushell, D. M. I., Elworthy, S., Ingham, P. W., & Whyte, M. K. B. (2006). A transgenic zebrafish model of neutrophilic inflammation. *Blood*, *108*(13), 3976-3978. https://doi.org/10.1182/blood-2006-05-024075

Reschly, E. J., Ai, N., Ekins, S., Welsh, W. J., Hagey, L. R., Hofmann, A. F., & Krasowski, M. D. (2008). Evolution of the bile salt nuclear receptor FXR in vertebrates. *J Lipid Res*, *49*(7), 1577-1587. https://doi.org/10.1194/jlr.M800138-JLR200

Reyniers, L., Del Giudice, M. G., Civiero, L., Belluzzi, E., Lobbestael, E., Beilina, A., Arrigoni, G., Derua, R., Waelkens, E., Li, Y., Crosio, C., Iaccarino, C., Cookson, M. R., Baekelandt, V., Greggio, E., & Taymans, J. M. (2014). Differential protein-protein interactions of LRRK1 and LRRK2 indicate roles in distinct cellular signaling pathways. *J Neurochem*, *131*(2), 239-250. https://doi.org/10.1111/jnc.12798

Reynolds, D. S., & Morton, A. J. (1998). Changes in blood-brain barrier permeability following neurotoxic lesions of rat brain can be visualised with trypan blue. *J Neurosci Methods*, *79*(1), 115-121. https://doi.org/10.1016/s0165-0270(97)00168-4

Rhodes, J., Hagen, A., Hsu, K., Deng, M., Liu, T. X., Look, A. T., & Kanki, J. P. (2005). Interplay of pu.1 and gata1 determines myelo-erythroid progenitor cell fate in zebrafish. *Dev Cell*, *8*(1), 97-108. https://doi.org/10.1016/j.devcel.2004.11.014

Richardson, C. D., Ray, G. J., DeWitt, M. A., Curie, G. L., & Corn, J. E. (2016). Enhancing homology-directed genome editing by catalytically active and inactive CRISPR-Cas9 using asymmetric donor DNA. *Nature Biotechnology*, *34*(3), 339-344. https://doi.org/10.1038/nbt.3481

Rink, E., & Wullimann, M. F. (2001). The teleostean (zebrafish) dopaminergic system ascending to the subpallium (striatum) is located in the basal diencephalon (posterior tuberculum). *Brain Res*, *889*(1-2), 316-330. https://doi.org/10.1016/s0006-8993(00)03174-7

Rink, E., & Wullimann, M. F. (2002). Development of the catecholaminergic system in the early zebrafish brain: an immunohistochemical study. *Brain Res Dev Brain Res*, *137*(1), 89-100. https://doi.org/10.1016/s0165-3806(02)00354-1

Robu, M. E., Larson, J. D., Nasevicius, A., Beiraghi, S., Brenner, C., Farber, S. A., & Ekker, S. C. (2007). p53 activation by knockdown technologies. *PLoS Genet*, *3*(5), e78. https://doi.org/10.1371/journal.pgen.0030078

Rocha, E. M., De Miranda, B. R., Castro, S., Drolet, R., Hatcher, N. G., Yao, L., Smith, S. M., Keeney, M. T., Di Maio, R., Kofler, J., Hastings, T. G., & Greenamyre, J. T. (2020). LRRK2 inhibition prevents endolysosomal deficits seen in human Parkinson's disease. *Neurobiol Dis*, *134*, 104626. https://doi.org/10.1016/j.nbd.2019.104626

Ross, O. A., Soto-Ortolaza, A. I., Heckman, M. G., Aasly, J. O., Abahuni, N., Annesi, G., Bacon, J. A., Bardien, S., Bozi, M., Brice, A., Brighina, L., Van Broeckhoven, C., Carr, J., Chartier-Harlin, M. C., Dardiotis, E., Dickson, D. W., Diehl, N. N., Elbaz, A., Ferrarese, C., Ferraris, A., Fiske, B., Gibson, J. M., Gibson, R., Hadjigeorgiou, G. M., Hattori, N., Ioannidis, J. P., Jasinska-Myga, B., Jeon, B. S., Kim, Y. J., Klein, C., Kruger, R., Kyratzi, E., Lesage, S., Lin, C. H., Lynch, T., Maraganore, D. M., Mellick, G. D., Mutez, E., Nilsson, C., Opala, G., Park, S. S., Puschmann, A., Quattrone, A., Sharma, M., Silburn, P. A., Sohn, Y. H., Stefanis, L., Tadic, V., Theuns, J., Tomiyama, H., Uitti, R. J., Valente, E. M., van de Loo, S., Vassilatis, D. K., Vilariño-Güell, C., White, L. R., Wirdefeldt, K., Wszolek, Z. K., Wu, R. M., & Farrer, M. J. (2011). Association of LRRK2 exonic variants with susceptibility to Parkinson's disease: a case-control study. *Lancet Neurol*, *10*(10), 898-908. https://doi.org/10.1016/s1474-4422(11)70175-2

Ruiz-Martínez, J., Gorostidi, A., Ibañez, B., Alzualde, A., Otaegui, D., Moreno, F., López de Munain, A., Bergareche, A., Gómez-Esteban, J. C., & Martí Massó, J. F. (2010). Penetrance in Parkinson's disease related to the LRRK2 R1441G mutation in the Basque country (Spain). *Mov Disord*, *25*(14), 2340-2345. https://doi.org/10.1002/mds.23278

Russell, D. W. (2003). The enzymes, regulation, and genetics of bile acid synthesis. *Annu Rev Biochem*, *72*, 137-174. https://doi.org/10.1146/annurev.biochem.72.121801.161712

Russo, I., Kaganovich, A., Ding, J., Landeck, N., Mamais, A., Varanita, T., Biosa, A., Tessari, I., Bubacco, L., Greggio, E., & Cookson, M. R. (2019). Transcriptome analysis of LRRK2 knock-out microglia cells reveals alterations of inflammatory- and oxidative stress-related pathways upon treatment with α-synuclein fibrils. *Neurobiol Dis*, *129*, 67-78. https://doi.org/10.1016/j.nbd.2019.05.012

Ryan, K. J., White, C. C., Patel, K., Xu, J., Olah, M., Replogle, J. M., Frangieh, M., Cimpean, M., Winn, P., McHenry, A., Kaskow, B. J., Chan, G., Cuerdon, N., Bennett, D. A., Boyd, J. D., Imitola, J., Elyaman, W., De Jager, P. L., & Bradshaw, E. M. (2017). A human microglia-like cellular model for assessing the effects of neurodegenerative disease gene variants. *Sci Transl Med*, *9*(421). https://doi.org/10.1126/scitranslmed.aai7635

Ryu, J. K., Kim, S. U., & McLarnon, J. G. (2004). Blockade of quinolinic acid-induced neurotoxicity by pyruvate is associated with inhibition of glial activation in a model of Huntington's disease. *Exp Neurol*, *187*(1), 150-159. https://doi.org/10.1016/j.expneurol.2004.01.006

Ryu, S., Mahler, J., Acampora, D., Holzschuh, J., Erhardt, S., Omodei, D., Simeone, A., & Driever, W. (2007). Orthopedia Homeodomain Protein Is Essential for Diencephalic Dopaminergic Neuron Development. *Current Biology*, *17*(10), 873-880. https://doi.org/https://doi.org/10.1016/j.cub.2007.04.003

Samii, A., Etminan, M., Wiens, M. O., & Jafari, S. (2009). NSAID use and the risk of Parkinson's disease: systematic review and meta-analysis of observational studies. *Drugs Aging*, *26*(9), 769-779. https://doi.org/10.2165/11316780-000000000-00000

Saunders, J. A. H., Estes, K. A., Kosloski, L. M., Allen, H. E., Dempsey, K. M., Torres-Russotto, D. R., Meza, J. L., Santamaria, P. M., Bertoni, J. M., Murman, D. L., Ali, H. H., Standaert, D. G., Mosley, R. L., & Gendelman, H. E. (2012). CD4+ Regulatory and Effector/Memory T Cell Subsets Profile Motor Dysfunction in Parkinson's Disease. *Journal of Neuroimmune Pharmacology*, *7*(4), 927-938. https://doi.org/10.1007/s11481-012-9402-z

Scheperjans, F., Aho, V., Pereira, P. A. B., Koskinen, K., Paulin, L., Pekkonen, E., Haapaniemi, E., Kaakkola, S., Eerola-Rautio, J., Pohja, M., Kinnunen, E., Murros, K., & Auvinen, P. (2015). Gut microbiota are related to Parkinson's disease and clinical phenotype. *Movement Disorders*, *30*(3), 350-358. https://doi.org/https://doi.org/10.1002/mds.26069

Schildt, A., Walker, M. D., Dinelle, K., Miao, Q., Schulzer, M., O'Kusky, J., Farrer, M. J., Doudet, D. J., & Sossi, V. (2019). Single Inflammatory Trigger Leads to Neuroinflammation in LRRK2 Rodent Model without Degeneration of Dopaminergic Neurons. *J Parkinsons Dis*, *9*(1), 121-139. https://doi.org/10.3233/jpd-181446

Schormair, B., Kemlink, D., Mollenhauer, B., Fiala, O., Machetanz, G., Roth, J., Berutti, R., Strom, T. M., Haslinger, B., Trenkwalder, C., Zahorakova, D., Martasek, P., Ruzicka, E., & Winkelmann, J. (2018). Diagnostic exome sequencing in early-onset Parkinson's disease confirms VPS13C as a rare cause of autosomal-recessive Parkinson's disease. *Clinical Genetics*, *93*(3), 603-612. https://doi.org/https://doi.org/10.1111/cge.13124

Schulte, E. C., Altmaier, E., Berger, H. S., Do, K. T., Kastenmüller, G., Wahl, S., Adamski, J., Peters, A., Krumsiek, J., Suhre, K., Haslinger, B., Ceballos-Baumann, A., Gieger, C., & Winkelmann, J. (2016). Alterations in Lipid and Inositol Metabolisms in Two Dopaminergic Disorders. *PLoS ONE*, *11*(1), e0147129. https://doi.org/10.1371/journal.pone.0147129

Schwiertz, A., Spiegel, J., Dillmann, U., Grundmann, D., Burmann, J., Fassbender, K., Schafer, K. H., & Unger, M. M. (2018). Fecal markers of intestinal inflammation and intestinal permeability are elevated in Parkinson's disease. *Parkinsonism Relat Disord*, *50*, 104-107. https://doi.org/10.1016/j.parkreldis.2018.02.022

Sejwal, K., Chami, M., Rémigy, H., Vancraenenbroeck, R., Sibran, W., Sütterlin, R., Baumgartner, P., McLeod, R., Chartier-Harlin, M. C., Baekelandt, V., Stahlberg, H., & Taymans, J. M. (2017). Cryo-EM analysis of homodimeric full-length LRRK2 and LRRK1 protein complexes. *Sci Rep*, *7*(1), 8667. https://doi.org/10.1038/s41598-017-09126-z

Seo, D. R., Kim, K. Y., & Lee, Y. B. (2004). Interleukin-10 expression in lipopolysaccharide-activated microglia is mediated by extracellular ATP in an autocrine fashion. *Neuroreport*, *15*(7), 1157-1161. https://doi.org/10.1097/00001756-200405190-00015

Sharma, M. K., Liu, R. Z., Thisse, C., Thisse, B., Denovan-Wright, E. M., & Wright, J. M. (2006). Hierarchical subfunctionalization of fabp1a, fabp1b and fabp10 tissue-specific expression may account for retention of these duplicated genes in the zebrafish (Danio rerio) genome. *Febs j*, *273*(14), 3216-3229. https://doi.org/10.1111/j.1742-4658.2006.05330.x

Sheng, D., Qu, D., Kwok, K. H., Ng, S. S., Lim, A. Y., Aw, S. S., Lee, C. W., Sung, W. K., Tan, E. K., Lufkin, T., Jesuthasan, S., Sinnakaruppan, M., & Liu, J. (2010). Deletion of the WD40 domain of LRRK2 in Zebrafish causes Parkinsonism-like loss of neurons and locomotive defect. *PLoS Genet*, *6*(4), e1000914. https://doi.org/10.1371/journal.pgen.1000914

Sheng, D., See, K., Hu, X., Yu, D., Wang, Y., Liu, Q., Li, F., Lu, M., Zhao, J., & Liu, J. (2018). Disruption of LRRK2 in Zebrafish leads to hyperactivity and weakened antibacterial response. *Biochem Biophys Res Commun*, *497*(4), 1104-1109. https://doi.org/10.1016/j.bbrc.2018.02.186

Sheng, Z., Zhang, S., Bustos, D., Kleinheinz, T., Le Pichon, C. E., Dominguez, S. L., Solanoy, H. O., Drummond, J., Zhang, X., Ding, X., Cai, F., Song, Q., Li, X., Yue, Z., van der Brug, M. P., Burdick, D. J., Gunzner-Toste, J., Chen, H., Liu, X., Estrada, A. A., Sweeney, Z. K., Scearce-Levie, K., Moffat, J. G., Kirkpatrick, D. S., & Zhu, H. (2012). Ser1292 autophosphorylation is an indicator of LRRK2 kinase activity and contributes to the cellular effects of PD mutations. *Sci Transl Med*, *4*(164), 164ra161. https://doi.org/10.1126/scitranslmed.3004485

Shi, W., Meininger, C. J., Haynes, T. E., Hatakeyama, K., & Wu, G. (2004). Regulation of tetrahydrobiopterin synthesis and bioavailability in endothelial cells. *Cell Biochem Biophys*, *41*(3), 415-434. https://doi.org/10.1385/cbb:41:3:415

Shiau, C. E., Kaufman, Z., Meireles, A. M., & Talbot, W. S. (2015). Differential requirement for irf8 in formation of embryonic and adult macrophages in zebrafish. *PLoS ONE*, *10*(1), e0117513. https://doi.org/10.1371/journal.pone.0117513

Shimura, H., Hattori, N., Kubo, S.-i., Mizuno, Y., Asakawa, S., Minoshima, S., Shimizu, N., Iwai, K., Chiba, T., Tanaka, K., & Suzuki, T. (2000). Familial Parkinson disease gene product, parkin, is a ubiquitin-protein ligase. *Nature Genetics*, *25*(3), 302-305. https://doi.org/10.1038/77060

Shutinoski, B., Hakimi, M., Harmsen, I. E., Lunn, M., Rocha, J., Lengacher, N., Zhou, Y. Y., Khan, J., Nguyen, A., Hake-Volling, Q., El-Kodsi, D., Li, J., Alikashani, A., Beauchamp, C., Majithia, J., Coombs, K., Shimshek, D., Marcogliese, P. C., Park, D. S., Rioux, J. D., Philpott, D. J., Woulfe, J. M., Hayley, S., Sad, S., Tomlinson, J. J., Brown, E. G., & Schlossmacher, M. G. (2019). Lrrk2 alleles modulate inflammation during microbial infection of mice in a sex-dependent manner. *Sci Transl Med*, *11*(511). https://doi.org/10.1126/scitranslmed.aas9292

Si, M., Goodluck, H., Zeng, C., Pan, S., Todd, E. M., Morley, S. C., Qin, X., Mohan, S., & Xing, W. (2018). LRRK1 regulation of actin assembly in osteoclasts involves serine 5 phosphorylation of L-plastin. *J Cell Biochem*, *119*(12), 10351-10357. https://doi.org/10.1002/jcb.27377

Si, M., Zeng, C., Goodluck, H., Shen, S., Mohan, S., & Xing, W. (2019). A small molecular inhibitor of LRRK1 identified by homology modeling and virtual screening suppresses osteoclast function, but not osteoclast differentiation, in vitro. *Aging (Albany NY)*, *11*(10), 3250-3261. https://doi.org/10.18632/aging.101977

Singh, K., Han, K., Tilve, S., Wu, K., Geller, H. M., & Sack, M. N. (2018). Parkin targets NOD2 to regulate astrocyte endoplasmic reticulum stress and inflammation. *Glia*, *66*(11), 2427-2437. https://doi.org/https://doi.org/10.1002/glia.23482

Skaggs, K., Goldman, D., & Parent, J. M. (2014). Excitotoxic brain injury in adult zebrafish stimulates neurogenesis and long-distance neuronal integration. *Glia*, *62*(12), 2061-2079. https://doi.org/10.1002/glia.22726

Sliter, D. A., Martinez, J., Hao, L., Chen, X., Sun, N., Fischer, T. D., Burman, J. L., Li, Y., Zhang, Z., Narendra, D. P., Cai, H., Borsche, M., Klein, C., & Youle, R. J. (2018). Parkin and PINK1 mitigate STING-induced inflammation. *Nature*, *561*(7722), 258-262. https://doi.org/10.1038/s41586-018-0448-9

Smith, W. W., Pei, Z., Jiang, H., Moore, D. J., Liang, Y., West, A. B., Dawson, V. L., Dawson, T. M., & Ross, C. A. (2005). Leucine-rich repeat kinase 2 (LRRK2) interacts with parkin, and mutant LRRK2 induces neuronal degeneration. *Proceedings of the National Academy of Sciences of the United States of America*, *102*(51), 18676. https://doi.org/10.1073/pnas.0508052102

Sorgdrager, F. J. H., Vermeiren, Y., Van Faassen, M., van der Ley, C., Nollen, E. A. A., Kema, I. P., & De Deyn, P. P. (2019). Age- and disease-specific changes of the kynurenine pathway in Parkinson's and Alzheimer's disease. *J Neurochem*, *151*(5), 656-668. https://doi.org/10.1111/jnc.14843

Spilker, C., & Kreutz, M. R. (2010). RapGAPs in brain: multipurpose players in neuronal Rap signalling. *European Journal of Neuroscience*, *32*(1), 1-9. https://doi.org/https://doi.org/10.1111/j.1460-9568.2010.07273.x

Spillantini, M. G., Crowther, R. A., Jakes, R., Hasegawa, M., & Goedert, M. (1998). alpha-Synuclein in filamentous inclusions of Lewy bodies from Parkinson's disease and dementia with lewy bodies. *Proc Natl Acad Sci U S A*, *95*(11), 6469-6473. https://doi.org/10.1073/pnas.95.11.6469

St'astný, F., Skultétyová, I., Pliss, L., & Jezová, D. (2000). Quinolinic acid enhances permeability of rat brain microvessels to plasma albumin. *Brain Res Bull*, *53*(4), 415-420. https://doi.org/10.1016/s0361-9230(00)00368-3

Staudinger, J. L., Goodwin, B., Jones, S. A., Hawkins-Brown, D., MacKenzie, K. I., LaTour, A., Liu, Y., Klaassen, C. D., Brown, K. K., Reinhard, J., Willson, T. M., Koller, B. H., & Kliewer, S. A. (2001). The nuclear receptor PXR is a lithocholic acid sensor that protects against liver toxicity. *Proc Natl Acad Sci U S A*, *98*(6), 3369-3374. https://doi.org/10.1073/pnas.051551698

Steger, M., Diez, F., Dhekne, H. S., Lis, P., Nirujogi, R. S., Karayel, O., Tonelli, F., Martinez, T. N., Lorentzen, E., Pfeffer, S. R., Alessi, D. R., & Mann, M. (2017). Systematic proteomic analysis of LRRK2-mediated Rab GTPase phosphorylation establishes a connection to ciliogenesis. *Elife*, *6*. https://doi.org/10.7554/eLife.31012

Steger, M., Tonelli, F., Ito, G., Davies, P., Trost, M., Vetter, M., Wachter, S., Lorentzen, E., Duddy, G., Wilson, S., Baptista, M. A., Fiske, B. K., Fell, M. J., Morrow, J. A., Reith, A. D., Alessi, D. R., & Mann, M. (2016). Phosphoproteomics reveals that Parkinson's disease kinase LRRK2 regulates a subset of Rab GTPases. *Elife*, *5*. https://doi.org/10.7554/eLife.12813

Stence, N., Waite, M., & Dailey, M. E. (2001). Dynamics of microglial activation: A confocal time-lapse analysis in hippocampal slices. *Glia*, *33*(3), 256-266. https://doi.org/https://doi.org/10.1002/1098-1136(200103)33:3<256::AID-GLIA1024>3.0.CO;2-J

Stone, T. W., & Perkins, M. N. (1981). Quinolinic acid: a potent endogenous excitant at amino acid receptors in CNS. *Eur J Pharmacol*, *72*(4), 411-412. https://doi.org/10.1016/0014-2999(81)90587-2

Struhar, D., Kivity, S., & Topilsky, M. (1992). Quinacrine inhibits oxygen radicals release from human alveolar macrophages. *International Journal of Immunopharmacology*, *14*(2), 275-277. https://doi.org/https://doi.org/10.1016/0192-0561(92)90040-R

Su, X., Maguire-Zeiss, K. A., Giuliano, R., Prifti, L., Venkatesh, K., & Federoff, H. J. (2008). Synuclein activates microglia in a model of Parkinson's disease. *Neurobiology of Aging*, *29*(11), 1690-1701. https://doi.org/https://doi.org/10.1016/j.neurobiolaging.2007.04.006

Suzzi, S. (2017). *Loss of lrrk2 impairs dopamine catabolism, cell proliferation, and neuronal regeneration in the zebrafish brain* [Dissertation, Dresden University of Technology]. https://d-nb.info/114073525X/34

Suzzi, S., Ahrendt, R., Hans, S., Semenova, S. A., Chekuru, A., Wirsching, P., Kroehne, V., Bilican, S., Sayed, S., Winkler, S., Spieß, S., Machate, A., Kaslin, J., Panula, P., & Brand, M. (2021). Deletion of lrrk2 causes early developmental abnormalities and age-dependent increase of monoamine catabolism in the zebrafish brain. *PLoS Genet*, *17*(9), e1009794. https://doi.org/10.1371/journal.pgen.1009794

Takanashi, M., Funayama, M., Matsuura, E., Yoshino, H., Li, Y., Tsuyama, S., Takashima, H., Nishioka, K., & Hattori, N. (2018). Isolated nigral degeneration without pathological protein aggregation in autopsied brains with LRRK2 p.R1441H homozygous and heterozygous mutations. *Acta Neuropathol Commun*, *6*(1), 105. https://doi.org/10.1186/s40478-018-0617-y

Tamura, T., Nagamura-Inoue, T., Shmeltzer, Z., Kuwata, T., & Ozato, K. (2000). ICSBP directs bipotential myeloid progenitor cells to differentiate into mature macrophages. *Immunity*, *13*(2), 155-165. https://doi.org/10.1016/s1074-7613(00)00016-9

Tan, A. H., Mahadeva, S., Thalha, A. M., Gibson, P. R., Kiew, C. K., Yeat, C. M., Ng, S. W., Ang, S. P., Chow, S. K., Tan, C. T., Yong, H. S., Marras, C., Fox, S. H., & Lim, S. Y. (2014). Small intestinal bacterial

overgrowth in Parkinson's disease. *Parkinsonism Relat Disord*, *20*(5), 535-540. https://doi.org/10.1016/j.parkreldis.2014.02.019

Tan, E. K., Peng, R., Teo, Y. Y., Tan, L. C., Angeles, D., Ho, P., Chen, M. L., Lin, C. H., Mao, X. Y., Chang, X. L., Prakash, K. M., Liu, J. J., Au, W. L., Le, W. D., Jankovic, J., Burgunder, J. M., Zhao, Y., & Wu, R. M. (2010). Multiple LRRK2 variants modulate risk of Parkinson disease: a Chinese multicenter study. *Hum Mutat*, *31*(5), 561-568. https://doi.org/10.1002/humu.21225

Tanaka, K. F., Kashima, H., Suzuki, H., Ono, K., & Sawada, M. (2002). Existence of functional beta1- and beta2-adrenergic receptors on microglia. *J Neurosci Res*, *70*(2), 232-237. https://doi.org/10.1002/jnr.10399

Tang, Y., Li, T., Li, J., Yang, J., Liu, H., Zhang, X. J., & Le, W. (2014). Jmjd3 is essential for the epigenetic modulation of microglia phenotypes in the immune pathogenesis of Parkinson's disease. *Cell Death Differ*, *21*(3), 369-380. https://doi.org/10.1038/cdd.2013.159

Tao, Y., Yang, Y., Jiao, Y., Wu, S., Zhu, G., Akindolie, M. S., Zhu, T., Qu, J., Wang, L., & Zhang, Y. (2020). Monobutyl phthalate (MBP) induces energy metabolism disturbances in the gills of adult zebrafish (Danio rerio). *Environ Pollut*, *266*(Pt 1), 115288. https://doi.org/10.1016/j.envpol.2020.115288

Tariq, M., Khan, H. A., Al Moutaery, K., & Al Deeb, S. (2001). Protective effect of quinacrine on striatal dopamine levels in 6-OHDA and MPTP models of Parkinsonism in rodents. *Brain Res Bull*, *54*(1), 77-82. https://doi.org/10.1016/s0361-9230(00)00427-5

Tavares, R. G., Schmidt, A. P., Abud, J., Tasca, C. I., & Souza, D. O. (2005). In vivo quinolinic acid increases synaptosomal glutamate release in rats: reversal by guanosine. *Neurochem Res*, *30*(4), 439-444. https://doi.org/10.1007/s11064-005-2678-0

Tavares, R. G., Tasca, C. I., Santos, C. E., Alves, L. B., Porciúncula, L. O., Emanuelli, T., & Souza, D. O. (2002). Quinolinic acid stimulates synaptosomal glutamate release and inhibits glutamate uptake into astrocytes. *Neurochem Int*, *40*(7), 621-627. https://doi.org/10.1016/s0197-0186(01)00133-4

Tavares, R. G., Tasca, C. I., Santos, C. E., Wajner, M., Souza, D. O., & Dutra-Filho, C. S. (2000). Quinolinic acid inhibits glutamate uptake into synaptic vesicles from rat brain. *Neuroreport*, *11*(2), 249-253. https://doi.org/10.1097/00001756-200002070-00005

Tay, T. L., Ronneberger, O., Ryu, S., Nitschke, R., & Driever, W. (2011). Comprehensive catecholaminergic projectome analysis reveals single-neuron integration of zebrafish ascending and descending dopaminergic systems. *Nat Commun*, *2*, 171. https://doi.org/10.1038/ncomms1171

Taylor, J. P., Hulihan, M. M., Kachergus, J. M., Melrose, H. L., Lincoln, S. J., Hinkle, K. M., Stone, J. T., Ross, O. A., Hauser, R., Aasly, J., Gasser, T., Payami, H., Wszolek, Z. K., & Farrer, M. J. (2007). Leucine-rich repeat kinase 1: a paralog of LRRK2 and a candidate gene for Parkinson's disease. *Neurogenetics*, *8*(2), 95-102. https://doi.org/10.1007/s10048-006-0075-8

Tejera-Parrado, C., Jesús, S., Periñán, M. T., Buiza-Rueda, D., Oliva-Ariza, G., Adarmes-Gómez, A. D., Macías-García, D., Gómez-Garre, P., & Mir, P. (2019). A replication study of GWAS-genetic risk variants associated with Parkinson's disease in a Spanish population. *Neurosci Lett*, *712*, 134425. https://doi.org/10.1016/j.neulet.2019.134425

Thanvi, B., Lo, N., & Robinson, T. (2007). Levodopa-induced dyskinesia in Parkinson's disease: clinical features, pathogenesis, prevention and treatment. *Postgrad Med J*, *83*(980), 384-388. https://doi.org/10.1136/pgmj.2006.054759

The NINDS NET-PD Investigators, P. (2008). A pilot clinical trial of creatine and minocycline in early Parkinson disease: 18-month results. *Clin Neuropharmacol*, *31*(3), 141-150. https://doi.org/10.1097/WNF.0b013e3181342f32

Thévenet, J., Pescini Gobert, R., Hooft van Huijsduijnen, R., Wiessner, C., & Sagot, Y. J. (2011). Regulation of LRRK2 expression points to a functional role in human monocyte maturation. *PLoS ONE*, *6*(6), e21519. https://doi.org/10.1371/journal.pone.0021519

Thirtamara-Rajamani, K., Li, P., Escobar Galvis, M. L., Labrie, V., Brundin, P., & Brundin, L. (2017). Is the Enzyme ACMSD a Novel Therapeutic Target in Parkinson's Disease? *J Parkinsons Dis*, *7*(4), 577-587. https://doi.org/10.3233/jpd-171240

Thomas, B., & Beal, M. F. (2007). Parkinson's disease. *Hum Mol Genet*, *16 Spec No. 2*, R183-194. https://doi.org/10.1093/hmg/ddm159
Thomas, D. M., Francescutti-Verbeem, D. M., & Kuhn, D. M. (2006). Gene expression profile of activated microglia under conditions associated with dopamine neuronal damage. *The FASEB Journal*, *20*(3), 515-517. https://doi.org/https://doi.org/10.1096/fj.05-4873fje
Ting, K. K., Brew, B. J., & Guillemin, G. J. (2009). Effect of quinolinic acid on human astrocytes morphology and functions: implications in Alzheimer's disease. *Journal of Neuroinflammation*, *6*(1), 36. https://doi.org/10.1186/1742-2094-6-36
Titz, B., Low, T., Komisopoulou, E., Chen, S. S., Rubbi, L., & Graeber, T. G. (2010). The proximal signaling network of the BCR-ABL1 oncogene shows a modular organization. *Oncogene*, *29*(44), 5895-5910. https://doi.org/10.1038/onc.2010.331
Tomás-Camardiel, M., Rite, I., Herrera, A. J., de Pablos, R. M., Cano, J., Machado, A., & Venero, J. L. (2004). Minocycline reduces the lipopolysaccharide-induced inflammatory reaction, peroxynitrite-mediated nitration of proteins, disruption of the blood–brain barrier, and damage in the nigral dopaminergic system. *Neurobiology of Disease*, *16*(1), 190-201. https://doi.org/https://doi.org/10.1016/j.nbd.2004.01.010
Tomkins, J. E., Dihanich, S., Beilina, A., Ferrari, R., Ilacqua, N., Cookson, M. R., Lewis, P. A., & Manzoni, C. (2018). Comparative Protein Interaction Network Analysis Identifies Shared and Distinct Functions for the Human ROCO Proteins. *Proteomics*, *18*(10), e1700444. https://doi.org/10.1002/pmic.201700444
Tong, Y., Yamaguchi, H., Giaime, E., Boyle, S., Kopan, R., Kelleher, R. J., 3rd, & Shen, J. (2010). Loss of leucine-rich repeat kinase 2 causes impairment of protein degradation pathways, accumulation of alpha-synuclein, and apoptotic cell death in aged mice. *Proc Natl Acad Sci U S A*, *107*(21), 9879-9884. https://doi.org/10.1073/pnas.1004676107
Toyofuku, T., Morimoto, K., Sasawatari, S., & Kumanogoh, A. (2015). Leucine-Rich Repeat Kinase 1 Regulates Autophagy through Turning On TBC1D2-Dependent Rab7 Inactivation. *Mol Cell Biol*, *35*(17), 3044-3058. https://doi.org/10.1128/mcb.00085-15
Tozzi, A., Tantucci, M., Marchi, S., Mazzocchetti, P., Morari, M., Pinton, P., Mancini, A., & Calabresi, P. (2018). Dopamine D2 receptor-mediated neuroprotection in a G2019S Lrrk2 genetic model of Parkinson's disease. *Cell Death Dis*, *9*(2), 204. https://doi.org/10.1038/s41419-017-0221-2
Tran, T. A., Nguyen, A. D., Chang, J., Goldberg, M. S., Lee, J. K., & Tansey, M. G. (2011). Lipopolysaccharide and tumor necrosis factor regulate Parkin expression via nuclear factor-kappa B. *PLoS ONE*, *6*(8), e23660. https://doi.org/10.1371/journal.pone.0023660
Tremblay, M.-È., Lecours, C., Samson, L., Sánchez-Zafra, V., & Sierra, A. (2015). From the Cajal alumni Achúcarro and Río-Hortega to the rediscovery of never-resting microglia [Review]. *Frontiers in Neuroanatomy*, *9*(45). https://doi.org/10.3389/fnana.2015.00045
Tsarouchas, T. M., Wehner, D., Cavone, L., Munir, T., Keatinge, M., Lambertus, M., Underhill, A., Barrett, T., Kassapis, E., Ogryzko, N., Feng, Y., van Ham, T. J., Becker, T., & Becker, C. G. (2018). Dynamic control of proinflammatory cytokines Il-1β and Tnf-α by macrophages in zebrafish spinal cord regeneration. *Nat Commun*, *9*(1), 4670. https://doi.org/10.1038/s41467-018-07036-w
Turcotte, K., Gauthier, S., Tuite, A., Mullick, A., Malo, D., & Gros, P. (2005). A mutation in the Icsbp1 gene causes susceptibility to infection and a chronic myeloid leukemia-like syndrome in BXH-2 mice. *J Exp Med*, *201*(6), 881-890. https://doi.org/10.1084/jem.20042170
Turnbull, S., Tabner, B. J., Brown, D. R., & Allsop, D. (2003). Quinacrine acts as an antioxidant and reduces the toxicity of the prion peptide PrP106-126. *Neuroreport*, *14*(13), 1743-1745. https://doi.org/10.1097/00001756-200309150-00017
Umeno, J., Asano, K., Matsushita, T., Matsumoto, T., Kiyohara, Y., Iida, M., Nakamura, Y., Kamatani, N., & Kubo, M. (2011). Meta-analysis of published studies identified eight additional common susceptibility loci for Crohn's disease and ulcerative colitis. *Inflamm Bowel Dis*, *17*(12), 2407-2415. https://doi.org/10.1002/ibd.21651
Valente, E. M., Abou-Sleiman, P. M., Caputo, V., Muqit, M. M. K., Harvey, K., Gispert, S., Ali, Z., Del Turco, D., Bentivoglio, A. R., Healy, D. G., Albanese, A., Nussbaum, R., González-Maldonado, R., Deller, T., Salvi, S., Cortelli, P., Gilks, W. P., Latchman, D. S., Harvey, R. J., Dallapiccola, B., Auburger, G.,

& Wood, N. W. (2004). Hereditary Early-Onset Parkinson's Disease Caused by Mutations in PINK1. *Science*, *304*(5674), 1158-1160. https://doi.org/10.1126/science.1096284

Van der Perren, A., Macchi, F., Toelen, J., Carlon, M. S., Maris, M., de Loor, H., Kuypers, D. R., Gijsbers, R., Van den Haute, C., Debyser, Z., & Baekelandt, V. (2015). FK506 reduces neuroinflammation and dopaminergic neurodegeneration in an α-synuclein-based rat model for Parkinson's disease. *Neurobiol Aging*, *36*(3), 1559-1568. https://doi.org/10.1016/j.neurobiolaging.2015.01.014

Vandresen-Filho, S., Martins, W. C., Bertoldo, D. B., Mancini, G., De Bem, A. F., & Tasca, C. I. (2015). Cerebral cortex, hippocampus, striatum and cerebellum show differential susceptibility to quinolinic acid-induced oxidative stress. *Neurological Sciences*, *36*(8), 1449-1456. https://doi.org/10.1007/s10072-015-2180-7

Vandresen-Filho, S., Severino, P. C., Constantino, L. C., Martins, W. C., Molz, S., Dal-Cim, T., Bertoldo, D. B., Silva, F. R. M. B., & Tasca, C. I. (2015). N-Methyl-d-aspartate Preconditioning Prevents Quinolinic Acid-Induced Deregulation of Glutamate and Calcium Homeostasis in Mice Hippocampus. *Neurotoxicity Research*, *27*(2), 118-128. https://doi.org/10.1007/s12640-014-9496-6

Vardar, G., Chang, S., Arancillo, M., Wu, Y.-J., Trimbuch, T., & Rosenmund, C. (2016). Distinct Functions of Syntaxin-1 in Neuronal Maintenance, Synaptic Vesicle Docking, and Fusion in Mouse Neurons. *The Journal of Neuroscience*, *36*(30), 7911-7924. https://doi.org/10.1523/jneurosci.1314-16.2016

Venkatachalam, A. B., Thisse, C., Thisse, B., & Wright, J. M. (2009). Differential tissue-specific distribution of transcripts for the duplicated fatty acid-binding protein 10 (fabp10) genes in embryos, larvae and adult zebrafish (Danio rerio). *Febs j*, *276*(22), 6787-6797. https://doi.org/10.1111/j.1742-4658.2009.07393.x

Vielhaber, G., Pfeiffer, S., Brade, L., Lindner, B., Goldmann, T., Vollmer, E., Hintze, U., Wittern, K. P., & Wepf, R. (2001). Localization of ceramide and glucosylceramide in human epidermis by immunogold electron microscopy. *J Invest Dermatol*, *117*(5), 1126-1136. https://doi.org/10.1046/j.0022-202x.2001.01527.x

Vigo, C., Lewis, G. P., & Piper, P. J. (1980). Mechanisms of inhibition of phospholipase A2. *Biochemical Pharmacology*, *29*(4), 623-627. https://doi.org/https://doi.org/10.1016/0006-2952(80)90386-X

Vilas, D., Fernández-Santiago, R., Sanchez, E., Azcona, L. J., Santos-Montes, M., Casquero, P., Argandoña, L., Tolosa, E., & Paisán-Ruiz, C. (2017). A Novel p.Glu298Lys Mutation in the ACMSD Gene in Sporadic Parkinson's Disease. *J Parkinsons Dis*, *7*(3), 459-463. https://doi.org/10.3233/jpd-171146

Vitner, E. B., Salomon, R., Farfel-Becker, T., Meshcheriakova, A., Ali, M., Klein, A. D., Platt, F. M., Cox, T. M., & Futerman, A. H. (2014). RIPK3 as a potential therapeutic target for Gaucher's disease. *Nature Medicine*, *20*(2), 204-208. https://doi.org/10.1038/nm.3449

Vlachakis, D., Labrou, N. E., Iliopoulos, C., Hardy, J., Lewis, P. A., Rideout, H., & Trabzuni, D. (2018). Insights into the Influence of Specific Splicing Events on the Structural Organization of LRRK2. *Int J Mol Sci*, *19*(9). https://doi.org/10.3390/ijms19092784

Vliegenthart, A. D. B., Wei, C., Buckley, C., Berends, C., de Potter, C. M. J., Schneemann, S., Del Pozo, J., Tucker, C., Mullins, J. J., Webb, D. J., & Dear, J. W. (2017). Characterization of Triptolide-Induced Hepatotoxicity by Imaging and Transcriptomics in a Novel Zebrafish Model. *Toxicol Sci*, *159*(2), 380-391. https://doi.org/10.1093/toxsci/kfx144

Volta, M., Beccano-Kelly, D. A., Paschall, S. A., Cataldi, S., MacIsaac, S. E., Kuhlmann, N., Kadgien, C. A., Tatarnikov, I., Fox, J., Khinda, J., Mitchell, E., Bergeron, S., Melrose, H., Farrer, M. J., & Milnerwood, A. J. (2017). Initial elevations in glutamate and dopamine neurotransmission decline with age, as does exploratory behavior, in LRRK2 G2019S knock-in mice. *Elife*, *6*. https://doi.org/10.7554/eLife.28377

Wang, D., Tang, B., Zhao, G., Pan, Q., Xia, K., Bodmer, R., & Zhang, Z. (2008). Dispensable role of Drosophila ortholog of LRRK2 kinase activity in survival of dopaminergic neurons. *Mol Neurodegener*, *3*, 3. https://doi.org/10.1186/1750-1326-3-3

Wang, G., Nola, S., Bovio, S., Bun, P., Coppey-Moisan, M., Lafont, F., & Galli, T. (2018). Biomechanical Control of Lysosomal Secretion Via the VAMP7 Hub: A Tug-of-War between VARP and LRRK1. *iScience*, *4*, 127-143. https://doi.org/10.1016/j.isci.2018.05.016

Wang, H., Lee, C. H., Qi, C., Tailor, P., Feng, J., Abbasi, S., Atsumi, T., & Morse, H. C., 3rd. (2008). IRF8 regulates B-cell lineage specification, commitment, and differentiation. *Blood*, *112*(10), 4028-4038. https://doi.org/10.1182/blood-2008-01-129049

Wang, J., Zhao, H., Lv, K., Zhao, W., Zhang, N., Yang, F., Wen, X., Jiang, X., Tian, J., Liu, X., Ho, C.-T., & Li, S. (2021). Pterostilbene Ameliorates DSS-Induced Intestinal Epithelial Barrier Loss in Mice via Suppression of the NF-κB-Mediated MLCK-MLC Signaling Pathway. *Journal of Agricultural and Food Chemistry*, *69*(13), 3871-3878. https://doi.org/10.1021/acs.jafc.1c00274

Wang, L., Li, N. N., Lu, Z. J., Li, J. Y., Peng, J. X., Duan, L. R., & Peng, R. (2019). Association of three candidate genetic variants in ACMSD/TMEM163, GPNMB and BCKDK /STX1B with sporadic Parkinson's disease in Han Chinese. *Neurosci Lett*, *703*, 45-48. https://doi.org/10.1016/j.neulet.2019.03.019

Wang, S., Chu, C.-H., Stewart, T., Ginghina, C., Wang, Y., Nie, H., Guo, M., Wilson, B., Hong, J.-S., & Zhang, J. (2015). α-Synuclein, a chemoattractant, directs microglial migration via H₂O₂-dependent Lyn phosphorylation. *Proceedings of the National Academy of Sciences*, *112*(15), E1926-E1935. https://doi.org/10.1073/pnas.1417883112

Wen, L., Wei, W., Gu, W., Huang, P., Ren, X., Zhang, Z., Zhu, Z., Lin, S., & Zhang, B. (2008). Visualization of monoaminergic neurons and neurotoxicity of MPTP in live transgenic zebrafish. *Dev Biol*, *314*(1), 84-92. https://doi.org/10.1016/j.ydbio.2007.11.012

Werner, Ernst R., Blau, N., & Thöny, B. (2011). Tetrahydrobiopterin: biochemistry and pathophysiology. *Biochemical Journal*, *438*(3), 397-414. https://doi.org/10.1042/bj20110293

West, A. B., Moore, D. J., Biskup, S., Bugayenko, A., Smith, W. W., Ross, C. A., Dawson, V. L., & Dawson, T. M. (2005). Parkinson's disease-associated mutations in leucine-rich repeat kinase 2 augment kinase activity. *Proceedings of the National Academy of Sciences of the United States of America*, *102*(46), 16842. https://doi.org/10.1073/pnas.0507360102

West, A. B., Moore, D. J., Choi, C., Andrabi, S. A., Li, X., Dikeman, D., Biskup, S., Zhang, Z., Lim, K. L., Dawson, V. L., & Dawson, T. M. (2007). Parkinson's disease-associated mutations in LRRK2 link enhanced GTP-binding and kinase activities to neuronal toxicity. *Hum Mol Genet*, *16*(2), 223-232. https://doi.org/10.1093/hmg/ddl471

Westerlund, M., Belin, A. C., Anvret, A., Bickford, P., Olson, L., & Galter, D. (2008). Developmental regulation of leucine-rich repeat kinase 1 and 2 expression in the brain and other rodent and human organs: Implications for Parkinson's disease. *Neuroscience*, *152*(2), 429-436. https://doi.org/10.1016/j.neuroscience.2007.10.062

Whiffin, N., Armean, I. M., Kleinman, A., Marshall, J. L., Minikel, E. V., Goodrich, J. K., Quaife, N. M., Cole, J. B., Wang, Q., Karczewski, K. J., Cummings, B. B., Francioli, L., Laricchia, K., Guan, A., Alipanahi, B., Morrison, P., Baptista, M. A. S., Merchant, K. M., Ware, J. S., Havulinna, A. S., Iliadou, B., Lee, J. J., Nadkarni, G. N., Whiteman, C., Daly, M., Esko, T., Hultman, C., Loos, R. J. F., Milani, L., Palotie, A., Pato, C., Pato, M., Saleheen, D., Sullivan, P. F., Alföldi, J., Cannon, P., & MacArthur, D. G. (2020). The effect of LRRK2 loss-of-function variants in humans. *Nat Med*, *26*(6), 869-877. https://doi.org/10.1038/s41591-020-0893-5

Widner, B., Leblhuber, F., & Fuchs, D. (2002). Increased neopterin production and tryptophan degradation in advanced Parkinson's disease. *J Neural Transm (Vienna)*, *109*(2), 181-189. https://doi.org/10.1007/s007020200014

Williams, G. P., Schonhoff, A. M., Jurkuvenaite, A., Thome, A. D., Standaert, D. G., & Harms, A. S. (2018). Targeting of the class II transactivator attenuates inflammation and neurodegeneration in an alpha-synuclein model of Parkinson's disease. *Journal of Neuroinflammation*, *15*(1), 244. https://doi.org/10.1186/s12974-018-1286-2

Witoelar, A., Jansen, I. E., Wang, Y., Desikan, R. S., Gibbs, J. R., Blauwendraat, C., Thompson, W. K., Hernandez, D. G., Djurovic, S., Schork, A. J., Bettella, F., Ellinghaus, D., Franke, A., Lie, B. A., McEvoy, L. K., Karlsen, T. H., Lesage, S., Morris, H. R., Brice, A., Wood, N. W., Heutink, P., Hardy, J., Singleton, A. B., Dale, A. M., Gasser, T., Andreassen, O. A., & Sharma, M. (2017). Genome-

wide Pleiotropy Between Parkinson Disease and Autoimmune Diseases. *JAMA Neurol*, *74*(7), 780-792. https://doi.org/10.1001/jamaneurol.2017.0469

Wong, D., Prameya, R., & Dorovini-Zis, K. (1999). In vitro adhesion and migration of T lymphocytes across monolayers of human brain microvessel endothelial cells: regulation by ICAM-1, VCAM-1, E-selectin and PECAM-1. *J Neuropathol Exp Neurol*, *58*(2), 138-152. https://doi.org/10.1097/00005072-199902000-00004

Wu, D. C., Jackson-Lewis, V., Vila, M., Tieu, K., Teismann, P., Vadseth, C., Choi, D. K., Ischiropoulos, H., & Przedborski, S. (2002). Blockade of microglial activation is neuroprotective in the 1-methyl-4-phenyl-1,2,3,6-tetrahydropyridine mouse model of Parkinson disease. *J Neurosci*, *22*(5), 1763-1771. https://doi.org/10.1523/jneurosci.22-05-01763.2002

Wu, R. S., Lam, II, Clay, H., Duong, D. N., Deo, R. C., & Coughlin, S. R. (2018). A Rapid Method for Directed Gene Knockout for Screening in G0 Zebrafish. *Dev Cell*, *46*(1), 112-125.e114. https://doi.org/10.1016/j.devcel.2018.06.003

Xenias, H. S., Chen, C., Kang, S., Cherian, S., Situ, X., Shanmugasundaram, B., Scesa, G., Chan, C. S., & Parisiadou, L. (2020). Pathogenic LRRK2 R1441C mutation is associated with striatal alterations. *bioRxiv*, 2020.2003.2011.986455. https://doi.org/10.1101/2020.03.11.986455

Xing, W., Liu, J., Cheng, S., Vogel, P., Mohan, S., & Brommage, R. (2013). Targeted disruption of leucine-rich repeat kinase 1 but not leucine-rich repeat kinase 2 in mice causes severe osteopetrosis. *J Bone Miner Res*, *28*(9), 1962-1974. https://doi.org/10.1002/jbmr.1935

Xu, J., Zhu, L., He, S., Wu, Y., Jin, W., Yu, T., Qu, J. Y., & Wen, Z. (2015). Temporal-Spatial Resolution Fate Mapping Reveals Distinct Origins for Embryonic and Adult Microglia in Zebrafish. *Dev Cell*, *34*(6), 632-641. https://doi.org/10.1016/j.devcel.2015.08.018

Yamashita, A., Deguchi, J., Honda, Y., Yamada, T., Miyawaki, I., Nishimura, Y., & Tanaka, T. (2019). Increased susceptibility to oxidative stress-induced toxicological evaluation by genetically modified nrf2a-deficient zebrafish. *Journal of Pharmacological and Toxicological Methods*, *96*, 34-45. https://doi.org/https://doi.org/10.1016/j.vascn.2018.12.006

Yan, A., Liu, Z., Song, L., Wang, X., Zhang, Y., Wu, N., Lin, J., Liu, Y., & Liu, Z. (2018). Idebenone Alleviates Neuroinflammation and Modulates Microglial Polarization in LPS-Stimulated BV2 Cells and MPTP-Induced Parkinson's Disease Mice. *Front Cell Neurosci*, *12*, 529. https://doi.org/10.3389/fncel.2018.00529

Yang, Y., Davis, I., Matsui, T., Rubalcava, I., & Liu, A. (2019). Quaternary structure of α-amino-β-carboxymuconate-ϵ-semialdehyde decarboxylase (ACMSD) controls its activity. *J Biol Chem*, *294*(30), 11609-11621. https://doi.org/10.1074/jbc.RA119.009035

Yanguas-Casás, N., Barreda-Manso, M. A., Nieto-Sampedro, M., & Romero-Ramírez, L. (2014). Tauroursodeoxycholic acid reduces glial cell activation in an animal model of acute neuroinflammation. *Journal of Neuroinflammation*, *11*(1), 50. https://doi.org/10.1186/1742-2094-11-50

Yanguas-Casás, N., Barreda-Manso, M. A., Pérez-Rial, S., Nieto-Sampedro, M., & Romero-Ramírez, L. (2017). TGFβ Contributes to the Anti-inflammatory Effects of Tauroursodeoxycholic Acid on an Animal Model of Acute Neuroinflammation. *Mol Neurobiol*, *54*(9), 6737-6749. https://doi.org/10.1007/s12035-016-0142-6

Yao, Y., Lin, J., Yang, P., Chen, Q., Chu, X., Gao, C., & Hu, J. (2012). Fine structure, enzyme histochemistry, and immunohistochemistry of liver in zebrafish. *Anat Rec (Hoboken)*, *295*(4), 567-576. https://doi.org/10.1002/ar.22416

Yoshida, Y., Yoshimi, R., Yoshii, H., Kim, D., Dey, A., Xiong, H., Munasinghe, J., Yazawa, I., O'Donovan, M. J., Maximova, O. A., Sharma, S., Zhu, J., Wang, H., Morse, H. C., 3rd, & Ozato, K. (2014). The transcription factor IRF8 activates integrin-mediated TGF-β signaling and promotes neuroinflammation. *Immunity*, *40*(2), 187-198. https://doi.org/10.1016/j.immuni.2013.11.022

Younis, N., Zarif, R., & Mahfouz, R. (2020). Inflammatory bowel disease: between genetics and microbiota. *Mol Biol Rep*, *47*(4), 3053-3063. https://doi.org/10.1007/s11033-020-05318-5

Yu, Q., Huo, J., Zhang, Y., Liu, K., Cai, Y., Xiang, T., Jiang, Z., & Zhang, L. (2020). Tamoxifen-induced hepatotoxicity via lipid accumulation and inflammation in zebrafish. *Chemosphere*, *239*, 124705. https://doi.org/https://doi.org/10.1016/j.chemosphere.2019.124705

Yu, T., Guo, W., Tian, Y., Xu, J., Chen, J., Li, L., & Wen, Z. (2017). Distinct regulatory networks control the development of macrophages of different origins in zebrafish. *Blood*, *129*(4), 509-519. https://doi.org/10.1182/blood-2016-07-727651

Yun, S. P., Kim, D., Kim, S., Kim, S., Karuppagounder, S. S., Kwon, S.-H., Lee, S., Kam, T.-I., Lee, S., Ham, S., Park, J. H., Dawson, V. L., Dawson, T. M., Lee, Y., & Ko, H. S. (2018). α-Synuclein accumulation and GBA deficiency due to L444P GBA mutation contributes to MPTP-induced parkinsonism. *Molecular Neurodegeneration*, *13*(1), 1. https://doi.org/10.1186/s13024-017-0233-5

Zecca, L., Zucca, F. A., Wilms, H., & Sulzer, D. (2003). Neuromelanin of the substantia nigra: a neuronal black hole with protective and toxic characteristics. *Trends Neurosci*, *26*(11), 578-580. https://doi.org/10.1016/j.tins.2003.08.009

Zhang, C. X., Engqvist-Goldstein, Å. E. Y., Carreno, S., Owen, D. J., Smythe, E., & Drubin, D. G. (2005). Multiple Roles for Cyclin G-Associated Kinase in Clathrin-Mediated Sorting Events. *Traffic*, *6*(12), 1103-1113. https://doi.org/https://doi.org/10.1111/j.1600-0854.2005.00346.x

Zhang, F. R., Huang, W., Chen, S. M., Sun, L. D., Liu, H., Li, Y., Cui, Y., Yan, X. X., Yang, H. T., Yang, R. D., Chu, T. S., Zhang, C., Zhang, L., Han, J. W., Yu, G. Q., Quan, C., Yu, Y. X., Zhang, Z., Shi, B. Q., Zhang, L. H., Cheng, H., Wang, C. Y., Lin, Y., Zheng, H. F., Fu, X. A., Zuo, X. B., Wang, Q., Long, H., Sun, Y. P., Cheng, Y. L., Tian, H. Q., Zhou, F. S., Liu, H. X., Lu, W. S., He, S. M., Du, W. L., Shen, M., Jin, Q. Y., Wang, Y., Low, H. Q., Erwin, T., Yang, N. H., Li, J. Y., Zhao, X., Jiao, Y. L., Mao, L. G., Yin, G., Jiang, Z. X., Wang, X. D., Yu, J. P., Hu, Z. H., Gong, C. H., Liu, Y. Q., Liu, R. Y., Wang, D. M., Wei, D., Liu, J. X., Cao, W. K., Cao, H. Z., Li, Y. P., Yan, W. G., Wei, S. Y., Wang, K. J., Hibberd, M. L., Yang, S., Zhang, X. J., & Liu, J. J. (2009). Genomewide association study of leprosy. *N Engl J Med*, *361*(27), 2609-2618. https://doi.org/10.1056/NEJMoa0903753

Zhang, M.-q., Chen, B., Zhang, J.-p., Chen, N., Liu, C.-z., & Hu, C.-q. (2020). Liver toxicity of macrolide antibiotics in zebrafish. *Toxicology*, *441*, 152501. https://doi.org/https://doi.org/10.1016/j.tox.2020.152501

Zhang, Q., Pan, Y., Yan, R., Zeng, B., Wang, H., Zhang, X., Li, W., Wei, H., & Liu, Z. (2015). Commensal bacteria direct selective cargo sorting to promote symbiosis. *Nat Immunol*, *16*(9), 918-926. https://doi.org/10.1038/ni.3233

Zhang, W., Wang, T., Pei, Z., Miller, D. S., Wu, X., Block, M. L., Wilson, B., Zhang, W., Zhou, Y., Hong, J.-S., & Zhang, J. (2005). Aggregated α-synuclein activates microglia: a process leading to disease progression in Parkinson's disease. *The FASEB Journal*, *19*(6), 533-542. https://doi.org/https://doi.org/10.1096/fj.04-2751com

Zhang, W., Zecca, L., Wilson, B., Ren, H. W., Wang, Y. J., Wang, X. M., & Hong, J. S. (2013). Human neuromelanin: an endogenous microglial activator for dopaminergic neuron death. *Front Biosci (Elite Ed)*, *5*, 1-11. https://doi.org/10.2741/e591

Zhang, X., Li, C., & Gong, Z. (2014). Development of a convenient in vivo hepatotoxin assay using a transgenic zebrafish line with liver-specific DsRed expression. *PLoS ONE*, *9*(3), e91874. https://doi.org/10.1371/journal.pone.0091874

Zhang, Y., Cen, J., Jia, Z., Hsiao, C. D., Xia, Q., Wang, X., Chen, X., Wang, R., Jiang, Z., Zhang, L., & Liu, K. (2019). Hepatotoxicity Induced by Isoniazid-Lipopolysaccharide through Endoplasmic Reticulum Stress, Autophagy, and Apoptosis Pathways in Zebrafish. *Antimicrob Agents Chemother*, *63*(5). https://doi.org/10.1128/aac.01639-18

Zhang, Y., Jiao, Y., Tao, Y., Li, Z., Yu, H., Han, S., & Yang, Y. (2021). Monobutyl phthalate can induce autophagy and metabolic disorders by activating the ire1a-xbp1 pathway in zebrafish liver. *Journal of Hazardous Materials*, *412*, 125243. https://doi.org/https://doi.org/10.1016/j.jhazmat.2021.125243

Zhang, Y., Yuan, B., Takagi, N., Wang, H., Zhou, Y., Si, N., Yang, J., Wei, X., Zhao, H., & Bian, B. (2018). Comparative Analysis of Hydrophilic Ingredients in Toad Skin and Toad Venom Using the UHPLC-HR-MS/MS and UPLC-QqQ-MS/MS Methods Together with the Anti-Inflammatory Evaluation of Indolealkylamines. *Molecules*, *24*(1). https://doi.org/10.3390/molecules24010086

Zhang, Y., Zhang, Z., & Ge, W. (2018). An efficient platform for generating somatic point mutations with germline transmission in the zebrafish by CRISPR/Cas9-mediated gene editing. *J Biol Chem*, *293*(17), 6611-6622. https://doi.org/10.1074/jbc.RA117.001080

Zhao, F., Shi, Y., Huang, Y., Zhan, Y., Zhou, L., Li, Y., Wan, Y., Li, H., Huang, H., Ruan, H., Luo, L., & Li, L. (2018). Irf8 regulates the progression of myeloproliferative neoplasm-like syndrome via Mertk signaling in zebrafish. *Leukemia*, *32*(1), 149-158. https://doi.org/10.1038/leu.2017.189

Zhao, J., Molitor, T. P., Langston, J. W., & Nichols, R. J. (2015). LRRK2 dephosphorylation increases its ubiquitination. *Biochem J*, *469*(1), 107-120. https://doi.org/10.1042/bj20141305

Zhao, N., Guo, M., Wang, K., Zhang, C., & Liu, X. (2020). Identification of Pan-Cancer Prognostic Biomarkers Through Integration of Multi-Omics Data. *Front Bioeng Biotechnol*, *8*, 268. https://doi.org/10.3389/fbioe.2020.00268

Zhou, F., Ju, J., Fang, Y., Fan, X., Yan, S., Wang, Q., Wei, P., Duan, F., Miao, F., Hu, Z., & Wang, M. (2019). Salidroside protected against MPP(+) -induced Parkinson's disease in PC12 cells by inhibiting inflammation, oxidative stress and cell apoptosis. *Biotechnol Appl Biochem*, *66*(2), 247-253. https://doi.org/10.1002/bab.1719

Zhou, J., Gu, X., Fan, X., Zhou, Y., Wang, H., Si, N., Yang, J., Bian, B., & Zhao, H. (2019). Anti-inflammatory and Regulatory Effects of Huanglian Jiedu Decoction on Lipid Homeostasis and the TLR4/MyD88 Signaling Pathway in LPS-Induced Zebrafish. *Front Physiol*, *10*, 1241. https://doi.org/10.3389/fphys.2019.01241

Zhou, N., Liu, K., Sun, Y., Cao, Y., & Yang, J. (2019). Transcriptional mechanism of IRF8 and PU.1 governs microglial activation in neurodegenerative condition. *Protein Cell*, *10*(2), 87-103. https://doi.org/10.1007/s13238-018-0599-3

Zimprich, A., Biskup, S., Leitner, P., Lichtner, P., Farrer, M., Lincoln, S., Kachergus, J., Hulihan, M., Uitti, R. J., Calne, D. B., Stoessl, A. J., Pfeiffer, R. F., Patenge, N., Carbajal, I. C., Vieregge, P., Asmus, F., Muller-Myhsok, B., Dickson, D. W., Meitinger, T., Strom, T. M., Wszolek, Z. K., & Gasser, T. (2004). Mutations in LRRK2 cause autosomal-dominant parkinsonism with pleomorphic pathology. *Neuron*, *44*(4), 601-607. https://doi.org/10.1016/j.neuron.2004.11.005

Zoodsma, J. D., Chan, K., Bhandiwad, A. A., Golann, D. R., Liu, G., Syed, S. A., Napoli, A. J., Burgess, H. A., Sirotkin, H. I., & Wollmuth, L. P. (2020). A Model to Study NMDA Receptors in Early Nervous System Development. *J Neurosci*, *40*(18), 3631-3645. https://doi.org/10.1523/jneurosci.3025-19.2020